The Sixth
International Conference on
Cold Fusion

PROGRESS IN NEW HYDROGEN ENERGY

October 13-18, 1996
JAPAN

New Energy and Industrial Technology Development Organization
The Institute of Applied Energy

Proceedings VOL.2

The Sixth International Conference on Cold Fusion

PROGRESS IN NEW HYDOROGEN ENERGY

Edited by Makoto OKAMOTO

■

October 13-18, 1996
JAPAN

Published by:
New Energy and Industrial Technology Development Organization
The Institute of Applied Energy

Supported by:
The Agency of Natural Resources and Energy of
the Ministry of International Trade and Industry

Proceedings VOL. 2

Contents

Volume 1

Fundamental Session

Helium and Heat Correlation

NHE Session

Excess Heat

Contents

Material Science Studies

Contents

Nuclear Physics Approach

Contents

Contents

Appendix

Contents

Volume 2

Excess Energy and Nuclear Products

Contents

Innovative Approach

Contents

Special Session

CETI Session

Contents

Transmutation

Russian Activities

Summary

Appendix

Organizing Committees

International Advisory Committee

Prof. Bressani, T.	(University Torino, Italy)
Prof. Fleischmann, M.	(IMRA Europe, U.K.)
Prof. Ikegami, H.	(NIFS, Japan)
Mr. Jaeger, F.	(ENECO, U.S.A.)
Dr. McKubre, K.	(SRI International, U.S.A.)
Prof. Okamoto, M.	(Tokyo Institute of Technology, Japan)
Prof. Pons, S.	(IMRA Europe, France)
Prof. Preparata, G.	(University Milano, Italy)
Prof. Samsonenko, N.	(PFUR, Russia)
Prof. Sánchez, C.	(University Autonoma, Spain)
Dr. Scaramuzzi, F.	(ENEA, Italy)
Dr. Srinivasan, M.	(BARC, India)
Prof. Li, X. Z.	(Tsinghua University, China)

Local Organizing Committee

Prof. Okamoto, M.	(Chairperson)
Dr. Asami, N.	(Vice-chairperson, NHE Sapporo)
Prof. Ikegami, H.	(NIFS)
Director Omura, T.	(NEDO)
Prof. Ota, K.	(Yokohama National University)
Prof. Takahashi, A.	(Osaka University)

Conference Information

Name of Conference

The Sixth International Conference on Cold Fusion

Period

Conference: October 13-17, 1996
Technical Tour: October 18, 1996

Venue

Hotel Apex Toya, Hokkaido
Aza-Shimizu, Abuta-machi, Abuta-gun, Hokkaido 049-57, Japan

Conference Secretariat

c/o NHE-Center, IAE
Shinbashi TS Building, 1-22-5 Nishi-Shinbashi, Minato-ku, Tokyo 105, Japan
Tel: +81-3-3508-8901 Fax: +81-3-3508-8902 E-mail: mac@iae.or.jp

Official Language

English

Fundamental Session

Excess Energy and Nuclear Products
Innovative Approach

Click here for a more readable copy of this paper

Radiationless Cold Fusion: Why Small "Crystals" Are Better, N_{cell} Requirement, and Energy Transfer to Lattice

Talbot A. Chubb and Scott R. Chubb

Oakton International Corporation
5023 N. 38th Street, Arlington, VA 22207, U.S.A.

Abstract
The Ion Band State Theory describes Fleischmann and Pons cold fusion phenomena. It is based on application of solid state band theory physics, many-body physics, and the known quantum behavior of hydrogen in metals. Important assumptions are that charge neutrality exists in each unit cell and that the reactive quantum states, which are stationary Bloch states, are describable as symmetric sums over complete sets of non-stationary, particle-like Wannier states. Consequences are that D^+-D^+ wave function overlap occurs for crystals possessing a sufficiently large number $N_{cell} >\sim 10^4$ of unit cells. Once this condition is met, small crystals provide more power per cc than larger crystals. Energy-transfer from the product state to the lattice electrons results from a change in the quantum of mass and resulting inelastic scattering due to charge distribution changes in the boundary region. The theory also predicts that the primary product is ^{4}He, as observed.

Observations of Fusion in PdD_X Explained by Ion Band State Theory

This paper is concerned with theory developed to explain Fleischmann and Pons (FP) type cold fusion. FP cold fusion is radiationless. Despite much study there has been no direct link established between emission of particles or □-rays and the observed production of heat in PdD_X. This lack of radiation distinguishes FP cold fusion from muon catalyzed cold fusion and from any fusion that might occur due to transients producing "temperatures" and/or densities enabling hot fusion reactions.

FP cold fusion theory must take into account at least 3 other realities. Cold fusion does not occur in D_2 or any deuterided molecules. It is restricted to metals to which deuterium has been added, i.e., to deuterided metal lattices. Second, there is the substantial evidence provided by Arata and Zhang[1] that deuterided ultrafine Pd powder produces substantial heat under conditions that correspond to lower deuterium chemical potential than those employed by Fleischmann and Pons. Third, Arata and Zhang have established that ^{4}He is the primary, if not sole, nuclear product.

The Ion Band State (IBS) Theory[2] has had singular success in providing a framework that can explain radiationless release of nuclear energy. This paper describes the IBS Theory and summarizes its assumptions. These assumptions include rules that are based on how quantum mechanics can apply in a periodic lattice in order for the effect to take place. They are not meant to be a minimum set of requirements for FP cold fusion; alternatively they could be incomplete. However, acceptance of the assumptions seems to lead logically to the conclusions (1) that there is a minimum "crystal" size enabling fusion, (2) that at significantly larger crystal

sizes small crystals are better, (3) that there are symmetry-preserving means by which available nuclear energy can by dissipated in deuterided metal lattices without radiation, and (4) the nuclear product is 4He.

Language Problems: Different Names for Same Thing

Before discussing IBS theory, we address a language problem that may have confused readers of our earlier papers. We have used different names from different disciplines to describe the same thing. Equivalent names are listed below with the ones most used in this paper listed in bold type:

deuteron = d = D^+ = D^+ ion = deuterium nucleus

stationary state = eigenstate = time-independent state

density distribution function = $|\psi(\mathbf{r})|^2$ = probability distribution function for Compton scattering type interactions = "ion orbital"

band state = Bloch function state = Bloch state = [state for which $|\psi(\mathbf{r}+\mathbf{R}_n)| = |\psi(\mathbf{r})|$] = [state for which $|\psi(\mathbf{r}+\mathbf{R}_{Bravais})| = |\psi(\mathbf{r})|$] = periodic amplitude state = lattice symmetric state = state having unbroken lattice symmetry = wavelike state = state resembling a standing wave = "periodic" state

Also, we use the term D^+_{Bloch} to mean a deuteron in a Bloch function state, i.e., with a spread-out charge distribution and having periodic symmetry.

Ion Band States on Surfaces

Both experiment and theory have shown that some of the excited states of hydrogen ions on metal surfaces are ion band states[3]. Also, ground state hydrogen on the relatively closely packed (111) surface of Ni appears to be a band state. The ground state hydrogen distributions on Ni (100), (110), and (111) have been calculated by Puska and Nieminen (1985). These calculations assume that the ion

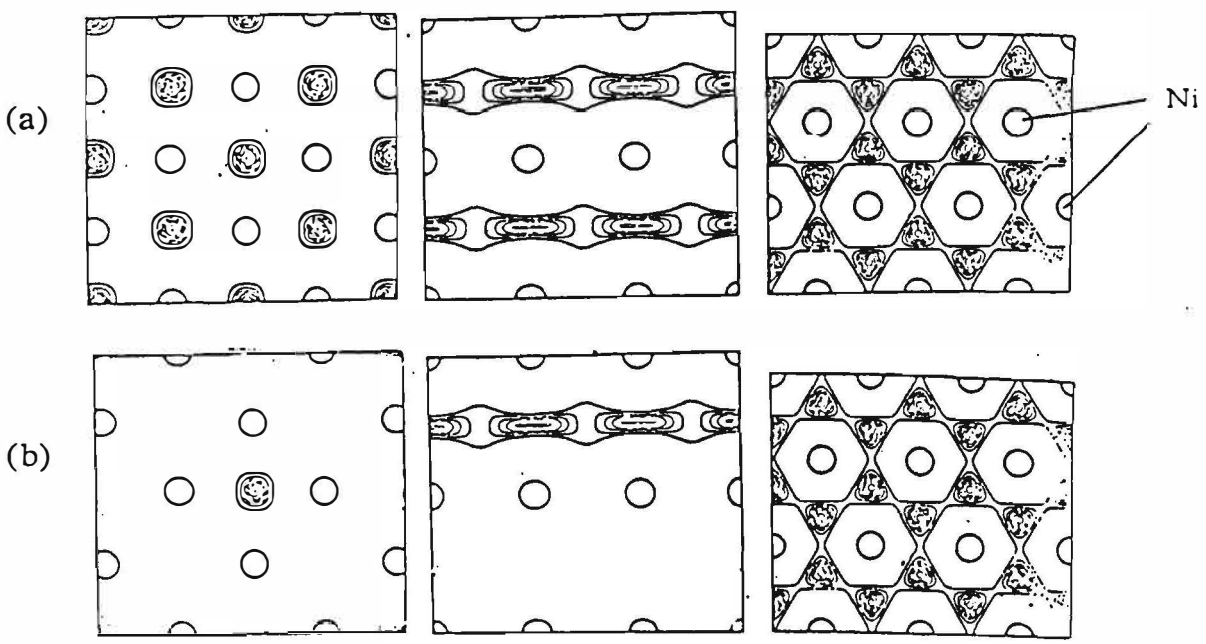

Fig. 1. (a) Calculated lattice-symmetric ground state H^+ density distributions on Ni (100), (110), and (111) taken from Nieminen (1992)[3]. (b) Distributions reachable from a localized particle configuration.

wave functions are Bloch functions. In Fig. 1 we use these calculations to show the difference between localized (chemical) states and ion band states. We also show how, when H^+ is locally

deposited on a surface, the wave function can remain localized, or alternatively, if the localized configuration sufficiently overlaps its neighbor, the wave function can spread out over the metal's surface so that the H^+ becomes uncertain in its position. The H^+ then becomes, or transitions to, a band state ion, effectively having unbroken lattice symmetry.

The plots in Fig. 1 illustrate 1- and 2-dimensional band states. The FP reaction in PdD_x is believed to be a 3-dimensional band state reaction, although the theory also applies to 2-dimensional states. The states supporting FP cold fusion will be assumed to be 3-dimensional.

Assumptions of the Ion Band State Theory

1. The active ingredient undergoing fusion is "paired" band-state deuterons which are part of a matter system described by a many-body wave function.
2. The system is describable by Schroedinger equation quantum mechanics as applied to indistinguishable particles. The 2-body point-particle correlation is fully described by the 2-body wave function.
3. "Paired" band state deuterons are describable by a 6-degrees-of-freedom 2-ion Bloch function in "center-of-mass, separation" coordinates. The Bloch condition applies to both "center-of-mass space" and "separation space".
4. The quantum mechanics superposition[4] principle applies in the sense that the 2-particle stationary state can be expressed as a sum over particle-like states, i.e. Wannier states[5] (virtual states in which identifiable whole ions occupy identifiable unit cells. Wannier states lack periodic symmetry.).
5. Each unit cell has net neutral charge.
6. The effect of electron screening on the stationary state is described by its effect on the 2-ion Wannier states, in accord with Assumptions 4 and 5.
7. Fusion rates can be calculated by time-dependent perturbation theory, which uses stationary initial and final state wave functions.
8. The nuclear and electrostatic portions of the stationary 2-ion wave function preserve a symmetry requirement that it be impossible to identify a specific location of a nuclear reaction.
9. The nuclear reaction couples to the lattice through a coherent release of energy and redistribution of small but equal amounts of charge from each unit cell within the bulk to the surface boundary region.

How Process Works

Broadly speaking, FP cold fusion occurs because deuterons occupying band states have their charge spread out and subdivided within a dominating periodic potential provided by a metal crystal. The IBS process does not work by confining 2 deuterons to a small volume, such as occurs in muon-catalyzed fusion. The IBS process requires that only a small fraction of the deuterons in PdD_x (< 0.0001) be in Bloch configuration states to explain observed power rates.

Properties of Quantized Matter

Sometimes quantum mechanics is described as attributing a mix of particle-like and wave-like properties to matter. Such a picture is appropriate for unbound particles. Here we describe quantum mechanics applied to bound systems as attributing a mix of particle-like and quantized-matter-field-like properties to matter. Sometimes quantized matter is mostly particle-like with some matter field properties. Sometimes quantized matter is mostly field-like with some particle-like properties. These behaviors are illustrated in Fig. 2, using modifications of the surface band state distributions calculated by Puska and Nieminen.

Excess Energy and Nuclear Products

It is important to note that both distributions 2a and 2b apply to a single band state H^+ ion. The second key point to note is that 2b and 2d show single particles and double Bloch-function particles as having identical distributions in space on Ni (111). This behavior would be expected if there were no D^+_{Bloch}-D^+_{Bloch} repulsion. However, it is also true, as we will show, if the D^+_{Bloch}-D^+_{Bloch} repulsion is sufficiently weak, provided that the assumptions of the IBS Theory apply.

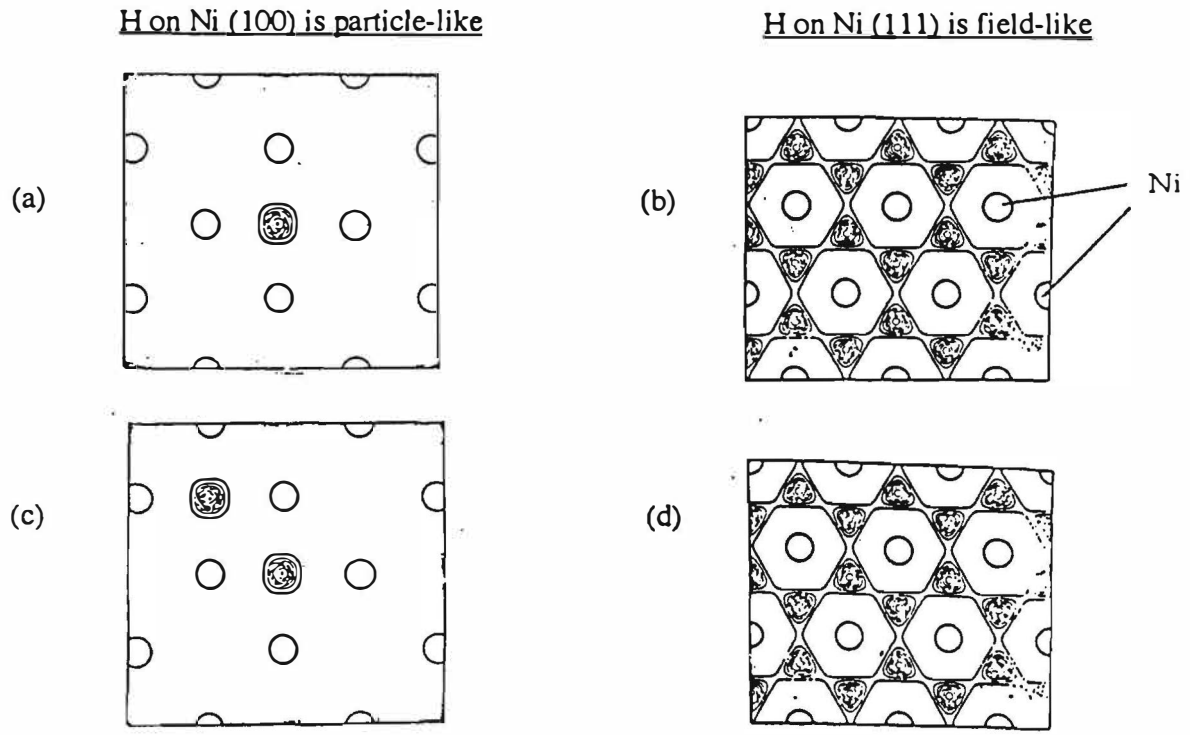

Fig. 2 Calculated charge density distributions of H^+ on Ni surfaces. (a) Single proton on Ni (100); (b) Single proton on Ni (111); (c) Two adjacent protons on Ni (100); (d) Di-proton on Ni (111)

The 2-D^+ Band State Wave Function

If the D^+ see only the periodic potential of the lattice and one neglects D^+-D^+ repulsion, the exchange-symmetrized Schrodinger 2-body band state wave function is:

$$\Psi(\mathbf{r}_1,\mathbf{r}_2) = \frac{1}{\sqrt{2}}\left[\psi_1(\mathbf{r}_1)\ \psi_2(\mathbf{r}_2) + \psi_1(\mathbf{r}_2)\ \psi_2(\mathbf{r}_1)\right] \quad .$$

Here we are assuming that the periodic symmetry imposed by the lattice requires that $\Psi(\mathbf{r}_1,\mathbf{r}_2)$, $\psi_1(\mathbf{r}_1)$, and $\psi_2(\mathbf{r}_2)$ be Bloch functions. $\Psi(\mathbf{r}_1,\mathbf{r}_2)$ is a function of 6 dimensions (6 degrees of freedom), i.e., $\mathbf{r}_1$ and $\mathbf{r}_2$ are independent vector variables. IBS theory assumes that ψ_1 and ψ_2 are independent functions. The Bloch function requirement then means that the amplitude distribution $|\Psi(\mathbf{r}_1,\mathbf{r}_2)|$ does not change if $\mathbf{r}_1 \rightarrow \mathbf{r}_1 + \mathbf{R}_i$ and/or $\mathbf{r}_2 \rightarrow \mathbf{r}_2 + \mathbf{R}_j$. Here $\mathbf{R}_i$ and $\mathbf{R}_j$ are independent Bravais lattice vectors.

When D^+-D^+ repulsion is included but kept weak, and provided each D^+ is screened by its neutralizing charge on length scales that are small compared to unit cell dimensions (which is true for two IBS D^+ in PdD), Ψ can be expressed in terms of position, separation vectors $\mathbf{r}_{cm} = (\mathbf{r}_1+\mathbf{r}_2)/2$ and $\mathbf{r}_{12} = \mathbf{r}_1 - \mathbf{r}_2$:

$$\varphi(\mathbf{r}_{cm}, \mathbf{r}_{12}) = \psi_{cm}(\mathbf{r}_{cm})\ g_{12}(\mathbf{r}_{12}) \quad ,$$

where ψ_{cm} and g_{12} are Bloch functions, i.e., $|\psi_{cm}(\mathbf{r}_{cm}+\mathbf{R}_n)| = |\psi_{cm}(\mathbf{r}_{cm})|$; $|g_{12}(\mathbf{r}_{12}+\mathbf{R}_m)| = |g_{12}(\mathbf{r}_{12})|$; and $\mathbf{R}_n$ and $\mathbf{R}_m$ are independent lattice vectors. Here vector $\mathbf{r}_{cm}$ defines a position in real space. Vector $\mathbf{r}_{12}$ defines a separation magnitude and direction in "separation space". As required by Schroedinger quantum mechanics for the general 2-particle case $\varphi(\mathbf{r}_{cm}, \mathbf{r}_{12})$ has 6 degrees of freedom. The assumptions that $\varphi(\mathbf{r}_{cm}, \mathbf{r}_{12})$, $\psi_{cm}(\mathbf{r}_{cm})$, and $g_{12}(\mathbf{r}_{12})$ are Bloch functions is in accord with Assumption (3) of the IBS Theory. This condition is consistent with the assumed independence of Bloch functions $\psi_1(\mathbf{r}_1)$ and $\psi_2(\mathbf{r}_2)$ in the normal configuration-coordinate formalism of the Schroedinger theory. $\varphi(\mathbf{r}_{cm}, \mathbf{r}_{12})$ is a function of 3 dimensions of real space and 3 dimensions of separation space.

The Bloch function requirement for $g_{12}(\mathbf{r}_{12})$ means that the interaction point $\mathbf{r}_{12} = 0$ is repeated in each unit cell of separation space, since $g_{12}(\mathbf{R}_m) = g_{12}(0)$ where $\mathbf{R}_m$ is any Bravais lattice vector in separation space. The points $[\mathbf{r}_{12} = 0, ..., \mathbf{R}_m, ...]$ are thus assumed to be coherently linked (as a consequence of periodic, order-preserving symmetry) in separation space, as are points $[\mathbf{r}_{cm}, ..., \mathbf{r}_{cm} + \mathbf{R}_n, ...]$ in real space.

In the $\psi_{cm}(\mathbf{r}_{cm})\ g_{12}(\mathbf{r}_{12})$ representation, $|\psi_{cm}(\mathbf{r}_{cm})|$ is called the "matter-field strength" and $|\psi_{cm}(\mathbf{r}_{cm})|^2$ is called the "matter-field density". The quantity $e\,|\psi_{cm}(\mathbf{r}_{cm})|^2$ is the charge density. $g_{12}(\mathbf{r}_{12})$ is called the "dimming function". $|g_{12}(\mathbf{r}_{12})|$ modulates the amplitude of wave function φ everywhere in real space based on the value of $\mathbf{r}_{12}$ in separation space. $g_{12}(\mathbf{r}_{12})$ is also called the "cusp function" because it has a cusp at $\mathbf{r}_{12}=0$ and all equivalent points.

Visualization of the 2-D^+ Band State Wave Function

It is helpful to have a visual representation of the 2-D^+ band state wave function $\varphi(\mathbf{r}_{cm}, \mathbf{r}_{12}) = \psi_{cm}(\mathbf{r}_{cm})\ g_{12}(\mathbf{r}_{12})$. Since φ has 6 degrees of freedom, it is best shown in two 3-dimensional drawings. To simplify the author's task, each of these 3-dimensional drawings is illustrated by a sketch of wave function amplitude versus position along a line through an idealized crystal lattice. This amplitude vs. position function is shown in Fig. 3a. This selected line is taken to pass through a sequence of saddle points in the electrostatic potential provided by the lattice. The saddle points are the minima in the potential barrier that localized interstitial D^+ ions must overcome to diffuse through the crystal. The accompanying dimming function in separation space is shown in Fig. 3b.

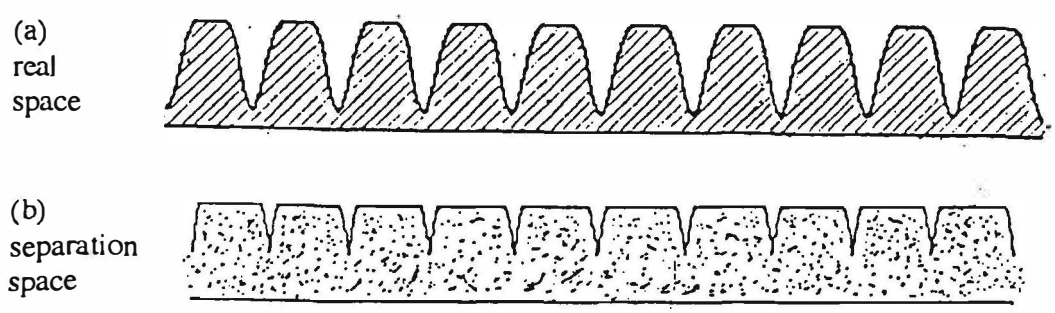

Fig. 3. (a) $|\psi_{cm}(\mathbf{r}_{cm})|^2$ vs. position $\mathbf{r}_{cm}$ along a line through a row of saddle points in an idealized cubic lattice. $\mathbf{r}_{cm}$ describes positions in real space inside a metal crystal lattice. (b) $g_{12}(\mathbf{r}_{12})$ vs. separation vector $\mathbf{r}_{12}$. $|g_{12}(\mathbf{r}_{12})|$ reduces the amplitude of the 2-ion wave function φ as $\mathbf{r}_{12} \rightarrow 0$. $\mathbf{r}_{12} = \mathbf{r}_1 - \mathbf{r}_2$ is the separation between coherently linked particle positions.

Excess Energy and Nuclear Products

In the IBS Theory each reaction occurs throughout the crystal in real space and at N_{cell} coherently-linked cusp points in separation space. The crystal is assumed to be made up of N_{cell} identical unit cells.

The starting point for the IBS 2-ion wave function is the pure matter field picture that models the band state ions in a lattice when D^+-D^+ repulsion is neglected. Here a field means an entity that has a defined value at every point in 3-dimensional space, i.e., is a function of the position vector in real space. Only 3-dimensions are required to describe the matter field. As the D^+-D^+ point-particle repulsion is turned-on, the quantized matter field changes into a 6-dimensional 2-body wave function. A dependency in separation space is created and the cusps shown in Figure 3b begin to grow. If the repulsion potential is permitted to grow to its real value, cusps grow to a magnitude that is determined by minimization of total system energy. Calculations[2] show that the energy-minimizing cusp amplitude is a function of N_{cell}. The cause of the N_{cell} dependence is a reduction in the point-particle interaction potential for Bloch function D^+ from its free space value, caused by the existence of multiple cusps in separation space. As described in ICCF5 (Chubb and Chubb, 1995) the point particle interaction potential calculated in accord with Assumptions 4 and 5 of the IBS Theory, which is appropriate for metals, is $e^2/(r_{12} N_{cell})$. Ideally, at some N_{cell} lower limit less than $\sim 10^4$, the cusps reduce the amplitude of the wave function to zero and no wave function overlap and cold fusion can occur. With still smaller crystals the cusp picture is no longer valid and the energy-minimized wave function splits into a diatomic molecule-like configuration in which negligible overlap occurs. The N_{cell} lower limit is the minimum N_{cell} requirement for cold fusion.

Why Small Crystals Are Better

Once metal crystals are sufficiently large that N_{cell} exceeds the minimum value required for D^+-D^+ wave function overlap and fusion, still larger crystals are detrimental in that they reduce heat production per cc. This reduction is a consequence of the matter field character of the FP fusion reaction. Effectively, because the reactant is derived from the 2-particle terms in the many-body wave equation describing a D^+ matter field which is confined to a single crystal, each crystal is a separate reactor. The other important factor is microscopic reversibility, which is expressed in the interaction matrix element identity $|V_{if}| = |V_{fi}|$ of the Fermi Golden Rule reaction rate equation. Microscopic reversibility means that the final state is as important as the initial state in reaction rate calculations. The final state wave function corresponds to a field strength of one $^4He^{++*}_{Bloch}$ excited-product Bloch function ion per crystal, regardless of crystal size. At the same D^+_{Bloch} concentration per unit volume, each crystal produces heat at the same rate per crystal. Since each crystal produces the same heat, the more crystals per cc, the higher the heat generation rate per cc. However, as described previously[2], the theory may not be applicable for crystals with $N_{cell} < 10^9$, because only when $N_{cell} \gtrsim 10^9$ is sufficient periodic order present to justify in a rigorous fashion that the ion band state theory apply.

d-d "Field" Reaction Rates; (Self-Interaction Reactions of a Matter Field)

Here we show more details for 2-particle matter field self-interaction fusion reactions. Reaction rate is calculated on a per-crystal basis. The matter field density is expressed in terms of normalized wave function densities. The matter field density of each particle integrated over a unit cell is $1/N_{cell}$ because each particle wave function is normalized at 1 particle per crystal. Hence the field of each particle decreases with crystal size, but the number of pairs equally increases with crystal size. The result of the calculation is described below:

Excess Energy and Nuclear Products

Reaction Parameters::

$\dot{N} \equiv$ [reactions s^{-1} $crystal^{-1}$]

Field pair-density of 2-D^+_{Bloch}: $|\psi_{cm,ij}|^2$. Fraction of deuteron $pair_{ij}$ per unit cell $\propto |\psi_{D,i}|^2 \; |\psi_{D,j}|^2 = 1/N_{cell}^2$

Field density of $^4He^{++*}_{Bloch}$: 0 in initial state

$|\psi_{cm,He}|^2$ in final state. Fraction of He per unit cell $= 1/N_{cell}$

Reactions rate per unit cell

$$\frac{\dot{N}}{N_{cell}} \propto |\psi_D|^4 \; |\psi_{He^*,\,final}|^2 \; \text{number of pairs}$$

$$\propto 1/N_{cell}^2 \; 1/N_{cell} \; N_D(N_D-1)$$

$$\tilde{\propto} \; 1/N_{cell} \; c_{D,Bloch}^2 \; s^{-1} \; unit\text{-}cell^{-1}$$

Reaction rate per crystal

$$\dot{N} \; \tilde{\propto} \; c_{D,Bloch}^2 \quad [s^{-1} \; crystal^{-1}]$$

We have used the approximation $N_D^2 \cong N_D(N_D-1)$ and the relation $N_D = c_{D,Bloch} N_{cell}$. Concentration $c_{D,Bloch}$ is the number of D^+_{Bloch} per unit cell. Both initial and final state field densities enter the reaction rate per unit cell because of quantum mechanics microscopic reversibility, which appears in the Fermi Golden Rule reaction rate equation. To get the reaction rate for the crystal as a whole we have summed over the unit cells in a single crystal.

Because the fusion rate is the same for big and small crystals, the smaller the crystals, the more fusions per cc.

Heat Generation: Coupling between the Nuclear Reaction and the Lattice

In a quantized matter field as shown in Figs. 2 and 3, paired D^+ as seen in each unit cell are constrained relative to each other to a volume of atom/molecular dimension, as opposed to nuclear dimension. Because energy minimization has eliminated the coulomb barrier, the remaining strong force attraction between antiparallel nuclear spin deuterons leads to coalescence[2] (i.e., to a reversible form of the interaction matrix element $|V_{if}|$) by which the nuclear components of the wave function are constrained relative to each other to a volume of nuclear dimension. This coalescence is reversible until some small amount of energy is transferred to the lattice. The $^4He^{++*}_{Bloch}$, which is the product of the coalescence (Chubb and Chubb, 1991), constitutes a new matter field which has a different quantum of mass and a different set of Bloch eigenstates than those of the D^+_{Bloch}. The coalescence process occurs coherently throughout the crystal, and occurs equally and simultaneously in each unit cell and in the boundary region. As an example of volume change, if the change from mass-2, charge-1 to mass-4, charge-2 occurred for ions in a 3-dimensional harmonic well, the decrease in volume of the ground state wave function would be a factor of 8.

It is assumed that the coalescence process occurs without disturbing periodic order and without altering the charge distribution within the crystal bulk. However, in the boundary region, which is coherently connected to the bulk, there is a change in charge distribution caused by the reduced coherence length associated with the $^4He^{++*}_{Bloch}$ quantum of mass. To be specific, the ion wave

function in the boundary region, which is required to match the bulk solution at the surface, is forced to die out by a rising potential on opposite sides of the bulk. In this rising barrier region the $^4He^{++*}$ wave function falls off more rapidly than the D^+ wave function at locations extending away from regions corresponding to the lower potential that characterizes the crystal bulk.

Throughout the crystal the band state ions are coupled to the many-body electron system which provides the potential minimum within which the D^+ reside in each unit cell. A change in the charge distribution within the boundary region inelastically scatters the band state electrons into empty states above the fermi level. The scattering process is the same scattering process that accompanies current flow (resistive heating). Once any electron scattering takes place, the reaction goes to completion in the boundary region with the release of energy in the solid totaling 23.8 MeV. The electron coherence volume extends beyond the ion coherence volume. As a result, for embedded crystals the many-body electron system extends beyond the ordered region of a single embedded crystallite and the heating effect extends beyond the N_{cell} volume.

In addition to energization of the band state electrons, there is a transfer of the He^{++} charge with its neutralizing electrons from the bulk to the boundary region, a slight shrinkage of the crystal, and a generation of phonons.

Indirectly accessible Bloch states

A candidate state for FP cold fusion is a 3-dimensional analog of the H^+-on-Ni (100) Bloch state illustrated in the left panel of Fig. 1a. Such a state is not directly accessible, or not easily accessible, from a localized occupied state, but is indirectly accessible through the occupation of an overlapping spread-out state. Occupation from a more accessible spread-out, excited state (Arata's "spillover" deuterium?) should involve a heat of transition and impose strict Bloch symmetry on allowed selection rules. The transition would likely be exothermic. Calculated fusion rates would be higher than in more spread-out states because of a smaller occupied volume prior to coalescence. Difficulty of depopulating indirectly accessible Bloch states may be responsible for the FP "heat after death" phenomenon.[6]

References

1. Y. Arata and Y-C Zhang, *Proc. Japan Acad.* **70B**, 106 (1994); *Proc. Japan Acad.* **71B**, 98 (1995); *Proc. Japan Acad.* **71B**, 304 (1995); *Fusion Technol.*, in press (1996).
2. T. A. Chubb and S. R. Chubb, *Fusion Technol.* **20**, 93 (1991); Proc. ICCF5, 315 (1995);S. R. Chubb and T. A. Chubb, *Fusion Technol.* **24**, 403 (1993).
3. M. J. Puska, R. M. Nieminen, M. Manninen, B. Chakraborty, S. Holloway, and J. K. Norskov, *Phys. Rev. Lett.* **51**, 1081 (1983); M. J. Puska and R. M. Nieminen, *Surf. Sci.* **157**. 413 (1985); R. Nieminen, *Nature* **356**,289 (1992):; Astaldi, A Bianco, S. Modesti, and E. Tosatti, *Phys. Rev. Lett.* **68**, 90 (1992).
4. P. W. Anderson, *Science* **177**, 393 (1972). D. J. Goss, *Phys. Today*, 46 (Dec. 1995).
5. J. M. Ziman, *Principles of Theory of Solids*, (Cambridge University Press, London, 1972).
6. S. Pons and M. Fleischmann, *Trans. Fusion Technol.* **26**, 87 (1994)

Excess Energy and Nuclear Products

MEASUREMENTS OF EXCESS HEAT AND NUCLEAR PRODUCTS IN Pd-D_2O SYSTEM USING TWIN OPEN TYPE ELECTROLYSIS CELLS

H. Fukuoka, T. Ikegawa[†], K. Kobayashi[‡], A. Takahashi
Department of Nuclear Engineering, Osaka University,
2-1 Yamadaoka, Suita, Osaka, 565, Japan
[†] Present affiliation, HITACHI Co.Ltd.
[‡] Present affiliation, University of Tokyo

Abstract

Measurements of excess heat, X-rays and neutrons to study possible correlation between excess heat and nuclear products during the electrolysis of LiOD heavy water electrolyte using Pd cathodes were carried out. Two open type electrochemical cells with two sets of X-ray and neutron detection systems were formed to be twin type. Therefore, two experiments being carried out by two cells at the same time were compared at any time and false signals in coincidence for two cells were able to be rejected as accidental noises. No excess heats were observed out of seven runs after ICCF5. But weak excess X-rays and neutron burst were observed at the same time in one case. And only soft X-rays were detected during electrolysis of heavy water using Pd cathodes in two cases and one case for electrolysis of light water.

1.Introduction

Since "cold fusion" phenomenon was reported by Fleishmann and Pons[1], excess heat and nuclear products during heavy water electrolysis were reported by many groups. However, it was difficult to reproduce this phenomenon in most of the groups[2]. We reported slight excess heat (5-7%) with weak neutron emission in energy over 3MeV at ICCF5[3]. The aim of this study was to reproduce our last results and to perform more reliable measurements to search the correlation between excess heat and nuclear products. If nuclear reaction with heat generation takes place in solid without neutrons, high energy (several MeV) charged particle emissions are usually expected. Therefore, emissions of characteristic X-rays and bremsstrahlung X-rays will be caused by slowing-down of the charged particles in material. Since most of these emissions will be characteristic X-rays, charged particles can be detected indirectly by the detection of the characteristic X-rays. Pd has been used as the cathode of the heavy water electrolysis in our group. Because characteristic X-rays

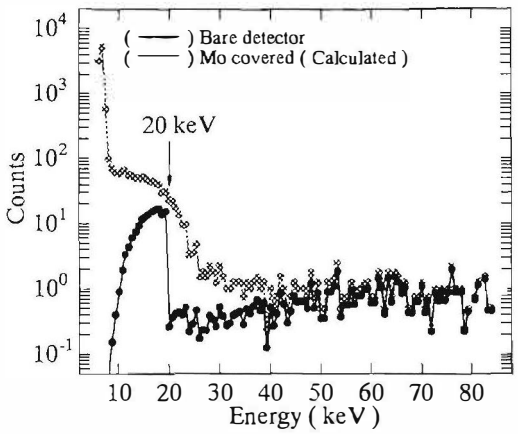

Figure 1 X-ray spectrum of bare CdTe detector and calculated spectrum of Mo-covered CdTe detector

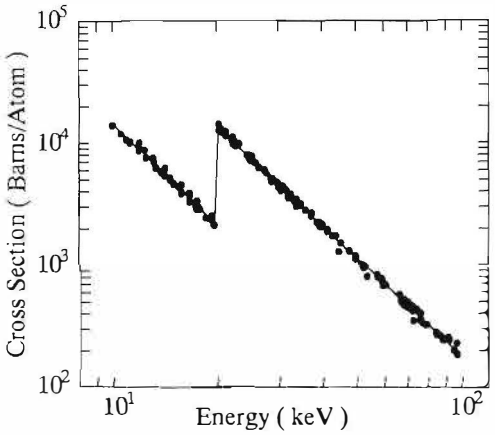

Figure 2 X-ray attenuation cross section of molybdenum (atomic number = 42)

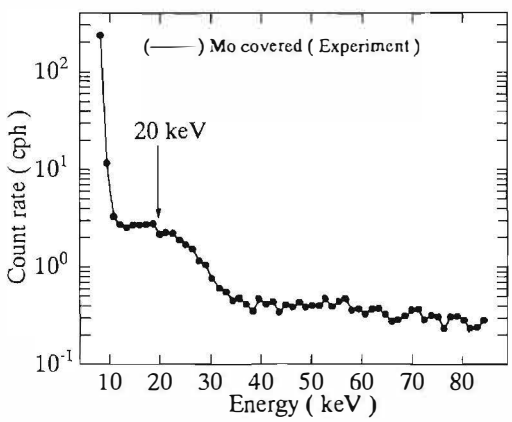

Figure 3 Measured X - ray energy spectrum of Mo-covered CdTe detector

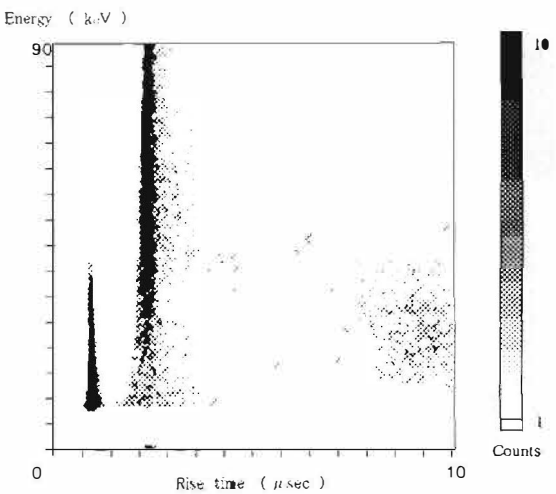

Figure 4 Two dimensional X - ray background spectrum

of Pd K $_{\alpha}$ and K $_{\beta}$ are 21-23keV, it is necessary to measure the X-rays of this energy range. A CdTe solid state detector was chosen to detect these X-rays because of its high efficiency in the energy less than 90keV and its compatibility to be used at room temperature.

CdTe detector picks up electromagnetic noise or mechanical noise easily will give a bad influence upon the accurate measurements. Figure 1 shows the X-ray spectrum of the bare CdTe detector compared with that of calculated spectrum with CdTe detector covered with molybdenum foil during a heavy water electrolysis run with Ni cathode. If the origin of this spectrum was due to X-rays, the spectrum of CdTe detector covered with molybdenum foil should look as the lower spectrum in Figure 1, because X-ray attenuation cross section of molybdenum is like Figure 2[4]. But actually measured X-ray spectrum using the molybdenum covered detector during the heavy water electrolysis was obtained as shown in Figure 3, from which we could find that the origin of this spectrum was not totally X-rays. We introduced them two-dimentional pulse-shape and pulse height analysis to reject the noise signals. Figure 4 shows background X-rays in two dimensional spectrum which was plotted for rise time of pulse as the axis of abscissa and pulse height on the vertical line. The

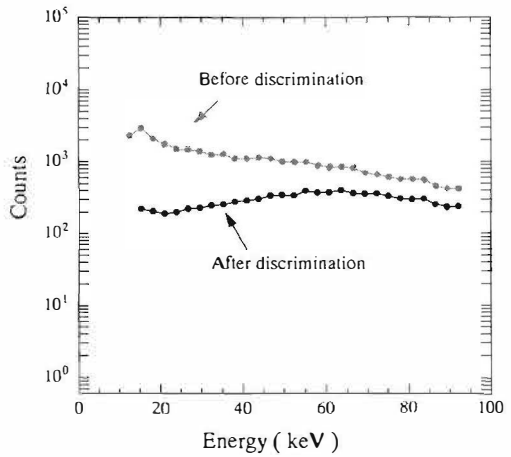

Figure 5 Rejection of noise signals

signals of which rise time were ~2 μ sec were accepted as X-ray signals, and the signals <1 μ sec were rejected as noise signals. Figure 5 shows background spectrum before rise time discrimination and background spectrum after rise time discrimination. This rise time discrimination could reject most of noise signals and slower rise-time events of X-rays. The electrical circuit of rise time discrimination of CdTe signals is shown in the next section.

On the other hand, calorimetry and neutron measurements were performed, too. The electrochemical cells and measurement systems were twin type, and two type experiments were able to be practiced at the same time, for example heavy water electrolysis and light water electrolysis using Pd cathodes for both cells. The advantage of this twin experimental system was that simultaneous events happening in both cells could be rejected as the noises. Using this system, the accurate comparative experiments of cold fusion could be performed for foreground/background or /blank runs.

2.Experimental

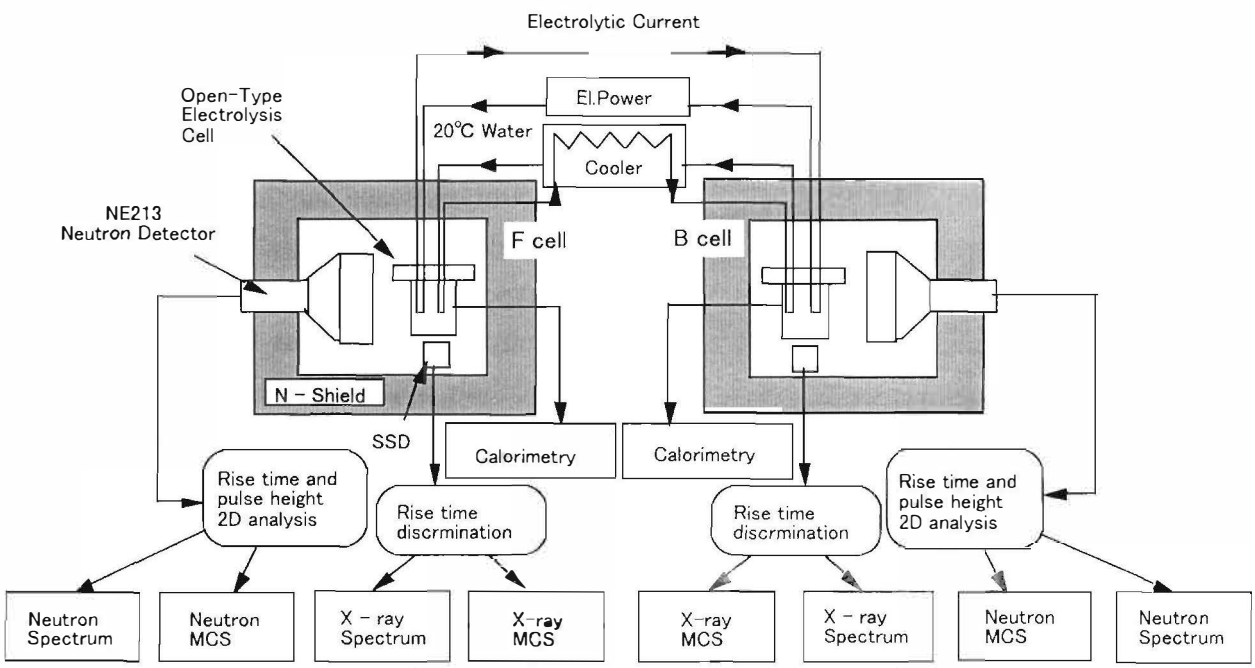

Figure 6 Schematic diagram of twin-type experimental system

The twin open-type cells and measurements systems were designed as shown in Figure 6. The system included two open-type electrolysis cells called F cell and B cell, two X-ray spectroscopy systems using CdTe detectors, and two fast neutron spectroscopy systems with NE213 detectors.

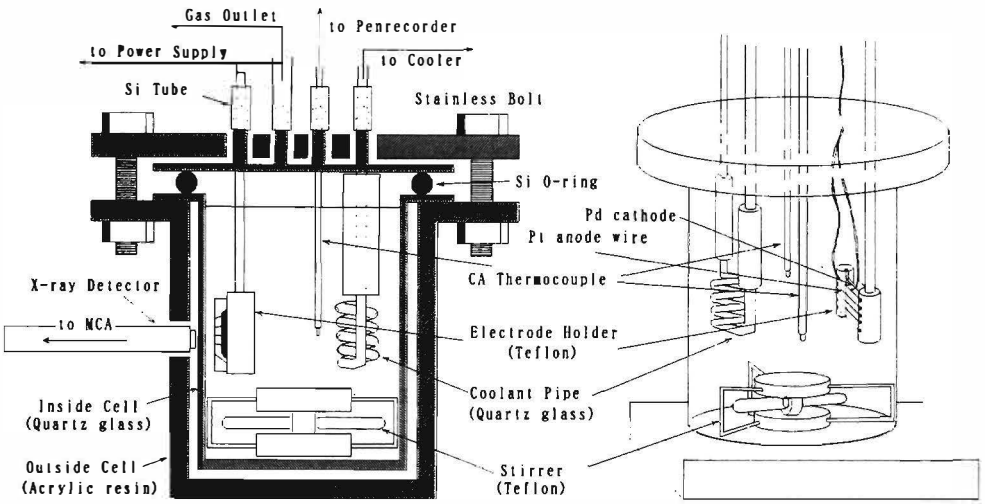

Figure 7 Structure of open type cell

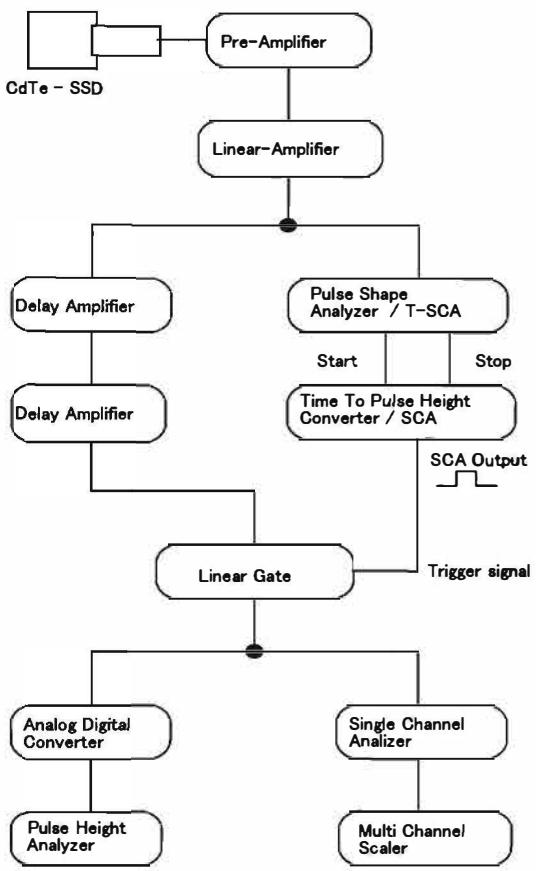

Figure 8 Block diagram of X-ray measurment system

One power supply was connected two cells in series and supplies the same electric current. Coolant (H_2O,20 ± 0.1℃) flow was connected two cells also in series.

Figure 7 shows the structure of open type cell. Inner cell wall was made of glass and outer cell wall was made of acrylic resin. The plate cathode (25×25×1mm) was hold by Teflon electrode holder which rolled up the anode wire (1mm φ). Coolant flowed in the coolant pipe which was made of glass and temperature distribution of the electrolyte was kept uniform by stirrer. The effluent gas (D_2, H_2 and O_2) which were generated by the electrolysis went out through the gas outlet. The electrolyte temperature was measured by K-type thermocouples. The output power of electrolysis was linear function of the thermocouple outputs, and the coefficients of the linear function were determined by the calibration run using Ni cathode in every experiment. The excess energy was determined by the difference between output power and input power to the electrolyte. The input power was expressed by ((cell voltage - 1.5) ×electrolytic current) because of gas generation.

Figure 8 shows the X-ray measurement system. The CdTe detector (2×2mm) was placed in front of the cell. Using this system, noise components in CdTe signals were distinguished by the rise time and separated from real X-ray signals. The measurement range of the system was about 6-90keV in

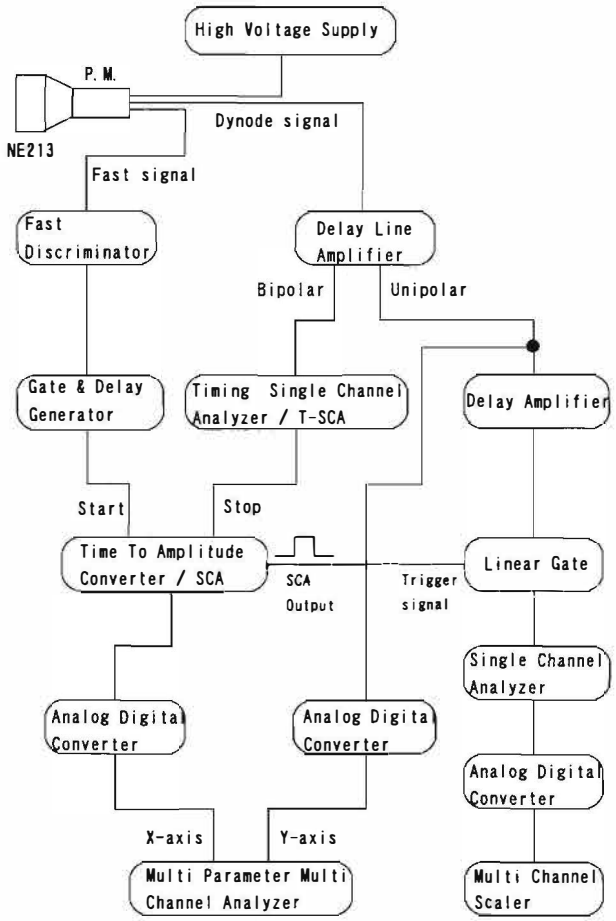

Figure 9 Block diagram of neutron measurment system

energy. The detection efficiency of K_α and K_β X-rays was 0.076% and the measurement system could detect one event per minute when Pd cathode emitted 1300 photons of this energy per minute. X-ray events are counted every 4 minutes besides spectroscopy. For F cell at Run 7, high resolution Si-SSD which was cooled with Peltier device was used instead of CdTe detector to detect lower energy X-rays than 6keV.

The n-γ pulse separation technique was applied to the neutron measurement using an NE213 fast neutron spectrometer, which was placed in front of the cell, as shown in Figure 9. The γ-ray component and noise component could be separated completely by this diagram. The measurement range of neutron is 0-9MeV in energy. But one of the NE213 detectors (for B cell) could not perform right measurement in low energy (<3MeV) because of containment α-particle emitters which are included in this NE213 detector, so it was used exclusively for higher energy. Neutron events were also counted every 4 minutes in addition to spectroscopy.

At most of experiments, the electrolysis current density was changed periodically from LOW (160 or 280mA/cm^2) to HIGH (608 or 640 mA/cm^2) or the reverse in every 3 or 6 hours (L-H mode) in order to give dynamic change of deuterium accumulation in Pd metal. But for a week at the beginning of electrolysis, the electrolysis current density was kept to be 160mA/cm^2 constantly (Constant Mode) in order to keep Pd cathodes from cracking, except for Runs 1-3. The electrolyte was 0.2M LiOD/heavy water solution.

3.Results and Discussions

Excess Energy and Nuclear Products

Table 1 shows the summary of the experiments. In the table, Yes means that anomalous events were observed.

No	Period	Cell	Cathode		Treatment	Particular treatment	Electrolyte	Electrolytic current (mA/cm^2)	Excess heat	X-ray	Neutron
Run 1	51days	F	Pd	NHE	Annealed		LiOD	208～608		Yes	
		B	〃	〃	〃		LiOH	〃			
Run 2	20days	F	〃	〃	〃		LiOD	〃			
		B	〃	〃	〃		LiOH	〃		Yes	
Run 3	30days	F	〃	〃	Cold worked	Cu coating after H or D accumulation	LiOD	〃			
		B	〃	〃	〃	〃	LiOH	〃			
Run 4	17days	F	〃	〃	〃	〃	LiOD	〃			
		B	〃	〃	〃	〃	LiOH	〃			
Run 5	43days	F	〃	〃	Annealed		LiOD	160～640		Yes	Yes
		B	〃	〃	〃		LiOH	〃			
Run 6	43days	F	〃	〃	〃	Etching	LiOD	〃			
		B	〃	〃	Cold worked	〃	〃	〃		Yes	
Run 7	19days	F	〃	IMRA	〃	Add Boron 0.2%at	〃	〃			
		B	〃	〃	〃		〃	〃			

Table 1 The summary of experiments

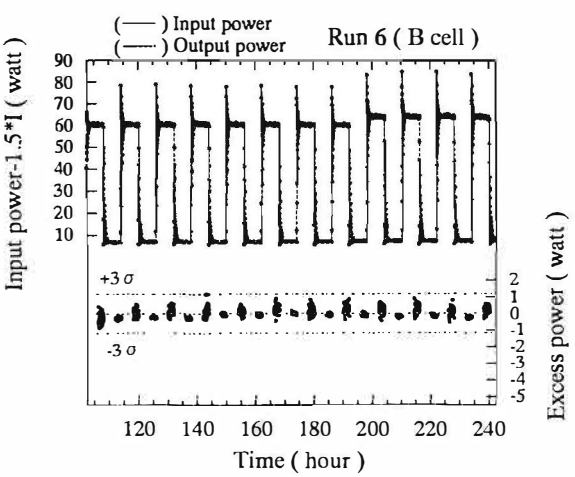

Figure 10 Typical example of heat balance (at Low-HIgh mode)

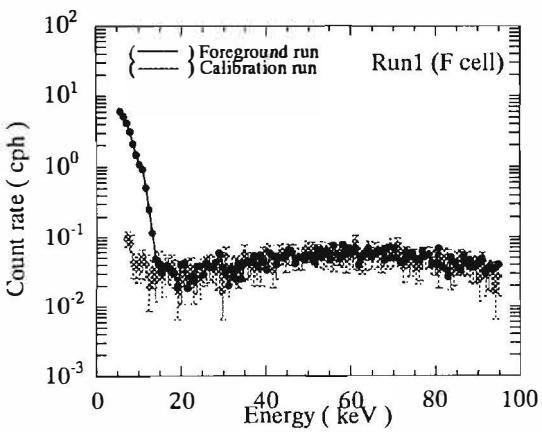

Figure 11 X - ray energy spectra using CdTe detector

Excess Energy and Nuclear Products

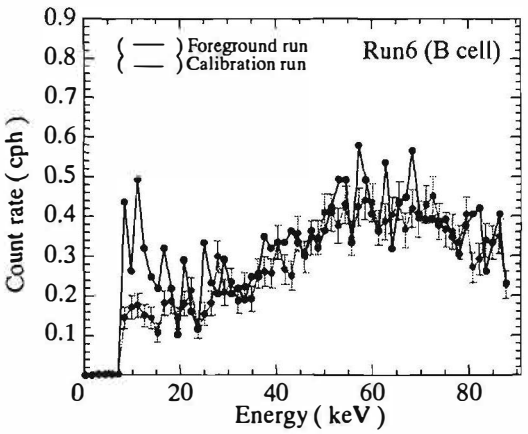

Figure 12 X-ray energy spectra using CdTe detector

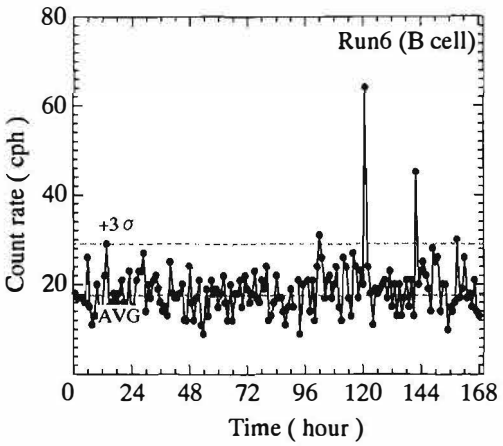

Figure 13 X-ray MCS data using CdTe detector

Figure 10 shows the typical data of heat balance when the current density was changed from 160mA/cm^2 (L-mode) to 640mA/cm^2 (H-mode) or the reverse in cycle. The excess power during thermal equilibrium was fluctuated around zero and not exceeding 99% confidence level (+3 σ and -3 σ).

Figure 11 shows the X-ray energy spectrum of Run 1 during heavy water L-H mode electrolysis at the first week of the electrolysis. This spectrum rising up in the low energy region is regarded as somewhat similar to electromagnetic noise signals, but it might be soft X-rays of the nuclear bremsstrahlung by charged particles. The similar spectrum was observed at Run 2 during light water electrolysis. These results may suggest the possibility of the production of low energy (less than 200keV) charged particles which generate no characteristic X-rays but do bremsstrahlung X-rays. At Run 6, the different X-ray spectrum was obtained at first week of Constant Mode electrolysis for the heavy water electrolysis using Pd cathode which was pre-processed by chemical etching, as shown in Figure 12. The MCS data is shown in Figure 13, where we see X-ray events caused as bursts. The events might be noise signals because

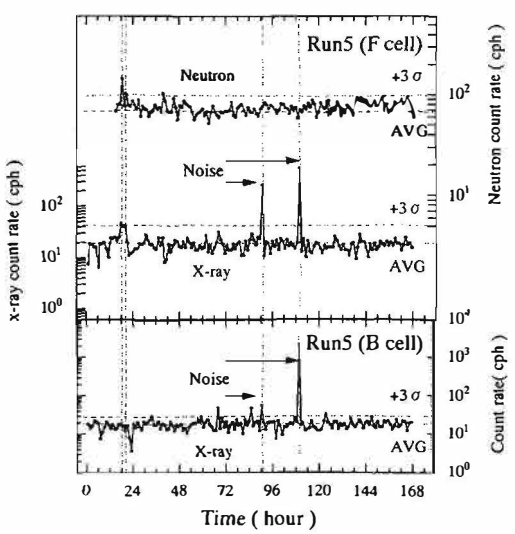

Figure 14 X - ray and neutron MCS data

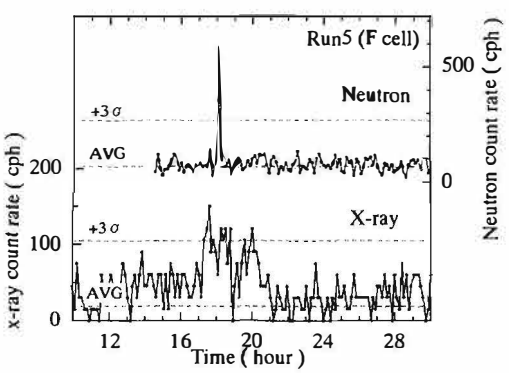

Figure 15 Correlation of X-ray and neutron MCS data

noise signals always appeared as bursts. Figure 14 shows the MCS data at Run 5 during the Constant Mode heavy water electrolysis using annealed (900℃, 10 hour) Pd cathode. Only for the F cell which electrolyte was LiOD heavy water solution, neutron and X-ray increased simultaneously around the time 17hr. Much larger X-ray burst-events after that event were probably noise signals because there were two simultaneous burst-events for the B cell which electrolyte was LiOH light water solution. Figure 15 shows the expanded-scale data for the neutron and X-ray coincident event. Because the time variation of neutron count rate is not identical to that of X-ray's, the origin of these events would not be the same reaction if these events were signals of some nuclear reactions. But there is possibility that the triggering conditions of two events will be the same solid-state or chemical conditions of the Pd cathode. Corresponding spectra of X-ray and neutron could not be identified, because counts in spectrum channels didn't exceed the statistical error level.

The helium-4 analysis of the gas in used Pd sheet at Run 5 for the F cell by quadrupole mass spectrometer was performed with the gas extraction condition Pd sheet was kept 1150℃ for 10 hour after electrolysis. Helium-4 peak was appeared slightly but that was very marginal and uncertain level, because of the problem of leaking of air into the gas storage part of the spectrometer oven during a long heating up process for the Pd sheet.

4.Conclusion

In order to study the correlation between excess heat and nuclear products, the measurements of heat balance, X-rays and neutrons during heavy water and/or light water electrolysis using Pd cathodes were performed. In this work, the reliable twin system was used. Above all, the X-ray measurement system for the correlation study was improved.

As a result, no excess heat beyond 3 σ level was observed. But for only heavy water electrolysis, X-ray and neutron event occurred simultaneously. Other three X-ray events were observed out of seven runs for both of heavy water electrolysis and light water electrolysis. And all of them occurred at the first week of the electrolysis. The energy spectra of X-ray were not characteristic X-ray's but looked like the bremsstrahlung's. But these X-ray spectra were also similar to noise signal's. The simultaneous X-ray measurements by a bare detector and a detector covered with metal foil as described at introduction will be needed in future to prove that these X-rays were not noise signals but genuine soft X-ray signals.

References

1) M. Fleischmann, et al., 1989, J. Electroanal.Chem., 261, 301

2) E. Storms, "Critical Review of the "Cold Fusion "Effect", 1995

3) A. Takahashi, et al., 1995, Proc. 5th Conf. on Cold Fusion,

4) E. B. Saloman, et al., 1988, Atomic Data and Nuclear Data Tables, 38, 1

Excess Energy and Nuclear Products

Excess Heat Production and Nuclear Ash in PdO/Pd/PdO Heterostructure after Electrochemical Saturation with Deuterium

A. G. Lipson, B. F. Lyakhov, D. M. Sakov, Y. A. Kuznetsov, T. S. Ivanova
Institute of Physical Chemistry.
The Russian Academy of Sciences. Moscow 117915 Russia

Abstract

Heat production nuclear ash and electrophysical processes in PdO/Pd/PdO (Au/Pd/PdO) heterostructures electrochemically saturated with deuterium (hydrogen) have been investigated. It was shown in after electrolysis period a strong heat flash with duration of 2-7 s and energy density of 60-100 J/cm^2 was observed for Pd/PdO:D(H) sample placed in air atmosphere. The thermal energy of each flash was approximately 2-5 times higher than the energy supplied to the sample during electrolysis. Neutron- and γ-emissions accompanying the heat production have been investigated.

1. Introduction

The results of 6-years cycle of investigations that was trained on determination of the nature of excess heat and nuclear ash generation in Pd/PdO(Au/Pd/PdO) heterostructure electrochemically saturated with hydrogen (deuterium) will be presented. In contrast to traditional (for CF-experiments) systems that are massive Pd samples saturated with D [1-3] the system under consideration has some essential advantage in terms of obtaining or reproducible and controllable results:

a. short saturation time and absence incubation period. that precedes to excess energy generation;

b. low current density in electrolysis process: control of H(D)-content in Pd-sample at any time;

c. high reproducibility of excess (in contrast to applied in electrolysis) energy in each cycle of saturation of Pd-sample with H(D);

d. possibility of H(D) concentration in a small volume onto Pd-PdO interface, that is cause of high loading ratio (x) as well as local high elastic energy density in Pd lattice i.e. non-equilibrium phonon generation [4].

Therefore, application of thin Pd/PdO heterostructure as a cathode in CF-experiments can bring some advantage to achieve minimum distance between deuterons (protons) and, simultaneously, high concentration of non-equilibrium phonons. Both effects lead to increase of nuclear reactions probability in Pd-lattice with D(H)participation.

2. Experimental

Electrolysis was carried out in a glass cell was subdivided cathodic and anodic spaces (electrolyte volume of about 250 cm^3). The electrolytes used: 1 M KOH or H_2O for Pd/PdO:H_x production: 1 M NaOD in D_2O for Pd/PdO:D_x production. Current density used of about j=10-30 mA/cm^2.

Samples: cold-rolled Pd-foils with thickness 30-50 μm and working area of about S= 4.5 cm^2 for PdO/Pd/PdO (S=2.2 cm^2 for Au/Pd/PdO).

Samples preparation: 1) annealing in vacuum at temperature 600°C for 3 hours with slow cooling (1°C/min) to room temperature; 2) metered annealing and oxygen flame at a temperature of about 1000°C That leads to PdO layer formation having a thickness of about 200-500 Å; 3) electrochemical deposition of Au on the one side of PdO/Pd/PdO heterostructure: thickness of gold coating of about 2000 Å.

Research methods

l. H(D)-concentration in the samples was determined by vacuum thermodesorption technique at 400°C and $P=10^{-6}$ mm Hg.

2. A gas thermometer was applied to record the afterelectrolysis thermal effect. The schematic diagram of that gas thermometer is presented in Fig.1. The quantity of heat (Q), evolved by the sample in the pulse regime, was recorded by a U-shaped mercury pressure gauge with an analytical volume of the exposure chamber (2), V=69 cm^3 which was filled either by air or by O_2 or Ar under atmospheric pressure. The value Q of the Pd-samples was estimated by integrating over the pressure-time (P-τ) curve within a range limited by the pulse origin moment, and by the moment of intersection by it of the time axis τ. Thereafter, for the purpose of quantitative estimation, a comparison of pulses, being obtained on thermal bursts with calibration pulses from a nichrome spiral (8) was carried out. The measurement error of Q did not exceed ±20%.

3. A specially developed set up on the basis of electromagnetic displacement transducer with sensitivity of about $2.5*10^{-6}$ cm was applied to determine in situ changes in the length of thin Pd samples m the hydrogenation-dehydrogenation processes.

4. A block of 7 proportional NWI-62 neutron counters ($B_{10}F_3$) placed into a tank containing vacuum oil and covered by Cd sheet l mm thickness, was used to neutron detection in deuterated Au/Pd/PdO samples (neutron detection efficiency: $\varepsilon_n=3.9*10^{-2}$).

5. To detect a γ-radiation upon thermal effect in afterelectrolysis period semiconductor γ-detector (pure Ge) GEM-20180P by- EG&G ORTEC was used (efficiency of γ-detection $\varepsilon\gamma=3*10^{-3}$).

3. **Experimental results**

Excess energy

On the electrolysis process, at the electrolysis time l<40 min in Au/Pd/PdO τ<40 min in Au/Pd/PdO heterostructure the one-side bending of sample is observed (Fig.2). The degree of bending is depend upon dectrolysis time. This bending is a cause of deuterium (H) storage on the Pd-PdO interface [5]. At electrolysis time τ>40 min the straighten of sample takes place due to deuterium (H) breakdown into the sample bulk.

The free energy (elastic deformation) stored up in the sample due to electrolysis may approximately be estimated with the formula [6]

$$F = \int \psi_2(U_{\alpha\beta})\, ds$$

where $U_{\alpha\beta}$ is 2-dimension deformation tensor; $\psi_2=Eh(\xi/l)4$ here E - is Young modulus of Pd, h - sample thickness; ξ - sample mean deflection, l - length of the sample. For $h=3*10^{-3}$ cm, l=4.5 cm, s=4.5 cm^2 and electrolysis time τ=30 min we have ξ=5 mm (Fig. 2). And then F=76 cal/cm^2. It should be noted that the energy value applied upon electrolysis time was E_{el} =7.8 cal/cm^2. Therefore the elastic energy stored up by Au/Pd/PdO:Dx (Hx) sample is excess

of electrolysis energy applied about one order of magnitude.

When the electrolysis is interrupt at pause (τ<40 min for h=50 μm) after the drying of sample there takes place the thermal burst (in air, Ar , atmosphere or vacuum). Which is accompanied by the heating of sample up to temperature a of 900 °C (Fig.3a).

In the case of electrolysis carried out for 5 hours (Fig.3a, curve 4), the monotonous increase in the pressure of the gas thermometer is due to movable excess hydrogen which easily leaves the Pd lattice have been took place.

When the hydrogenated Pd/PdO samples are placed into the chamber at t=20°C. the dependence ΔP- τ is of the extremum character (Fig.3a, curves 1,2,3). The retardation of the thermal effect (when O_2 or air is present in the chamber) is limited by the sample drying time. and may range from a few seconds to several minutes. The pressure increase being accompanied by the visible heating of the Pd sample (e.g red or white glow) up to temperatures higher than 900°C (the thermocouple reading) during 3 to 4 seconds, and by its axial bending. Then the chamber is evacuated, which is due to the consumption of O_2 for the reaction with hydrogen in the Pd sample, and for condensation of water vapor.

The Pd/PdO system. which has been electrolytically deuterated for the same time intervals, behaves itself somewhat differently (Fig. 3b). When a sample is put into the analytical volume at room temperature, strong deformations take place in it, as well as in hydrogenated samples; however, no thermal burst is observed. When the sample is preheating by the aid of an electric lamp up to a temperature of 35 to 40°C the behaviour of the Pd/PdO:D samples becomes similar to that of the Pd/PdO:H samples at room temperature. In this case, the character of a thermal pulse is more prolonged, the growth time about 7 to 10 sec, the vanishing time about 40 sec), while the integral thermal effect is approximately by a factor of 1,3 to 1,4 higher than that in the Pd/PdO:H system.

The integral mean values of heat evolution, Q both for Pd/PdO:H system (at t=20°C) and for the Pd/PdO:D system (at t=40 °C), were estimated by carrying at calibration measurements with a nichrome spiral. For 100 thermal bursts, these are equal to Q_H =15,1 ±3,5 cal/cm^2 , Q_D =20,3 ±4,8 cal/cm , respectively. The reproducibility of the effect is extremely high, so that one sample gives not less than 150-200 thermal bursts in succession with consecutive hydrogenation cycles. In Fig.4 are presented in the form of histograms the results obtained for 100 bursts in succession on one of the Pd/PdO:H samples. In 5 cases from 100 there were observed very powerful bursts attaining the value of 40 to 45 cal/cm^2 . Let us note that the energy transmitted to the sample directly on electrolysis W_E =8,0 ±1,5 cal/cm^2 . Therefore, the observable thermal effect $Q_{H,D}$ may be considered as being anomalous.

The magnitude of thermal effect can be increased essentially when specific surface of heterostructure samples will be strongly increased too. For this purpose it was Pd-black (r^{-4}=10 cm) deposited by electrochemical method onto PdO surface. At saturation time τ =30 min, the mean Q value is increased of about 2 times (in contrast to samples without Pd black) and became of about 35 ±3.6 cal/cm^2 (Fig.5). The reproducibility of this thermal burst at room temperature is equal to 100 %.

Nuclear ashes

To determine correlation between thermal and nuclear processes in Au/Pd/PdO:D(H) heterostructure the simultaneous detection of excess heat production and nuclear radiations was carried out. The registration was began from the moment

of sample's drying and was finished to the moment of total gas desorption from the sample.

The experiments have shown no statistically noticeable emission of neutrons is observed on the Au/Pd/PdO:H control samples (with the thermal effect), while the distribution of neutron events is well consistent with the Poisson distribution of the natural (cosmic) background (Fig.6, curve 2).

In the same time thermal effect (and deuterium desorption) from the sample Au/Pd/PdO:D_x is accompanied by a neutron emission (Fig.7). The maximum of neutron counts is observed in the beginning of D-pressure jump, when strong plastic deformation of sample is taking place. In this time interval the neutron bursts are observed with multiplicity i=6-17 (in the time gate of about 1 ms) or with intensity n=100-500 n/(s*cm^2) Pd (Fig.6, curve 1). The residual plastic deformations that occurs on the D_2O condensation process are accompanied by weak neutron emission too. The neutron emission decay to background level takes place after 5-6 min (from the beginning of D-gas desorption). After finishing of the process the loading ratio value is $x \sim 10^{-3}$ [7]. However, neutron emission can be prolongated during 15-20 min, if Au/Pd/PdO sample will be loaded by mechanical stress (by hanging up to the one end of the sample a weight of about M=40 g). The rate constant of dd-reaction in Au/Pd/PdO:D_x heterostructure $\lambda_{DD} = 2*10^{-21}$ s^{-1} per dd-couple (for x=0.72) and $\lambda_{DD} = 10^{-18}$ s^{-1} per dd-couple (for $x=10^{-3}$). It should be noted that the sample with $x \sim 10^{-3}$ posses of residual elongation of about 1/3 from elongation at x=0.72, accordingly with the date obtained from electromagnetic displacement's transducer measurements. It has been discovered that this elongation is due to quasimetallic clusters of hydrogen [7].

The same samples of Au/Pd/PdO:D_x and Au/Pd/PdO:H_x (x=0,72) after electrolysis procedure was used for γ-emission tests in the energy range of 2.0-10.0 MeV. In the spectrum of Au/Pd/PdO:D_x samples (Fig. 8) there are 3 plainly expressed maxima with positions $(E_\gamma)_1 = 2.225 \pm 0.005$ MeV; $(E_\gamma)_2 = 3.8 \pm 0.5$ MeV; $(E_\gamma)_3 = 6.3 \pm 0.3$ MeV. The narrow line $(E_\gamma)_1$ (half width of about 10 keV) could be ascribed to p+n reaction, because its position is in a good agreement with γ -line (E=2,225 MeV) obtained upon PE-irradiation by thermolized neutron from Cf^{252} -source (Fig.9). The $(E_\gamma)_3$ maximum can be give rise to γ-quanta from d+n reaction (E_γ=6.25 MeV). In fact this peak increases of about 2 times upon the sample irradiation by thermalized neutrons. The nature of $(E_\gamma)_2$ maximum is not clear. However as it was proposed earlier [8] the E_γ =3.8 MeV peak can be exhibition of the first excited state of He nucleus that may form with phonon participation [9].

In contrast to deuterated heterostructure the samples of Au/Pd/PdO:H generate only one - maximum with position of about $E_\gamma = 4.6 \pm 0.3$ MeV. Under the irradiation of the sample by thermalized neutrons the maximum E_γ =4.6 MeV is increasing in intensity more than 5 times and shifted on 0.3 MeV into the high energy band. The nature of this γ-emission is unknown now.

Therefore excess energy generation in Au/Pd/PdO:D(H) heterostructure is accompanied by γ-emission. The γ-emission intensity depends upon the thermal neutron background [10].

Moreover, as it shown by A.Roussetski (this volume of ICCF-6 Proceedings) desorption process in heterostructure of Pd/PdO type (both H and D saturated) is accompanied by emission of charged particles (protons and possibly α-particles). Intensity of proton emission of about I_p =0.8 proton/s in 4π .

4.Conclusion

Simultaneous generation of excess energy and weak nuclear radiation in Au/Pd/PdO:D_x (H_x) heterostructure as well as strong plastic deformation in it are indicate on the possibility of phonon laser action in system of this type. Really, the main process that determines heterostructure's properties in afterelectrolysis time is an intensive exothermic desorption of hydrogen (D) from the sample. This effect, from other side, is a main condition to phonon laser operation on Pd-PdO interface in the high loading ratio zone (clusters of quasimetallic hydrogen [7]). In this zone coherent multiphonon excitations can initiate an anomalous energy transfer and, simultaneously lead to coherent neutron transfer reactions [11]. As result, both excess heat and weak nuclear radiation are observed. In this connection the short electrolysis process for heterostructure saturation with H(D) can be considered as pumping up procedure of phonon laser.

References

1. Fleischmann M, Ponce S, Hawkins M J.Electroanal. Chem. 261 , p.301 (1989).
2. McKubre, M.C.H, Crouch-Baker S, Hauser A.K. Proc. of ICCF-5, Monte-Carlo, p.17 (1995).
3. Storms E. // Fusion Tech. 20 , p.433 (1991).
4. Hagelstein P.L. // Trans. Fusion Tech. 26 , p.461 (1994).
5. Yamaguchi E., Nishioka T. // Jap.J.Appl.Phys (Part 2) 29, (4), p.L666 (1990).
6. Landau L.D., Lifshitz E.M. Theory of Elasticity Moscow, Nauka, s.202 (1965).
7. Lipson A.G., Lyakhov B.F., Sakov D.M., Kuznetsov V.A. // Rus. Solid State Phys, 38 (6), 1657 (1996).
8. Lipson A.G., Bardyshev I.I., Sakov D.M. // Rus.J.Tech.Phys.Lett. 20 (23), p.53 (1994).
9. Takahashi H. in Anamalous nuclear Effects in Deuterium/solid systems, Ed by S.E.Jones et. al, AIP.Conf.Proc. N 228, p.884, New York (1991).
10. Kozima H. // Nuovo Cimento 27A , 1781 (1994).
11. Hagelstein P.L. // Proc. of ICCF-5, Monte-Carlo, p.327 (1995).

Captions to figures

Fig. 1. Experimental set up with gas thermometer and neutron detector: 1 - PE(Co) ; 2 - chamber with atmosphere ; 3 - gas thermometer (Mcleod) ; 4 - sample ; 5 - neutron counters ; 6 - moderator ; 7 - Cd; 8 - heater.

Fig. 2. Au/Pd/PdO sample: initial (a) and deformed (b) after electrochemical hydrogenation during τ =30 min ; ξ - is mean deflection.

Fig. 3a. Thermal bursts for Au/Pd/PdO:H_x : saturation time : 10 min - curve 1 ; 20 min - curve 2 ; 30 min - curve 3 ; 5h - curve 4 ; calibrating pulse from nichromium coil - curve 5.

Fig. 3b. Thermal burst for Au/Pd/PdO:D_x saturation time : 30 min - curve 1 ; 5h - curve 2 ; calibrating pulse - curve 3.

Fig. 4. Distribution of the heat production events (n_Q) with respect to the heat evolution energy Q for Au/Pd/PdO:H_x -system.

Fig. 5. Distribution of n_Q with respect to Q for [Au/Pd/PdO+Pd-black]:H_x system.

Fig. 6. Distribution of the number of neutron events (n_i) with respect to the multiplicity of neutron pulses (i) for Au/Pd/PdO:D_x heterostructure for $\Delta\tau$=120 s time intervals preceding the heat burst (N=100 experiments) - curve 1 ; Poisson distribution for neutron events with N=100 - curve 2.

Fig. 7. Excess heat generation (curve 1) and neutron emission (curve 2) in Au/Pd/PdO:D_x heterostructure (simultaneous registration) for 100 experiments. Locations of neutron bursts with n>100 n/cm^2 marked by vertical lines (curve 3).
Fig. 8. γ-emission for Au/Pd/PdO:D_x heterostructure after 30 min electrolysis (with subtraction of γ-background) in cosmic neutron background (curve 1); during irradiation by thermal neutron (I_n ~2 n/s*cm^2) (curve 2).
Fig. 9. γ-spectrum of 2.225 MeV maximum (curve 1) and γ-peak from thermal neutron capture and polyethylene (curve 2).
Fig. 10. γ-spectrum for Au/Pd/PdO:H_x heterostructure after 30 min electrolysis (with subtraction of γ-background) in cosmic neutron background (curve 1); during irradiation by thermal neutron (curve 2).

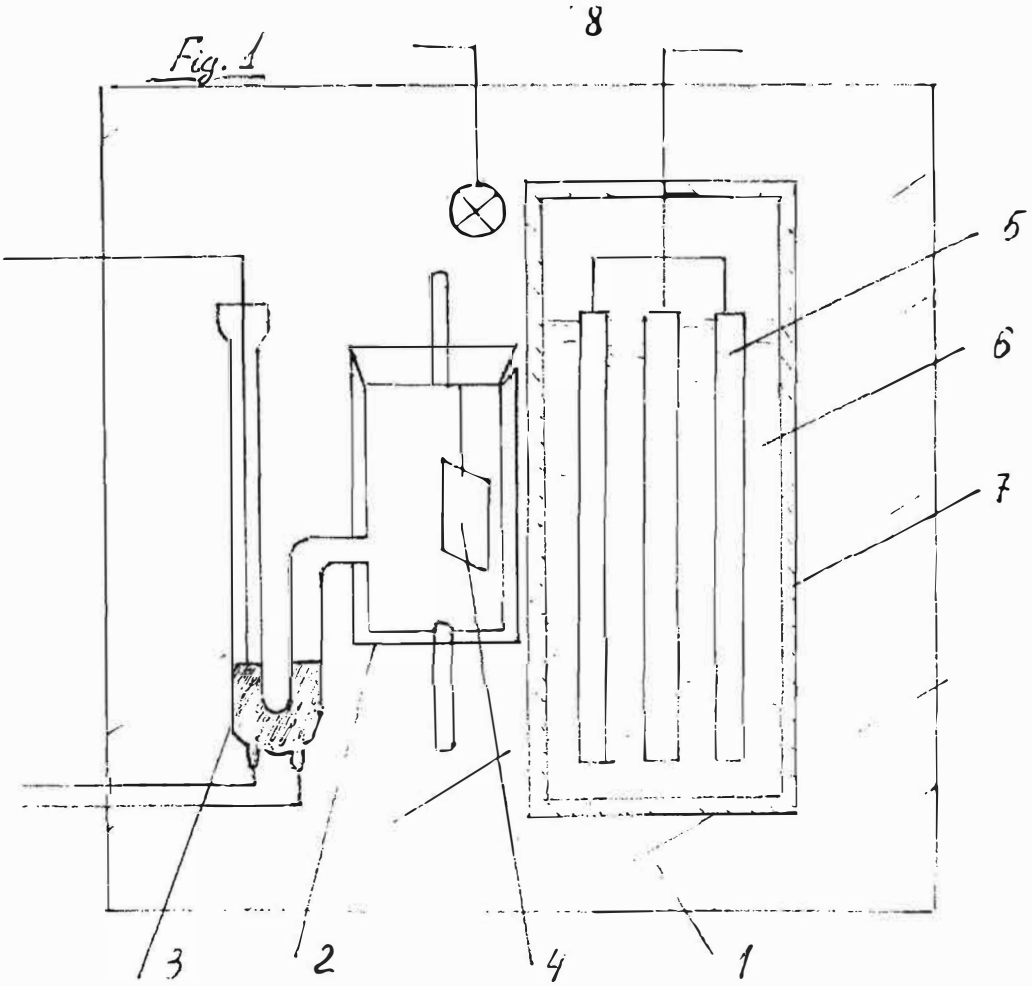

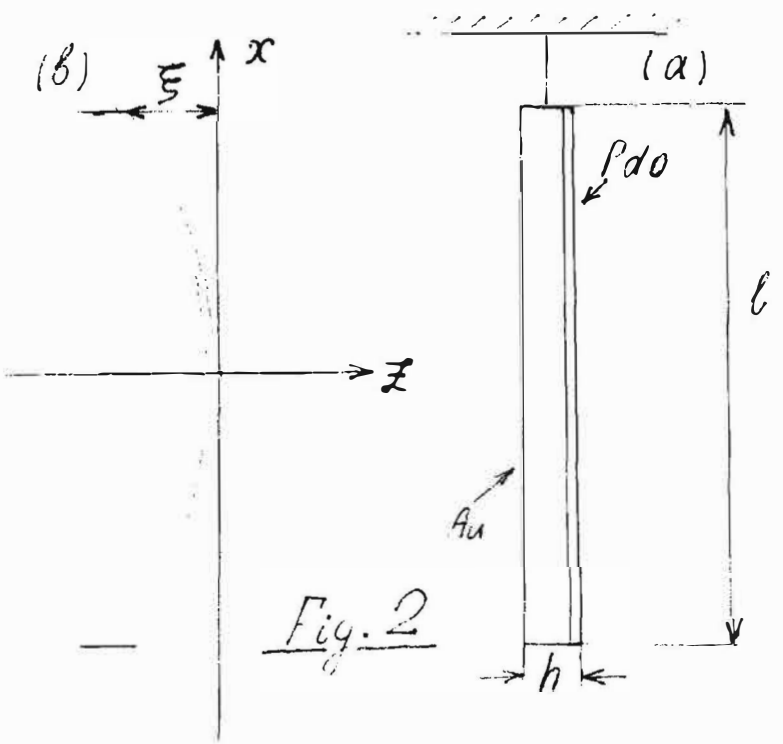

Fig. 2

Excess Energy and Nuclear Products

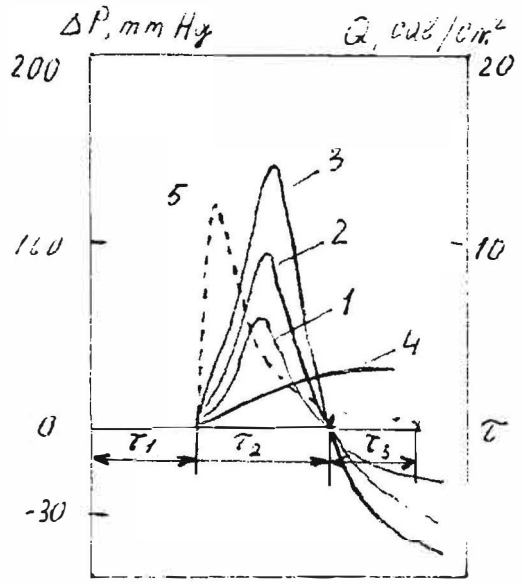

Fig. 3a

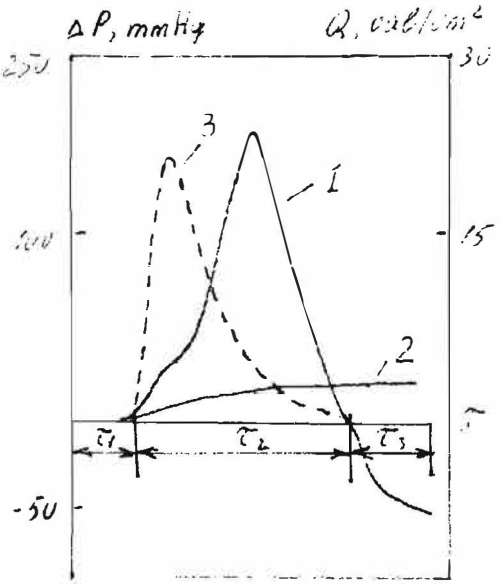

Fig. 3b

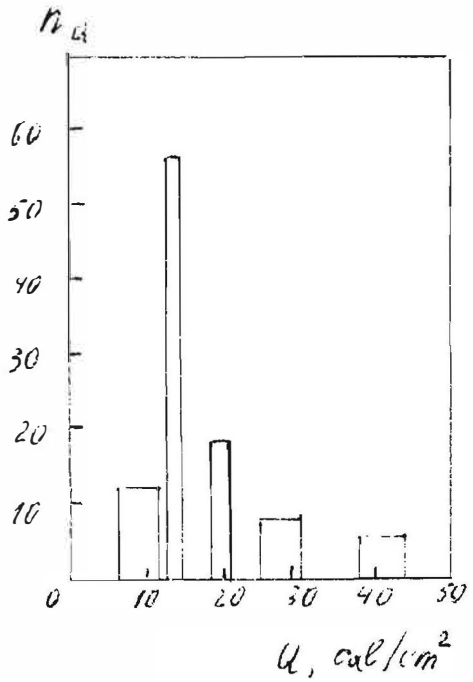

Fig. 4

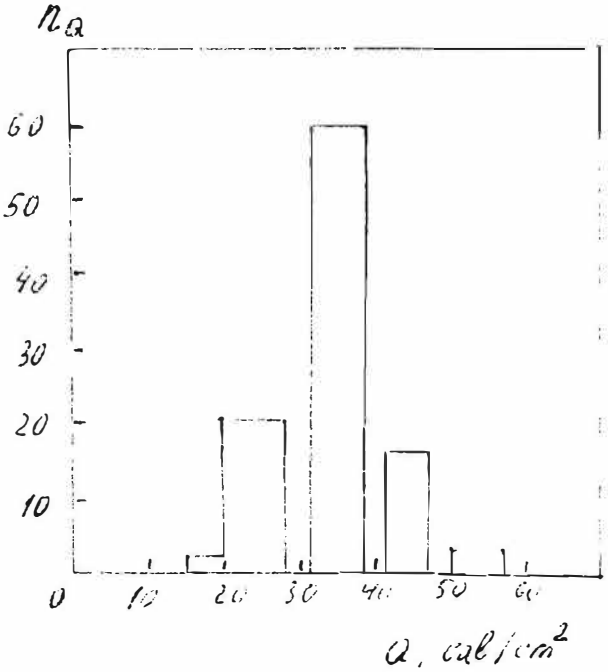

Fig. 5

Excess Energy and Nuclear Products

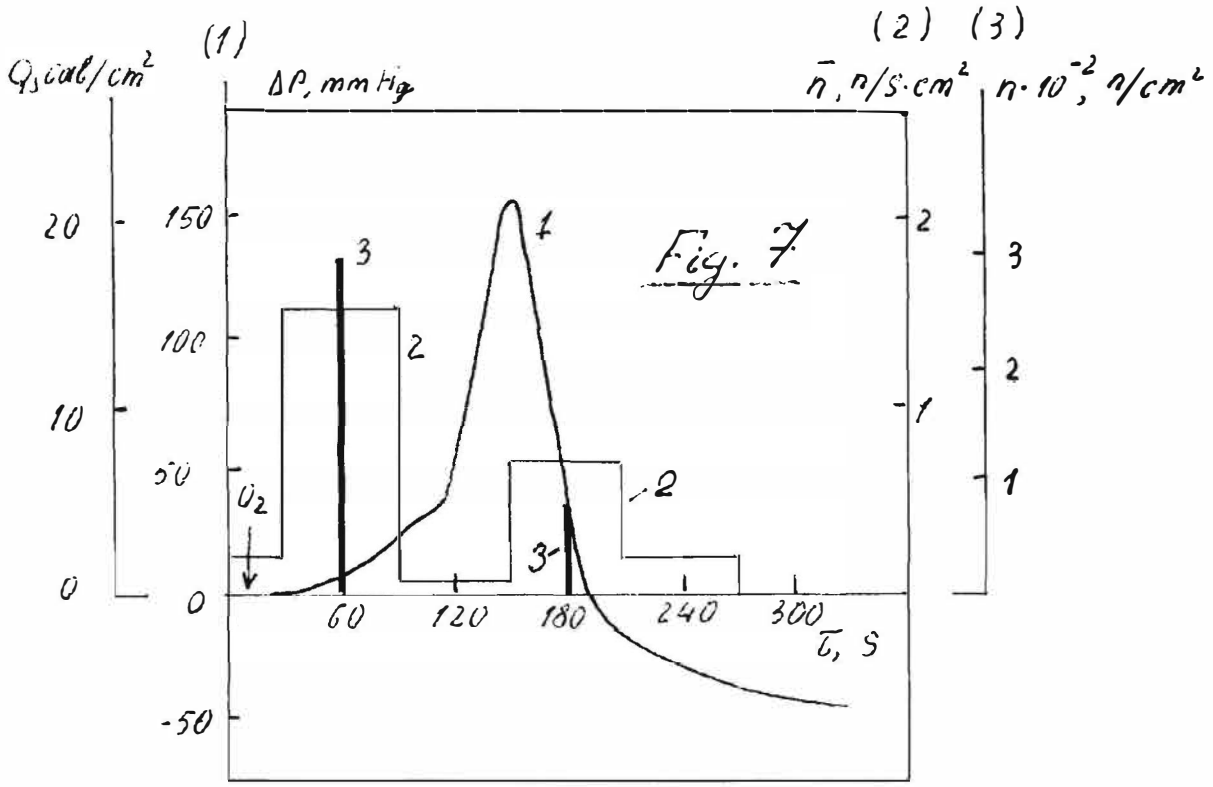

Fig. 7

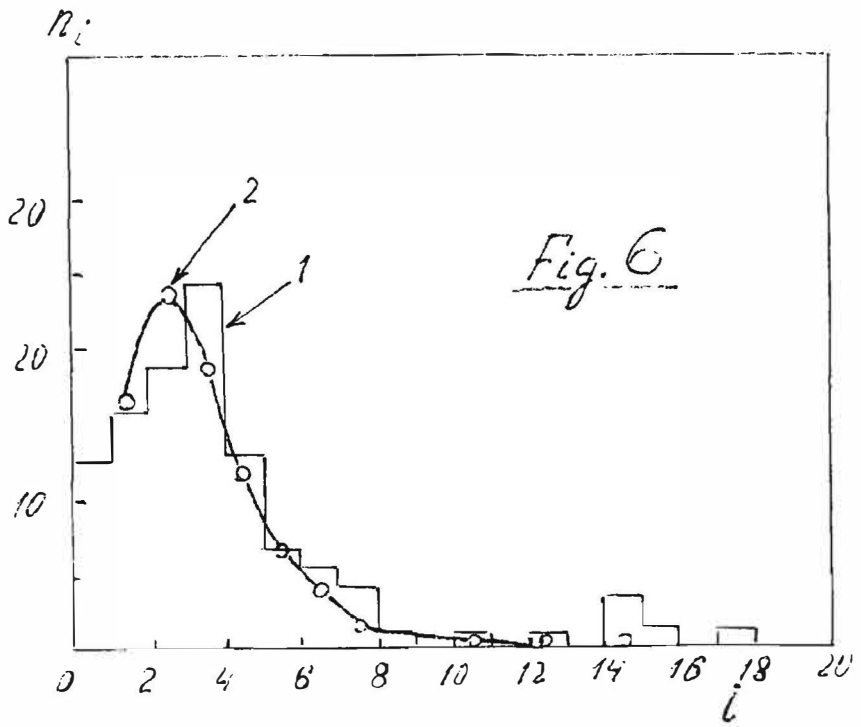

Fig. 6

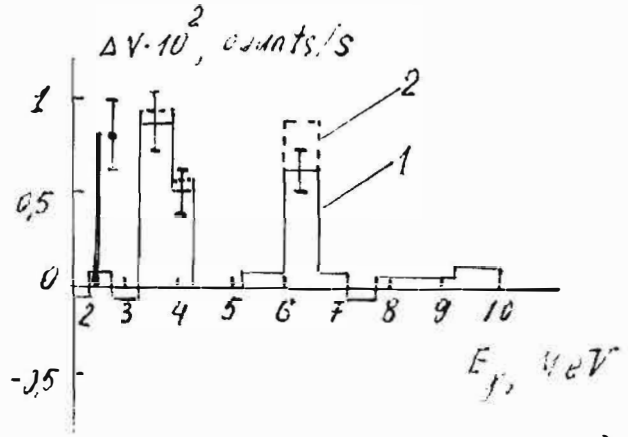

Fig. 8

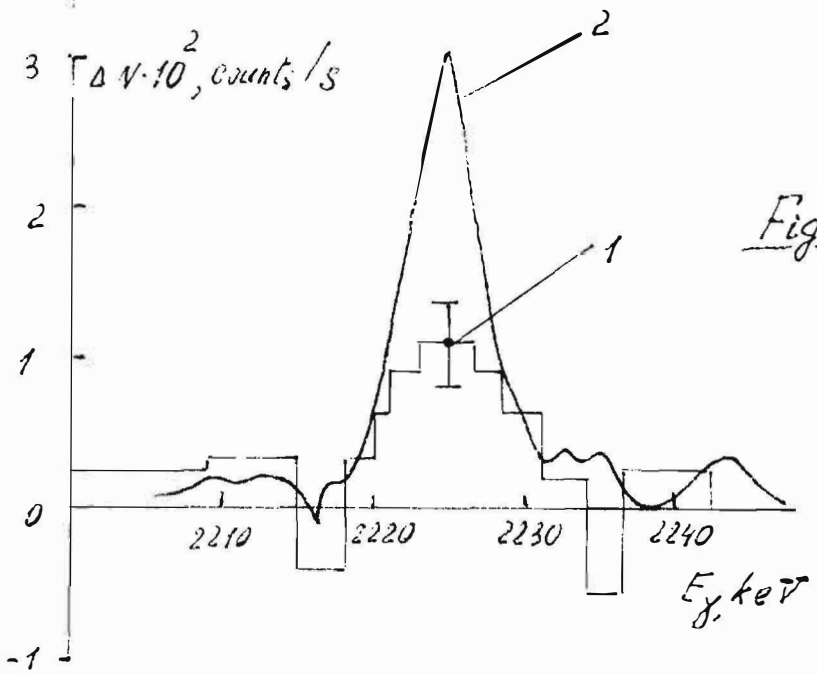

Fig. 9

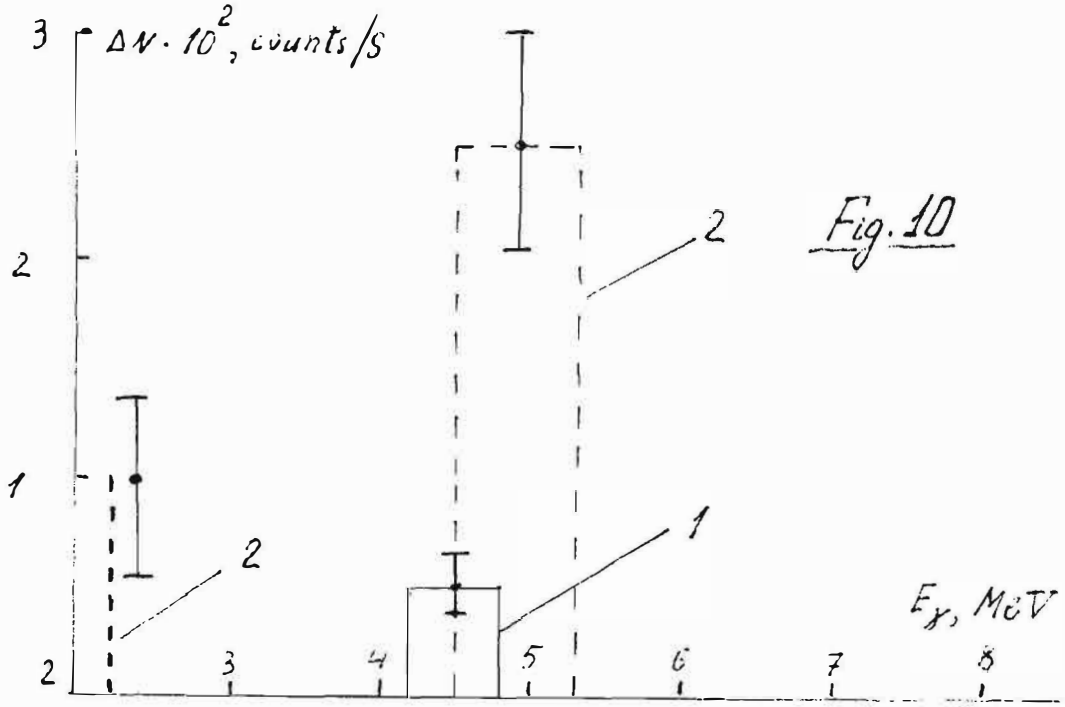

Fig. 10

DYNAMIC MOVEMENT OF HYDROGEN ISOTOPES IN PULSE MODE ELECTROLYSIS

Y.Oya, H.Ogawa, O.Aruga, T.Ono, M.Aida and M.Okamoto
Res. Lab. Nucl. Reactors, Tokyo Institute of Technology
Ookayama, Meguro-City, Tokyo 152 Japan
Tel: 81-3-5734-3065, Fax: 81-3-5734-2959

Abstract

The movement of the hydrogen isotopes in Pd-LiOD(H) electrolysis has been studied by monitoring the hydrogen loading ratios based on the electro-resistance measurement. The movement of the hydrogen isotopes in Pd was found to be influenced strongly by the conditions of the electrolysis, such as the current density, the repetition time. The dynamic absorption/desorption movement can be realized by the pulse mode electrolysis with the current density higher than 200mA/cm^2 and the repetition time longer than 3 hours. In these dynamic movement of the hydrogen isotopes, anomalous isotope effects have been observed and discussed with respect to the new hydrogen energy research.

Introduction

As has been discussed, the anomalous accumulation of deuterium in Pd surface and the dynamic movement of deuterium in the surface should be recognized as the key factors to initiate the deuterium based on nuclear reactions and the anomalous phenomena as new hydrogen energy[1]. The dynamic movement of deuterium has been also discussed in SRI empirical equation for the excess energy generation with the term of δ X/ δ t and they reported the dynamic movement of deuterium in their stepwise rise up of the current density in their electrolysis[2]. While we and Takahashi et al. have applied the square pulse mode electrolysis to elucidate the correlation between the excess energy generation and the nuclear effects, resulting the high reproducibility of the new hydrogen energy production[3][4][5][6].

In the present work, the movement of the deuterium and hydrogen in Pd electrode has been studied by means of the monitoring of the loading ratios (D/Pd, H/Pd) based on the electric resistance method to determine the conditions of the pulse mode electrolysis for realization of the dynamic movement of the hydrogen isotopes, to find the isotope effects in such a dynamic movement of the hydrogen isotopes, and to understand the threshold value of the current density discussed in the SRI empirical equation.

Experimental

Excess Energy and Nuclear Products

The block diagram of the experimental system is shown in Fig.1. The electric resistance was measured by use of a milli-ohm meter PH4338A purchased by HEWLETT PACKARD Co. Ltd. The resistance measurement was performed with 4 points method as shown in Fig.2. The electrolyte volume in the electrolysis cell was kept to be 100 mℓ by addition of the electrolyte throughout the electrolysis. The cell was placed in a thermostat water bath with a constant temperature of 23℃. The Pd electrodes used were 4N Pd plates and were annealed for 2 hours under vacuum (< 10-8Pa) before use. The size of the Pd electrodes was 25mm × 10mm × 0.5mm. The electrolyte was 1 mole/ ℓ LiOD or LiOH. The loading ratios were evaluated by use of the calibration curves reported by Kunimatsu et al. from the electric resistance data[7].

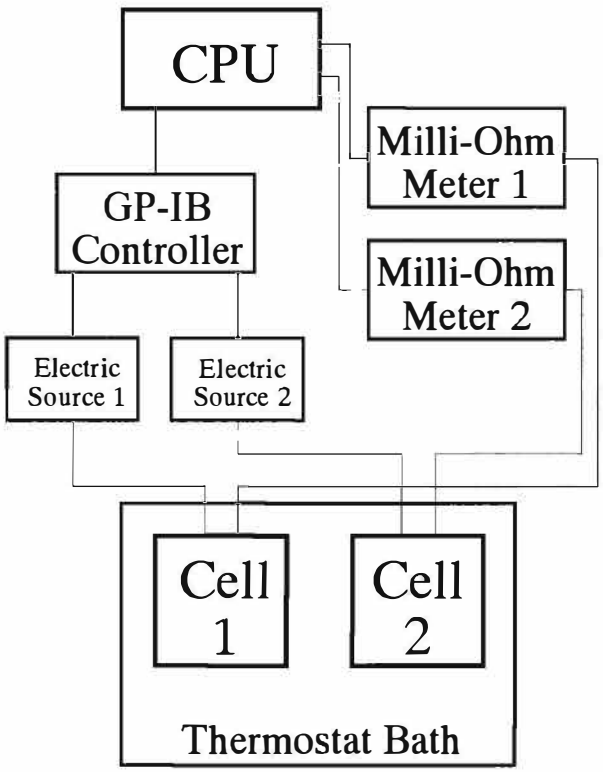

Fig.1 Schematic drawing of experimental system.

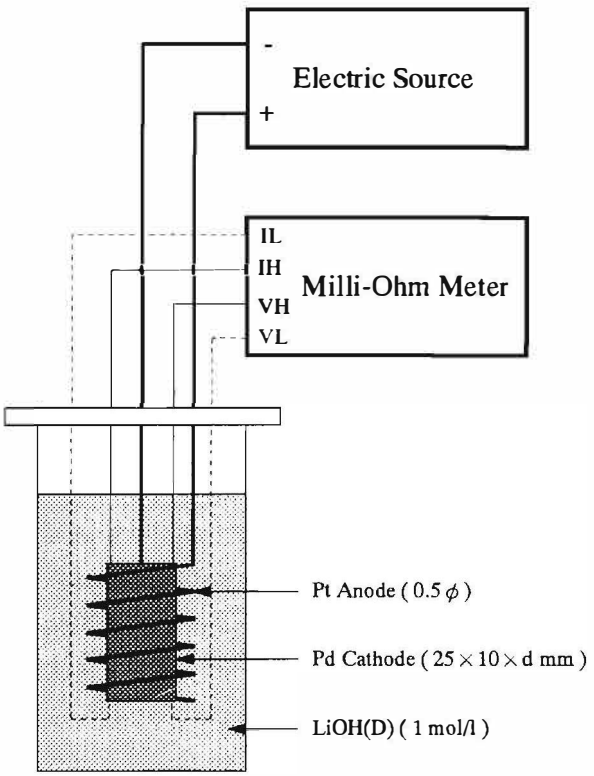

Fig.2 Electrolysis Cell for Pd resistance measurements

Results and discussion

To confirm the performance of the above technique of the loading ratio evaluation, a series of on-off mode electrolysis has been carried out using the Pd plates with the thickness of 0.5mm and 1.0mm at the several current densities from 40 to 800mA/cm² in LiOH or LiOD electrolyte. The dynamics of the loading ratios obtained are illustrated in Fig.3 and Fig.4 , for LiOH and LiOD respectively.

From these curves in these figures, it can be said that the present technique for the evaluation of the loading ratio has adequate response as the monitor of the dynamic movement of the hydrogen isotopes in Pd-LiOD or LiOH electrolysis. The loading rates were evaluated from the first stage of the loading process, the linear part of the loading curves, and the rates are plotted vs the current

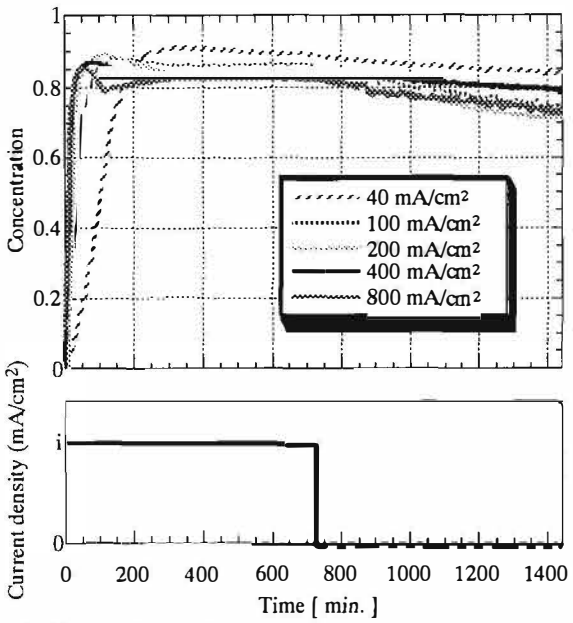

Fig.3 Concentration H/Pd versus time.
Specimen thickness = 0.5 mm,
Constant current density i = 40, 100, 200, 400, 800 mA/cm².

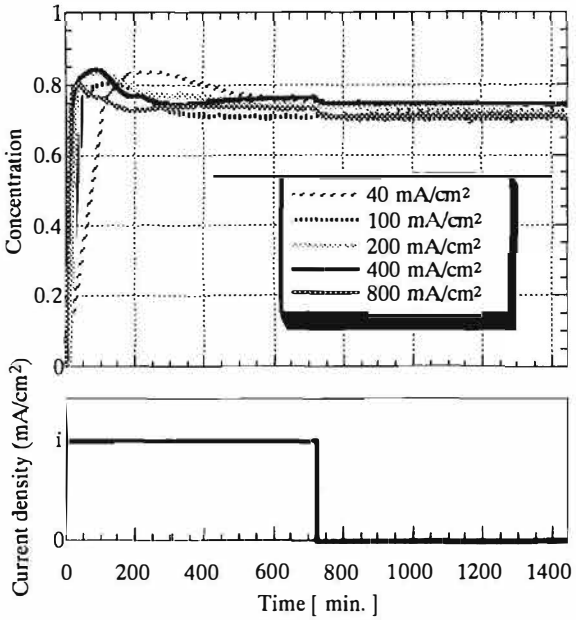

Fig.4 Concentration D/Pd versus time.
Specimen thickness = 0.5 mm,
Constant current density i = 40, 100, 200, 400, 800 mA/cm².

density in Fig.5. The solid line with no marks represents the loading rate calculated by the Faraday`s law. The loading rates obtained in the current density lower than 200mA/cm² correspond to the solid line, while the rates over the current density. This fact indicates that the current density of 200mA/cm² is a critical current density in the our electrolysis as discussed by SRI group. The reason why the loading rates become constant over the 200mA/cm² is now under study.

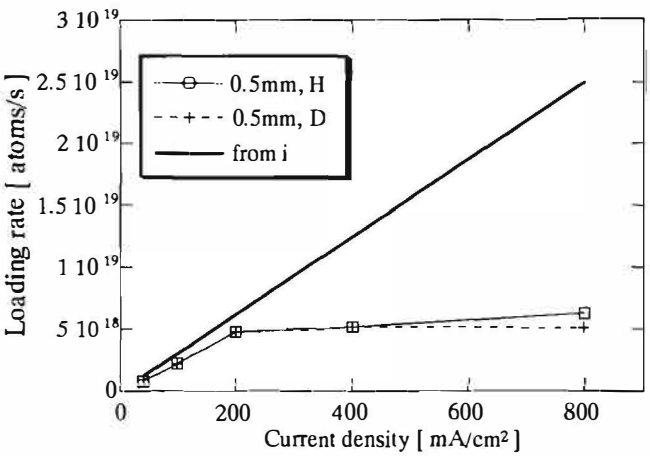

Fig.5 Loading rate versus current density curve.

The loading ratios observed in a series of pulse mode electrolysis are displayed in Fig. 6 for LiOD and LiOH. The electrolysis were carried out in two high-low pulse modes with 20mA/cm²-200mA/cm² and 40-400, and the repetition time was three hours. From these curves, we can find very interesting points as follows.

(1) The loading ratios obtained in LiOH electrolysis are larger than those obtained in LiOD electrolysis as usual.

(2) The loading ratios obtained in 20-200mA/cm² pulse mode electrolysis are almost constant without any response of the high-low pulse mode in LiOH and LiOD.

(3) The loading ratios obtained in the higher current density pulse mode, ie 40-400mA/cm², indicate the evident dynamic movement with clear response to the high-low current density in LiOD electrolysis, while in LiOH electrolysis, the dynamic movement is slight with reversal response to the high-low current density as just opposite to LiOD electrolysis. It can be said that the evident

dynamic movement of deuterium can be realized by the electrolysis of LiOD with Pd cathode with 40-400mA/cm² high-low pulse mode and with 3 hours repetition time. These facts should be recognized as the anomalous hydrogen isotope effects occurred in Pd-LiOD(H) electrolysis.

To confirm the reliability of the 3 hours repetition time, the Pd-LiOD electrolysis has been carried out with the same high-low pulse mode but with 6 hours repetition time. The result obtained here is displayed in Fig.7 along with the above data of the 3 hours repetition time. In the case of the 6 hours repetition time, the dynamic movement of the deuterium in Pd electrode could be observed as shown in Fig.7. However, the direction of the response is just opposite to that of 3 hours repetition. It means that in the case of the 6 hours repetition pulse mode the deuterium was desorbed at the high current density and was absorbed at the low current density electrolysis. This movement can not be explained by the bases of the electrochemistry. From the facts mentions above, it can be concluded that the conditions; high/low pulse mode electrolysis of LiOD with Pd cathode, high current density over 400mA/cm² and 3 hour repetition time which have been employed by the present authors to perform the deuterium based anomalous phenomena are reasonable.

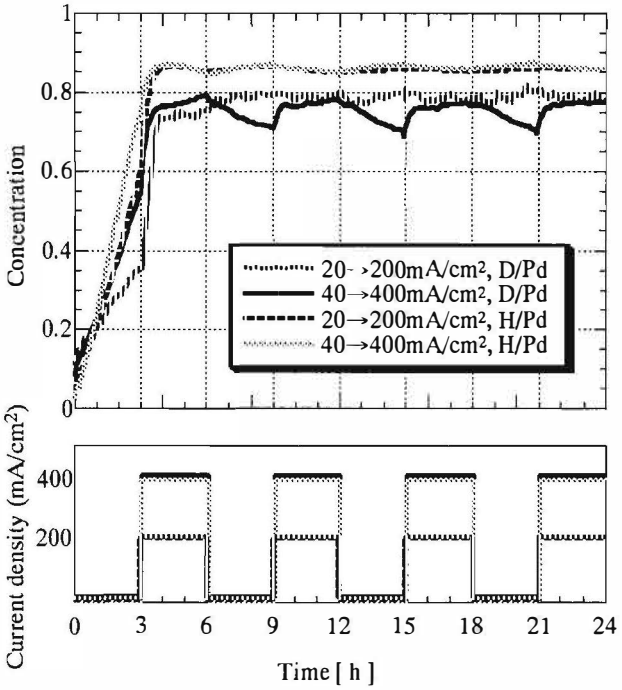

Fig.6 Concentration H(D)/Pd versus time on pulse mode. Specimen thickness = 0.5 mm, high current density = 200 mA/cm², low current density = 20 mA/cm², and high current density = 400 mA/cm², low current density = 40 mA/cm²

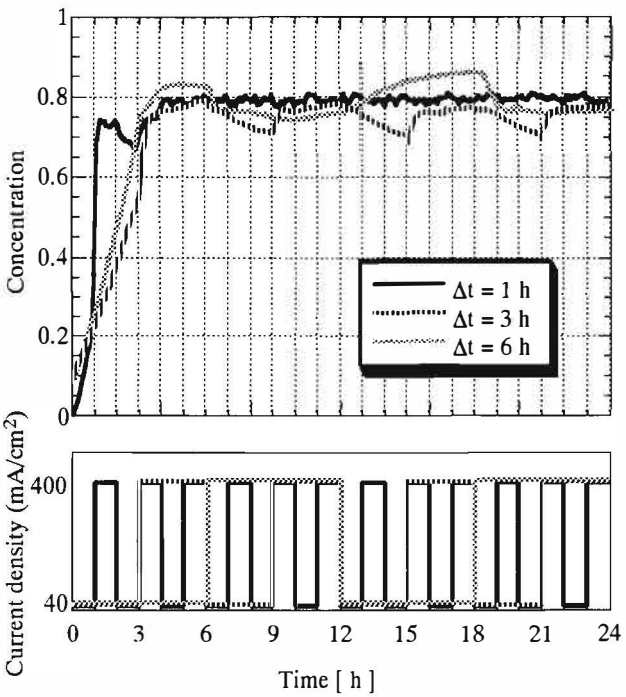

Fig.7 Concentration D/Pd versus time on pulse mode. Specimen thickness = 0.5 mm, high current density = 400 mA/cm², low current density = 40 mA/cm², and Pulse period Δt = 1, 3, 6 hour.

Conclusion

The reliability of the dynamic movements of the hydrogen isotopes in LiOD(H)-Pd electrolysis have been investigated under the high/low pulse mode electrolysis by varying the current density and the repetition time. The very clear and reasonable response of the loading ratios to the pulse mode could be confirmed in LiOD electrolysis with 3 hours repetition time and high current density like 400mA/

cm^2. While only the slight and reversal direction responses were detected in LiOH electrolysis and longer repetition time like 6 hours even in LiOD electrolysis gave clear response but with reversal direction.

The evidently different response between LiOD and LiOH is significant to elucidate the anomalous phenomena occurred in LiOD-Pd electrolysis.

The conditions realized the dynamic movement of the deuterium in Pd electrode were identified and found to be well consistent with high reproducibility of the anomalous reported by the present authors[8].

Reference

[1] M.Nakada, T.Kusunoki and M.Okamoto, "Energy of the Neutrons Emitted in Heavy Water Electrolysis", Frontiers of Cold Fusion, Tokyo: Universal Academy Press Inc., 581～586 (1992) [Book]

[2] M.C.H.McKubre, S.Crouch-baker, A.K.Hauser, S.I.smedley, F.L.Tanzella, M.S.Williams, S.S.Wing, "Concerning Reproducibility of Excess power Production", Proceedings of the Fifth International Conference on Cold Fusion, 17～33 (1995)

[3] M.Okamoto, Y.Yoshinaga, M.Aida and T.Kusunoki, "Excess Heat generation, Voltage Deviation and Neutron Emission in D_2O-LiOD Systems", Proceedings of Fourth International Conference on Cold Fusion, EPRI, **2**, 3-1～3-6 (1994)

[4] M.Okamoto, T.Kusunoki, Y.Yoshinaga, H.Ogawa and M.Aida, "Excess Heat Generation, Neutron Emission and Cell Voltage Change in D_2O LiOD-Pd Systems", Trans. Fusion Tech., **26**, 176～179 (1994)

[5] H.Ogawa, S.Yoshinaga, Y.Yoshida, M.Aida and M.Okamoto, "Correlation of Excess Heat and Neutron Emission in Pd-Li-D Electrolysis", proceedings of The Fifth International Conference on Cold Fusion, 116～119 (1995)

[6] H.Miyamaru, Y.Chimi, T.Inokuchi and A.Takahashi, "Search for nuclear Products of Cold Fusion", Proceedings of Fourth International Conference on Cold Fusion, EPRI, **2**, 2-1～2-10 (1994)

[7] J.Minato, T.Nakata, S.Denzumi, Y.Yamamoto, A.Takahashi, H.Aida, Y.Tsuchida, H.Akita and K.Kunimatsu, "Materials/Surface Aspects of Hydrogen/Deuterium Loading into Pd Cathode, Proceedings of the Fifth International Conference on Cold Fusion, 383～410, (1995)

[8] In this Proceedings

Excess Energy and Nuclear Products

CORRELATION OF EXCESS HEAT GENERATION AND NEUTRON EMISSION IN Pd-LiOD ELECTROLYSIS

H.Ogawa, Y.Oya, T.Ono, M.Aida, and M.Okamoto
Research Laboratory for Nuclear Reactors, Tokyo Institute of Technology
Ookayama, Meguro-City, Tokyo 152 Japan
Tel: 81-3-5734-3065, Fax: 81-3-5734-2959

Abstract

The correlation of the excess heat generation and the neutron emission in Pd-LiOD electrolysis has been investigated by use of a pair of experimental systems consisted of the same equipments in principle and operated coincidentally. Three pairs of electrolysis runs have been performed on the coincidental experiment systems, resulting clear time correlations between the excess heat generation and the excess neutron emissions. The reproducibility of the anomalous phenomena occurred in the present electrolysis could be accomplished completely in the series of experiments by a pretreatments of the Pd electrodes and the special purity control of the electrolyte used.

Introduction

The correlation between the excess heat generation and the excess neutron emission has been discussed based on the data obtained by the background runs with the light water and the foreground runs with the heavy water which were operated reciprocally under the same electrolysis conditions. In the course of the discussion, some uncertainty arouse on the neutron detection that came from the different date of the operation between the background runs and the foreground runs. To avoid such an uncertainty, especially in the excess neutron evaluation, two sets of the experimental systems have been assembled with the possibly same equipments such as the excess heat monitoring systems and the neutron detection systems of NE213 liquid scintillation counters.

In the present work, by use of the experimental systems, the background runs with the light water and the foreground runs with heavy water have been carried out conincidentally under the same conditions which gave us the positive results with high reproducibility to confirm the time correlation between the excess heat generation and the excess neutron emission and to check the reproducibility of the anomalous phenomena occurred in the deuterium-Pd system.

Experimental

The blockdiagram of the coincident experiment systems used are illustrated in Fig.1. The systems consists of the same equipments in principle. However, there might be some little differences in their characteristics especially in the excess heat monitoring systems and the neutron counting systems.

Excess Energy and Nuclear Products

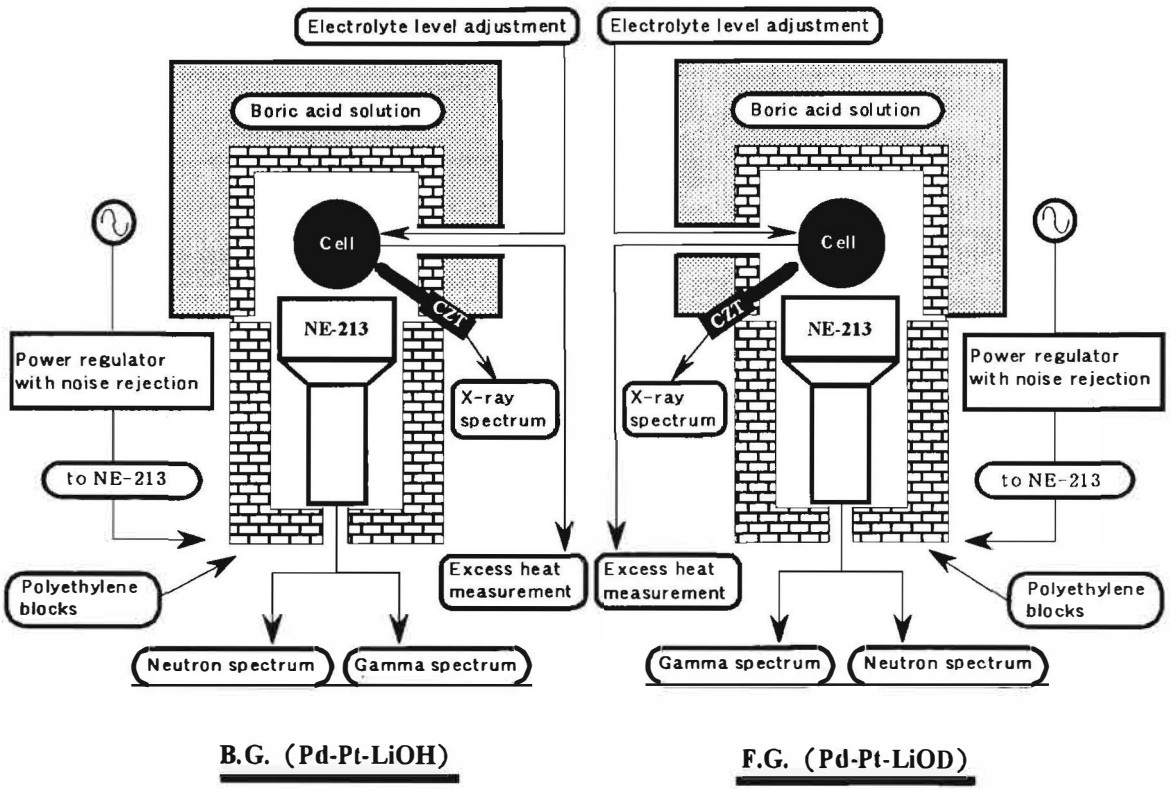

Fig.1 Coincident operating systems

The machine factors on the two systems have been checked before and after the every electrolysis operation. The details of the NE213 neutron counting systems were described in the previous papers.[1]

The schematic view of the electrolysis cell system is illustrated in Fig.2. The details of the electrolysis cell are same as described in the previous papers except the automatic electrolyte supplier. By this, the level of the electrolyte could be adjusted at a constant level throughout the electrolysis.

The ambient temperature was controlled at 24 ± 1℃ and the temperature of the cooling water was kept at 24 ± 0.1℃. The fluctuation of the electrolyte temperature caused by the supplying the electrolyte became negligible throughout the operations.

The data acquisition were performed on a personal computer in every thirty seconds

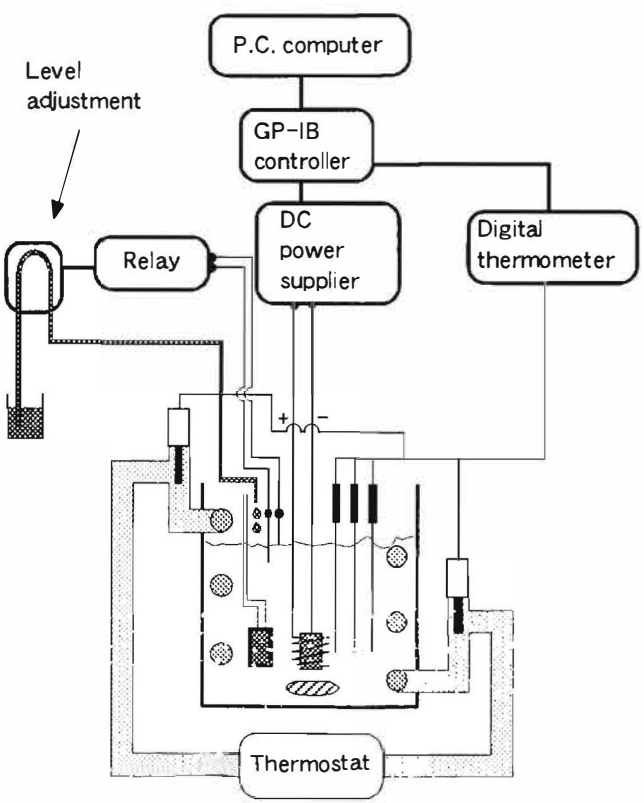

Fig.2 Electrolysis cell and Calorimetry system

Table1 Experimental conditions

		Cathode size	Pretreatment	Electrolysis mode
Run 1	B.G.	Pd 0.8 mm × 10 mm × 25 mm	Mechanical polishing 1 mm → 0.8 mm ⇩ Vacuum annealing 850 ℃, 10 hours	B.G. (LiOH) F.G. (LiOD) 1 M High / Low 800 / 20 (mA/cm²) 3 / 3 (hours)
	F.G.			
Run 2	B.G.			
	F.G.			
Run 3	B.G.			
	F.G.			

for the electrolyte temperature and in every hour for the neutron counting, the γ ray counting and the X ray counting, respectively.

The experimental conditions are listed in Table 1. The Pd cathodes used were four nine purity Pd plates manufactured by Tanaka Kikinzoku Co. Ltd. and supplied from NHE Center of Institute of Applied Energy as the standard material in New Hydrogen Energy Project. Before use, the surfaces of Pd plates were mechanically polished to the mirror surface, so 0.1 mm from the initial surface of the Pd electrodes was lost for each sides. The electrolyte used was 1 mole/dcm^3 LiOD or LiOH. The light water and the heavy water were distilled three times before use. The electrolysis was performed under the square pulse mode with 3 hours repetition, and with high current density of 800mA/cm^2 and low current density of 20mA/cm^2 as shown in Table 1. The electrolysis operations were carried out for four weeks or more. The excess power evaluation was performed by means of inner standard calibration method by use of a standard electrical resistance placed in the cells, and the details were described in the previous papers. [2]

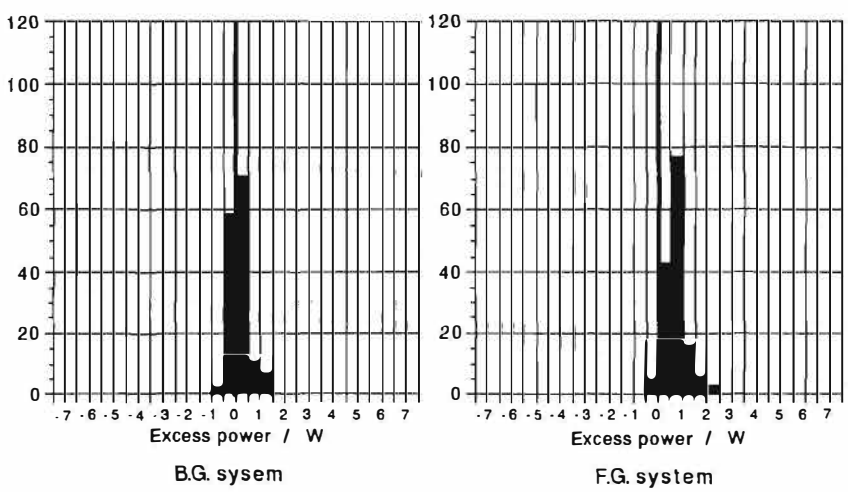

Fig.3 Histgram of the excess power for Run 1

Results and discussion

Excess power

The excess power obtained in the present series of the experiments are demonstrated by the

statistical histgrams in Fig.3, Fig.4, and Fig.5 for Run 1, Run 2, and Run 3, respectively. In these figures, the left hand side histgrams represent the results obtained in the background runs with the light water and the right handside histgrams represent the results obtained in the foreground runs with the heavy water.

The distributions of the histgrams indicate that the foreground runs with the heavy water gave the clear excess power generation except Run 2, while the background runs did not give any excess power as reported previously. The excess power generation can replicate in Run 1 and Run 3, but did not in Run 2. The reason why Run 2 did not give the excess power will be discussed later in this paper.

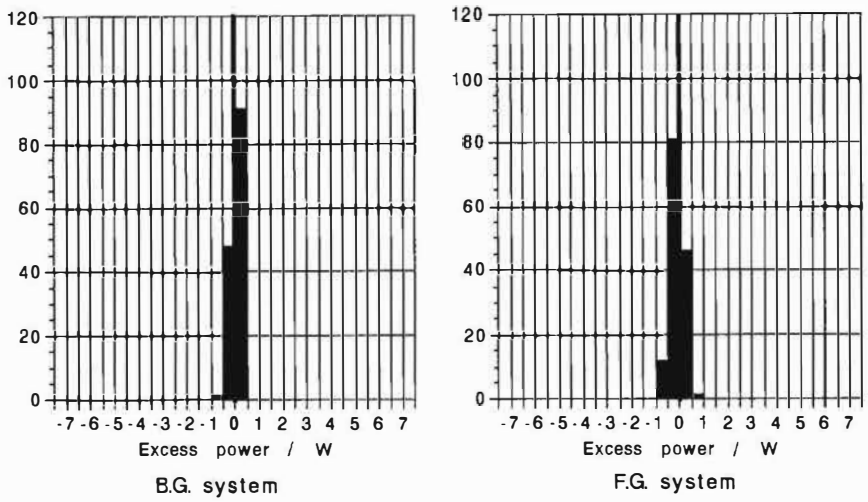

Fig.4 Histgram of the excess power for Run 2

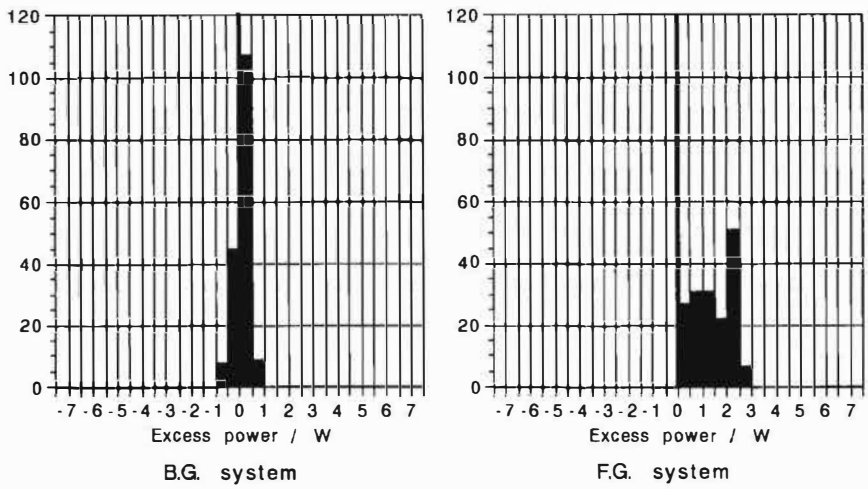

Fig.5 Histgram of the excess power for Run 3

Excess neutron

The neutron energy spectrum evaluated by the neutron ratios between the neutron counting rates in the background runs and the foreground runs are shown in Fig. 6. The error bars represent 3 σ . When the neutron ratios were over unity, it was concluded that the excess neutrons were detected in the corresponded bit of the PHA. It can be said from these spectrum that the excess neutrons were observed in Run 1 and Run 2, but did not observed in Run 2. The fact well corresponds with the results for the excess power as mentioned above. The reason why the Run 2 did not give any excess neutrons will be also discussed later in the paper. In Fig.7, the time correlation between the excess power generation and the excess neutron emission are demonstrated for Run 3. The time correlation is very clear from the start of the electrolysis to the termination of the operation. The intensities of the neutron ratios increased with increase of the magnitudes of the excess power. The clear time correlation between the two events is firstly reported in the new hydrogen energy project and other related researches.

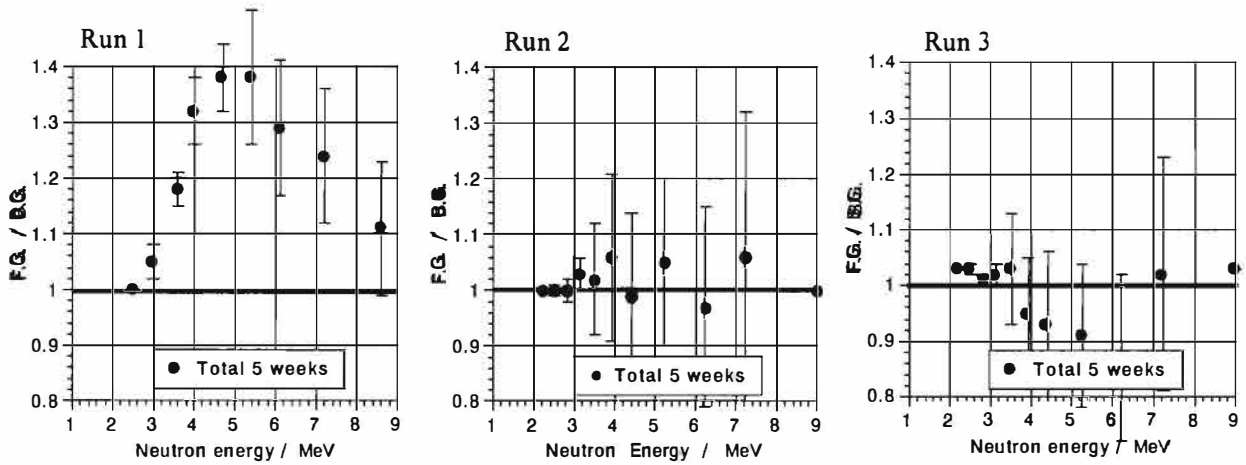

Fig.6 Neutron energy spectra of Run 1,Run 2 and Run 3

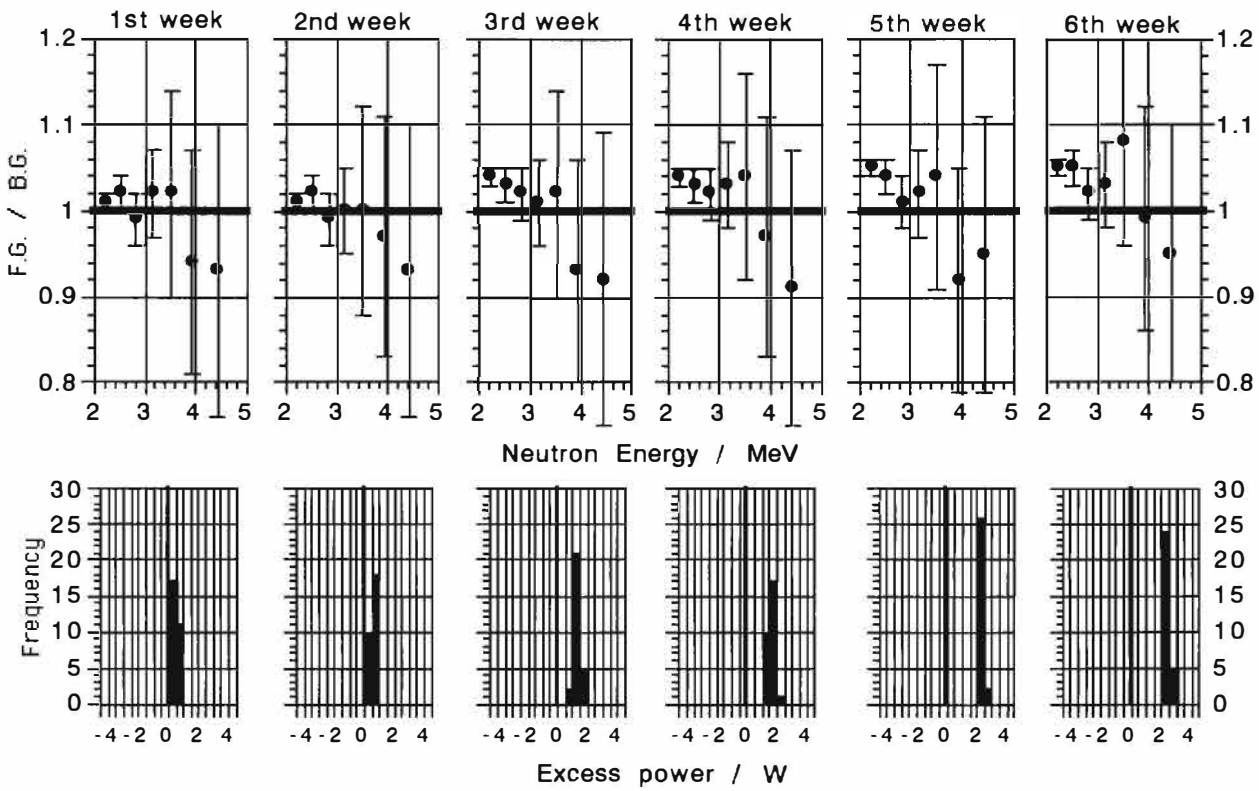

Fig.7 The time correlation between the excess power generation and the excess neutron emission

Cell voltage (open circuit voltage)

As discussed in the previous papers,[3] the cell voltage was recognized as one of the key factors to elucidate the mechanisms of the anomalous phenomena occurred in LiOD-Pd electrolysis process. The cell voltages have been also measured in the present series of experiments. The data are shown in Fig. 8 for the three runs.

The cell voltages changed with some nonlinear fractions in Run 1 and Run 3 comparing with the curves observed in the background runs in all of the runs, while Run 2 gives almost straight linear curves even in the foreground run. The similar nonlinear fractions have been observed in the previous experiments by the authors, resulting the excess heat generation and the excess neutron emission. [1] It can be said that the previous findings have been strongly confirmed by the present results obtained

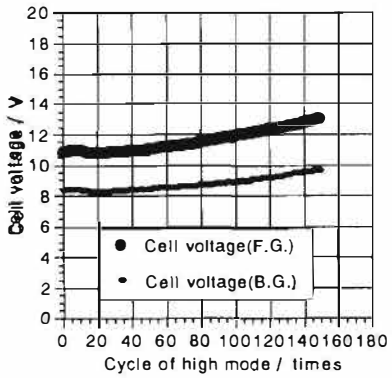

Fig.8-a Cell voltage for F.G and B.G. of Run 1

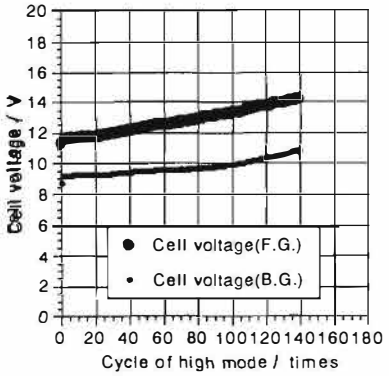

Fig.8-b Cell voltage for F.G. and B.G. of Run 2

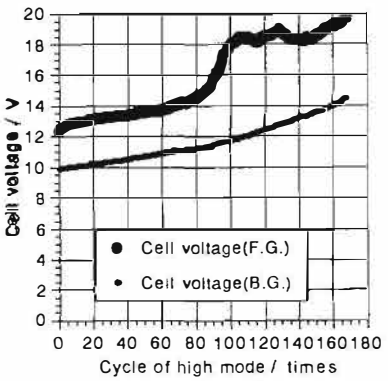

Fig.8-c Cell voltage for F.G. and B.G. of Run 3

from the couple of the coincidental electrolysis operations. The nonlinear fraction in the Run 3 is tremendously anomalous as has been never found in the present authors studies.

Combining the three findings of the excess power generation, the excess neutron emission and the nonlinear fraction of the cell voltage, it can be concluded that the larger deviation with larger nonlinear fraction from the curves obtained in the background runs gave larger excess power and more clear excess neutron emission.

At the last part of the present work, the authors should describe the reason why Run 2 gave no anomalous events. In fact, there was a different procedure in Run 2 from the other two runs. The Pd electrodes in Run 2 were placed in the electrolyte for two weeks before the electrolysis operation start to check the machine factors. Only this point is unique point for Run 2 in the all of the experimental conditions. It can be said that the Pd electrode should be employed for the electrolysis immediately after the cooling of the Pd electrodes in annealing chamber.

Conclusion

A pair set of the experimental systems to avoid the uncertainty caused from the different date of the background runs and foreground runs has been assembled to study the correlation between the excess power generation and the excess neutron emission in LiOD-Pd electrolysis. By use the systems and the well controlled conditions, the time correlation was observed clearly. The well controlled conditions was found to replicate the anomalous phenomena based on the deuterium. The anomalous nonlinear fraction observed in the cell voltage in the heavy water electrolysis was confirmed as one of significant factors to elucidate the new hydrogen energy process. The further investigations should be carried out to clarify the mechanisms of the anomalous phenomena including the nonlinear fraction occurred in the cell voltage.

Acknowledgments

The authors acknowledge financial support from 20 Japanese industries for the Basic Research Program for the New Hydrogen Energy Project, and express their many thanks to whom concerned to the Basic Research Program.

Excess Energy and Nuclear Products

References

[1] M.Nakada, T.Kusunoki and M.Okamoto, "Energy Emitted in Heavy Water Electrolysis", Frontiers of Cold Fusion, Tokyo: Universal Academy Press Inc., 581～586 (1992) [Book]
[2] H.Ogawa, S.Yoshinaga, Y.Yoshida, M.Aida and M.Okamoto, "Correlation of Excess Heat and Neutron Emission in Pd-Li-D Electrolysis", Proceedings of The Fifth International Conference on Cold Fusion, 116～119 (1995)
[3] M.Okamoto, T.Kusunoki, Y.Yoshinaga, H.Ogawa and M.Aida, "Excess Heat Generation, Neutron Emission and Cell Voltage Change in D_2O-LiOD Systems", Trans. Fusion Tech., **26**, 176～179 (1994)

Excess Energy and Nuclear Products

"Excess Heat" Measurement in Gas-loading D/Pd System

Xing Zhong Li, Wei Zhong Yue, Gui Song Huang
Hang Shi, Lan Gao, Meng Lin Liu, Feng Shan Bu*

Department of Physics, Tsinghua University
Beijing 100084, CHINA

*Beijing General Research Institute for Non-Ferrous Metals
Beijing 100088, CHINA

Abstract
A gas-loading D/Pd system has been designed to measure the "excess heat". The preliminary result has shown that the calorimetric feature of the D/Pd system is distinct from that of its twin H/Pd system. The difference between these twin systems can be attributed to the "excess heat" of the order of watts per cubic centimeter of palladium.

1. Introduction

The "heat after death" phenomenon [1] has revealed a fact that the electrolysis is not necessary for "excess heat" phenomena. Provided that enough deuterons are absorbed in the palladium crystal lattice, we may expect to see the "excess heat" in a gas-loading system as well. We are particularly interested in the gas-loading system, because we have been engaged in the gas-loading system for several years[2-7]. Early in 1993, Manduchi et al. [8] showed that the palladium samples might be soldered together during the gas-loading process with the deuterium gas. It was explained as an evidence of "excess heat" in this gas loading system. Manduchi's experiments worked out with both the Russian palladium and the British palladium samples. It seems that the only important pre-treatment in his experiment is the annealing at the high temperature (900 °C) in vacuum. This is consistent with the early basic research on the gas loading experiments. Oats and Flanagan [9] did the gas loading experiments early in 1971. They showed that the only pre-treatment was just the flame heating before use. The loading ratio was as high as 0.94 in their experiments as a matter of routine. The even surprising point was that the gas-loading was done at low hydrogen pressure (1.5 Torr, 25 °C). The key element was a heated tungsten wire which dissociated the hydrogen molecules into hydrogen atoms. These features of operating under the low pressure and heating by a tungsten wire facilitate the combination of a calorimetric system with a gas-loading system.

2. Experimental Apparatus.

The low pressure feature makes thin wall stainless steel dewar system applicable for a closed gas-loading system (Fig.1). Palladium wire of ϕ 0.34mm is wound on a quartz frame. A pair of such quartz frames with palladium wire winding are made for D_2-loading and H_2-loading, respectively. They are put into a electrical oven to be heated to 900 °C in vacuum (10^{-3} Pa). Then they are cooled gradually with the oven. Before they are put into the stainless steel dewar, a piece of tungsten filament (ϕ 0.1mm) is mounted at the center of the quartz frame. The resistance of the palladium wire is measured by the four-lead method in order to determine the loading ratio (D/Pd and H/Pd) *in situ*. The leads for palladium wire and for tungsten filament can be used for both heating the dewar vessel and measuring their resistance. A platinum thermometer is put into the gap between the tungsten filament and the palladium wire in order to measure the temperature change during the process of gas-loading and the calorimetric heating. A manometer is monitoring the gas pressure to evaluate the loading ratio, and a diffusion pump is used to pump out the air to 7×10^{-4} Pa.

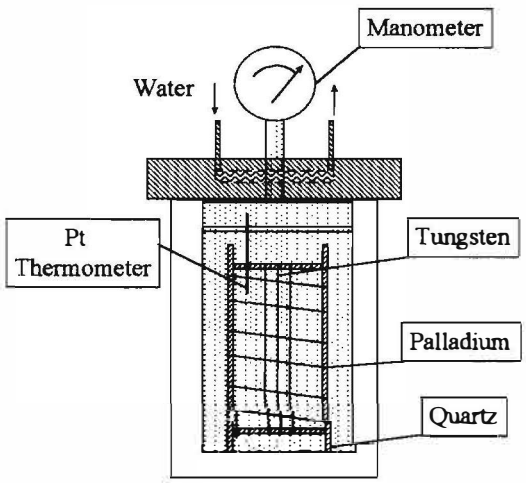

Fig.1 A Combination of a Calorimeter with a Gas-loading System

3. Calorimetric Feature.

This stainless dewar vessel is different from the glass or quartz dewar electrolytic cell in Fleischmann and Pons experiments. In stead of radiation, the heat conduction plays the dominant role in the heat transfer. Fig.2 shows the temperature, θ, in the dewar as a function of time. It can be described by the following equation

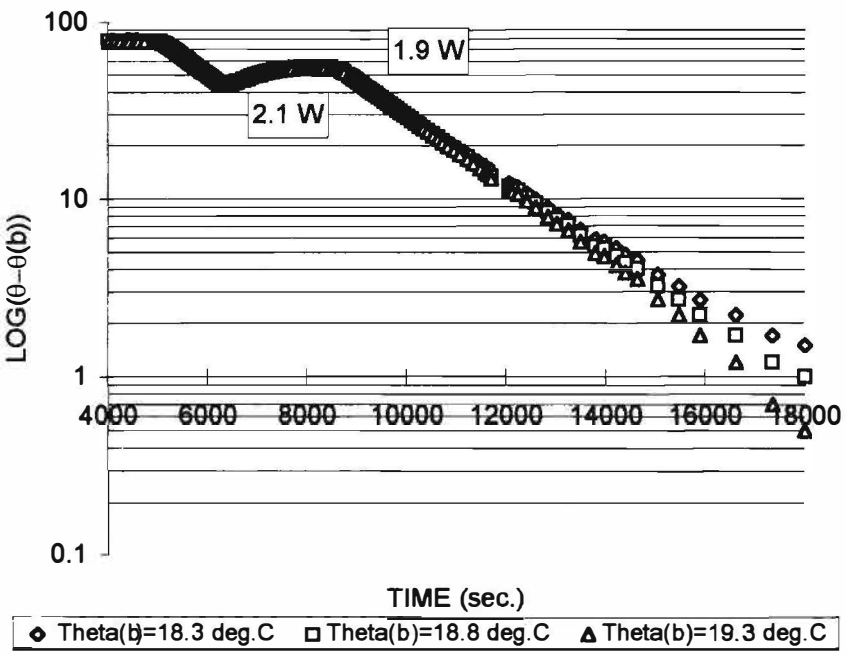

Fig.2 Calorimetric Feature of the Stainless Steel Dewar System

$$MC_p \frac{d\theta}{dt} = -k(\theta - \theta_b) + S \tag{1}$$

when the heat source, S, is a constant source; the temperature in the platinum thermometer, θ, approaches a constant value θ_f

$$\theta_f = \theta_b + \frac{S}{k} \tag{2}$$

Here, k is the heat conduction coefficient in the Newton's Law of heat transfer. θ_b is the room temperature. The relaxation time of this system is determined by the reduced heat conduction coefficient:

$$\hat{k} = \frac{k}{MC_p} \tag{3}$$

MC_p is the equivalent heat capacity of the calorimetric system. The equation can be written as

$$\frac{d\theta}{dt} = -\hat{k}[\theta - (\theta_b + \frac{S}{k})] \tag{4}$$

When S is a constant

$$\theta = (\theta_b + \frac{S}{k}) + [\theta_0 - (\theta_b + \frac{S}{k})]e^{-\hat{k}(t-t_0)} \tag{5}$$

or

$$\log[\theta - (\theta_b + \frac{S}{k})] = -\hat{k}(t - t_0) + \log[\theta_0 - (\theta_b + \frac{S}{k})] \tag{6}$$

Here, θ_0 is the initial temperature of the dewar system at time t_o. This is the straight line section shown in Fig.2. The slope of the straight line gives the value of the reduced heat conduction coefficient, $\hat{k}$; the constant $(\theta_b + \frac{S}{k})$ may include the information for both the applied heat source, P; and the internal heat sources, Q. The applied heat source, P, is the heating power given by the experimentalist; however, the internal heat sources, Q, may include the "excess heat" which is what we are searching for.

There are two ways to determine ($\theta_b + \frac{S}{k}$):

(1) Heating method: Given a constant heating power (e.g. a constant current through the tungsten wire), the temperature, θ, approaches a constant value, θ_f .

$$\theta_f = \theta_b + \frac{S}{k} \tag{7}$$

(2) Cooling method: When we plot the Fig.2 using the experimental data, we have to have a correct value for $\theta_b + \frac{S}{k}$ in order to make a straight line for cooling part. Fig.2 shows that the least squares fit is able to find the value of $\theta_b + \frac{S}{k}$ with a precision better than 3%. 0.5 °C change in $\theta_b + \frac{S}{k}$ may make the straight line visibly distorted (i.e; bent upward or downward, if the $\theta_b + \frac{S}{k}$ is not a correct number.)

Fig.2 shows also the sensitivity of our calorimetric system. When a small power of 2.73W is applied onto the calorimetric system through a current in the tungsten wire, the temperature goes up to a constant value of 96.0 °C. Then the current is shut off, and we see a straight line of cooling curve with no heat source (see equation (6)). Later we turn on the current in the tungsten wire again with a power of 2.55W, a clear inflection point appears to stop the straight line, and levels to a new constant value. Particularly, the curve goes up continuously at a power of 2.1W and turns horizontal at a power of 1.9W. Thus, we are confident that this system is able to detect the "excess heat" at the level of 1 W per c.c. palladium while we put 0.234 c.c. palladium wire into this calorimetric system.

4. Temperature Difference between Twin Systems

A calibration is necessary to quantify the "excess heat"; however, if we are able to show that there are sharp differences in the calorimetric feature between the H/Pd and D/Pd twin systems; then, we may qualitatively show the evidence of the "excess heat".

To load the hydrogen or deuterium gas into the

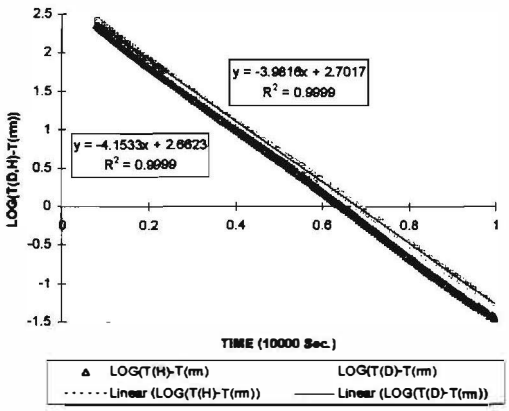

Fig.3(a) Cooling Feature for D/Pd & H/Pd Systems
(43—32 Deg.C for D; 41—31 Deg.C for H)

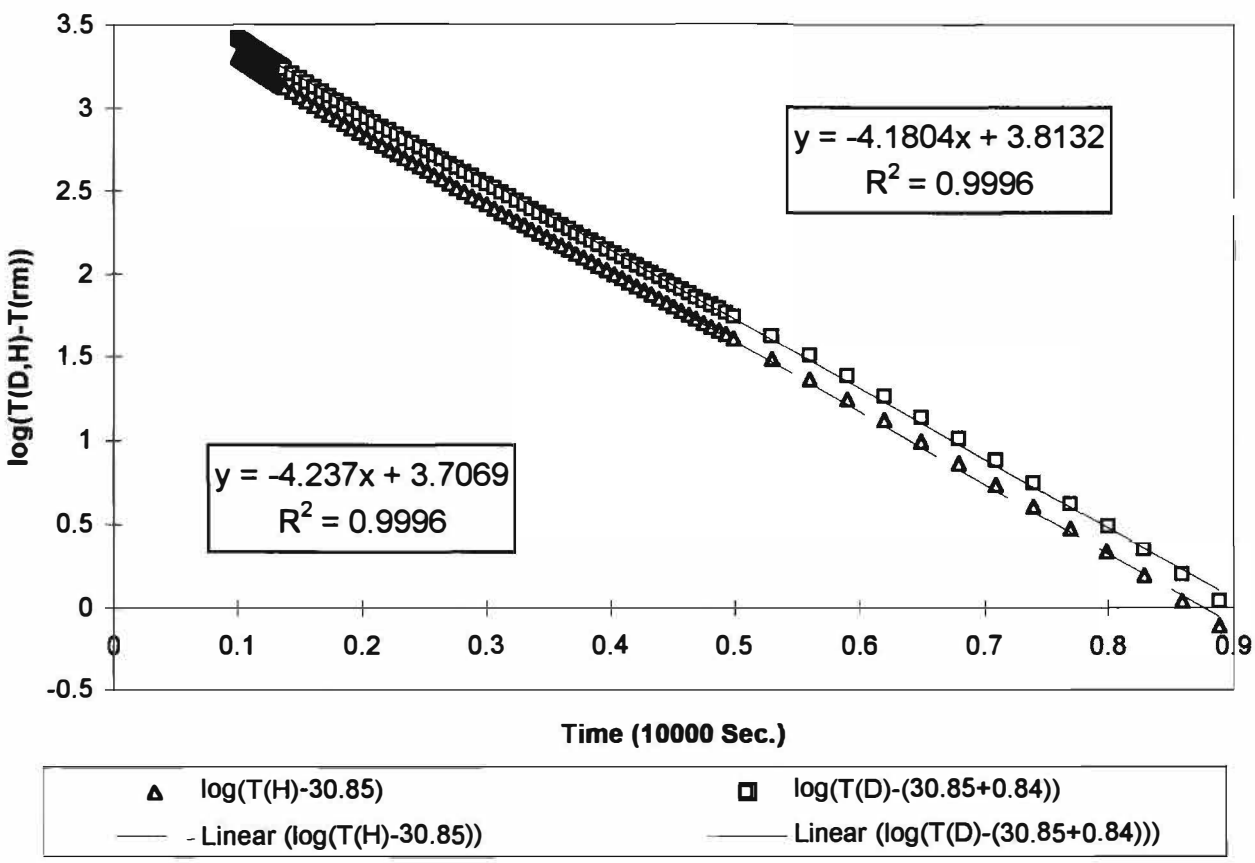

Fig.3(b) Cooling Feature of D/Pd and H/Pd Systems
(62-–33 Deg.C for D; 58---32 Deg.C for H)

palladium, electrolytic cell was supposed to be necessary to provide the enough "chemical potential"; otherwise, the high pressure and low temperature was supposed to be necessary. R.F. power, a piece of incandescent tungsten wire (2000 °C), or D.C. discharge were found to be able to provide the hydrogen or deuterium atoms in stead of the electrolytic current. However, we found that even if the tungsten wire was turn-off, as long as the correct pre-treatment of the palladium wire was done, the loading ratio (H/Pd or D/Pd by atom number) might achieve 0.74 at a pressure much less than 1 atm. This is discussed in two associated papers [10] and [11]. Here, we just discuss the calorimetric feature of the gas-loading system.

In order to detect the possible "excess heat" in a D/Pd system, we intentionally built a pair of twin systems. No.1 bottle is for deuterium loading, and No.2 bottle is for hydrogen loading. These two systems have same dewar structure, and similar quartz frames. The palladium wires in both bottles are cut from same batch (ϕ 0.34mm); and have been pre-treated with same procedures. The weight of palladium wires in two bottles are 2.846g. and 2.844g., respectively. The tungsten wires are cut from same batch (ϕ 0.1mm). The resistance of tungsten wire are 4.1Ω (in D bottle), and 4.3Ω (in H bottle) , respectively. After being pumped to 10^{-3}Pa, the No.1 bottle was filled with deuterium gas up to 660 mmHg; and the No.2 bottle was filled with hydrogen gas up to 660 mmHg also. Fig.3 shows the cooling curves for bottles No.1 and No.2. A straight line is drawn to fit the experimental data using the least squares fit. From this straight line, the reduced heat conduction coefficient, $\hat{k}_D$ and $\hat{k}_H$, is calculated. To maximize the correlation coefficient R^2, we may determine the value of $(\theta_b + \frac{S}{k})$ for that straight line. Table 1 gives the corresponding values for the reduced heat conduction coefficients $\hat{k}_D$ and $\hat{k}_H$; the constants $(\theta_b + \frac{S}{k})_D$ and $(\theta_b + \frac{S}{k})_H$; and the correlation coefficients R_D^2 and R_H^2.

Table 1 Calorimetric Feature for Cooling Curve of D/Pd and H/Pd Systems

Temperature Range °C		Reduced Heat Conduction Coefficient $\hat{k}$ sec^{-1}	$\theta_b + \frac{S}{k}$ °C	R^2
41.456→ 31.173	H	$(4.15 \pm 0.02) \times 10^{-4}$	30.94	0.9999
42.785→ 31.803	D	$(3.98 \pm 0.02) \times 10^{-4}$	30.94+0.579	0.9999
58.047→ 31.741	H	$(4.24 \pm 0.04) \times 10^{-4}$	30.85	0.9996
62.161→ 32.728	D	$(4.18 \pm 0.03) \times 10^{-4}$	30.85+0.84	0.9996

It is clearly shown that the reduced heat conduction coefficients are same for both bottles with the precision better than 5%. However, the constants, $\theta_b + \frac{S}{k}$, are different for D/Pd and H/Pd

systems. The difference between them increases, when the temperature range expands. Since the information of "excess heat" is included in this constant, $\theta_b + \frac{S}{k}$, we investigated further by another method: i.e. we heat the systems using the electrical current in the tungsten wire. Through the constant current at 0, 0.1965A, 0.359A, 0.464A, 0.601A, 0.753A and 0.801A; the D/Pd and H/Pd systems are heated to different temperatures. From these temperatures, we may have another estimate of the constant, $\theta_b + \frac{S}{k}$. Table 2 list the results of these heating experiments. The difference of $\theta_f - \theta_b = \left[\left(\theta_b + \frac{S}{k}\right) - \theta_b\right]$ gives the $\frac{S}{k} \equiv \frac{P+Q}{k}$.

In the experiments, the tungsten wires in the D/Pd and H/Pd are connected in series such that the electrical current, I_w, is same in both tungsten wires. This heating power enhances the temperature, θ, in both bottles, and eventually makes a steady state value, θ_f. We can measure the temperature difference at the steady state between the inside and the outside of the dewar, $\theta_f - \theta_b$, which should be equal to the constant $\frac{S}{k} = \frac{P+Q}{k}$. In this case, P is the heating power in tungsten wire, Q is the possible "excess power", k is the heat conduction coefficient. It is interesting to notice that when the heating power increases, the temperature difference, $\theta_f - \theta_b$, in D/Pd system increases much faster than that in H/Pd system. This could be attributed to the possible "excess power" in the D/Pd system. In order to estimate this "excess power", we need the value for heat

Table 2 Calorimetric Feature for Heating Curve of D/Pd and H/Pd System

I_w	D		H		
	P_w^D	$\theta_f - \theta_b = \left[\frac{P_w + Q_{ex}}{k}\right]_D$	P_w^H	$\theta_f - \theta_b = \left[\frac{P_w + Q_{ex}}{k}\right]_H$	$Q_{ex}^D = \frac{\left[\frac{P_w + Q_{ex}}{k}\right]_D}{\left[\frac{P_w + Q_{ex}}{k}\right]_H} P_w^H - P_w^D$
(A)	(W)	(°C)	(W)	(°C)	(W)
0.197	0.161	2.44	0.173	2.48	0.009
0.359	0.551	8.34	0.569	7.70	0.065
0.464	0.960	14.2	0.977	12.9	0.115
0.601	1.73	24.6	1.71	21.5	0.227
0.753	2.99	39.8	2.93	33.9	0.450
0.801	3.51	41.8	3.45	33.3	0.821

conduction coefficient, k_D. Since the reduced heat conduction coefficients, $\hat{k}_D$ and $\hat{k}_H$ for D/Pd and H/Pd are almost same (see table 1). It is reasonable to assume that the heat conduction coefficients, k_D and k_H, are same also. Based on this assumption, the "excess power" in the D/Pd system is calculated. It may achieve up to 0.821W (see the last column in table 2) while the heating power is about 3.5W. An additional evidence of this "excess power" in D/Pd system is the change of the resistance of the tungsten wire. Initially, the resistance of the tungsten wire in H/Pd system (4.46 Ω) is a little higher than that of D/Pd system(4.15 Ω). When the heating power is increased to ~ 3.5W, the resistance of the tungsten wire in H/Pd system (5.38 Ω) becomes smaller than that of D/Pd system (5.47 Ω). Using the resistance temperature coefficient $\alpha_W = 4.8 \times 10^{-3} K^{-1}$ for tungsten wire, we have the temperature for the tungsten wires in the H/Pd and D/Pd system, 73.5 °C and 96.9 °C, respectively. The temperature in D/Pd system is much higher than that of H/Pd system . This is consistent with the former calculation of the "excess power" inside the D/Pd system.

5 Concluding Remarks:

While a pair of twin calorimetric systems are heated by the same amount of electrical power, the systems approach different temperatures at steady state. The D/Pd system is hotter than the H/Pd system. The temperature difference may achieve the value of 8.5 °C measured by the platinum thermometer. Since the cooling curves have shown the reduced heat conduction coefficients for both systems are same, this temperature difference means that there must be an "excess heat" source in the D/Pd system.

We are using platinum resistance thermometers and the Keithley digital multi-meter to measure the temperature. The precision of the measurement is better than 0.1 °C. Hence, we are confident about the existence of this temperature difference. This is a qualitative proof of the "excess heat" in D/Pd system.

To quantify this excess heat, we need two assumptions: First the heat conduction coefficient is assumed to be same for the twin systems; second, the excess heat in the H/Pd system is assumed to be zero. The first assumption is supported by the equality of $\hat{k}_D = \hat{k}_H$; and the second assumption just makes a conservative estimate on "excess heat". If there is any "excess heat" in the H/Pd system also; then, the "excess heat" in D/Pd system should be greater than this estimate. It is at least at a level of 1W per c.c. palladium. We have observed this excess heat for more than 5 months. (from April, 20 to September 29, in 1996) in a D/Pd system with 2.846g. of palladium. It is about 10^3eV for each palladium atom, which is very difficult to be attributed to any chemical resource. This gas-loading system has the advantage of being operated at a higher temperature which is essential to enhance the heat energy efficiency as an energy source.

6. Acknowledgments.

Excess Energy and Nuclear Products

This work is supported by the State Commission of Science and Technology, the Natural Science Foundation of China, the Basic Research Fund of Tsinghua University. Many thanks to Mr. Karl Chang, the co-founder of VeriFone Inc., for his generous support .

References

1. S.Pons and M.Fleischmann, "Heat after Death", Transactions of Fusion Technology, Vol.26, 87, (1994)
2. X. Z. Li, et al., "The Analysis of the Neutron Emission from the Glow Discharge in Deuterium Gas Tube and the Gas Loading in Palladium", Transactions of Fusion Technology, Vol.26, 384, (1994)
3. X. Z. Li, et al., "Anomalous Nuclear Phenomena and Solid State Nuclear Track Detector" Nucl. Tracks Radiat. Meas. 22, 599 (1993)
4. X. Z. Li, et al., "The Precursor of 'Cold Fusion' Phenomenon in Deuterium/solid System". AIP Conference Proceedings 228, Anomalous Nuclear Effects in D/Pd System, Provo, Utah, Oct 22-25, 1990, edited by S.E. Jones, et al., (New York, 1991) p.419.
5. D. W. Mo, X. Z. Li, et al., "Search for Precursor and Charged Particles in 'Cold Fusion'". Italian Physical Society Conference Proceedings Vol.33, the Science of Cold Fusion, Proceedings of II Annual Conference on Cold Fusion, edited by T.Bressani, et al., Como, 29 June--4 July 1991 (Bologna, Italy, 1991) p.123.
6. D. W. Mo, X. Z. Li, et al., "Real Time Measurements of the Energetic Charged Particles and Loading Ratio (D/Pd)," Frontiers of Cold Fusion, Proceedings of the Third International Conference on Cold Fusion, Oct. 21-25, 1992, Nagoya, Japan, edited by H.Ikegami (Universal Academy Press, Inc. Tokyo, Japan, 1993), p.535.
7. G. S. Huang, X. Z. Li, et al., "The Measurements and the Control of the Loading Ratio of Deuterium in Palladium", Proceedings of the Fourth International Conference on Cold Fusion, Lahaina, Hawaii, USA, Dec.6-9, 1993, Vol.I, 20-1.
8. C.Manduchi, et al., "Anomalous Effects During the Interaction of Subatmospheric $D_2(H_2)$ with Pd from 900 °C to Room Temperature." Nuove Cimento, Vol.107A, N.2. (1994) p.171.
9. W.A. Oates and Ted B. Flanagan, "Formation of Nearly Stoichiometric Palladium-Hydrogen Systems" , Nature Physical Science , Vol.231, 19, (1971)
10. F.S. Bu and X. Z. Li, "Loading Ratio Study in a Gas-Loading System", (see Proceedings of ICCF-6, 1996)
11. G.S. Huang and X. Z. Li, "A Possible Phase Transition in a Gas-Loading D/Pd System", (see Proceedings of ICCF-6, 1996)

Excess Heat Registration in High Current Density Glow Discharge with Varrous Cathode Materials

Alexander Karabut

Scientific Industrial Association "Luch"
24 Zheleznodorozhnaya St., 142100 Podolsk, Moscow Region,
Russian Federation

ABSTRACT

Experimental facts and results of heat and electric power measurements (including nuclear products) with various cathode materials are presented.

1. INTRODUCTION

Excess heat was registered with various cathode materials and high current density glow discharge in D_2, H_2, Ar using a continuous flow calorimeter. These measurements confirmed our previous results [1]. A continuous flow calorimeter measured excess heat in the glow discharge using system of measurements with better precision.

2.EXPERIMENTAL METHOD

Experimental device "Calorimeter-2" consists of vacuum chamber having a volume of 1200 cm^3, a gas pumping system, a water cooling system, a power supply and a measuring system [1]. The system of the measurements and methods was represented [1]. The system for excess power heat measurement was improved. The termoresistors were pairs of five silicon KTS 395A transistors. The water flow was stabilized in each channel. In experiments of a system Pd-D2, Pd-H2, Ni-H2, Ni-D2, Nb-H2 (cathode samples- a gas) were used. The various kinds of the pulses current were applied.

3.EXPERIMENTAL RESULTS

Excess heat was not observed by use the pulses current up to 100 A and duration up to 3-5 μs. Excess heat in a kind of thermal bursts was observed in a range of a current 20-60 mA. The frequency of the recurrence of thermal bursts changes for these currents from 6 minutes till 5-8 seconds (Fig.1-2). Large excess heat were registered for a system Ag-D2 at density of a current 20-50 mA / cm2 (Fig.2). Excess heat was observed for systems Ni-H2, Nb-H2 (cathode sample- - plasma gaze). Large excess heat for simple Pd samples are registered at the large loading D2 in Pd at small currents and at large currents (Fig.3). Excess heat is increased monotony with a increase of density of a current for special Pd samples (Fig.3). We presented before possible nuclear reactions of the fission [2] at energy 3-20 MeV on one reaction. The manufacture stable isotope- impurity is observed in Pd cathode samples (Fig.4).

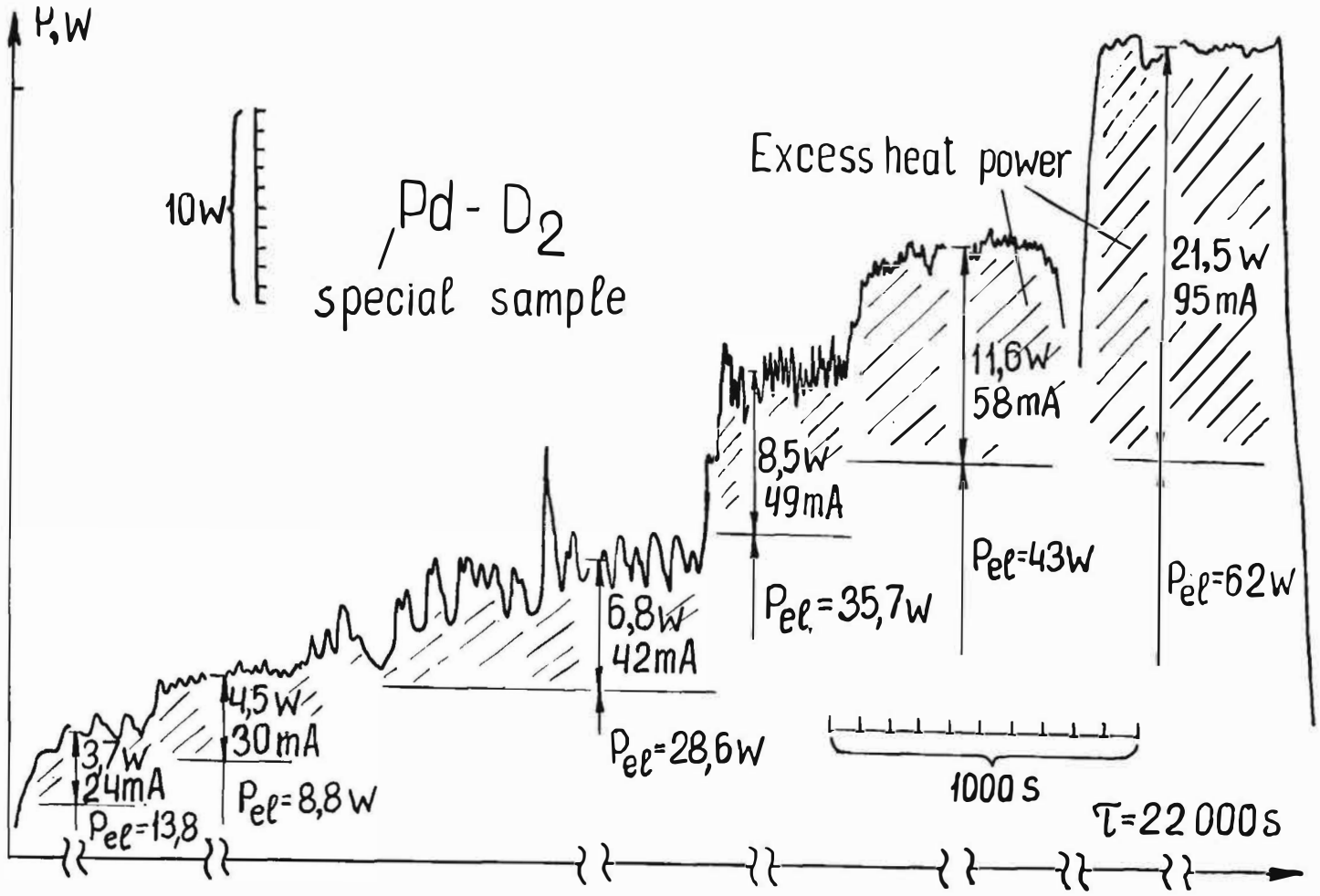

Fig. 1. Typical time dependence of heat power (Pd-D2) in continuous flow calorimeter.

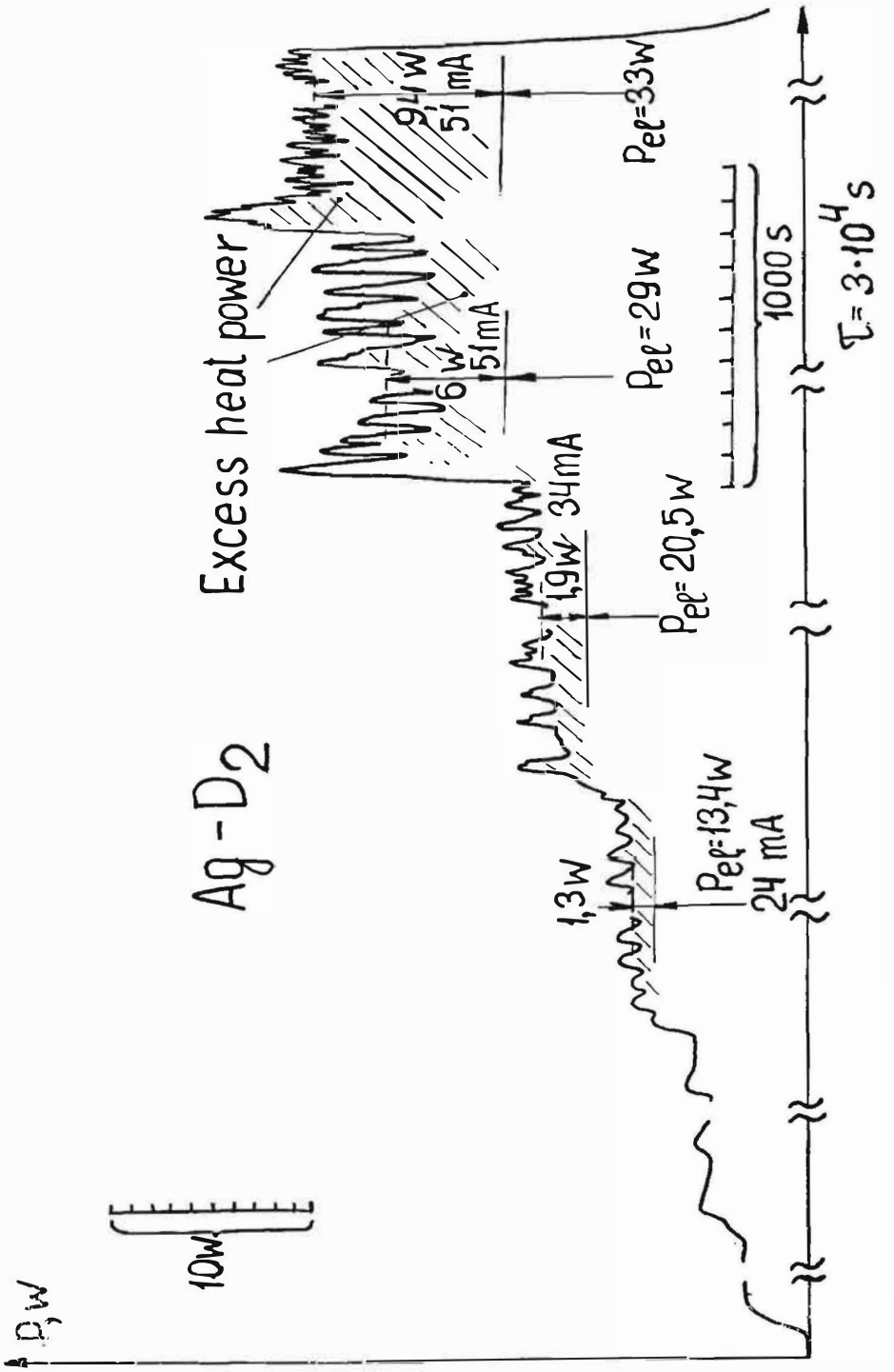

. Fig. 2. Typical time dependence of heat power (Ag-D2) in continuous flow calorimeter.

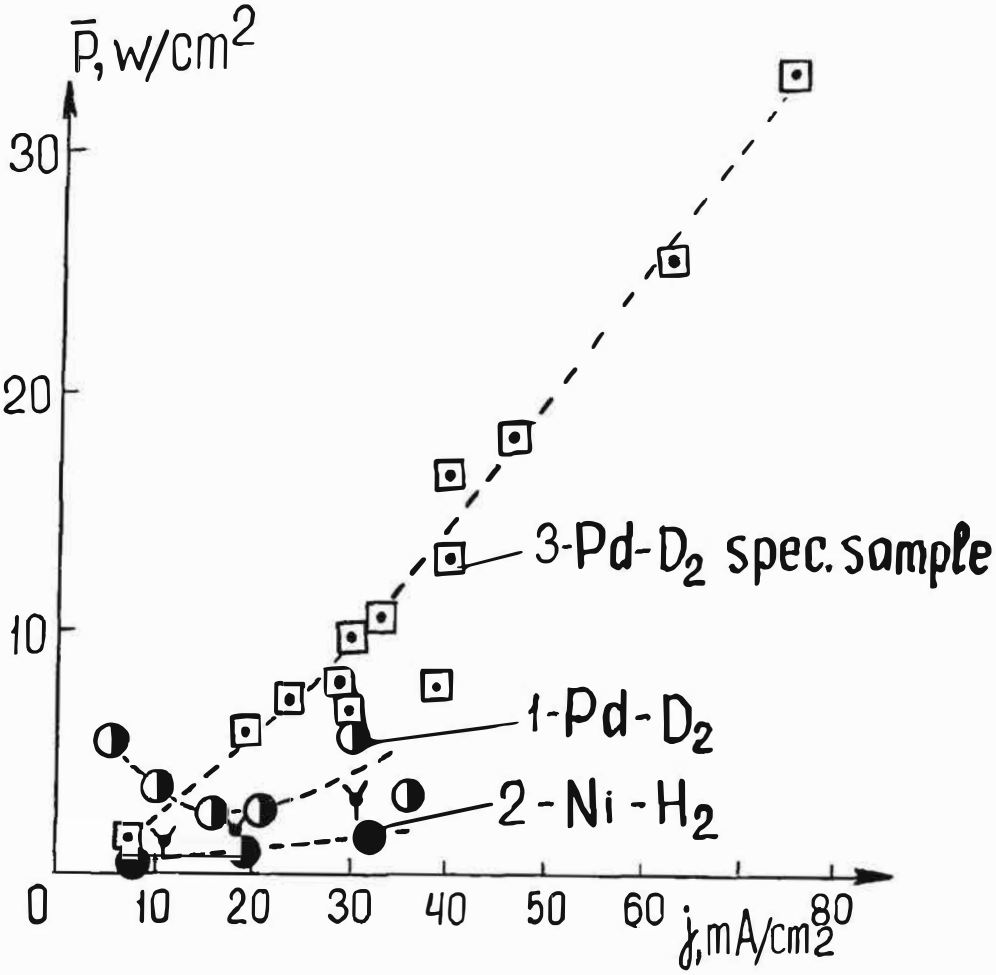

Fig. 5. Dependence of excess heat power on current density.

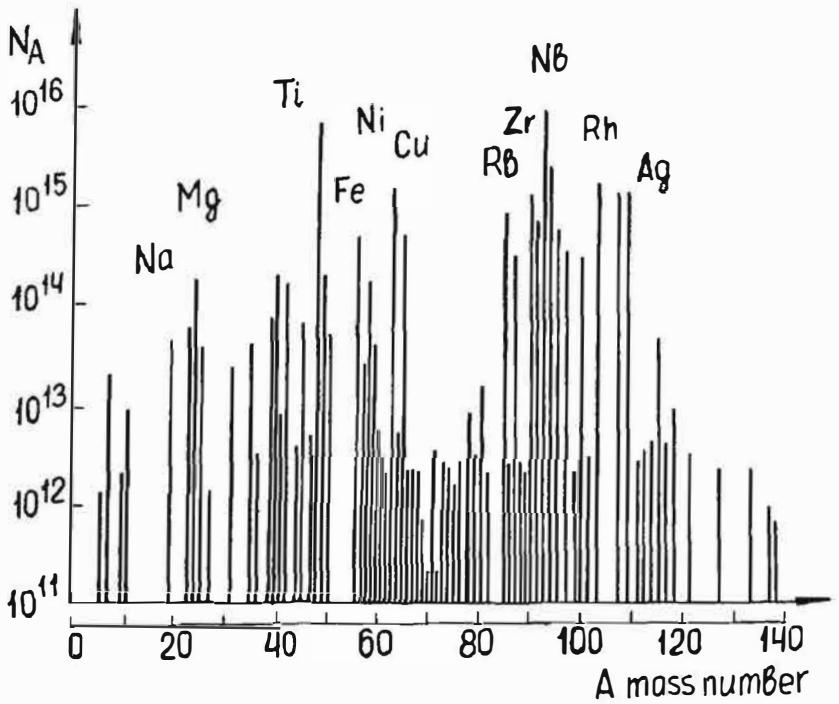

Fig. 6. Impurity in Pd-cathode after glow discharge.

4.CONCLUSIONS

The quantity of impurity corresponds to the complete value of excess heat. The comparison excess heat and of nuclear products (stable isotope) shows, that two types of nuclear reactions are observed: 1- with formation radioactive nuclides, which are observed practically for any working gases including Ar and cathode samples from the majority of metals with intensity 10^{2}-10^{3} s^{-1} , 2- reactions proceeding for some metals with H_2 and with D_2 by intensity 10^{11}-10^{12} s^{-1} and forming stable nuclides with excess heat without decelerated γ- radiation .

REFERENCES

1. A.B. Karabut, Ya.R. Kucherov, I.B. Savvatimova, "Excess heat measurements in glow discharge using flow "Calorimeter-2" *Proc, of the* 5th *International Conf. on Cold Fusion*, April 9-13, 1995, Monte-Carlo, Monaco, p.223-226.

2. A.B. Karabut, Ya.R. Kucherov, I.B. Savvatimova, "Possible nuclear reactions mechanisms at glow discharge in deuterium", Frontiers of cold fusion , *Proc, of the Third International Conf. on Cold Fusion*, October 21-25, 1992, Nagoya, Japan, p. 165.

Excess Energy and Nuclear Products

Registration of High-Energy Products in High Current Density Glow Discharge

Alexander Karabut

Scientific Industrial Association "Luch"
24 Zhelesnodorozhnaya St., 142100 Podolsk, Moscow Region,
Russian Federation

Abstract

The experimental results of the High-Energy Products registration are presented in this paper. In our previous experiments with glow discharges in deuterium [1,2,3] excessive heat release, neutron, gamma and charged particle emission have been observed. Results of research high-voltage (up to a few tens kV) and high current (up to hundreds A) pulses of a nanosecond duration are submitted. Amplitude spectra of a voltage of pulses for the discharge in H_2, D_2, Ar are received. Results of measurement electronic and x-ray emission cathode samples after switch off of a discharge current in the area from 2 keV up to 1 MeV are indicated.

1. Introduction

In previous experiments with glow discharges in deuterium [1,2,3] neutron, gamma and charged particle emission have been observed. We modified the experimental facilities. The purpose of experiments was determination of possible gears of conversion low energy ions of discharge in high energy.

2. Methods

A glow discharge device (continuous flow calorimeter) [3] filled with deuterium, hydrogen or inert gases was used. Cathodes were made of Pd, Zr, Nb, Mo and other materials. The typical gas pressure in the chamber was 2-10 Torr, the discharge voltage 300-800 V and the discharge current 5-100 mA. A schematic diagram of the experimental device is given in Fig. 1.

Electric probe measurements

Electric probe measurements were conducted to study high voltage pulses of a short duration which are generated in the discharge area. The consisted of Mo cylinder placed in quartz tube with one end open, the probe was placed at 1 mm from the cathode. The spacing between anode and cathode was 2-5 mm.

Leading edge was 35-40 ns and independent of the sort of gas (H_2,D_2,Xe,Ar) (Fig.2). The spectrum of probe voltage pulses consists of pronounced lines (Fig.3). The line character of the probe voltage spectrum indicates that electrons have fixed energies and can be conversion electrons.

Registration of fast electrons

We used x-ray film RT-1V (SVEMA) with various degrading screens to register x-rays and fast electrons. The films were exposed during run-times of 4000-15000 s. The film exposure was analyzed using a densitometer. In our experiments the film exposure can be caused by gamma, x-ray or fast electron emission The

results are still preliminary and the contribution of each specific component is not evaluated yet, but the results of the probe measurements (see below) indicate presence of electrons.The x-ray films were placed out side the vacuum chamber.
The registration beta of activity samples after experiment.
Beta the activity (or x-ray) was made with the help Si-Li detector, cooled by a to liquid nitrogen. Si-Li detector had a crystal by thickness 5 mm. There was a opportunity to register fast electrons up to 4 MeV. Emission is registered from samples after experiment in the field of 1 -1000 keV (Fig.5.). The activity Pd samples is higher after Ar discharge, than after D2 discharge.

The spot film exposure can be caused by electron beams. Energy of the beams depends upon the cathode material and the working gas. The beams pass through 5 mm quartz in the case of palladium cathode and registreted (Fig. 4) bay multiplication effect in plastic. Such beams can consist of electrons with energies ranging from hundreds of keV to units of MeV.

The exposure spots are clear and non diffused in spite of long-term exposure (up to 15000 s). This indicates that quite intensive beams are emitted within short-term intervals.

Discussion

Judging by the time dependence of probe and cathode voltages and cathode current, the registered pulses are generated by the spontaneous release of bunches of 0.01-0.23 MeV electrons. It is estimated that there are 10^8-10^{11} electrons in a bunch. The line character of the probe voltage spectrum indicates that electrons have fixed energies and can be conversion electrons. Made experiments show, that there is a gear of transformation low energy ions of the discharge in high energy metastable of levels in solid.

References

1. Karabut A.B., Kucherov Ya.R., Savvatimova I.B. "Nuclear reaction on the cathde in gas discharge", *Pisma v GETF (Sov. Tech. Phys. Lett.)*, v. 16, release 12, 1990, p 53-57.
2. Karabut A.B., Kucherov Ya.R., Savvatimova I.B. The Investigation of Deuterium Nuclear Fusion at Glow Discharge cathode. *Fusion Technology*, December 1991, v.20, #4, part 2, p. 924.
3. Karabut A.B., Kucherov Ya.R., Savvatimova I.B. Nuclear Product Ratio for Glow Discharge in Deuterium. 1992. *Physics Letters A*, 170, p.265.
4. F. W. Walker, J. R. Parrington, F. Feiner. *Chart of the Nuclides*. General Electric, San Jose, 1988.
5. Karabut A.B., Kucherov Ya.R., Savvatimova I.B. Possible Nuclear Reactions Mechanisms at Glow Discharge in Deuterium. *Frontiers of Cold Fusion, Proc. of the Third International Conf. on the Cold Fusion*, October 21-25,1992, Nagoya, Japan, University Academy Press, Inc., Tokyo, Japan, p165-168
6. Savvatimova I.B., Karabut A.B., Kucherov Ya.R., "Cathode Material Change after Deuterium Glow Discharge Experiments", *Transaction of Fusion Technology*, v.26, 1994, pp. 389-394.

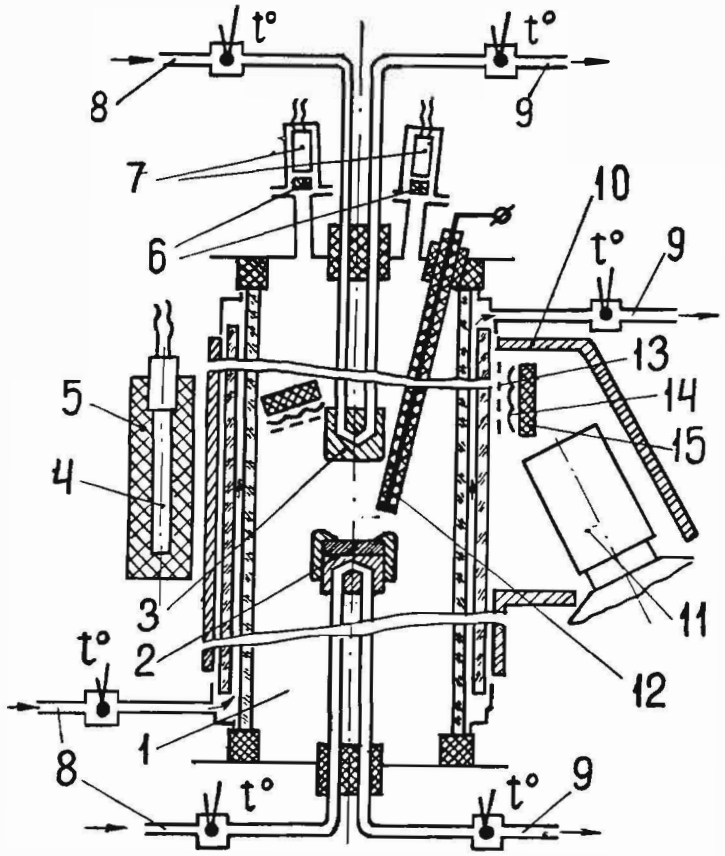

Fig.1. Experimental device: 1-vacuum chamber, 2-cathode, 3-anode, 4-He3 neutron detector, 5-moderator, 6-windows with attenuating foils, 7-Si-Au detectors, 8-, 9-Be window 10-lead shielding, 11-Ge-Li detector, 12-probe 13-x-ray film, 14- attenuating foils, 15- multiplicater

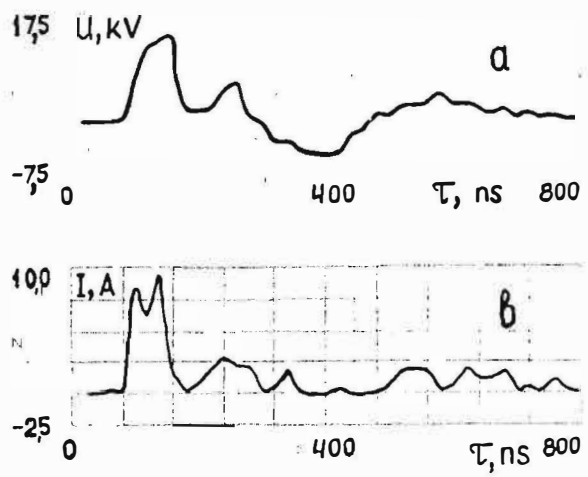

Fig. 2.Oscillogram of probe voltage and current in the cathode circuit. (Pd, D_2).

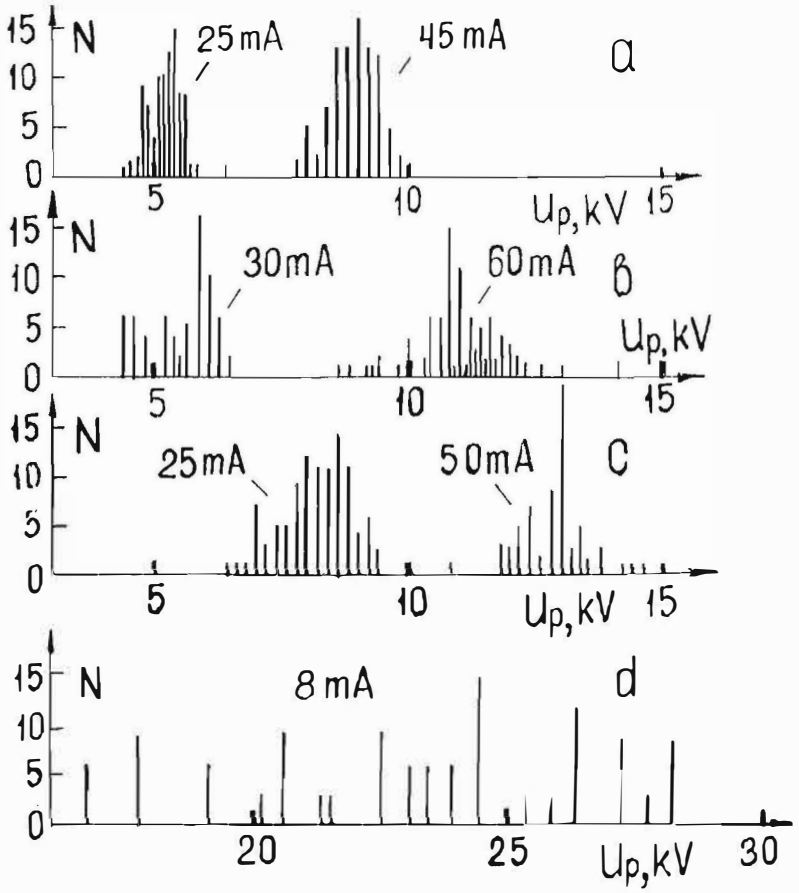

Fig.3. The spectrum of probe voltage pulses; a- Pd-Ar, b- Pd-D2, c- Pd-H2, d- Pd-D2, high loading D/Pd

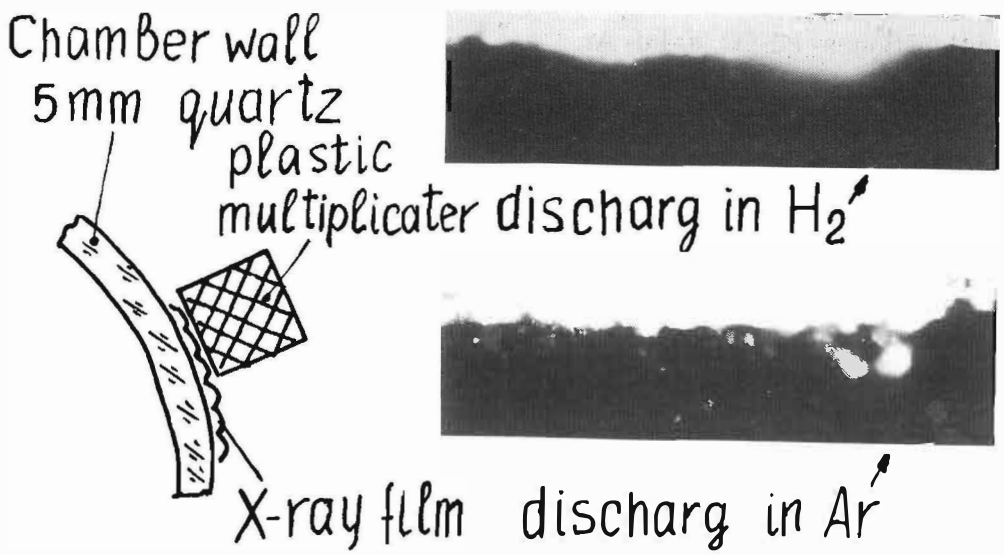

Fig.4. Schematic diagram of registration of radiation emission outside the chamber using an X-ray film and positive image of the film, Pd-cathode.

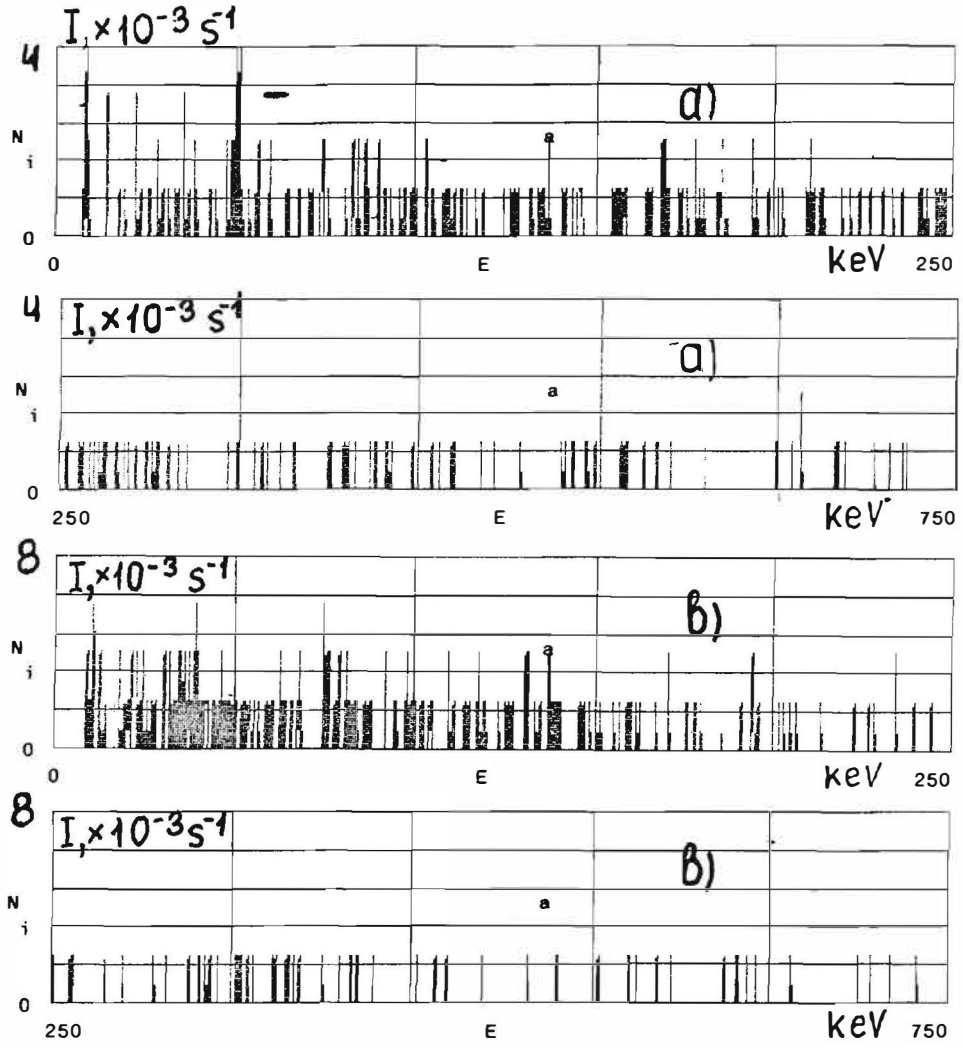

Fig.5. Background-corrected beta-spectra of cathode samples after discharge termination; a- Pd-D2, b- Pd- Ar.

Excess Energy and Nuclear Products

Possible Phenomenologycal Model of Initiation of Nuclear Reactions in Solid

Alexander Karabut, SIA "Luch", Podolsk, Moscow region, Russian Federation.

On the basis of experimental results possible model of processes of transformation of energy of a flux low energy ions in a solid is considered, which includes: generation optical pole phonons with energy 1-500 eV, in a solid at the expense of components of nuclear deceleration of a ions flux, multicascade unharmonic processes of the third and fourth orders (merge two and three phonons in one with a increase of frequency) and formation of populated level of nucleuses with effective phonon in temperature up to a few tens and hundreds keV (a phonon laser of P. Hagelstein), Interaction populated of phonon levels with electrons and generation of fast electron beams (electronic laser) is discussed. Opportunity of realization between nucleuses with such phonons by excitation of nuclear reactions of a following type is considered: $A + B = C^* + D^*$ These reactions can be resonant (long-haul acting) under a following condition: the difference between energy of reaction by received new nucleuses C^* and D^* and energy of excited nuclear levels C^* and D^* is size small (up to a few tens keV).

It is possible to mark two types of nuclear reactions: 1- with formation radioactive nuclides, which are observed practically for any working gases including Ar and cathode samples from the majority of metals with intensity 10^2-10^3 s^{-1} , 2- reactions proceeding for some metals with H_2 and with D_2 by intensity 10^{11}-10^{12} s^{-1} and forming stable nuclides with excess heat without decelerated γ- radiation.
The removal of energy from the excited levels C^* and D^* can be to realization by the way electron - multiphonons of interaction (inradiative transitions in a solid), when the energy is transmitted to a plenty of thermal phonons of a crystal lattice.

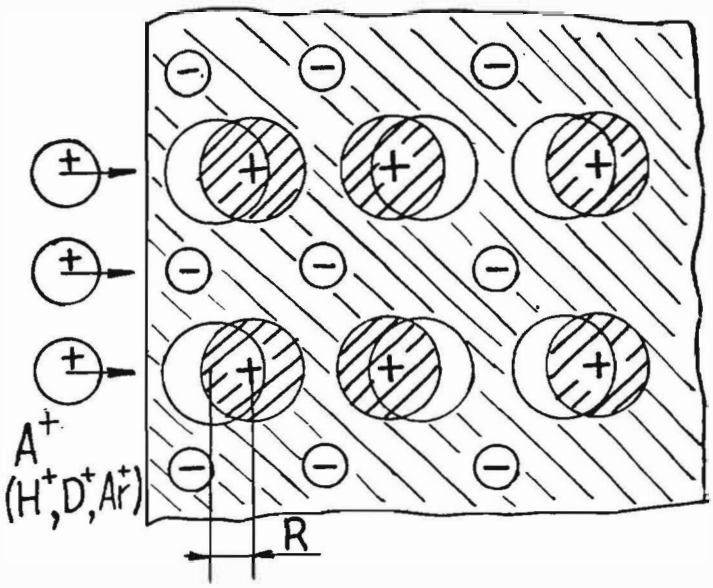

Fif.1. Generation of optical pole phonons.

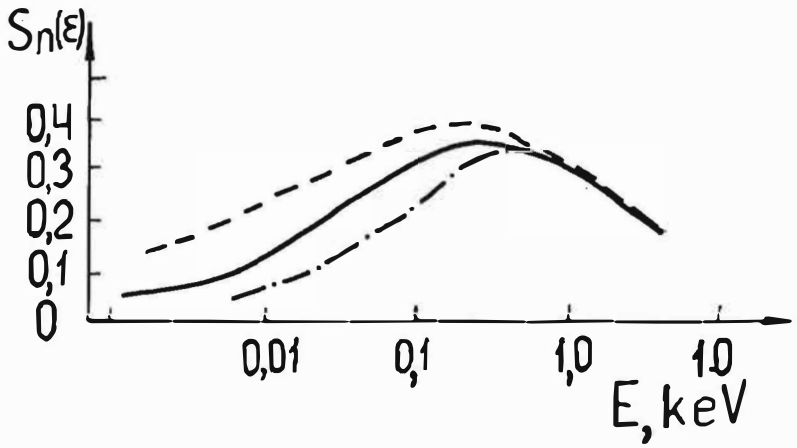

Fig.2. Efficiency of nuclear deceleration of a ions flux.

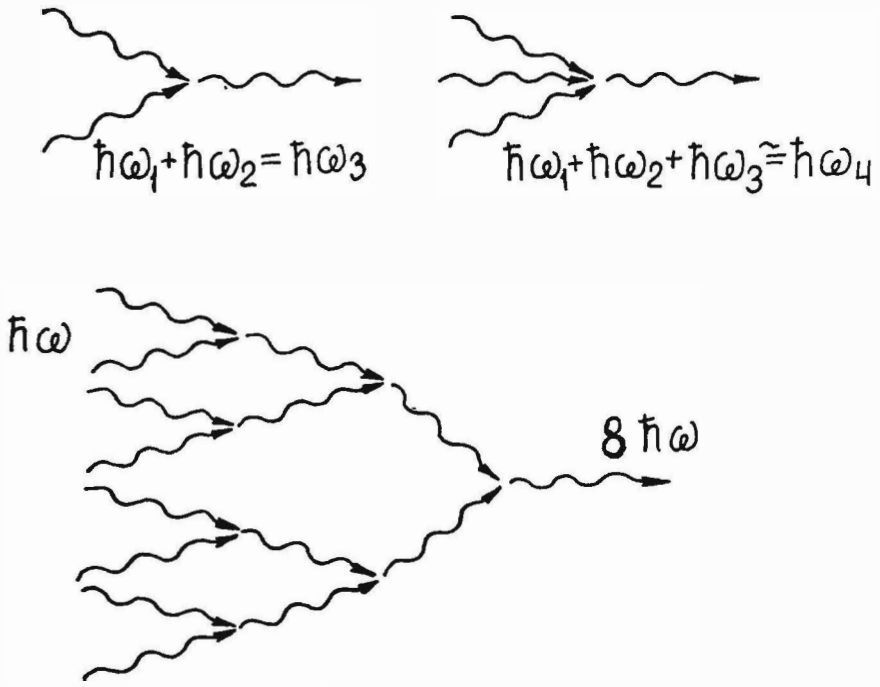

Fig.3. Multicascade unharmonic processes.

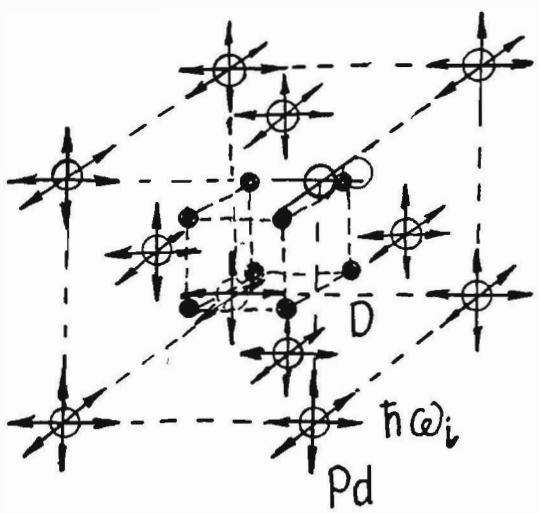

Fif.4. Formation of populated levels of nucleuses,
T(crystal lattice) = 20-300°C, T(optical phonons) = 10-1000 keV.

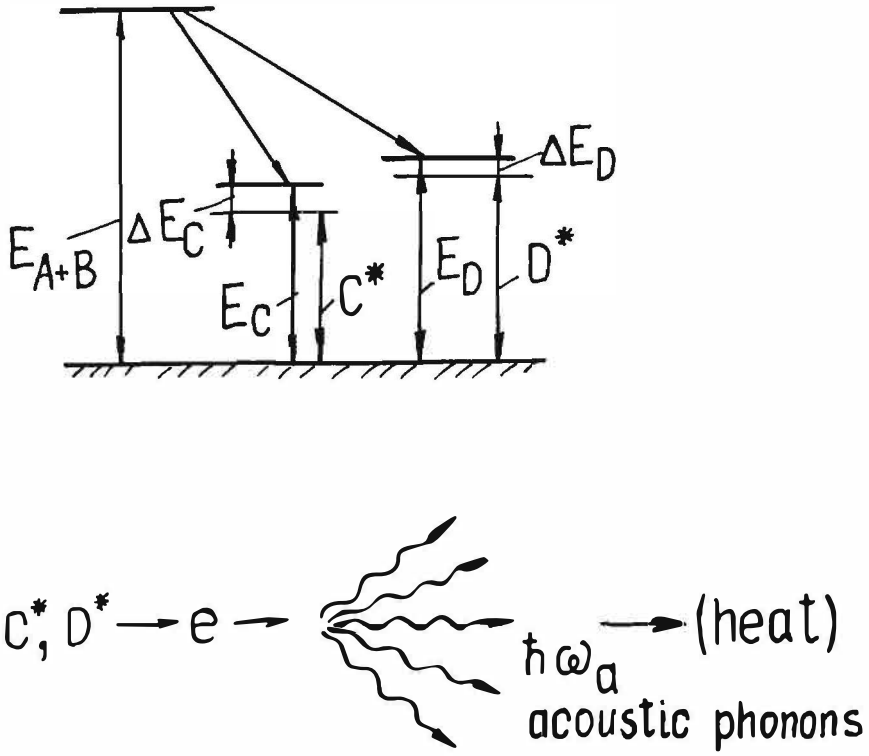

Fig.5. Schematic diagram of resonant (long-haul acting) nuclear reactions.

Excess Energy and Nuclear Products

CHEMICAL CHANGES AND EXCESS HEAT CAUSED BY ELECTROLYSIS WITH H2SO4-D2O ELECTROLYTE

J. Dash
Physics Dept., Portland State University
Portland, OR 97207, USA

ABSTRACT. Preliminary mass spectrometer analysis showed that a palladium foil which had been electrolyzed for 12 minutes had greater abundance of Pd108 than Pd106, whereas the unelectrolyzed control showed the reverse, expected natural abundances.

After about 20 hours of electrolysis, a Pd cathode produced excess heat at the rate of about 5 watts per gram. After about 70 hours of electrolysis. the Pd electrode no longer produced excess heat, but a Pt cathode began to produce excess heat.Similar localized concentrations of unexpected elements were found on both the Pd and the Pt cathodes.

INTRODUCTION. We have previously reported results of electrolysis of palladium cathodes with a H2SO4-D2O electrolyte (1-3). Further results have now been obtained with improved calorimetry. In addition, mass spectrometry is now being used to compare the chemical makeup of the Pd before and after electrolysis.

EXPERIMENTAL METHODS AND RESULTS. Cold rolled Pd foil was used as the cathode in an electrolyte containing 0.06 mol fraction H2SO4 and 0.94 D2O. A Pt foil anode was used, and electrolysis was performed for 12 minutes on 4-24-89. A piece of the same Pd foil which had not been electrolyzed and the electrolyzed Pd cathode were then analyzed by microscopy to determine the surface topography (1). The same samples were analyzed in Oct. 1996 with a secondary ion mass spectrometer (SIMS), using a 3 KV Ce ion beam and a quadrapole mass analyzer. Pd was sputtered at a rate of about 1 angstrom per second for 50 minutes.

Fig. 1 shows preliminary SIMS results. It should be noted that the mass numbers given in the figure result from combination of Cs ions and the Pd isotopes indicated. The spectra in Fig. 1a from the Pd foil control (unelectrolyzed) shows that the relative intensities of the Pd isotopes are approximately in proportion to their natural abundances.However, Fig. 1b shows that the Pd isotope of mass 108 is more abundant than Pd 106 in the electrolyzed foil., whereas the natural abundance of Pd 108 is 26.46% and that of Pd 106 is27.33% (4).The difference in these two abundances decreases with increased depth into the sample. After sputtering for 50 minutes to a depth of about 0.3 μm, these two isotopes have the same abundance.

Two closed cells of 25 ml capacity were constructed. Both had Pt anodes, an electrolyte with 0.06 mol fraction H2SO4 in D2O, and recombination catalyst suspended above the electrolyte. One cell had a Pd foil (0.055 g) cathode, and the other had a Pt foil cathode of similar mass. Each cell was placed in an identical insulated

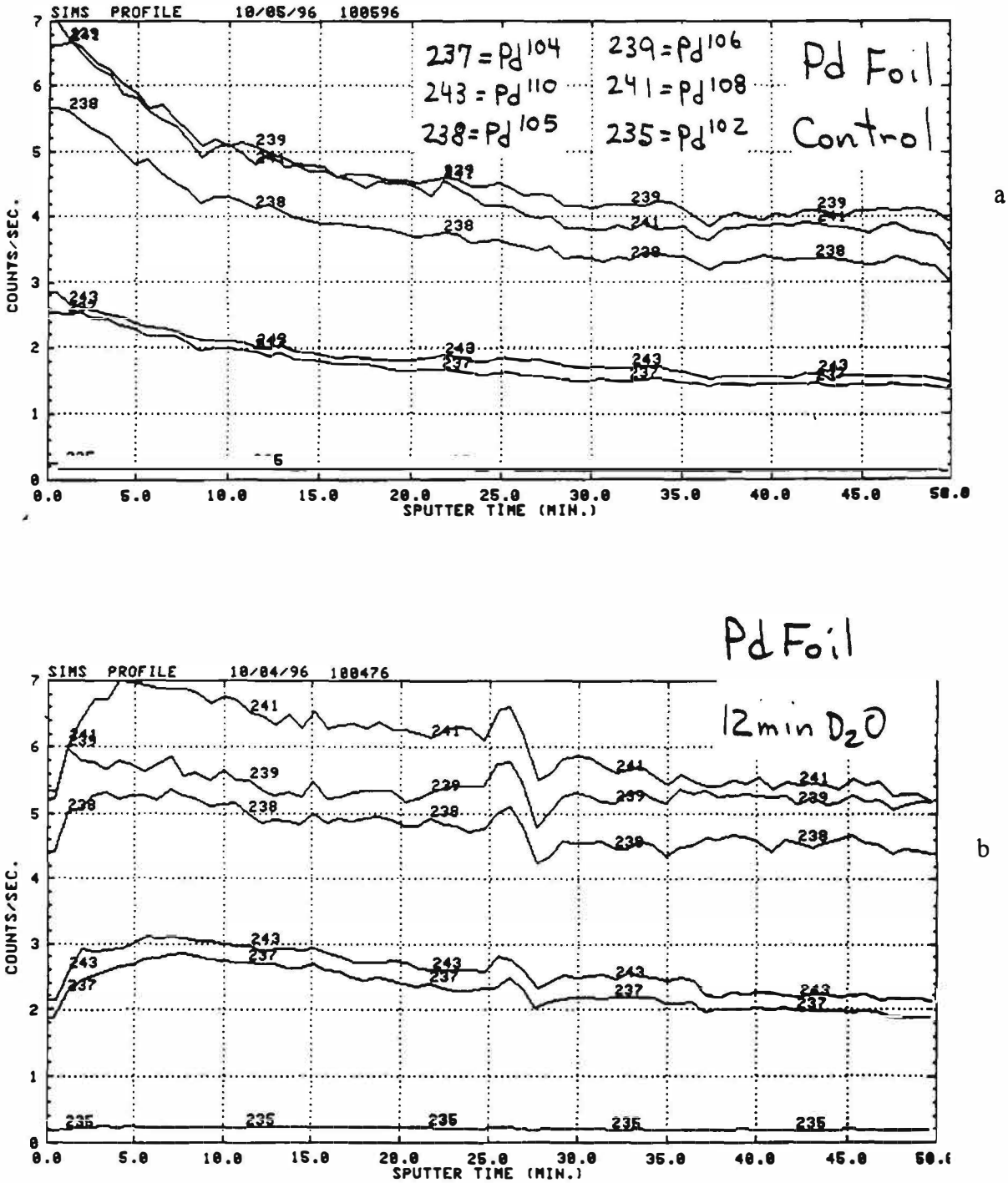

Fig. 1. SIMS spectra for six palladium isotopes. (a) Spectra from the Pd foil control (not electrolyzed). The Pd isotope responsible for each line on the graph is given in the upper center. (b) Spectra from the Pd foil cathode which was electrolyzed for 12 minutes on 4-24-89.

container. The cells were connected in series, and electrolysis was performed at constant current density of about 0.25 A/sq. cm. The cell voltages were almost the same. The temperature of the air surrounding the cells inside the

insulated containers and the ambient temperature were monitored.

During the first 20 hours of electrolysis, there was no difference in heat output of the two cells. For most of the next 50 hours of electrolysis, the cell with the Pd cathode produced more heat (as much as 0.3 watt more) than the Pt cathode cell. A typical result is given in Fig. 2.

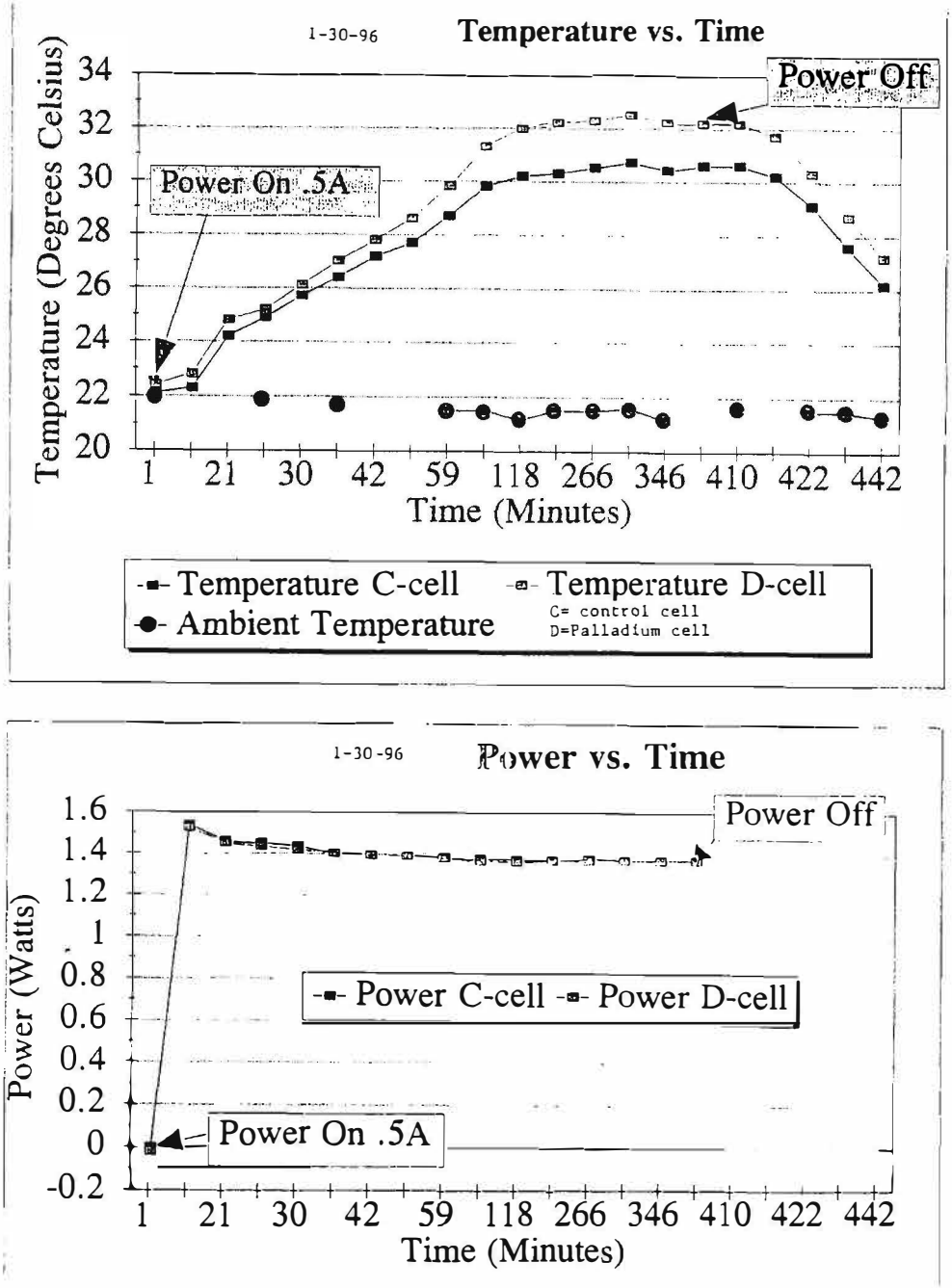

Fig. 2. Temperature-time and power-time graphs for electrolysis with a platinum cathode (C) cell in series with a palladium cathode (D) cell. At the steady-state temperature the D cell produced about 0.3 watt more energy than the C cell.The precision of measurement was ±0.1 C and ±0.01 V.

the Pd deteriorated and a solid black substance accumulated at the bottom of the cell. The Pt cathode did not appear to change.

After lying dormant for 75 days, electrolysis was again performed. In five consecutive experiments totaling 20 hours over a period of two weeks, the cell with the Pt cathode produced more heat (as much as 0.3 watt more) than the Pd cathode cell.

These results suggest that a Pt cathode, under suitable conditions, can serve to catalyze excess heat, consistent with the work of Ohmori and Enyo(6).

After electrolysis for about 90 hours, both a Pd and a Pt cathrode were cleaned ultrasonically in deionized water and studied with a scanning electron microscope (SEM) and an energy dispersive spectrometer (EDS). Fig. 3 shows the electrolyzed parts of both cathodes. The width of each cathode is less than the original width due to sputtering which occurred during electrolysis. It was shown previously that Pd is inert in the sulfuric acid-heavy water electrolyte (1), and it is likely that this is also true for Pt. The extent of this sputtering is greater on the Pd than on the Pt cathode. For example, the original square corners of the Pd cathode are now rounded, whereas the corners of the Pt cathode remain almost square.

The arrow on each electrode indicates a place where the same, unexpected elements were found by EDS. The spectra are shown in Fig. 4. Both show unexpected concentrations of sulfur and chlorine. A large concentration of chlorine was detected previously on a Pd cathode after electrolysis (5).

DISCUSSION OF RESULTS. The data in Fig. 1 present clear evidence that a nuclear process occurs at the surface of a palladium cathode during electrolysis in heavy water. Otherwise, how could the observed isotopic shifts occur over a thickness of about 0.3μm ? Chemical explanations for the excess heat observed for both the Pd and the Pt cathodes are also unlikely. The chlorine observed on these electrodes may be the result of transmutation of sulfur which is present in the electrolyte.

REFERENCES.

1. D. S. Silver, J. Dash, and P.S. Keefe, "Surface Topography of a Palladium Cathode After Electrolysis in Heavy Water", Fusion Tech. 24, 423 (1993).
2. J. Dash, G. Noble, and D. Diman, "Surface Morphology and Microcomposition of Palladium Cathodes After Electrolysis in Acidified Light and Heavy Water: Correlation with Excess Heat", Trans. Fusion Tech. 26, part 2, 399 (1994).
3. S. Miguet and J. Dash, "Microanalysis of Palladium after Electrolysis in Heavy Water", J. New Energy 1, 23 (1996).
4. CRC Handbook of Chemistry and Physics, D.R. Lide, Editor-in-chief, 74th Ed. (1993), p. 11-64.
5. J. Dash, G. Noble, and D. Diman, "Changes in Surface Topography and Microcomposition of a Palladium Cathode Caused by Electrolysis in Acidified Light Water", Cold Fusion Source Book, Hal Fox, Editor (Fusion Information Center, Salt Lake City, UT 84158, 1994).
6. T. Ohmori and M. Enyo, J. New Energy, 1, 15 (1996).

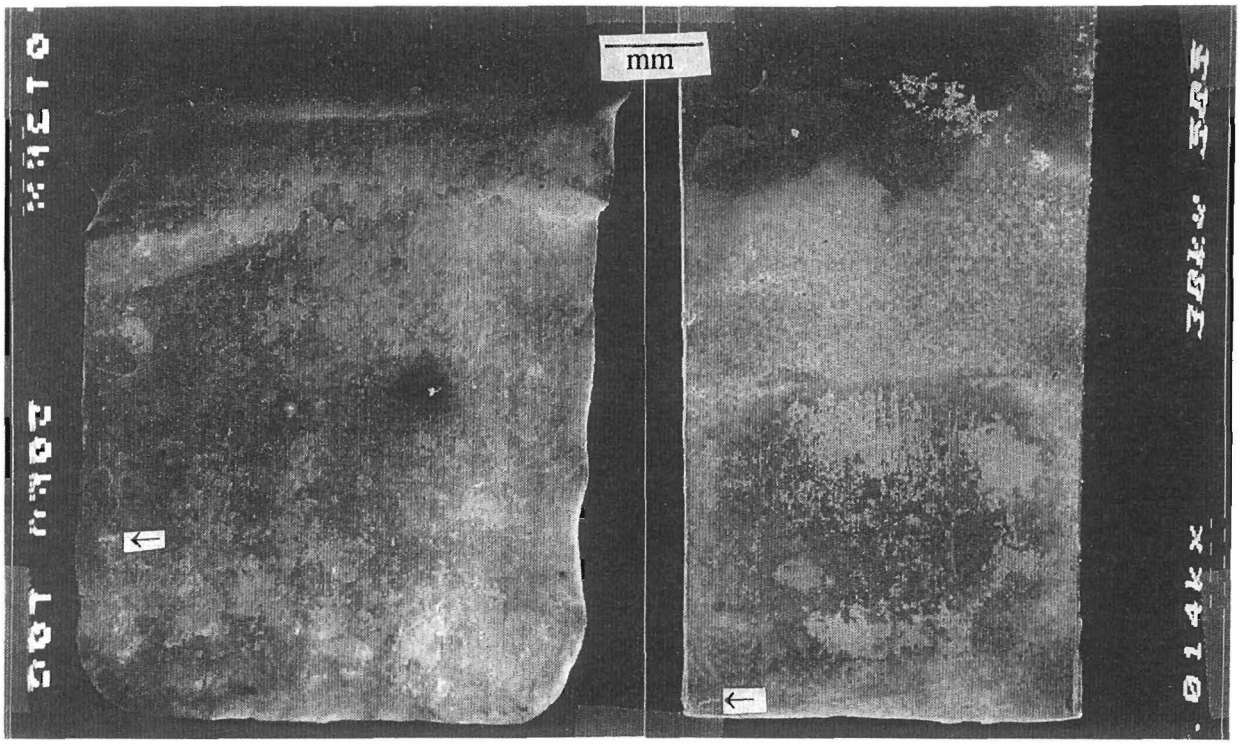

Fig. 3. Pd cathode (left) and Pt cathode (right) after electrolysis for about 90 hours.

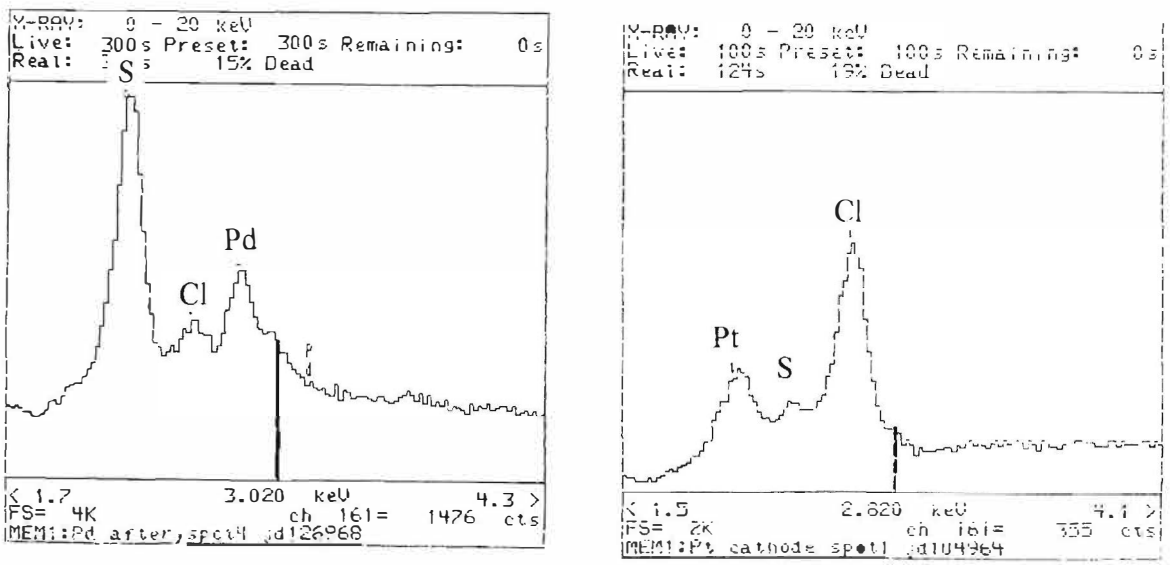

Fig. 4 EDS spectra (left) from the spot indicated by the arrow on the Pd cathode in Fig. 3, and (right), from the spot indicated by the arrow on the Pt cathode.

ACKNOWLEDGEMENT The SIMS spectra were obtained by Douglas L. Jones of Omega Analytical Services, Aloha, OR. We are grateful for his assistance in interpretation of the data.

Excess Energy and Nuclear Products

FROM "COLD FUSION" TO "HYDREX" AND "DEUTEX" STATES OF HYDROGEN

Jacques DUFOUR, Jacques FOOS, Jean Paul MILLOT and Xavier DUFOUR

SHELL/CNAM, Laboratoire des Sciences Nucléaires.
Conservatoire National des Arts et Métiers, Paris, France.

Abstract

Based on experimental results, the possibility of formation of new bound states between an electron and a proton (deuteron) is discussed. These bound states (HYDREX and DEUTEX) result from the equilibrium between the attractive Coulombic force and the repulsive weak electro-nuclear force. These species could account for all data obtained in field of Cold Fusion".

Introduction

Seven years ago, the announcement [1], that nuclear fusion of deuterium had been obtained at room temperature by electrolysing heavy water with a palladium cathode, raised much interest but also much controversy. Although the phenomenon is now denied by most scientists, a number of more and more reliable experimental data, point to a real phenomenon, but still very surprising and difficult to explain.

A number of those puzzling experimental data have been obtained by striking sparks or ozonizer discharges through an hydrogen isotope [2,3] (hydrogen and deuterium were used), in contact with a palladium electrode :

- excess energy production, in amounts far above any known chemical reactions that could take place in the systems used [4,5,6].
- unexplained disappearing of hydrogen [6,7].
- emission of ionizing radiations (X Rays, γ Rays ?) that can be observed even after the electrical current is cut off [4].
- production of exceedingly small amounts (if any) of the known ashes of the classical fusion reactions between hydrogen isotopes, which cannot explain the amount of excess energy observed (by several powers of ten) [6].
- possible nuclear synthesis of lithium from helium and deuterium.

The last experimental results obtained with an ozonizer type of discharge are presented. A description is then given of possible bound states of a proton and an electron, resulting from the combined action of the attractive Coulombic force and the repulsive weak electro-nuclear force. These hypothetical bound states will be called HYDREX (when a proton is involved) and DEUTEX (in the case of a deuteron). It will be seen that the properties of these hypothetical species can account for all experimental data observed in the field of so-called "Cold Fusion" [1], including transmutations [8,9]. The existence of HYDREX and DEUTEX, when proven, is likely to be the actual reason why the TNCF phenomenological model gives a very approximate description of the phenomenon [10].

Experimental results

The most interesting results obtained when an ozonizer (or a spark) discharge is struck through hydrogen isotopes, contacting a palladium electrode, will now be summarised. The experimental devices used have been previously described [4,5,6,7].
Emphasis will be laid on results obtained with pure hydrogen (ALPHAGAZ quality U $H_2 > 99.995$ %) and pure palladium (Johnson Matthey quality Puratronic, metal impurities less than 20 ppm weight) (see table 1 in annex for detailed compositions of the palladium), as this system is the most simple and clean.

Excess Energy and Nuclear Products

Excess energy

Very significant excess energy production have been observed, on long periods.

⇨ excess power up to 10 W (representing 7 % of the input power) have been obtained [6,7]. The standard deviation of the calorimetric system being 1W, this result is very significant. This excess power production has been obtained on long periods ($3x10^6$ to $10x10^6$ s) and increases when the input power is increased. Fig.1 in annex, gives the evolution with time of this excess power for the system hydrogen/palladium (note that for deuterium, the excess power is higher : 14 W, representing 10 % of the energy input).

⇨ unexplained disappearing of hydrogen (deuterium) which cannot be explained by leakage, diffusion through the walls of the reactor or combination with elements present in the reactor [7]. The loading ratio of the palladium after experiment (measured by heating the electrode and measuring the volume of hydrogen -deuterium- recovered) is 0.85 to 0.9. Fig.2 in annex, gives the evolution with time of the "apparent" loading ratio of the palladium during the experiment (calculated from the amount of palladium present in the reactor and the quantity of hydrogen injected in this reactor to keep its pressure constant). It can be seen that this "apparent" loading ratio reaches values up to 5, which is impossible. Hydrogen is thus lost in the experiment.

⇨ very high excess energy per atom : Fig.3 in annex, is a plot of the cumulative excess energy ($\int_0 E_P(t)dt$, $E_P(t)$ being the excess power in Watt at time t) as a function of the cumulative quantity of hydrogen lost ($\int_0 F_H(t)dt$, $F_H(t)$ being the flow of hydrogen into the reactor, in mMole H per second at time t), for the above mentioned experiment with hydrogen and palladium. The slope of the curve is the overall excess energy per mMole H (W/mMole H). It can be seen from Fig.3, that :

① the mean value of the overall excess energy is very high ; expressed in eV/atom H : 7,100 eV/H (to be compared to 1 eV/H for the combustion of hydrogen). This value is shown on Fig.3 by the straight line.

② this value increases with time as can be seen from the curvature of the curve Fig.3.

Table 2 below summarises the results obtained with the system hydrogen/palladium :

Table 2 Period	Duration (second)	H consumed (mMole H)	Excess energy on period (J)	Mean excess power (W)	Exc.Ene. eV per atom H	Power input (W)
CAL	230 000	0	0			Calib.
INC	695 000	9.88	1 737 500	2.5	1 800	Increasing
I	1 390 000	9.63	5 838 000	4.2	6 300	115
II	342 000	1.41	1 846 000	5.4	13 600	150
III	767 000	5.44	6 596 000	8.6	12 600	150
Total	3 424 000	26.36	16 018 300	4.7	9 000	

Note that the combustion of all the hydrogen used in the experiment (26.36 mMole H) would have yielded 6,400 J, to be compared with 16,018,300 J actually obtained.

Emission of low energy radiations

During the experiments carried out with sparks [4], observations were made, that can be related to the emission of low energy X Rays :

⇨ light tight films placed in the reactor were found completely blackened after experiments with hydrogen and deuterium. In contrast, experiments carried out in the same conditions, but using nitrogen as sparking gas yielded no blackening of the film.

⇨ after cut-off of the spark a strange phenomenon was observed : by polarising the electrodes gap (100 V for a gap of 1 cm), **after an experiment**, the gap being filled with the hydrogen that had been submitted to the sparks (hydrogen pressure round 900 mbar), a current was measured with values up to

25 nA for hydrogen experiments 700 nA for deuterium ones. The current was observed on periods of several days, with a fast decrease for deuterium (hours) and a slower one for hydrogen (days). Similar measurements carried out with hydrogen and palladium **before sparking**, yielded current values lower than 10 pA. Fig.4 in annex, shows the evolution of this unexplained current with time (for a D_2/Pd experiment).

These two sets of observations can be explained by the production of low energy X Rays, the intriguing thing being the long persistence (several days) of the phenomenon after cut-off of the discharge.

Possible synthesis of new elements in the palladium matrix (transmutation)

A complete analysis of the palladium electrode used for the experiment with hydrogen above mentioned (ozonizer discharge), was carried out. The **palladium electrode** was a wire (diameter 0.25 mm) **weighing 120 mg**.The electrode was completely dissolved and the following analysis were carried out (sample 3H06):

- atomic emission spectrometry with plasma torch (ICP/AES) for Fe, Ru , Rh and Ag.
- mass spectrometry with plasma torch (ICP/MS) for the other impurities and for the isotopic composition of the palladium.

Similar analytical procedure was carried out on a virgin palladium wire from the same batch, the same roll of wire and of the same weight as sample 3H06 (sample Blank) .

The complete results of the analysis are given in annex (Table 1). From Table 1 it can be seen that variations from sample Blank to sample 3H06 are observed for the elements :
Li, Mg, Al, Cr, Mn, Fe, Ni, Cu, Zn, Ir, Pt and Au. Table 3 gives the variations of these elements (expressed in number of atom) :

Table 3 :

Element	3H06	Blank	3H06 - Blank
Li	5.2×10^{14}	1.0×10^{14}	4.2×10^{14}
Mg	2.5×10^{17}	2.2×10^{16}	2.3×10^{17}
Al	7.2×10^{16}	2.7×10^{15}	7.0×10^{16}
Cr	1.1×10^{16}	1.3×10^{15}	9.7×10^{15}
Mn	3.9×10^{14}	2.6×10^{14}	1.3×10^{14}
Fe	2.8×10^{16}	1.3×10^{16}	1.6×10^{16}
Ni	3.3×10^{15}	2.5×10^{15}	8.6×10^{14}
Cu	4.7×10^{15}	1.8×10^{15}	2.8×10^{15}
Zn	4.8×10^{16}	4.8×10^{15}	4.3×10^{16}
Ir	2.3×10^{14}	1.9×10^{14}	3.8×10^{13}
Pt	3.0×10^{14}	5.2×10^{14}	-2.2×10^{14}
Au	2.9×10^{14}	4.0×10^{14}	-1.1×10^{14}

From table 1 (annex) it can also be seen that there is no significant variation of the isotopic composition of the palladium. This table also shows that the precision on the measure of Ag is low (1.3×10^{16} atoms), so any nuclear generation of Ag lower than this quantity are not detectable.

From these data, following conclusions can be drown :

- the total amount of new atoms that appear in the sample (some 2.4×10^{17}) is much higher than the total amount of atoms that disappear from the sample (some 3.3×10^{14}). No nuclear reaction, either fusion or fission, can explain this fact. So the bulk of the new atoms in sample 3H06 comes from contamination and indeed all the new elements found (except Li), can be traced back in the various components of the reactor. The case of Li will be discussed below.
- assuming that all new elements found in sample 3H06 originate from a nuclear reaction with an exothermicity of 5 MeV, it can be calculated that the total amount of energy produced would have been 3×10^{5} J, which represents only 1.9 % of the total amount of excess energy produced in the experiment (some 16×10^{6} J).

⇨ case of Li : a contamination of sample 3H06 by Li could not be found obviously. Although the precision of the analysis carried out to trace it back, cannot completely rule it out, a nuclear origin of Li found, is plausible. The detailed nuclear reaction proposed to account for that will be discussed below (*Reactions of HYDREX with nuclei of the metal*). The overall reaction could be written :

$$^4_2He + {}^2_1H = {}^6_3Li + 1.4\ \text{MeV} \qquad (0)$$

The origin of ^4_2He in the palladium could be ionic implantation of ^4_2He from the hydrogen gas phase of the reactor : during the search for fusion ashes [6], the amount of ^4_2He in the gas phase (H2 bottle) was found to be $4.4\text{x}10^{13}$ atoms per cm^3, which, for the experiment reported (26.36 mMole H) , gives a total of $1.3\text{x}10^{16}$ atoms. The amount of lithium formed ($4.2\text{x}10^{14}$) can thus originate from ^4_2He present in the experiment. The data gathered [6] allows an evaluation of the order of magnitude of the reaction rate of reaction (0). The equilibrium amount of ^4_2He in the metal was found to be 10^{13} atoms. From the deuterium content of the H2 used, we can assume that the amount of deuterium in the palladium is $2.5\text{x}10^{19}$ atoms. Given the volume of the palladium wire ($1.3\text{x}10^{-3}$ cm^3), the concentration of the reacting nuclei are thus: for ^4_2He $7.69\text{x}10^{15}$ and for ^2_1H $1.92\text{x}10^{22}$ $atom.cm^{-3}$. The total duration of the experiment being $3{,}4\text{x}10^6$ s, the average formation rate of lithium is : $9.5 \cdot 10^{10}$ $atom.s^{-1}.\ cm^{-3}$. The average first order reaction constant for (0) is thus :

$$k_0 = 6.4 \cdot 10^{-28}\ (s^{-1}) \cdot (atom \cdot cm^{-3})^{-1}$$

which expressed in $(s^{-1})\text{x}(Molexcm^{-3})^{-1}$ yields $3.85\text{x}10^{-4}$, which is the order of magnitude of the fastest nuclear reactions occurring in the sun.

Conclusion on the experimental results

Three main conclusions can be drown from the experimental results :

① a sizeable amount of excess energy is produced, and hydrogen is lost.

② if a small part of this excess might come from nuclear reactions, the bulk cannot have this origin, but is much higher than any known chemical reaction.

③ ionizing radiations (X Rays ?) are produced during the experiment. They are persistent (for periods of hours to days) after cut-off of the experiment.

All this is extremely puzzling and a **strong and simple lead is necessary** to order all these data.

Theoretical arguments have thus been developed to show the possible existence of **new bound states between a proton** (deuteron) and **an electron**, resulting from the **equilibrium** between the **attractive Coulombic force and the repulsive weak electro-nuclear force**. The properties of these bound states, when there existence is proven, can account for all data obtained in the field of "Cold Fusion".

Physical basis of the model

A good overall description of the hydrogen atom is given by the Bohr model that quantifies the interaction between the Coulombic force and the resulting kinetic energy of the electron. Another interaction is possible between the proton and the electron, the endothermic synthesis of a neutron :

$$p^+ + e^- = n + \nu - Q\ , \quad \text{with } Q = \left(M_n - M_h\right)c^2 \qquad (1)$$

M_n and M_h being respectively the masses of the neutron and of the hydrogen atom and c the velocity of light. $Q = 1.2583 \times 10^{-13}$ J. No (or extremely small amounts) of neutrons are produced in "Cold Fusion" experiments. (1) is thus likely to yield only virtual states of the neutron.

Contrary to the Coulombic force or the centrifugal force, the weak electro-nuclear force has no macroscopic description. Nevertheless a very broad description of its possible interaction with the Coulombic force can be achieved by using the basic principles of quantum mechanics.

To start with, it can be noted that the Bohr model deals with a system consisting of a single proton and a single electron in vacuum. Considering the electron starting from infinite, the formation of the hydrogen atom can be described as the electron approaching the proton, with a kinetic energy ruled by the intensity of

the Coulombic force and successively meeting the various excited states of the hydrogen atom to finally end up in the ground state of this atom.

In a metallic hydride forming metal, the hydrogen is partly in the form of protons. Conduction electrons could interact with these protons in a way which is likely to be very different from the previous one. It is well known [11] , that the behaviour of the conduction electrons in a metal can be precisely described by the void cation model, where the Coulombic potential from the cation is replaced by a much lower "pseudo potential" (with practically 0 value) in the close vicinity of the cation (from 0 to 1.66 Bohr radius / see Fig.5 in annex). This is due to the periodic character of the cation lattice and means that the conduction electrons can move in the vicinity of the cations without feeling their Coulombic attraction. Note that this model is not meant to describe the very close vicinity (some fm) of the cation, where the real Coulombic potential should apply. In a metallic hydride, if all the sites available are occupied by hydrogen, a similar phenomenon could occur, between the conduction electrons and the lattice formed by the hydrogen cations (which is a "moving lattice", because it is known that protons can migrate across the metal lattice under the influence of an electrical field).

A model of the hypothetical interactions between protons trapped in a metallic lattice and the conduction electrons of this "proton lattice" can thus be obtained by considering the system formed by one proton and one electron, **the electron starting its motion** towards the proton at **a very short distance** from it (some fm) **with 0** (or very low) **kinetic energy**, this very short distance being the distance beyond which the void cation model is valid and the pseudo potential very low.

The HYDREX (DEUTEX) model

As usually the proton is considered to be fixed. Let R_0 be the distance from the center of the proton, from which the electron starts its motion towards it and R_a the distance at which the electron impacts the proton. R_0 being supposed very small, the interaction between the spins of the 2 particles should favour "head on" collisions.

The exchange of energy between the 2 particles can be described in 3 steps :

❶ - acceleration of the electron towards the proton. At the impact R_a , the kinetic energy of the electron is :

$$E_c = \frac{e^2}{4\pi\varepsilon_0}\left[\frac{1}{R_a} - \frac{1}{R_0}\right] \qquad (2)$$

❷ - nuclear interaction between the electron and the proton to yield a virtual neutron, that reverts into an electron and a proton according to the scheme :

$$p^+ + e^- = n + \nu = p^+ + e^-$$

Theoretical arguments to justify the possibility of such a reaction have already been proposed[12]. Note that they suppose a very small mass of the neutrino (10^{-3} to 10^{-1} eV).

The life time of the virtual state of the neutron is limited by Heisenberg uncertainty relations :

$$\Delta T \cdot \Delta E \geq \hbar$$

ΔE being equal to $(Q - E_c)$, ΔT can be expressed as :

$$\Delta T = \frac{k\hbar}{(Q - E_c)} \qquad (3)$$

with $k > 0$ and integer and $(Q - E_c) > 0$, reflecting the virtual state of the neutron.

❸ - ejection of the electron from the neutron, when the neutron reverts to the proton, with a kinetic energy $E_c^{'}$ given by the energy balance of step 2 :

$$E_c^{'} = Q - (Q - E_c) = E_c$$

The electron is then back to its initial state (distance R_0 from the proton, kinetic energy very low) and steps ❶,❷ and ❸ repeat indefinitely, yielding the HYDREX bound state of hydrogen.

A very broad description of the various levels of this bound state can be obtained by considering step ❷ is an elastic collision between the electron and the proton, with duration ΔT and impact energy E_c. The quantification of the product $E_c.\Delta T$ gives :

$$E_c.\Delta T = n\hbar \quad , \quad \text{n being an integer} \qquad (4)$$

Replacing E_c and ΔT by (2) and (3) and Q by its value (1) in (4), yields :

$$\frac{1}{R_a} - \frac{1}{R_0} = \frac{n}{n+k} \frac{4\pi\varepsilon_0 c^2}{e^2} \left(M_n - M_h\right) \qquad (5)$$

(5), with the condition that R_0 is positive, gives a broad estimation of the values of the radii of the different states of HYDREX, provided an hypothesis is made on the values of k, that is on the actual duration of the virtual state of the neutron (note that this value could be k' different from k in the case of DEUTEX where a virtual di-neutron is formed, and that the quantity Q' corresponding to Q is also different - see below for an estimation of Q' -).

Discussion. Possibilities and limitations of the model

To choose the above mentioned values of k, we have to take into account the limitations set previously :

$$k > 0 \text{ integer} \quad , \quad \text{(virtual state of the neutron)} \qquad (6)$$

$$\left(Q - E_c\right) > 0 \quad , \quad \text{(virtual state of the neutron)} \qquad (7)$$

$$1/R_0 > 0 \quad , \quad (R_0 > 0) \qquad (8)$$

Combining (3) and (4) shows that (7) is satisfied for all values of $k > 0$:
Combining (5) and (8) yields the condition :

$$k > n.\left[R_a \frac{4\pi\varepsilon_0 c^2}{e^2}\left(M_n - M_p\right) - 1\right] \qquad (9)$$

For $R_a = 1.2$ (radius of the proton), (9) yields $k > -0.4372 . n$. This is always true if n and k are positive integers, which are the only 2 conditions left.

Description of the HYDREX state of hydrogen

To describe HYDREX, an hypothesis has to be made on the value of R_a. It is commonly admitted that the radius of the free proton is 1.2 fm. This value has been taken for R_a (parametric calculations have shown that the basic description of HYDREX is not much modified when R_a varies from 1 to 1.5 fm).

The ground state is obtained for n = 1. As mentioned above, nothing is known on k, which describes the life of the virtual state of the neutron (note that for k infinite, the radius of HYDREX is $R_0 = R_a$, and the model is no longer valid).

A parametric calculation yields the following values for the ground state :

k	1	2	3	4	5
R_0 (fm)	1.78	1.53	1.43	1.38	1.35

The highest excited state (end of the continuum) is obtained for n infinite, where the influence of low values of k are negligible. The radius of this state is :

$$R_0^{\infty} = 3.47 \text{ fm}$$

Given the physical way HYDREX is supposed to be formed, **these highest excited states are likely to be the first obtained.** To analyse the way they deexcite, the energies of the various transitions have to be calculated. Let $\Delta E_{n,k}^{n+1,k}$ and $\Delta E_{n,k}^{n,k+1}$ be the transitions for k fixed and n fixed respectively. The way the binding energy of HYDREX is disposed of will be discussed later. The transition energies can be calculated from the values of the potential energies of the electron at R_0, $E_p\left(R_0\right)$:

$$E_p(R_0) = \frac{e^2}{4\pi\varepsilon_0}\left(\frac{1}{R_a} - \frac{n}{n+k}\right)(M_n - M_h)c^2 \qquad (10)$$

From (10) :

$$\Delta E_{n,k}^{n+1,k} = \frac{k}{(n+1+k)(n+k)} \cdot (M_n - M_h)c^2 \qquad (11)$$

$$\Delta E_{n,k}^{n,k+1} = \frac{-n}{(n+k+1)(n+k)} \cdot (M_n - M_h)c^2 \qquad (12)$$

(12) shows that transitions $\Delta E_{n,k}^{n,k+1}$ are forbidden. This means that once HYDREX is formed with a given duration quantum of the virtual neutron state, this duration is kept constant during all the deexcitation process. This reduces the limitations of the model and allows a representative description of HYDREX to be made, by taking k = 1 (it should be kept in mind that k could differ from 1 and be different for HYDREX and DEUTEX).

Three other quantities have to be taken into account to describe HYDREX :

- the life time of the virtual state of the neutron. Replacing $(Q - E_c)$ by its value (5) and (1) in (3) yields :

$$\Delta T = (n+k)\frac{\hbar}{(M_n - M_h)c^2} \qquad (13)$$

- the endothermicity of this virtual state, obtained from (1) and (5) :

$$(Q - E_c) = \frac{k}{n+k}(M_n - M_h)c^2 \qquad (13')$$

- the velocity on the electron at the impact with the proton. The electron being relativistic, its velocity v_e is , by combining (2) and (5) (with M_e the rest mass of the electron) :

$$v_e = c\sqrt{1 - \frac{1}{\left(1 + \frac{n}{n+k}\frac{M_n - M_h}{M_e}\right)^2}} \qquad (14)$$

Table 4 gives the main features of HYDREX, for $k = 1$ and for n varying from 1 to infinite.

Table 4 n	R_0 (fm)	$\Delta E_{n,1}^{n+1,1}$ (keV)	Virtual neutron life (10^{-21}s)	Time for 1 electron oscillation (10^{-23} s)	Ratio Neutron/ (p+e) states (s/s)	Binding energy (keV)
1	1.78	130.90	1.67	2.10	80	392.69
2	2.13	65.45	2.51	2.87	85	261.79
3	2.36	39.27	3.35	3.38	100	196.35
4	2.51	26.18	4.19	3.74	110	157.08
5	2.63	18.70	5.03	4.01	125	130.90
6	2.73	14.02	5.87	4.22	140	112.20
7	2.81	10.91	6.70	4.39	150	98.17
8	2.86	8.72	7.54	4.53	165	87.26
9	2.92	7.13	8.38	4.64	180	78.54
20	3.20	1.70	18.40	5.23	350	35.69
100	3.41	0.077	84.62	5.73	1475	7.77
500	3.46	3.1×10^{-3}	419.90	5.87	7150	1.56
1000	3.47	0.8×10^{-3}	838.9	5.87	14290	0.078
10^6	3.47	7.8×10^{-7}	8.4×10^5	5.87	1.42×10^7	7.8×10^{-4}

It can be seen that :

⇨ the radius R_0 of HYDREX increases from 1.78 to 3.47

⇨ the transitions between levels are in the order of tens of keV for the first values of n and decrease to values of a few eV when n increases.

⇨ in all cases, HYDREX is more often in the form of a virtual neutron + virtual neutrino than in the form of a proton + electron. This is shown in column (Neutron/(p+e) states) which gives the ratio of the duration of the virtual state of the neutron (ΔT) to the duration of the motion of the electron to and from the proton (calculated from the velocity of the electron, considering that its average velocity is half its velocity v_e at the impact of the electron on the proton).

At that stage, HYDREX can be described as an oscillation between two states : one is the proton, surrounded by an electron cloud at very short distance (few fm) and the other a virtual neutron state surrounded by an oscillating virtual neutrino.

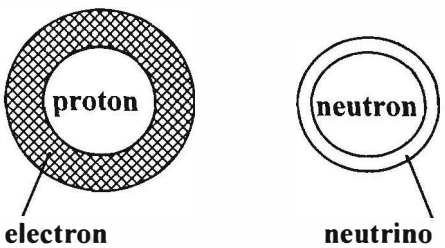

$$H\left(\left|{}^{e}_{p}\right.\right) \quad \Leftrightarrow \quad H\left(\left|{}^{\nu}_{n}\right.\right) \qquad (15)$$

HYDREX can thus be noted as $H\left(\left|{}^{e}_{p}\right., \left|{}^{\nu}_{n}\right.\right)$, resulting from the oscillation between the two states written in (15)

This scheme gives a clear understanding of what is the binding energy of the system. This binding energy, given in the last column of table 4, is equal to $(Q - E_c)$. It is the amount of energy that has to be given to the system either in the form $H\left(\left|{}^{\nu}_{n}\right.\right)$ to yield a real neutron and neutrino :

$$H\left(\left|{}^{\nu}_{n}\right.\right) + (Q - E_c) = \mathrm{n} + \nu$$

or in the form $H\left(\left|{}^{e}_{p}\right.\right)$, to yield a proton and an electron at a distance beyond the stability limit of HYDREX :

$$H\left(\left|{}^{e}_{p}\right.\right) + (Q - E_c) = \mathrm{p} + \mathrm{e}$$

The description of the way HYDREX may deexcite and may react with nuclei will give more insight on its properties and shed light on the field of "Cold Fusion".

Before this description is given, two limitations of the model should be emphasised :

⇨ **no indication are available on the value of k. This is due to the lack of knowledge on the weak electro-nuclear force**. The situation might be improved if the models proves to represent an actual new combination of a proton and an electron.

⇨ the second is more fundamental : **the existence of a virtual neutrino implies that the neutrino has a mass**. The order of magnitude of the required mass can be evaluated by writing the momentum and energy conservation equations. It can thus be calculated that this mass should be in the order of $\mathbf{10^{-1}}$ **to** $\mathbf{10^{-3}}$ **eV**.

Deexcitation of HYDREX and possible nuclear reactions

Deexcitation of HYDREX

As previously mentioned, HYDREX is formed in its higher excited states. The way the binding energy is emitted, is very similar to classical electron capture : emission of a neutrino, with the difference that the neutrino is virtual. The electron which is bound, comes from the conduction band of the palladium. If ΔE_f is the energy of the Fermi level of palladium + hydrogen (deuterium), HYDREX is formed in a state n such that :

$$\Delta E_n^{\infty} \geq \Delta E_f$$

A photon of energy ΔE_f is emitted when a new electron replaces the HYDREX bound electron in the conduction band (UV range) and this emitted energy can be small compared to ΔE_n^{∞}.

Further deexcitation can occur when HYDREX, in its $H\left(\left|{}^{\nu}_{n}\right.\right)$ state, collides with an electron e_L more energetic than the conduction band electrons (deeper levels of the electronic structure of the atom). If ΔE_L is the energy of the corresponding level of the electron, a transition of HYDREX from level n to level m (m<n), can occur if :

$$\Delta E_m^n \geq \Delta E_L$$

and the only visible energy production is the emission of a photon (or a cascade of photons) of energy ΔE_L. Note that, here again, ΔE_m^n can be much higher than ΔE_L and that unknown selection rules can limit some HYDREX transitions. The deexcitation process can be written as :

$$H\left(\left|{}^{\nu}_{n}\right.\right) + e_L \Rightarrow H\left(\left|{}^{e_m}_{p}\right.\right) + e_n + \text{X photon}$$

The formation and deexcitation of HYDREX should thus be visible, first through emission of **UV photons characteristic of the Fermi level of the metal used** and through **emission of X photons characteristic of the atoms present in this metal**.

This can explain X Ray emission during the formation and deexcitation of HYDREX and also the fact that the X Ray emission can go on even after the discharge has been cut-off.

Furthermore, the very small dimension of HYDREX explains that it readily diffuses through any material and is thus very quickly lost from the reactor.

Reactions of HYDREX with nuclei of the metal

When sufficiently stable, HYDREX in its $H\left(\left|{}^{\nu}_{n}\right.\right)$ state could react with a nucleus to yield neutron induced transmutations, provided that the endothermicity of the virtual neutron state is lower than the exothermicity of the neutron induced transmutation. It should be noted that the cross sections of these reactions should be in the order of magnitude of those occurring with real neutrons, which combined with the high diffusivity of HYDREX, should limit transmutation reactions in currently used experimental set-up.

The endothermicity of the virtual neutron state is equal to the binding energy of HYDREX. Equation (13') shows that this energy is always lower than 784 keV. Thus all neutron induced transmutation having an exothermicity higher than this value are possible. Put in an other way, it can be said that any reactions implying the addition of an atom of hydrogen (or deuterium) to a nucleus and that would be impossible (for Coulombic barrier reason), are possible with HYDREX (DEUTEX), provided this reaction is exothermic. As an example, the reaction with deuterium should yield tritium according to the scheme :

$${}^{2}_{1}H + H\left(\left|{}^{\nu}_{n}\right.\right) \Rightarrow {}^{3}_{1}H + \nu \qquad (16)$$

because the reaction :

$${}^{2}_{1}H + n \Rightarrow {}^{3}_{1}H + \nu \qquad (17)$$

has an exothermicity of some 6260 keV, higher than the highest binding energy of HYDREX. But this reaction (16) should have a rate severely limited by cross section and diffusion reasons.

Another example is the production of lithium that may have been observed in our experiments. Reaction (0) can be written :

$$ {}^{4}_{2}He + D\left(\left|{}^{\nu}_{2n}\right.\right) \Rightarrow {}^{6}_{2}He + \nu \Rightarrow {}^{6}_{3}Li + \beta^{-} + \bar{\nu} \qquad (0') $$

$D\left(\left|{}^{\nu}_{2n}\right.\right)$ being the virtual (di-neutron,neutrino) state of DEUTEX - $D\left(\left|{}^{e}_{d}, {}^{\nu}_{2n}\right.\right)$ -.

In the case of DEUTEX, Q' is equal to :

$$ Q' = \left(M_{2n} - M_d\right)c^2 = \left(2M_n - M_d\right).c^2 $$

assuming that the di-neutron has no binding energy (M_d being the mass of the deuterium atom, M_{2n} the mass of the di-neutron and M_n the mass of the neutron). Q' is thus equal to 3.11 MeV. The radius R'_a of the deuteron is taken as 2.5 fm. It can be seen from the relations (5) to (15), that stable states of DEUTEX, with values of R'_0 in the order of 25 fm (that is still meeting the condition that head-on collisions between the electron and the deuteron are dominant), can be found for $k' \approx 10^2$ (for DEUTEX relation (9) implies $k \geq 4.4.n$). This means that DEUTEX is likely to be easier to form than HYDREX. Moreover the bound states thus formed have a much higher binding energy than HYDREX, and their first deexcitation steps are also more energetic. All this might explain that more positive results are obtained with deuterium than with hydrogen and could account for the production of lithium in our experiment, according to (0'), because reaction (0) is exothermic (1.40 MeV) .

Conclusion

The model described in this paper, based on experimental results, can account precisely for all results obtained in the field of "Cold Fusion". It is hoped that it will be a strong guidance for further progress in the field.

Tables and figures in annex

Table 1 : Composition of virgin and activated palladium sample.
Figure 1 : Excess power generation as a function of time.
Figure 2 : Apparent loading ratio as a function of time.
Figure 3 : Excess energy per atom hydrogen as a function of time.
Figure 4 : Ionizing radiations after cut-off as a function of time.
Figure 5 : The pseudo-potential in the void cation model.

References

Ref.1 M. Fleischmann, S. Pons and M. Hawkins, "Electrochemically Induced Nuclear Fusion of Deuterium", *J. Electroanal. Chem.* **261**, p. 301 (1989)

Ref.2 J. Dufour Patent **WO 91/01036** "Energy source system", Filed 11 July 1989. International publication date : 24 January 1991

Ref.3 J. Dufour Patent **WO 94/10688** "Energy source system and process", Filed 26 October 1992, International publication date 11 May 1994

Ref.4 J. Dufour "Cold Fusion by sparking in Hydrogen Isotopes", *Fusion Technology*, **24**, p. 205 (1993)

Ref.5 J. Dufour, J. Foos, J.P. Millot "Cold fusion by sparking in Hydrogen isotopes. Energy balances and search for fusion by-products. A strategy to prove the reality of cold fusion" *Proceedings : fourth international conference on cold fusion.* **Volume 1 : Plenary session papers**, p 9-1 (1993)

Ref.6 J. Dufour, J Foos, J.P Millot "Excess energy in the system palladium/hydrogen isotopes. Measurement of the excess energy per atom hydrogen" *Proceedings ICCF5 April 9-13 1995*, p. 495 (1995)

Ref.7 J. Dufour, J. Foos, J.P Millot, X. Dufour "Interaction palladium/hydrogen and palladium/deuterium. Measurement of the excess energy per atom for each isotope" *Accepted for publication in Fusion Technology.*

Ref.8 I.B. Savvatimova, Ya.R. Kucherov, A.B. Karabut "Cathode material change after deuterium glow discharge experiment". *Proceedings : fourth international conference on cold fusion.* **Vol. 4 : Nuclear measurement papers**, p 16-1 (1993)

Ref.9 D. Tuggler, T. Claytor, S. Taylor "Tritium evolution from various morphologies of palladium". *Transactions of Fusion Technology : fourth international conference on cold fusion.* **Vol. 26**, p 221 (1994)

Ref. 10 H. Kozima, " Trapped Neutron Catalysed Fusion of Deuterons and Protons in Inhomogeneous Solids",*Trans. Fusion Technology (Proc. ICCF4)* **26**, p.508 (1994)

Ref.11 Charles KITTEL Introduction to solid state physics John Wiley and Sons Inc., New York. French edition, p 268

Ref.12 J.L. Russel "Virtual electron capture in Deuterium" *Ann.Nucl.Energy* **Vol. 18**, p.75 (1991).

Annex

FIGURE 5

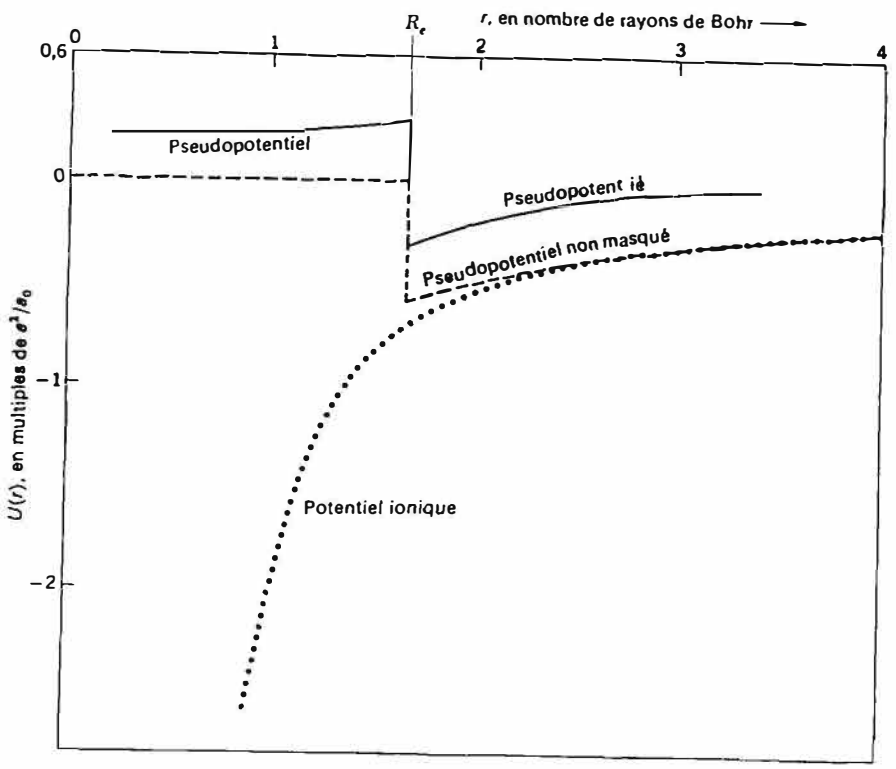

Figure 22 Pseudopotentiel du sodium métallique, basé sur le modèle du cation vide et masqué par la fonction diélectrique de Thomas-Fermi. Les calculs ont été réalisés pour un rayon $R_c = 1{,}66\,a_0$, où a_0 est le rayon de Bohr, et pour un rayon d'écran $\lambda a_0 = 0{,}79$. La courbe en tirets représente le potentiel non masqué, d'après l'équation [21]. La courbe en pointillés est le potentiel réel du cation ; en-dessous de $r = 1$, ce potentiel $V(r)$ prend les valeurs − 4,6, − 11,6 et − 50,4 pour $r = 0{,}7$, 0,4 et 0,15 respectivement. Par conséquent le potentiel réel de l'ion (ajusté pour correspondre aux niveaux d'énergie de l'atome libre) est bien plus grand que le pseudopotentiel, dans un rapport 200 pour $r = 0{,}15$.

Excess Energy and Nuclear Produc ts

TABLE 1 *Chemical composition of 3H06 Pd sample and virgin Pd sample (amount expressed in ppm per mass)*

Element	Pd of 3H06	Virgin Pd sample
H	***43 ± 7***	***28 ± 10***
Li	***0.05 ± 0.02***	***≤ 0.01***
Be	≤ 0.01	≤ 0.01
B	≤ 0.08	≤ 0.08
Na	nm	nm
Mg	***85 ± 9***	***7.3 ± 0.8***
Al	***27 ± 3***	***≤ 1***
Si	nm	nm
P	nm	nm
K	nm	nm
Ca	*	*
Ti	≤ 0.1	≤ 0.1
V	≤ 0.2	≤ 0.2
Cr	***7.9 ± 0.8***	***0.9 ± 0.3***
Mn	***0.3 ± 0.1***	***≤ 0.2***
Fe	***22 ± 10***	***≤ 10***
Co	≤ 0.05	≤ 0.05
Ni	***2.7 ± 9***	***≤ 2***
Cu	***4.1 ± 0.4***	***1.6 ± 0.2***
Zn	***43 ± 5***	***4.3 ± 1.5***
Ga	≤ 0.05	≤ 0.05
Ge	≤ 0.7	≤ 0.7
As	*	*
Se	≤ 8	≤ 8
Rb	≤ 0.15	≤ 0.15
Sr	≤ 0.15	≤ 0.15
Y	≤ 0.05	≤ 0.05
Zr	≤ 0.1	≤ 0.1
Nb	≤ 0.1	≤ 0.1
Mo	≤ 0.6	≤ 0.6
Ru	≤ 80	≤ 80
Rh	≤ 10	≤ 10
Pd	bulk	bulk
Ag	≤ 20	≤ 20

Element	Pd of 3H06	Virgin Pd sample
Cd	0.7 ± 0.2	0.7 ± 0.2
Sn	*	*
Sb	*	*
Te	*	*
Cs	≤ 0.05	≤ 0.05
Ba	≤ 0.07	≤ 0.07
La	≤ 0.15	≤ 0.15
Ce	*	*
Pr	≤ 0.07	≤ 0.07
Nd	*	*
Sm	≤ 0.4	≤ 0.4
Eu	≤ 0.01	≤ 0.01
Gd	≤ 0.1	≤ 0.1
Tb	≤ 0.02	≤ 0.02
Dy	≤ 0.08	≤ 0.08
Ho	*	*
Er	≤ 0.05	≤ 0.05
Tm	≤ 0.01	≤ 0.01
Yb	≤ 0.08	≤ 0.08
Lu	***0.05 ± 0.02***	***0.02 ± 0.01***
Hf	≤ 0.15	≤ 0.15
Ta	≤ 2	≤ 2
W	≤ 0.15	≤ 0.15
Re	≤ 0.1	≤ 0.1
Ir	***0.6 ± 0.2***	***0.5 ± 0.2***
Pt	***0.8 ± 0.1***	***1.4 ± 0.2***
Au	***0.8 ± 0.1***	***1.1 ± 0.1***
Hg	0.4 ± 0.1	0.4 ± 0.1
Tl	≤ 0.04	≤ 0.04
Pb	≤ 0.08	≤ 0.08
Bi	≤ 0.05	≤ 0.05
Th	≤ 0.15	≤ 0.15
U	≤ 0.05	≤ 0.05

* not measured ⇨ interference ; **nm** : not measured

Isotopic composition (expressed in atomic %)

Pd isotopes	Pd of 3H06	Virgin Pd sample	* Natural Pd
Pd 102	0.86 ± 0.10	0.87 ± 0.10	0.96
Pd 104	10.2 ± 1.0	10.2 ± 1.0	10.97
Pd 105	21.4 ± 1.5	21.5 ± 1.5	22.23
Pd 106	27.5 ± 2.0	27.5 ± 2.0	27.33
Pd 108	29.0 ± 2.0	28.9 ± 2.0	26.71
Pd 110	11.0 ± 1.0	11.0 ± 1.0	11.81

* Handbook of Chemistry and Physics - David R. Lide - 1994 - 1995 - CRC Pres

Excess Energy and Nuclear Products

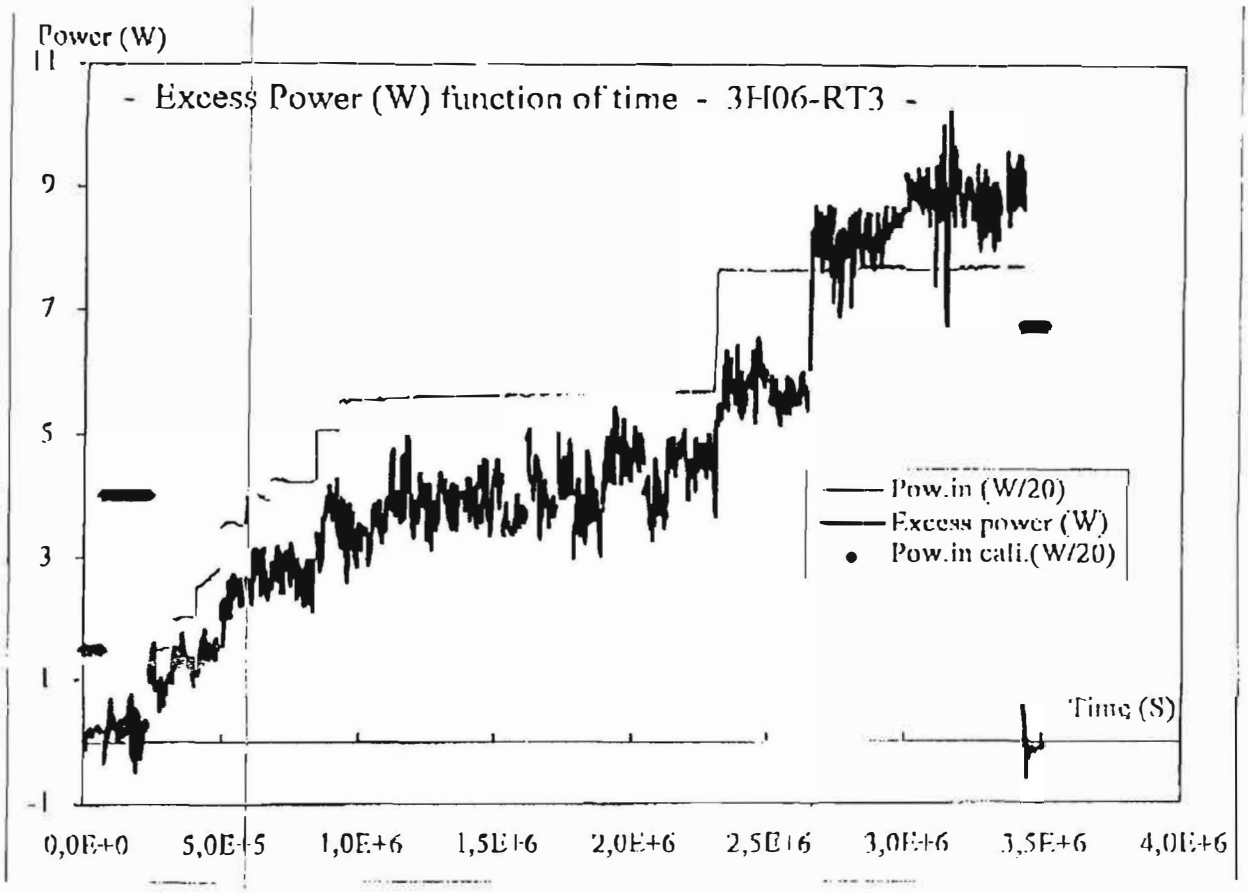

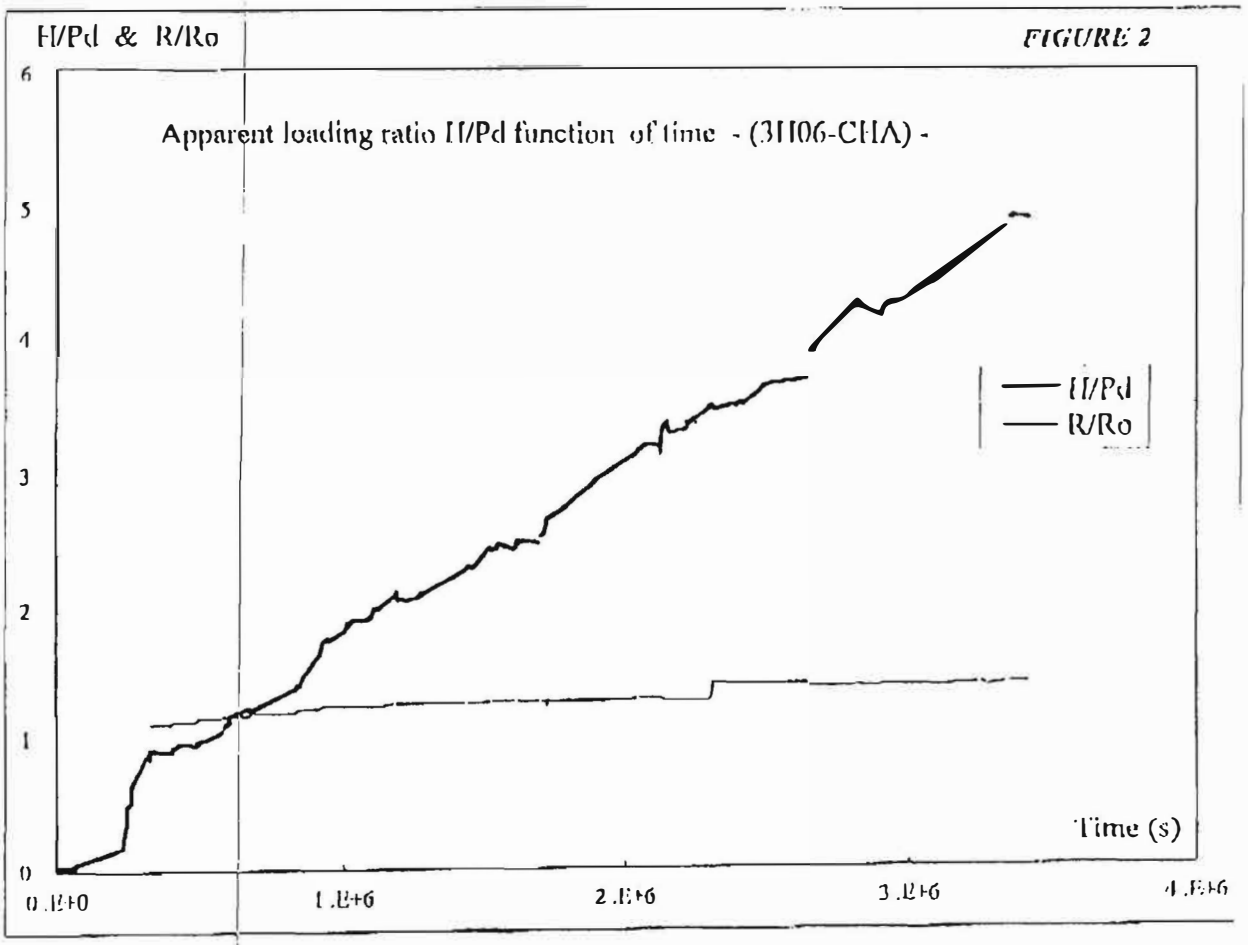

FIGURE 2

Excess Energy and Nuclear Products

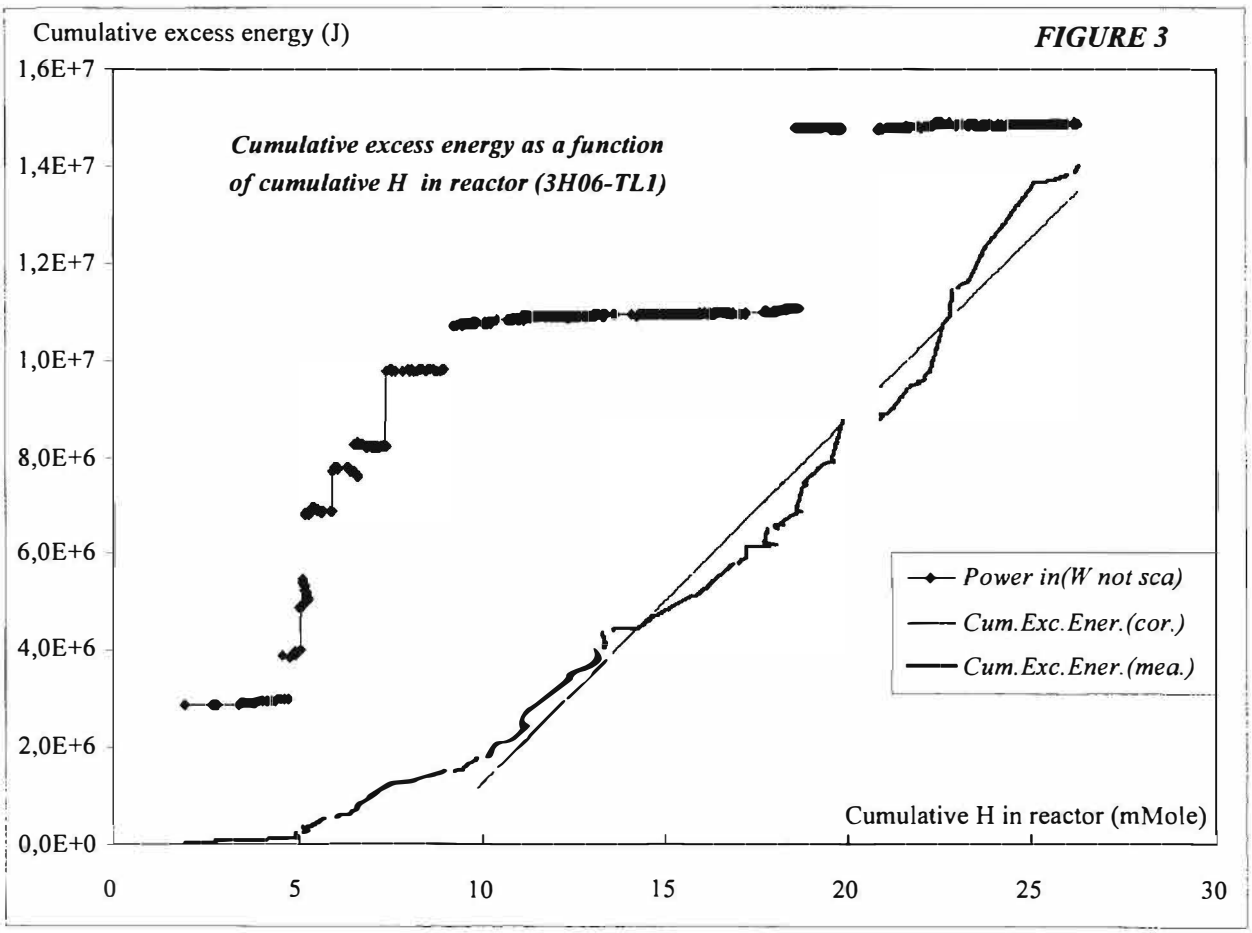

FIGURE 3

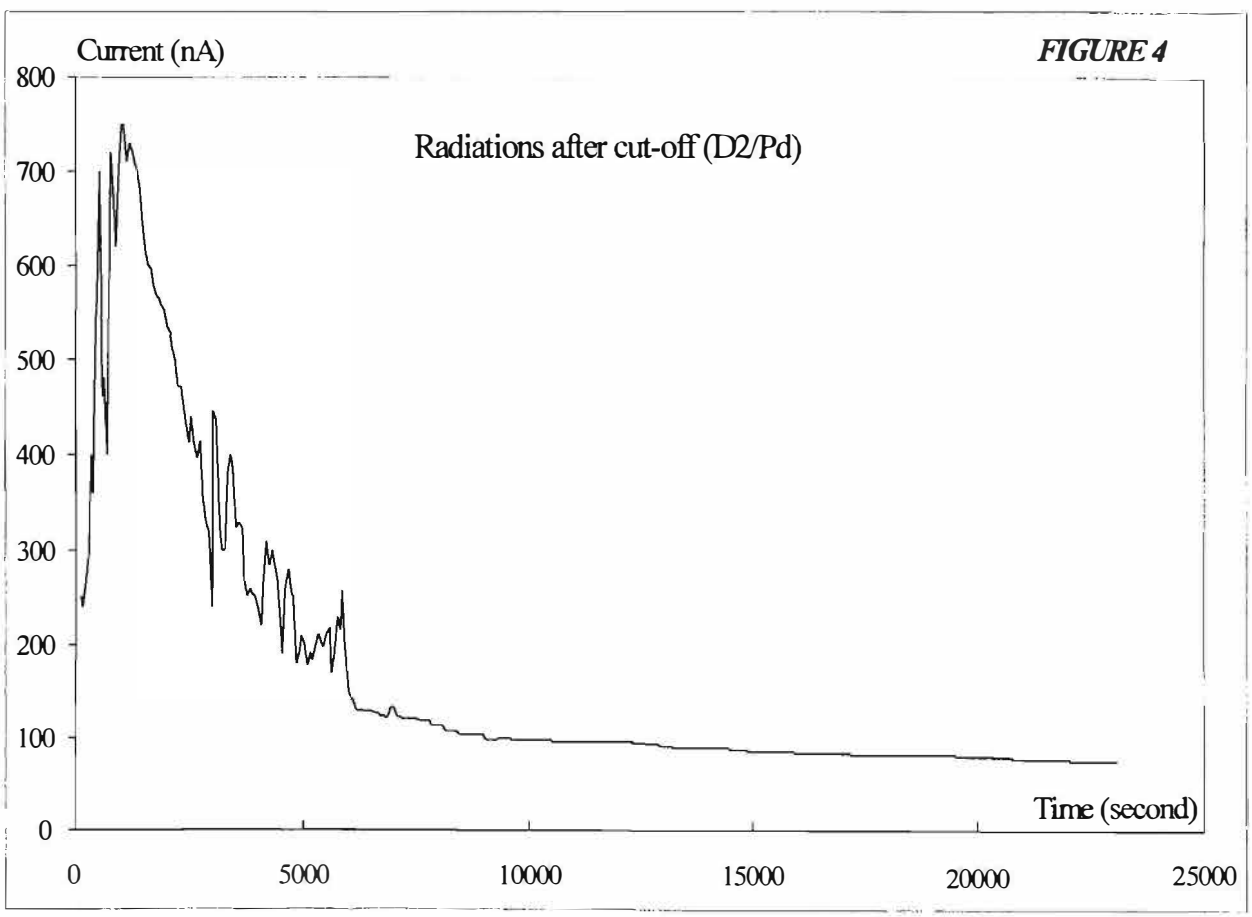

FIGURE 4

Excess Energy and Nuclear Products

Improved, Open Cell, Heat Conduction, Isoperibolic Calorimetry

Melvin H. Miles and Kendall B. Johnson

Chemistry & Materials Branch, Research & Technology Division
Naval Air Warfare Center Weapons Division
China Lake, CA 93555-6100, USA

Abstract
Significant calorimetric improvements have been realized at our laboratory. These improvements include the calorimetric hardware design, theoretical modeling, computerized experimental control, data acquisition, and extensive averaging of experimental measurements. The absolute calorimetric accuracy for operating over the entire temperature range from bath temperature to near boiling temperatures (0 to 5 watts of input power) was better than ±10 mW or ±1%, whichever is larger. This improved calorimetry yielded a short-term precision of ±0.2 mW or ±0.1% of the input power. The noise level (±0.1% or ±0.2 mW, peak to peak) is very low compared to other known calori-metric systems in use. Control experiments consisting of silver cathodes in 0.1 M LiOD showed no excess heat to within experimental error. In live experiments using palladium and palladium-boron alloys as cathodes, the exothermic heat of loading of deuterium into the metal is readily measurable. Small amounts of sporadic excess power were seen in one experiment using a palladium cathode.

1. Introduction

Accurate, sensitive calorimetry that is appropriately scaled to the electrode size and that has sufficient time resolution is essential to the study of the Fleischmann-Pons excess heat effect in the palladium-LiOD + D_2O system. As a general rule, the calorimetry must be capable of readily detecting an excess power level of about one watt per cubic centimeter of palladium that is used.[1] Accurate calorimetry is also needed to show the exothermic loading of deuterium into the palladium.[2] Finally, Jones et al.[3] have suggested possible energy storage in the cell and phase transitions to explain excess heat measurements. Our improved calorimetry shows that there is no energy storage mechanism in the Fleischmann-Pons type experiments.

2. Experimental

Our basic electrochemical calorimetric cell design is described in previous publications.[4,5] The use of the appropriate equations along with a room temperature correction yields an error range of ±20 mW or ±1% of the input power (whichever is larger) for our integrating, open isoperibolic calorimetry.[1] Based on our extensive previous experience with this calorimetry, various improvements were made to eliminate or minimize most of the error sources. This new calorimetry and improvements are illustrated in Figure 1. The major new improvements include a copper inner jacket that acts as the integrator and replaces the H_2O jacket used previously. An insulating box over the cell top and bath greatly reduces the effect of changes in the room temperature. Furthermore, the lead wires coming out of the cell top are thermally staked to the bath itself, thereby further reducing the effect of the room temperature. A copper outer jacket contacts the bath and minimizes bath level effects by virtue of its high thermal conductivity. This outer jacket helps form an isothermal outer surface that makes the calorimetry less sensitive to air temperature change over the bath.

Approved for public release; distribution is unlimited.

Excess Energy and Nuclear Products

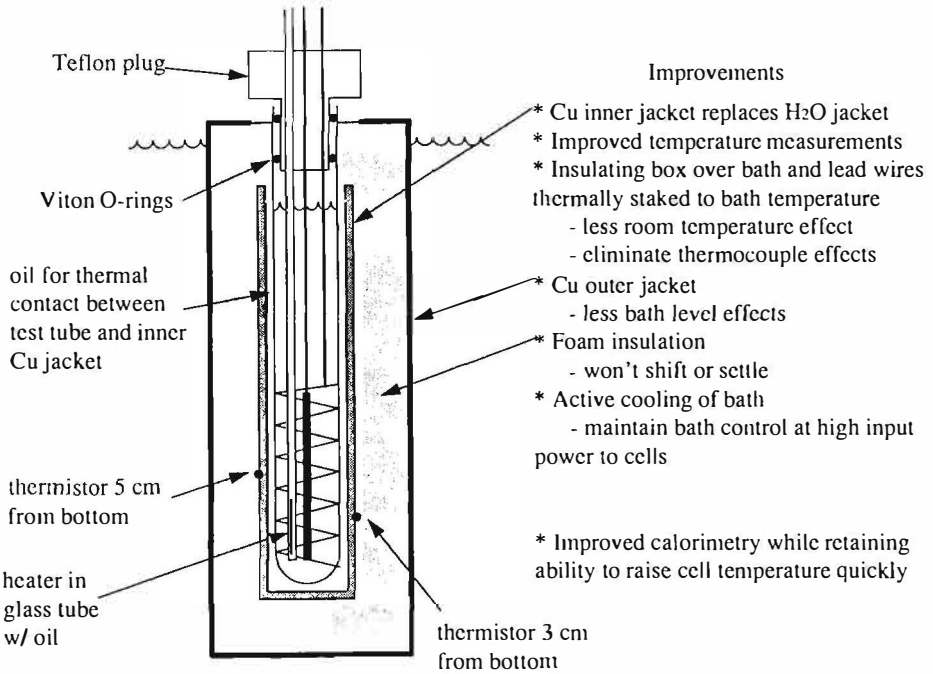

Figure 1. Improved design for integrating, open, isoperibolic calorimeters developed at China Lake.

The electrochemical cell shown in Figure 1 is a Pyrex test tube with an 18-mm outer diameter and a 15 cm length. The cell top consists of a machined Teflon plug with Viton O-rings. The 1-mm nickel lead wires are covered with double-walled shrink Teflon tubing. Spot-welding was always used to join the lead wires and electrodes. The shrink Teflon tubing extends over the spot weld and prevents any exposure of the nickel lead wire to the solution. The cathodes tested were 1-mm and 2-mm diameter wires and rods consisting of palladium, palladium-boron, and silver (for calibrations) ranging from 4 to 4.3 cm in length. The counter electrodes were made from 0.5 mm diameter platinum wire, 100 cm in length and coiled to 5 cm from top to bottom of the coil. The cell volume was 19 mL of 0.1 M LiOD + D_2O when full, while 10 mL was the smallest volume allowed during calorimetric measurements.

The inner copper jacket shown in Figure 1 is a very important improvement. This jacket consists of 3/4 inch copper plumbing pipe cut to 12 cm in length. The use of this jacket greatly reduces the electrolyte level dependence of heat conduction through the sides of the calorimeter. Ideally, the inner copper jacket makes an isothermal surface whose dimensions do not change with the changing electrolyte level. Mineral oil is used for the thermal contact between the glass electrochemical cell and the inner copper jacket. Two thermistors are set in groves in the inner copper jacket for temperature measurements. This has several important advantages over calorimeters that measure the temperature in the electrolyte. First, the temperature is smoothed over time so that any rapid fluctuations in cell temperature are integrated to yield lower noise and more accurate temperature readings. The noise in the temperature measurements is typically about 0.001°C for the calorimetry shown in Figure 1. This allows very smooth and accurate derivatives of the cell temperature versus time to be calculated. Second, mixing of the electrolyte is no longer an issue when the temperature is measured in the isothermal jacket. Although local temperatures in the cell may be of interest for understanding heat production within the cell, the temperature of the isothermal jacket remains the only temperature of interest for calorimetric measurements. The only exception to this is for very rapidly changing cell temperatures such as during D_2O additions or changes in the cell input power.

Common foam tubing insulation for plumbing pipe is used for insulation between the inner and outer copper jackets shown in Figure 1. An appropriate size for a tight fit is selected so that no

shifting is possible. This allows these calorimeters to be disassembled and reassembled without any change in dimensions.

A 100-ohm constantan wire is used for an additional calibration and temperature control heater in the cell as seen in Figure 1. This heater wire is coiled in a 3-mm outer diameter Pyrex tube containing mineral oil for thermal contact. These heaters were carefully constructed to provide good thermal contact and accurate voltage measurements.

Two calorimetric cells were always connected in series. These cells were also connected in series with two resistors that provided accurate and redundant measurements of the cell current. These resistors were a 10-ohm constantan wire with Teflon insulation and a 1-ohm commercial power resistor. Voltage measuring leads were attached and the connections sealed. These resistors were immersed in the bath to maintain them at constant temperature in order to minimize errors from resistance changes due to temperature. This provided for very accurate current measurements (±0.01%). The heaters for the two cells were also connected in series. Furthermore, they were also connected in series with another pair of resistors, identical to those described above, that provided accurate measurements of the current through the heaters.

The two calorimetric cells connected in series were immersed in a constant temperature bath set to approximately 22°C. Active cooling of the bath allows the controller to operate with a more uniform power load that provides better bath temperature control and keeps the bath temperature from rising during high cell input powers. Short term (1 hour) fluctuations in the bath temperature were less than ±0.01°C.

The thermally insulating box built over the bath to control the air temperature above the bath contained a small fan to circulate the air. This box was continually purged with a low flow rate of nitrogen gas that was conditioned to bath temperature by passing it through a coil of copper tubing immersed in the bath. This served to reduce the humidity in the box as well as providing a safety measure to prevent deuterium and oxygen gases from accumulating in the box in the event of a leak in the cell gas discharge tubes. This insulating box reduced the air temperature fluctuation to 1/8 of the normal daily fluctuation (1-3°C) of the air temperature in our laboratory.

3. Data Acquisition and Control System

The data acquisition and control system consisted of a 486 PC computer connected via GPIB connections to a Keithley Model 7002 switch system, a Keithley model 193, 6 and 1/2 digit digital multimeter (DMM), an EG&G PAR 273 Potentiostat/Galvanostat (cell power source), and a Keithley 228 voltage/current source (heater power source). The Keithley Test Point software was used and extensively programmed to provide complete instrument control, data acquisition, and display of data in real time, both digitally and graphically. The Keithley switch system was used to connect the various electrical connections to the K193 DMM. This included 10 temperature channels (1—air, 2—box air, 3—bath, plus two temperature measurements for each cell) and 8 voltage channels. Thermistors were used in all temperature measurements. Their resistances were measured directly with the K193 DMM which were then converted to temperatures. There was negligible self-heating of the thermistors. Extreme care was taken so that all quantities (temperatures, cell voltage, cell current) could be measured to four digits of accuracy. This is very important when attempting to measure 1 mW accuracy at 5 W input power. This was our goal for this new calorimetry.

Computer averaging and appropriate data collection are very important for this calorimetry. Under constant current conditions, cell voltages vary erratically and often quite widely during electrochemical experiments due to bubble formation and release.[1] This is especially true for the high current densities (≥ 100 mA/cm^2) required for excess heat effects.[6] These voltage fluctuations often

exhibit a periodicity on the order of a minute. It is extremely important that the cell voltages are sampled often and averaged over a sufficiently long time period in order that the cell input power is measured accurately. The input power measurements limit the performance of many calorimetric systems, both in accuracy and noise.

For our system, data is collected as fast as the switch and DMM settling time allows. The measurements of cell voltages and currents are made 14 times as often as the other 14 measurements (10 temperatures, 2 heater voltages, and 2 heater current resistor voltages). The measurements are averaged and recorded to disk every five minutes. During this 5-minute period, there are typically 112 measurements of each cell voltage and current along with 8 measurements of the other calorimetric quantities such as temperature. This provides sufficient averaging for smooth and accurate input power measurements.

4. Calorimetric Modeling

Heat conduction, isoperibolic calorimeters are generally modeled with a $K\Delta T$ term for heat conduction from the cell to the bath.[1,4,5] However, for the new caloriemter shown in Figure 1, it was found that the use of a $K_{3/2}\ (T^{3/2}_{cell}-T^{3/2}_{bath})$ term provided a better fit of the experimental data over a wide temperature range for the cell. The foam insulation used in this calorimetric system (Figure 1) approximates heat conduction through a motionless gas. The heat conduction for a motionless gas is proportional to $T^{1/2}$ which yields the $T^{3/2}$ term when integrated through the thickness of the wall of the caloriemter.[7] Therefore, the set of equations used for modeling the calorimeter shown in Figure 1 are as follows:

$$P_{excess} = P_{out} - P_{in}$$

$$P_{in} = (V_{cell} - E_h(T))I_{cell} + V_{heater}I_{heater}$$

$$P_{out} = P_{conduction} + P_{Cp} + P_{evap}$$

$$P_{conduction} = K_{3/2}\ (T^{3/2}_{cell} - T^{3/2}_{bath})$$ -heat conduction through foam insulation

$$+ K_2\ (T_{cell} - T_{bath})^2$$ -additional term added experimentally for improvement

$$+ K_{\Delta L}\ \Delta L\ (T_{cell} - T_{bath})$$ -changing heat conduction through lead wires with electrolyte level

$$+ C$$

$$P_{Cp} = C_{p(D2O)}(T)\ dT/dt\ (M_o + \Delta M)$$ - heat capacitance term, - power required to change the temperature of the calorimeter

$$P_{evap} = L_{(D2O)}(T)\ (0.75\ I/F)\ (P_{D2O}/(P_{atm} - P_{D2O}))$$ - latent heat of evaporation

where

ΔM = molar loss of electrolyte (due to electrolysis and evaporation) since the cell was last filled

ΔL = distance of electrolyte level below full level

dT/dt = derivative of Temperature with respect to time, calculated from the previous, current, and next points

The temperature dependence of the terms $L_{(D2O)}(T)$, $C_{p(D2O)}(T)$, P_{D2O}, $E_h(T)$ is given elsewhere.[1] The constants, $K_{3/2}$, K_2, $K_{\Delta L}$, M_o, C are calculated from calibration run data. Typical constants for cell 1 are $K_{3/2}$ = 0.0027295 $W \cdot K^{-3/2}$, K_2 = 0.000060611 $W \cdot K^{-2}$, M_o = 2.0819 mol, $K_{\Delta L}$ = 0.00069436 $WK^{-1}cm^{-1}$, and C = -0.0020172 W.

5. Calorimetric Results

Results using this new calorimetric system are presented elsewhere.[1,2] For example, Figure 1 of Reference 2 presents the measurement of the exothermic heat of absorption of deuterium into a palladium wire. This yields 5 mW of power over a two-hour period which can be readily measured to within ±0.2 mW using the new calorimetry. The measured exothermic heat of absorption correlates very well with that calculated for the palladium volume used assuming loading to $PdD_{0.6}$. This accurate calorimetry proves that there is no energy storage or phase transitions in the cell as suggested by Jones et al.[3] to explain excess heat measurements.

Figure 2 shows a fluctuating excess power effect for a 1-mm Johnson-Matthey wire cathode (1 mm x 4.3 cm) that was apparently triggered by a change in the cell temperature. About 50 mW of excess power was measured. This corresponds to 1.5 W per cubic centimeter of palladium which is approximately the level of excess power expected.[1,8] This result demonstrates how this more sensitive calorimetry can be used to study events that may trigger or kill the excess-power effect.

Four experiments were conducted using palladium-boron alloy electrodes with this new calorimetric system. Despite previous studies which showed a high success rate for excess heat with these alloys,[8] no excess power was measured. However, these alloy electrodes had swaged, folded-over metal regions and had to be machined prior to use to remove these defects. The poor quality of these palladium-boron cathodes may explain the lack of excess heat.

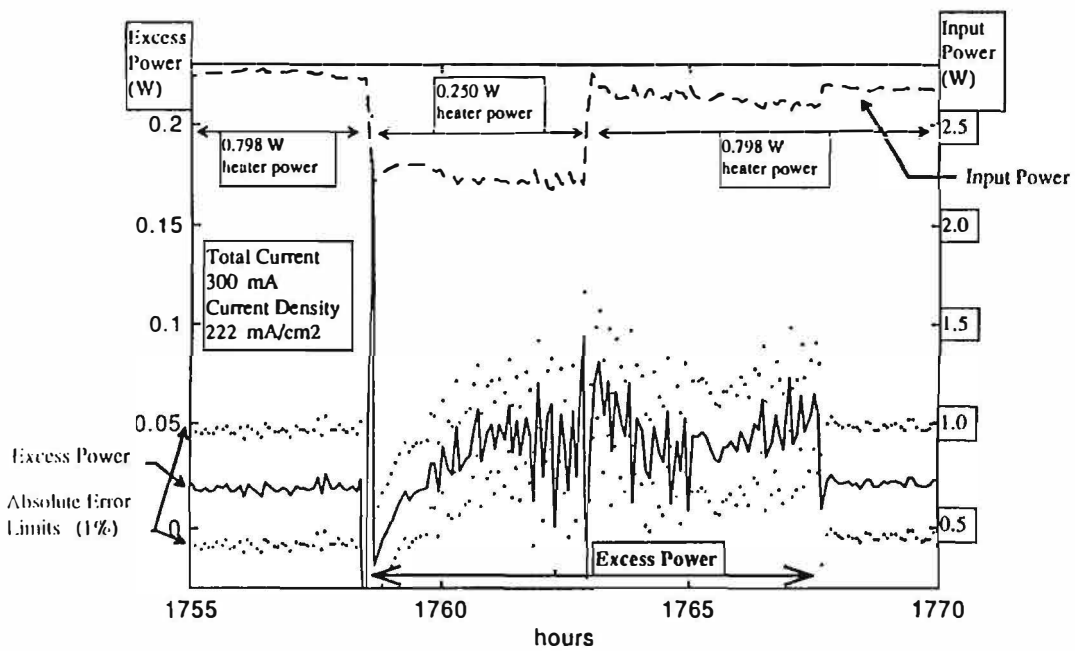

Figure 2. Fluctuating excess power effects for a 1-mm Johnson-Matthey wire cathode (1 mm x 4.3 cm). The onset of excess power began shortly after the reduction in the heater power which changed the cell temperature.

6. Conclusions

The following specifications were realized for this new calorimetric system: The absolute accuracy is better than ±1% or ±10 mW over the entire operating temperature range (bath temperature to near boiling temperatures). The short term precision is better than ±0.1% or ±0.2 mW. The peak-to-peak noise level is less than ±0.1% or ±0.2 mW. The percent limit is based on the input power and is always used when it becomes larger than the mW limit. The time resolution is 5 minutes point-to-point. Numerous readings are always averaged per point. The heat of absorption of deuterium into the palladium is always observed and is readily measurable with this calorimetry. Small amounts of sporadic excess power was observed in one experiment using a palladium cathode.

7. References

1. M. H. Miles, B. F. Bush, and K. B. Johnson, "Anomalous Effects in Deuterated Systems," NAWCWPNS TP 8302 (September 1996).
2. M. H. Miles, K. B. Johnson, and M. A. Imam, "Electrochemical Loading of Hydrogen and Deuterium into Palladium and Palladium-Boron Alloys" in Proceedings of the Sixth International Conference on Cold Fusion, Hokkaido, Japan, 13-18 October 1996 (submitted).
3. S. E. Jones and L. D. Hanson, *J. Phys. Chem.*, **99**, 6966 (1995).
4. M. H. Miles, K. H. Park, and D. E. Stilwell, *J. Electroanal. Chem.*, **296**, 241 (1990). See also M. H. Miles, "The Extraction of Information From an Integrating open Calorimeter in Fleischmann-Pons Effect Experiments" in Proceedings of the Fifth International Conference on Cold Fusion, Monte-Carlo, Monaco, 9-13 April 1995, pp. 97-104.
5. M. H. Miles, B. F. Bush, and D. E. Stilwell, *J. Phys. Chem.*, **98**, 1948 (1994).
6. M. H. Miles, "Reply to S. E. Jones and L. D. Hanson Concerning Claims of Miles, et al. in Pons-Fleischmann-Type Cold Fusion Experiments" in Proceedings of the Sixth International Conference on Cold Fusion, Hokkaido, Japan, 13-18 October 1996 (submitted).
7. J. P. Holman. "Heat Transfer," 6th Edition, McGraw-Hill Book Company, New York, 1986, pp. 6-10.
8. M. H. Miles, K. B. Johnson, and M. A. Imam, "Heat and Helium Measurements Using Palladium and Palladium Alloys in Heavy Water" in Proceedings of the Sixth International Conference on Cold Fusion, Hokkaido, Japan, 13-18 October 1996 (submitted).

Excess Energy and Nuclear Products

Slow Nuclear Excitation Model

Yan Kucherov
ENECO, Inc.391-B Chipeta Way, Salt Lake City, Utah, 84108

Abstract
Phonon modes in a two - component lattice produce an oscillating non- uniform electric field that interacts with nuclear quadrupole moment. This dipole- quadrupole interaction in combination with nuclear spin alignment and a presence of a vacancy in a light sublattice can produce very significant energy transfer from the phonon mode to the nucleus. Accumulated energy can exceed nuclear reaction barrier

1. Introduction

The idea that nuclear reactions in solids can be related to lattice phonon system was suggested by J.Schwinger and P. Hagelstein in 1989 - 1990 [1, 2]. If we accept that nuclei excitation comes through the phonon system, there should be a specific phonon mode which allows excitation of nuclear reactions. As phonons are lattice vibrations, probably this excitation can be imagined as nuclei parts interaction with an oscillating lattice electric field. To large extent this situation has an optical analogy with solid state lasers, i.e. Nd^{+++} in glass. Phonon interaction with atomic quantum levels resulting in energy up - conversion is described in [3]. Most of the optical formalisms can be applied to phonon interaction with a nucleus. One of the obvious cases is the Anderson's localization theorem [4]. It states that for interactions decreasing faster than distance in minus third power (dipole - dipole interaction) energy transfer can happen only with high density of (phonon) population. Application of this principle to nucleus - phonon system requires intensive phonon mode in order to get energy transfer. The other sequence of this principle is the existence of a threshold excitation below which the effect goes away. Nuclear acoustic resonance (between spin and quadrupole levels) achieved by AC magnetic field showed anomalies in line shape with TaH system [5]. Anderson's condition was not realized in this experiment and lattice oscillations were random.

2. Nuclear excitation model

Stable nuclei do not have dipole moment and there are no dipole interaction. To feel oscillating field nucleus must be non-spherical, i.e. it must have a pronounced quadrupole moment. According to [6] a list of naturally abundant nuclei with quadrupole moment looks like: ^{2}H; $^{6,7}Li$; ^{9}Be; ^{11}B; ^{17}O; ^{23}Na, ; ^{25}Mg; ^{27}Al; ^{33}S; $^{35,37}Cl$; $^{39,41}K$; ^{43}Ca; ^{45}Sc; $^{47,49}Ti$; ^{53}Cr; ^{55}Mn; ^{59}Co; ^{61}Ni; $^{63,65}Cu$; ^{67}Zn, ^{73}Ge, 75As, $^{79,81}Br$; ; ^{85}Rb; ^{87}Sr; ^{91}Zr; ^{93}Nb; ^{97}Mo; ^{101}Ru; ^{105}Pd; and nuclei with charge numbers 57- 71 which includes most of lantanoids, $^{177,179}Hf$; ^{181}Ta; $^{185,187}Re$; ^{189}Os; $^{191,193}Ir$; ^{197}Au; $^{199,201}Hg$; ^{209}Bi; ^{235}U. The champions among this group are ^{179}Hf, ^{181}Ta, and lantanoids ^{165}Ho, ^{167}Er, ^{173}Yb, and ^{175}Lu, having quadrupole moment around 3×10^{-24} cm^2 (barns). It should be noted that deuteron has quadrupole moment (0.0028 barn) and though it is 2 - 3 orders smaller than that of most of listed metals, in principle it can be excited as well.

Let us now address the issue of how the excitation can be transferred to the nuclei. The nucleus itself is a slow system and estimations from quadrupole gamma - transitions half life

times [7] give oscillation time constant at 1 KeV energy of 10 - 10^3 s. In a lattice we have a slow oscillations of a heavy nuclei system and fast reaction of electron system. Nuclear oscillations create distortions in electronic field, thus creating charge displacement, which in its turn create dipole electric field. Electric field change due to nuclei system harmonic oscillations will be effectively screened by electrons distances larger than lattice parameter and it is highly unlikely that neighboring sites will have strongly different sustained phonon modes as they will tend to attenuate each other. It can happen with anharmonic modes but it is difficult to visualize sustainable anharmonic modes. The situation is different when we have two - component lattice. In this case neighboring sites have nuclei with different mass and harmonic oscillations frequencies (phonon spectra) of each sublattice are basically different, providing strong oscillating electric field at nucleus location. As is known, it is impossible to transfer energy in an ideal lattice, so to get coupling to the heavy component there must be a vacancy in the light component. From geometric considerations ideal case in a lattice with cubic symmetry, i.e. PdH_x corresponds to x = 0.875 or x = 0.125, the former is much more preferable in many aspects (not discussed here). The situation is illustrated in fig. 1. We can consider that heavy nucleus has a fixed coordinate, which is an extremely good approximation for Pd-H system, where for a given phonon energy nucleus displacement differs by a factor of 50. The trouble is that the heavy nucleus is not oriented and net transfer is zero. To change the situation magnetic field must be applied. All the listed nuclei have spins (quadrupole moment exists only for nuclei with spin $S \geq 1$.) and application of a sufficient magnetic field orients it. The problem of magnetic field strength will not be treated here, but depending on various parameters it is in the interval between 0.5 and 100 Oe, and can be easily achieved. If we align orientations of magnetic field and phonon oscillations we obtain a situation preferable to energy coupling into the nucleus which is illustrated in fig. 2 . Here an electric field of three light atoms and a vacancy is modeled by one oscillating electric charge. This charge is created by a combination of electronic and ionic electric fields. As electronic system is much faster than ionic, it oscillates with the same frequency. Electric field gradient on the nucleus itself is about the same as in the absence of the electrons or larger due to antishielding effect [5] Typical values of electic field gradient are 10^{20} - 10^{22} V/m^2 [5], which is about 10^{10} times more than in any other experimental situation, except direct nuclear interactions.

Dipole moment of a nucleus in the ground state is zero, and the nucleus dipole interaction with oscillating electric field does not exist. The situation is different for the quadrupole interaction which gives additional energy [8]:

$$E = \frac{e_o D}{6} \cdot \frac{\partial^2 \varphi_o}{\partial\alpha\partial\beta}, \qquad (1)$$

where D - quadrupole moment e_o - elementary charge, α, β - coordinates and φ_o - electric potential at the beginning of coordinates, in our case at the lattice site. With this model slow nuclear deformation looks at fast oscillations of asymmetric electric field and if the field is sustained we simply build this energy on and on. Integration of (1) gives time dependence for energy transfer to the nucleus:

$$E(\tau) = \frac{4e_o e^* D\omega}{x_o^3} \cdot \frac{\hbar\omega}{E_v} \cdot \tau, \quad (2)$$

were τ is time, ω - phonon frequency; x- axis corresponds to xx components of both nuclear quadrupole and electric field gradient tensors, x_o - distance from the nucleus to the vacancy, e* - vacancy effective charge, E_v - vacancy formation energy, $\hbar$ - Plank's constant. Evaluations using

formula (2) for an intense phonon resonance in $PdH_{0.87}$ lattice and ^{105}Pd isotope component are given in the table 1.

ω, Hz	ΔE,eV	$\partial E/\partial\tau$, eV/s
10^{11}	10^{-10}	10
10^{12}	10^{-9}	10^{3}
10^{13}	10^{-8}	10^{5}

Here ω - phonon frequency, ΔE - energy transfer in one phonon oscillation and $\partial E/\partial\tau$ - energy transfer rate. I.e. 1 MeV can be accumulated in 10 seconds. Evaluations of phonon energy replenishment from neighboring lattice sites (from phonon dipole - dipole interaction and phonon spectral density) give maximum values of energy transfer about 10^{-4} eV. Phonon density is a limiting factor here and requires excitation to meet Anderson's condition.

Building a phonon resonator is within known engineering and will not be discussed here. From quantum mechanics point of view, in the absence of magnetic field (degenerate levels) energy levels due to thequadrupole interaction look like [5]:

$$E_o = \frac{e_o D q}{4I(2I-1)} \qquad (3)$$

where $q = \frac{\partial^2 \varphi}{\partial x^2}$, electric field gradient, I - nuclear spin, D - quadrupole moment, e_o - elementary charge. Number of levels is I + 1/2. Level spacing is 10^{-10} - 10^{-8} eV.

When Anderson's condition is met, on top of the levels (3) new levels will be accumulated in each cycle:

$$E_i = \frac{e_o D q}{4\pi I(2I-1)} \cdot N, \qquad (N = \pm 1, \pm 2 \ldots). \qquad (4)$$

Quantum number N is the integer part of ωt, where ω - phonon frequency and t - time. Time dependent quantum number N represents virtual energy levels. Total number of levels will be $(I + 1)2^N$, or in the presence of a magnetic field $(I + 1)2^{N+1}$.

3. Excitation relaxation

The described kind of excitation is entirely different from normal situation, when nuclear reactions occur at large energy portions transfer, allowing for energy relaxation on unoccupied energy levels. With a slow excitation all nuclear energy levels are being gradually filled from the nuclear ground level, thus forbidding energy relaxation in the form of gamma - emissions. On top of usual selection rules slow excitation probably requires stable nuclear shells for resulting products, as they have a lot of time to form a state with minimum energy (stable shells). Nevertheless, conservation of energy, momentum, spin, parity must be observed in all cases. Out of about 70 isotopes listed above, only four allow energy release with beta - decay (Re, Pm, In, Mo), but all are forbidden by both Fermi and Gamov - Teller selection rules, so no betas.

Alpha - decay with positive energy release (Q) is allowed in some cases and can give positive Q, i.e.:

^{197}Au (s=3/2) --> α + ^{193}Ir (s=3/2) + 1.045 MeV. (5)

Resulting iridium is a stable isotope. It is known that alpha - decay is very sensitive to low level excitations, at least for ^{235}U, where 10 KeV excitation changes decay rate dramatically. Probably the same is true here.

With atomic mass less than 145 alpha - decay has negative Q even if it is allowed. The examples of negative Q alpha - decay are ^{105}Pd --> $^{101}Ru + \alpha$ - 2.9MeV; ^{135}Ba --> $^{131}Xe + \alpha$ -1.87 MeV.

Paradoxical situation happens with isotopes for which all three channels of energy relaxation are forbidden and they are cornered into nuclear fission. Fission will also compete with alpha - decay that requires high negative Q, i.e. for ^{105}Pd isotope fission reactions

^{105}Pd --> $^{25}Mg + ^{80}Se$ + 2.53 MeV. (6)

^{105}Pd --> $^{17}O + ^{88}Sr$ + 0.311 MeV (7)

are about 10^2 times more probable than alpha - decay at low excitation level from barrier considerations.

For some elements even normal fission is forbidden and something like multi - particle decay can be expected, which can be the source of tritium etc.

When transfer process is stopped with energy accumulation short of nuclear reaction level, there is one fast relaxation process with low probability - through the electron system. In this case low level emissions of photons and Auger electrons can happen. Two other possibilities are quadrupole - dipole relaxation and quadrupole - spin relaxation. Spin relaxation requires oscillating magnetic field and can only be done artificially. Dipole relaxation is associated with electric field potential at vacancy location due to nuclear quadrupole of 10^5 - 10^6 times weaker than other way around with expected relaxation times longer by the same factor. To de - excite one single level from (4), assuming I = 5/2, the following condition must be met:

$$5 \cdot 10^{-2}\, e_o q D = h\omega_o(n + 1/2), \qquad (8)$$

where ω_o - lattice phonon frequency, h - Plank' constant, n - quantum number for dipole oscillations. Even for n = 0, ω_o corresponds to 10^6 - 10^8 Hz , where the phonon density is very low. This process requires a decay of higher frequency phonons to populate this region, i.e. lattice thermal non - equilibrium.

Conclusion

The proposed slow nuclear excitation model allows the explanation of most of the experimental data accumulated to date, i.e. excess heat in nickel- hydrogen system is the result of impurities, like ^{197}Au or ^{105}Pd "burning", as shown in equations (5)-(7). ^4He accumulation is the result of induced alpha - decay rather than d-d fusion, etc.. Engineering for energy generation on the basis of nuclear resonance in solids (not discussed here) becomes straightforward and understandable.

References

1. J. Schwinger. Trans. Fusion. Technology, 26 (1994).
2. P. Hagelstein. ibid., pp. 461-73.
3. F. Ausel. in: Radiationless Processes, NY, Plenum, 1979, pp. 250-286.
4. P.W. Anderson. Phys. Rev. 109, (1958) 1492.
5. D.I. Bolef, R.K. Sundfors. Nuclear Acoustic Resonance, Acad. Press., 1993.
6. CRC Handbook of Chemistry and Physics, 73rd edition, 1992-93.
7. K.N. Mukhin. Introduction to Nuclear Physics. Atomizdat, Moscow, 1965.
8. L.D. Landau, E.M. Livschitz. Field Theory. Nauka, Moscow, 1967.

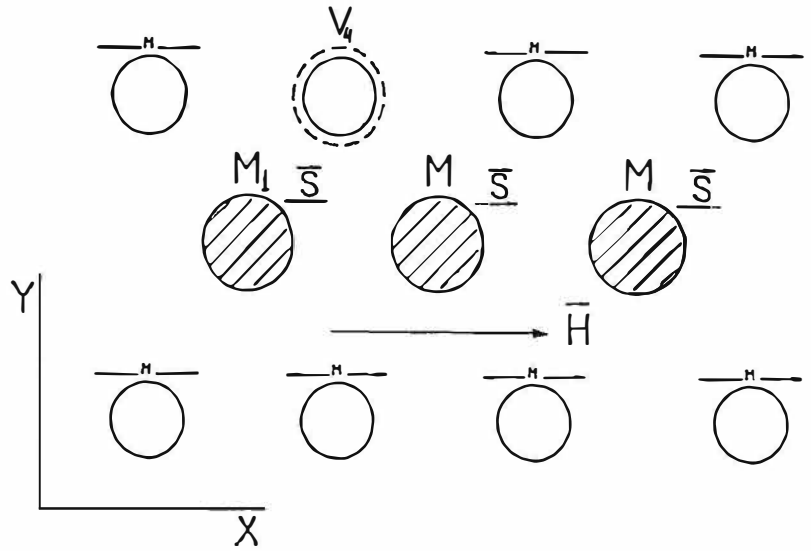

Fig. 1. Illustration of a two - component lattice, having a heavy component element M (i.e. palladium 105 isotope), which has a nucleus with a quadrupole moment, with nuclear spin S aligned along the magnetic field vector H, and a light component m (i.e. hydrogen), with phonon oscillations oriented along the X - axis, and having a stable vacancy V_4 .

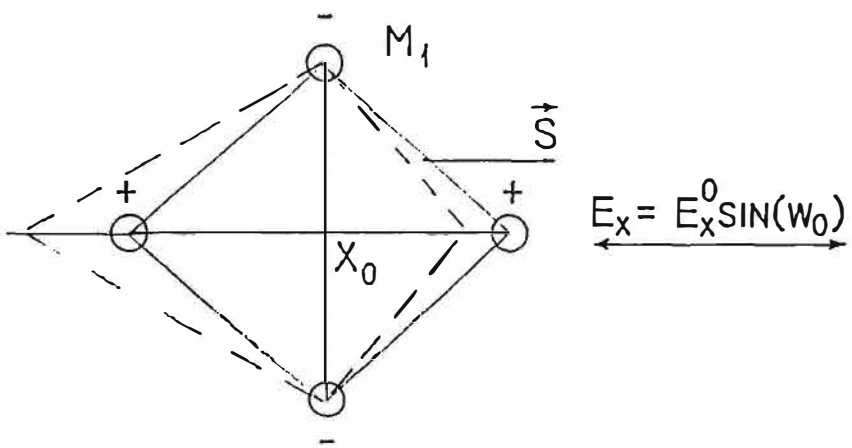

Fig. 2. Illustration of a nucleus M_1 from fig. 1, shown as quadrupole in the oscillating electric field gradient created by a vacancy. Dotted line shows quadrupole deformation caused by this field.

"Fine Tuning" Mechanism for Resonance Tunneling in D/Pd Systems

Xing Zhong Li, Hai Feng Huang, Zhi Gang Bian
Department of Physics, Tsinghua University, Beijing 100084 CHINA
Jie Fu Yang
Department of Physics, Hunan Normal University Changsha, 410081, CHINA

Abstract
A "Fine Tuning" parameter is introduced to describe how an extremely narrow energy level in the nuclear potential well is able to keep itself in resonance with the energy level in the lattice potential well. The good agreement between theoretical expectation and the experimental observation provides an additional evidence for the "resonance penetration of Coulomb barrier via lattice confined deuterons", and suggests the key to enhance the reproducibility of "excess heat".

1. Introduction

The assumption of a narrow nuclear energy level solves the puzzle of "excess heat" without commensurate neutron and Gamma radiation[1]. This assumption is supported by the "heat after death" and "heat after life" experiments; however, a question remains, i.e. how an extremely narrow energy level is able to be in resonance with the narrow energy level of a lattice confined ion. A "fine tuning" mechanism in terms of "self-lock" is proposed to solve this remaining problem.

2. Theoretical Expectation —"Fine Tuning" parameter.

The characteristic time in "heat after death" experiments (10^4 seconds), and the fact of "excess heat without commensurate neutron radiation" have revealed a low energy resonance d-d state with an energy width of 10^{-19}eV. On the other hand, the lattice confined deuterons are distributed on the energy band in the palladium lattice potential well. If the density of state in that energy band is greater than $\rho_c(E) \approx 10^{19}$/eV; then, the resonance penetration of Coulomb barrier would be more probable since the energy band width in the palladium lattice may be greater than 1 meV. This requirement on density of state turns out to be a requirement on the grain size in the Pd crystal: i.e. the grain size should be greater than 50 ~100 microns.

However, the dynamics of resonance requires more than a grain size. The extremely narrow energy level may resonance with one of the energy levels in the lattice energy band, but the heat released in this resonance may quickly push themselves away from the resonance due to the thermal expansion which shifts the energy band. If we would like to keep them in resonance, there has to be a

restoring force to pull them back. The variation of the density of state, $\rho(E)$, may provide such a restoring force, if $\frac{d\rho(E)}{dE} < 0$. (E is the energy of the relative motion of d-d state). In Fig.1 it shows schematically an energy band with a negative derivative of density of state. When the thermal expansion lowers the energy band, the resonance nuclear energy level, E_N, will see a higher energy level in that energy band; hence, see a less density of state. This difference in the density of state in an energy band will reduce the heat released by the resonance, and reduce the thermal expansion. In other words, the negative derivative, $\frac{d\rho(E)}{dE} < 0$, will provide a negative feed-back to pull back the energy band and restore the resonance between the nuclear energy level, E_N, and the lattice energy level, E_L. It is very similar to the "self-lock" phenomenon in "fine tuning" mechanism of a radio receiver.

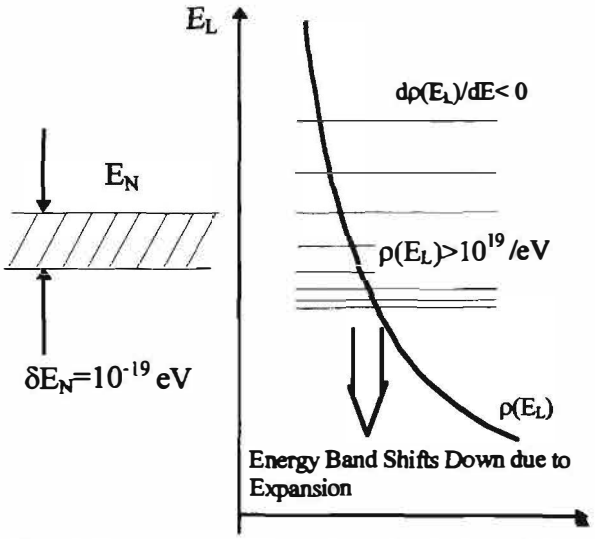

Fig.1 Energy Band Structure in Pd Crystal

There is a critical derivative of the density of state, $\left(\frac{d\rho}{dE}\right)_c$, in order to make this "fine tuning" work. Any power perturbation inside the calorimeter, $\Delta\tilde{p}$, will result a thermal expansion, $\frac{\Delta\lambda_L}{\lambda_L} = \frac{\Delta\tilde{p}}{k_c}\cdot\alpha$. Here, λ_L is the lattice constant k_c is the heat transfer coefficient of the D/Pd system (0.1 ~ 0.7 W/K for most of "excess heat" experiments); α is the linear expansion coefficient ($\approx 11.8\times10^{-6}$ K^{-1} for palladium). The shift of the energy band due to this expansion is about $\Delta E_L = 2\frac{\Delta\lambda_L}{\lambda_L}E_L$. The energy band shift ΔE_L will change the number of resonance states from $\rho(E_L)\Delta E_N$ to $\rho(E_L+\Delta E_L)\Delta E_N$. Here, ΔE_N is the width of the nuclear energy level. This change will reduce the "excess heating" power by an amount of $\Delta E_N\left(\frac{d\rho}{dE}\right)_{E_L}\cdot\Delta E_L\cdot\frac{E_F}{\tau_{ex}}$. Here, E_F is the "fusion energy" released by a pair of d-d resonance state during their life-time τ_{ex}. $E_F \approx 23.8 MeV$ and $\tau_{ex} \approx 10^4$ seconds. Thus the restoring power is

$$\left|\frac{\Delta\tilde{p}}{k_c}\cdot\alpha\cdot 2E_L\cdot\Delta E_N\cdot\left(\frac{d\rho}{dE}\right)_{E_L}\cdot\frac{E_F}{\tau_{ex}}\right| > |\Delta\tilde{p}|$$

This restoring power has to be greater than the initial power perturbation, $\Delta\tilde{p}$, in absolute value but opposite in their signs in order to keep this resonance. In other words, the derivative of the density of the state has to be negative but its absolute value has to be greater than a critical value:

$$\left|\frac{d\rho}{dE}\right| > \frac{k_c \cdot \tau_{ex}}{\alpha \cdot 2E_L \cdot \Delta E_N \cdot E_F}$$

Since the density of the state in a Pd sample is proportional to its volume, V_{Pd} ; it is evident that the ratio of V_{pd} to k_c will determine the restoring force for the fine tuning mechanism. We may define $(\frac{V_{pd}}{k_c})$ as a "fine tuning" parameter

$$F \equiv (\frac{V_{pd}}{k_c})$$

The greater the "fine tuning" parameter, F, is, the more stable the resonance between the nuclear energy level and the lattice energy band, provided that the derivative of the density of the state less than zero, i.e.

$$\frac{d\rho(E)}{dE} < 0$$

3. Experimental Observation

The experiments have verified the first requirement ($(\rho_c(E) > 10^{19} eV^{-1})$ by the metallography of the annealed Pd samples[2] [3] and the positive annealing fact[4] . Now we examine the "fine tuning" parameter in various experiments. Table 1 lists some of these early positive "excess heat" experiments, and the recent negative experiment completed by Quickenden et al.[5].

Table 1 "Fine Tuning" Parameter in Various Experiments

	Heat Transfer Coefficient (W/°C)	Volume of Palladium (cm^3)	"Fine Tuning" Parameter ($cm^3 \cdot °C$ /W)
Quickenden[5]	0.71	0.0251	0.0354
Mckubre[6]	0.46	0.353	0.767
Kunimatsu [7]	0.2	0.232	1.16
Miles [8]	0.14	0.343	2.45
Fleischmann & Pons [9]	0.0648	0.0392	0.605
Xing Z.Li [2]	0.1	0.234	2.34
Lewis [10]	0.0714	0.073	1.02

It is noticed that in that negative experiment their "fine tuning" parameter is much less than those of all other positive experiments. Particularly, it is interesting to notice that the "fine tuning" parameter in the early "negative" experiment of Lewis is relatively large, there should have been "excess heat" as pointed out by Dr. Miles in 1994. However, it was reported as a negative one.

An important test on this "fine tuning" mechanism is the sign of the derivative, $\frac{d\rho}{dE}$. Although it is difficult to calculate its exact number, it is possible to determine its sign according to the shape of the lattice potential well. The quantum mechanics gives the qualitative conclusion that the derivative of the density of state will be

$$\frac{d\rho}{dE}\begin{cases} < 0 & \text{(square - well)} \\ = 0 & \text{(harmonic well)} \\ > 0 & \text{(Trumpet - like well)} \end{cases}$$

as schematically shown in Fig.2. The inelastic neutron scattering experiment showed that the lattice potential well in Pd is a square-well-like one because its anharmonicity parameter is positive (see Fukai [11]).

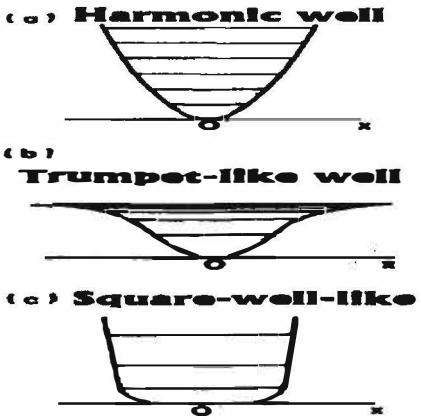

Fig.2 Three types of well with different sign of dρ/dE

Our gas-loading experiment provides an additional evidence on this "fine tuning" mechanism. In Fig.3 , the upper line shows the temperature difference between the twin D/Pd and H/Pd systems and the lower curve shows the derivative of the temperature of the D/Pd system with respect to the time (in an enlarged scale), When the heating power through the tungsten wire is shut off, the temperatures of the twin systems are changing with the room temperature, but the temperature of the D/Pd system (T(D)) is always higher than that of H/Pd system due to the possible "excess heat" source in the D/Pd system. It is interesting to observe that this "excess heat" source changes in day and night also. The maximum of [T(D)-T(H)] appears at the point where the T(D) drops quickest, and the minimum of [T(D)-T(H)] appears at the point where T(D) rises quickest. This behavior implies a heat source in D/Pd system, which is proportional to (-dT(D)/dt). A possible explanation of this behavior is just that the density of state in the resonance energy band decreases with the energy, i.e. $\frac{d\rho}{dE} < 0$. When the T(D) is dropping, the D/Pd system will see a higher density of state in resonance. This is equivalent to adding an additional "heat source" into the D/Pd system. The quicker the T(D) drops, the stronger this additional "heat source", which enlarges the temperature difference between the D/Pd and H/Pd systems.

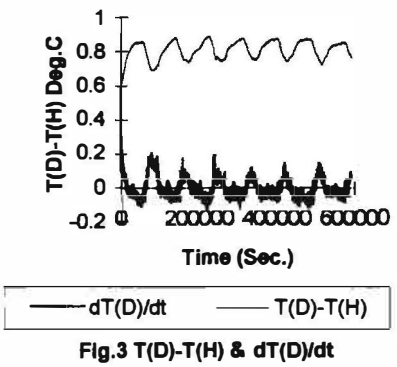

Fig.3 T(D)-T(H) & dT(D)/dt

4. Conclusion.

The "fine tuning" mechanism supports the theory of penetration of the Coulomb barrier via lattice confined ions, and the experiments support this "fine tuning" mechanism by three facts:

$$\rho(E) > \rho_c(E), \qquad \frac{d\rho}{dE} < 0, \qquad \text{and} \qquad \frac{V_{pd}}{k_c} > F_c.$$

A critical "fine tuning" parameter, F_c, is introduced to qualitatively describe this negative feed-back for the "fine tuning" mechanism. In order to make the "excess heat" reproducible, it is important to use large Pd sample (large V_{pd}), good insulation of calorimeter (less k_c), suitable annealing to increase the $\rho(E)$, keep the square-well-like potential field in the Pd ($\frac{d\rho}{dE} < 0$), and keep the high population on that resonance energy level.

Acknowledgments

This work is supported by the State Commission of the Science and Technology, the Natural Science Foundation of China, the Basic Research Fund of Tsinghua University. Many thanks to Mr. Karl Chang, the Co-founder of the VeriFone Inc., for his generous support.

References

[1] X. Z. Li, "Solving the Puzzle of Excess Heat without Strong Nuclear Radiation", Proceedings of ICCF-5, April 9-13, 1995, Monte-Carlo, Monaco, p.285.

[2] X. Z. Li, et al. "Excess Heat Measurement in Gas-loading D/Pd System", Presentation on ICCF-6, Oct. 13-17, 1996, Toya, Hokkaido, Japan.

[3] F. S. Bu, X. Z. Li, "Loading Ratio Study in a Gas-Loading System", Presentation on ICCF-6, Oct. 13-17, 1996, Toya, Hokkaido, Japan.

[4] M.C.H. Mckubre et al., "Concerning Reproducibility of Excess Heat Production", Proceedings of ICCF-5, April 9-13, 1995, Monte-Carlo, Monaco, p.17.

[5] T.A. Green, T.I. Quickenden, "Calorimetric Studies of Highly Loaded Deuterides and Hydrides of Palladium", J.Electroanal. Chem, 389(1995), 91.

[6] M.C.H. Mckubre et al., "Excess Power Observation in Electrochemical Studies of the D/Pd System; the Influence of Loading", Proceedings of ICCF-3, Oct. 21-25, 1992, Nagoya, Japan, p.5.

[7] K. Kunimatsu, N. Hasegawa et al. "Deuterium Loading Ratio and Excess Heat Generation during Electrolysis of Heavy Water by a Palladium Cathode in a Closed Cell Using a Partially Immersed Fuel Cell Anode," ibid. p.31.

[8] M. H. Miles, et al., "Heat and Helium Production in Cold Fusion Experiments", Proceedings of ICCF-2, June 29-July 4, 1991, Como, Italy, p.353; J. of Physical Chem. 98 (1994) 1948.

[9] M. Fleischmann, S. Pons. "Calorimetry of the Pd-D_2O system: from Simplicity via Complications to Simplicity", Physics Letters A, 176 (1993)118.

[10] N.S. Lewis, et al., "Searches for Low-Temperature Nuclear Fusion of Deuterium in Palladium", Nature, 340 (1989)525.

[11] Y. Fukai, "The Metal-Hydrogen System", Spring-Verlag Berlin, Heidelberg (1993) p.148.

Excess Energy and Nuclear Products

Cold Fusion and Electrophysical Processes in Ferroelectric Deuterated Crystalls. Influence of Thermal Neutron BackgroundLevel, D-H Substitution and Crystal Mass

A.G.Lipson, V.A.Kuznetsov, D.M.Sakov, E.I.Saunin

Institute of Physical Chemistry,
The Russian Academy of Sciences, Moscow 117915 Russia

Abstract

Change in neutron flux intensity upon the passing through $K(D_xH_{1-x})_2PO_4$ crystals in the vicinity of Curie point depending on thermal neutron background level, its mass and D-H substitution index (x) has been studied. The semi-empirical equition that describes neutron emission processes in DKDP crystals near T_C quite correctly, has been proposed.

1.Introduction

As it was shown earlier [1-3], upon the transition through Curie point in $K(D_xH_{1-x})_2PO_4$ crystals (DKDP) with x=0.98; 0.96 and 0.80 at the conditions of external thermal neutron background irradiation, the excess emission of fast neutron is observed. In common case it may be amplification or attenuation of external thermal neutron flux passing through crystal in the vicinity of Curie point. As result emission of neutron in these crystals can get positive or negative sign (with subtraction of background value). Simultaneously in DKDP crystals the suppression of spontaneous deformation, defects and cracks formation are observed. In present work we will demonstrate that absolute value of neutron emission and its sign (positive or negative one) is depend upon external thermal neutron flux, crystal mass and its D-H substitution degree.

2. Experimental part

The samples consisted of ferroelectric single crystals of $K(D_xH_{1-x})_2PO_4$ with x=0.96 and x=0.80. Their Curie points are T_C=219 K and T_C=190 K in accordance with calorymetric measurments. Samples with mass from $5*10^{-2}$ g up to 11.0 g were cut from single-crystalline plate in (001) direction. The temperature position and polarization reversal of ferroelectric phase transition were monitored by the registration of pirocurrent signals in the non-polarized samples near T_C with the help thermostimulated depolarisation (TSD) technique. The samples were heated and cooled in a linear regime at a rate of 0.15 K/s.

To determine change in a neutron flux and to create flux of

thermal neutrons one the experimental set up shown in fig.1 has been used. A Cf^{252} source of neutrons with intensity ~ 200 n/s in solid angle of 4 π was used for experiments with neutron fluxes of different intensity. The source was placed at a distance r_1=6 cm from the surface of the sample, which in turn was located at a distance r_2=6 cm from the neutron detector. The change in detector's neutron background (N_x) was reached by change in free space volume inside the PE box (addition or removal of "neutrostop" blocks). Measurements show, that in the range of neutron detector background values of $1 \le N_x/N_o \le 270$ (where N_o - is a detector counts for a cosmic neutron background) the flux of thermal neutron passing through DKDP crystal is in a range of $0.1 \le I_x \le 25$ n/s*cm^2 (where I_o=0.1 n/s*cm^2 - cosmic background flux).

Typical results of simultaneous measurments of a neutron emission and TSD in DKDP crystals with x=0.96 and x=0.80 are shown in fig.2,3. In the case of DKDP with x=0.96 m=2 g (fig.2a) at background I_x/I_o=100 the amplification of neutron emission intensity (ΔN) has place. The emission intensity is about of 20 times more than for crystal temperature cycled in the cosmic background conditions. Moreover in the TSD spectrum the changes are observed, that indicate on change in domain structure of DKDP (x=0.96) under the action of ultraweak thermal neutron flux (fig.2, curve 1,2).

In the case of DKDP (x=0.80 m=4 g) in the cosmic background conditions a weak positive neutron emission is observed ($\Delta N>0$). But at I_x/I_o=100 the sign of ΔN is changed, that is indicate on appearance of attenuation of external thermal neutron flux effect. The change in TSD spectrum at $I_x/I_o>100$ in contrast to cosmic background conditions is corresponding to suppression of spontaneous deformations in partialy deuterated DKDP crystals [1].

3.Discussion

The balance of amplification-attenuation processes in DKDP crystal near T_C upon the passing through it of external thermal neutron flux is deutermining by:

a) the process of inelastic scattering of thermal neutrons on lattice deuterons, that is lead to "positive" neutron emission"$\langle N_{ef} \rangle$ (in reference to background flux);

b) the process of capture of background thermal neutrons by the [DH] complex located in crystal, i.e. by the "negative" neutron emission $\langle N_{ef} \rangle^-$.

Taking to account a previous work data [3] it can be shown that

$$\langle N_{ef} \rangle^+ = x P_D P_n I_n \qquad (1)$$

where P_D - is probability of background thermal neutron

scattering on lattice DKDP deuteron; P_n - is probability of deuteron-donor splitting by coherent multiphonon excitation (CME) with taking to account neutron diffusion depending on I_x/I_o or probability of dd-reaction initiation by the neutron Mossbauer effect [4,5].
I_n - neutron yield (n/cm^3*s) in thermonuclear dd-reaction, to be occur on the spheres surrounding CME (on the isoenergetic surface ε=22.5 keV [3]).

The captured in DKDP crystal part of neutron flux $\langle N_{ef} \rangle$ can be obtained by the next way:

$$\langle N_{ef} \rangle = \frac{6\, P_n(DH)\, F_x}{V_c^{1/3}} \qquad (2)$$

where $P_n(DH)$ - is a probability of thermal neutron capture by [DH] complexes with taking to account thermal neutron diffusion, which depends upon the I_x/I_o ; F_x - is a thermal neutron flux passing through the crystal; V_c - is a volume of crystal.

Therefore the total expression for balance of neutron effects in DKDP crystal near T_C depending on relative value of thermal neutron background (I_x/I_o); D-H substitution index (x) and crystal mass ($m=V_c\rho$) will assume the form:

$$\langle N_n \rangle = x\, P_D\, P_n(D)\, I_n - \frac{6\, P_n(DH)\, F_x\, \rho^{1/3}}{m^{1/3}} \qquad (3)$$

This semiempirical equation is valid only for DKDP crystal with mass more than some crytical value [3]:

$$m_{crit} \geq \left[\frac{n\, \rho^{2/3}}{6\, I_o\, k\, [1-P_n(D)]\, [1-P_n(DH)]} \right]^{3/4} \qquad (4)$$

where $n \sim (N_x/N_{max})^{1/2}$ - is a minimum number of thermal neutrons (passing through the crystal for ferroelectric phase transition time) that can initiate "effect" N_n (3) more than 1 standard diviation σ higher then background; here N_x - is a current indication of detector which corresponds to flux I_x N_{max} - a maximum indication of detector in used geometry of experiment. Semiempirical equation (3), with taking to account condition (4) makes it possible to compute theoretical dependences of $N_n(I_x/I_o)$ $N_n(x)$ and $N_n(m)$, which are in a good agreement with experimental results (fig. 4-8).

4. Conclusion

Data obtained, make it possible to conclude that to observe non-zero neutron effects in deuterated non-equilibrium crystals

it is necessery, in each case, to optimize crystal parameters and external thermal neutron background. At $m>m_{crit}$ as well as corresponding values I_x/I_o and x with taking to account crystal structure perfection, it is possible to obtain reproducible results, that, in fact, are a value of balance between amplification and attenuation of external (background) neutron flux.

References

1. Lipson A.G., Sakov D.M., Saunin E.I. // JETP Lett. 62 (10) 828 (1995).

2. Lipson A.G., Sakov D.M., Saunin E.I. // Rus J.Tech.Phys.Lett. 22(2) 8 (1996).

3. Lipson A.G., Sakov D.M., Saunin E.I., Kuznetsov V.A. // Rus.J.Tech.Phys. 1996 (to be published).

4. Kozima H // Nuovo Cimento A27 , 1781 (1994).

5. Hagelstein P.L. // Trans Fusion Tech. 26T , 461 (1994).

Captions to figures

Fig.1. Experimental arrangement 1 - Polyethlene (Co), 2 - detector; 3 - counters; 4 - silicone oil; 5 - Cd foil; 6 - cryostat with DKDP crystal (TSD cell), 7 - Cf^{252} neutron source

Fig. 2. TSD spectra and neutron emission intensity for DKDP (x=0.96) crystals cooling (heating) in the vicinity of T_C: curves 1 - TSD spectra for N_x/N_o=100 condition; curves 2 (dashed line) - TSD spectra for cosmic neutron background conditions (N_x/N_o=1); curves 3 - neutron emission intensity with subtraction of background (counts obtained out $T>T_C$ and $T<T_C$).

Fig. 3a. TSD spectra and neutron emission intensity for DKDP (x=0.80) crystals upon cooling in the vicinity of T_C: curve 1 - TSD spectrum for cosmic background condition (N_x/N_o=1) : curve 2 - neutron emission intensity with subtraction of background.

Fig. 3b. Just the same as fig.3 a, but for N_x/N_o=100 (TSD peak is shifted on 4K in the field of lower temperatures (curve 1); ΔN was negative sign (curve 2).

Fig. 4. Neutron yield versus crystal mass at cosmic thermal neutron background (N_x/N_o=1) for DKDP crystals (x=0.96; 0.80; 0.60) upon the transition through T_C. Theoretical curves derived from equations (3), (4) (Points with standard deviations are obtained from experiment).

Fig. 5. Neutron yield versus crystal mass for DKDP (x=0.96 and x=0.80) upon the transition through T_C at thermal neutron background N_x/N_o=100. Theoretical curves derived from (3), (4) (Points with standard deviations are obtained from experiment).

Fig.6. Neutron yield versus background conditions (N_x/N_o) for DKDP (x=0.96, m=2 g) crystal upon the transition through T_C.

Fig. 7. Neutron yield versus D-H substitition index (x) in cosmic background conditions (N_x/N_0=100, m=3 g).

Excess Energy and Nuclear Products

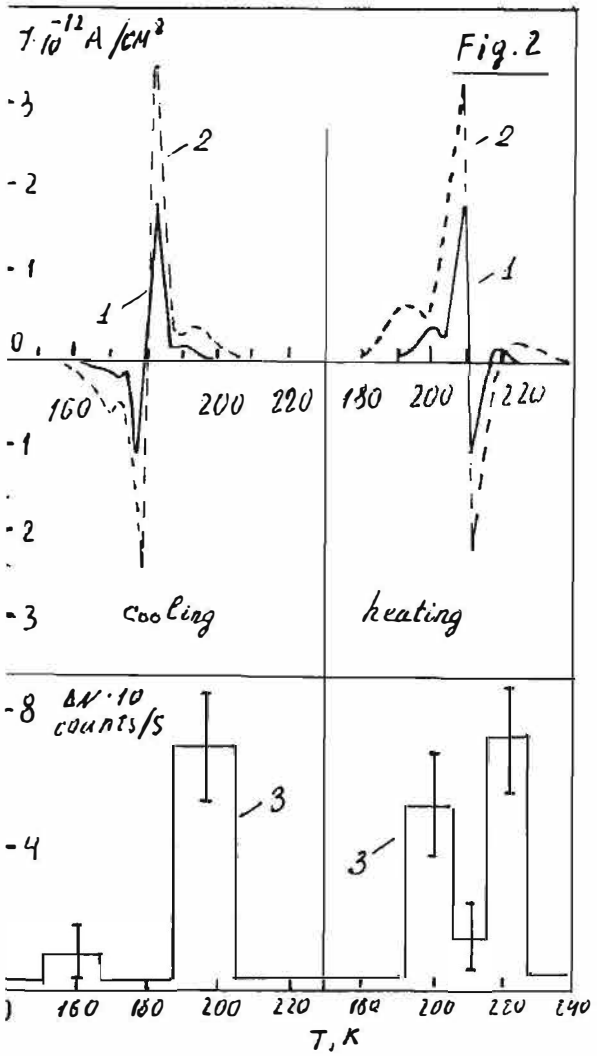

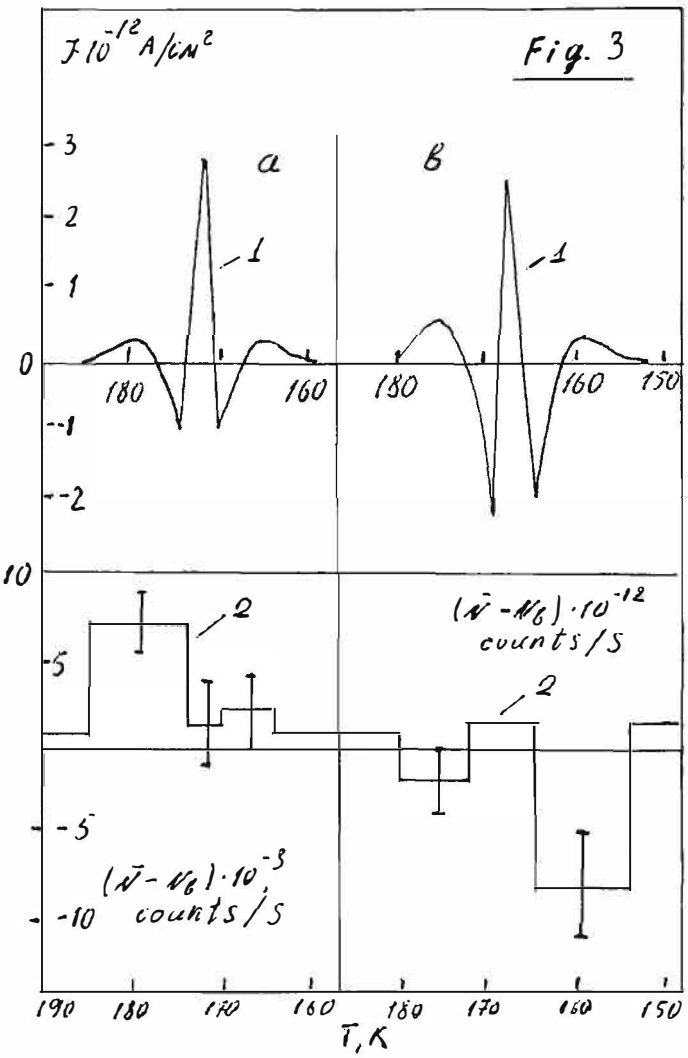

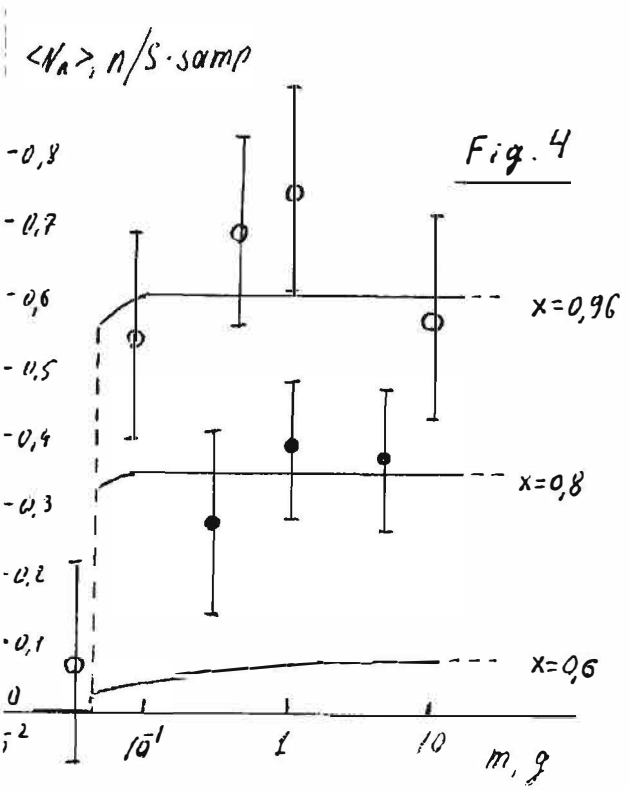

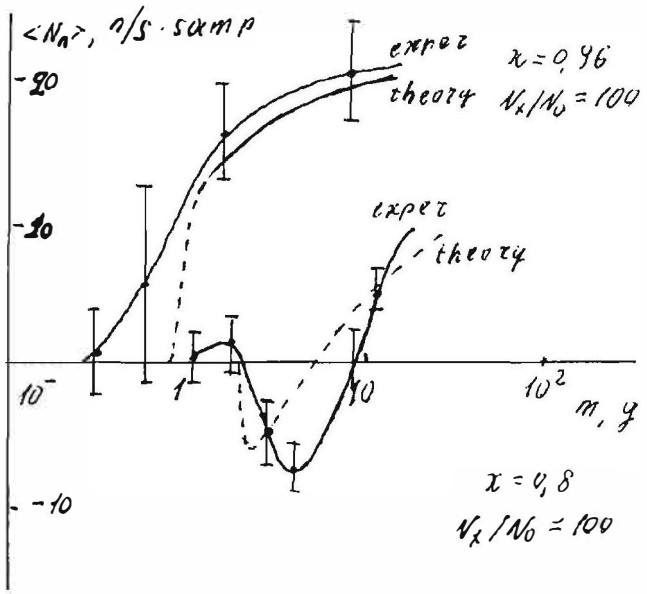

Fig. 5

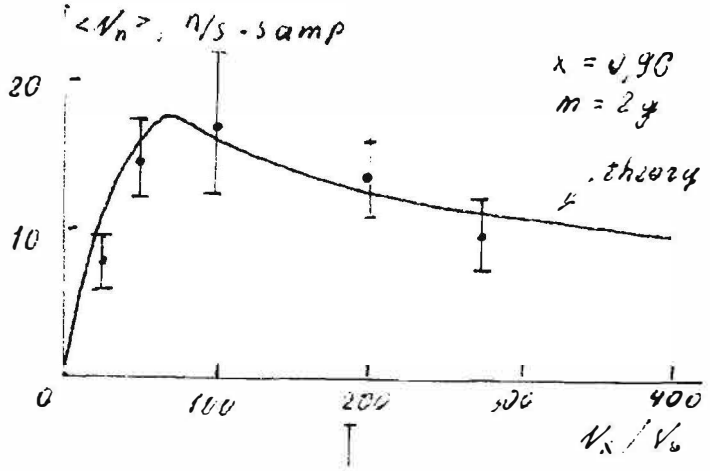

Fig. 6

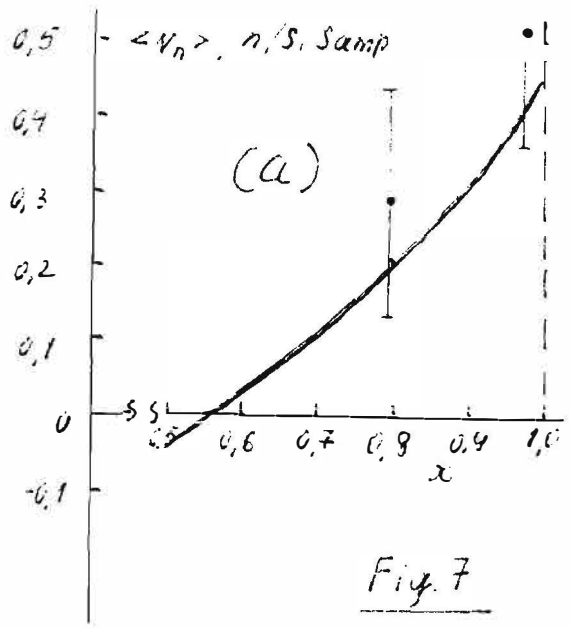

Fig. 7

Fig. 1

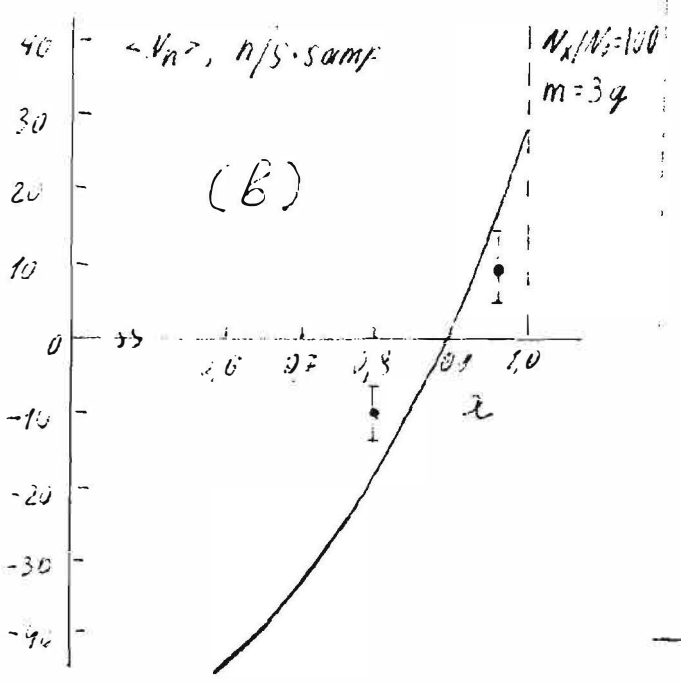

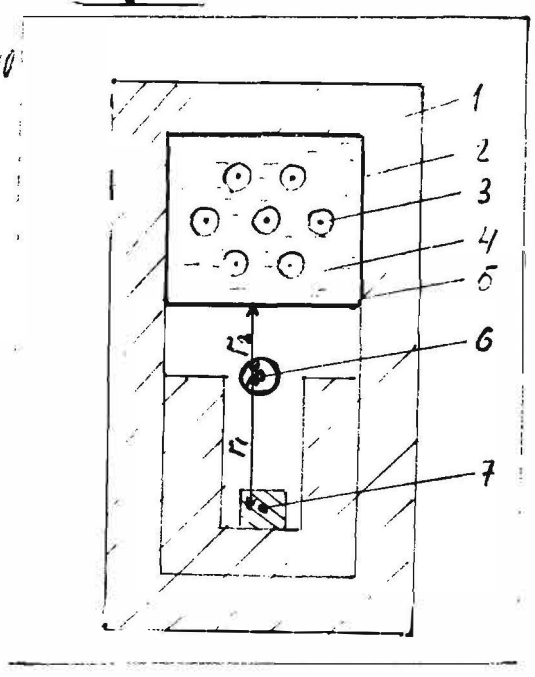

Electron-ion bound state and its introducing of nuclear fusion and solar flare

Lu Runbao

Institute of Applied Physics and Computational Mathematics,

P. O. Box 8009, Beijing 100088, CHINA

Abstract **A strict description of quantum mechanics on electron-ion bound state three-body system and two approximate solutions are given, which are (1) corresponding to monoenergetic X rays emission from p-e-p bound state with $E_P \approx$ 12.5 keV, and (2) emission from D^+-e-D^+ bound state with $E_D \approx$ 25 keV, which also introduces a little D-D fusion to give out neutrons, protons, tritium, ^{3}He, ^{4}He, and Gamma rays. In this paper some experiments such as Ni-H, deuterium gas glow discharge, are explained. The energy about the excess heat is just a large quantity of X rays release from two electron-ion bound states mentioned above, and only (D^+-e-D^+) bound state can introduce nuclear fusion. The author further analyses a large quantity of the measurement of solar flare energy spectrum and points out that the solar flaring also contains the processes of emitting monoenergetic X rays of 12.5keV and 25keV and the latter introduces a little (D-D) fusion.**

1 Introduction

In this paper the author discusses two questions: (1) the generation mechanism of so called "cold fusion" can be discribed by "electron-ion bound state and its introducing of nuclear fusion"; (2)the solar flare and "cold fusion" are same physical process essentially.So the author contributes new concept and new research field.

2 Description of electron-ion bound state with quantum mechanics

This problem can be considered through quantum mechanics. The distances between particles in the (p,e,p) and (D^+,e,D^+) systems are approximate or less than Bohr radius under the special condition of bound states [1]. Because of the strong electromagnetic interaction, Born-Oppenheimer approximation is now unsuitable for this problem, which

approximation is now unsuitable for this problem, which must be calculated with three-body problem. Reference [1] simplified the three-body problem to two-body problem in accordance with an approximation of average potential.

Let the coordinates of particles be $x_1, x_2 and\ x_3$, respectively, and $x_3 > x_2 > x_1$, which can be shown as follows:

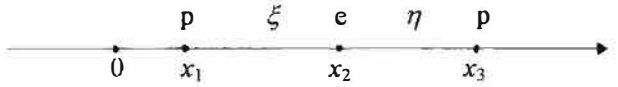

Hamiltonian of this system, without regard to nuclear force, can be written as:

$$\hat{H} = -\frac{\hbar}{2}\sum_{i=1}^{3}\frac{1}{m_i}\frac{\partial^2}{\partial x_i^2} + \frac{e^2}{x_3 - x_1} - \frac{e^2}{x_2 - x_1} - \frac{e^2}{x_3 - x_2} \qquad (1)$$

where subscripts i=1,3 represent protons or deuterium ions and i=2 represents electrons.

To remove the center-of-mass motion [2], we suppose

$$X = \frac{1}{M}\left(m_1 x_1 + m_2 x_2 + m_3 x_3\right), \quad M = m_1 + m_2 + m_3$$
$$\xi = x_2 - x_1, \quad \eta = x_3 - x_2, \quad x_3 - x_1 = \xi + \eta$$

On the new coordinates representation, we have

$$\sum_{i=1}^{3}\frac{1}{m_i}\frac{\partial^2}{\partial x_i^2} = \frac{1}{M}\frac{\partial^2}{\partial X_i^2} + \left(\frac{1}{m_1} + \frac{1}{m_2}\right)\frac{\partial^2}{\partial \xi^2} + \left(\frac{1}{m_3} + \frac{1}{m_2}\right)\frac{\partial^2}{\partial \eta^2} - \frac{2}{m_2}\frac{\partial^2}{\partial \xi \partial \eta} \qquad (2)$$

Substituting Eq.(2) to Eq.(1) and removing the part of center-of-mass motion (which has no effects on the formation of material structure), Schrodinger equation on the new coordinate system can be written as:

$$-\frac{\hbar^2}{2}\left[\left(\frac{1}{m_1} + \frac{1}{m_2}\right)\frac{\partial^2}{\partial \xi^2} + \left(\frac{1}{m_3} + \frac{1}{m_2}\right)\frac{\partial^2}{\partial \eta^2} - \frac{2}{m_2}\frac{\partial^2}{\partial \xi \partial \eta}\right]\Psi$$
$$-e^2\left[\frac{1}{\xi} + \frac{1}{\eta} - \frac{1}{\xi + \eta}\right]\Psi = E\Psi \qquad (3)$$

From the selection of coordinates we know that: $-e^2\left[\frac{1}{\xi} + \frac{1}{\eta} - \frac{1}{\xi + \eta}\right] < 0$, which means that the system always has a negative potential. As a result, the system has negative energy levels, i.e., the existence of bound states.

To remove the cross differential operator, we introduce a coordinate transformation: $\xi = \left(1/\sqrt{2}\right)\left(\xi' - \eta'\right), \quad \eta = \left(1/\sqrt{2}\right)\left(\xi' + \eta'\right)$. Substituting them to Eq.(3), for p-e-p system (m_1 =

$m_3 = m_p$, $m_2 = m_e$, $1/m_p + 2/m_e \approx 2/m_e$), we obtain

$$-\frac{\hbar^2}{2}\left[\frac{1}{m_p}\frac{\partial^2}{\partial\xi'^2}+\frac{2}{m_e}\frac{\partial^2}{\partial\eta'^2}\right]\Psi-\sqrt{2}e^2\left(\frac{1}{\xi'-\eta'}+\frac{1}{\xi'+\eta'}-\frac{1}{2\xi'}\right)\Psi = E\Psi \quad (4)$$

Eq.(4) is a standard Schrodinger equation, which always has a negative potential. Strict solution of this equation will be carried out in future. To find its physical meanings we consider a quasi-stationary state, i.e. $|\eta'| << \xi'$.

After some approximate process, we can get [3]

$$E_{p,n} = -\frac{m_e e^4}{2\hbar^2}\frac{1}{2}\frac{m_p}{m_e}\frac{1}{n^2} \qquad (12.1)$$

$$E_{e,n} = 0 \qquad (12.2)$$

For the ground state, $E_{p,1} = -\frac{1}{2}\frac{m_p}{m_e}\frac{m_e e^4}{2\hbar^2}$, where $\frac{m_e e^4}{2\hbar^2} = 13.55\,\text{eV}$ is the ground state energy of hydrogen, which results that $E_p \approx$ -12.5keV.

Similarly, for D^+-e-D^+ system the energy is about

$$E_D \approx -25\,\text{keV}.$$

These two energies are just the released monoenergetic X rays energies from electron-ion bound states in p-e-p and D^+-e-D^+ systems. The latter can also initiate a little D-D fusion[1], emitting high energy γ Rays, neutrons, protons, tritium, ^{3}He and ^{4}He. Reference [1] discussed the bound states and fusion initiation probability. Probability of bound state formation (i.e., probability of producing X rays) was about 10^4-10^6 times to that of fusion initiation. It is upon this basis that the author interprets that excess heat release from so-called cold fusion is mainly the X rays energy release from bound states. Those two bound states mentioned above are independent processes, which can take place in an independent or adjoint way according to various conditions.

3 Interpretation of so-called cold fusion experiments

3.1 Piantelli experiment[4] (Ni-H system)

There are two results obtained from this experiment, which are (1) excess heat release, with 15g-Ni and 1g-H, producing enough energy for 30-40 W lamp about three months, and (2) that there are not any neutrons or γ-rays recorded, we can estimate the mass of hydrogen according to the p-e-p bound state with emission about 12.5kev x-ray.

$$Q_{emission} = (30 \sim 40)\text{J/s} \times (3 \times 30 \times 24 \times 3600)\ \text{s}$$
$$= (1.46 \sim 19.4) \times 10^{27}\ \text{eV}$$
$$N_p = 2[Q_{thermal} / 12.5\,\text{keV}] = 2(1.46 \sim 19.4) \times 10^{27}\text{eV} / 12.5 \times 10^3$$
$$= 2(0.117 \sim 0.155) \times 10^{24}$$
$$m_p = 2(0.117 \sim 0.155) \times 10^{24} / 6.02 \times 10^{23}\ /\text{g}$$
$$= 0.39 \sim 0.51\ \text{g}$$

Only a half of hydrogen ions formed bound states. I believe that x-rays willl be certainly observed.

3.2 Deuterium gas glow discharge experiment

Wang Dalun *et al*[5] carried out a well-known experiment on deuterium gas glow discharge. There are the following results:(1)energies of monoenergetic x-rays are all about 26.7kev measured with three methods,while the earlier mean energy is about 27kev ; (2)this experiment has also given a stable neutron emission density about 10^4/s, x-ray about 10^9/s.

4 Solar Flare

On the basis of great deal of observed facts the author points out the following:

(1)x-ray emission with monoenergy about 12.5kev is the main component of soft x-ray in solar flares[6]

(2)x-ray emission with monoenergy about 25kev is the main component of hard x-ray in soalr flares[7]

(3)the (d,d) fusion existence is proved by observation of proton spectrum, 2.223Mev γ-line, ^{3}He-rich ...[8]

(4)the x-ray in solar flare comes from formation of p-e-p or d^+-e-d^+ bound state,there are not nonthermal electrons by which the impulsive component of x-ray is produced during flash phase. Observed leakage electrons are produced in process of Compton scattering[9]

(5)delay of energetic x-ray emission in solar flare[10] and "heat after death"[11,12], "rediation after death"[13,14] have common cause that comes from secondary effects of (d,d) fusion.

Acknowledgment

The author wishes to thank Qian Xueshen, Chen NengKuan and Hong MingYuan for their encouragement and help; and Wu Yanbing, director of editorial department of High Power Laser Particle Beams, for his useful comments and discussions in the final revision of this manuscript.

This work is supported by the Natural Science Foundation in China and China Engineering Physics Academy.

References

1. Lu Runbao, *High Power Laser & Particle Beams*, **6**(4):615-621, 1994
2. Zeng Jinyan, *Quantum Mechanics*, Science Press , Beijing, 1989
3. Lu Runbao, electron ion bound state and its introducing of nuclear fusion, to be published in *High Power Laser & Particle Beams*, *1996*
4. Focardi S, Habel R, and Piantelli F, IL *Nuovo CIMENTO*, 107A(1), 1994
5. Wang Dalun, Chen Suhe, et al, *Trends in Nuclear Physics*, **12**(4), 1995
6. Lu Runbao, X-ray emission with monoenergy about 12.5kev in solar flares, manuscript submit to *ACTA Astronomica Sinica*
7. Lu Runbao, X ray emission with monoenergy about 25kev in solar flares, manuscript submit to *ACTA Astronomica Sinica*
8. Lu Runbao, The (d,d) fusion in solar flares, manuscript submit to *ACTA Astronomica Sinica*
9. Lu Runbao, Nonthermal electrons in solar flares, manuscript submit to *ACTA Astronomica Sinica*
10. Lu Runbao, Delay of energetic X ray emission in solar flares, manuscript submit to *ACTA Astronomica Sinica*
11. S.Pon`s and H.Fleischmann, ICCF4, C2.12.1994
12. Y.Arata and Yue-Chang Zhang, ICCF4, C2.3.1994
13. Liu,Hung-qiuan et al, Report on national symposium on "normal temperature nuclear fusion" in China 1996
14. LI.Xing-zhong, Infinite Energy 1995.11-1996.2 p59

Excess Energy and Nuclear Products

Reply to S. E. Jones and L. D. Hansen Concerning Claims of Miles, et al. in Pons-Fleischmann-Type Cold Fusion Experiments

Melvin H. Miles

Chemistry & Materials Branch, Research & Technology Division
Naval Air Warfare Center Weapons Division
China Lake, CA 93555-6100 USA

Abstract

The simultaneous measurements of power and the rate of evolution of the electrolysis gases in our experiments prove that faradaic efficiencies less than 100% cannot account for our reports of excess heat. Furthermore, our calorimetric results are strikingly similar to reports from other laboratories including measurements in closed calorimetric systems where faradaic efficiencies are not a factor. Excess enthalpy for the Pd/D_2O system generally involves high current densities that exceed 100 mA/cm^2; therefore, the report by S. E. Jones et al. of low faradaic efficiencies using current densities of only 1 to 2 mA/cm^2 is not applicable to cold fusion experiments. Based on experiments at our laboratory, there is compelling evidence that the anomalous excess heat is correlated with helium-4 production. For example, 30 out of 33 heat and helium studies yielded either excess helium when excess power was measured or no excess helium when no excess power was present. The probability of obtaining this result by random errors in our heat and helium measurements is very small. Permanent laboratory records always defined the presence or absence of excess power prior to any helium measurement. The measurement of helium in the electrolysis gas samples at three different laboratories places our rate of helium-4 production at 10^{11} to 10^{12} atoms/s per watt of excess power. This is the correct magnitude for typical deuteron fusion reactions that produce helium-4 as a product.

1. Introduction

This paper is a response to S. E. Jones and L. D. Hansen[1] who critically examined our claims of excess heat and helium-4 production during electrolysis of the Pd/D_2O + LiOD system.[2] Excess enthalpy for the Pd/D_2O system generally involves high current densities that exceed 100 mA/cm^2. Therefore, the report by S. E. Jones et al.[3] of low faradaic deficiencies using current densities of only 1 to 2 mA/cm^2 is not applicable to cold fusion experiments.

2. Excess Heat Production

Many scientists attribute reports of excess power production in cold fusion experiments to calorimetric errors. This is reflected in the publications by S. E. Jones et al.[1,3] However, it is nearly impossible to explain how calorimetric errors could lead to practically identical results between independent laboratories. For example, the major conclusions from the China Lake calorimetric experiments are almost identical to those reported by M. McKubre et al. at SRI.[4,5] The excess power measurements in the China Lake experiments can be summarized by the following conclusions:

Approved for public release; distribution is unlimited.

Excess Energy and Nuclear Products

1. The excess power effect is typically 5 to 10% larger than the input power. The largest excess power effect was 30%.
2. The excess power in terms of the palladium volume typically yields 1 to 5 W/cm^3.
3. Long electrolysis times are required before the onset of the excess power effect. This time period usually ranges from 6 to 14 days of electrolysis for 1 to 6 mm diameter palladium rods.
4. Excess power production requires a threshold current density of 100 mA/cm^2 or larger.
5. Most experiments produced no evidence of any excess power. Overall, only 30% of our experiments yielded evidence for excess power.
6. Our success ratio in obtaining excess power varied greatly with the source and batch of palladium used.

The SRI results typically yielded 5 to 10% excess power with a maximum of 28% excess power, the excess power in terms of the palladium volume was 1 to 5 W/cm^3 on the average, the initiation time was on the order of 300 hours for 1 to 4 mm diameter Pd wires, the threshold current density ranged from 100 to 400 mA/cm^2, and the success rate varied greatly with the source of the palladium.[4,5] This striking agreement between the China Lake and SRI results simply cannot be explained by calorimetric errors. Furthermore, the calorimeters used at China Lake and SRI are totally different. China Lake used an open, isoperibolic calorimetric system[2] while SRI employed a closed, isothermal flow calorimetric design.[5]

The China Lake calorimetric results are also very similar to those reported by M. Fleischmann et al.[6] when the excess power density (W/cm^3) in terms of the palladium volume is compared with the experimental current density. Both China Lake and M. Fleischmann et al.[6] report approximately 1 W/cm^3 of palladium at current densities of 100 to 200 mA/cm^2. In a review by E. Storms,[7] the China Lake calorimetric excess heat effects are shown to be very similar to those reported by many other laboratories. This leaves the unanswered question of how calorimetric errors could yield this correlation of our excess heat results with various other laboratories.

The accuracy of our calorimetry is illustrated in Figure 1 that features one of many experiments that never displayed any evidence for excess power. The measured output power tracks very closely to the electrochemical input power. Approximately 70% of our experiments never displayed any evidence for excess power. These studies, therefore, served as controls for our calorimetry.

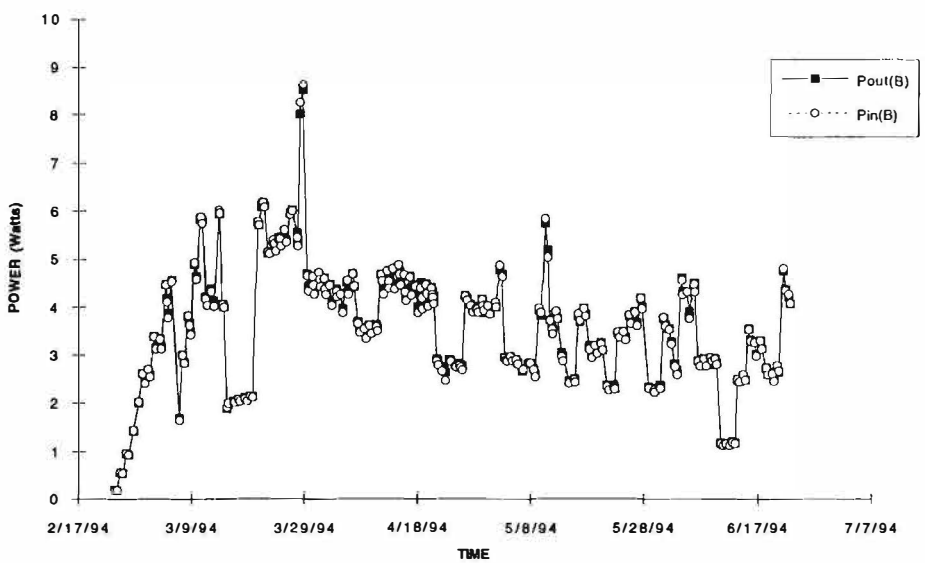

Figure 1. Electrochemical Input Power and Calorimetrically Measured Output Power for a Palladium Cathode That Produced No Excess Power.

Excess Energy and Nuclear Products

Many experiments have proved that the recombination of D_2 and O_2 electrolysis gases does not occur to any significant level for typical cold fusion studies using high current densities and solid, fully-submerged palladium cathodes.[2,7] Some scientists, however, ignore this evidence and continue to claim that the excess heat effect can be explained by faradaic efficiencies less than 100% ($\gamma < 1$).[3] The recombination effects for Ni and Pd cathodes reported by Jones et al.[3] used current densities of only 1 to 2 mA/cm^2. Such studies are irrelevant since excess heat effects for the Pd/D_2O system require a threshold current density of about 100 mA/cm^2 or higher. This requirement of high current densities was reported by M. Fleischmann et al.[6] in 1990. Lowering the current density in water electrolysis experiments will always decrease the current efficiency due to the slower gas evolution that allows the product at one electrode to more readily invade the vicinity and react at the opposing electrode. Furthermore, the current fraction consumed by the electrode reaction of impurities becomes larger at smaller current densities. Contrary to the comments by Jones and Hansen,[1] we always measured the current efficiency at the time of collection of an electrolysis gas sample for helium analysis. This was done volumetrically by measuring the rate of the displacement of water by the electrolysis gases.[2]

Several other measurements and observations provided secondary checks for any recombination of D_2 and O_2 in our experiments. The volume of D_2O added to replenish the cell was always recorded to provide another test for any significant recombination effects. Furthermore, the rate of the electrolysis gases passing through the oil bubbler could always be directly observed. If recombination of D_2 and O_2 within the electrolysis cell occurs, this would slow or even stop the evolution of gases through the bubbler.[8]

3. Helium-4 Production in Electrolysis Cells

A major point raised by S. E. Jones and L. D. Hansen[1] was that our helium-4 detection limit was first reported as 10^{12} atoms/500 mL of effluent gases and then later increased to 10^{13} ^{4}He atoms/500 mL. Our earlier limit was based on measurements at the University of Texas laboratory where 10 mTorr air in 500 mL of nitrogen gas yielded the observation of helium-4 at the detection limit of the mass spectrometer.[9] We originally used a conservative value because we did not want to overstate the amount of helium-4 produced in our experiments.

Solid evidence that we should have originally reported considerably higher helium-4 production rates was obtained in later studies where the electrolysis gas samples were collected in metal flasks rather than in Pyrex glass flasks and then analyzed by a commercial laboratory.[10] For six control experiments yielding no excess power, the mean background helium concentration in our system was 4.5 ± 0.5 ppb or $5.1 \pm 0.6 \times 10^{13}$ ^{4}He atoms/500 mL.[10,11] These values, therefore, accurately define a minimum helium-4 detection limit for our original studies. In order to clearly resolve this helium-4 detection limit issue, exactly the same procedures and apparatus were used in these experiments except for the replacement of the glass flasks with the metal flasks. This eliminated the diffusion of atmospheric helium into the sample flasks. These quantitative commercial measurements of background helium-4 concentrations in our calorimetric system dictated an upward revision of our original helium reports.

In retrospect, the higher helium-4 detection limit resolves the issue of atmospheric helium diffusion into our glass flasks and is consistent with the detection limits reported by a commercial laboratory.[10,11] Furthermore, this higher helium-4 detection limit yields helium production rates of 10^{11} to 10^{12} ^{4}He/s•W, which is the correct magnitude for typical fusion reactions that yield helium as a product.[10] The consistent merging of these various results would have been highly improbable if our initial measurements were due to errors or atmospheric contamination. Nevertheless, the revision in our helium-4 detection limit was a major issue raised by S. E. Jones and L. D. Hansen[1] in their criticism of our work. Our explicit explanations for this change[10] were completely ignored.

Excess Energy and Nuclear Products

S. E. Jones and L. D. Hansen[1] report that our designation of an experiment as a "control" is done after the experiment is run, not before. Neither Jones nor Hansen has been in our laboratory, hence they have no basis for such a statement. Permanent laboratory records always defined the amount of excess power prior to any helium measurements. In general, excess power was consistently produced in experiments that yielded excess helium-4 production, while no excess power was detected in experiments that served as controls.

Based on experiments at our laboratory, there is compelling evidence that the anomalous excess heat is correlated with helium-4 production. For example, 30 out of 33 heat and helium studies yielded either excess helium when excess power was measured or no excess helium when no excess power was present.[8,11] A statistical treatment shows that the odds are approximately one in 750,000 that our complete set of heat and helium results could be this well correlated due to random experimental errors in our calorimetry and helium measurements.[8,11] It is even more unlikely that random errors would consistently yield helium-4 production rates in the appropriate range of 10^{11} to 10^{12} atoms/s per watt of excess power.

4. Conclusions

Although S. E. Jones and L. D. Hansen[1] presented many harsh comments about our experiments, we were never officially informed about their paper by the authors, reviewers, or editors involved. Even after we requested a delay of this publication to allow a response to be published back-to-back, the authors and editors refused our request. Our detailed response to this attack by Jones and Hansen has been submitted but has not yet been accepted for publication.[12]

S. E. Jones and L. D. Hansen[1] ignored our previous explanation on many issues that are contained in our publications. Their mixture of facts, distortions, and misunderstandings regarding our work certainly does not facilitate any scientific resolution of the cold fusion controversy.

Jones et al.[3] used current densities of only 1 to 2 mA/cm^2 in their studies of faradaic efficiencies during water electrolysis. Excess enthalpy for the Pd/D_2O system involves much larger current densities that exceed 100 mA/cm^2. It is essential that Jones et al.[3] use current densities in the right ballpark if they wish to investigate faradaic efficiencies in cold fusion experiments. The arguments of Jones et al.[3] are not relevant for the large current densities used in cold fusion experiments.

5. Acknowledgment

Appreciation is extended to the Office of Naval Research for support of this work.

6. References

1. S. E. Jones and L. D. Hansen, *J. Phys. Chem.*, **99**, 6966 (1995).
2. M. H. Miles, R. A. Hollins, B. F. Bush, and J. J. Lagowski, *J. Electroanal. Chem.*, **346**, 99 (1993).
3. J. E. Jones, L. D. Hansen, S. E. Jones, D. S. Shelton and J. M. Thorne, *J. Phys. Chem.*, **99**, 6973 (1995).
4. M. C. H. McKubre, S. Crouch-Baker, A. K. Hauser, S. I. Smedley, F. L. Tanzella, M. S. Williams and S. S. Wing in Proceedings of the 5th International Conference on Cold Fusion, Monte Carlo, Monaco, 9-13 April 1995, pp. 17-33.
5. M. C. H. McKubre, S. Crouch-Baker, R. C. Rocha-Filho, S. I. Smedley and F. L. Tanzella, *J. Electroanal. Chem.*, **368**, 55 (1994).
6. M. Fleischmann, S. Pons, M. W. Anderson, L. J. Li and M. Hawkins, *J. Electroanal. Chem.*, **287**, 293 (1990).
7. E. Storms, *Fusion Technol.*, **20**, 433 (1991).
8. M. H. Miles, B. F. Bush and K. B. Johnson, "Anomalous Effects in Deuterated Systems," NAWCWPNS TP 8302 (September 1996).
9. B. F. Bush, J. J. Lagowski, M. H. Miles and G. S. Ostrom, *J. Electroanal. Chem.*, **304**, 271 (1991).
10. M. H. Miles and B. F. Bush, *Transactions Fusion Technol.*, **26**, 156 (1994).
11. M. H. Miles, K. B. Johnson and M. A. Imam, "Heat and Helium Measurements Using Palladium and Palladium Alloys in Heavy Water" in Proceedings of the Sixth International Conference on Cold Fusion, Hokkaido, Japan, 13-18 October 1996 (submitted).
12. M. H. Miles, *J. Phys. Chem.* (submitted).

Excess Energy and Nuclear Products

Field Screened Long Range Nuclear Reactions by Thermal Protons

Heinrich Hora, George H. Miley* and Jak C. Kelly
School of Physics, Univ. of New South Wales, Sydney 2052, Austrnlia;
*Fusion Studies Lab., Univ. Illinois, Urbana 6 l 801, USA.-

Abstract
Confirmation of the model of field screened long range nuclear reactions has been obtained from the isotopes produced by nuclear Reactions In a Film-Excited CompleX (RIFEX) using nickel and nickel/palladium films, electrolytically loaded with hydrogen. The isotopes result from thermal proton (or deuterium or triton) reactions. The process is based on high Coulomb screening including the Swimming Electrons of the double Layer (SEL) at the surface of metals or at the interfaces between different metals due to the differences of the Fermi levels. These long range reactions for the low energy (nearly thermal) impact nuclei permits very long interaction times at the large distances. The quantum relations for the values of the energies, distances and times involved are discussed and compared with the situation for the high energies at shorter distances in the usual hot fusion and MeV nuclear reactions. Comparing these long range reactions with fission thermal reactions leads to the suggestion that the missing exchange of large momenta lead to the emission of lower energy gammas. from rotational and vibrational or surface states of the daughter nuclei. These may account for the large amount of energy of the exothermic reactions measured in the RIFEX experiments.

I. Introduction

The recent measurement of nuclear reactions in 2000-Angstrom films of nickel or nickel-palladium, electrolytically loaded with very high concentrations of hydrogen [1] are believed to be due to long range nuclear reactions with thermal protons. These reactions of hydrogen (or its isotopes) with medium or heavy weight nuclei are basically different from the cold fusion reactions [3] for which the long range nuclear reactions at very large Coulomb screening theory was developed [3]. This treatment suggests consideration of other possible reactions between nuclei over large distances, picometers (pm) compared with the usual few femtometers (fm) of nuclear reactions when hadrons or light nuclei of MeV energy or more and heavy nuclei of more than 100 MeV energy collide.

The usual hot fusion reactions, involving nuclei with energies in the 1-10 keV range are reproducible and well understood. We consider a screening model which in certain metals allows 11uch closer nuclear approach than the usual binding conditions [3]. We derive a limiting condition, calculating interaction times to distances, for the nuclear reaction interaction parameters determined by Quantum mechanics It can be proved that these conditions are obeyed by the long-range interactions [3]. Finally we consider long-range nuclear reactions in metals where high concentrations of isotopes have been produced (nuclear transmutations by thermal protons) which are different from the cold fusion reactions in platinum or similar metals. We suggest a mechanism which results in the production of softer gammas of short range hadrons or betas rather than the usual reaction products, MeV neutrons or gammas.

2. The Long Range Anomaly for Hot Fusion

Consider the minimum nuclear reaction distance r to which nuclei approach under central collision for a point like Coulomb repulsion. The kinetic energy of the particles E is then equal to the potential Coulomb energy E_c (in cgs units)

$$E = E_c = e^2/r \qquad (1)$$

where the electron charge e is 4.806×10^{-10} cgs units. If the energy of collision E is 1 MeV, the distance r is 1.43 fm, about the radius of the deuteron. A cross section of this radius corresponds to 64 mbarns, just the value common to nuclear reactions with colliding energies of dozens of MeV.

What is evident is that r = 14.3 fm for a collision energy E of 100 keV corresponds to the cross section of the DT reaction at the 100 keV with the well known cross section radius (impact parameter) r_c = 12.61 fm. This cross section is considered as an exceptionally large value due to "resonances" etc.. We know from the electron scattering experiments after Hofstadter [4][5] that the entire radius of the chargedistribution of deuterons is in the range of 1 fm.

While this view of resonances may still be acceptable, we know that fusion reactions can occur - with low probability - at collision energies of 10 keV though the radius of the collision cross section (impact parameter) for DT is then down to a value r_c = 0.25 fm. What is astonishing is that the minimum reaction distance r, Eq. (1), for central collision at this 10 keV energy E is 142 fm = 0.142 pm, in the order of hundred times the entire radius of the deuteron! How can such a nuclear reaction happen [if there were a Gamov factor one has to realize that $\exp(-100)=10^{-43}$]. Hot fusion reactions measured every day show that it does happen however.

As we had shown before [3], this real measured value and the reaction time together with the distance for the hot fusion of the D and T can be compared with the measurements of a myonic fusion reaction. It can further be compared with the measured reaction time combined with the separation of D and T in a hydrogen molecule and the expected reaction time of 10^{80} s [3]. The result is a straight power law arriving in a reaction probability time U, in seconds, for a distance r, in picometers,

$$U = 8.139 \times 10^4 r^{34.8} \qquad (2)$$

We use this relation below for reactions at larger distances than r = 0.142 pm and up to one order of magnitute larger than in the case of the measured myonic fusion reaction (r = 0.45 pm). Time U and length r are indeed large number quantum statistical values as knwon e.g. from the time of nuclear decay.

3. High Coulomb Screening and the Swimming Electron Layer

The following model was developed [3] to explain some of the reversibly measured cold fusion results of Yamaguchi et al [7] and of Prelas et al [8]. The highly concentrated 50% to 200% hydrogen or deuterium loaded into metals as palladium or titanium [9] is assumed to be not located at fixed points in the crystal, as ligands or other kinds of chemical bond, but to behave like a Maxwellian gas. The degenerate conduction electrons are at least acting as a Coulomb screen and one may assume that the lower bound metal electrons are causing less interaction where the hydrogen or deuterium ions are penetrating, similar to the Ramsauer effect.

While the reduction of the Coulomb field within the bulk material may be of a considerable magnitute, there is a further screening by the swimming electron layers at clean or neutral surfaces (i.e. free of adsorbed molecules or of oxide) or stable and clean interfaces between hydrogen absorbing metals of different kinds. These can be constructed as a series of layers, e.g. nickel-palladium, iron-titanium, nickel-platinum or similar combinations chosen to have the highest

possible Fermi level difference [3][9]. These swimming electron layers are the result of a plasma model of the surface tension for metals, in analogy to a plasma surface or interface. The faster degenerate electrons like to leave the lattice of the metal ions until they are stopped by the generated high electric field. This generates an electric double layer which becomes equal to the electrons' exit potential, the work function. The surface tension calculated on this quantum mechanical basis is in good agreement with experimental values [10]. The surface tension always produces positive values unlike some other previously used phenomenological models.

These electron layers, of about 1 Angstrom thickness, should be sufficient to permit a very high suppression (screening) of the Coulomb repulsion of the positive charges of the hydrogen or deuterium ions. Using Eq. (2) above and the very few fully reproducible cold fusion experiments with D-D reactions [7][8] concluded that this screening reduces the Coulomb repulsion by a factor of 14. We further concluded that the distance r of the reacting deuterons is in the range of 3 pm. The screening means that the deuterons behave as if they had an energy of 470 eV, an adequate value for hot fusion, but with a real energy of only 2.3 eV. Only the very few ions, in the Maxwell tail of the energy distribution, which exceed the 2.3 eV will react. This agrees then with room temperature measurements. Higher temperatures, 100°C or more, can well increase the reactivity [3].

The high screening by a factor 14 is not unusual even for bulk materials as plasma theory indicates [11] but the swimming electron layer [10] may strongly help in arriving at the factor 14. The distance of r = 3 pm between the reacting deuterons come from detailed comparison with experimental parameters and are comparable with basically different other models of Preparata and the theory of Vigier, see [3]. Our swimming electron model motivated us to look for experiments with large surfaces and to use multilayers e.g. Ni/Pd for fully reversible low energy nclear reactions [1]. The experiments with 5 g palladium black (0.4 mm diamter) producing large amounts of ^{4}He in cells with deuterium electrolysis [12], can be evaluated to arrive at r = 2 pm. The details of the nuclear reaction e.g. of protons within the swimming electron layer has been carefully elaborated by Kim et al [13]. The increase of d-d reaction cross sections (though at 2 keV energy) due to screening of the Coulomb field has been measured [14].

4. A Quantum Condition for the Long Range of Interaction

Cold fusion observations indicate that nuclear reactions may occur at inter nuclear separations 21.1 times greater than those common to hot fusion. Myonic fusion also occurs at large separations. We should like to consider the quantum mechanical implications of these interaction processes at distances in the range of 3 pm.

There is a mathematical physics way "how to understand quantization"[15]. It describes reality by observables and states. With this "natural language we can say that quantum mechanics is a deformation of classical mechanics in a framework...where Planck's constant is the deformation parameter".

A less mathematically formal way is to understand quantum theory form the empirical fact that all quantities with the dimension of an action can occur only as multiples of Planck's constant h (or h/2p). If a free moving electron in a zero potential has a momentum $p = mv = (2mE_o)^{1/2}$ with a mass m, velocity v and kinetic energy E_o, it has a de Broglie wave length l_{dB} where the product of momentum p times length l_{dB} has the dimension of an action and has to be equal to h or multiples of it. This results in the de Broglie wave length

$$l_{dB} = h/p = h/(2mE_o)^{1/2} \qquad (3)$$

It should be realized that the de Broglie wave length l_{dB} and the electron energy E_o are well defined, no inaccuracy ranges or error bars etc., but simple numbers.

The quantization has to be expressed by the h in the case of the de Broglie wavelength, Eq. (3). For the atom mechanics of Bohr's planetary model the quantity of the action had to be h/2p. A modified Bohr model can be used where the problem of orbiting and therefore dipole radiation emitting electrons in the s-state can be avoided and only in p- and higher states orbiting and radiation emission is possible. This model [16, Section 2.3] asks why does an electron not fall into the positive atomic nucleus. There is Coulomb energy gained from the reduction of the distance r between electron and nucleus. On the other hand there is quantum energy E_q (Fermi-Dirac) to be increased if the radius r

$$r(2mE_q)^{1/2} = h/2\pi \qquad (4)$$

is becoming smaller. For a simply charged nucleus, both energies are equal at a radius equal to the Bohr radius $r_B = (h/2\pi)^2/(me^2)$. It is important to note that in the case (4) the quantization is not given by h but by $h/2\pi$. Using multiples n = 1,2,3,... of the right-hand side of Eq. (4) one arrives at energies E_n equal to the Rydberg terms.

One should be aware that the meaning of quantum mechanics is simply the atomistic structure of action. This appears indeed also in Born's statistical interpretation by functional analytical expressions. If a quantum state is given by

$$\Psi(\mathbf{r},t) = \int A(\mathbf{p})\exp\{(2\pi\imath/h)[\mathbf{p}\cdot\mathbf{r}-(\mathbf{p}^2/2m)t]\}d\mathbf{p} \qquad (5)$$

a localization can be expressed by a width Δr for the density distribution $\Psi(r)$ of a state in the configuration space determined by the spectrum A(p) of a momentum distribution. The functional analytical relation between the states Ψ and p is given by an integral equation of the first kind (in the case of Eq. (5) as a Fourier's integral equation solved by Fourier transform). It was the discovery of Heisenberg with his uncertainty relation to realize that the widths of the spectra

$$\Delta r\, \Delta p = ah \qquad (6)$$

where the number a is in the order of unity. If the spectrum of A(p) is a Gaussian error function, the spectrum of $\Psi(r)$ is also Gaussian and both distributions (spectra) have the narrowest width, resulting in an $a = 1/4\pi$. If Ψ is a box, the spectrum of p is a type of a (1/u)(sin u) function and a=1/2.

The Fourier transform defines widths which can well vary with the resulting a. It is no surprise that the rule of quantization *also* refers to these spectral widths of functional analytical distribution functions as seen in Eq.(6) but this does not exclude that quantization also refers to simple numbers as e.g. in Eq. (3). Hermann Weyl's transformation theory explained the relation between the Schrödinger picture (expressed by eigenvalues of differential equations) and the Heisenberg picture (expressed by the elements of the matrix evolution of the integral equations corresponding to the differential equations) as explained by Johann von Neumann [17]. In the Heisenberg picture the initial access to quantization was the non commutative matrix product of space [r] and momentum [p] matrices to be

$$[r][p] - [p][r] = ih/2\pi \qquad (7)$$

and in the Schrödinger case it was the question of Debye in Schrödinger's seminar report about de Broglie's results (3) in 1924 "if there are electron waves with a wave length and frequency, where is the related wave equation?" The later answer was then the Schrödinger equation which also can be derived in mathematical symbolics of quantization [16, Appendix A]. In the latter case one defines the operator for the momentum $p = -i(h/2\pi)d/dx$ and the energy $E=i(h/2\pi)d/dt$ derived as a symbolic product $p\,dx$ = "h" and $E\,dt$ = "h" to be substituted in the classical Hamilton function where the resulting Hamilton operator defines a differential equation resulting in distributions functions Ψ to determine expectation values in the sense of statistics.

5. Soft Gamma Emission of the Reaction Energy

We now consider the quantum mechanical concepts in the preceding section applied to long range nuclear reactions. The question involves energies E and times t (or the corresponding velocities v) for nuclear reactions at distances r, as large as 3 pm, such that $Et = h/2\pi$. Expressing $E = (h/2\pi)v/(2r)$ with the assumption that the incident particle has a velocity v and the interaction with another particle (nucleus or atom) appears within the length of two radii (2r), we find a limiting energy for the quantum interaction between the incident particle of mass m and the other particle

$$E > (h/2\pi)^2/(2mr^2) \qquad (8)$$

For electrons the energy E for interaction over a distance of $r = 10^{-8}$cm has to be lager than 3.7 eV. This indeed seems to be the limit below which no (inelastic) quantum interaction of electrons with atoms appears and the electrons move through atoms without interaction (Ramsauer effect). Interaction is possible only with larger entities, e.g. when the conduction electrons in a metal or semiconductor are colliding and causing ohmic resistivity; in this case the entity of collision is e.g. a lattice vibration, characterized by an acoustic wave length of 10nm permitting the transfer of energy above 0.37 meV. In general, any particle needs to have a deBroglie wave length

$$l_{dB} < r/(2\pi) \qquad (9)$$

otherwise it will not perform an inelastical quantum interaction with an object of radius r.

For alpha particle interaction with particles within a radius r of 1 fm (nuclear dimension) one arrives at E > 1.27 MeV. This is reasonable since it is well known that alphas with energies above MeV may produce nuclear reactions. No nuclear reactions at all are possible for alphas of lower energy, if not a larger interaction length r is considered. For deuterons taking a value r = 143 fm, the central collision distance at 10 keV energy, the limit is E > 500 eV, in agreement with observed fusion reactions. For deuterons at a distance of 3 pm, as derived for the cold fusion reactions [3], the limit is E > 1.13 eV. This value is in agreement with the concluded [3] energy of 2.3 eV of deuterons in the energetic tail of the Maxwellian distribution which result in the cold fusion reactions. This restriction to the energetic protons or deuterons in the same way also for the following other long range nuclear reactions is a natural controll against too hefty reactions. The energy output of a mutlilayer energy source with up to kW/cm^3 power density could be controlled by the temperature using heat exchangers and by the concentration of the protons.

We have to distinguish between the cold fusion reactions where only isotopes of hydrogen are involved from the present long range nuclear reactions where thermal hydrogen isotopes react with heavy nuclei, resulting in a nuclear transmutation. The first indication of this kind of reactions came from cold fusion experiments [18]. However this may have been an Oppenheimer-Williams neutron swapping (or hopping) process [3]. There was an alteration of the ratio of the isotopes in the outermost layers near the surface of the palladium, indicating that a (d,p) reaction had taken place

for exothermic reactions. Deeper layers of the palladium showed the unchanged isotope ratio. Contrary to this, the observation of RIFEX [1] or the similar case of strong heat generation at palladium nickel interfaces [19] resulted in the generation of nuclei with different atomic number. This type of measurements with long range nuclear reactions were observed [1] where high concentrations of hydrogen in palladium reacted and produced silver isotopes and other elements. These reactions at distances r of few fm, are governed by Eq. (8) and involve Coulomb screening, especially with swimming electron layers SEL [3] at the clean surface at intermetallic interfaces.

No MeV neutrons nor energetic gammas have yet been observed, only some thermal energy has been measured in these long range nuclear reactions[1]. It may be asked whether the resulting nucleus loses energy in the form of only larger numbers of low energy gammas or of usual short range alphas or betas. The energies involved are rather large, e.g.

$$Pd^{108} + p = Ag^{109} + 6.664\ MeV \quad (10)$$

$$Pd^{106} + p = Ag^{107} + 5.957\ MeV \quad (11)$$

There seems to be a similarity to the reaction of thermal neutrons with U^{238} where the momentum transfer is small because of the thermal energy and - since no fission occurs for compensating the momenta of MeV reaction products - one has to follow up gamma emissions. One may speculate whether lower energetic rotational states or surface oscillations are involved as indicated from the surface energy of the nuclei [20]. This may be different when a long range nuclear reaction in a metal, with a high hydrogen concentration, results in a nuclear fission, e.g. with deuterium in platinum

$$Pt^{196} + H^2 = Xe^{136} + Mn^{60} + 2n + 104.3\ MeV \quad (12)$$

since there are several branches for compensating the momenta.

Stiumulating discussions with Dr. James A. Patterson and partial support by Clean Energy Technology, Inc., Dallas, Texas, 75240, are very gratefully acknowledged.

References

[1] G.H. Miley, G. Marne, M.J. Willimas, J.A. Patterson, J. Nix, C. Cravens, and H. Hora, 6th Int. Conf. Cold Fusion Hokkaido 1996; Jerry E. Bishop, Wall Street Journal 29 Jan. 1996, p. A9A

[2] M. Fleischmann and S. Pons, J. Electroanalyt. Chem. **251**. 301 (1989)

[3] H. Hora, J.C. Kelly, J.U. Patel, Mark A. Prelas, G.H. Miley, and J.W. Tompkins, Phys. Lett. **A175,** 138 (1993; G.H. Miley, H. Hora, E.G. Batyrbekov, R.L. Zich, Trans. Fusion Technol. **26**, 4T, Part 2, 313 (1994)

[4] R. Hofstadter, Ann. Rev. Nucl. Sci **7** (1957) 231; Australian Physicist **24**, 236 (1987)

[5] T. Meyer-Kuckuk, *Kernphysik* (Stuttgart 1984) p. 28

[6] H. Hora, G.H. Miley, L. Cicchitelli, A. Scharmann, W. Scheid, Nuovo Cimento **D12** (1990) 393

[7] E. Yamaguchi, and J. Nishioka, *Frontier of Cold Fusion* H. Ikegami ed. (Universal Academy Press, Tokyo) p. 179

[8] M. Prelas, F. Boody, W. Gallaher, E. Leal-Quiros, D. Mencin, S. Taylor, J. Fusion Energy, **9** (1990) 309

[9] H. Hora, G.H. Miley, M. Ragheb, and A. Scharmann, in *Proc. 8th World Hydrogen Conf. July 1990, Cold Fusion Symposium* (Hawaii Natual Energy Inst., Univ. Hawaii, 1990) p. 169

[10] H. Hora, Gu Min, S. Eliezer, P. Lalousis, R.S. Pease, and H. Szichman, IEEE Trans. Plasma Sci. **PS-17** (1989) 290

[11] S. Ichimaru, Rev. Mod. Phys. **65** (1994) 255

[12] Yeong E. Kim and A.J. Zubarev, 6th Int.Conf. Cold Fusion, Hokkaido 1996, 0-033

[13] Y. Arata and Y.C. Zhang, 6th Int. Confl Cold Fusion, Hokkaido 1996, 0-003

[14] J. Kasagi et al 6th Int. Conf. Cold Fusion, Hokkaido 1996, 0-032

[15] L.D. Faddeev, Physik. Blätter **52** (1996) 689

[16] H. Hora, *Plasmas at High Temperature and Density* (Springer, Heidelberg 1991)

[17] Johann von Neumann, *Mathematische Grundlagen d.Quantenmechanik* (Springer, Berlin 1933)

[18] D.R. Rollison, W.O. Grady, R.J. Doley and P.T. Trzaskoma, Progr. 1st Ann. Conf Cold Fusion, Salt Lake City, March 1990 (Nat. Cold Fusion Inst. 1990) p. 36

[19] S. Szpak, P.A. Mosier-Boss, Phys. Letters **A221**, 141 (1996)

[20] H. Hora, *Plasma model of Surface Tension of Nuclei and the Phase Transition to the Quark Plasma*, CERN-PS/DL-Note-91/05, August 1991

Excess Energy and Nuclear Products

HEAT MEASUREMENT DURING THE ELECTROLYSIS USING MODIFIED PALLADIUM CATHODE

Ken-ichiro OTA, Taichi KOBAYASHI, Hiroki KABUMOTO,
Kazuhiko YAMAKI, Naobumi MOTOHIRA and Nobuyuki KAMIYA

Department of Energy Engineering, Yokohama National University
79-5 Tokiwadai, Hodogaya-ku, Yokohama 240, JAPAN

ABSTRACT

The heat balances during the electrolysis using 2 types of Pd cathodes (B controlled Pd and Ni coated Pd) in 1M LiOD heavy water solution have been measured using the flow calorimeter system. The excess heat was observed at 6 runs out of 14 experiments for B controlled specimen. Among them, the heat burst was observed at 2 runs. For Ni coated specimen the small excess was observed at 4 runs out of 9 experiments. Further study is necessary to improve the reproducibility and to confirm the phenomena.

1. INTRODUCTION

Many positive or negative reports have been published since the announcement of M.Fleischman and B.S.Pons about the excess enthalpy production(the cold fusion) during the electrolysis in LiOD heavy water solution using palladium cathode[1]. However, the phenomena is not clear and many people could not believe it mostly from the theoretical point of view. At least a scientifically precise experiments and reliable data are necessary in order to confirm the phenomena

As far as the heat measurement concern, a direct measurement or an absolute measurement should be applied considering the scientific importance of the results. From that point we are applying the flow calorimeter using the thermochemically closed cell from the start of this study in 1989.

The reproducibility is crucial and most important for this. Several other groups also reported the excess heat using Pd cathode[2-4]. However, their reproducibility is not enough to confirm the phenomena. The experimental

recipe to get the excess enthalpy for everyone who wants to do should be presented. There are many factors to think of to get the reproducible results; materials, the electrolysis conditions an so on. Among them we think the Pd material is most important. From this standpoint we have reported the effect of the mechanical treatment, the heat treatment and the effect of some additives[5-7].

In this paper we will report our recent results of heat measurements during the electrolysis in LiOD heavy water solution using 2 types of Pd electrodes; boron controlled Pd and Ni coated Pd.

2. EXPERIMENTAL

The electrolysis cell was made by acrylic resin in order to avoid the effect of alkaline solution. Figure 1 shows the schematic drawing of the cell. The recombination catalyst was placed on the upper part of the cell where the recombination reaction (D_2+O_2 or H_2+O_2) proceeded completely up to 4A. The recombination catalyst was Teflon treated fine Pd powder on alumina. The flow calorimetry was applied to the measurement of heat balance during the electrolysis. The copper tubing was surrounded the electrolysis cell and picked up the generated heat by the electrolysis and the recombination reaction. The increase of the temperature of cooling water was measured by CA thermocouple or Pt resister. The temperature of cooling water was 296 K or 288 K.

2 types of the heat measuring system have been constructed. One is the electrolysis cell in a box of ceramic wool insulator where the heat recovery was up to 99 %. The other is the cell in the newly developed fine temperature controlled bath where inside temperature was controlled ± 0.01K at the temperature range from 283 to 333 K and the heat recovery was 96 %.

The cathodes were Pd rods(4 mm ϕ x 15 mm) containing B (mostly 500 ppm) and Ni coated Pd rod(2 mm ϕ x 15 mm) where Ni was electrically plated using sulfamate solution. These materials are obtained from IMRA Material(IM), Tanaka Kikinzoku Kogyo(TNK) and Tokuriki Corp.. The anode was Pt wire(1 mm ϕ) which was surrounded the Pd cathode.. The electrolyte was mostly 1 M LiOD heavy water solution which was made by LiOD-D_2O(99 at% D) powder.

The constant power electrolysis was applied in order to get clear heat balance using a constant power generator. The temperature of the electrolyte was between 293 and 323 K during the electrolysis.

3. RESULTS AND DISCUSSION

Table 1 shows the heat balance of B controlled Pd specimens. N1 and N2

in the first column means the heat measurement using the fine temperature controlled bath. The electrolyses were conducted mostly at the fixed power of 5 W and the current density ranged from 300 to 1100 mA/cm^2. The average heat balance means the ratio of (total output heat)/(total input power) throughout the electrolysis. The maximum excess heat means the maximum excess power during the electrolysis when the excess heat was observed.

Among 14 runs we observed excess heat 6 times. During the run N1-03 we observed the heat burst 2 times using 500 ppm B containing Pd cathode. The result is shown in Fig.2. The heat burst took place at 225 h and 1020 h and we got maximum excess of 1.8 W at 1020 h for a half hour. The temperature of electrolyte and the cell voltage(or current) changed owing to the heat burst. This kind of abrupt heat burst did not observed at other runs and could not be reproduced even using the same Pd specimen.

Table 2 shows the result of the heat balance during the electrolysis using the Ni coated Pd cathode. In these experiments we want to see the effect of Ni/Pd interface, although the amount of absorbed deuterium(hydrogen) decreased. We observed small excess heat for 4 runs out of 9 runs. These excess heat appeared continuously during the electrolysis. Figure 3 shows the typical excess heat using the Ni plated Pd cathode. Since these excess are so small and very close to the error limit, further study is necessary to confirm this.

4. CONCLUSION

We observed excess heat several times using B controlled Pd and Ni coated Pd. However, the excess heat is mostly very small and the reproducibility has not been improved with applying these treatments. The essential factor to produce excess heat is stll not clear. Further study is necessary to improve the reproducibility and confirm the phenomena.

Acknowledgment

The financial support from the New Hydrogen Project through the Institute of Applied Energy is greatly appreciated.

REFERENCE

1) M.Fleischmann, S. Pons,et al; J. Electroanal. Chem., 289, 293 (1990)
2) M.C.H.McKubre, et al: "Frontiers of Cold Fusion" Ikegami Ed., p.5 (1992) University Academy Press Inc. Tokyo
3) K.Kunimatsu, et al; ibid, 31 (1992)
4) A.Takahashi, et al; ibid, 79 (1992)

5) K.Ota, et al; ibid, 71 (1992)

6) K.OTA, et al., Trans. Fusion Tech., **26**, 138 (1994)

7) K.Ota, et al., Proc. 5th Int.Conf. Cold Fusion, 132 (1995) Monaco

Table 1. Results of electrolysis using B containing Pd.

Run	Pd sample	Current density (mA/cm2)	Win (W)	Heat balance Ave.(%)	Excess heat (W) Max	Temperature (℃)
23	B 500ppm (IM)	750～300	5	103.5	0.29	
25	B 127ppm (TNK)	850～440	5	99	-	
29	B 500ppm (IM)	750～360	5	101	0.22	
31	B 267ppm (TNK)	900～540	5	101	0.14	
33	B 500ppm (IM)	740～660	5	102	0.14	23
34	B 500ppm (IM)	1180～500	5.1	100	-	
37	B 1000ppm (TNK)	1040～950	5	100		
48	B 500ppm (IM)	910～840	5	101	0.16	
49	B 500ppm (IM)	1020～900	5	99	-	
N1-03	B 500ppm (IM)	590～560	5	101	1.8	15
N2-01	B 267ppm (TNK)	810～780	5	99	-	15
N2-02	B 500ppm (IM)	640～320	5	100	-	23
N2-03	B 500ppm (IM)	750～700	5	100		15
N2-04	B 500ppm (IM)	700～530	5	99	-	15

Table 2. Results of electrolysis using Ni coated Pd.

Run	Pd sample	Current density (mA/cm2)	Win (W)	Heat balance Ave.(%)	Excess heat (W)	Temperature (℃)
46	Ni-coated (10 μm, D_2O)	1230～490	5	103	(0.28)	
47	Ni-coated (10 μm, D_2O)	1090～700	5	100	0.23	
50	Ni-coated (10 μm, H_2O)	1530～1310	5	100	-	
51	Ni-coated (10 μm, D_2O)	1380～530	5	99		23
52	Ni-coated (10 μm, D_2O)	1210～460	5	100	-	
53	Ni-coated (10 μm, H_2O)	1660～1340	5.8.6	102	(0.19)	
54	Ni-coated (10 μm, H_2O)	Testing now	5	100		
55	Ni-coated (1 μm, D_2O)	Testing now	5	100	-	
N1-06	Ni-coated (10 μm, D_2O)	1040～700	5	101	(0.1)	23

Excess Energy and Nuclear Products

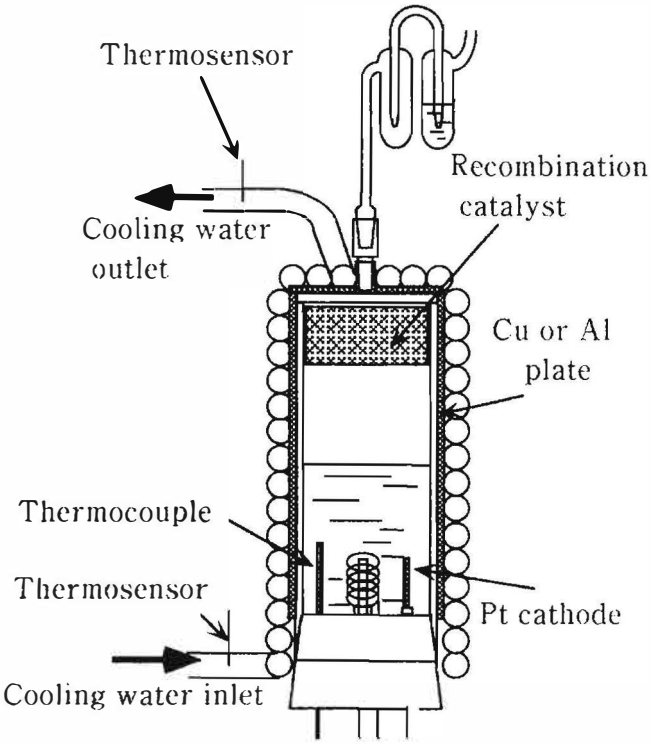

Fig.1. Electrolysis cell.

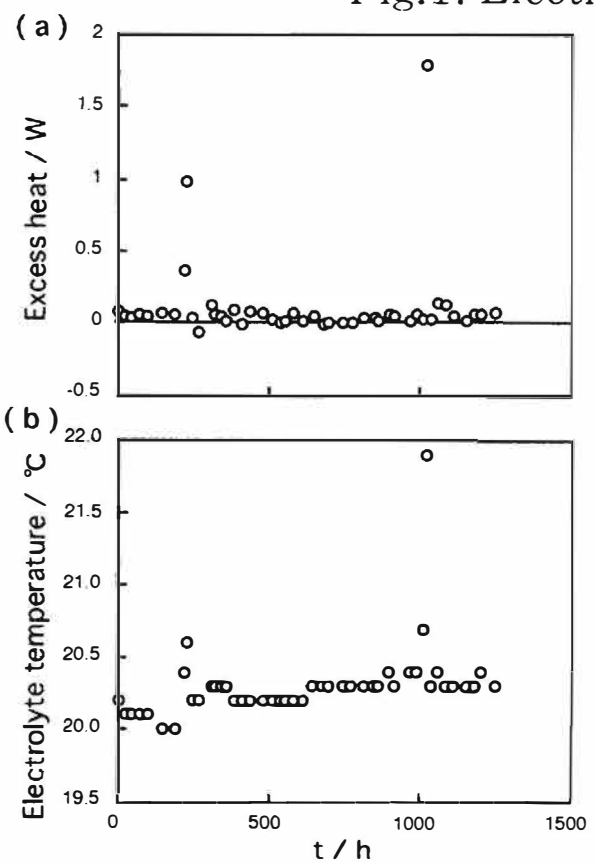

Fig.2. (a) Excess heat (b) Electrolyte temperature of N1-03 (B 500ppm)

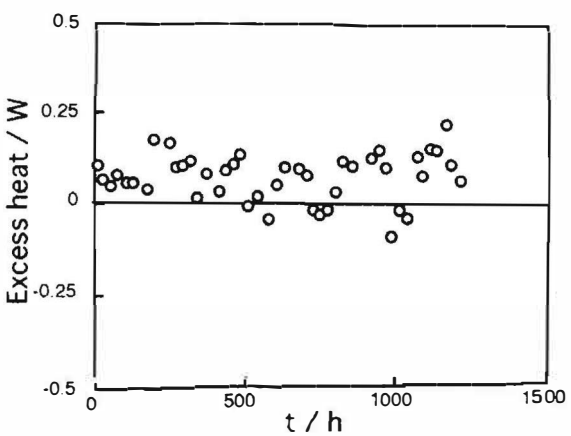

Fig.3. Excess heat of Run-46 (Ni-coated 10 μ m).

TRIODE CELL EXPERIMENTS FOR CONTROLLED FLEISCHMANN/PONS EFFECT

Evan L. Ragland
***the Boiler Works*, Diamondhead, MS, 39525, USA**

ABSTRACT

Experimental research and evaluation of three electrode (triode) cold fusion electrolysis cells is reported herein. Apparatus development began, after patent application, 05 June 1995. The triode apparatus introduces controlled loading and operation of Fleischmann/Pons-type (F/P) cells. In August 1995 excess heat generation was observed in initial triode apparatus experiments conducted by Dr. Dennis Cravens in his New Mexico laboratory. In November 1995 *the Boiler Works* laboratory in Diamondhead began experimental evaluation of the triode apparatus. A series of experiments in December, January and February led to development of a functioning triode fusion reactor. The reactor was put into operation 20 March 1996 and operated continuously until 23 August 1996. Over the five months of operation of the reactor several experiments were preformed and over 65,000 data points were recorded. This data base is being applied in further triode apparatus developments.

A second reactor test bed for "quick change" cathode specimen evaluation is in operation. Thin film cathode specimens prepared by the Materials Science and Engineering Laboratory of the University of Alabama in Birmingham are presently being evaluated. These include Pd film on Ag, Al, Cu, and quartz substrates and Pt films on Si bead specimens. Engineering design of a 2 KW reactor cell is underway.

Details of triode apparatus operation, control, and experimental results are reported. The general design approach to the 2 KW reactor is described. It is concluded that sufficient experimental and theoretical understandings of cold fusion exist for engineering design and development of water heating appliances.

1. Introduction

The concept of the triode cell and the laboratory experiments reported herein are all guided by the Crowded Deuterium Model (CDM) construct presented by the author at ICCF-3 in Nagoya, Japan in 1992. The reader should be informed that while CDM theory enjoys significant peer review and critique that it is not a generally accepted concept nor is it rigorously proven in principle. Nevertheless, it has proved to be a useful tool for the visualization of F/P mechanics and for the design of devices and experiments. The CDM concept teaches that F/P is a bulk effect occurring within structural domains encompassed by at least one or more palladium hydride envelop(s); that often such domains occur naturally in polycrystalline palladium (Pd) saturated with nuclei of the hydrogens; that if hydrogen nuclei are sufficiently rich in deuterons; if the

geometry of the structure is appropriate; and the random distribution of polycrystalline boundaries internal to the domain are propitious; that then deuterons may be crowded to nuclear fusion within the structure. Satisfying this set of particular conditions makes F/P experiments difficult to preform and extremely difficult to repeat. Furthermore, even when all other conditions are positive the last condition, favorable boundaries within the domain, is of such low probability that most domains reach internal Coulomb equilibrium and *block* before enough deuterons are absorbed to crowd to fusion. Finally, even with favorable boundary distributions, deuteron loading and sustainment of fusion may be erratic; i.e., sometimes rapid, sometimes sluggish, and sometimes *blocked* until equilibrium is internally or externally disturbed.

Fleischmann and Pons taught diode electrolysis of *heavy water* could be used to achieve low temperature nuclear fusion using a Pd cathode in a diode cell. Numerous experiments have since demonstrated generation of excess heat using various methods of electrolysis, gas discharge, and solid state with diode apparatuses. All methods encounter the conditional difficulties previously described. The diode characteristic of common anode/cathode current affords limited possibilities for control. The triode apparatus - two anodes; one cathode - improves methods to load, ignite, sustain, and control the F/P effect. Most important; triode control overcomes *blocking*. Diode and triode apparatus characteristics are schematically illustrated in Fig. 1.

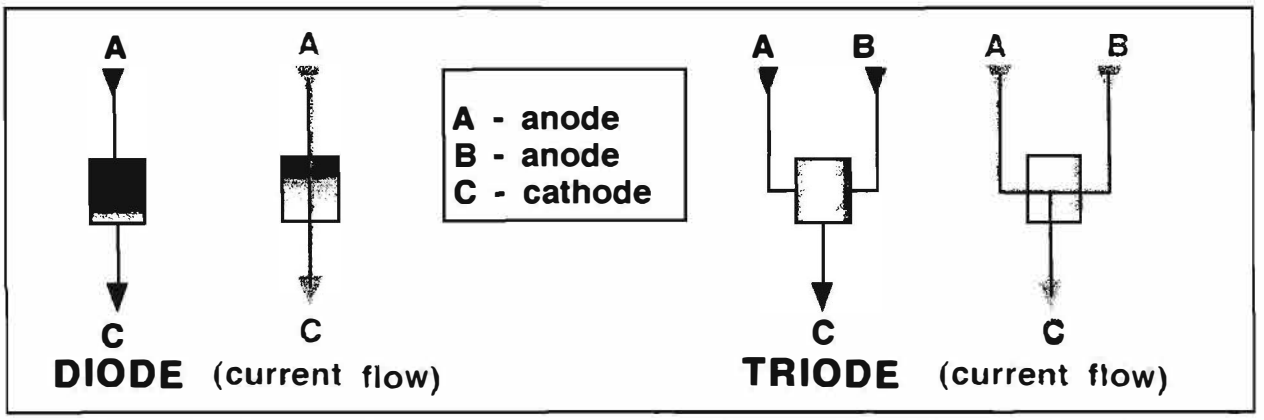

Figure 1. Diode vs. Triode electrical connections and electric current paths.

2. Methods

Cell shadings in Figures 1 and 2 illuminate electrostatic gradients from positive, *dark*, to negative, *light*. Diodes are limited to cathode current control whereas *the triode* can be modulated by varying the anode voltages A and B as well as by manipulation of the cathode current. This is particularly meaningful when one contemplates the relatively uniform current density characteristic of cathode surfaces in most electrolysis and gas discharge, and many solid state devices. In Figure 2, four examples schematically illustrate gradient control across a triode cathode cross section with independent anodes A and B at different operating potentials. Figures 2(a) and 2(d) illustrate the conventional method of cathode current modulation where anode voltages A and B are at the same potential. Figures 2(b) and 2(c) show how voltage potentials to anodes A and B may be alternated so as to cause the cross section gradient to sweep, or vary sinusoidally, exponentially, in step function, or in other manner. Switching and frequency rates can also be varied. These modulation methods enhance loading, ignition, sustenance, and control of F/P fusion cells by overcoming Coulomb equilibrium.

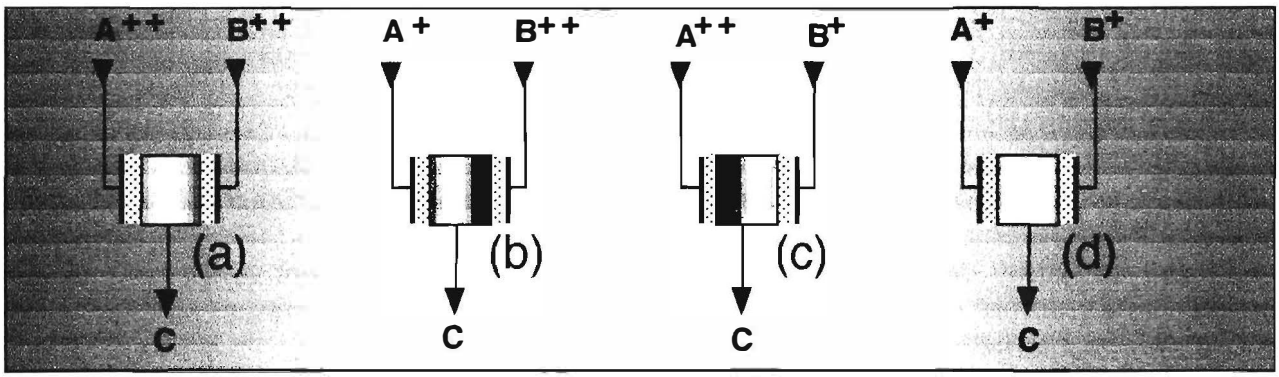

Figure 2. Current control [(a) and (d)]; Voltage control [(b) and (c)].

A simplified electrode configuration for a F/P triode cell is depicted in Figure 3 (a) and (b). *the Boiler Works* experimental cells are designed to mount cathode specimens 2.5 x 2.5 x 0.1 centimeters or smaller in a Teflon cathode frame. The cathode frame inserts between Teflon anode frames with eleven 0.051 centimeter diameter platinum wires. Other geometries are possible; the preferred embodiment is of different geometry.

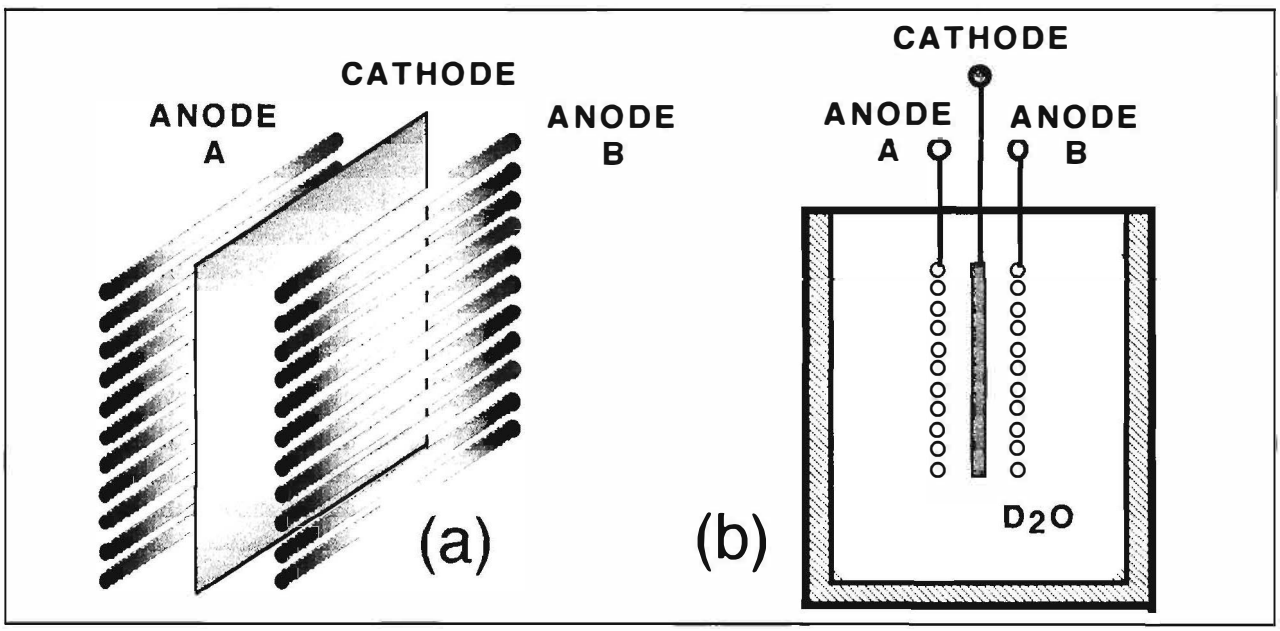

Figure 3. (a) Triode electrode configuration; (b) Triode cell cross section.

Two laboratory test beds are in operation. The block diagram of Figure 4 identifies the functional elements and organization of the long term facility. These are two *hp* 361XA constant current power supplies, a function generator which programs the *hp* 361XA

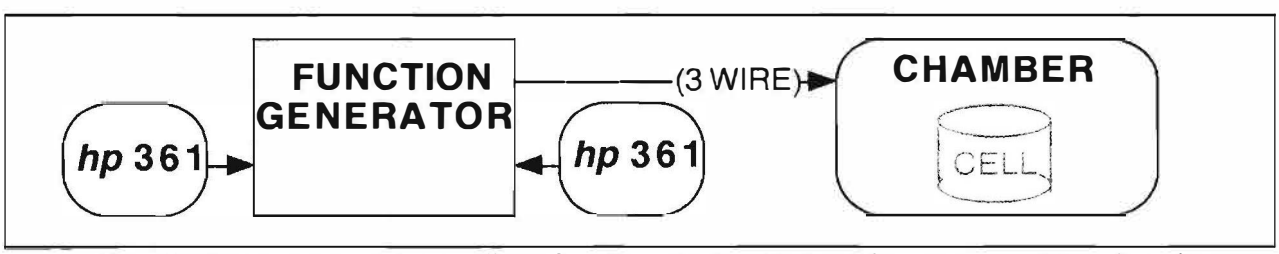

Figure 4. ***hp*** current supplies, function generator and environmental chamber.

current levels and the three (A, B, and C) output currents to the triode cell, and an environmental chamber. The "quick change" cathode test bed, is not described herein.

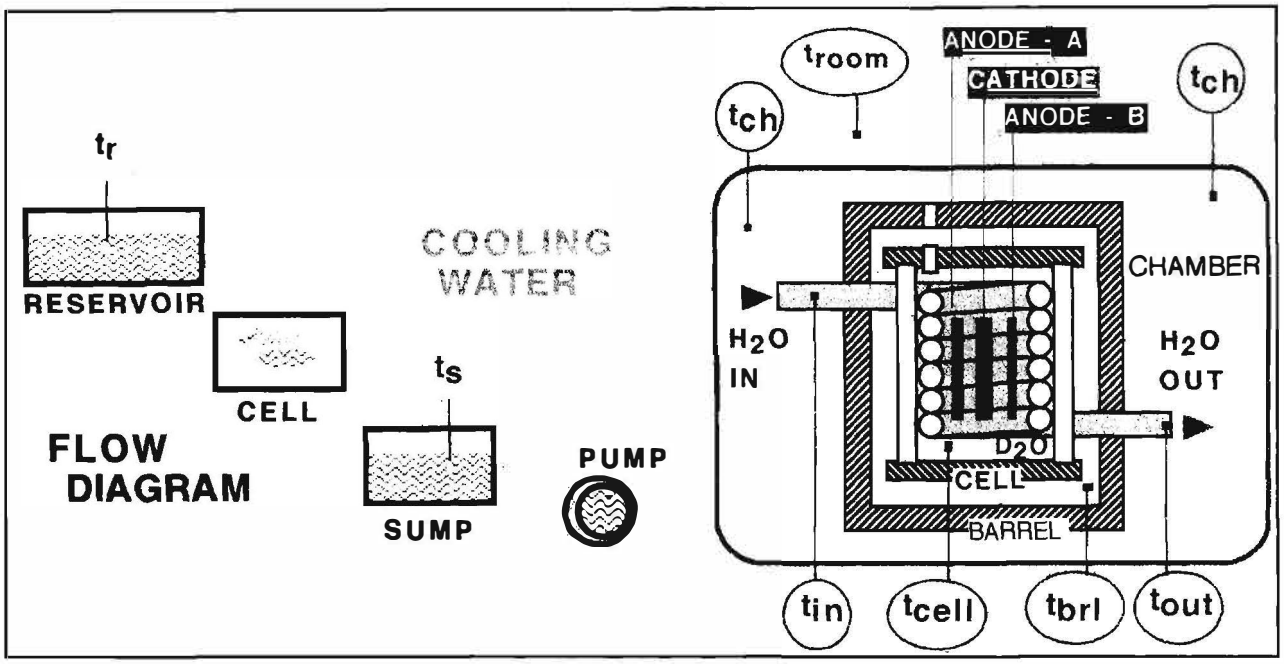

Figure 5. Flow.through heat exchanger and environmental chamber organization.

Long term testing utilizes flow through calorimetry in which gravity fed clean water flows into the chamber, through the cell heat exchanger, and discharges into a sump. A pump returns water to the reservoir. The background diagram in Figure 5 shows this circulation system. The foreground of Figure 5 illustrates details of the chamber, the cell, and temperature sensor locations. Cooling water flow rate is regulated by a valve and discharge is manually measured and recorded with each set (see Figure 5) of temperature data. The cell is thermally isolated within the chamber in a "barrel" enclosure. The chamber further isolates this enclosure from the laboratory environment. Chamber temperature is regulated and is stabilized by a two liter tank of ballast water. In the cell the triode structure is mounted inside the heat exchanger coil and both structures are completely immersed in heavy water. Gasses are vented through ports in the cell, the barrel, and the chamber enclosure. The electrolyte is 99.9% D_2O diluted with 0.1 mol of LiOH. Volume is 80 ml., replenished periodically when reaching a 70 ml. level.

3. Results

Patent application on the triode apparatus was filed 05 June 1995. A test cell was designed at *the Boiler Works* in June. Parts for two cells were fabricated in Houston, Texas in July. In late July the first F/P effect cell was assembled and calibrated by Dr. Dennis Cravens in his Cloudcroft , New Mexico laboratory. The first calibrated open cell test began loading on Thursday, 27 July. At 10:52 AM, MDT, Tuesday 01 August cell resistance began to drop and cell temperature began to rise. At 12:13 PM excess heat was measured at 40%; at 12:29 PM at 84%, and at 01:18 PM after cell temperature was stabilized excess heat was calculated at 267%. On 02 August the cell was restarted. Maximum excess heat measured was 40%. Subsequent tests on 03 August produced null results. Bipolar triode and fibrous nickel cathode tests were also inconclusive.

Excess Energy and Nuclear Products

In November *the Boiler Works* laboratory in Diamondhead began calibrated open cell experimental evaluation of triode apparatuses. These experiments were inconclusive. At 08:03 PM, 13 December temperature began to rise rapidly in a cell test begun on 10 December. By 12:02 AM, 14 December, with cell temperature at 200 degrees Fahrenheit, input power was switched to a minimal level. Efforts to repeat the anomaly went empty. The test was terminated on 15 December to clear the chamber for a test cell with a 5 micron Pd on silver (Ag) substrate cathode. This test, the first flow through calorimetry experiment, began on 23 December. The test was fraught with unexpected complications, miscalculations, and learning; however all new instrumentation worked precisely and excellent records were logged. The vexatious problem was absolute absence of any evidence of excess heat. This experiment terminated on 13 January. A second Pd on Ag cathode cell was calibrated on 07 February and put on test on 10 February. This experiment ended on 13 March, again without evidence of excess heat.

These experiments informed, albeit they evidenced no excess heat. In all tests versatility of triode control accelerated loading. A ranging investigation of F/P cathode characteristics through adjustments of triode voltages and switching rates provided experimental results to compare with theory. This review suggested the design of solid Pd cathodes be revisited. New Pd cathodes were designed. The first of these went on test at 08:28 PM, 20 March. At 02:03 AM, 21 March excess heat generation was observed. During the next week of operation cell output was 200% of input. Gain gradually increased to 500% with operation and better informed control. The reactor was in continuous operation until deliberately shut down 23 August 1996.

Evaluation of thin film cathodes is in progress in a reactor test bed dedicated to "quick change" cathode specimen testing. Thin film cathode specimens prepared by the Materials Science and Engineering Laboratory of the University of Alabama in Birmingham include Pd film on Ag, Al, Cu, and quartz substrates and Pt films on Si bead specimens. To date, these experiments have not exhibited generation of excess heat.

In June engineering design of a prototype modular cell for application in water heating appliances was begun. The design goal is a 2 KW equivalent thermal output reactor cell for battery application in water heating systems. Market study, equipment specifications, cost analysis, and engineering layout were initiated in late July. Figure 6 illustrates the design approach which elaborates on the basic cell design of the March to August tests.

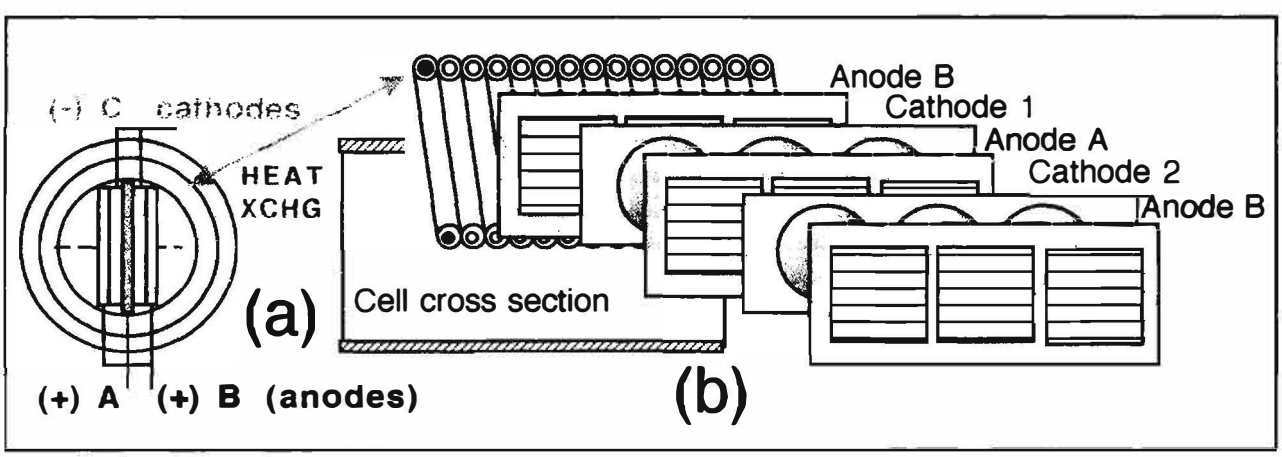

Figure 6. End (a) and exploded (b) views of 2 kilowatt cell design approach .

4. Discussion

Conceptually triode apparatus mechanics avail means to overcome and control *blocking* during F/P cell loading and operation. Experimental success in improved loading and control tend to confirm the concept. Longevity, stability, and cell control demonstrated in the March through August experiment were particularly encouraging. Data gathered during this experiment create an extensive operational data base for advanced apparatus design. It is further encouraging that other laboratories plan to conduct triode experiments.

A second reactor test bed for "quick change" cathode specimen evaluation is in operation. Thin film cathode specimens prepared by the Materials Science and Engineering Laboratory of the University of Alabama in Birmingham are presently being evaluated. These include Pd film on Ag, Al, Cu, and quartz substrates and Pt films on Si bead specimens. Engineering design of a 2 KW reactor cell is underway.

5. Conclusion

Triode control accelerates loading, overcomes F/P cell blocking, and relieves experimental uncertainties heretofore attributed to cathode specimen incongruities. Triode experiments should lead to faster, more certain, and consistent results. Elimination of the "reproducibility" paradox should speed development and acceptance of F/P technology. Much remains to be done in development of cathode materials and fabrication techniques. Additionally, the state and behavior of condensed matter in the fusion locale is not well understood and must be further investigated. Nevertheless, sufficient experimental and theoretical understanding exists to begin engineering design and development of water heating appliances for practical uses.

5. Acknowledgments

The author wishes to thank Drs. Bruce Cain, Dennis Cravens, Michael Rigsbee, and Edmund Storms for their technical audience; Mrs. Theo Vaughey for her help in audit and review; and the many others for their encouragement, support, and counsel.

6. References

[1] Fleischmann, M., Pons, S., and Hawkins, M., Electrochemically Induced Nuclear Fusion of Deuterium, J. of Electroanal.. Chemistry, 261, 301 (1989).
[2] Ragland, E., Theory of Crowding Fusion, Nuclear Physics Review, Mississippi State University, May (1991).
[3] Bush, R., Cold Fusion Report, ICCF-2, Como, Italy, June (1991)
[4] Takahashi, A., Nuclear Products by D_2O/Pd Electrolysis and Multibody Fusion, Proc. Int. Symp. Nonlinear Phenom. In Electromagnetic Fields, ISEM, Nagoya, 1992
[5] Ragland, E., Cain, B., and Gu, A., Transport of the Hydrogens in Transition Metals, National Science Foundation, Washington, D.C., April, (1992).
[6] Tamaki, M. and Tasaka, K., Field Formation of the Condensed Matter Fusion by Electro-Transport of Deuterium in Palladium, ICCF-3, Nagoya, Japan, October (1992).
[7] Ragland, E., A Physical Description of Cold Fusion, ICCF-3, Nagoya, Japan, October (1992).

Excess Energy and Nuclear Products

ANOMALOUS INCREASE IN EXCESS HEAT IN ELECTROLYSIS OF HEAVY WATER AND LIGHT WATER FOR USE OF DRILLED CATHODE OF CHARCOAL

Ryoji Takahashi
(University of Tokyo)
Setagayaku Seta 2-26-21,Tokyo 158 Japan

Abstract
The excess heat measured for the use of charcoal cathode in the electrolysis of heavy water reached about 150% of the input power by preparing a notched hole in the surface of the cathode. The experimental condition was as follows. The cathode used was very hard charcoal. The anode was 0.3mm Pt wire. The electrolyte was 50cc of D2O or H2O with 0.25N LiOH.The anode and the cathode were set up in the electrolyte so as the Pt wire to locate near the diameter of the hole. Making a hole as small as 0.3mm produced excess heat of 70%.Making a notch at the hole edge enhanced the excess heat higher than 100%. The excess heat for the use of H2O was about a half of that for D2O. The current showed oscillation when the excess heat was large.A SEM examining of the charcoal showed that many uniform holes,as small as 1 micron,distributed inside the vessels are responsible for this anomalous increase in the excess heat.

1.Introduction

The use of the charcoal cathode for the electrolysis of D2O and H2O was reported in the preceding paper(1) that it produces chemical substance and the excess heat as well,as expected from the structure of charcoal. These results suggested that if very hard charcoal ,carbonized at temperatures higher than 1000 degrees,would be used the excess heat might be possibly increased. Because,the very hard charcoal decreases the synthesis of material by the high chemical stability,so the synthesis of ions,the cause of the cold fusion, becomes relatively increased.
This paper describes how the excess heat production was improved for the use of the very hard charcoal.After many experiments,making a hole in the cathode was found to be a reliable method which provides anomalous excess heat. A SEM study of specimens with good results showed that micro-holes distributing regularly inside the vessels are responsible for this anomalous increase in excess heat.

2.Methods

At the first stage of the experiment,the obtained excess heat was only several percent for every trial.It was noticed that as long as the anode and the cathode are apart,1 or 2 cms,the electrolysis at the cathode is done mostly in the limited part of the surface where the current is concentrated,so the share of the electrolysis in the vessels is poor.Then it occurred that how to increase the current flow to the vessels is a key factor. Soon it was found that the excess heat was much improved by shortening the distance between the anode and the cathode and by modifying the surface of the

cathode against the anode.
After all,making a hole in the cathode surface was found to be a reliable methode of improving the excess heat. The arrangement of the cathode and the anode is illustrated in Fig.1. The anode should

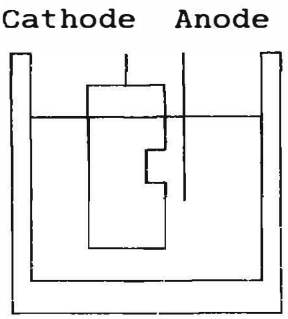

Fig.1. Arrangement of drilled cathode and anode wire in the cell.

be located as near as possible to the diameter of the hole so as to converge the current to the hole edge. The length of the anode should be short enough to cover the hole to decrease the waste current. The electrolysis should be done just under the level of the electrolyte also to decrease the waste current. The drilling effect is sure on the cross section of the charcoal rod,i.e.the vessels are parallel to the drilling direction.
Making a notch at a hole edge was done by filing,and the form was as illustrated in Fig.2.

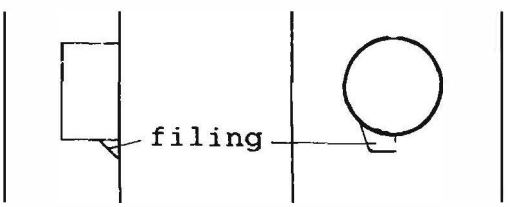

Fig.2. Illustration of making a notch at hole edge in cathode.

3.Results
The excess heat measured for various sizes of the diameter of the holes are shown in Table 1.The excess heat in Table 1 shows a mean

Table 1

Hole diameter(mm)	0.3	0.5	1	1.8	3	5
Excess heat(%)	70	40	70	70	55	20

value for the corresponding diameter of the hole. Table 1 shows the excess heat is almost independent of the hole diameter less than 3 mm. The increase in the temperature of the electrolyte, ΔT, and the electrolysis current i measured for the elapsing time are shown in Fig.3(A)and 3(B), respectively for D2O and H2O. The heat production

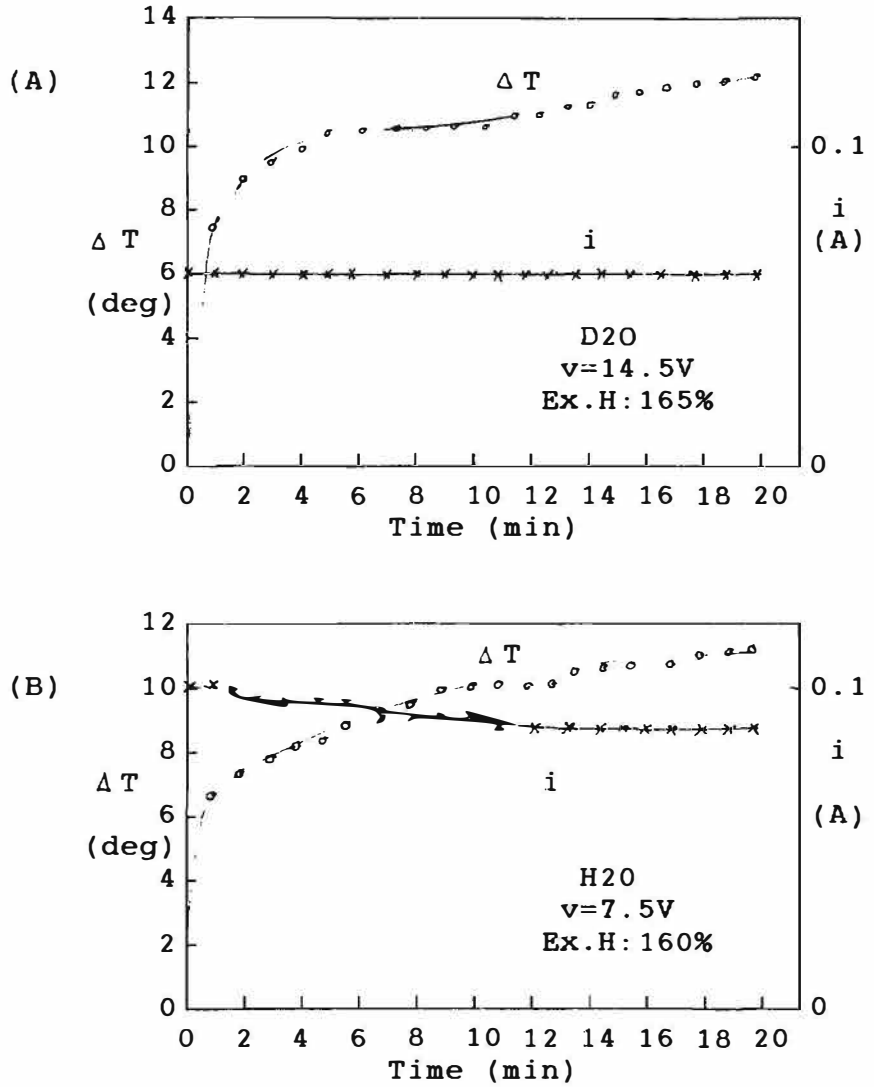

Fig.3 Temperature increase and current change after start of electrolysis for drilled charcoal cathode, with 3mm diameter hole and a notch. (A)is for D2O and (B)is for H2O.

in one or two minuits after the start of the electrolysis is very large. The value of ΔT in the begining two minuits determines the final ΔT, so the temperature dependence of the excess heat was estimated by measuring the ΔT(2min) for the elevated temperatures of the electrolyte in the cell. The results showed that the value at the room temperature decreases to about the half at 90°C.

Excess Energy and Nuclear Products

4.SEM observation
The distribution of the big vessels,observable by lupe,in a cross section of the very hard charcoal is shown in Fig.4. Big vessels are surrounded by small vessels,one order smaller in the diameter, as shown in Fig.5. A big vessel has many fine uniform holes in the wall as shown in Fig.6.

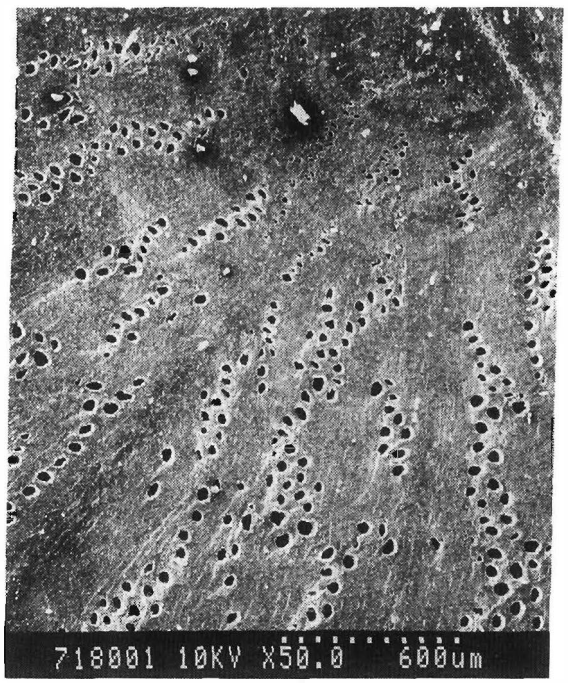

Fig.4. Distribution of big vessels serial from the center.

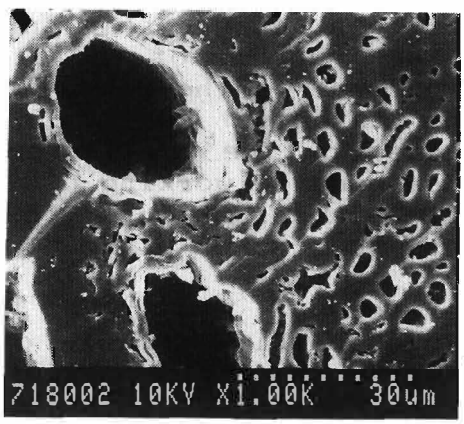

Fig.5. Small vessels surrounding big ones.

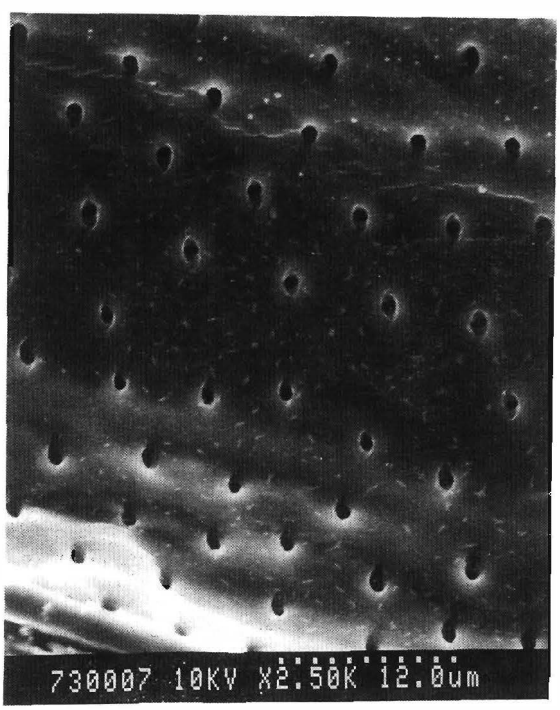

Fig.6. Distribution of micro-holes in inside wall of big vessels.

5.Discussion
A drilled hole in a cathode surface converges the electrolysis current to its edge,so if there are micro-channels at the edge,the excess heat can be well enhanced. A SEM examining showed that favorable micro-channels are present in the inside wall of the big vessels as shown in Fig,6. Making a hole in the cross sectional surface surely exposes the inside wall of the big vessels. An adition of a notch at the hole edge clearly exposes the micro-holes to much more extent to the electrolyte.Another significant role of the notch is to cause disturbance or turbulence in the liquid between the electrodes.In practice,the current shows a oscillatory behavior for the large value,because of the irregular form of the notched hole. The turbulency increases the diffusion of the electrolyte into the micro-holes. The osillatory mode of the current increases the working of the micro-drops in the micro-holes(2).

6.Conclusion
1.The presence of the micro-holes in the cathode is necessary for the excess heat production.
2.The concentration of the electrolysis current to the micro-holes is necessary to enhance the excess heat production.
3.Making a notched hole in a cross sectional surface of the cathode provides numbers of the micro-holes and effective concentration of the current to the micro-holes.
4.The turbulent flow of the liquid between the electrodes,as detected by the oscillatory current,enhances the current concentration and the working of the microdrop.
5.After satisfaction of these condition,an anomalous increse in the excess heat takes place.

References
(1)R.Takahashi:Synthesis of substance and generation of heat in charcoal cathode in electrolysis of H2O and D2O using various hydrooxides,Proc.5th Int.Conf.on Cold Fusion (1995),619.
(2)R.Takahashi:Cold fusion explained by negentropy theory of microdrop of heavy water,Proc.4th Int.Conf.on Cold Fusion (1993),Vol.4, 29-1.

Acknowledgement
The electron micrographs were taken in the SEM laboratory in the Faculty of Engineering,Univ.of Tokyo. The author wishes to express his thanks to Mrs.Tsuta Takahashi for her skillful aids in the operation.

Excess Energy and Nuclear Products

The Relationship of Crystal Structure Transition of Ti-Cathode and "Excess Heat" on Cold Fusion

Zhang Qingfu, Gou Qingquan, Zhu Zhenghe
Liu Fusheng, Luo Jiaoming, Sun Yue, Chen Licai

The Institute of Atomic and molecular Science at High Temperature and High Pressure, Sichuan Union University, Chengdu, 610065 China

Abstract

This paper presents an experiment result of crystal structure transition of Ti-cathode due to "excess heat" of cold fusion. It has been found that the crystal structure of Ti-cathode is changed from hexagonal to face-centered cube structure after cold fusion with "excess heat". On the contrary, there will be no observable change for that without "excess heat".

Key Word: Deuterium, Titanium, Structure of Lattice.

1. The x-ray analysis of Ti-Cathode before electrolysis experiment.

Before the electrolysis, the surface of Ti-rod was analyzed by x-ray, which showed that it was indeed oxidized into TiO_2 (Fig. 1) identified by x-ray spectral lines: (1) 0.3201nm, (2) 0.2500nm, (3) 0.2305nm, (4) 0.2203nm, (5) 0.2200nm, (6) 0.1695nm in good agreement with the standard x-ray spectral lines of TiO_2: (1) 0.324nm, (2) 0.249nm, (3) 0.229nm, (4)

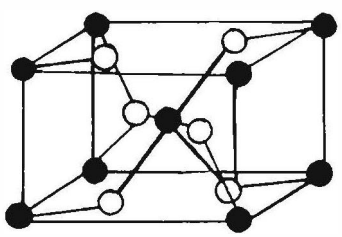

Fig. 1 The Crystal structure of TiO_2

0. 219nm, (5)0. 206nm, (6)0. 169nm. (Fig. 2). It was also examined by x-ray analysis that the inner part of Ti-rod is α-Ti(Fig. 3)identified by x-ray spectral lines: (1) 2. 563nm, (2) 2. 343nm, (3) 2. 240nm, (4) 1. 726nm comparable with the standard lines: (1) 0. 2558nm, (2) 0. 2341nm, (3) 2. 244nm, (4)1. 729nm of hexagonal α-Ti. (Fig. 4)

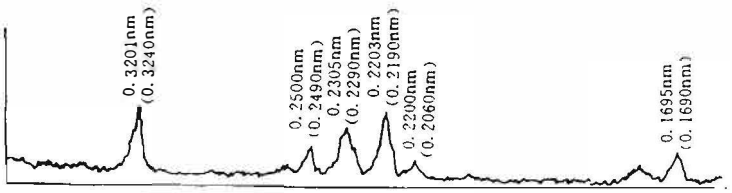

Fig. 2 The x-ray spectral lines of the surface of Ti-rod

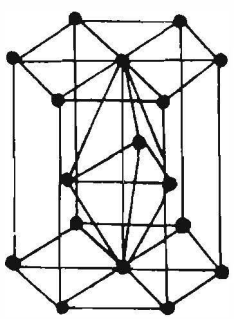

Fig. 3 The hexagonal crystal structure of α-Ti

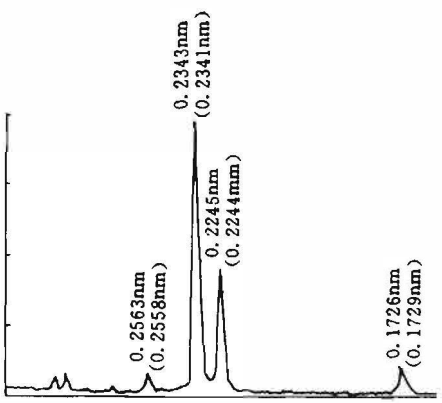

Fig. 4 The x-ray spectral lines of the inner part of Ti-rod

2. The crystal structure analysis of Ti-Cathode without "excess heat" during the electrolysis experiment.

The electrolytic solution was prepared to be a mixture of low purity D_2O and H_2O, therefore, it was not observed the "excess heat" after more than 20 days of electrolysis experiment. The Ti-rod we used was pretreated, so the x-ray analysis showed that the Ti-rod is α-Ti, and it was no change after

electrolysis. (Fig5. and Fig. 6)

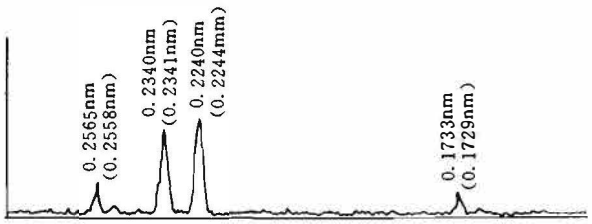

Fig. 5 The x-ray spectral lines of Ti-cathode before electrolysis

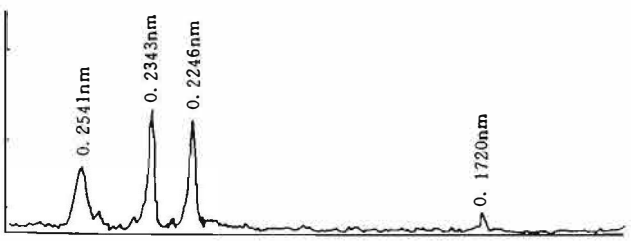

Fig. 6 The x-ray spectral lines of Ti-cathode after electrolysis without "exess heat"

3. The crystal structure analysis of the Ti-rod with "excess heat" during electrolysis.

The Ti-rod was pretreated, and the electrolytic solution consists of D_2O with 0. 1N (NaOD). After 70 hours or more, the "excess heat" happened. The effect of temperature ascent lasted on the Ti-cathode for more than 24 hours, where the highest temperature ascent is 24℃. (Fig. 7) Having been pretreated before the experiment, the surface stucture of Ti-cathode is that of α-Ti. (Fig. 8) However, x-ray analysis showed that surface structure of the Ti-rod changed into that of TiH_2, if there was "excess heat" effect happened.

Standard spectral lines of Ti-H_2 are: (1) 0.25nm, (2) 0.221nm, (3) 0.156nm, (4) 0.133nm, (5) 0.121nm, (6) 0.110nm, (7) 0.101nm.

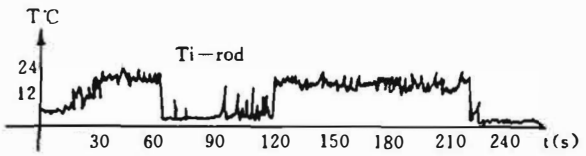

Fig. 7 The highest Temperature ascent of Ti-cathode on cold fusion

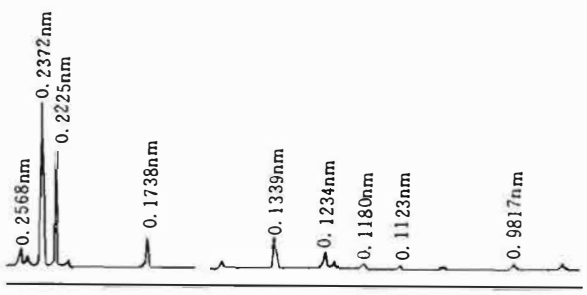

Fig. 8 The x-ray spectral lines of Ti-cathode before electrolysis

The spectral lines of Ti-fod after"excess heat" are: (1) 0.2533nm, (2) 0.2119nm, (3) 0.1535nm, (4) 0.1323, (5) 0.1261nm, (6) 0.1101nm, (7) 0.1008nm. (Fig. 9)

These 7 spectral lines correspond to the standard ones. We could say that the surface of Ti-cathode had been cahanged into Ti-D_2 structure. (Fig. 10)

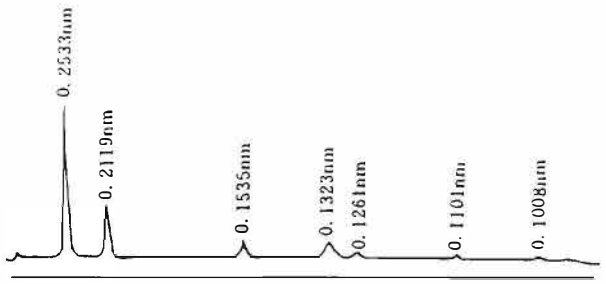

Fig. 9 The x-ray spectral lines of Ti-rod after electrolysis

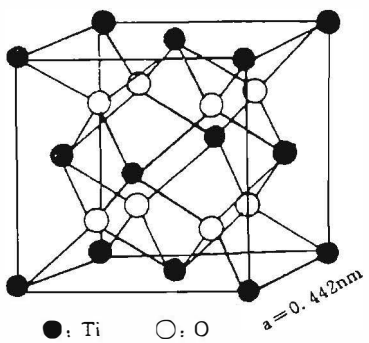

Fig. 10 The crystal stractrue of Ti-D_2

4. Conclusion

From the experiment, we could come to the conclusion that Ti-cathode absorbs D and then changes its crystal structure from hexagonal to the face-centered cube of TiD_2 owing to the electrolysis in D_2O. Because of these, the probability of collision will increase, which leads to nuclear fusion accompanied with remarkable "excess heat" effect.

References

[1] Q. Q. Gou, Z. H. Zhu. Q. F. Zhang, (1990) 《Chinese Journal of ATomic and Molecular Physics》 7. 3. 1491—1495.

[2] Q. F. Zhang, Q. Q. Gou, Z. H. Zhu et al, 《Frontiers Science Series》 No. 4. (1993) P. 531

[3] Q. F. Zhang, Q. Q. Gou, Z. H. Zhu, et al, 《Fusion Facfs》 Vol. 5. Number7. (1994) P28.

* The Project Supported by National Natural Science Foundation of China

Innovative Approach

A CONFIRMATION OF ANOMALOUS THERMAL POWER GENERATION FROM A PROTON CONDUCTING OXIDE

R.A. Oriani
Departent of Chemical Engineering and Materials Science
University of Minnesota
Minneapolis, MN 55455, USA

Abstract

The claims of Mizuno and collaborators, and the earlier claims of Biberian and Forrat, that excess thermal power can be developed by proton-conducting oxides held in deuterium gas at elevated temperatures are important because thermal power generated at high temperatures can be converted to other forms of power with greater Carnot efficiency than thermal power at lower temperatures. Therefore, a Seebeck calorimeter operating at 400°C was constructed to attempt to verify these claims. This calorimeter, whose operation is independent of the spatial distribution of power sources and of the thermal conductivity of the gas, is described.

The calorimeter was used with specimens of nominal composition $SrCe_{0.9}Y_{0.08}Nb_{0.02}O_{2.97}$ supplied by Dr. T. Mizuno. Two of these specimens produced positive deviations from the calibration curve by more than four standard deviations so that thermal power was produced that was greater than the d.c. power of alternating polarity supplied to the specimen. In several episodes excess power was produced without supplying any d.c. power.

Verification of the claims has been achieved. It remains to increase the reproducibility and the power output of the technique, as well as to achieve understanding of the underlying mechanism of the phenomenon.

Introduction

Beginning with the initial work of Pons and Fleischmann (1), a number of reliable calorimetric determinations have been carried out (2,3) that have demonstrated that in a variety of processes it is possible to obtain more thermal power than can be accounted for by the electrical power put into the system. At the Fourth International Conference on Cold Fusion, T. Mizuno (4) announced the generation of excess thermal power from a perovskite oxide held in deuterium gas at temperatures about 400°C (see also (5)). In these experiments the oxide specimen bathed by D_2 gas is maintained at the desired temperature by measured, constant electrical power delivered to a small furnace inside of a gas-tight enclosure. Then a voltage whose polarity is alternated at a frequency between 10^{-4} and 1 Hz is applied across the specimen thickness, generating a small, measured electrical power in the specimen. In some, but not all such experiments (about 12 out of 80 attempts), the specimen temperature was observed to rise considerably above the value consistent with the electrical power furnished to the specimen.

Because thermal power generated at high temperatures can be converted to other forms of power with greater Carnot efficiency than thermal power at lower temperatures, Mizuno's generation of excess power is particularly interesting. In addition, Biberian (6) following earlier work by Forrat (7) has also claimed to have generated excess power with $LaAlO_3$ in D_2 gas by a similar process. For these reasons it has seemed important to attempt to verify claims of the production of excess power from perovskite oxides. The present work has been done with a newly constructed Seebeck calorimeter using specimens of nominal composition $SrCe_{0.9}Y_{0.08}Nb_{0.02}O_{2.97}$ made and supplied by Dr. T. Mizuno of Hokkaido University.

Innovative Approach

The Seebeck Calorimeter

The principle of Seebeck calorimetry is the generation of a thermoelectric emf by a large number of thermocouple junctions connected in series in response to a temperature difference, ΔT, across the walls of an enclosure that totally surrounds a source of thermal power. The multiple thermocouples are arranged such that junctions of one polarity lie on the outside surface (that contacting a heat sink) of the enclosure, and junctions of the opposite polarity lie on the inside surface of the enclosure. If the thermocouple junctions completely and densely surround the source of thermal power and the thermal conductivity of the material of the enclosure is K, the thermal power transmitted to the constant temperature heat sink is $P_{out} = K\Delta T$, where ΔT is the average temperature difference across the enclosure walls as integrated by the multiple thermocouples, and at steady state P_{out} = thermal power generated within the enclosure. In practice it is, of course, impossible to cover the entire wall area of the enclosure since power leads, gas ducts, etc., must have access to the interior of the enclosure. Hence, in general at steady state $P_{source} = P_{out} = K\Delta T + a(T_i - T_s) + b(T_i - T_L)$, where T_i, T_s, and T_L are the temperatures of the source, the heat sink, and the laboratory, respectively. With proper design, the second and third terms can be rendered small, and the relation between P_{source} and the Seebeck signal, E_s, (which is linear in ΔT) can be established by calibration by using a known heat source.

The apparatus consists of three principal units. These are a gas-tight envelope for the specimen and furnace, the Seebeck thermoelectric device, and the thermostatted environment. These are discussed separately. The envelope (the reactor) for the specimen is a stainless steel closed cylinder welded to a stainless steel flange which mates via a copper gasket with another stainless steel flange through which enter the power leads for the small furnace that surrounds the specimen, and for the specimen and for an auxiliary heater, as well as a chromel-alumel thermocouple and a stainless steel tube which leads via swagelock fittings to a vacuum and gas-handling system made entirely of metal. The perovskite disc specimen, sandwiched between either thin palladium or platinum discs, is supported by perforated copper plates within the furnace made of nichrome wire wound on a spirally grooved ceramic tube. The specimens supplied by Dr. T. Mizuno measure about two cm in diameter by about 1 mm in thickness. The faces of the disc have been thinly coated with metal, either Pd or Pt Mo. Within the furnace is also a small coin-shaped ceramic cast about a spirally wound nichrome wire made and supplied by Mr. Jeff Driscoll. This device serves as an auxiliary heater used for calibration of the calorimeter. The junction of the chromel-alumel thermocouple is in the gas phase between the specimen and the inside of the furnace tube.

The Seebeck calorimeter itself is a parallelopiped enclosure made of machineable ceramic, and it surrounds the reactor on five sides. The sixth side, its base, rests on insulating ceramic. Through 1/16 inch diameter holes in each of the five sides a continuous wire of alternating chromel and alumel segments is threaded in such a way that the inside surface of the ceramic parallelopiped has 355 thermoelectric junctions and the outside surface has an equal number of junctions of opposite polarity. The thermoelectric emf developed by the temperature difference between the inside and the outside surfaces, integrated over the five sides, is measured both by a digital millivoltmeter and by a sensitive strip chart recorder. The latter continually records the difference between the thermoelectric emf and an applied adjustable constant voltage in order to increase the sensitivity of the recorder to small variations of the thermoelectric emf. The purpose of the strip chart recorder is to have a record of the time dependence of the thermoelectric signal, E_s. About 5 hours are required to attain steady state. Because of the greater sensitivity of the digital voltmeter, its readings of E_s at steady state are taken for plots of E_s vs. input power and subsequent analysis.

At steady state, that is when temperatures everywhere in the system are time independent, the thermoelectric emf is a measure of the power generated within the reactor. Clearly this necessitates a time-independent temperature of the environment that serves as a heat sink. This is accomplished by an insulated cylinder that envelopes the Seebeck calorimeter. It is fitted with a large-area heater and an air fan driven by a constant-speed motor. The average temperature of the air within this insulated jacket is maintained constant by a controller, operating between two adjustable power levels, which uses the output of four thermocouples connected in series as the distributed sensing element. In order to make the Seebeck calorimeter less sensitive to fluctuations in air movement between regions of different temperatures, the Seebeck box is closely surrounded by a five-sided enclosure made of copper sheet which causes the Seebeck system to "see" the average temperature of the circulating air.

Innovative Approach

All wire connections and the tube for evacuation of the retort and admission of gases to it are led out below the retort through an opening in the insulated platform that supports all of the systems described above. The platform in turn is supported by a stand which is entirely surrounded by an insulating skirt. A constant-current d.c. power supply furnishes power to the furnace within the retort. Separate d.c. power supplies furnish power to the auxiliary heater and to the specimen. In all cases the power delivered is measured by digital ammeters and voltmeters, taking care that the same instruments and settings are used both in calibrations and in the experimental runs. The signal from the thermocouple within the reactor is read by a digital millivoltmeter. The temperature of the circulating air is continuously recorded and also occasionally measured by a hand-held Fluke voltmeter.

Calibration of the calorimeter is accomplished by furnishing measured electrical power to the furnace and to the auxiliary heater and measuring E_s at steady state. By varying the ratio between the power supplied to the furnace and that supplied to the auxiliary heater it was verified that E_s is independent of the spatial distribution of the power sources, whereas the reading of the internal chromel-alumel thermocouple depends upon that distribution. The calibration is found to yield a linear E_s (P) relation, where P is the total input power. Furthermore, the E_s (P) relation does not depend on the thermal conductivity of the gas within the reactor , whereas the reading of the internal thermocouple is a strong function of the nature of the gas phase, and also of the spatial distribution of the sources of power. The regression lines fitted to the calibration data are characterized by very small standard deviations of the order of 0.1 mV for signals of the order of 70 mV.

Results and Discussion

The initial experiments with the Seebeck calorimeter were done by first establishing the E_s (P) relation with D_2 gas without the perovskite specimen in place. The reason for this precaution is that in earlier work with an isoperibolic calorimeter some results seemed to show generation of excess power before d.c. power was supplied to the specimen. After calibration without the specimen, the specimen was put in place within the reactor, the apparatus was reassembled and an experimental run was carried out. Generation of excess power is judged by comparing the E_s produced by a given value of P with the E_s value given by the calibration line for that value of P. The experimental run with a specimen in the reactor consisted of heating the reactor by means of the furnace while continually evacuating the reactor by means of a mechanical pump. After reaching a temperature in excess of 400°C deuterium gas was admitted to a pressure between 0.1 and 0.3 atm and a steady state was allowed to be attained. Direct current of alternating polarity was then applied to the specimen and steady state was again awaited. The frequency of alternation of polarity was between 0.1 and 0.003 Hz. The temperature of the air surrounding the Seebeck box was maintained constant at 106°C.

Many experiments were done in this fashion while the performance of the calorimeter was continually improved. Although some indications of the generation of excess power were obtained during this period none can be considered reliable. Final modifications of the calorimeter produced reliable operation. At this stage an experiment was carried out which yielded excess power (Experiment X). First a calibration was carried out, without the specimen in place, with deuterium gas in the reactor. Then the apparatus was totally disassembled, re-assembled and another calibration, again without a specimen in the reactor, was made. The two calibrations for E_s(P) agree with each other and can be fitted by a straight line characterized by $r = 0.9988$ and standard deviation $\sigma = 0.116$ mV. A perovskite specimen was then mounted within the reactor and an experimental run at about 410°C was carried out which is detailed in Table 1. The first point established without d.c. current into the specimen falls within one standard deviation from the calibration line, giving confidence that the calibration is valid for the experiment with the specimen in place. After this, 0.009 W of d.c. power with its polarity alternating at about 0.008 Hz was supplied to the specimen; the power to the furnace was adjusted attempting, unsuccessfully, to keep the total input power constant. This produced an E_s value above the calibration line, and the positive deviation persisted after the d.c. power to the specimen was turned off. After this, the experiment was continued at times with, and at other times without, d.c. power to the specimen. The steady-state points are all considerably above the calibration line. One can have considerable confidence that the six data points in Table 1 that lie at more than four sigma values above the calibration line exhibit the generation of

excess power. For orientation, a deviation, δ, of +0.6 mV represents excess power equal to 0.65 W which is considerably larger than the d.c. power into the specimen ranging from 0.047 to zero watt. Table 4 displays the values of excess power calculated from the positive deviations from the calibration line. The episodes characterized by more than 4σ deviation from the calibration line produced excess power over a cumulative time of 90 hours.

During the period leading to the successful experiment described above it was noted that now and then an $E_S(P)$ calibration was obtained after a disassembly/re-assembly sequence that was somewhat different from what had been obtained prior to that operation despite great care to reproduce exactly all features of the assembly. To avoid this possible source of uncertainty, it was decided to calibrate with a specimen already within the reactor, but using helium within the reactor to avoid the possible generation of excess power during calibration. Then without disturbing the apparatus the helium was evacuated and replaced by deuterium for the search for excess power generation.*

Six experiments were carried out as described, each one with a calibration using helium for which the standard deviation, σ, was calculated. The distribution of the deviations of the individual calibration points, characterized by the number, n, of sigmas, is shown in Table 2 in which the calibration data of experiment X are also included for completeness. The distribution of the n-values of all the calibration points is roughly Gaussian. Table 2 also displays the distribution of n-values for the individual data points of the power runs with deuterium of the six determinations that had been preceded by calibrations with helium, as well as for the data of Table 1. It is noted that all but one entry represent positive deviations, and that the distribution is heavily weighted toward large values of n. Most of the large values arise in two experimental runs, the one labeled X and detailed in Table 1, and run B, detailed in Table 3, from the sequence of six experiments that employed helium for the calibrations. Table 4 displays the values of excess power calculated from the positive deviations given in Table 3. Again, we pay attention only to the data characterized by more than 4σ deviation from the calibration line and note that excess power can be developed even without alternating d.c. power into the specimen. It is worthwhile to remark that the same perovskite specimen was used in experiment X (Table 1) first, then later in experiment B. This specimen was coated by Dr. Mizuno with 300 nm of platinum by sputtering. It is also worth recording that run B developed excess power only after some days during which the determinations were on the calibration line, after which a lengthy, high-temperature continuous evacuation of the reactor and heating of the vacuum lines were carried out. After obtaining the data given in Table 3 for Run B, the calorimeter was calibrated again with the specimen undisturbed in place and under helium, yielding points on the same calibration line as before.

These data provide strong evidence that under some conditions this strontium-cerium based oxide in an atmosphere of deuterium gas can produce thermal power, as claimed by Mizuno and collaborators. However, it is clear that the ratio of experiments with which success in generating excess power can be claimed to those which yield only points lying on the calibration line is small. Mizuno et al. have reported a similar experience. The factors that lead to this lack of reproducibility are unknown, but it is suspected that they are related to details of specimen preparation. In the present experiments much variation among the specimens was noted in the electrical resistance across the thickness of the specimens as well as of the faces of the discs, and also in the appearance of the metallic coatings on the disc faces. It is believed that success in developing reproducibility depends on learning how to produce the required characteristics in the perovskite, whether these be composition, dopant distribution, crystallite size, grain boundary structure and composition, etc. It is emphasized that the calorimetric method employed in this kind of work should not depend upon a measurement of temperature because the thermal conductivity of the ambient gaseous phase depends markedly upon its composition and this can change in the process of experimentation, leading to incorrect conclusions.

The magnitude of the thermal power generated in these experiments is small and clearly not interesting from a technological point of view. However, at the present stage establishment of the phenomenon is important. Much work is needed to increase the reproducibility and the power output, as well as to achieve understanding of the mechanism which is currently completely mysterious.

---

* I am indebted to my son, Steven R. Oriani, for suggesting this procedure.

Acknowledgments

The kindness and spirit of cooperation displayed by Dr. T. Mizuno in making specimens available are deeply appreciated. Grateful thanks are also extended to Dr. Francis Guillaume of the University of Minnesota for the construction of control electronics. Mr. Mark Hugo lent assistance during the early phase of this work. Mr. Dinh Ba Le is thanked for preparing some of the figures. Dr. John C. Fisher gave valuable advice relevant to the statistical treatment of the data.

References

1. M. Fleischmann and S. Pons, *J. Electroanal. Chem.* **261**, 301 (1989).
2. Edmund Storms, "Review of experimental observations about the cold fusion effect," *Fusion Technology* **20**, 433 (1991).
3. R.A. Oriani, J.C. Nelson, S. Lee, and J.H. Broadhurst, *Fusion Technology* **18**, 652 (1990).
4. T. Mizuno, M. Enyo, T. Akimoto and K. Azumi, Proc. 4th Intnl. Conf. on Cold Fusion, Vol. 1, p. 14-1, Electric Power Institute (1994).
5. T. Mizuno, T. Akimoto, K. Azumi, M. Kitaich, K. Kurokawa and M. Enyo. to appear in *Fusion Technology*, May 1996.
6. J.P. Biberian, Fifth Intnl. Conf. Cold Fusion, Monaco 1995.
7. F. Forrat, Patents F8907703 and F9008360, France.

TABLE 1
Details of Experiment X

d.c. power W	P, Total Input Power, W	E_s, mV	Duration of episode, h	δ, mV	n
0	65.20	73.60		+0.11	1
0.009	65.14	73.75		+0.32	2.7
0	64.83	73.72	17	+0.57	4.9
0.015	64.765	73.75	7	+0.66	5.7
0	64.77	73.74	16	+0.65	5.6
0.036	64.656	73.63	10	+0.64	5.5
0	63.44	72.12		+0.24	2.1
0	66.88	75.55	23	+0.52	4.5
0	68.22	76.61		+0.36	3.1
0	68.31	76.63		+0.30	2.6
0.039	68.36	76.67		+0.29	2.5
0.047	68.18	76.74	17	+0.52	4.5

Notes: E_s = Seebeck emf

δ = deviation of measured E_s of the poewr run from E_s calculated from regression line, E_s = 13.187 + 0.9152 P, for the calibration specific to this power run, for which r = 0.9988 and σ = 0.116 mV.

n = δ/σ

The tabulated numbers are listed in the order of experimental measurement.

TABLE 2
Distributions of n values ($n = \delta/\sigma$)

	For Power Experiments of Runs X and B		
n-values	all calibration points	Experiment X	Six D_2 runs
7.0 to 7.5			2
6.5 to 7.0			
6.0 to 6.5			
5.5 to 6.0		3	
5.0 to 5.5			
4.5 to 5.0		2	1
4.0 to 4.5			1
3.5 to 4.0			1
3.0 to 3.5		1	2
2.5 to 3.0		3	
2.0 to 2.5		1	4
1.5 to 2.0	1		2
1.0 to 1.5	5	1	4
0.5 to 1.0	5		4
0 to 0.5	10		5
-0.5 to 0	6		
-1.0 to -0.5	6		1
-1.5 to -1.0	2		
-2.0 to -1.5	4		

Notes: The second column refers to the data points of eight calibration runs. The third column refers to the data points (episodes) of power run X which followed two calibration runs using D_2 gas without the specimen in place. The fourth column refers to data points (episodes) of the six power runs each of which was preceded by a calibration run using He gas with the specimen in place.

TABLE 3
Details of Experiment B

d.c. power, W	P, total power, W	E_s, mV	Duration of episode, h	δ, mV	n
0	72.11	77.31		+0.073	1.3
0.25	72.49	77.61		+0.086	1.5
0.25	72.60	77.61		+0.003	0.05
0	79.423	82.87		+0.125	2.2
0.399	79.896	83.33	16	+0.229	4.1
0.432	79.876	83.49	24	+0.404	7.3
0.484	79.903	83.50	25	+0.393	7.1
0	79.40	82.98	16	+0.252	4.5
0	79.40	82.78		+0.052	0.9

Notes: E_s = Seebeck emf
δ = deviation of measured E_s from E_s calculated from regression line, $E_s = 22.93 + 0.75312$ P, for the calibration specific to this experiment, for which $r = 0.99982$ and $\sigma = 0.0556$ mV.
$n = \delta/\sigma$, where $\sigma = 0.0556$ mV.
The tabulated numbers are listed in the order of experimental measurement.

TABLE 4
Excess Power Energy Calculated for the Episodes Exhibiting Large Positive Deviations From the Calibration Line

Input d.c. Power, W	n, the Number of Standard Deviations Above the Calibration Line	Excess Power, W	Duration of Episode, h	Integrated Excess Energy, kJ
		Experiment X		
0	4.9	0.62	17	37.9
0.015	5.7	0.72	7	18.1
0	5.6	0.71	16	40.9
0.036	5.5	0.70	10	25.2
0	4.5	0.57	23	47.2
0.047	4.5	0.57	17	34.9
		Experiment B		
0.399	4.1	0.30	16	17.3
4.32	7.3	0.54	24	46.7
0.484	7.1	0.52	25	46.8
0	4.5	0.33	16	19.0

Innovative Approach

SOLID PROTONIC CONDUCTORS: CONDUCTIVITY, STRUCTURE, PROTON TRAPS, PHASE TRANSITIONS, EXCESS HEAT AND NEUTRON ANTI-EFFECT

A.L.Samgin, S.V.Vakarin, V.S.Andreev, V.A.Khokhlov, E.S.Filatov and V.P.Gorelov

Institute of High-Temperature Elecrochemistry
Russian Academy of Sciences
Ekaterinburg 620219, S.Kovalevskoy 20, RUSSIA

Abstract
In our study of high temperature proton conductor (HTPC) it is shown that thermal and radiation effects can be correlated to a set of peculiarities of their structural and electric properties. These materials may be considered as model object to be searched for the elucidation of mechanism of anomalous phenomena in solid/deuterium systems. The ceramics are in specific cases superior to palladium. Our experiments were conducted with ceramic sandwich-like structure on the base of strontium cerate, espesially synthesized, with porous platinum or palladium coating. Analysis of some peculiarities of conductivity nature of HTPC shows that conductivity can not be satisfactorily explained without considering interaction between protons as well as protons and crystal lattice environment. The available electrochemical data on ionic (in this case on hydrogen nuclei) transport suggest that processes of nuclear interaction simultaneously occur which may result in cold fusion phenomena. The phase transition at 445°C and similar behavior at other points in the range to 1000°C were found. We have established that pass through a region of phase transition is correlated to heat effect. A transition from exothermic to endothermic effect during cooling and heating of ceramic has been found. Analysis of X-ray studies shows that processes of explosive character inside lattice of sample, which give rise to the neutron and heat effects, can occur. We observed a incomprehensible influence of background on neutron emission, as well as a decay of neutron background inside the protection container with the sample.

1. Introduction

This study is the continuation of the investigation of anomalous phenomena in high temperature protonic conductors (HTPC) / deuterium systems, which have been submitted to the 3-th, 4-th and 5-th International Conferences on Cold Fusion. We reported about both discovered excess heat and neutron generation effects in such systems, and new physical properties of protonic conductors (e.g. the reduction of the ceramics at some conditions or the availability of unknown phase transition in samples, based on $Sr(Ba)CeO_3$, in the neighbourhood of 450°C), connected with manifestation of those effects. This suggests that the HTPC offer the greatest promise for cold fusion investigations.

In [1-4] the observations of excess heat and neutron emission in solid protonic conductors such as bronzes and $ACedO_3$ ceramics (where A is Sr or Ba, d is dopant, such as Nd, Dy Yb etc.) have been reported. In [5] the appearance of radioactive isotopes in the ceramics has been announced. In particular, as perspective materials for investigation of anomalous phenomena the different HTPC - Pd and HTPC - Pt sandwichs were used.

Innovative Approach

In [2] we proposed the hypothesis about the vital role of conductivity nature for such anomalous behavior. Furtheover, many cold fusion effects in solids can be considered with universal viewpoint based on proton conduction. In [2, 4] we found some examples of correlations of excess heat and conduction properties in doped $SrCeO_3$ ($BaCeO_3$) - Pt(Pd) systems.

This paper reports the subsequent investigation of possible correlation between anomalous effects in proton conductors and their electrical and structure properties.

2. Methods, results and discussion

Neutron measurements

The samples were prepared from protonic conductors based on the doped $SrCeO_3$ or $BaCeO_3$, with Pt or Pd porous electrode covers, in the form of discs as that is described in [4] .

The principal neutron registration system consists of two thermal neutron detector rings, with 15 counters in each ring, placed in a paraffin moderator (see fig.1 in ref. [4]). The plant well is of diameter 200 mm, the external ring is 350 mm in diameter, the internal ring is 250 mm in diameter. The cell with ceramic sample is installed in the well. The registration system is placed in a radiation shielding box, which consistes of polyethylene bricks contained 3 percent of boron.

The nuclear electronics simultaneously allows the displaying of amplitude distribution of events registered as result of nuclear reaction with boron nuclei in the counters, and time information on the neutron detector signals appearing, as well as result distribution of time intervals between events, successively registered both the neutron detector rings and the additional flat neutron detector placed on top of the box, within 1 ms. The signals from each detector system have been amplified by the preamplifier. The signal was sent to the spectrometric amplifier with shaping time constant 2mks, then it was treated by the analog-to-digital converters with conversion time less than 4 mks. A pulse amplitude code and pulse time mark have been written into intermediate memory by help of the synchronizator. The information was stored by means of CAMAC in PC-486 for further analysis, based on the methods developed in Los Alomos [6] and Dubna JINR [7] . The principal analysis involves the fitting of time distributions obtained in effective and background exposures.

To determine the efficiency of the detector ring a calibration with a Pu-α-Be neutron source (12000 ± 2500 n/s intensity into 4π angle) was made. The efficienty of the ring measurement was 1.5 ± 0.4 percent with a certain type of used counters. The measurement of the background by this system without voltage on the sample during two day was shown counts rate to be 0.08 1/s. It was established that for reliable analysis it is necessary to consider pulses in the range from 31 to 128 channels in the amplitude distribution, the rest part may be connected with detectore noise, electronic hindrance, electric and acoustic signals.

The experiments were described in references [4, 8]. In a serie of experiments during cooling the solid electrolytes to room temperature, after its electrolysis in deuterium atmosphere and thermal treatment by cooling-heating, the pulse count rate was observed as follows:

Pulse time, mks	Channel Number	Pulse time, mks	Channel Number
3 032 804	73	12 104 138	36
4 305 050	49	12 104 218	110
12 104 026	42	12 669 726	158
12 104 052	28	12 923 576	119
12 104 076	83	12 923 768	>255
12 104 098	28	12 957 710	160
12 104 114	33	12 975 742	>255

Pulse time, mks	Channel Number	Pulse time, mks	Channel Number
13 407 850	163	13 836 316	>255
13 407 884	>255	14 381 008	233
13 836 264	195		

The analysis of amplitude spectrum and time distribution of the events does not permit to make unambiguous conclusion about the nature of the observed burst. It may be in principe explained as: i) "sly" electrical hindrance, ii) neutron burst, in which time interval between the acts of neutron registrations may be less than 20 mks. The second explication is fully justified. The observed value of pulse count was insignificant greater than background level. The maximum background value, obtained after a number of measurements, has been shown as 9 pulses for measurement period of 16.8s. The "successful" obtained pulse count time distribution in the mentioned experiment in the time interval was fixed as 21 events.

Excess heat measurements

The method was described in [4]. Nontheless, basic information will be replicated below. As calorimeter the metall (Al) cylinder was used for the most part, and in some cases we conducted the excess heat measurements with the use of Calvet-type microcalorimeter.

We used a inner heater, placed in metallic cylinder, for two purposes: 1) for calibrating the calorimeter, 2) for creating strongly non-equilibrium conditions which manifest itself in the formation of temperature gradient at the sample.

The power was determined with the calibrating curves found for direct (U=10 V) and reverse pulse load (U=10 V or 40 V) of electrolysis of solid electrolytes under hydrogen/deuterium atmosphere at high temperature. This investigation has been conducted with particular reference to the pass through temperature region of phase transition in the cerate samples. The heat power given out during electrolysis in the case of reverse current can not be directly detected by this method without a special updating. That is why, the electrolysis power was calculated in line with maximum current.

The results of our large body of research are typical for the results presented at ICCF-5. Little doubt can be that a unknown heat excess effects exist, but their nature to be investigated. The heat excess exceeds power spent to producing electrolytic processes over 10 - 1000 percent depending on way of loading by deuterium. The thermal effect was greater for reverse current than for direct current, it was less for hydrogen atmosphere than for deuterium one.

The microcalorimetric investigations showed that both processes of output of heat pulses and decay of heat at such electrolysis take place. We found some regions in the temperature range from 250°C to 800°C connected with abnormal heat spike like behavior clearly defined for these doped ceramics, in particular near 500°C and 630°C (see typical curve 4 in [4]). The voltage of 10 V was applied to the sample. During the cooling of the sample we observed enough noticeable summary endothermic effect, while during heating of the ceramic, inversely, the exothermic effect has been found, both for hydrogen and deuterium atmosphere (greater for deuterium). This may indicate phase transition or other unknown process in the ceramic lattice. It should to note that in the period after our presentation at ICCF-5 the similar spike heat liberation and heat decay have been observed in clean barium cerate [13]. In contrast to that experiment we found this effect in doped ceramic. It is essential since the proton conduction exist precisely in doped samples of such composition resulted in a manifestation of cold fusion phenomenon.

As to nuclear products, the most likely exess heat is not correlated with neutron emission. But the mechanism of heat effect remains unclarified. In hydrogene atmosphere the exceeding

of neutron background was not observed. This probleme has aroused considerable interest in connection with investigation of phase transitions in HTPC, as it will be discussed below.

Conductivity

The experimental studies of conduction of electrolytes such as $SrCeO_3$ or $BaCeO_3$-based doped ceramics are summarized as follows [2, 4, 9, 10] : i) these oxides have p-type conduction in atmosphere free from hydrogen, ii) in hydrogen atmosphere they exhibit pure protonic conduction at temperature of 500° - 900°C, the conductivity is of 0.001 - 0.01 S/cm, iii) the protons are formed as results of processes:

$$H_2O + V_0'' \Leftrightarrow O_0^{\times} + 2H^{\bullet} \qquad (1)$$

$$V_0'' + 1/2O_2 \Leftrightarrow 2h^{\bullet} + O_0^{\times} \qquad (2)$$

$$H_2O + 2h^{\bullet} \Leftrightarrow 2H^{\bullet} + 1/2O_2 \qquad (3)$$

$$H_2 + 2h^{\bullet} \Leftrightarrow 2H^{\bullet} \qquad (4),$$

when V_0'' - oxygen vacancies, $O_0^{\times}$- oxide ion in the lattice, $h^{\bullet}$- hole, $H^{\bullet}$- proton, iV) in relation to gas pressure the reduction of sample may occurs resulted in the appearence of n-type electronic conduction.

It was been established that these conditions are sensible for manifestation of anomalous phenomena in ceramic-deuterium systems. The electrochemical observations are the most important for elucidation of the mechanism of cold fusion processes, which evidence that the nature of conduction can not be explained without idea of interactions of protons with lattice environment. The process of proton hops in the lattice formed the conductivity mechanism, is unknown in details. The appreciable energy-charge transfer processes may take place. It follows that conditions for nuclear interactions into ceramics can be realised resulting in so-colled cold fusion. This question will be described more thoroughly in the other papers.

Structure and structure changes

This problem is more complex in character than it seems. We conducted the analysis of X-ray structure data both pre- and after experiment with the samples by DRON-3 diffractometer. Our X-ray study shows that the sample based on $SrCeO_3$ has the orthorombic structure. However the structure can be strongly distinct even with identical composition depending from preparation of sample [13]. The chemical purity of ceramics, its microstructure pecullarities, its thermal history could favor one or the other of the possible conductivity mechanisms [14]. Some indications exist that the structural modifications of the lattice can take place during thermocycling when phase transitions are also considered. This can drastically affected the deuteron distribution, the splitting of the deuteron positions and their migration. We observed also the production of the additional phases such as $SrCO_3$ and CeO_2 in the test specimens, and the oscillations of electrical charasteristics . This can have a direct influence with non-reproducibility of cold fusion results.

The latest our investigations show that the samples, used to advantage in experiments on heat and neutron detection, have sever structural changes, which give an insight into mechanism of processes. A sharp decrease of the volume of elementary cell of the sample generating heat pulse has been found by X-ray method. As an example, the SrCeO3-based ceramic characterized by excess heat has in value $V=314,9\pm 0,1$ Å^3 before the beginning of experiment, and $V=313,8\pm 0,1$ Å^3 [11]. For oxide sodium tungsten bronzes resulted in neutron burst, this decreasing is more evident. All the crystals for which neutron emission was not observed, have the volume of the elementary cell enlarged or not changed [12,15]. From these results logical deductions are drawn that the process of compression happens in the

lattice. In this connection it is well to bear in mind that the test conditions with ceramics (electrolysis voltage U < 100 V, reverse current frequence f is of several of Hz or of a fraction of Hz) are similar to conditions of P.Bridgman's reological explosion under pulse electrical loading of materials. It is common knowledge that in conditions of Bridgman's explosion the many of chemical and physical processes in solid can go through the other mechanism as compared with normal conditions. This point will be corrected in a future study.

3. Ceramics as model object for cold fusion

Phase transitions

The role of phase transition is active discussed with "classical" scheme pertaining to PdD. But for cold fusion with protonic conductors the influence of this factor is taking new twists.

An important unexpected result of our research of electrical dc and ac conduction consist in the realisation of conditions for rupture change of conductivity charasteristics in doped $ACedO_3$ - ceramics under deuterium atmosphere. This testifies that unknown processes in lattice can occur contributed finally to phenomena observed. Our investigations of current dependences and calorimetric study enable the phase transition in doped ceramic to be found at 445°C [4]. Recently the availability of structural phase transition induced by the temperature variation was confirmed in undoped $BaCeO_3$ by other authors [13, 14]. Thus, the lattice ordering, fluctuations of some characteristics and even non-reproducibility of normal electric properties can be observed. In the latest experiments we obtained some indications on the availability of behavior, which is a close match to phase transition, at other points in the range from 200°C to 1000°C. Of special note is the very large correlation between pass through such temperature points and manifestation of anomalous phenomena.

As mentioned above, during cooling the sample, saturated with deuterium at electrolysis with voltage U = 10 V, we observed a endothermic effect, whereas during a heating the same sample the exothermic pulse process has been detected by the scan microcalorimeter. In line to our method [4], in all experiments the such order of the principle steps was used for heat generation as thermal cycling by means of the inner and outer heaters. This proves conclusively the advantage of the availability of phase transitions in the ceramics. As regards to possible "feedback" for nuclear reactions, the problem of this sort exists. To be sure, the "perfect" structure of the crystal lattice (of the conduction channels) is of vital importance in processes of energy transfer. One possibility of "positive feedback" for the heat generation in PdD systems is described by M.Fleishmann in [16].

Proton traps

A model of multibody fusion for deuteron clustering exists for Pd-deuterium system which looks supportive to some experiments [17]. The problems of particle traps in PdD also have aroused considerable interest. It is interesting to note in this connection that currently striking evidence for the association of protons in doped $SrCeO_3$ was observed using site-selective spectroscopy technique [18]. The quasielastic neutron scattering study of $SrCe_{(0,95)}Yb_{(0,05)}H_{(0,02)}O_{(2,985)}$ was shown, that a sequence of free diffusion and trapping-escape events of protons takes place [19]. The traps with radius of 2,6 Å can immobilize the protons. The nature of proton transport in solids is seen to be not fully understand. Thus their investigation brings us closer to elucidation of cold fusion effect.

Crack formation

The intensive crack formation on the ceramic samples has been observed in all our experiments shown excess heat [2, 4]. This can be du to the compression, to the structure changes or to the existence of shock wave into the sample.

4. Neutron "anti-effect"

Innovative Approach

We would like to call attention to one paradox event. Our investigations of neutron emission have shown the influence of background on yield of neutrons from ceramic.

Furthemore, during electrolysis in deuterium atmosphere depending from conditions and chemical purity of ceramic we have observed new neutron "anti-effect". Both before and after experiment we have measured the background during two days. It has adhered to normal distribution. But at thermocycling the abrupte changes in neutron counts rate were fixed into the shielding box with the cell (typical situation is presented on the fig.1). This decay appears near the points of phase transitions and lasts a few tens of seconds, followed by neutron burst. Analogous effect has been observed in the experiments with molten salt according our method, which is described in [20]. The nature of this phenomenon to be investigated.

We have discussed here some examples of use of ceramics as model object to name only a few.

References

1. K.A.Kaliev, A.N.Baraboshkin, A.L.Samgin et al. Proc. of III Intern. conf. on cold fusion, Japan, Nagoya, 1992. Universal Academy Press, p.241-244; Phys. Lett., 1993, v.A172, p.199-202.
2. A.L.Samgin, A.N.Baraboshkin, I.V.Murigin et al. Proc. of IV Intern. conf. on cold fusion, USA, Palo Alto, 1994, v.3, p.5-1 - 5-7.
3. T.Mizuno, M.Enyo, T.Akimoto et al. Ibid., v.2, p. 14-1 - 14-4. 4. A.L.Samgin, O.Finodeyev et al. Proc. of V Intern. conf. on cold fusion, 1995, France, Valbonne, p.201-208.
5. T.Mizuno, K.Inoda, T.Akimoto et al. Infinite Energy, 1995, Sept.-Oct., p.9 - 11.
6. V.A.Tsarev. Uspechi fisitches. nauk (in Russian), 1992, v.162, N.10, p.63-91.
7. V.I.Artyukhov et al. Preprint of Joint Institute for Nuclear Research, Russia, Dubna, 1991, D15-91-289.
8. A.L.Samgin, V.S.Andreev et al. Presentation on the Minsk intern. cold fusion conference, 1994, May, 21-26; Fusion facts, USA, 1994, v.6, N.4, p.16.
9. H.Iwahara. Sol.State Ionics, 1988, v.28-30, p.573-578.
10. N.V.Arestova, V.P.Gorelov. Electrochemistry (in Russian), 1994, v.30, N.8, p.988-990.
11. A.L.Samgin, S.V.Vakarin, V.S.Andreev et al. Proc. of III Russian conf. on cold fusion, 1996, Sotchi (in press).
12. S.V.Vakarin, A.L.Samgin, V.S.Andreev. Sent to J.Techn. Phys.Lett. 1996 (in Russian).
13. Yu.M.Baykov, V.M.Egorov, N.F.Kartenko et al. Ibid., 1996, v.22, p.91-94.
14. S.Loridant, L.Abello, E.Siebert et al Solid State Ionics, 1995, v.78, p.249-258.
15. S.V.Vakarin, A.L.Samgin, V.S.Andreev. In these proceedings.
16. M.Fleischmann. Proc. of the V Intern. conf. on cold fusion, 1995, France, Valbonne, p.140 - 151.
17. A.Takahashi. Proc. of the Fourth Inern. conf. on cold fusion, USA, 1994, v.4, p. 12-1 - 12.8.
18. A.S.Nowick, Yang Du. Solid State Ionics, 1995, v.77, p.137 - 146.
19. R.Helpelmann, Ch.Karmonik, Th.Matzke et al. Ibid., p.152 - 156.
20. V.A.Khokhlov, E.S.Filatov, A.L.Samgin et al. Abst. of ICCF-5, 1995, Monte-Carlo, p.209; Proc. of 2 Russian conf. on cold fusion, Sotchi, 1994, p.117-122.

Innovative Approach

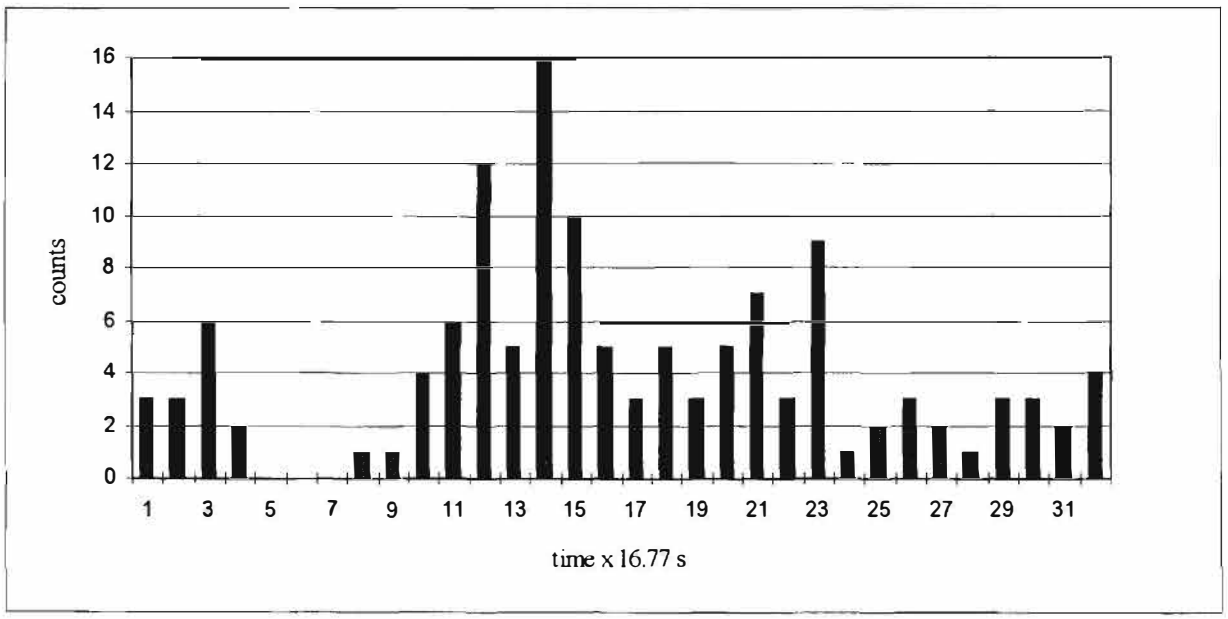

Fig. 1
Yield of neutrons as function of time for one of the experiments.

Innovative Approach

X-RAY DIAGNOSIS IN GAS DISCHARGE

Chen Suhe, Wang Dalun, Cui Gaoxian, Li Yijun, Wang Mei, Fu Yibei
Institute of Nuclear Physics and Chemistry,
China Academy of Engineering Physics,
P.O.Box 525-74, Chengdu 610003, P.R.China
Zhang Xinwei, Zhang Wushou
Institute of Applied Physics and Computational Mathematics,
Beijing 100088, P.R.China

ABSTRACT

It was found that X rays were yielded when the anomalous phenomenon in the metal loaded with deuterium was studied by the gas discharge method. The X-ray energy spectrum was measured and X rays were confirmed existing by the absorption method, the characteristic X-ray approach and the NaI scintillation counters. The average X-ray energy (26.9 ± 2.2 keV) measured by the absorption method is in agreement within the error range with X-ray one (26.0 ± 2.4 keV) detected by NaI scintillation counters. The X-ray intensity measured roughly by use of the ^{7}Li thermoluminescent foils is about 10^{9}-10^{10} s^{-1}.

KEY WORDS Nuclear fusion at normal temperature, Gas discharge, X-ray

1. INTRODUCTION

Considering the electromagnetic interferences involved in gas discharge, X-ray energy is measured firstly by use of the ^{7}Li thermoluminescent foils combined with the absorption method. As soon as the average X-ray energy (27 keV) is obtained, the characteristic X-ray approach is used to testify the above results. Finally the X-ray energy (27 keV) is measured again by the NaI scintillation counters and proven to be monoenergetic. The results given by the methods mentioned above are self-consistent.

2. X-RAY DIAGNOSIS AND RESULTS

2.1 Absorption Method

The sensitivity of a set of ^{7}Li thermoluminescent foils chosen is caliberated. The counts of the thermoluminescent foils irradiated are normalized by the sensitivity and corrected by background. The average X-ray energy derived from gas discharge is measured by the absorption method.

If the thermoluminescent foils have the same thickness and uniform density, the total mass attenuation coefficient $\mu_m(T)$ (cm^2/g) can be derived from the counts N_0 before and N_d after X rays through the foils:

Innovative Approach

$$\mu_m(T) = \frac{1}{\rho \cdot d} \ln \frac{N_d}{N_0} \qquad (1)$$

where ρ and d refer to the density and thickness of foils respectively.

Given the experimentally measured $\mu_m(T)$ and the relation between $\mu_m(T)$ and X-ray energy, the X-ray energy yet to be measured will be given by interpolation.

1) Measurement with different absorption foils: Cu, $(CH_2)_n$-polyethylene, Cd and LiF were chosen as the absorption foils, and then used to measure the X-ray energy in gas discharge.

2) Measurement of the X ray from discharging of various materials loaded with deuterium: The X-ray energy was measured in gas discharge by the absorption method when Ta, Ti, Pd, Nb, Zr and Fe were used as electrode.

3) Measurement of self-absorption of detector: Being taken as detectors and as absorbents of X rays, several of the ^{7}Li thermoluminescent foils were arranged into a string as shown in Fig. 1 when the counts N_n referes to the *n* th foil, thus $\mu_m(T)$ can be expressed in relation:

$$\mu_m(T) = \frac{1}{\rho \cdot d} \ln \frac{N_{n-1}}{N_n} \qquad (2)$$

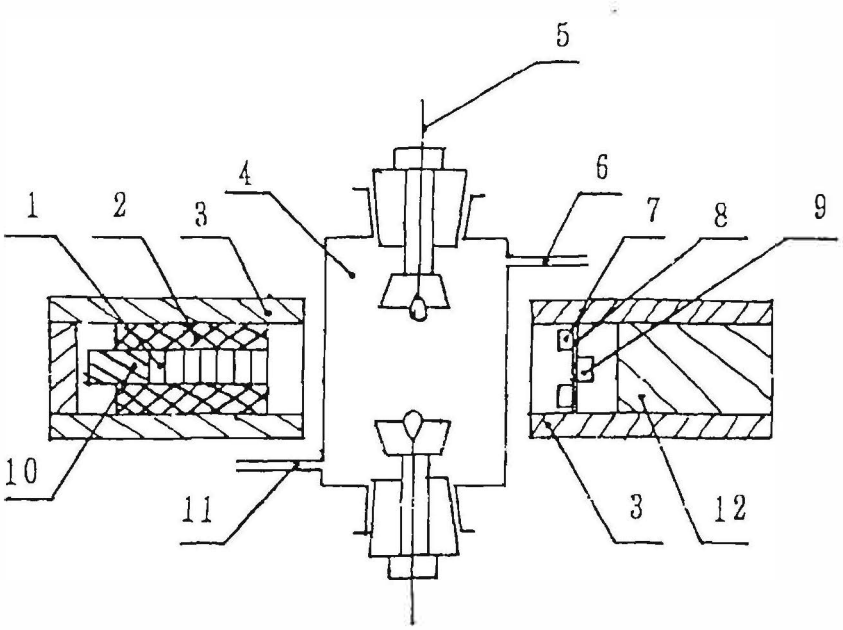

Fig. 1 Arrangement of thermoluminescent foils and absorption foils irradiated

1. ^{7}Li thermoluminescent foils; 2. polyfluortetraethylene sheath; 3. Pb shielding case
4. discharge chamber; 5. electrode; 6. gas inlet; 7. N_0 thermoluminescent foils; 8. absorption foils
9. N_d thermoluminescent foils; 10. plug; 11. To vacuum system; 12. Pb plug

The measured results in different conditions mentioned above are listed in table 1.

Table 1 The measured results of X ray average energy in gas-discharge

order	Measuring conditions		Average energy of X ray
1	Voltage : 11 kV, Gas of D_2, Different metal electrode	Ti	26.8± 2.2
		Ta	27.4± 1.6
		Pd	27.8± 3.2
		Nb	28.2± 4.3
		Zr	28.1± 5.8
		Fe	28.8± 4.7
2	Electrode of Ta, Voltage 11.5 kV; Different gas	3/4 D_2+1/4 H_2	28.2± 5.3
		99% D_2 +1% H_2	27.5± 4.7
		H_2	26.8± 5.3
		D_2	26.9± 4.6
3	Gas of D_2, Electrode of Ta, Voltage : 11kV; Measured results of Different absorbent	Cu	27.7± 1.2
		Cd	28.2± 1.1
		C_2H_4	28.1± 1.8
		^7LiF	26.6± 2.4

The average X-ray energy measured by the self-absorption method is listed in table 2.

Table 2 The average energy of X rays measured by the self-absorption method

Measuring conditions	Voltage . 11kV, electrode of Ta or Ti, gas of deuterium							
Order	1	2	3	4	5	6	7	8
Average energy of X rays (keV)	28.0± 2.4	28.2± 4.0	29.5± 2.6	26.2± 4.3	24.4± 4.0	28.8± 8.0	27.2± 5.8	29.3± 3.6
Order	9	10	11	12	13	14	15	
Average energy of X rays (keV)	29.1± 3.6	26.7± 3.0	22.5± 9.7	25.4± 6.2	23.6± 5.9	28.6± 6.1	26.0± 4.6	
Average value	26.9± 2.2							

2.2 Characteristic X-ray Approach

The specific absorption energy of cadmium is 26.7 keV and there is abrupt reduction of photon mass absorption coefficient nearby the energy. We can make use of this feature to identify whether or not the X-ray energy is 27 keV in gas discharge. In our experiments, the ^7Li thermoluminescent foils wrapped with Cu and Cd (both 0.5 mm in thickness) respectively were irradiated by X-rays emitted from the gas discharge facility. The experimental results are listed in table 3.

Table 3 The counts of ^{7}Li thermoluminescent foils wrapped with Cu or Cd

Experimental conditions	Wrapped with Cd (0.5 mm in thickness)	Wrapped with Cu (0.5 mm in thickness)	Background
Counts of ^{7}Li thermoluminescent foils (mGy)	0.412± 0.167	0.031± 0.004	0.018± 0.002

2.3 Measurement of NaI Scintillation Counters

The value 26.9± 2.2 keV given by the absorption method is the average X-ray energy. However by using NaI scintillation counters and an ^{243}Am γ source to measure and calibrate the X-ray energy, the X-ray energy yielded through gas discharge can be identified. Under three kinds of amplifying factor (k_1, k_2, and k_3), the pulse height spectra of X-ray yielded in the NaI scintillation counters are shown in Fig. 2.

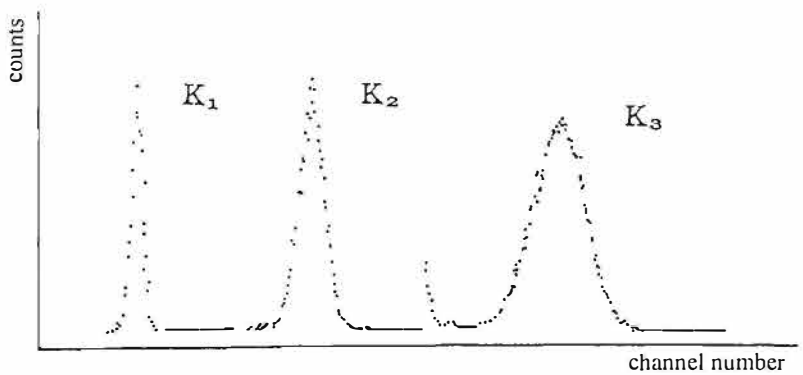

Fig. 2 X-ray spectra yielded by gas-discharge

3. DISCUSSION

Several points can be concluded from the diagnosis for X rays yielded in deuterium-filled gas discharge:

(1) In gas discharge, there exists a monoenergetic X-ray (27 keV) of which the energy is higher than the discharging voltage (11 kV). The repetition rate of the effect is 100% .

(2) X-ray energy varies independent of electrode material.

(3) X-ray energy is in no relation to the kind of discharging gas.

(4) How is the X ray yielded: Is it yielded in normal way or abnormal way? Problems remain to be investigated experimentally further.

REFERENCES

1 Karabut A B, et al. , Phys. Lett. , 1992 A 170 265.

2 Tasreev V A, et al. , Fusion Technology, 1992, 22 138.

3 Wang Dalun, Chen Suhe, Li Yijun, et al. , High Power Laser and Particle Beams, 1993 5(3) 333.

4 Wang Dalun, Chen Suhe, Li Yijun, et al. , Chinese Joural of Atomic and Molecular Physics, 1993, 10(3) 2789.

Innovative Approach

Transmutation Phenomena in the Palladium Cathode after Ions Irradiation at the Glow Discharge

Savvatimova I.B., Senchukov A. D.

SIA "Lutch", 142100, Russia, Podolsk, Moscow Region,
Zheleznodoroznaya St., 24

Chernov I.P.
Polytechnic University, Russia, Tomsk.

Abstract

It was shown that the change of impurity elemental and isotopic composition after irradiation of the Pd cathode by glow discharge plasma ions depends on the structure of the cathode material, contents of the working environment, ion flux density and the location of the analyzed layer relative to the surface. Secondary Ion Mass Spectrometry (SIMS) and microprobe x-ray analysis (EDS) were used.

The largest change of isotope ratio on the Pd cathode in comparison with a natural abundance appeared after irradiation with xenon and argon ions. The ^{104}Pd concentration increased two times in comparison with protium irradiation.

The dependence of the ratio of impurity elements and concentration upon the type of irradiating ions has been found. But a group of a certain impurity repeated after irradiation under similar condition by H, D, Xe + Ar ions. Elements such as Cl, P, Sc, Ti, V, Br, Ge, As, Kr, Sr, Y, Cd, In, Xe were observed. The quantity of additional impurity elements after ion irradiation decreased in the following order: D, H, Xe + Ar.

The maximum increase of impurities qualitatively correlated with the maximum in excess heat during of ion irradiation of palladium cathodes in a glow discharge.

Introduction

In previous works it was found that the elemental and isotopic composition changes on Pd cathodes after deuteron irradiation during glow discharges /1-8/. Weak radioactivity of the samples was observed. Weak radioactivity caused the blackening of the x-ray film located in contact with the samples after irradiation by deuterons, protons, argon and xenon ions. Activity of the samples (including foils of Pd, Ti, Ag, Nb and other materials), either directly irradiated by ions, or located below the irradiated materials (up to 7 layers of thickness 100 microns each) was registered / 4, 5 /.

The content of individual impurity elements increased by 2-4 orders according to spark mass-spectrometry, x-ray microprobe analyses. The increase of mass 107 and mass 109 (Ag) after irradiation from 2×10^{-3} at. % up to 5.10^{-1} at. % by spark mass-spectrometry method in a layer with a 10 micron thickness was observed. Impurity elements were observed which had been outside the sensitivity of microprobe x-ray analyses method before the experiment.

The presence of the high-energy and low-energy radioactive isotopes on Pd cathode after ion irradiation at the glow discharge was found by the radiography analysis / 4,5/.

Innovative Approach

The isotope shift tendency of the Pd cathodes and helium formation in Pd cathodes after deuterons irradiation was shown in previous research / 1, 3, 7, 8/.
The emission of γ-quanta, neutrons and charged particles were registered during the glow discharge and after termination of the discharge /1-3,6/ and under certain conditions excess heat was observed/ 7/. Observable effects were suggested to be possibly due to fission-fusion reactions (disintegration of the excited palladium, formation of Pd + xD complexes and the disintegration into lighter elements)/ 2/.

In this work the surface layers of 99.9% pure Pd cathodes before and after irradiation with deuterium, protium, argon and xenon ions were investigated. Particular attention was paid to the study of elemental and isotopic changes depending on the kind of the bombardment ions.

2. Methods

The installation included a vacuum chamber with cathode and anode units. It was equipped with devices for diagnostic and calorimetric measurement, as described in detail previously /1, 3/. A chamber evacuated to 10^{-2} Pa was filled with a working gas up to 300-1000 Pa. Deuterium, protium, argon and xenon and their combinations were used as the working gas. The irradiation of the samples was carried out at a current density of 10-50 mA·cm^{-2} and 50-600 volts. The duration of the glow discharge lasted 1-4 hours. The cathode samples were 20 mm diameter, and 100 microns thick, with an irradiation zone ≅ 1 cm^2. Multilayer cathodes consisting of several foils with a thickness ≅ 100 microns each were used to obtain more information.

Analysis of elemental and isotopic changes of the cathodes were conducted by SIMS and microprobe x-ray methods /EDS/. Research of the elemental composition of cathode materials was conducted using a Hitachi S-800 scanning electronic microscope with a Link Analytical LS-5 device for spectral analysis. The analysis was conducted in ions bombardment zone. The zone of the analysis was ~30 x 30 micron (in contrast to previous results which covered an area of ~1 micron diameter), with a depth of ~1 micron for the analyzed layer. The method sensitivity was 10^{-2} atom %.

The elemental impurity concentration was based on the most intense lines of x-ray spectra. Spectra before experiment were subtracted from the spectra after the experiment to create "difference" spectra as shown in Fig. 1. Spectra for three different places from the surface of each initial sample and the samples, irradiated under various irradiation conditions by the SIMS were received.

SIMS studies were conducted an MC-7201 M device. The samples were irradiated by argon ions with energy 6 keV. The zone of the irradiation was an ellipse with axes 1.5 and 3 mm. A layer of about 100 nm was removed from the samples during the analysis. The elements from structural equipment and residual atmosphere were not included in this measurement.

The second group of results was obtained using a special SIMS device. In this case, a record of the mass spectrum was conducted after removal of a surface layer of about ~100 nm depth by an ion beam before the analysis. A beam of ions N^{2+} with 4.5 keV energy and a current density of 10^{-5} A·cm^{-2} for sputtering of a target was applied. Masses from 1 to 27 and from 92 to 250 were recorded. The isotope change was calculated from the relation of individual isotope intensity to the sum of intensities of the all Pd isotopes. ^{102}Pd was excluded because its small intensity.

3. Results

The change in the natural abundance after Pd cathode irradiation by deuterium, protium, argon and xenon and their combinations was evaluated using a SIMS technique. The relative Pd isotopes intensity (104, 105, 106, 108 and 110 masses) before and after irradiation by deuterium and protium did not exceed 20% under different current and voltage parameters Fig 1. In other experiments, different ions (such as argon and xenon) produced isotope shifts in excess of possible measurement error, as shown in Fig. 3. The ^{104}Pd quantity after protium irradiation was ~ 8%, and after xenon and argon ions irradiation ~16.4 % under similar experimental conditions. For the initial sample the ^{104}Pd quantity was ~10.8%.

The quantity of the impurity elements changed under various experimental conditions such as the type of the bombardment ions. Another group of elements appeared. The spectra received from different sites of various samples (EDS methode) for similar conditions of experiments are essentially similar Fig. 4 shows the impurity elements of irradiated zone samples by deuterium, protium, argon and xenon ions.

Innovative Approach

Diagrams were constructed according to the maximum intensity of individual elements in "difference " spectra . This shows that the quantity of the impurity elements in Pd cathode depend on the kind

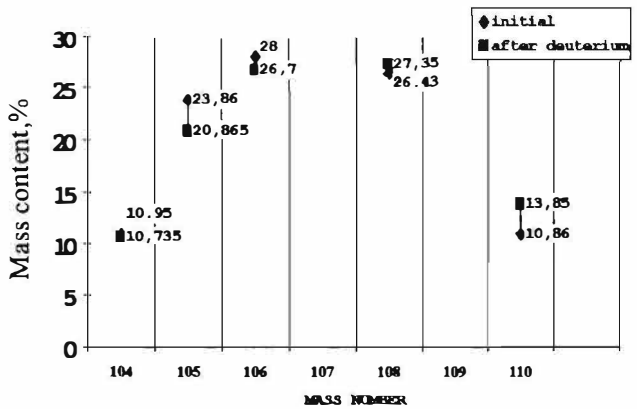

Fig. 1. Isotope composition onf palladium cathode before and after irradiation by deuterons.

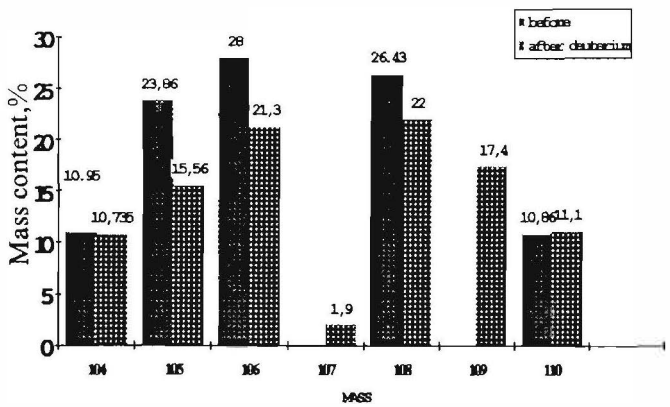

Fig. 2. Isotope composition of palladium cathode before and after irradiation by deuterons with 107 and 109 masses.

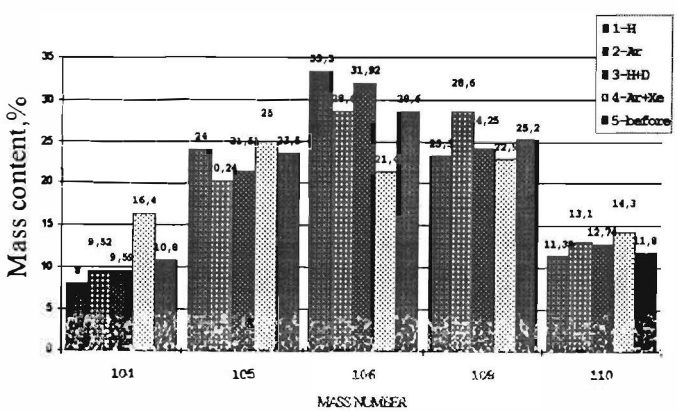

Fig. 3. Isotope composition of palladium cathode before and after irradiation by protons, deuterons, argon ions, and mixtures of argon and xenon ions, for similar irradiation conditions

of bombardment ions. The amplitude proportional to the quantity pulses of the maximum intensity for each element was taken. The data of intensity for several specters of each element (for five deuterium spectra) are not averaged and are represented in one interval on axis of abscissa. The largest quantity of impurity elements is found in Pd after deuterium ions irradiation. The predominating impurities were: Al, P, Zn, Ga, Ge, Br, Kr, Rb, Sr, Y, Zr, Ru, Ag, Cd, Yn, Sb, Xe, Cs, Ba. Such elements as Al, P, Zn, Br, Kr, Ag, Cd were 0.1- 1(Ag)%. Lower quantities are found after protium irradiation, and less still after irradiation by argon and xenon.

The such elements as Sc, V, Cd, In, P, Cl, Br, Ge, As, Kr, Sr, Y, Ru are never present in the discharge chamber. Xenon was not present in the chamber before experiments with deuterium.

The presence of the listed elements was not detected in non-irradiated samples.

4. Discussion

We noted, that the Pd cathodes impurities change Fig. 4 for different bombardment ions have:

1. Similarity of EDS spectra after irradiation by the same kinds of ions.
2. Reproducibility of the main registered elements;
3. Correlation EDS with SIMS results and previously published results using the spark mass-spectrometry method (SMS);
4. The maximum observed increase in impurities corresponded to the maximum measured excess heat in the process of irradiation Pd by deuterons / 6/.

If the increase in impurity content is explained by preferentia sputtering or diffusion of separate elements, the dependence of registered elements quantity on a type bombardment of ions should be different.

Innovative Approach

The maximum sputtering and separation effect would be found on Ar and Xe irradiated samples. This further suggests that nuclear reactions may be responsible.

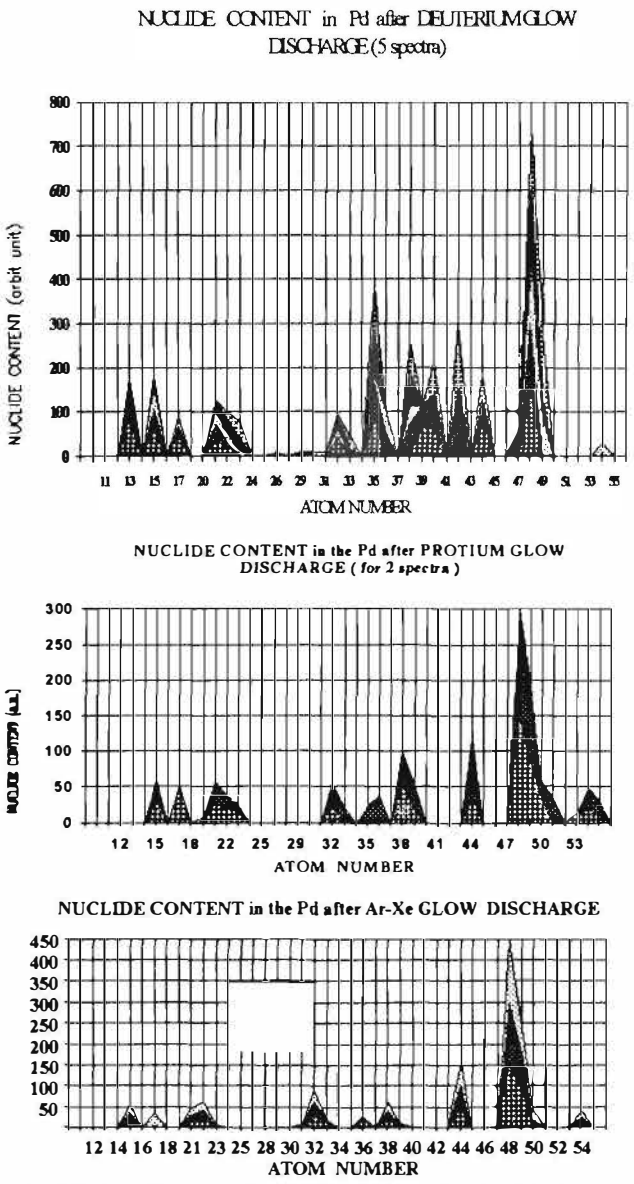

Fig. 4 Impurity content of the Pd cathode after experiments in glow discharge: a) deuterium; b) protium; c) argon and xenon ions.

The main group of impurity elements, including Sc, Ti, V; Ag, Cd, In; P, Cl, Br, Ge, As, Kr, Sr, Y, Ru, Xe was observed for all ion types. The elements with charge number Z=26-31 (Fe, Cu, Zn, Ga) and Zr are found under conditions of deuteron irradiation. Cs and I are observed more after proton irradiation. There are elements with charge number Z + (2 ± 1), Z/(2 - 1); Z - (12 ± 2); Z - (8 ± 2); Z + (8±1) on all diagrams.

It is possible that transmutation reactions were the results of the low energy ion irradiation, including fusion reaction (Pd + xD) and disintegration of "excited" Pd and clusters of formations of the different type (Pd + xD and probably others).

The SMS analysis results of the isotope ratio change after Pd cathode irradiation by deuterium, protium, and simultaneous protium and deuterium ions were previously published. Several elements were observed using SMS with an isotope ratio deviating from the natural isotope abundance by a factor of two or three, such as $^{10}B/^{11}B$; $^{12}C/^{13}C$; $^{60}Ni/^{61}Ni/^{62}Ni$ /; $^{40}Ca/^{44}Ca$; and $^{90}Zr/^{91}Zr$ /ref. 4/. Deviation from the natural ratio of Ag isotopes (109/107 as 3/1 to 9/1) in palladium cathode and change of the Pd isotope ratios was observed using SIMS / 4 /. The maximum of the 109 mass intensity was smaller in the analysis with a 100 nm "removed" surface layer.

As can be seen, ^{105}Pd decresed and ^{110}Pd increased for deuterium experiments. The observed isotope Pd shift essentially exceeded the change for comparable experimental regime of other ion types.

So, after irradiation by protium ions the ^{104}Pd content was 8 %, and after irradiation by argon and xenon ions the ^{104}Pd content was 16.4 % (Fig. 3.)..

The irradiation by low energy ions in a glow discharge plasma changes in structural and mechanical properties of the material. The mobility of elements of the matrix and impurities increases. Such defects as vacancy-poor zones, bubbles, dislocations, with loops and "roll" of the dislocation congestion are formed. The defects of the type: bubbles, rolls dislocation and dislocation of grids are high-temperature traps for such elements as hydrogen and the elements for the replacement. This fact can contribute to the phonon interactions in the crystal lattice. Besides, previously the authors showed that the crystal lattice existed as a pseudo-melted state during ions bombardment at glow discharge with high ion density for temperature less than 0.5 of the melting temperature /11-13/.

Increasing current density, results in increased density of dislocations, being high-temperature hydrogen traps. However, the temperature of the cathode and, accordingly, deuterium mobility and desorption is increased also. After deuterium desorption from the cathode the output of nuclear reactions products was not detected. The process of nuclear conversions on the glow discharge cathode is a complex phenomenon and the material structure influences this process only partially. The main factors are: non-stationary process (non-equilibrium conditions), type bombardment ions and ion flux density.

We notice maximum impurity elements change in all cases on samples after irradiation by deuterium ions. The isotope ratio violation is observed mainly in the layers near the surface, and accordingly, suggests that nuclear reactions occur mainly within ~1 micron of the surface. As was shown, the comparison of results obtained using various analytic methods indicated that the isotope ratio violation of 107 and 109 masses cannot be explained by formation of a hydrate or deuterate of a Ag isotope. But it is possible to suppose that 107 and 109 masses might be the palladium isotopes (Fig.2). The half life of Pd^{109} is 13.5 hours which roughly correlated to the decreased ability of the post-experiment sample to expose x-ray film /5/. Some samples showed gamma emissions from 10 to 70 times background in the range of several tens of keV and about twice times background values up to 1 MeV, as measured by a Ge-Li detector within ~15 minutes after extracting the cathode from the chamber.

In samples which were analyzed by the SIMS method a few weeks after irradiation in argon and xenon, both mass 107 and 109 mass with various isotopes ratio were found. They do not correspond to natural abundance. In samples analyzed some months later, only mass 107 was found. If this is due to Pd^{107}, the half-life would be > 10^6 years. This tends to suggest the existence of a nuclear reaction.

The changes of the elemental and isotopic composition of the cathode after electrolysis has also been observed by other researchers / 9,10 /. These researchers as well as the present authors have observed the formation of light and heavy elements group at the cathode after experiments.

The authors assume, that the majority of nuclear reactions take place mainly with the formation of stable isotopes.

5. Conclusion

There are some interesting theories that attract the attention of the present authors. The theory of Prof. Peter Hagelstein explains atomic and nuclear reactions as a mechanism resulting from decay of highly excited lattice. The unitary quantum theory of Prof. L. Sapogin and the slow nuclear excitation model of Ya.Kucherov, are very promising. Wave process and field interaction is supposed to play an importent role in New Hydrogen Energy, in the opinion of the authors.

The results of the investigations obtained for several series of the samples using various analysis methods, in author's opinion are well outside of the bounds of experimental error. The transmutation phenomenon exists, but it is nessasary to take attantion for more detail research.

References.

1. Karabut A. B., Kucherov Ya. R., Savvatimova I.B. Physics Letters A, 170, 265-272 (1992).
2. Karabut A.B., Kucherov Ya.R., Savvatimova I.B.Proc. ICCF-3,1992, Nagoya, p.165.
3. Karabut A. B., Kucherov Ya. R., Savvatimova I.B. Fus.Tech., Dec. 1991, v. 20(4.), part 2, p.294.
4. Savvatimova I., Kucherov Ya. and Karabut A., Trans. of Fus. Tech.: v.26, 4T(1994), pp. 389-394
5. Savvatimova I.B , Karabut A. B. Proc., ICCF5, Monte-Carlo, 1995, p.209-212; p.213-222
6. Karabut A.B, Kucherov Ya. R., Savvatimova I.B ICCF5, Monte-Carlo, 1995, p.223-226; p.241.
7. Savvatimova I.B, Karabut A. B. Poverhnost (Surface), V. 1, Moscow: RAN, 1996, p.63-75;.76-81
8. Savvatimova I.B Proc.of 3 Rus.Conf. Cold Fus.& Nuc.Transm., Sochy-95, Moscow,1996, p.20-49
9. Tadahiko Mizuno, Tadayoshi Ohmori, Michio Enyo. Journal Physical chemistry.
10.Reiko Notoya. Proc. ICCF-5 Monte-Carlo, 1995, p.531.
11. Savvatimova I.B, Karabut A. B. Mat. 2 Russia Conf. On Cold Nucl. Fus. and Trans.mutation of nucleuses. -Sochy, Sep. 19-23 1994, Moscow, 1995, page 184.
12. Babad-Zahryapin A.A., Savvatimova I.B., Senchukov A.D. Diffusion in monocrystals Mo and SiC at processing by low energy ions irradiation in glow discharge. Atomic energy, 48, v. 2, 1980, P.98
13. Babad-Zahryapin A.A., Savvatimova I.B., Physics and chemistry of processing of materials, N6,1981

Innovative Approach

Concentrated Energy and Micro Nuclear Fusion

Xing-liu Jiang and Li-jun Han
Department of Applied Mathematics and Physics
Beijing University of Aeronautics and Astronautics
Beijing 100083, P.R.China

Wen Kang
Department of Modern Physics
Lanzhou University, Lanzhou 730000, P.R.China

Abstract

For a electrolysis cell, high persistent electrical fields($>10^7$ V/cm) and large equivalent capacitance on cathode surface lead to a high concentrated energy density in the double layer. The enhancement of localized fields due to normally existing protrusion or cracks after long period loading with deuterium on the palladium cathode surface conducts high transient current density. Nonequilibrium conditions lead to the occurrence of energy concentration, the current filamentation and the chaotic processes in the lattice for the fusion reaction to occur.

Key words: Cold fusion, Electrolysis, Field enhancement, Concentrated energy

I. Introduction

Cold nuclaer fusion appears to be a sporadic, nonequilibrium processes in the Pd-D, Ti-D or Ni-D systems.[1,2,3] A highly concentrated energy is required for the area where nuclear fusion reaction occurs. For an electrolytic cell, one can see that bubble chains of hydrogen gas come out mostly from the protrusion of the cathode. This phenomena implies that denser electron flux appears on protrusions of cathode surface due to the tip effect similar to the point discharge of the electrodes in air or in vaccum. The high energy densities and high charge densities occur on the tips due to high electric field.

Innovative Approach

Increasing current density, results in increased density of dislocations, being high-temperature hydrogen traps. However, the temperature of the cathode and, accordingly, deuterium mobility and desorption is increased also. After deuterium desorption from the cathode the output of nuclear reactions products was not detected. The process of nuclear conversions on the glow discharge cathode is a complex phenomenon and the material structure influences this process only partially. The main factors are: non-stationary process (non-equilibrium conditions), type bombardment ions and ion flux density.

We notice maximum impurity elements change in all cases on samples after irradiation by deuterium ions. The isotope ratio violation is observed mainly in the layers near the surface, and accordingly, suggests that nuclear reactions occur mainly within ~1 micron of the surface. As was shown, the comparison of results obtained using various analytic methods indicated that the isotope ratio violation of 107 and 109 masses cannot be explained by formation of a hydrate or deuterate of a Ag isotope. But it is possible to suppose that 107 and 109 masses might be the palladium isotopes (Fig.2). The half life of Pd^{109} is 13.5 hours which roughly correlated to the decreased ability of the post-experiment sample to expose x-ray film /7/. Some samples showed gamma emissions from 10 to 70 times background in the range of several tens of keV and about twice times background values up to 1 MeV, as measured by a Ge-Li detector within ~15 minutes after extracting the cathode from the chamber.

In samples which were analyzed by the SIMS method a few weeks after irradiation in argon and xenon, both mass 107 and 109 mass with various isotopes ratio were found. They do not correspond to natural abundance. In samples analyzed some months later, only mass 107 was found. If this is due to Pd^{107}, the half-life would be > 10^6 years. This tends to suggest the existence of a nuclear reaction.

The changes of the elemental and isotopic composition of the cathode after electrolysis has also been observed by other researchers / 9,10 /. These researchers as well as the present authors have observed the formation of light and heavy elements group at the cathode after experiments.

The authors assume, that the majority of nuclear reactions take place mainly with the formation of stable isotopes.

5. Conclusion

There are some interesting theories that attract the attention of the present authors. The theory of Prof. Peter Hagelstein explains atomic and nuclear reactions as a mechanism resulting from decay of highly excited lattice. The unitary quantum theory of Prof. L. Sapogin and the slow nuclear excitation model of Ya.Kucherov, are very promising. Wave process and field interaction is supposed to play an importent role in New Hydrogen Energy, in the opinion of the authors.

The results of the investigations obtained for several series of the samples using various analysis methods, in author's opinion are well outside of the bounds of experimental error. The transmutation phenomenon exists, but it is nessasary to take attantion for more detail research.

References.

1. Karabut A. B., Kucherov Ya. R., Savvatimova I.B. Physics Letters A, 170, 265-272 (1992).
2. Karabut A.B., Kucherov Ya.R., Savvatimova I.B.Proc. ICCF-3,1992, Nagoya, p.165.
3. Karabut A. B., Kucherov Ya. R., Savvatimova I.B. Fus.Tech., Dec. 1991, v. 20(4.), part 2, p.294.
4. Savvatimova I., Kucherov Ya. and Karabut A., Trans. of Fus. Tech.: v.26, 4T(1994), pp. 389-394
5. Savvatimova I.B , Karabut A. B. Proc., ICCF5, Monte-Carlo, 1995, p.209-212; p.213-222
6. Karabut A.B, Kucherov Ya. R., Savvatimova I.B ICCF5, Monte-Carlo, 1995, p.223-226; p.241.
7. Savvatimova I.B, Karabut A. B. Poverhnost (Surface), V. 1, Moscow: RAN, 1996, p.63-75;.76-81
8. Savvatimova I.B Proc.of 3 Rus.Conf. Cold Fus.& Nuc.Transm., Sochy-95, Moscow,1996, p.20-49
9. Tadahiko Mizuno, Tadayoshi Ohmori, Michio Enyo. Journal Physical chemistry.
10.Reiko Notoya. Proc. ICCF-5 Monte-Carlo, 1995, p.531.
11. Savvatimova I.B, Karabut A. B. Mat. 2 Russia Conf. On Cold Nucl. Fus. and Trans.mutation of nucleuses. -Sochy, Sep. 19-23 1994, Moscow, 1995, page 184.
12. Babad-Zahryapin A.A., Savvatimova I.B., Senchukov A.D. Diffusion in monocrystals Mo and SiC at processing by low energy ions irradiation in glow discharge. Atomic energy, 48, v. 2, 1980, P.98
13. Babad-Zahryapin A.A., Savvatimova I.B., Physics and chemistry of processing of materials, N6,1981

Innovative Approach

Concentrated Energy and Micro Nuclear Fusion

Xing-liu Jiang and Li-jun Han
Department of Applied Mathematics and Physics
Beijing University of Aeronautics and Astronautics
Beijing 100083, P.R.China

Wen Kang
Department of Modern Physics
Lanzhou University, Lanzhou 730000, P.R.China

Abstract

For a electrolysis cell, high persistent electrical fields($>10^7$ V/cm) and large equivalent capacitance on cathode surface lead to a high concentrated energy density in the double layer. The enhancement of localized fields due to normally existing protrusion or cracks after long period loading with deuterium on the palladium cathode surface conducts high transient current density. Nonequilibrium conditions lead to the occurrence of energy concentration, the current filamentation and the chaotic processes in the lattice for the fusion reaction to occur.

Key words: Cold fusion, Electrolysis, Field enhancement, Concentrated energy

1. Introduction

Cold nuclaer fusion appears to be a sporadic, nonequilibrium processes in the Pd-D, Ti-D or Ni-D systems.[1,2,3] A highly concentrated energy is required for the area where nuclear fusion reaction occurs. For an electrolytic cell, one can see that bubble chains of hydrogen gas come out mostly from the protrusion of the cathode. This phenomena implies that denser electron flux appears on protrusions of cathode surface due to the tip effect similar to the point discharge of the electrodes in air or in vaccum. The high energy densities and high charge densities occur on the tips due to high electric field.

Innovative Approach

II. Electrochemical Double Layer and Point-effect

For an electrolysis cell, the electrolyte with high conductivity ,and the electrochemical double layer with large layer capacity lead to a typical structure of the cathode potential distribution similar to the cathode potential drop of glow discharge in low gas pressure (Fig. 1).

For a compact layer, the thickness of double layer equals to one ionic layer and across which is a linear fall of potential .Thus a high electric field appears on the surface of the cathode.

The local enhancement of electric field on the cathode surface winthin the dou ble layer is related to the protrusions and cracks similar to the tip effect of discharge in air or in vaccum. The current distribution depend strongly on the surface roughness and the work function of the electron emis.-sion. A high transient current density ($>10^6 A/cm^2$) could be expected due to the enhanced field.

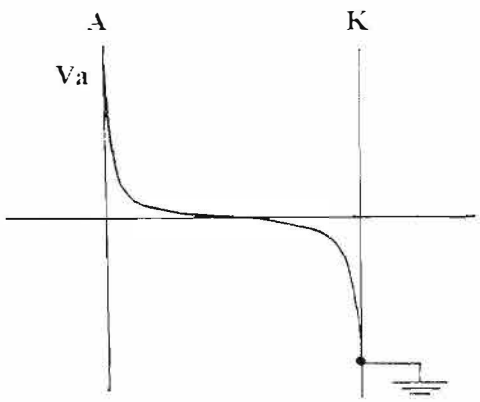

Fig.1 Potential distribution of electrolysis cell with high conductivity of electrolyte.
A: Anode; K: Cathode; Va: Applied voltage.

III. Concentrated Energy and Cold Fusion

On the cathode surface the high persistent electrical fields ($>10^7 V/cm$),and large equivalent capacitance($>250\mu F/cm^2$)[4] lead to a high energy concentration in the double layer.The concentrated field on the tips of the protrusions or cracks after long period loading with deuterium on the palladium cathode surface creats a high transient electron flux because of the large distributed capacitance and the negligible inductance in a localized discharge mini-network(Fig. 2).

As electron flux with high current density is extracted from the tips of cathode surface.A tiny vortex of cluster containing electrons and deuterons could form in the interface between the cathode and the electrolyte of heavy water. The experimental data show that the locus of the cold fusion reactions is the surface of some metallic deuterides(hydrides). The reactions take place only in some restricted areas that have specific properties.The idea of micro fusion due to some effects of the tip effect,the formation of bubbles and cracks leading to the energy concentration and the deuteron flux focusing could be used to explain cold fusion.

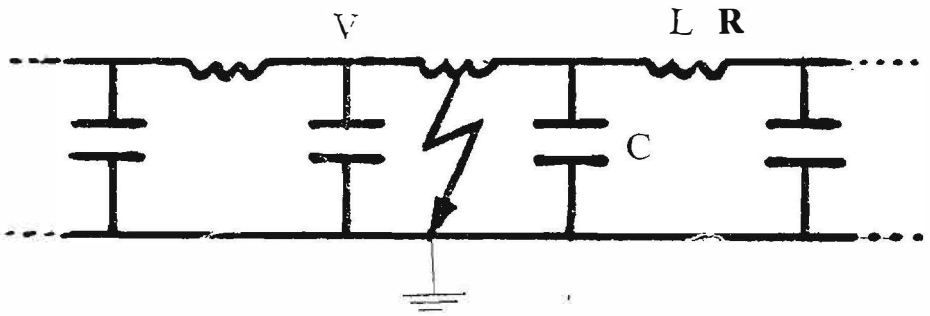

Fig.2 Equivalent RLC mini-network of the electrochemical double layer.
R: Resistance; L: Inductance; C: Capacitance.

IV. Nonlinear Processes

In metal deuterids there exist a possible transient dynamic process which may generate the close pairs and clusters of deuteron in the motion to induce a strong screen effect on the repulsive barrier. There is a variety of nonlinear processes which could be taken into consideration.

a. Work function changing due to loading ratio of D/Pd

b. Electrical conductivity changing due to loading ratio of D/Pd

The experimental results prove that the resistance of Pd with a loading ratio of D/Pd over 0.85 decreases eventually. Such a behaviour could conduct cascade effect in a tiny area with concentrated deutron flux .

c. Temperature raises locally.

Higher temperature occurs in the tiny area due to Joule heating by locally high current density. This factor leads to a transient deuteron flux in the phase boundary area.

d. Influerence of magnetic field on the distribution of deuterium .

Azimuth magnetic field created by transient electron current with high flux density causes redistribution of the deuterons inside the palladium lattice.

e. Polarization and coherence effects

High persistent field in addition of the transient electric and magnetic fields lead to the polarization and coherence of the deuterons with quadrupole momentum

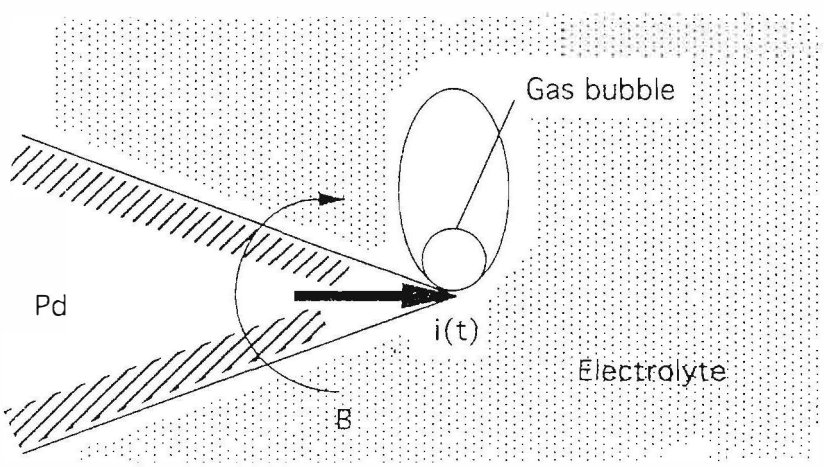

Fig.3 Triplet region of protrusion in the electrochemical double layer.

f. Triplet region (Fig3.)

The transient processes of triplet of the interface of the palladium lattice ,the electrolyte and the gas bubble should be taken into carefully examination due to its complicated situation .

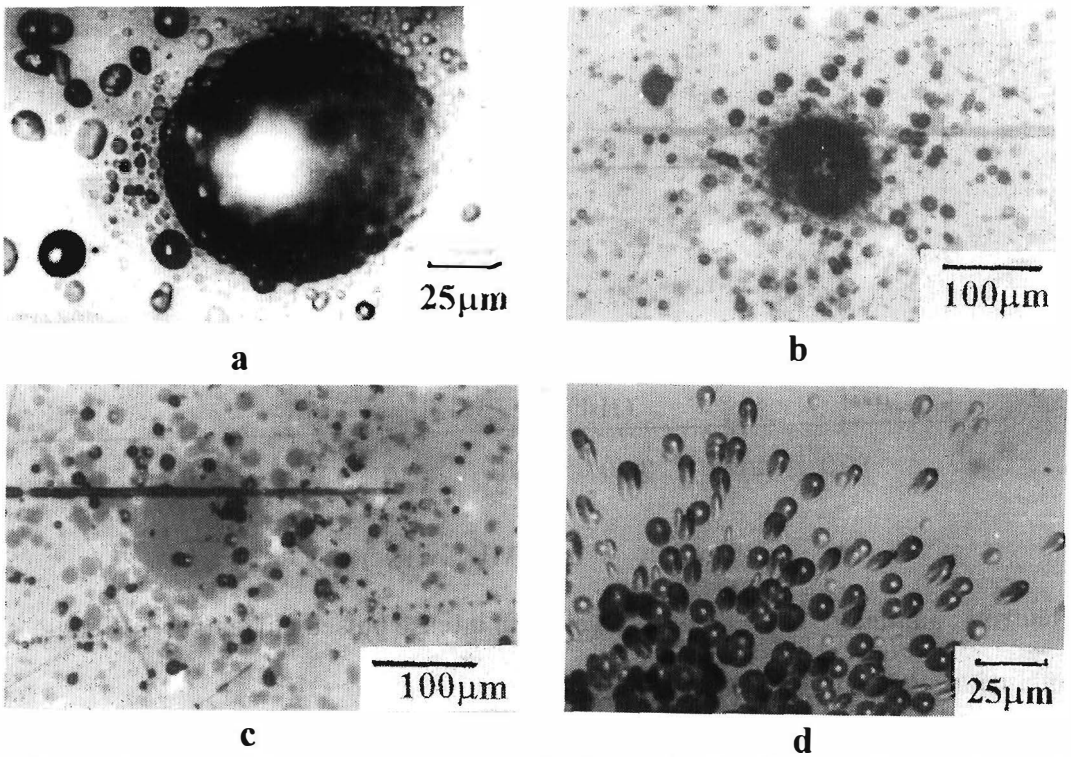

Fig.4 The tracks on the CR-39 detector, a: track cluster; b: distribution of enegetic particles caused tracks; c: back side of the track cluster on the same region with case b; d: typical tracks of background radiation.

V. Experiment

The CR-39 plastic films possessing with a high degree of optical clarity and isotopy in track response,and sensitive to n,p,t,alpha particles were used to detect the products of CF.The films of CR-39 were immersed in the NaOH electrolyte of heavy water and placed adjacent to the tips of the cathode .After 110 hous electrolyte experiment with the applied 1V and the current 2mA,the CR-39detectors were taken out of the electrolysis cell and then etched by 6.25N NaOH solution in 70°C for 11 hours, The photo micrograph in Fig.4 shows the cluster of tracks forming a circle crater with ~ 100μm in diameter and ~ 25μm in depth .According the etching condition,the energies of the most of particles of the fusion products p,t,Alpha are estimated roughly to be in the range of 1-4MeV.From the tiny track cluster of ~ 100μm in diameter,one can easily deduce that the fusion reaction area should be smaller ,and we could draw a conclusion on this ,the case of tiny fusion area is closely related to the point -effect

For the enhancement of the point-effect and energy concentration ,the high voltage pulse(30KeV) have been applied on the eletrolysis electrodes,the total electrolysis currents are more than 100A, neutron bursts have been detected (Fig.5).

Innovative Approach

From Fig.5,one can see that for the similar electrolysis cell ,the neutron counts are slightly higher than background counts.When higher currents have been applied,higher counts have been detected. The rapid movements of deuterium inward and outward of the palladium lattice are believed to be beneficial for nuclear fusion.

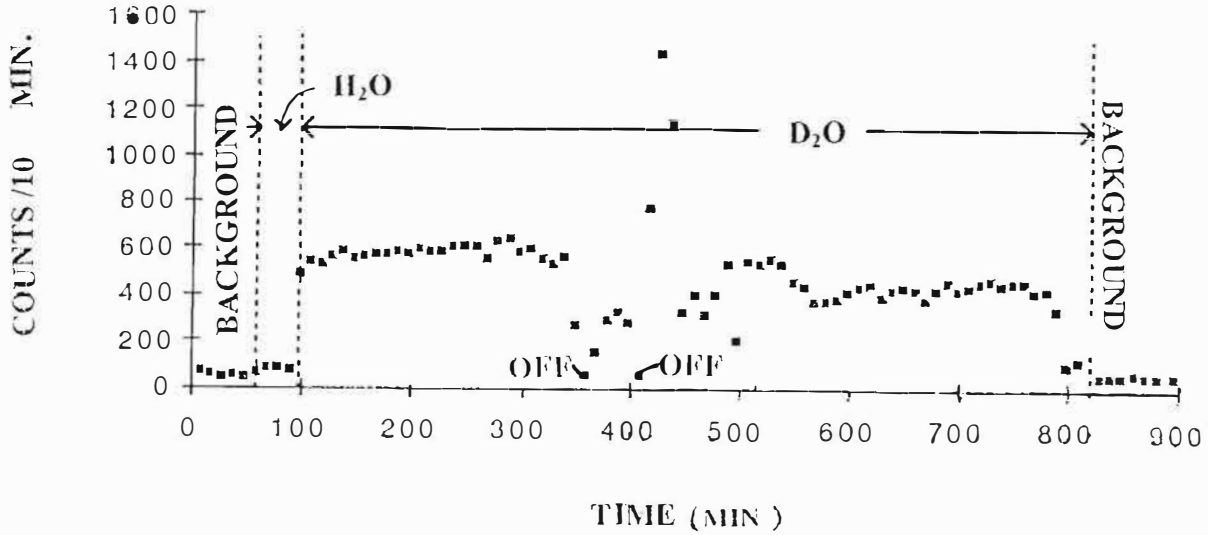

Fig.5 Neutron counting of the electrolysis cell with intense pulsed currents by BF_3 detector.

VI. Conclusion

As the researchers, theorytisians or experimentists of cold fusion should pay great attention on the general process of the electrolysis to find the key points which could play major role of the transit from the electrochemical processes to the electromagnetic processes.and further to the nuclear processes. For authors`s point of view,the evolution of double layers is of importance to understand the anomalous effects.

AKNOWLEDGMENT

The subject is supported by the National Natural Science Fundation of China.

REFERENCES

1. M. Fleischmann and S. Pons, "Electrically Induced Nuclear Fusion of Deuterium",J. Electroanal. Chem.,261,301(1989).

2. Proc. 3rd Int. Conf. Cold Fusion, Nagoya, Japan, 1992, Universal Academy Press(1993).

3. X.L.Jiang,N.Xu, and L.J.Han, "Point Effect and Nonequilibrium Conditon in Electrolysis Experiments." Proc. Anomalous Nuclear Effects in Deuterium/Solid System, Provo, Utah, Oct.22-23, 1990, p.228, American Institute of Physics(1991).

4. G.Korluem and J.O'M. Bockris, Textbook of Electrochemistry,Vol.II, Elsevier Publishing Company, Amsterdam,1951,p.364.

Innovative Approach

TRITIUM GENERATIONS AT TRANSFUSION OF HYDROGEN ISOTOPS THROUGH TARGET IN PLASMA OF POWERFUL GLOW DISCHARGE

V.A.ROMODANOV, V.I.SAVIN,*Ya.B.SKURATNIK

StateSRI SPA "LUTCH", Zheleznodorozhnaya 24, Podolsk, Moscow reg.142100, RUSSIA.
T.:095-137-9258, F.:095-137 9384, E-m.: luch@adis.msk.su
*StateSC RF "Karpov SRPCI", Vorontsovo pole 10, Moscow, 103064, RUSSIA.

Abstract

The valuation on influence of formation hydrogen complexes for tritium generation rate, by means of use the flow return of gas in side to plasma is conducted. Is shown, that deuterium transfusion through sample in plasma for V, Nb, Ta has not rendered the appreciable influence on tritium generation rate. For samples from molybdenum singlecristal and polycristal the deuterium transfusion resulted in increase of tritium generation rate in two times, in comparison with stationary conditions.

At long researches (more 1000 h) with transfusion return of hydrogen isotops through samples from molybdenum polycristal is established, that the influence of deuterium transfusion on tritium generation rate had the casual nature, while protium transfusion was resulted in significant reduction of spread and stabilization of results.

1 INTRODUCTION

At registration for allocation of hydrogen isotops from metals it is necessary to take into account the isotops effect, which for majority of metals is displayed that more heave of hydrogen isotops penetrate in metal worse than light isotops. However, in metal heave isotops and leave its in last turn. Such dependence can deform the results for measurements of tritium contents in metals, at analysis of gas tests, if the reliance is not present, that was managed to extract tritium whole. For some metals, for example, palladium, is observing the reverse isotops effect, when heave isotops of hydrogen is leave the metal better than lights. One of methods, helping to extract of heave isotops from metals, is the creation of diffusion flow for more lights isotops through metal. This method, in kind counter transfusion, us early was used for increase of safety of storage tritium in volume of thermo-nuclear reactors [1]. The first experiments with deuterium transfusion through samples of vanadium, niobium, and zirconium have shown the significant influence of such effect on occurrence in spectrum of mass to heave complexes and on quantity tritium recording [2,3] In [4,5] the assumption is stated, that the formation of complexes isotops to hydrogen can facilitate further going of nuclear reactions and to increase, thus, the tritium generation rate. Transfusion of hydrogen isotops light through sample can increase the reproducibility of tritium registration and safety of determination to characteristics of behaviour for hydrogen in metals.

The present work is devoted to increase of reproducibility for tritium registration, at effect of hydrogen isotops on metals from plasma powerful glow discharge, for transfusion through sample more light isotops.

Innovative Approach

2. Methods

The equipment and technique of experiments on interactions accelerated of hydrogen isotops, from plasma of powerful glow discharge, with metal samples are adduced in [6,7]. The scheme of experiments with transfusion of hydrogen through sample is shown on Fig.1. The hermetically sample - cathode 2 in kind of glass, was welding to flange 4, through transition tube 3. The samples with flanges permited to make the fast replacement with preservation of tightness. The discharge was ignition between anode 1 of molybdenum and sample-cathode 2 of studied materials. The zone of burning for discharge was limited by quartz isolator. The samples were produced of vanadium, niobium, molybdenum and tantalum, with general contents of impurity less than one percent. The outside diameter of samples was within the limits of 14 - 25 mm, and thickness of wall 1 - 5 mm.

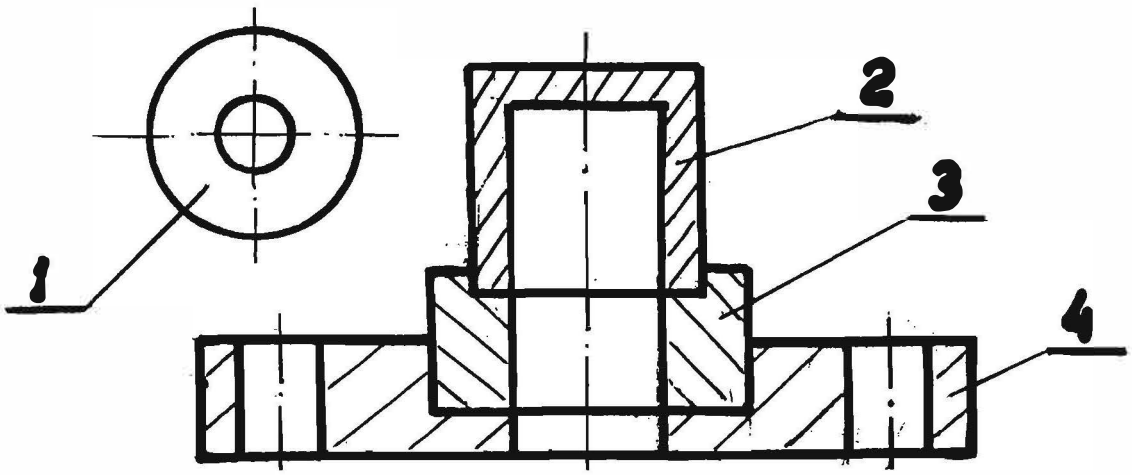

Fig 1.The scheme of cathode unit for glow discharge with transfusion of hydrogen. 1-Anode; 2-sample-cathode; 3-transition tube; 4-flange.

Tritium measured by liquid scintilation method, take away the plasma-forming gas from chamber of installation, on parts, two - three times during one experiments [3]. The error of measurement for tritium concentration was not exceeded 50 %.

The pressure of hydrogen in chamber changed in limits $(5 - 60)\cdot10^{0}$ Pa, and in volume of sample supported from two to ten time more high, than in chamber.

3. Results and Discussion

For hydride-forming materials of V, Nb, Ta the influence of return deuterium flow on tritium generation rate to put on record was not managed (Tab.1). For samples of singlecristal and polycristal molybdenum nearly the double excess for tritium generation rate was fixed at return deuterium flow through sample, in comparison with stationary conditions. The surface of all samples, teatment in discharge, was pure and, on visible, influence surface films on tritium generation was insignificant one. In these conditions, more significant was the influence of deuterium concentration in molybdenum, has appeared which is very small (about $1\cdot10^{-7}$ mole/mole) and depended on the pressure in degree 0.5.

Further have conducted the series of experiments, with deuterium pressure in volume of sample of molybdenum polycristal in limits $(70 - 130)\cdot10^{5}$ Pa, for determination of tritium generation efficiency at pressure of plasma-forming gas (deuterium) in limits $(5 - 20)\cdot10^{5}$ Pa (Fig. 2). Most the high tritium genera-

Innovative Approach

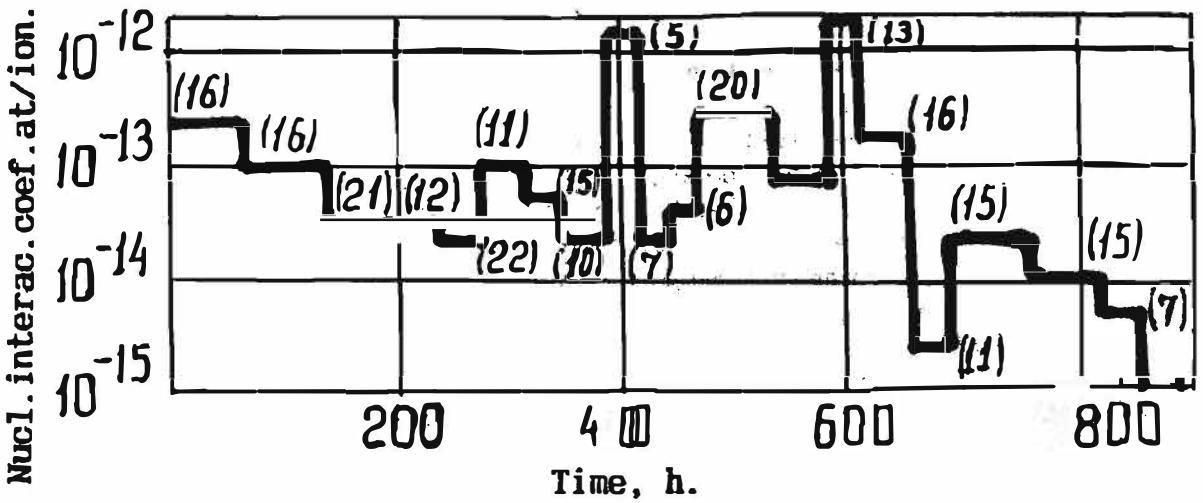

Fig. 2. The dependence of nuclear interaction coefficient for sample of molybdenum polycristal processed by deuterium plasma from time. Brackets mentioned the pressure in Pa, x 10^{-3}.

Table 1

The results of influence return deuterium transfusion through sample on tritium generation rate at processing in glow discharge

Material	Parameters of experiment							Results	
	Temperature	Voltage	Current density	Time	Pressure in cham	Pressure in samp	Flow of deuterium	Tritium generation rate	Nuclear interaction coefficient
	K	V	A/cm^2	h	Pa, x10^{-3}	Pa, x10^{-3}	mole/g, x10^{-7}	atom/s	atom/ion
Vanadium	1450	560	0.09	72	17	100	3.5	$2.3\cdot10^{5}$	$3.1\cdot10^{-14}$
	1450	500	0.09	71	15	15	-	$2.1\cdot10^{5}$	$2.7\cdot10^{-14}$
Niobium	1460	600	0.05	46	21	100	2.3	$3.5\cdot10^{5}$	$4\cdot10^{-14}$
	1470	600	0.05	48	20	20	-	$5.2\cdot10^{5}$	$5.5\cdot10^{-14}$
Molybdenum									
MN3<111>	1740	720	0.09	70	16	100	0.84	10^{6}	$9.1\cdot10^{-14}$
MN3<111>	1740	620	0.1	70	16	16	-	$4.4\cdot10^{5}$	$3.5\cdot10^{-14}$
MCVP-Polycrist.	1770	780	0.08	84	16	100	1.1	$2.9\cdot10^{6}$	$1.9\cdot10^{-13}$
	1760	790	0.08	72	16	16	-	$1.5\cdot10^{6}$	$9.6\cdot10^{-14}$
Tantalum	1370	600	0.08	68	16	100	2.4	$2\cdot10^{5}$	$2.6\cdot10^{-14}$
	1370	620	0.08	70	16	16	-	$1.9\cdot10^{5}$	$2.4\cdot10^{-14}$

Innovative Approach

tion rate, which reached 10^{7} - 10^{8} atom/s and are marked for lowered deuterium pressure in chamber. The coefficient of nuclear interaction, thus, reached 10^{-13} - 10^{-11} atom/ion. At the same time it is visible, that at excess of background significances, as the minimum on order, the rate and efficiency of tritium generation hesitated in three orders. With than such large fluctuations of efficiency until clearly, as far as the experiments are conducted in conditions, when the molybdenum surface was pure and free from surface films, pollution, and return transfusion of deuterium through sample excluded the accumulation of tritium in molybdenum. The summary time for this series experiments was exceed 8000 h. These results, as a whole have shown, that, at absence of surface pollution in processes ion bombardment, return transfusion of hydrogen and formation of complexes isotops was not present to increase of nuclear reactions rate and tritium generation, as it was assumed in [4,5]. Such conclusion is fair, as far as the best speed of passing for hydrogen through sample is fixed for vanadium (about $3.5 \cdot 10^{-7}$ mole/s), and least of all for molybdenum (about $(0.84 - 1.1) \cdot 10^{-8}$ mole/s).

The third series of experiments with transfusion have conducted on the same sample of polycristalline molybdenum on protium, which contained about $1.5 \cdot 10^{-3}$ % deuterium (Fig. 3). Have registered, unexpectedly the high of tritium generation rate after beginning series, which reached 10^{7} - 10^{8} atom/s, at coefficient

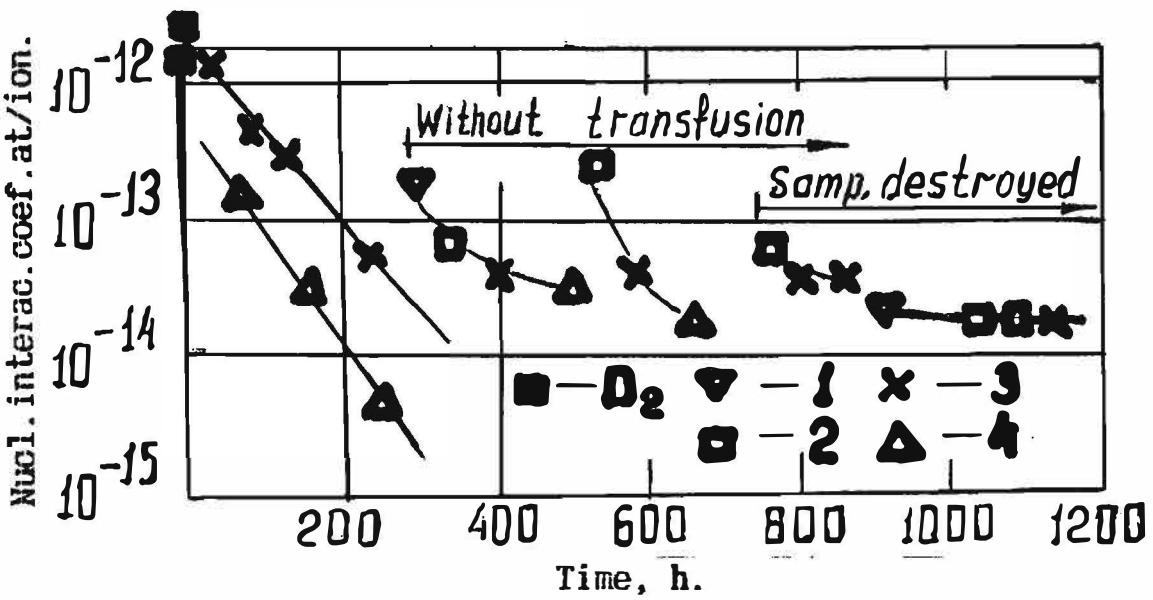

Fig. 3. The change of nuclear interaction coefficient for sample of molybdenum polycristal and plasma of protium with nature additive of deuterium at various pressure from times 1-Pressure-$6 \cdot 10^{-4}$ Pa; 2-pressure-4 10^{-4} Pa; 3-pressure-$2 \cdot 10^{-4}$ Pa; 4-pressure-$1 \cdot 10^{-1}$ Pa.

of nuclear interaction about 10^{-13} - 10^{-12} atom/ion. Then the rate during more of two hundred hours by degrees was reduced, that can testify about enough slow removal of deuterium remainders from sample. Through 300 h the protium transfusion was excluded and hereinafter the experiments were conducted in stationary conditions at various pressure of plasma-forming gas. For protium the tendency of increase efficiency for tritium generation with increase of pressure is found out. After the sample was destroyed on one side, on area 0,5 cm^2, afterwards 760

h the efficiency of tritium generation was stabilized, at the rate, roughly, on order background one. In this experiments deserved attention the high reproducibility of tritium generation, at use protium with nature additive of deuterium for plasma-forming gas.

4. Conclusions

4.1. The return transfusion of deuterium (flow is directed in opposite side to direction of fall for bombardments ions) has not rendered the significant influence on tritium generation rate for samples of vanadium, niobium and tantalum. For samples of polycristal and singlecristal molybdenum the efficiency of tritium generation was increased at transfusion, approximately, in two times.

4.2. It is shown, that the speed for passing of hydrogen isotops through membrane (formation of complexes) does not influence on the tritium generation rate. The speed of passing for deuterium was best at vanadium and reached 3.5 10^{-7} mole/s, and lesser at molybdenum (about 10^{-8} mole/s)

4.3. Fluctuations of tritium generation rate, for samples from polycristalline molybdenum, at in comparison identical conditions with transfusion and without, reached the three orders of size. Thus the minimum significances of rate exceeded background on order.

4.4. The tritium generation rate, for samples from polycrystalline molybdenum, at use of discharge on protium with nature concentration of deuterium, by degrees decreased from maximal significance for deuterium and was established on level of significances on orders exceeding background ones. The time of achievement of stationary significances on tritium generation rate exceeded 300 h.

References

1. V.A.Romodanov. "The Method For Suppression Of Tritium Outflow From Chamber Thermo-Nuclear Reactors".- Patent of Russia n. 4330994, from 08.10.1987. ICI G21 B 1/00. (in Russian).

2. V.A.Romodanov, V.I.Savin, M.V.Shakhurin et al.
Nuclear Fusion in a Solid.- Zhurnal Tekhnicheskoy Fiziki, 1991, v.61, is.5, p.122-125. (in Russian).

3. V.Romodanov, V.Savin, Ya.Skuratnik, V.Elksnin
Reproducibility Of Tritium Generetion From Nuclear Reactions In Condensed Media.- Proceedings; Fourth International Conference on Cold Fusion. TR-104188-V2, EPRI, 1994, p.15 (1-15).

4. J.P. Vigier.
New Hydrogen (Deuterium) Bohr Orbits In Quantum Chemistry And Cold Fusion Processes.- Cold Fusion Sourse Book. Salt Lake City, Uta FIC, 1994, p.99-104.

5. Ren-Bao Lu.
The X-Ray Emission From Elements Of First Period And Cold Fusion.-Cold Fusion Sourse Book. Salt Lake City, Uta.FIC, 1994.

6. V.Romodanov, V.Savin, Ya.Skuratnik, Yu.Timofeev.
Nuclear Fusion In Condensed Matter.-Frontiers of Cold Fusion. UAP Inc. Tokyo, Japan, 1993, p.307-319.

7 A.A.Babad-Zakhrjapin, V.A.Romodanov.
Hydrogen Permebility for Single-Cristal Molybdenum.- Questions Of Nuclear Sciences And Engineering. Ser.: Physics of radiation damages and radiation material science. 1991, n. 2 (56), p. 69-72. (in Russian).

Innovative Approach

NUCLEAR REACTIONS AT EFFECT OF IONS DEUTERIUM ON CERAMIC MATERIALS FROM PLASMAS OF GLOW DISCHARGE

V.A.ROMODANOV, V.I.SAVIN, *Ya.B.SKURATNIK

StateSRI SPA "LUTCH", Zheleznodorozhnaya 24, Podolsk, Moscow reg.142100. RUSSIA.
T.:095-137-9258. F.:095-137-9384. E-m.: luch@adis.msk.su
*StateSC RF "Karpov SRPCI", Vorontsovo pole 10, Moscow, 103064. RUSSIA.

Abstract

The high mechanical properties at increased temperatures permit to consider the ceramic materials as perspective, for targets special, high-loading of nuclear devices. It is shown, that the heaviest rate of tritium generation, of materials TiC, VC, ZrB_2, ZrC, ZrN, LaB_6, was observed at bombardment by deuterium ions from plasma of glow discharge for ZrB_2 and made $3.6 \cdot 10^7$ - $3.9 \cdot 10^7$ atom/s, at efficiency $2.5 \cdot 10^{-13}$ - $2.9 \cdot 10^{-13}$ atom/ion, that is comparable with results for metal targets.

The stability of compound materials at increased temperature in condition of hydrogen plasma of far below than in vacuum, that can result in failure discharge of glow form and transition of it in arcing. The transition of glow discharge form in arcing form resulted in reduction of tritium generation rate.

The measurements of accompanying gamma-radiation generations have shown, that its possible of generation rate was on three - six orders below, in comparison with generation rate of tritium.

1. Introduction

In [1,2] we state the assumption that the additives light of elements to metal targets should reduce the rate of nuclear reactions at interactions accelerated of hydrogen isotops with solid-state targets. Therefore the ceramic materials types of carbides or nitrides should have lesser of efficiency in stimulation of nuclear reactions. At the same time the ceramic materials can have complex physical, chemical and mechanical properties are unattainable for usual metals. In particular, high melting temperature, low scattering coefficient by accelerated ions, high mechanical properties at increased temperatures permit to consider the ceramic materials as perspective, for special targets, high-loading of nuclear devices. At the same time the compound materials are convenient objects for checks of transmutation opportunity lights of elements entering in structure compounds. On their bases it is possible select the optimum structure compound, consisting from of lights element, intended for transmutation, and heavy, which should stimulate the transmutation of lights [2]. Thus the light elements select from condition to opportunity of nuclear products registration (gamma-radiation, high-energy beta-radiation). So in combinations with boron and nitrogen is possible to be expected the registration bremsstraglung gamma-radiation from protons with energy 8,4 and 8 MeV accordingly or from beta E = 13,37 MeV for ^{12}B.

The purpose of work consisted in that, to determine for some boredes, carbydes nitredes the efficiency of tritium generation and opportunity to transmutation at effect accelerated of hydrogen isotops from plasma powerful of glow gischarge.

Innovative Approach

2. Methods

The scheme, equipment and technique of experiments on interactions accelerated of hydrogen isotops, from plasma powerful of glow discharge, with metal samples is adduced in [3,4]. In quality of ceramic samples used the pressured disks VC, TiC, ZrC with diameter of 25 mm and hight of 10 mm; ZrB_2-with diameter 35 mm and hight of 4 mm; ZrN-with diameter 40 mm and hight of 20 mm; LaB_6-with diameter 50 mm and hight of 5 mm. The composition of samples was close to stohiometric. The scheme of discharge unit with sample-cathode from ceramics is shown on Fig. 1.

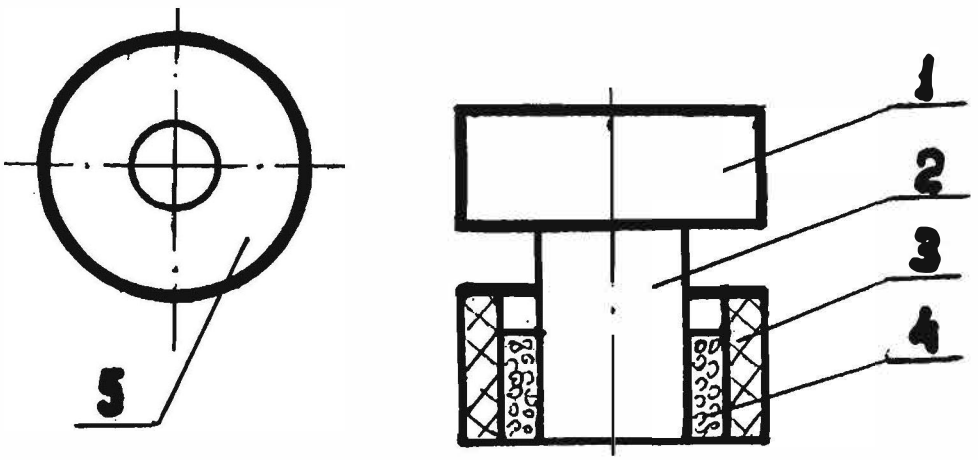

Fig.1. The scheme of experimental unit of glow discharge with sample-cathode of ceramics. 1- Sample-cathode of ceramic; 2-stand for heat transfered; 3-insulator; 4-fiber-cloth; 5-anode.

The unit consists of the sample-cathode from mentioned ceramics, which lies on stand 2 from molybdenum. The area of discharge is limited quartz tube 3 and fiber-cloth 4. The studied ceramics had the sufficient conductivity for ignitions of glow discharge at submission of high voltage on anode 5 from molybdenum. The voltage of glow discharge changed in dependence at material of sample, its temperature, pressure of gas and was within the limits of 500- 1250 V.

Gamma-radiation registered by devices SRP-88 with crystal NaJ, diameter of 25 mm and hight of 40 mm. The measurements conducted by differential method, alternately placing the gauge on close and remote distance from cathode unit (Fig. 2). The gauge 2 placed outside of vacuum chamber 3 on distance of 100 mm from cathode unit with ceramic sample. The other arrangement of gauge, accepted for base, had the distance to cathod unit in five times more. In the beginning conducted the record of twenty ten-second intervals on distances of 100 mm between sample and gauge, then such the measurements made on distance of 500 mm between gauges and sample. Such series of measurements conducted on ten time during two hours. For each regime and sample the two-hour series conducted numerously, afterwards that summarized the significances of gauge indications in each of situations and calculated the relation. The similar series of measurements conducted and at switched off installation, for receiption of background significances.

The measuring complex periodically was calibrated on external source radium (^{226}Ra) gamma-radiations and inside-cobalt. The bottom threshold of energy for registration of gamma-radiation by used measuring device made 50 KeV. The error of measurements of such technique and devices was not managed to lower

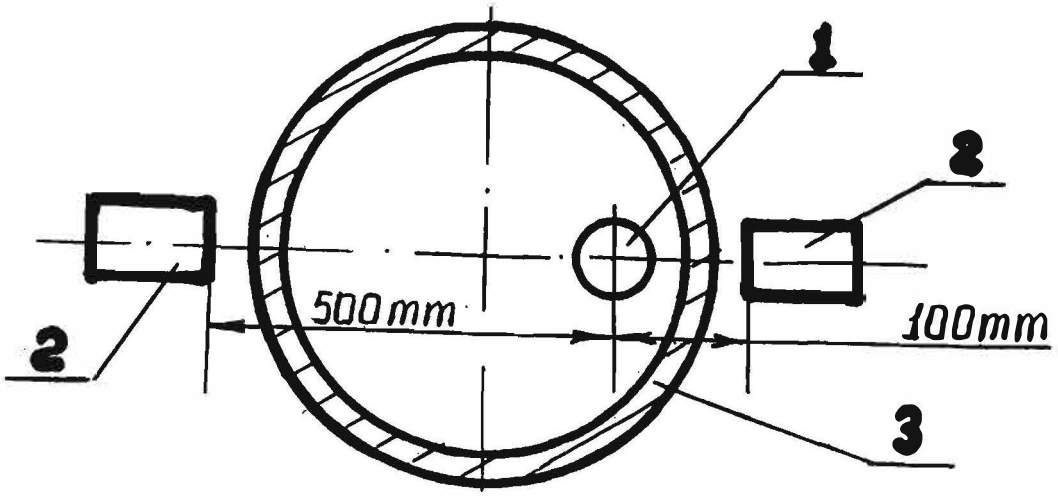

Fig. 2. The scheme of gamma-radiation measurement.
1-Sample-cathode; 2-gauge in two situations; 3-vacuum chamber.

less than 5 %. At availability transmutation in given experiments assumed to put on record bremsstraglung gamma-radiation from p (8.43 MeV) for ^{10}B and from ^{11}B (beta E = 13.37 MeV) for ^{11}B, as well as from p (8 MeV) for ^{14}N and p (7.5 MeV) or p (5.5 MeV) for ^{13}C and ^{12}C accordingly. If there is nuclear reactions, it is possible also to put on record characteristic radiation for ^{11}B (gamma E = 4.5 MeV) and for ^{14}N (gamma E = 6.13 MeV; E = 7.11 MeV).

The measurement of contents tritium in plasma-forming gas made by liquid, scintillation method, on fulfilled program with error not more 50 % [3,4].

3. Results and Discussion

The main results on measurements of tritium and gamma-radiations are submitted in Table 1 From table it is visible, that the tritium generation rate for all samples considerably exceeds background, which for given technique made about 10^{6} atom/s. The most high tritium generation rate, equal $(3.6 - 3.9)\cdot10^{7}$ atom/s, was observed for samples of ZrB_2, at which the coeffitient of nuclear interaction reached $(2.5 - 2.9)\cdot10^{-12}$ atom/ion. The tritium generation rate on carbide zirconium was also enough high. The samples from carbides titanium and vanadium have shown approximately identical and, in comparison, low tritium generation rate (about 10^{6} atom/s). The tritium generation rate for LaB_6 was not enough high, that, obviously, is connected with low stability of discharge. The low tritium generation rate for various samples pays attention, when the discharge passed in the arcing form. Nitride zirconium, on efficiency of nuclear reactions, taked intermediate rule, the tritium generation rate was about $(2.7 - 4.2)\cdot10^{6}$ atom/s.

At registration gamma-radiation of significant flows to put on record was not managed. Some excess above background (1 - 5 %) it is possible to note only for samples from ZrB_2. Thus, with account of gauge calibration on radium source gamma-radiation and expected energy in some MeV, maximal valuation may give the flux of possible gamma-radiation within the limits of $10 - 10^{3}$ s^{-1}. Thus, relation of gamma-radiation generation rate to tritium generation rate did not exceed $10^{-6} - 10^{-7}$. This circumstance puts under doubt of message about facts transmutation of heavy elements, at low energies of interacting particles and in absence of tritium registration.

Innovative Approach

Table 1
The results on measurements of tritium and gamma-radiation

Material	Parameters				Results					
	Current	Temperature	Pressure	Time	Coefficient of nuclear interaction	Tritium generation rate	Exceeding above base exper.	Exceeding above base backg.	Appraisal flux gam.	Relation flux. n/tr.
	A	K	Pa, $x10^{-3}$	h	atom/ion	atom/s	%	%	s^{-1}	
ZrB_2	2	1600	10	49	$6.6\cdot10^{-13}$	$3.2\cdot10^{6}$	-	-	-	-
	2	1850	20	47	$2.9\cdot10^{-13}$	$5.6\cdot10^{7}$	2.5	-	-	-
	2	1750	10	42	$5.7\cdot10^{-13}$	$7.1\cdot10^{6}$	3.8;2.8	3;3.6	10	10^{-6}
	2.2*	1900	40	20	$3\cdot10^{-14}$	$4.1\cdot10^{5}$	6.4;4.4	4;-1.3	10^{2}	10^{-3}
	2.1*	2000	32	20	-	-	1.1	-	-	-
	2.5	1970	20	22	$2.5\cdot10^{-12}$	$3.9\cdot10^{7}$	2.5;2.4	-	-	-
	2.5	1860	10	46	$9.6\cdot10^{-13}$	$1.5\cdot10^{7}$	2.3;2.2 2.3	-	-	
	2.5	1770	6	23	$4.8\cdot10^{-13}$	$7.5\cdot10^{6}$	2.7;2.5	1.7; -0.9;	10^{3}	10^{-4}
	2.1	1925	20	49	$3.9\cdot10^{-13}$	$5.1\cdot10^{6}$	3;2.7 1.5	-	-	-
	2.2	1950	17	73	$1.4\cdot10^{-13}$	$2\cdot10^{6}$	5.6	4.7	10^{2}	10^{-4}
	2.1	1910	20	71	$3.1\cdot10^{-14}$	$4.1\cdot10^{5}$	-1.4; 1.5;2.4	1.3	-	-
TiC	2.3	2020	20	56	$1.1\cdot10^{-13}$	$1.6\cdot10^{6}$	0.07	-	-	-
	2.3	1910	10	34	$8.1\cdot10^{-14}$	$1.2\cdot10^{6}$	-2.2; -1.7	-	-	-
VC	2.1	2030	20	52	$1.2\cdot10^{-13}$	$1.6\cdot10^{6}$	0.1; -1.3;	0.5	-	-
	2.1	1935	12	39	$2\cdot10^{-13}$	$2.6\cdot10^{6}$	2.1	-	-	-
ZrC	2	2060	29	60	$4.9\cdot10^{-13}$	$1.6\cdot10^{7}$	-1.7; -2.1	-	-	-
	1.8*	1580	7	72	$1.1\cdot10^{-13}$	$1.2\cdot10^{6}$	-	-	-	-
ZrN	2.5	2030	30	44	$2.7\cdot10^{-13}$	$4.2\cdot10^{6}$	-1.5;	-	-	-
	2.5	2240	20	48	$2.8\cdot10^{-13}$	$3.6\cdot10^{6}$	-1.4; 0.4;0.5	-	-	-
	2.4	1900	10	66	$1.6\cdot10^{-13}$	$2.7\cdot10^{6}$	-	-	-	-
LaB_6	1.2*	1730	30	20	-	-	-	-	-	-
	1.7	1650	11	47	$1.3\cdot10^{-13}$	$1.4\cdot10^{6}$	2.1;3.6	3.5	-	-

* - Failure of discharge.

Innovative Approach

It is necessary to note, that the restoring properties of hydrogen, considerably limited the working temperature of sample and pressure of plasma-forming gas at radiation in discharge, in comparison with isothermal heating. The restoration by hydrogen of metals in compounds resulted in anticipatory failure to regime of glow discharge and transition of it in arcing. The arcing regime reduced the stimulating opportunities of discharge and tritium generation rate will decreased. The most steady compounds in glow discharge on hydrogen isotopes have appeared ZrB_2 and ZrN. On sample of ZrN was managed of long work at temperatures about 2300 K and pressure about $3 \cdot 10^{4}$ Pa. The least steady to failure regime has appeared LaB_6, than the low results on tritium generation rate for given material are largely explained.

4. Conclusions

4.1 The significant tritium generation rate, is fixed at radiation by ions deuterium of samples from borides, carbides and nitrides of titanium, vanadium, zirconium and lantanum from plasma powerful of glow discharge. For samples of ZrB_2 the tritium generation rate reached ($3.6-3.9) \cdot 10^{7}$ atom/s.

4.2 The generation rate of gamma-radiation, accompanying tritium, is close to background and maximal valuation has made $10 - 10^{3}$ s $^{-1}$, at relation to tritium generation rate within the limits of $10^{-3} - 10^{-4}$.

4.3 The most proof of materials, at radiation in plasma of glow discharge, were ZrB_2 and ZrN, and the least proof samples of LaB_6.

References

1. V.Romodanov, V.Savin, Ya.Skuratnik, V.Elksnin.
Reproducibility Of Tritium Generetion From Nuclear Reactions In Condensed Media.- Proceedings; Fourth International Conference on Cold Fusion. TR-104188-V3, EPRI, 1994, p.15 (1-15).

2. V.Romodanov, V.Savin, Ya.Skuratnik, S.Korneev.
Consept Of Target Material Choice For Nuclear Reactions In Condensed Media.Ibidem. TR-104188-V3, EPRI, 1994, p.22 (1-13).

3. V.A.Romodanov, V.I.Savin, M.V.Shakhurin et al.
Nuclear Fusion in a Solid.- Zhurnal Tekhnicheskoy Fiziki, 1991, v.61, is.5, p.122-125 (in Russian).

4. V.A. Romodanov, V. Savin, Ya. Skuratnik and Yu.Timofeev.
Nuclear Fusion in Condensed Matter.- Frontiers of Cold Fusion. Proceedings of the Third International Conference on Cold Fusion. October 21-25, 1992, Nagoya, Japan. Ed. By H. Ikegami. UAP Inc., Tokyo, Japan, 1993, p.307-319.

Innovative Approach

ENERGY GENERATION PROCESSES AND COLD NUCLEAR FUSION IN TERMS OF SCHRODINGER EQUATION

Lev G. SAPOGIN

Department of Physics, Technical University (MADI)
Leningradsky pr. 64, A-319,125829, Moscow, Russia

Abstract:Proceeding from the complete Schrodinger equation at small energyes the classic variable charge particle motion equation has been obtained, the later providing a good explanation for CNF and the excessive energy.

In earlier works [1,2] an approximate motion equation for an individual oscillating charge particle was proposed. It adequately explains both the cold nuclear fusion phenomena [13,14] and the anomalous excessive energy [12] occurrences of a mysterious origin being observed in experiments of a number of researchers. Yet, the said equation has resulted from purely heuristic reasoning, not in rigorous terms, when determining the electric charge value and the fine structure constant [9,10] on the basis of the Unitary Quantum Theory (UQT). This invited right criticism of many research workers and caused personal deep dissatisfaction. Further it will be shown that the above equation may follow directly from the Schrodinger's equation for small energies.

Let us consider the entire Schrodinger's equation:

$$\frac{\hbar^2}{2m}\frac{\partial^2}{\partial x^2}\Psi(x,t) + i\hbar\frac{\partial}{\partial t}\Psi(x,t) = U(x)\Psi(x,t) \quad ; \qquad (1)$$

Its solution is to be expressed in wave function terms:

$$\Psi(x,t) = \cos(kx)\int \exp[i\,\mathrm{tg}(\phi)]dt \quad ; \qquad (2)$$

where $$\phi = \frac{m\,t}{2\hbar}\left(\frac{d\,x(t)}{dt}\right)^2 - \frac{m\,x(t)\,d\,x(t)}{\hbar\qquad dt} + \phi_0 \quad ; \qquad (3)$$

where ϕ_0 is an initial phase, x is an independent variable, and x(t) represents a non-related to x as yet unknown function which, as will be shown below, turns out to be a time-dependent coordinate. By substituting the latter into the Schrodinger's equation we arrive at:

$$i\hbar^2k^2\int \exp[i\,\mathrm{tg}(\phi)]dt + 2im\,U(x)\int \exp[i\,\mathrm{tg}(\phi)]dt + 2\hbar m\exp[i\,\mathrm{tg}(\phi)] = 0 \quad (4)$$

At small energies the value $\hbar^2k^2 \ll 2mU(x)$, the first integral being neglected. Having differentiated the resulting equation with respect to time and having reduced the common exponential factor we come to:

Innovative Approach

$$2\,\mathrm{U}(x)\cos^2(\phi)+2mt\frac{d\,\mathrm{x}(t)}{dt}\frac{d^2\,\mathrm{x}(t)}{dt^2}-m\left(\frac{d\,\mathrm{x}(t)}{dt}\right)^2-2m\mathrm{x}(t)\frac{d^2\,\mathrm{x}(t)}{dt^2}=0 \qquad (5)$$

It is evident that for short time stretches (or for small energies at elastic interactions when the velocity changes are small) the member $\mathrm{x}(t) \approx t\frac{d\,\mathrm{x}(t)}{dt}$. Then the second and third terms are reduced and we obtain the following:

$$\mathrm{U}(x)\cos^2(\phi)=\frac{m}{2}\left(\frac{d\,\mathrm{x}(t)}{dt}\right)^2 \qquad (6)$$

It is clearly seen that the left term is the potential energy oscillating according to the harmonics law, whereas the right one represents the conventional kinetic energy. Yet, the potential energy doesn't transform into the kinetic one as is the common case in the conservative systems of conventional mechanics. If one relates the potential energy oscillations to those of the electric charge existent in the Unitary Quantum Theory [3-11], as the potential energy always stands in direct proportion to the electric charge value, then one arrives at the oscillating charge equation of conventional mechanics. But in this case one's reasoning would naturally proceed from the necessary assumption on substitution of the independent variable x for the function $\mathrm{x}(t)$

Proceeding from this equation, by way of differentiation, one can readily come to the same oscillating charge equation of motion, the latter having been obtained [1,2] heuristically within the Unitary Quantum Theory based on quite different reasons.

$$m\frac{d^2}{dt^2}\mathbf{r}=Q\mathbf{GRAD}(\mathrm{U})\cos^2\varphi;\quad \text{where}\quad \varphi=\frac{mt}{2\hbar}\left(\frac{d\mathbf{r}}{dt}\right)^2-\frac{m\mathbf{r}}{\hbar}\left(\frac{d\mathbf{r}}{dt}\right)+\phi_0.$$

Let us clear up the validity of the resulting 1- st order equation (6). At first, we shall consider the motion within the plane condenser field. Let us insert the potential $\mathrm{U}(x) = G\,\mathrm{x}(t)$:

$$G\,\mathrm{x}(t)\cos^2(\phi)+\frac{m}{2}\left(\frac{d}{dt}\mathrm{x}(t)\right)^2=0 \qquad (7)$$

We shall look for a particular solution in the form of $\mathbf{x}(t)=at^2$. Having substituted this solution into the equation (7) we arrive at:

$$at^2\left(G\cos^2\phi_0+2am\right)=0. \qquad (8)$$

One can see clearly that the acceleration may be chosen to satisfy the equation. The motion will take place with the acceleration value of:

$$a=-\frac{G\cos^2\phi_0}{2m}$$

An interesting fact is discovered: the acceleration generated in one and the same field is dependent upon ... the initial phase ϕ_0

Let us consider now the diffusion motion within the dipole field $\mathrm{U}(x) = -G/\mathrm{x}(t)^2$, for which there is also a well-known analytical solution.

The substitution of the particular solution $\mathrm{x}(t) = r\sqrt{t}$ will result in:

$$\frac{1}{8tr^2}\left\{-8G\cos^2\left(\frac{3mr^2-8\hbar\phi_0}{8\hbar}\right)+mr^4\right\}=0$$

This transcendental equation will have a non-analytical decision, as the 4-th degree parabola will always intersect with the cosine squared. And again, the velocity of the resulting motion will depend upon the initial phase ϕ_0.

Unfortunately, at this point the possibility to solve these equations analytically seems to be exhausted.

In all the solutions the coordinate, velocity or acceleration is always dependent upon the initial phase value ϕ_0. As illustrated by the given examples, at some phase values the motion equations are in conformity with the energy conservation laws and are the same as within conventional mechanics, whereas at other phase values the motion will be different and, consequently, there is violation of the energy conservation law: the particle may gain or lose energy. The same phenomenon is true for the harmonic oscillator, which has been revealed at first numerically in [1,2], and both the cold nuclear fusion and the energy generation mechanisms in their considered approximation follow directly from the Schrodinger's equation. It is well-known, that the energy conservation laws are non-existent if the potential function is time-dependent. It should be noted that even in the conventional quantum mechanics the energy conservation laws are observed within the accuracy of uncertainty correlation. Previously it was shown numerically [1,2,13] that if one sums up the energy or momentum for an assembly of particles throughout all the phases, the resulting energy and momentum will be preserved which is the case in quantum mechanics, because it always regards particles in assemblies.

The energy conservation laws hold true only in selection of the initial phase particular value, which proceeds clearly from the equation's translational properties. Thus, the given examples prove the soundness of the earlier used approach and the validity of the oscillating charge motion equation, having been previously obtained heuristically on the basis of absolutely different assumptions.

We shall regard now the problem of the cold nuclear fusion. Let us express the equation of motion for two nuclei with charges Q and q. Let the heavy nucleus possessing the charge q be at rest, and let the other nucleus move in its direction with the velocity V from the point at the distance A. Then the equation of motion for the head-on collision may be expressed in the following way:

$$m\mathrm{x}(t)^2\frac{d^2}{dt^2}\mathrm{x}(t)=Qq\cos^2\varphi \quad \text{where} \quad \varphi=\frac{mt}{2\hbar}\left(\frac{d\mathrm{x}(t)}{dt}\right)^2-\frac{m}{\hbar}\mathrm{x}(t)+\frac{d\mathrm{x}(t)}{dt}+\phi_0; \qquad (9)$$

The accurate analytical solution for the above equation is hardly possible, yet, one may obtain a 4-th order series expansion of its solution:

$$\mathrm{x}(t)=A+Vt+\frac{Qq\cos^2\delta}{2mA^2}t^2-\frac{QqW\cos\delta}{6A^3m\hbar}t^3+\mathrm{O}(t^4)$$

where $W=\hbar V\cos\delta-mAV^2\sin\delta+2\hbar mAV^2\sin\delta+2Qq\hbar\cos^2\delta\sin\delta$;

$$\delta=\frac{mVA}{\hbar}-\phi_0.$$

Restricting our consideration by the first three terms of the obtained solution, we can find out that minimum x(*t*) occurs at:

$$t = -\frac{mVA^2}{Qq\cos^2\delta}$$

Then the minimal distance for which the nuclei will approach each other will be equal to:

$$x_{\min} = A - \frac{mV^2A^2}{2Qq\cos^2(\frac{mVA}{\hbar} - \phi_0)}$$

It is evident that by choosing the initial phase value at no matter how small energies and at any nuclei charge values, the minimal distance between the nuclei may be made no matter how small. This was shown numerically for the first time in [1,2]. Consideration of the next (cubic) component would not entail any principal changes in the solution and, therefore, is not cited here in because of its being too cumbersome. Such nuclei transmutations have been frequently observed. It is clear now that cold nuclear reactions may take place at any nuclei charge values. Naturally, the phase precipice width [13] will diminish in direct proportion to the charge value increase.

Full of mystery is a well-known energy shortage problem being observed in a number of bio-chemical reactions with enzymic participation. For instance, the well-studied polysaccharides breakdown reaction in the presence of a lysozyme involves the following: the polysaccharide molecule gets caught into a special cavern within the big lysozyme molecule, the remains of the former being thrown away after some time. In so doing the polysaccharide ties break energy is of the order of 5 eV, whereas the heat movement energy does not exceed 0.025 eV. Where the lysozyme takes energy for breaking the polysaccharide is still unclear. No satisfactory mechanism to explain this type of reactions (which are rather numerous) had been proposed and all these phenomena, as the physicists say, have been "swept under the carpet". Most intriguing is the fact that in all these cases (CETI elements, proton-conducting ceramics, cavitation devices of the Griggs-Potapov type, sonoluminescence, electric motors with new magnetic ceramics, etc.) the energy generation can be explained neither by chemical reactions nor by phase transitions. Sometimes these phenomena are accompanied by nuclear reactions (which is, in fact, impossible), but even the latter can be responsible only for a hundredth portion of the generated heat energy. Doubtless, all these phenomena belong to new physics, because their explanation is impossible in terms of rigorous science.

The energy generation processes may possibly help to explain the anomalous excess heat production phenomena occuring in proton-conducting ceramics, CETI elements, nickel electrolysis in light water, cavitation bubbles, hydrated metals, fermentative chemical reactions, etc. In such systems the proton (or some other particle), being incorporated into some kind of a cavity (potential well), will each time be reflected from its wall with the velocity greater than that of falling and take energy from the vacuum (the "maternity home" solution) [12].

It is most curiouse that if the magnetic momentum oscillates alongside with the electric charge (which, of course, must take place in UQT), then the solution of the problem of their orientation is reduced to similar equations and thus it makes possible to obtain energy from vacuum with the help of permanent magnets. There is an impression that these phenomena are observed in experiments. If Nature is actually designed so that there are no energy conservation laws for an individual particle, but there is one for an assembly of particles, then the generation of pollution free energy may be viewed as a relatively simple task both from theoretical and technical viewpoint as compared to hot nuclear fusion. Thus the mankind will be saved from energy shortages forever. Look for the detailed discussion of energy conservation problem in earlier publications [12].

Innovative Approach

I wish to express my grattitude my collegues Ryuichi Kubota, V.Boichenko, V.Dzhanibekov, prof. M.Mokoulsky and Dr. Nataly Famina, a remarkable translator. I also wish to thank Dr. Eugene F. Mallove for a prolonged scientific discussion at the Loews Hotel, Monte-Carlo, Monaco.

References

1. L.G.Sapogin, "Deuteron interaction in unitary quantum theory","On the mechanisms of cold nuclear fusion", Proceedings Fourth International Conference on Cold Fusion, Vol. 4, Theory and special topics papers TR-104188-V4, July (1994), (Hawaii).
2. L.G.Sapogin, "Deuterium interaction in unitary quantum theory", "On the mechanism of Cold nuclear fusion ", Fusion Source Book. International Symposium on Cold Fusion and Advanced energy sources, Belarusian State University. Minsk, Belarus, May 24-26, (1994).
3. L.G.Sapogin. "Unitary Field and Quantum Mechanics", Investigation of systems, (in Russian), Vladivostok, Academy of Science of the USSR, No. 2, p. 54, (1973).
4. L.G.Sapogin, "On Unitary Quantum Mechanics," Nuovo Cimento, vol. 53A, No. 2, p. 251, (1979).
5. L.G.Sapogin, "An Unitary Quantum Field Theory", Annales de la Fondation Louis de Broglie. vol. 5, No.4, 285, (1980).
6. L.G.Sapogin, "A Statistical Theory of Measurements in Unitary QuantumMechanics," Nuovo Cimento, vol. 70B, No.1, p.80, (1982).
7. L.G.Sapogin.,"A Statistical Theory of the Detector in Unitary Quantum Mechanics," Nuovo Cimento, vol. 71B, No. 3, p. 246, (1982).
8. V.A.Boichenko, L.G.Sapogin, "On the Equation of the Unitary Quantum Theory," Annales de la Fondation Louis de Broglie, vol. 9, No. 3, p.221, (1984).
9. L.G.Sapogin, V.A.Boichenko, "On the Solution of One Nonlinear Equation", Nuovo Cimento, vol. 102B, No.4, p.433, (1988).
10. L.G.Sapogin, V.A.Boichenko, "On the Charge and Mass of Particles in Unitary Quantum Theory," Nuovo Cimento, vol. 104A, No.10, p.1483, (1991).
11. L.G.Sapogin, "Clear-cut picture of micro worlds", Journal Technic for the young . (in Russian) No.1, p.41, (1983).
12.L.G.Sapogin, "On one of the Energy Generation Mechanisms in Unitary Quantum Theory". Infinite Energy [E.Mallove, editor], vol.1, No.2, p.38, (1995); Proceedings of the ICCF5, p.361, April 9-13, (1995), Monte-Carlo; Proccedings of the 2 Russian Conference CNFNT (in Russian) p.18-24, Sochi, September 19-23, (1994); Cold Fusion, No 11, p.10, (1995).
13.L.G.Sapogin, I.V.Kulikov,"Cold Nuclear Fusion in the Unitary Quantum Theory". Chinese Journal of Nuclear Physics, vol.17, No.4, p.360-370, (1995).
14.L.G.Sapogin, "Cold Nuclear Fusion and Energy Generation Processes in Terms of the Schrodinger Equation". Infinite Energy [E.Mallove,editor], vol.1, No 5,6, p.75, (1996).

Innovative Approach

New Experimental Results and Analysis of Anomalous Phenomenon in Gas Discharge

Zhang XinWei, Wu Jun, Zhang WuShou
Institute of Applied Physics and Computational Mathematics,
P.O.Box 8009, Beijing, 100088, P.R.China
Fu Yibei, Wang Dalun, Chen Suhe, Li Yijun
Institute of Nuclear Physics and Chemistry, China Academy of Engineering Physics,
P.O.Box 525–74, Chengdu, 610003, P.R.China
Long Heqing, Ying Wen
Institute of Sichuan Material and Technology
P.O.Box 538–14, Chengdu, 610007, P.R.China
Tang Hongqing, Li Ze, Shen Guanren, Zhou Zuying
Qi Bujia, Liu Yonghui, Wang Xiaozhong, Yang Yi
China Institute of Atomic Energy
P.O.Box 275, Beijing, 102413, P.R.China

Abstract

Counts and energy Spectrums of x–ray have been registered in gas glow discharge system [1], there were some anomalies in about 100 energy spectrums. When discharge voltage was 4–14kv, there were 30–300kev continuous x–ray, their intensities were 10%–1000% of background. According to registered energy spectrums the energy dependence of the mass attenuation cross section (μ / ρ) could be obtained, it was different than standard $(\mu / \rho)^*$, sometime negative absorption was detected. We suggested some explanation of above anomalies.

Keywords: Cold Fusion, gas discharge, anomaly of x–ray, negative absorption

Experiment:

Electrodes (Pd, Nb, Ta or other metal) were fixed to both ends of a glass reaction bulb. The thickness of the glass wall of bulb was 2.0 ± 0.2mm, the voltage V and current I of discharge were 4–18KV, 1–50mA(50Hz) respectively: The pressure of discharge gas (D_2, H_2, air, Ar•••) was dynamic (flowing) low pressure(< 100Pa).

The x–ray measurement system was composed of a high pure Ge detector (GMX200) made in ORTEC company of U.S.A., a pulse shape analyser (CANBERRA, 2160A) and a IBM–PC / XT computer. The detector sensitive volume was 102 cm^3, the measuring range was 5 KeV to 1.64Mev, the relative efficiency is 20%. The Ge detector was placed in a lead shielded cabin so that the background was 10～11counts / sec within 24 to 4096 channels. We used ^{152}Eu and ^{241}Am source to calibrate the energy Ex and detection efficiency ε_i of x–ray detector, the results were described as table 1, the error and the drift of energy during a week was less than 0.5KeV.

Using different thickness (L) metal attenuator (Cu, Al, Cd foil), the $(\mu / \rho)(Ex)$ of source x–ray could be obtained, it was consistent with the standard value [2] (error～ 15%). In air discharge there

was not anomaly of x–ray.

Results:

There were some anomalous phenomenon in many energy spectrums of x–ray, table 2–5 described the typical spectrums, there were high energy x–ray; in the energy interval $Ex / (\sqrt{2}ev) = 3 \sim 20$ (V denoted alternating voltage, e denoted electron charge), the intensities of x–ray were 10% ~ 1000% of background. To test the character of x–ray, we used different thickness (L) metal attenuating foil (Cu, Al, Pb, Cd foil) in front of the detector, the mass attenuation cross section $(\mu/\rho)(Ex)$ might be obtained (see table 6–9): $\frac{\mu}{\rho} = \frac{1}{\rho(L_1 - L_2)} lg\left[\frac{N_1(Ex) - N_0(Ex)}{N_2(Ex) - N_0(Ex)}\right]$, $N_1(Ex)$, $N_2(Ex)$ were the Intensities of x–ray of energy Ex as metal attenuating foil of thickness L_1, $L_2$was used respectively. $N_0(Ex)$ was the Intensities of background, ρ was the density of metal foil. In Comparison with the standard value $(\mu/\rho)^*$ of handbook [2], (μ/ρ) was very different: at low energy (<20KeV) $(\mu/\rho)/(\mu/\rho)^* \approx 0.01 \sim 0.5$, at high energy ($>30$KeV) $(\mu/\rho)/(\mu/\rho)^* \approx 2 \sim 100$, for some energy spectrums (μ/ρ) might be negative at some energy interval, and (μ/ρ) depended not only Ex and atomic number Z (as standard value $(\mu/\rho)^*$) but also V,L….

In some special cases (table 10), as $L_1 > L_2$, the corresponding total count rate of x–ray $\Sigma_1 > \Sigma_2 (\Sigma = \int \frac{dN(E_x)}{dE_x} dE_x)$. So the average effective attenuation cross section $(lg[(\Sigma_1 - \Sigma_0)/(\Sigma_2 - \Sigma_0)] / \rho(L_1 - L_2))$ was negative. It was very anomalous.

For reducing the electromagnetic disturbance effect upon measuring result, some steps were adopted. In short time interval (100~ 300sec) only changing the thickness L, the change of energy spectrum and intensity of x–ray was regular (not random) and might be repeated. This meant the counts of x–ray were not affected by electromagnetic disturbance obviously. For check and comparison, we also applied thermoluminescent dosimeters (TLD) and NaI detector to measurement of x–ray dose, TLD was not affected by electromagnetic noise. Using Pb attenuation foil of 5mm thickness , TLD recorded the intensity of 4 times background; Using Pb attenuation foil of 1,2,6mm thickness simultaneously, the discharge voltage was 14kV, TLD recorded the intensity of 77.6, 35.1, 8.6 mR (milli Rongen) respectively, the background was about 2.4 mR. So we might obtain the average mass attenuation cross section: $(\overline{\mu/\rho}) = 0.734(1 \sim 2mm), 0.367(2 \sim 6mm) cm^2/g$, the corresponding x–ray energy was 214 keV and 277 keV, this strongly supported above measuring results about there were 100~300keV high energy x–ray in the low voltage gas (D_2,H_2) discharge.

Analysis and discussion

From above measuring results. we might think that the x–ray emission spectrum N(Ex) included two parts: $N(E_x) = Nn(E_x) + Na(E_x)$, Nn(x) was the normal x–ray of gas discharge, or called beam–target x–ray, Na(Ex) was anomalous part, according to our supposition [3], some quasis table compact small deuterium (hydrogen) atom or molecule (denoted by De^*, Pe^* De^*De^*, Pe^*Pe^*, D denoted deuterium nucleus, P was proton, e^* was electron) Could be produced in the low voltage gas discharge, the dimension R of De^*, Pe^* was much more less than Bohr radius R_B, R / R_Bmight be 0.01~0.1 or less, so De^*, Pe^* could penetrate thick metal foil and interact with metal atom, when it broke up very nearby the nucleus of metal atom, the electron was accelerated by Coulomb field of nucleus, and x–ray were emitted, because electron might move very nearby nucleus and $Z >> 1$, so high energy x–ray could be emitted. In metal attenuation foil on the one hand x–ray were absorbed (mainly was photoelectric absorption), and on the other hand, x–ray were produced

simultaneously, in the result negative absorption might appear.

Supposing the current of quasi stable compact small neutral particle (De^*,Pe^*,•••) was n_0, its attenuation cross section was $\alpha(\omega)$, it depended some parameters ω (for example: radius, energy •••), the attenuation of neutral particle current in metal foil accompanied the emission of new x–ray: We might obtain the expression:

$$N_a(E_x,x) = n_0 \int G(\omega) g(\omega,E_x) \frac{e^{-\mu(E_x)x} - e^{-\alpha(\omega)x}}{\alpha(\omega) - \mu(E_x)} d\omega$$

$G(\omega)$ was the distribution function of small neutral particle, $g(\omega,E_x)$ was the distribution function of emitting x–ray when the neutral particle of ω–characteristic was attenuated. X denoted the thickness of metal attenuation foil.

In low energy, $Nn(E_x)$ and $Na(E_x)$ both contributed to x–ray emission spectrum $N(E_x)$ effectively (in many cases, $Nn(E_x)$ might be main), But in high energy interval, or when the metal attenuation foil attenuated the low energy x–ray to very great extent, then the measuring x–ray was $Na(E_x)$ mainly, the character of $Na(E_x)$ was represented by factor S(x) mainly

$$S(x) \equiv \frac{e^{-\mu(E_x)x} - e^{-\alpha(\omega)x}}{\alpha(\omega) - \mu(E_x)} = \begin{cases} \dfrac{e^{-\alpha(\omega)x}}{|\alpha(\omega) - \mu(E_x)|} & when \quad \mu \gg \alpha \\ \dfrac{e^{-\mu(E_x)x}}{|\alpha(\omega) - \mu(E_x)|} & when \quad \mu \ll \alpha \end{cases}$$

The value of S(x) was maximun at $x_m = lg[\mu(E_x) / \alpha(\omega)] / [\mu(E_x) - \alpha(\omega)]$. as $L_1 < L_2 < x_m$, $Na(E_x,L_1) < Na(E_x,L_2)$, so the negative absorption might appear.

In summary, because the existence of $Na(E_x,x)$, above anomalies of x–ray might be explained qualitatively.

In future, we should discriminate Nn(x) and Na(x) in detail, research the character of Na(x) and test the existence of quasi stable compact small neutral particle directly.

Acknowledgement

This work was supported by State Commission of Science and Technology, Natural Science Foundation of China and Foundation of China Academy of Engineering Physics. The authors express their thanks to Prof. Chen Neng Kuan, Wu Sheng, Wu Dong zhou and Xie Renshou for their discussion and supporting.

Reference

[1] Long He Qing, Zhang Xin Wei et al., Trans Fusion Tech. Vol.26, Dec. 1994, P.170

[2] W.J.Veigele, Handbook of Spectroscopy, P.28

[3] Zhang Xin Wei et al., Frontiers of cold Fusion, Ed.H.Ikegami, P.381; Science (Kexue, Chinese) Vol.46, No.1(1994)P.39

[4] M.Fleishmann, S.Pons and H.Hawkins, J.Electroanal chem, 261,(1989)P.310

[5] A.B.Karabut et al., Phys. Lett. A 170(1992)P.265

[6] S.Szpak et al., Phys. Lett. A 210(1996)P.382

Innovative Approach

Table 1 Detector efficiency

E KeV	13.9	17.8	20.8	26.35	39.91	59.54	121.78	244.7	344.3	778.9	964.1
ε_i	6.65^{-4}	1.445^{-3}	1.089^{-3}	1.648^{-3}	1.314^{-3}	1.587^{-3}	1.614^{-3}	9.205^{-4}	8.16^{-4}	3.47^{-4}	3.01^{-4}

Table 2. The Result of the experiment 122nd (X Ray counts per Second)

ΔE	6.4 →	10.1→	20.2 →	30.3 →	40.0 →	50.2 →	60.3 →	70.0 →	80.2 →	90.3 →	100 →
Pd122	69.22	526.37	75.682	21.710	4.572	2.014	1.258	1.152	0.944	0.742	2.988
B.G.	0.0882	0.274	0.175	0.152	0.160	0.156	0.171	0.219	0.223	0.231	1.184

(Continue)

150.3→	200.1→	250.0→	300.3→	350.1→	400.4→	450.2→	500.1→	550.3→	600.2→	650.1 →	700.3→ 750
2.240	1.882	1.506	1.332	1.154	0.816	0.652	0.596	0.454	0.406	0.400	0.300
1.075	0.924	0.701	0.564	0.469	0.388	0.333	0.327	0.270	0.250	0.267	0.192

Table 3. The Results of the experiments 125th,126th,127th,128th (X-Ray counts per Second)

ΔE	6.4 →	10.1 →	20.2 →	30.3 →	40.0 →	50.2 →	60.3 →	70.0 →	80.2 →	90.3 →	100. →	150.3 →	200.1 →250
Pd125	14.21	35.15	10.36	0.96	0.501	0.409	0.320	0.479	0.394	0.308	1.450	1.091	0.967
Pd126	2.077	3.387	1.950	0.217	0.189	0.191	0.239	0.364	0.321	0.279	1.333	1.133	0.928
Pd127	0.349	0.676	0.658	0.152	0.155	0.149	0.244	0.377	0.305	0.288	1.340	1.151	0.929
Pd128	0.128	0.389	0.343	0.144	0.168	0.170	0.210	0.366	0.318	0.286	1.330	1.085	0.952
B.G.	0.088	0.274	0.175	0.152	0.160	0.156	0.171	0.219	0.223	0.231	1.184	1.075	0.924

Table 4. The Results of the experiments 125th,126th,127th,128th (X Ray count per Second)

ΔE	6.4 →	10.1 →	20.2 →	30.3 →	40.0 →	50.2 →	60.3 →	70.0 →	80.2 →	90.3 →	100. →	150.3 →	200.1 →	250. →300
nb60	21.82	1.519	1.181	1.015	1.135	1.233	1.023	1.617	1.654	1.895	13.67	14.77	50.18	38.23
nb61	467.5	1398.	57.62	4.378	2.757	3.060	3.645	4.661	5.474	5.634	50.42	54.59	19.52	3.853
nb62	1.317	2.894	2.846	2.865	2.721	2.769	2.654	2.788	2.827	2.760	16.37	46.33	43.93	9.548
B.G	0.275	0.877	0.724	0.698	0.659	0.728	0.824	1.210	1.033	0.967	6.083	5.709	4.391	3.077

Table 5. The Results of the experiments 104th (X Ray count per Second)

ΔE	6.4 →	10.1 →	20.2 →	30.3 →	40.0 →	50.2 →	60.3 →	70.0 →	80.2 →	90.3 →	100 →	150.3 →	200.1 →	250. →	300.3 →350
Pd104	266.9	264.1	7.795	0.634	0.458	0.416	0.386	0.396	0.430	0.381	2.048	1.422	1.104	0.731	0.677
B.G	0.090	0.290	0.175	0.157	0.164	0.169	0.196	0.292	0.272	0.257	1.284	1.104	0.942	0.711	0.562

Table 6 (μ/ρ) (Cm^2/g) of Pb

E(KeV)	8.	15.	25.	35	45	55	65	75	85
Exp 1	4.45	5.95	3.16	0.89	0.677	1.13	1.15		
Exp 2	1.81	1.93	0.744	-0.312	-0.48	-0.35	-0.15	$2.54x10^{-3}$	0.085
Ref [2]	230	114	47.5	19	10.19	5.77	3.61	2.43	1.71

(Continue)

E(KeV)	95	125	175	225	275	325	375	425	475
Exp 1	1.60	1.71	0.98	0.95					
Exp 2	0.156	0.66	0.98	-0.25	-1.71	-1.19	-0.21	-0.035	0.144
Ref [2]	6.11	3.02	1.21	0.676	0.374	0.239	0.163	0.120	0.0912

Innovative Approach

Table 7 (μ/ρ) (Cm^2 /g) of Cu

E(KeV)	8.	15.	25.	35	45	55	65	75	85
Exp 1	13.15	8.688	9.47	10.01	8.85	7.87	4.99	4.80	4.25
Exp 2	14.93	43.54	11.28	7.92	7.26	5.00	4.23	4.89	4.64
Exp 3	17.82	30.45	22.46	37.02	29.1	22.54	21.52	14.51	15.55
Exp 4	3.28	7.83	4.97	2.34	1.64	1.84	2.40	2.73	2.98
Exp 5	19.02	22.01	15.02	26.58	22.65	15.76	10.03	5.52	4.56
Exp 6	25.58	27.85	19.15			5.38	-2.07	0.050	3.66
Exp 7	20.92	13.94	11.75			11.46	7.108	0.83	-1.66
Ref [2]	53.2	74.1	17.5	6.57	3.36	1.80	1.08	0.693	0.472

Continue

E(KeV)	95	125	175	225	275	325	375	425	475
Exp 1	3.79	3.39	4.52	4.66	5.49				
Exp 2	4.61	-0.034	-3.44	-4.75	-7.42				
Exp 3	22.83	19.54		30.89	45.2				
Exp 4	2.82	4.11	1.25	0.77	-3.60	-5.00	-4.60	-9.20	-3.43
Exp 5	-1.65	2.82	-18.77						
Exp 6	5.17	3.10	1.22	11.32					
Exp 7	0.36	0.81	22.33	-18.95					
Ref [2]	0.34	0.149	0.05273	0.026	0.0139	8.3×10^{-3}	5.36×10^{-3}	3.79×10^{-3}	2.75×10^{-3}

Table 8 (μ/ρ) (Cm^2 /g) of Al

E(KeV)	8.	15.	25.	35	45	55	65	75	85
Exp 1	28.6	26.15	9.23	10.39	12.78	18.83	24.8	28.66	
Exp 2	35.73	32.37	45.61	46.13	47.94	60.5	61.6	42.03	28.77
Ref [2]	49.6	7.47	1.54	0.532	0.26	0.133	0.077	0.0483	0.0321

Table 9 (μ/ρ) (Cm^2 /g) of Cd

E(KeV)	8.	15.	25.	35	45	55	65	75	85	95	125	175
Exp 1	1.21	0.43	0.12	-0.17	1.69	0.68	2.25			3.31	3.22	0.48
Exp 2	0.27	0.57	1.38	0.32	0.31	0.31	0.44	0.62	0.60	0.46	0.45	0.14
Ref [2]	225	39.6	9.68	25.1	13.4	7.51	4.63	3.10	2.12	1.53	0.704	0.261

Table 10, Average negative absorption of X-ray

E(KeV)	8.	15.	25.	35	45	55	65	75	85	95	175	$(\mu/\rho)_{av}$
$(\mu/\rho)_{Al}$	0.18	-8.70	-17.83	-6.46	-6.32	-13.24		-12.35	-25.57			-7.76
$(\mu/\rho)_{Al}$	1.08	-3.59	-9.52	-5.66	-4.96	0.23	0.89	0.65	2.01	-2.69		-1.43
$(\mu/\rho)_{Al}$	6.68	-12.31	19.37	27.40	-37.11	13.94	-3.81	-34.66	-57.35			-11.46
$(\mu/\rho)_{Cu}$	-6.19	-6.14	-4.29	-3.51	-3.52	5.58	7.24	3.04	0.41	1.19	-4.83	-5.18

Fig. 1 Average Counts of X-ray for Experiments Pd122nd and Pd125th

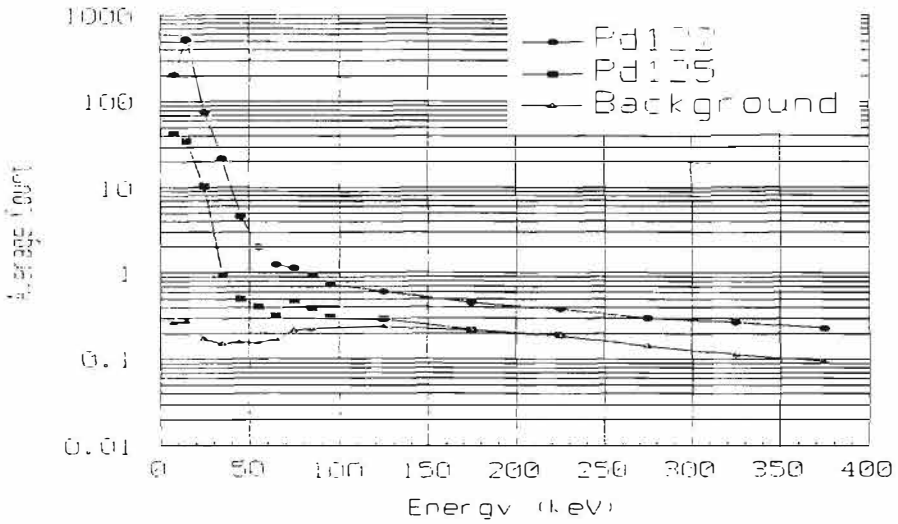

Fig. 2 Average Counts of X-ray for Experiments Nb60th

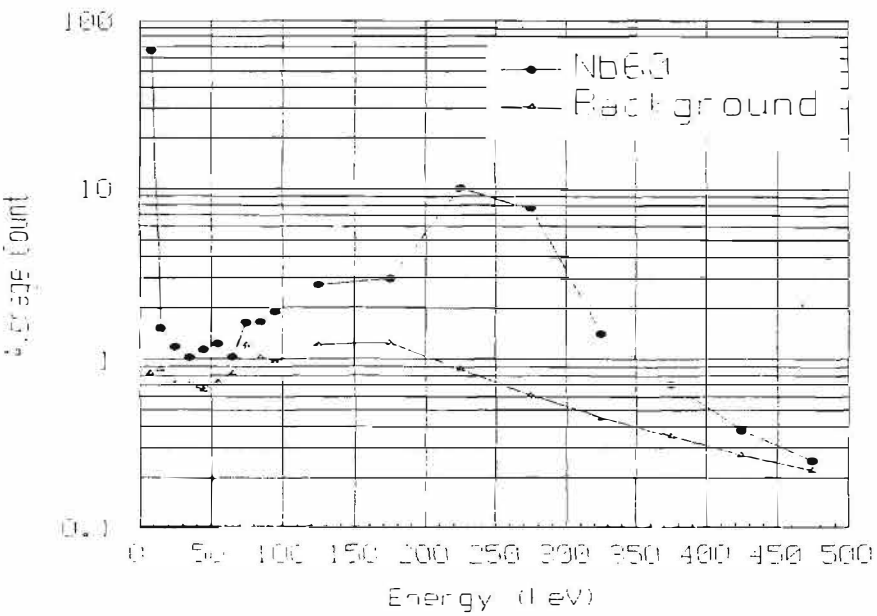

Innovative Approach

STRUCTURAL CHANGES OF SINGLE CRYSTALS IN NEUTRON GENERATION EXPERIMENTS

S.V.Vakarin, A.L.Samgin and V.S.Andreev

Institute of High-Temperature Electrochemistry
Russian Academy of Sciences
Ekaterinburg 620219, RUSSIAN FEDERATION

Abstract
This paper presents the results of new analysis of X-ray data (crystal lattice parameters and elementary cell volumes) both before and after experiments. On the basis of detection of structural changes, it is reasonable to suggest that the generation of neutrons occurs at the instant of disruption of channel structure of solid, associated with compression of crystal lattice. Perhaps the processes of explosive character inside the crystal, caused structure rebuilding, take place. Such changes may be considered as phase transition.

1. Introduction

Single crystal samples are capable to become perspective materials for cold fusion. Different experiments on reproducibility and search for neutron generation using single crystals of oxide tungsten bronze were run in the last years [1-5]. However, some experiences have not produced the positive result. This can be associated with failure to meet necessary requirements relative to preparation of experiment. Our numerous experiments with the use of two-ring detector and electronics in CAMAC-standard [4] have shown, that some events were registered to be considered as separate neutron bursts of duration of some tens of microseconds. We have shown [5], that neutron generation is observed with such crystals, which had sufficient perfection of the working plane in the beginning of the experiment. During experiment as well as at preparation for it, the perfection of crystals is subject to distortion, resulting in a disappearrance of effect.

2. Method

In this paper we propose a latest analysis of X-ray studies of single crystals of oxide bronzes. X-ray pattern of the samples was performed by DRON-3 diffractometer under Cu-k_α radiation (with the use of Ni-filter). The IBM computer processes from recorder X-ray data simultaneously concerning refinement of diffraction maxima position, analysis of phase composition, as well as information on parameters of crystal lattice and errors of their definition.

The primary objective is to investigate the structural changes of single crystals of oxide tungsten bronzes with cubic structure which are involved in neutron generation experiments. We used crystals grown by the electrolysis of molten salts. We carried out experiments using only crystals free from admixtures (polytungstates, tungsten etc.) on the surface.

Filming of X-ray patterns has been conducted from the same planes of crystal, just as before conduction of experiments, so also after them. This has allowed to record changes in a surface layer of the sample. In these experiments both positive results on registration of neutron events, and negative results were observed.

The neutron yield was found to be at most consistently 2-3 times above the maximally observable significance of background level (background was observed during two days

before experience). Registration of neutrons was conducted with the use of the two-ring detector containing 15 counters of SNMO type in each ring.

3. Results and discussion

Results of account of X-ray patterns of the Na_xWO_3 samples, when positive effect has been observed, are presented in table 1, and results in the case that positive effect was not found, are tabulated in table 2 . Here a_1 and a_2 are the respective parameters of the cubic lattice before and after experience, V_1 and V_2 are the respective volumes of the elementary cell before and after experience, X_1 and X_2 are the respective contents of the alkaline metal (Na) in surface layer of the crystal before and after experience, V/V_1 is the relative change of the volume of elementary cell during experience.

The quantities X_1 and X_2 are calculated with use of the known relation, connecting the parameter of the crystal lattice with the content of the alkaline metal (Na) in the bronze

$$a = 0.0819\,X + 3.7846\ (Å). \qquad (1)$$

Table 1

a_1(Å)	V_1 (Å^3)	a_2 (Å)	V_2 (Å^3)	X_1 / X_2	V/V_1 (%)
3.8539	57.24	3.8460	56.89	0.85/0.75	0.61
3.8546	57.27	3.8494	57.04	0.85/0.79	0.40
3.8526	57.18	3.8430	56.76	0.83/0.71	0.73

Table 2

a_1(Å)	V_1 (Å^3)	a_2 (Å)	V_2 (Å^3)	X_1 / X_2	V/V_1 (%)
3.8534	57.22	3.8532	52.21	0.84/0.84	0
3.8508	57.10	3.8509	57.11	0.81/0.81. ..	0
3.8587	57.45	3.8596	57.49	0.90/0.91	0.07
3.8526	57.18	3.8567	57.37	0.83/0.88	0.33

Trough the analysis of successful experiments it is possible to conclude, that elementary cell volume of the samples used in these experiments has been decreased. All the samples, for

which neutron effect was not found, were imperfect (with microblocks and strong tension). For them a decreasing of elementary cell volume was not found (within the limits of the error of definition dV = 0.02 Å^3), or this volume was increased.

The repeated use of the sample, the growth regime and the operations on its preparation can result in significant disorder of perfection and, as a consequence, in absence of neutrons emission and in nonreproducibility of the results. In particular, the generation of neutrons was found to be sensitive to water steam atmosphere. By a method of X-ray analysis we established, that in such atmosphere a disorder of crystal structure perfection of the single crystal surface takes place. This is due to the fact that the water molecules in a surface layer form hidrogen bonds with atoms (ions) of oxygen-tungsten octahedrons deforming them, and accordingly, deforming a channel structure formed by these octahedrons as a whole. Besides, the water steam can exert some influence on process of the nuclear reactions with neutrons, as the solid substence is in this case saturated not only with molecules of deuterium, but also with complexes HD and hydrogen molecules as well.

This clearly demonstrares the direct influence of insignificant (at first sight) conditions on reproducibility of results and the complexity of conduction of correct electrochemical experiments on cold fusion.

In this connection it must be note, that preliminary electrolysis pursued before experience for the purpose of creation of the channel structure in surface layers of single crystal, while is, as appear, a necessary procedure, can at the same time in itself bring into local reduction of elementary cell volume. This is thermodynamically due to the fact that under electrochemical extraction of sodium the defect in the centre of elementary cell of the Na_xWO_3 crystals will be formed. The regimes of electrolysis should thus be chosen with the special attention.

As appear, the degree of depletion of alkaline metal inside sample remainsto be optimum. On the one hand, at electrolysis it is necessary to extract from the bronze enough quantity of sodium for formation of channels absorbing atoms or molecules of deuterium. Thus the character of conductivity of surface layers depending on the content of alkaline metal can vary. On the other hand, the premature deformation of the lattice and structure violation involved in the composition change and in the their related change of bronze properties, should not hinder realization of processes, resulting in neutron generation.

A question remains to be answered, which factors cause significant reduction of elementary cell volume of those crystals which bring into existence the positive results during experience.

Based on conducted researches, we propose that the generation of neutrons occurs at the moment of distortion of the channel structure of substance, connected with compression of crystal lattice. Perhaps, the processes of explosive character inside the crystal, caused the structure rebuilding, take place. Such changes may be considered as phase transition.

References

1. K.A.Kaliev, A.N.Baraboshkin, A.L.Samgin et al. "Reproducible Nuclear Reactions during Interaction of Deuterium with Oxide Tungsten Bronze". Phys. Lett., 1993, v.A172, p.199-202; Frontiers of Cold Fusion / Nagoya Proc. of 3 Intern. Conf. on Cold Fusion, Universal Academy Press. Japan, 1992, p.241-244; Reports of Russian Academy of Sciences, 1993, v.330, N. 2, p.214-216.

2. A.Bertin, M.Bruschi, V.M.Bystrisky et al. "Negative result on the verification of reported "cold fusion" phenomena in Na_xWO_3 (D;D-T) system".J. of Nucl. Phys. (In Russian), 1996, v.59, N.5, p.789-794.

3. E.Yamaguchi. "Measurement of the Neutron Emission and Nuclear Products from Na_xWO_3 in the Deuterium DC Plasma Environment". Preliminary Progr. of the Sixt Intern. Conf. on Cold Fusion, 1996, October 13-18, Japan, p.10.

4. A.L.Samgin, V.S.Andreev, et al. " Electrolysis of Solid Deuteron Conducting Electrolytes in Deuterium Atmosphere: Microsecond Structure Analysis of Neutron Pulses by means of Two-Ring Detector". Progr. of Minsk Cold Fusion Conf., 1994, May 21-26; Fusion Facts, USA, 1994, v.6, N.2, p.14.

5. S.V.Vakarin, A.L.Samgin, V.S.Andreev, et al. "Influence of Perfection of Sodium Tungsten Bronze Single Crystals on Neutron Emission". Proc. of 5 Intern. Conf. on Cold Fusion. France, IMRA Europe, 1995, p.227-232.

Innovative Approach

Carbon Production on Palladium Point Electrode with Neutron Burst under DC Glow Discharge in Pressurized Deuterium Gas

H. Yamada, H. Nonaka, A. Dohi, H. Hirahara, T. Fujiwara, X. Li and A. Chiba

Faculty of Engineering, Iwate University, Morioka 020, Japan

Abstract

A point-to-plane electrode configuration in slightly pressurized deuterium gas for highly non-uniform electric field was employed to confirm the cold fusion phenomena under glow discharge condition. A neutron burst took place in 2 runs out of total 37 runs. Using an optical microscope, black deposit was observed to cover the tip surface of two positive electrodes. To the contrary, the tip surface of other 35 electrodes was observed to keep its beginning appearance. X-ray photo-electron spectroscopy have revealed the black deposit to be carbon, mixed with palladium at the surface of palladium point electrode. The total amount of carbon impurity in the palladium electrode and in environment deuterium gas dose not account for the large amount of carbon on the tip surface of electrode.

1. Introduction

Wada et al. have reported a spontaneous neutron emission from palladium(Pd) electrode in deuterium(D_2) gas during and after activation by flashover between electrodes[1]. The study shows that the nuclear reaction can takes place at solid in D_2 gas atmosphere[2,3] as well as in heavy water[4]. In this study, the nuclear reaction in D_2 loaded Pd point electrode in 2 atm D_2 gas under glow discharge condition has been investigated by neutron detection and X-ray photo-electron spectroscopy(XPS).

2. Methods

A neutron measurement system, including a ^{3}He thermal neutron detector , is used to detect the excess neutron from the nuclear reaction in Pd point electrode. A neutron moderating system of polyethylene block, as shown in Fig. 1, has a center cavity with a cylindrical shape of 140 mm in diameter and 100 mm high, enhance the efficiency of the ^{3}He counter by moderating fast neutron from a test cell. The test cell and the detector are positioned inside the center cavity. Signals from the detector are fed to the single channel analyzer through a preamplifier and an amplifier. The counts are stored on a floppy disk using a personal computer. The noise related to high-voltage application is avoided by adjusting the preamplifier gain and the

Innovative Approach

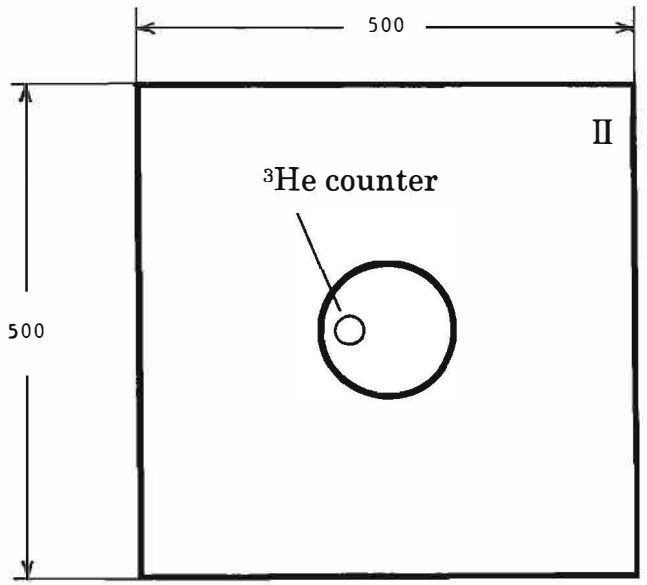

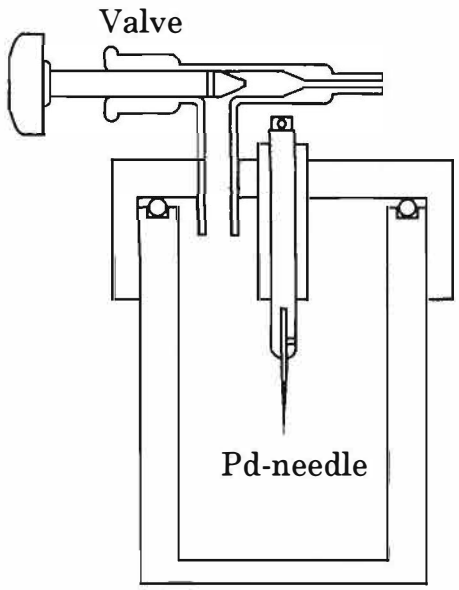

Fig. 2 Test cell

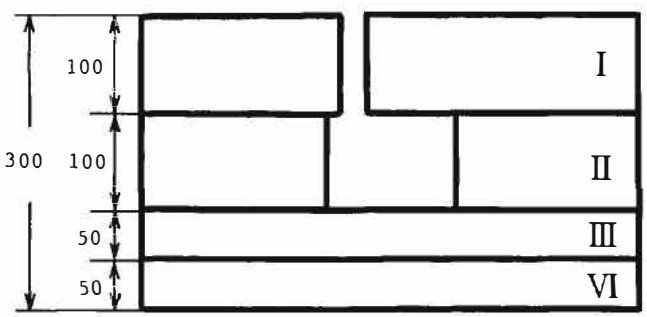

Fig. 1 Neutron moderating system

window of the single channel analyzer.

The test cell, shown in Fig. 2, have a cylindrical shape with volume capacity of 110 cm^3. The point-to-plane electrode system with gap spacing about 10 mm was employed in the closed cell to obtain highly non-uniform electric field. A Pd wire of 0.5 mm in diameter was cut to about 30 mm in length to be a point electrode. After polishing the surface with sandpaper, the Pd point electrode was vacuum annealed at 400℃ for 3 hours under a pressure about 10^{-4} Torr then cooled down to room temperature, followed by loading of D_2 gas under 2 atm pressure for 24 hours. Next, the Pd point electrode was set to the test cell, followed by filling the test cell with 2 atm D_2 gas. After positioning the cell and the detector inside the center cavity of moderating system, positive DC 4 or 8 kV was applied to the Pd point electrode. The neutron measurement started just after the voltage application and continued for 24-65 hours. The deuteron to Pd loading ratio was measured to be about 0.6.

The efficiency of the detector was measured to be approximately 1% using ^{252}Cf source. The average background of neutron flax without the test cell is about 25 counts per hour after the adjusting. The counting characteristics of background neutron has been stable over total about 3,500 hours of background measurement period for these 7 years.

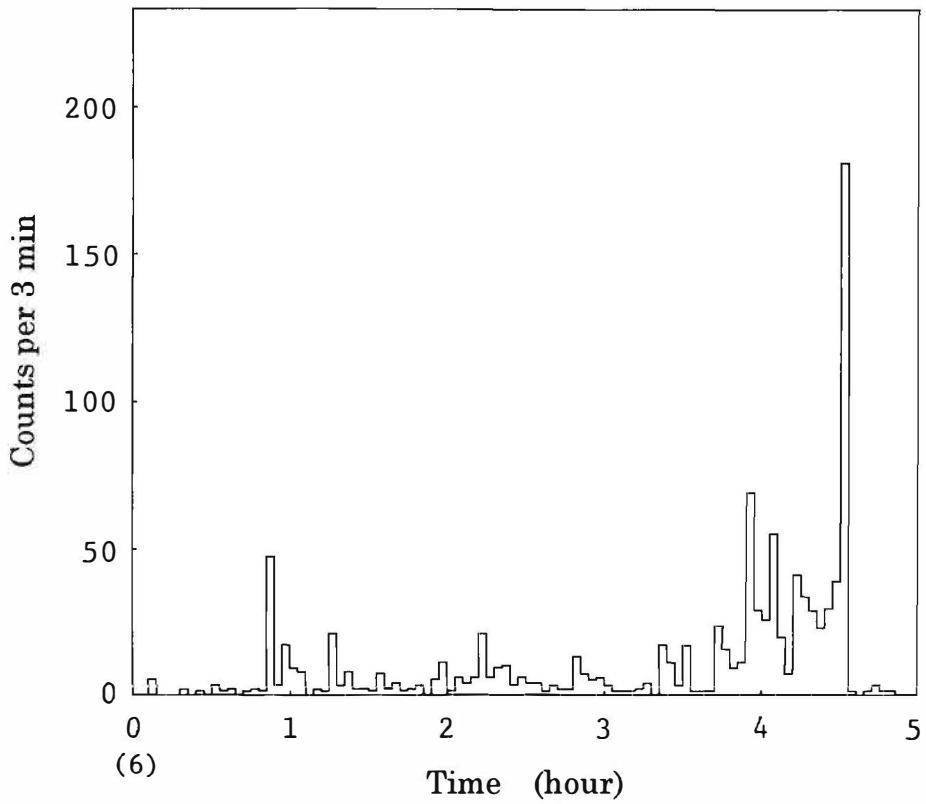

Fig. 3 Time dependence of the neutron counts from deuterium-palladium system

3. Results

The neutron burst was observed in 2 out of 37 runs. The electrodes used in the positive 2 runs are assigned to the names "Electrode-A" and "Electrode-B". The time behavior of the neutron emission rate for Electrode-A is shown in figure 3, where the emission started at 6 hours 48 min after the beginning of the 8 kV application and continued 3 hours 50 min. No excess count was observed for 30 hours after the emission ceased. The highest count rate of 180 counts per 3 min, observed just before the emission ceased, is 140 times larger than that of the background neutron. The number of total neutron counted was about 900. In the case of Electrode-B, The burst was started just after the voltage application and continued for about 15 min. The next burst started about 5 hours after the first burst and continued for 5 min. The number of neutron counted during the 2 bursts amounts to 3×10^4. The highest count rate of 2,700 per 5 sec was 9×10^4 times larger than that of the background neutron. The total number of excess neutron is estimated to be 35 times larger than that for the Electrode-A, even though the emission period was shorter than that for the Electrode-A. No excess neutron was observed for 65 hours after the second burst ceased.

The electrodes after the voltage application were viewed by an optical microscope. The tip surface of two positive electrodes was found to be covered with black deposit. Of particular interest is that several craters of about 10 μ m in diameter were formed on the tip surface of Electrode-A. The covered area was measured to be more than 0.32 mm^2 for Electrode-A. To the contrary, the tip surface

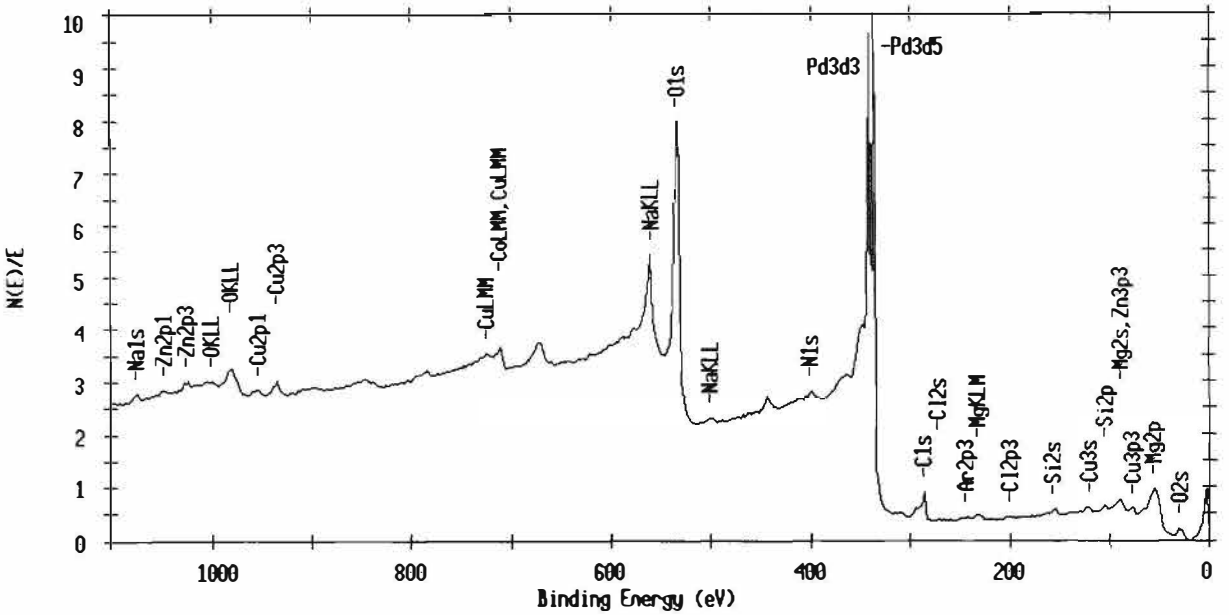

Fig. 4 XPS spectrum of the Pd point electrode before neutron emission

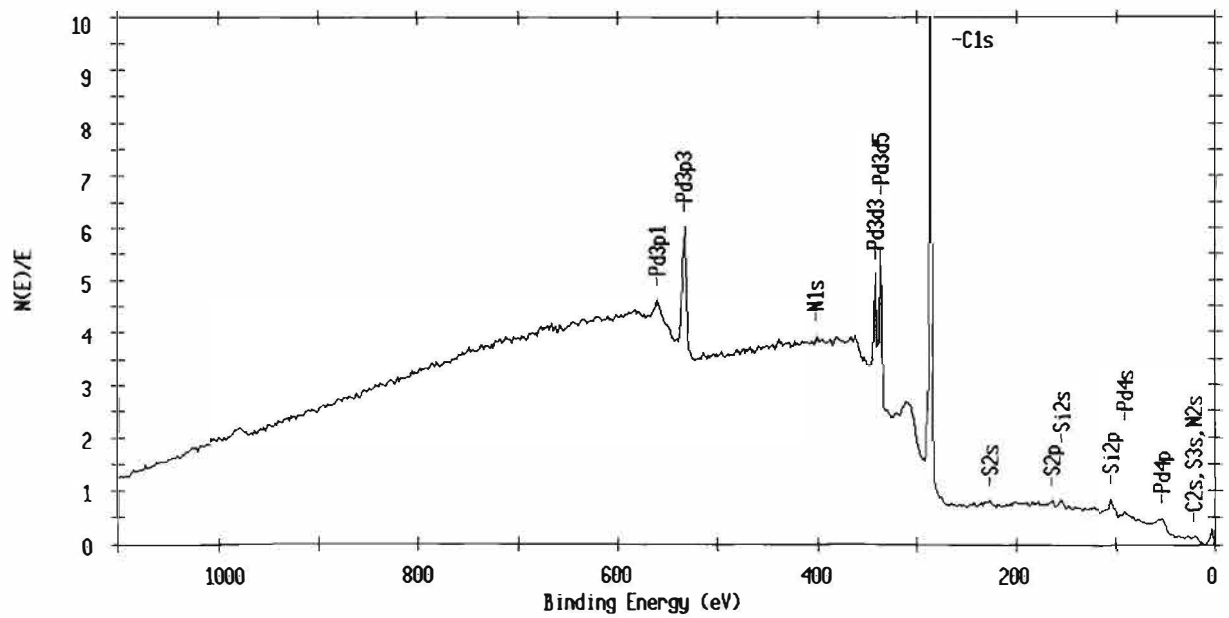

Fig. 5 XPS spectrum of the Pd point electrode after neutron emission

of negative 35 electrodes was observed to keep its beginning appearance.

An XPS spectrum for D_2 loaded Pd point electrode before the voltage application is shown in Fig. 4, where the tip of electrode was etched in about 0.5 nm depth with argon ion to remove molecules of air contamination. The figure shows a strong absorption of oxygen on the surface. To the contrary, a large carbon peak is seen in the XPS spectrum of the tip of Electrode-A after the neutron emission, as shown in Fig. 5. It seems that the carbon atoms were mixed with Pd atoms in the bulk region from the electrode surface to the depth in several atomic size at least .

4. Discussion

The Pd point electrode may include 1 PPM carbon at most. The point positive condition excludes the possibility that the carbon in the bulk of Pd point electrode was collected and condensed into the surface region by an electro-migration. Even though there exists another unknown mechanism for carbon impurity to migrate to the surface, the carbon collected should be 17 nm in thickness, based on that the deposit density of 1.5 and carbon impurity of 1 PPM. Whereas the thickness of the deposit should be more than 340 nm for the deposit to be seen black.

The environmental D_2 gas in the test cell includes 0.4 PPM CO , 0.6 PPM CO_2 and 0.1 PPM CH_4 at most. The total amount of carbon impurity in the gas can form carbon deposit of 250 nm in thickness. Thus, the carbon impurity both in the Pd electrode and in the environment D_2 gas does not account for the large amount of carbon on the surface of Pd point electrode.

The plausible explanation for the neutron burst and the carbon production is that the high current density at the point electrode and its fluctuation by glow discharge would stimulate the accumulation of deuterons to induce a fusion in the bulk near surface of Pd point electrode. The relatively low loading ratio of 0.6 allow us to conceive that high loading ratio is not always necessary but high current density is rather an important factor for the nuclear reaction. An atom such as helium would be produced from deuterons at first reaction step; carbon would be produced from the atoms next. However, the total excess neutrons estimated was considerably few compared with the estimated number of carbon atoms on the surface of Pd point electrode. This indicates that the first reaction would produce a large number of atoms such as helium but few neutrons.

5. Conclusion

The large amount of carbon deposit was observed at the tip of D_2 loaded Pd point electrode after neutron burst under glow discharge condition in 2 atm D_2 gas, even though the phenomena are rare. The phenomena could be explained in terms of a nuclear fusion at the Pd point electrode.

Acknowledgment

This work was supported in part by a Grant-in-Aid for Scientific Research from Ministry of Education, Science and Culture. It was also supported in part by a Grant-in-Aid for Scientific Research from The Thermal and Electric Energy Technology Foundation.

Reference

1) N. Wade and K. Nishizawa: Jpn. J. Appl. Phys. 28 (1991) 380
2) A. De Ninno et al. : Europhys. Lett. 9 (1989) 221
3) T. Mizuno et al. : Fusion Tech. 29 (1996) 385
4) A. Takahashi et al. : Fusion Tech. 19 (1991) 380

Innovative Approach

A Study of The Mechano-Nuclear Interaction Using Piezoelectric Material of $LiNbO_3$ in D_2 Atmosphere:

Dependence of D_2 Gas Atmospheric Pressure

M.Utsumi, M.Chiba[1], M.Fujii[2], T.Shirakawa[3], Y.Fujimoto[1], Y.Hayami[1], Y.Hayashi, T.Nobuhara, N.Sekino[1], T.Yokoyama, T.Yonekura, T.Hirose[1], H.Nakahara[2] , K.Sueki[2]

Department of Applied Physics, Faculty of Engineering, Tokai University
1117 Kitakaname, Hiratsuka-shi, Kanagawa, 259-12, Japan
[1]Department of Physics, Faculty of Science, Tokyo Metropolitan University
1-1 Minami-Ohsawa, Hachioji-shi Tokyo, 192-03, Japan
[2] Department of Chemistry, Faculty of Science, Tokyo Metropolitan University
1-1 Minami-Ohsawa, Hachioji-shi, Tokyo, 192-03, Japan
[3] Department of Social Information Processing, Otsuma Women's University
2-7-1 Karakida, Tama-shi, Tokyo, 206, Japan

Abstract

In order to clarify the detailed mechanism of neutron emission from $LiNbO_3$ crushing process in D_2 atmospher, *Mechano-Nuclear Reaction*, we measured the neutron emission rate with respect to D_2 gas pressure. In a low pressure region, the excess neutrons were not observed. While in a high pressure region, larger than 30 kPa, the excess neutrons were observed. We are also studying the difference in neutron emission between a single and a multi ferroelectric domain crystals of $LiNbO_3$.

Innovative Approach

1. Introduction

We have been studying neutron generation from piezoelectric material crushed in D_2 atmosphere[1,2,3,4]. We call this phenomenon as *Mechano-Nuclear Reaction*. Only in the system of $LiNbO_3$ with D_2 gas, the neutron emission was observed.

We specurate the mechanism of the reaction as follows; In crushing of piezoelectric material, surface charges appear on new birth surface caused by breaking of the chemical bonds of the material, with a generation of high electric field by piezoelectric effect. These surface charges activate the adsorbed substances.. Therefore D_2 molecules adsorbed on the surface are decomposed and excited by the charges. Thus, some of the excited particles are accelerated by the piezoelectric field along the chink of the crystal (Fig. 1) and collide with atmospheric D; then D-D fusion occurs[4].

In order to verify the mechanism of *Mechano-Nuclear Reaction*, we measured the neutron emission rate with respect to the D_2 gas pressure. Further we are studying the neutron emission in different structures of the $LiNbO_3$ crystal, *e.g.* a single- and a multi-domain crystals.

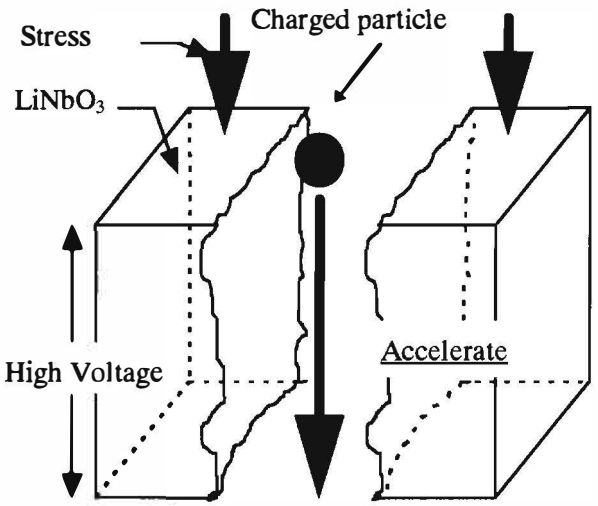

Fig. 1 Acceleration mechanism of the charged particle by piezoelectric effect

2.Experiments

Fig. 2 shows the schematic view of our experimental system. The crushing chamber was a 230 ml of stainless steel cup (inner diameter of 90 mm) with a hard steel ball of 50 mm in diameter (515g). The chamber was vibrated at the frequency of 50 Hz with the vertical amplitude of 3 mm (Vibromill VP-100, ITOH Co. Ltd.).

The emitted neutrons were detected by 16 ^{3}He proportional counters (Reuter-Stokes RS-P4-0806-207) arrayed in a cylindrical shaped paraffin block, 38 cm outer diameter and 10 cm inner diameter, around the crushing chamber. After thermalized by the paraffin, the neutrons reacted with ^{3}He nuclei in the counter making a proton and a tritium with a Q value of 760 keV. Each pulse height of the signal from ^{3}He gas counters was processed and digitized by CAMAC analog-to-digital converters (12bit ADC) indivisualy. The pulse height of the ^{3}He gas counters were calibrated by ^{252}Cf neutron source. The peak of full energy deposit signal in the ^{3}He gas counter by thermalized neutrons was set at 1500 channel of ADC by tuning each high voltage applied. In order to increase the signal

to noise ratio, counts between 600 to 1599 channels were selected. The detection efficiency was measured to be 5.8 %.

The experiment has been done in the low background facility at Nokogiri mountain of The Cosmic-ray Research Institute, The University of Tokyo (ICRR), which is located underground 100 m water equivalent at least[5].

The crushing process was proceeded for one hour duration. The crystal size of $LiNbO_3$ was about 3 mm initially. After one hour crushing process, it was reduced to about 1μm diameter.

The two types of $LiNbO_3$ crystal were employed. One was manufactured by Toshiba Co., for the experiment measuring gas pressure dependence in D_2, which was the end part of the single crystal block. Another was the wafer of about 600 μm in thickness and 3 inches in diameter manufactured by SUMITOMO METAL MINING Co. Ltd. for measuring the neutron emission rate with the single and the multi ferroelectric domain crystals.

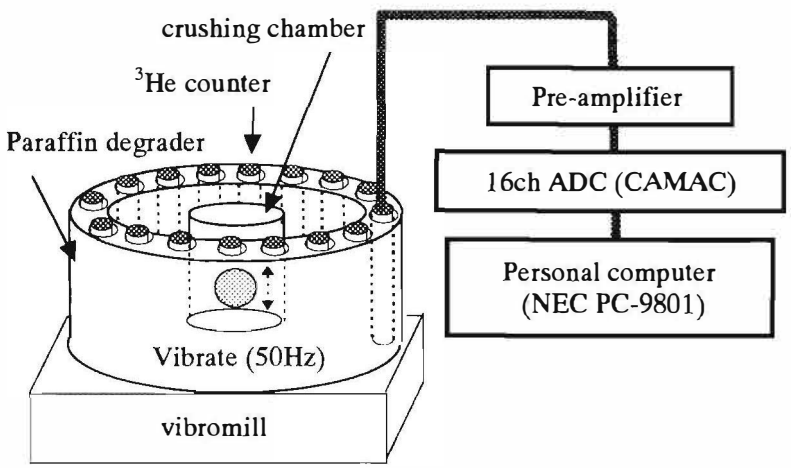

Fig. 2 Schematic view of our experimental system

3.Results

The neutron counts exceeded over the background rate is plotted in Fig. 3 with respect to the D_2 gas pressure. The background count rate was 10.01 ± 0.20 counts/hour except 101 kPa. Each data in the measurement of pressure dependence was obtained by the experiment of 5 hours, except 7.5, 25 and 101 kPa. The error bars are statistical only taking into account of the background count fluctuation. In the high pressure region, larger than 30kPa, the weighted mean value over the background rate is 2.79 ± 0.71 counts/hour and the lower pressure region, -0.04 ± 0.56 counts/hour. The result clearly shows that the existence of D_2 gas is indispensable for the neutron generation.

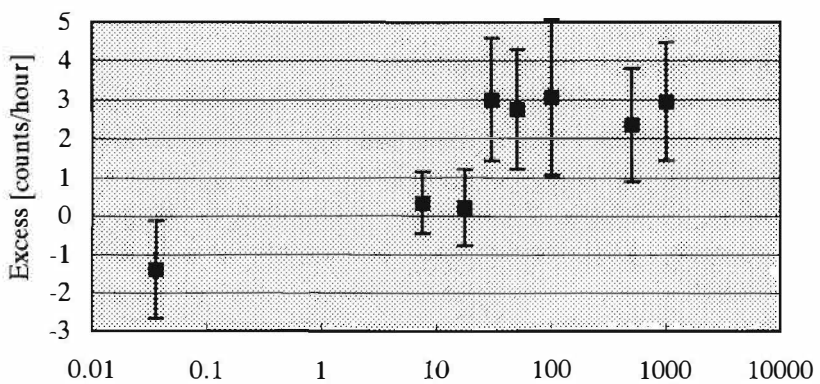

Fig. 3 Dependence of excess neutron on D_2 gas pressure
($LiNbO_3$ was manufactured by Toshiba Co.)

Innovative Approach

We are going to study the effect due to the characteristics of $LiNbO_3$ crystal itself. The wafer provided by the SUMITOMO METAL MINING Co. Ltd. is a single-domain crystal. We would like to measure the neutron generation rate by the crushing process of a multi-domain crystal. We have tried to make the multi-domain crystal by annealing the wafer at 1200°C for 30 hours. In order to clarify the boundary of each domain, the surfaces of the wafers are etched by mixed solution of HF and HNO_3. The micrographs of etched surfaces are presented in Fig. 4 (a) and (b). For the single-domain crystal Fig. 4(a), we can not find any boundaries due to the difference in the orientation of the dielectric polarization. On the contrary, we can find domain structure in the annealed sample in Fig. 4(b). We are planning to measure neutron generating rate by the annealed sample as well as the single-domain crystal.

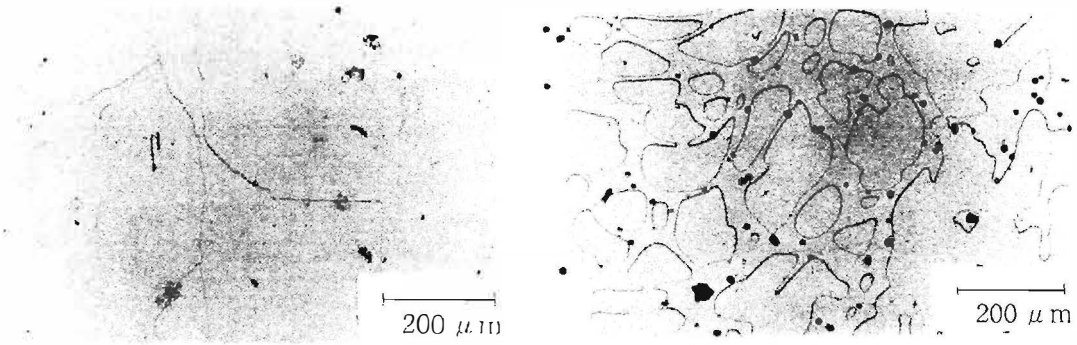

(a) single-domain crystal (b) multi-domain crystal

Fig. 4 The micrographs of etched surface of the single- and multi-domain crystal

4.Conclusion

We have observed the effect to the neutron generation by the pressure of D_2 gas, which means the presence of D_2 gas is necessary to generate the neutron. The result suggests that the neutrons come from D-D fusion processes. We are preparing to measure the effect on the neutron generation by $LiNbO_3$ ferroelectric domain structure. The acceleration of D ion could be depended on the characteristic of $LiNbO_3$ in the fusion process.

5.Acknowledgment

We would like to express our appreciation to the late Prof. K. Yamakoshi (ICRR) for his great support. This research was supported in part by Specific Research Fund from Tokyo Metropolitan University and NHE.

Reference

[1]T.Shirakawa, et al. *Chemistry Lett.*, 897, (1993).
[2]T.Shirakawa, et al. Frontiers of Cold Fusion (Universal Academy Press, Inc. Tokyo, 1993) 523
[3]T.Shirakawa, et al. Proceedings: Forth International Conference on Cold Fusion, **Vol. 3** (1994) 6.
[4]M.Chiba et al., *IL NUOVO CIMENT*, **108A**, 1277 (1995)
[5]T.Shibata, M.Imamura, S.Shibata, Y.Uwamino, T.Ohkubo, S.Satoh, K.Yamakoshi, N.Oyama, T.Ohsaka, N.Yamamoto, O.Hatozaki and N.Niimura, *Nucl. Instr. Meth. Phys. Res.*, **A316**,337(1992)

Innovative Approach

PRELIMINARY STUDY ON TRITIUM AND ELEMENTS TRANSMUTATION IN WATER UNDER SIMULATED AEROSPATIAL CONDITIONS

Chang B. Liu , Guo Z. Wang, Da W. Mo* , Xi Y. Li** , Xing Z . Li***

Beijing Yuan Heng Physicochemical High Scientific and Technology Corporation
Beijing 100083, China
*Institute of Nuclear Energy and Technology, Tsinghua University, Beijing 100084
**Institute of Semiconductor, Academia Sinica, Beijing 100083
***Department of Physics, Tsinghua University, Beijing 100084

Abstract
A series of unexpected phenomena have been discovered under simulated aerospatial conditions. The tritium-rich water passed through the aerospatial condition. The Beta-radiation of tritium was measured before and after this process in terms of liquid scintillation counter. It was found that the radiation from tritium decreased every time it passed through this simulated system. the amount is about 20%. The trace elements analysis was made for distilled water before and after the same process. It was found also that the change of the trace elements, for example K from 0.0045ppm to 0.008ppm.

1. Introduction

It is very strange that a series of unexpected phenomena have been discovered in the aerospatial condition in terms of the spaceships. An attempting has been started to mimic the aerospatial conditions as that in the F-2 ionosphere(vacuum, ionization, weightless, etc.) in the laboratory on the earth. At these mimic aerospatial conditions the tritium in water decreased, and the content of trace elements increased. All of these experimental phenomena should be introduced in this paper.

2. Experimental conditions

Temperature: ambient.
Work gas and pressure: Nitrogen, vacuum.
Environment: plasma, weightless and glow
Processing time : ~ 0.3 sec
Processing material : distilled water or natural water
The discharge power can be controlled , the glow might be selected.

3. Experiment

The water passed through the system of mimic aerospatial conditions, in which the discharge power can be changed, the appear or disappear of glow are able to be controlled, the vacuum and weightless are kept . The schematic drawing of this system (DST-1) was shown in Fig. 1

Innovative Approach

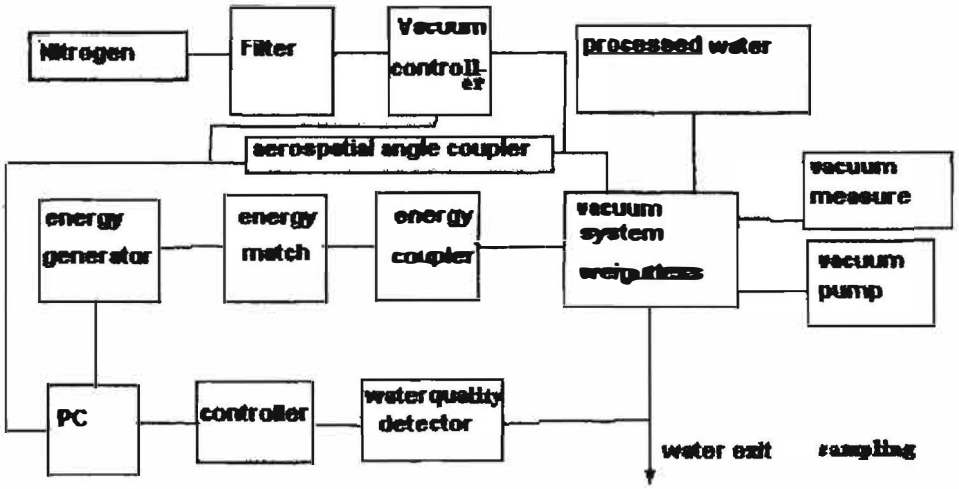

Fig.1 schematic drawing of mimic aerospatical system

For sake of more sensitive measurement, the tritium was added in natural water , the content is about 1000-1500 Bq/L. Owing to limitation of environment control, this amount is the largest, but it is not enough sensitive for experiment. The tritium measurement was carried out with 2550 type liquid scintillation counter (Park company). The content of trace elements were measured by P. E. 5000 type automatic atomic absorption spectroscopy, 2010 type ion exchange chromatography, and ORION. STA20 ionometer etc.

4. Results

4.1 Tritium measurement

4.1.1 Natural water

Before processing 63Bq/L

After processing 38Bq/L

4.1.2 Rich-tritium water (1)

Sample No.	Before processing Bq/L	Processing once Bq/L	processing twice Bq/L
1	1200	900	800
2	1200	1000	600
3	1200	700	500
4	1200	900	800

All of these samples are processed in different discharge power , without glow.

4.1.3 Rich-tritium water (2)

Sample No.	Before processing Bq/L	After processing Bq/L	processing
1	1450	1350	
2	1450	1300	
3	1450	1500	glow

4	1450	1600	glow
5	1700	1500	
6	1700	1400	glow +power
7	1700	1800	glow

These experiments used the different discharge power and glow. when glow was used, the tritium increased, conversely the tritium decreased.

4.1.4 Static experiment

Rich-tritium water was sealed in quartz ampoule, which was put in our system and processed. the result is following

Before processing 3590Bq/ml

After processing 3600Bq/ml

Of course this processing was done without vacuum, plasma in it. The content of tritium did not change.

4.2 Trace elements experiment

Sampling the processing distilled water and analyzing it with above-mentioned instruments, the results were shown in table 1.

Table 1 the content of trace elements(ppm)

Element	K	Na	Ca	Mg	Zn
Before processing	0.0045	0.098	0.04	0.006	0.0145
After processing	0.008	0.165	0.663	0.018	0.006

4.3 The other results

The other phenomena were observed, for example the processed natural water (poor-tritium) the temperature decreased, when the rich-tritium water was processed the temperature increased about 2¡æ.but it needs confirm precisely.

5. Discuss

1. All of this experiments are preliminary, it needs confirm, consummate.
2. From this work, the nuclear transmutation is possible at the suitable conditions.
3. Nuclear transmutation can be happened under some condition, how to understand it? We only can supply some phenomena.
4. Reifenschweiler's[1] work on tritium decay showed that the nuclear radiation might chang due to the variation of the enviroment. We have got the same conclusion in our experiment.

Acknowledgements

We want to acknowledge the important contribution to measurement and analysis given by Prof. Yi F. Guo, Prof. Xiu Q. Liu. We also like to thank Dr. Qing S. Cai , Dr. Jie wang ,They give us so much help about analyzing trace element and experiment.

Reference:

1. Reifenschweiler, ICCF-5 proceedings, 163(1995)

Innovative Approach

NUCLEAR PRODUCTS ASSOCIATED WITH THE PONS AND FLEISCHMANN EFFECT; HELIUM COMMENSURATE TO HEAT GENERATION, CALORIMETRY AND RADIATION.

B. F. Bush and J. J. Lagowski, University of Texas, Dept. of Chem., Austin, TX, 78712, USA. M. H. Miles, Naval Air Warfare Center, Weapons Division, China Lake, CA 93555, USA.

Abstract: The nature of the nuclear phenomena associated with the Pons and Fleischmann effect remains largely unexplored. The phenomena are reproducible, but the processes lack controllability. The circumstances of the electrolysis experiments do not produce the same nuclear product distribution as that expected during hot plasma D + D fusion experiments.

From our earliest qualitative heat versus helium nuclear products analyses[1] to our more recent quantitative helium analyses; the utmost care has been exercised with respect to the scientific rigor of our work. The correlation between the production of helium and the generation of excess heat has been reproduced in different laboratories and under different experimental protocols. Preliminary results are shown in Fig. 1. The quantitative correlation between the amount of energy generated and the helium produced is at the level that is expected for a high energy nuclear reaction, such as fusion. These results are underwritten by extensive ^{3}He:^{4}He:^{20}Ne control experiments.

Calorimetric quality is the foundation of this work. In our early work, isoperibolic calorimetry was used successfully. In our later work as depicted in Fig. 1, high performance Calvet calorimetry is used. This is the most rigorous method of calorimetry known, amounting to an integrated measurement of the total thermal flux. Electrolysis off-gas production rates were measured to determine the Coulombic efficiency of the electrolysis. Atmospheric helium contamination was precluded by use of all-metal sampling flasks and all-metal gas collection equipment with helium leak-tight Cajon VCR metal seals.

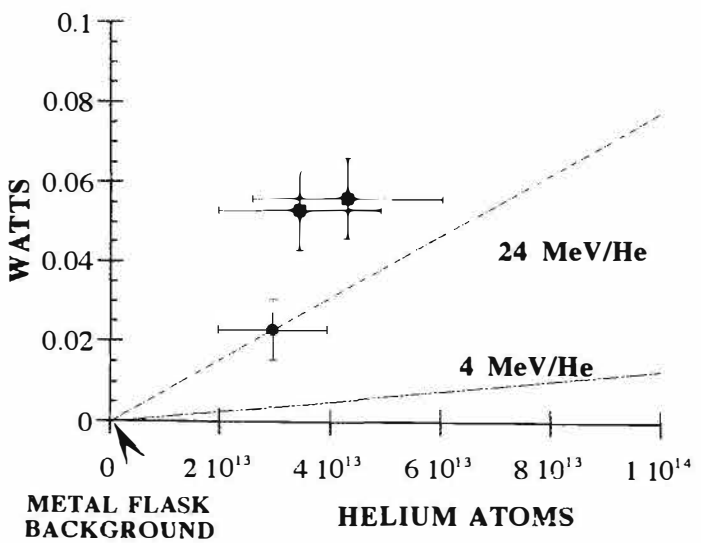

Figure 1. D + D --> ^{4}He + 24 MeV is the most energetic reaction known. The heat *versus* helium analysis can be used to attempt to identify the nuclear reaction pathway by comparing the quantity of helium produced to the amount of energy generated. Thus, the most energetic reaction known would generate 24 MeV/^{4}He, as depicted by the line in the plot. Likewise, the 4 MeV/^{4}He line is included to add perspective. These results were obtained with all-metal apparatus shown to be capable of eliminating atmospheric contamination.

Radiation monitoring suggested the presence of a weak source of high energy γ-radiation. The weakness of the source tended to confound the analysis because of the statistics of the minimum detectable activity associated with various radiation detectors. The cathodes used in these experiments were palladium electroplated on gold-flashed copper. No calorimetry was associated with these radiation experiments.

The ultimate goal of this effort is to identify explicitly which nuclear reactions result in the Pons and Fleischmann effect.

Innovative Approach

Introduction: The quantitative nuclear products study of excess heat generation versus ^4He production helped garner $750,000.00 of funding for SRI. This data, presented in Fig. 1 was the result of decisive application of the most rigorous methods of calorimetry and helium sample collection known. A collection of available data is shown in Fig. 2:

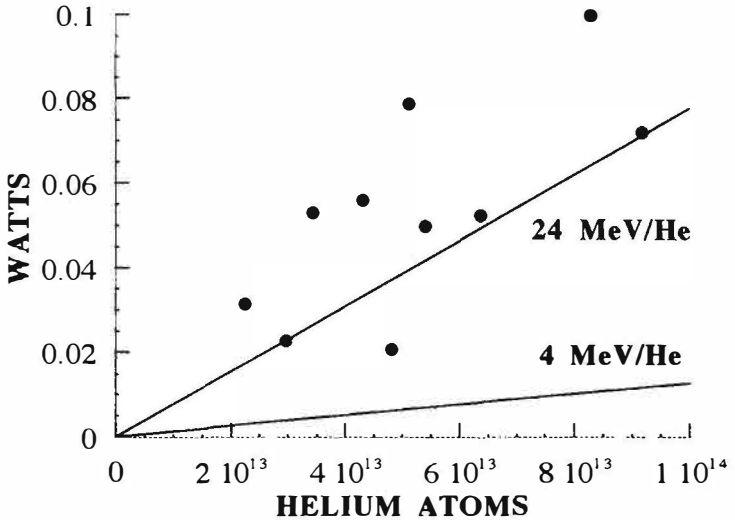

Figure 2. Quantitative heat *versus* helium analysis, using isoperibolic calorimetry.[1] Note that the data of Fig. 1 overlays; different calorimetric techniques are used but the same type of result is obtained. Helium sequestered by the cathode would result in an apparent increase in the energy per ^4He atom. Reaction at the cathode surface is suggested by the ^4He being found in the $D_2 + O_2$ off-gas.

Notice that the data appears to collect around the 24MeV/^4He line in Figs. 1 and 2. Nuclear reaction pathways can be identified by comparing the quantity of nuclear product (^4He) to the amount of energy generated (~Watts). The 24MeV/^4He line in Figs. 1 and 2 correspond to D + D --> ^4He + 24MeV, the most energetic reaction known. Theoretically, amount of energy (E) expected for the mass (m) lost in the reaction is given by the equation $E = mc^2$, where c is the speed of light. The mechanism can probably induce more than one nuclear reaction pathway, and so we are beginning the nuclear products analysis of the cathodes, in addition to continuing heat and helium studies.

Experimental: Our early finding of helium production during excess heat generation[1] was validated by control experiments; hence 8 excess heat events correlated to the detection of ^4He in the electrolysis off-gas, 6 control experiments produced samples of off-gas containing no detectable helium. The probability that these experiments are due to random causes is $(1/2)^{14}$=0.0061%; i.e. there is a 99.9939% probability that we observed a real phenomenon. The use of isoperibolic calorimetry and glass apparatus resulted in unwarranted criticism. We will now describe more rigorous methods, noting that the conclusions (Fig. 1) are similar to our earlier work (Fig. 2).

Helium does not diffuse through metals, as a practical matter. Thus, a rigorously all metal Seebeck calorimeter and all metal gas collection system was constructed to preclude atmospheric contamination. Our tactic has always been to use a self flushing system, electrolysis off-gas flushes out any contamination in a continuous manner, through D_2O and oil bubblers. The electrolysis energy input is corrected for the $2D_2 + O_2$ gas formation, and the validity of the energy input correction is checked periodically by measuring the $2D_2 + O_2$ gas production rate versus the electrolysis current to ensure that the $2D_2 + O_2$ gas is not recombining in the calorimeter to reform D_2O and thereby increasing the effective electrolysis energy input. The data was normalized to 525mA in Figs. 1 and 2. All metal gas collection flasks are baked out under vacuum and N_2 flushed repititiously, to remove any helium occluded in pores in the metal surface. A schematic of this rigorous system is shown in Fig. 3; use of this system resulted in the Fig. 1 data.

Seebeck calorimetry is, functionally, integrating thermal flux envelope calorimetry. The electrolysis cell is completely enclosed by a thermal flux transducer envelope, so that essentially all heat leaving the cell is measured. The thermal flux transduction envelope consists of series differential thermocouples set across a homogeneous thermally insulative layer (see Fig. 3). The heat flowing through the insulative layer sets up an electrical potential across each differential thermocouple pair; the series sum voltage of all the differential thermocouple pairs represents the total heat flow.

Seebeck calorimetry differs from Calvet calorimetry in that the insulative layer between

Innovative Approach

the differential thermocouple pairs, is a rather good conductor of heat; a high density of thermocouple pairs (about 30 pairs per cm^2) allows high sensitivity. Ease of heat flow to the thermostatic water bath minimizes unmeasured heat leakage, the effect of which is calibrated. Seebeck calorimetry has an enormous dynamic range, our 3X3X9 cm devices can measure from a few milliwatts to tens of watts with approximately ± 0.3% accuracy. For comparison: isoperibolic calorimetry used in our early work[1] had a dynamic range from about 1 to 4 Watts. Further, it takes about 3 hours for the isoperibolic calorimeters to achieve thermal equilibrium, while it takes only half an hour for the Seebeck.

Figure 3

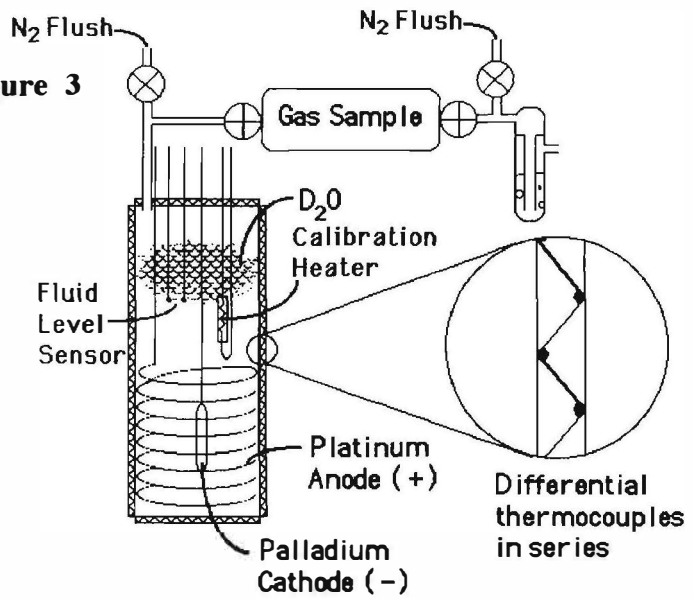

Seebeck calorimetry is high performance Calvet calorimetry. It combines the benefits of high sensitivity, enormous dynamic range, fast response and convenience of operation. Thermal homogeneity within the calorimeter is irrelevant, because all flux paths are covered by the thermal flux transduction envelope. Seebeck calorimetry is the most rigorous method of calorimetry known (note: Fig. 1).

An attempt was made to replace the Seebeck thermal flux transducers with cheaper Peltier devices.[2] Initially, the calorimeter seemed to give a reasonable response, and then it became more and more non-linear over time. Such an insidious failure appears to have occurred at the Naval Research Lab; and elsewhere.

Mass Spectral ^3He:^4He:^{20}Ne analysis has the advantages of helping identify the helium source and directly probing the branching ratio of the nuclear reaction. Tritium, which decays to ^3He can also be analyzed. ^3He analysis is blinded by the presence of HD (also mass 3), so all deuterium is removed prior to analysis.

^4He:^{20}Ne analysis (Fig. 4) is plotted with respect to 4 separate electrolysis systems. The ^4He analysis used in Fig. 1 had a detection threshold of 1 ± 1 parts per billion; the ^3He:^4He:^{20}Ne analysis now in use (Fig. 4) has a ^4He detection threshold in the low parts per trillion range. The ^3He:^4He isotope ratio associated with the data of Fig. 4 is about twice that expected for air, due to tritium decay. The ^3He:^4He:^{20}Ne electrolysis off-gas sampling manifold was constructed of metal and glass, sealed with viton o-rings, and is more than good enough to acquire the rigorous data of Fig. 1. Sampling flasks are all metal, in both studies. Hence, the contemporary data (Fig. 4) acts as a massively redundant control, validating our findings depicted in Fig. 1.

Figure 4: Note: multiply 7 X 10^{11} atoms ^4He by 10 = 7 X 10^{12} atoms, this corrects for sample flask volume differences. Now compare 7 X 10^{12} atoms with the rigorous helium analysis in Fig. 1. The different permeation rates of ^4He and ^{20}Ne accounts for their isotope ratio, ^{20}Ne diffuses slower than ^4He.

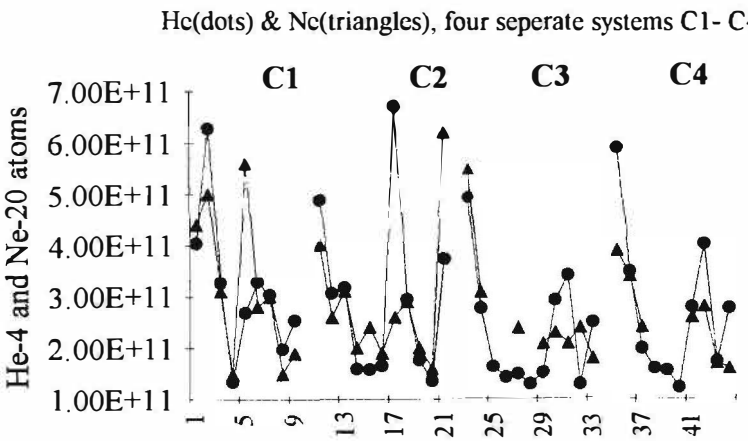

Innovative Approach

A small radiation signal was observed associated with 0.001" thick palladium plated onto gold flashed copper cathodes. We were unable to acquire spectra perhaps owing to broad band scatter.[3] Such broad band scatter might be taken to suggest a bremsstrahlung continuum spectrum[4] arising from "hot electrons" associated with the mechanism of energetic coupling between the nuclear reaction and the metal lattice.

The radiation was traced to the electrolytic cell by systematic displacement of the detector, using the fact that radiant intensity (I) decreases as the square of distance (D) from the source $I \propto 1/D^2$, in Fig. 5.

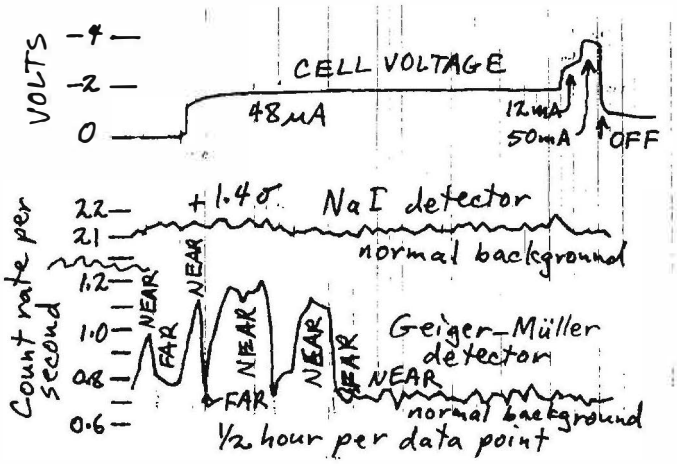

Figure 5: Plots of cell voltage and radiation count rate for a NaI detector and a G-M detector. Count rates are in counts per second average over 0.5 hour per data point.

This type of experiment was reproduced many times. Note that the less sensitive detector will detect a smaller radiant intensity than a more sensitive detector, because the less sensitive detector discriminates against background better. For a discussion of the Minimum Detectable Activity with respect to environmental background see: D. A. Gollnick.[5] The background at this location in the lab is well characterized.

Cathode analysis by Secondary Ion Mass Spec. (SIMS) must fail as a nuclear products analysis, because it does not analyze the bulk, and SIMS is prone to artifacts. Briefly, material from the surface of the cathode is sputtered by an ion beam, the secondary ions from the cathode surface are then analyzed by the mass spectrometer. Unfortunately, the ionization cross section of various elements is vastly different so that elemental quantification is relatively inaccurate. Even the isotopes of a single element suffer from ion fractionation,[6] and in dynamic SIMS the extent of ion fractionation changes with sputter hole depth.[7] Furthermore, it takes a considerable amount of instrumentation time to obtain meaningful precision. Large secondary ion intensities can overwhelm the detector, wildly skewing the isotope ratio observed; this is detector dead time, and has been particularly troublesome with respect to easily ionized elements, like lithium (^{6}Li:^{7}Li). A more insidious dead time effect occurs when spurts of ions overwhelm the detector, and again skew the isotope ratios. Although SIMS and other surface techniques (e.g. EDX and XPS) must fail for decisive nuclear products analysis, much useful information can be gained by their careful application.

Prompt Gamma Activation Analysis (PGAA) using a cold neutron beam is the method of choice; it provides a high sensitivity isotope specific bulk analysis, and is complemented by Neutron Activation Analysis (NAA). The cold neutron beam is essential, because it allows analysis far removed from the reactor cores' gamma ray field Fig. 6.[8] The cold neutrons also have a higher capture cross section, enhancing sensitivity. PGAA with thermal neutrons is futile due to the interference of the reactor cores' gamma ray field.

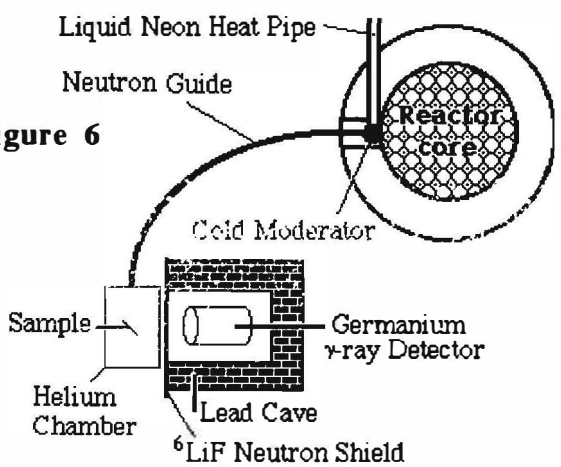

Figure 6

Innovative Approach

Thermal neutrons are moderated by liquid neon cooled 1,3,5-trimethylbenzene before being guided down the beam channel by total internal reflection off the ^{58}Ni coated silica walls, just like fiber optics. The cold neutrons expose the sample housed in a helium filled chamber, captured neutrons cause the sample to emit γ-rays characteristic of the isotope. The germanium γ detector of the spectrometer is housed in a lead cave, sheathed with ^{6}LiF sheets to adsorb scattered neutrons radiationlessly; thus effecting a very low background system.

Cold neutron beam PGAA represents the state-of-the-art. There are only two operational installations known in the USA.

Conclusions: The heat versus helium analysis is reproducible and appears to indicate that the Pons and Fleischmann effect induces the D + D --> ^{4}He + 24MeV reaction pathway (Figs. 1 and 2), by an unknown mechanism. Finding helium in the gas phase suggests that the reaction occurs at the surface of the cathode. Helium born within the cathode would be lost to analysis, and indeed isolated incidents of excess heat generation without helium production have been observed. Future helium analysis will investigate the branching ratio using state-of-the-art ^{3}He:^{4}He:^{20}Ne analysis and Seebeck calorimetry.

Rigor with regard to calorimetry is the experimental foundation in this field. Seebeck calorimetry is used because it is the most fundamentally rigorous method known, amounting to high performance Calvet calorimetry. Further, Seebeck calorimetry provides a complementary method, validating our isoperibolic results.

The solid state physics that allow radiationless reaction remains to be elucidated (See for example Y. Kim). Radiation, though occasionally observable, is not related quantitatively to excess heat. The minuscule amount of radiation intermittently observed suggests an efficient energetic coupling between the nuclear reaction and the metal lattice. The breakdown of the energetic coupling mechanism might result in bremsstrahlung,[4] and hence a continuum spectrum superimposed with characteristic peaks;[3] while efficient energetic coupling results in excess heat.

Isotope specific analysis of the cathodes by PGAA[8] is being pursued in conjunction with NAA and SIMS[6,7] to search for nuclear products in the cathode.

Outlook: A fundamental understanding of the solid state physics that results in the Pons and Fleischmann effect is to be gained through nuclear products analysis. Understanding the mechanisms will allow technological development.

Acknowledgments: Mr. Joe Bennett, Mr. Tom Davidson, Mr. Leigh Evans, Mr. John Fontanot, Dr. John Lupton, Dr. G. Bryant Hudson, Dr. Tom Passell, Mr. Ed Pylant, Dr. Kenan Unlu, and Dr. Bernard Wehring.

Funding by the following organizations is gratefully acknowledged: The Electric Power Research Institute, The Robert A. Welch Foundation, The American Society for Engineering Education, and The Office of Naval Research.

References:

1) a) B. F. Bush, et. al. J. Electroanal. Chem., 304, 271 (1991).
b) see also: M. H. Miles in Chem. Abstracts.
2) S. C. Barrows, et al., Proc. Fourth International Conference on Cold Fusion, (1994), EPRI TR-104188-V2, Vol 2, 21-1
3) S. Szpak, et. al., Phys. Lett A, 210 (1996) 382.
4) G. F. Knoll, Radiation Detection and Measurement, 2nd Ed., 1989, J. Wiley & Sons, p. 299.
5) D. A. Gollnick, Basic Radiation Protection Technology, 3rd Ed., April 1994, p. 517.
6) N. Shimizu, S. R. Hart, J. Appl. Phys. 53(3) (1982) 1303.
7) H. Gnaser, I. D. Hutcheon, Surface Science, 195 (1988) 499.
8) B. W. Wehring, K. Unlu, Proceedings, Physics at Advanced Pulsed Neutron Sources, PANS II, Dubna, June 14-16, 1994.

Special Session

CETI Session

QUANTITATIVE OBSERVATION OF TRANSMUTATION PRODUCTS OCCURRING IN THIN-FILM COATED MICROSPHERES DURING ELECTROLYSIS

G.H. Miley, G. Name, M.J. Williams, J.A. Patterson*, J. Nix*, D. Cravens*, and H. Hora‡
Fusion Studies Laboratory, U. of Illinois
103 S. Goodwin Avenue, Urbana, IL 61801-2984
Ph. 217-333-3772, Fax 217-333-2906
E-mail: g-miley@uiuc.edu

ABSTRACT

Several research groups previously identified new elements in electrodes that appeared to be transmutation products (Bockris et al., 1996a; 1996b). However, due to the low concentrations involved, the distinction from possible impurities has been difficult. Now, by using a unique thin-film electrode configuration to isolate the transmutation region, plus measurements based on neutron activation analysis, the authors have achieved, for the first time, a quantitative measure of the yield of transmutation products. Results from a thin-film (500-3000Å) nickel coating on 1-mm microspheres in a packed-bed type cell with 1-molar $LiSO_4$-H_2O electrolyte were reported recently at the Second International Conference on Low-Energy Nuclear Reactions (Miley and Patterson, 1996). Key new results are now presented for thin-film Pd and for multiple Pd/Ni layers. The transmutation products in all cases characteristically divide into four major groups with atomic number $Z \cong$ 6-18; 22-35; 44-54; 75-85. Yields of ~1 mg of key elements were obtained in a cell containing ~1000 microspheres (~½ cc). In several cases over 40 atom % of the metal film consisted of these products after two weeks' operation.

INTRODUCTION

Various nuclear transmutation products generated during electrolytic cell operation, typically employing Pd and heavy or light water with various electrolytes, have previously been reported, e.g., see the proceedings of the First and Second International Conferences on Low Energy Nuclear Reactions (Bockris and Lin, 1996a; Bockris, Miley, and Lin, 1996b). Most of these reports dealt with impurity-level quantities of elements, complicating the distinction from impurities. In sharp contrast, the thin (500-3000Å) films used in present work result in the transmutation of a significant percentage of the metal in the thin-film cathode. That result, combined with Neutron Activation Analysis (NAA) and Secondary Ion Mass Spectrometry (SIMS), provide a quantitative measure of the amounts of the various elements produced.

Over a dozen experiments with various thin-film coatings have been carried out in different cells. Thin-film coatings on 1-mm-diameter plastic microspheres, ranging from 500Å-thick single layers of Pd or Ni to multiple Ni/Pd layers, were used in a flowing packed-bed-type electrolytic cell with a 1-molar Li_2SO_4 light water electrolyte. Nuclear reaction products were obtained in all cases, with several runs resulting in concentrations of over 40 atomic % of the metallic film being Fe, Si, Mg, Cu, Cr, Zn, and Ag. Six key runs listed in Table 1 are presented here. A prior publication by Miley and Patterson, 1996, dealt exclusively with the Ni film (run #8) results, while the present paper adds important results for additional Ni runs, for Pd, and for multiple Pd/Ni layers. (The earlier paper, subsequently referenced as M-P 96, contains more

*Clean Energy Technologies Inc., Dallas, Texas 75240
‡University of New South Wales, Australia

Table 1. Summary of runs

Run ID	Packing*	Run 10.0 Duration (hours)	Excess Power (W)
5	#59 PS/NPNPN	520	~ 2 ± 0.5
7A	C1 PS/PN-E	197	~ 4 ± 0.8
8	#60 PS/N	311	~ 0.1-0.9
11	#63 PS/P	211	~ 0.1-0.9
13	#61 GL/N	293	~ 0.1-0.9
18c	#76 PS/N	358	~ 0.1-0.9

*see Table 2 for microsphere data

details about the experimental technique than could be included in the present space-restricted article. Thus, there are frequent references to it.)

The use of thin-film coatings originates from the "swimming electron layer" (SEL) theory proposed earlier (Hora, Miley, et al., 1993; Miley et al, 1993). It suggests that nuclear reactions are assisted by the high interface electron density in multilayer thin-films with alternating metals possessing large differences in Fermi energy levels. Initial experiments used thin-film Pd/Ti coatings sputtered onto a large stainless steel electrode (Miley, et al., 1994). Those experiments were abruptly terminated when the films separated from the substrate soon after loading and heating occurred. Still, high excess heat (estimated to be kW/cm^3 at the interface regions) was observed for minutes prior to loss of the thin-films. Subsequently, Patterson developed a unique electrode configuration using electrochemical deposition of "thick" (μm) metal coatings on mm diameter cross-linked polymer microspheres for use in a flowing packed-bed-type electrolytic cell. The coatings were found to be quite stable in this configuration, so experiments were undertaken to study reaction products using thin-films (500- to 3000-Å thick) laid down by a special sputtering process.

ELECTROLYTIC CELL DESCRIPTION AND OPERATION

The general configuration of the electrolytic cell is shown in Fig. 1. About 1000 microspheres (~0.5 cm^3 volume) were used in the packed-bed cell. Titanium electrodes were employed in most runs. The preheater allows control of the entering temperature of the electrolyte (1 molar $LiSO_4/H_2O$), with flow rates of ~11 ml/min. Voltages across the bed were held at ~2-3 V, with several mA of current, giving an electrical input power of approximately 0.06 W. Inlet-outlet thermocouples provided a measure of the temperature increase of the flowing electrolyte. Positive, but often very small, increases in temperature across the cell, ranging from 0.1 to 4 °C, were observed in all cases.

Loading of hydrogen into the thin-film is done at low (~25 °C) temperatures, requiring several hours, as observed by an initial increase in the voltage across the bed, followed by an eventual equilibrium voltage level of +2-3 V. Then the cell inlet temperature is slowly raised (over 4-8 hours) to the maximum allowed with the present plastic cell construction, near

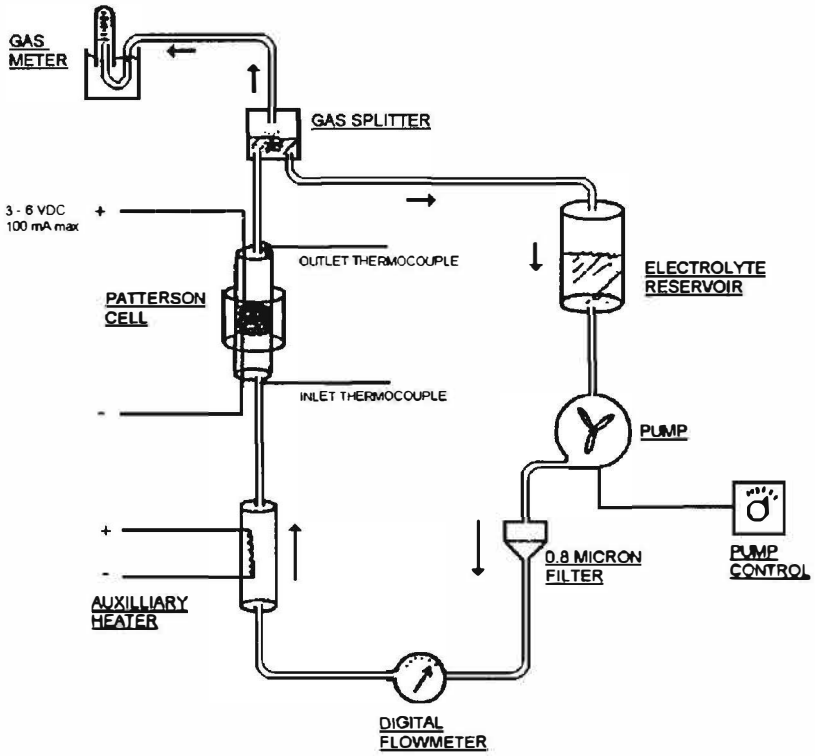

Figure 1. Schematic of flowing cell arrangement

60-70 °C. Run times of several weeks were typical (Table 1). Further details about the construction and operation of this type of cell are given in Patterson, 1996; Cravens, 1995; and Nix, 1996.

Initial runs (#5, 7A, 8) employed a cell with all plastic fittings with the exception of the pressure and flow meters and the pump. Later runs substituted all plastic components ("clean cell" design) except for the electrodes. A filter fitted with 0.8-μm pore size filter paper was employed in the loop (Fig. 1) to collect any fine particles entering the electrolyte, either from film surfaces or from other parts of the system.

THIN-FILM RUNS

Characteristics of the thin-film coated microspheres used are summarized in Table 2. The following nomenclature is adopted: P: palladium, N: nickel, PS: Polystyrene, G: glass. Thus a PS/P/N microsphere has a plastic core with a first coating of palladium and a second coating of nickel. All coatings were sputtered on, unless denoted as -E which used electroplating. The layer masses shown are based on "witness" plate weight measurements during sputtering, hence they are not considered highly accurate compared to element data taken by NAA after a run. Excess power measurements varied from run to run, but the PS/N run was typical for single coatings. It gave a temperature rise of the order of 0.6 °C throughout the run, representing an output of 0.5 ± 0.4 W. Multi-layers gave larger excess power,

approaching 4 W. Calibration corrections due to heat losses and flow-pattern variations limited the measurement accuracy. More precise calorimetry is in use in several laboratories studying excess power from the Patterson Power Cell™, but the present cell design focused on ease of reaction product measurements.

Scanning electron microscope (SEM), photographs of the microspheres confirmed that a very smooth surface was achieved but with a small-scale, rough structure uniformly distributed over it. (see Fig. 2e of M-P 96). Some erosion of small particles and occasional ejection of larger "flakes" from the film occurs during operation as detected by debris collected by the loop filter. Concurrently, various fragile looking bead-like and fiber-like structures are typically visible on the film surface after electrolysis (Fig. 2b of M-P 96). Some structures are perhaps miniature versions of the volcanic-like formations observed on solid electrodes producing transmutations (e.g., Ohmori and Enyo, 1996).

REACTION PRODUCT ANALYSIS METHODS

Reaction product measurements have utilized a combination of NAA, SIMS, Energy Dispersive X-ray (EDX) analysis, and Auger Electron Spectroscopy (AES). NAA can measure total quantities of elements in a sample containing multiple microspheres, while the other techniques are restricted to probing a local area on single microspheres. Due to variations among microspheres arising from location in the packed bed and other effects, this difference in technique is responsible for some of the variations in the results.

Table 2. Data for various thin-film microspheres

PS/N/P/N/P/N (#59; used in Run #5)

Layer	Volume (cc)	Mass of layer (g)	# of atoms
PS (core)	6.22E-04	6.09E-04	-
Ni(300A)	1.06E-07	9.41E-07	9.64E+15
Pd(500A)	1.76E-07	2.11E-06	1.19E+16
Ni(400A)	1.41E-07	1.25E-06	1.29E+16
Pd(800A)	2.82E-07	3.38E-06	1.90E+16
Ni(350A)	1.23E-07	1.10E-06	1.13E+16

PS/P/N-E (#C1; used in Run #7A)

Layer	Volume (cc)	Mass of layer (g)	# of atoms
PS (core)	6.22E-04	6.09E-04	-
Pd(1micron)	3.54E-06	4.24E-05	2.39E+17
Ni(0.5 micron)	1.76E-06	1.57E-05	1.61E+17

PS/N (#60; used in Run #8)

Layer	Volume (cc)	Mass of layer (g)	# of atoms
PS	6.22E-04	6.09E-04	-
Ni(2650A)	9.34E-07	8.31E-06	8.52E+16

PS/P (#63; used in Run #11)

Layer	Volume (cc)	Mass of layer (g)	# of atoms
PS (core)	6.22E-04	6.09E-04	-
Pd(2000A)	7.05E-07	8.46E-06	4.76E+16

G/N (#61; used in Run #13)

Layer	Volume (cc)	Mass of layer (g)	# of atoms
Glass (core)	6.22E-04	1.01E-03	-
Ni(850A)	3.00E-07	2.67E-06	2.73E+16

PS/N (#76; used in Run #18C)

Layer	Volume (cc)	Mass of layer (g)	# of atoms
PS	6.22E-04	6.09E-04	-
Ni(3000A)	1.06E-06	9.41E-06	9.64E+16

Diameter of PS base = 1.06E-01 cm

To distinguish from impurity contributions, both the microspheres and electrolytes were analyzed *before* and *after* the run. Sampling after a run was done by disassembling the cell and removing microspheres from the top (cathode end) layer of the packed bed. (The 1000 microspheres in the bed result in approximately 3-5 layers total). These microspheres were

selected due to accessibility and because the higher electric field in that region should make this layer most reactive. NAA of the microspheres was carried out at the University of Illinois' (UI) TRIGA research reactor (Landsberger, 1996), typically using samples of 10 microspheres. Techniques for short- and long-lived NAA (Parry, 1991) were performed to determine the presence of Ag, Cu, Al, Fe, Cr, Zn, Ni, Co, and V, subsequently termed **"NAA elements."** Typical detection limits were of the order of 2 ppm, with a precision of 2-10%. NAA was also employed to study key isotope ratios (e.g., Cu and Ag) for comparison to natural abundance. Calibration used certified liquid standards from the National Institute of Standards and Technology. Ores containing known quantities of these elements were analyzed simultaneously in all runs for quality control. Further details are described in M-P 96.

The SIMS analysis employed a Cameca IMS 5F unit operating with 8-keV oxygen primary beam in the positive ion mode (Wilson et al., 1989). Scans of key isotopes were made using single microspheres in a low-resolution (2,000 mass resolution) mode at several depths of interest (see Fig. 3a and b of M-P 96). High-resolution (40,000 mass resolution) scans were then done to resolve any interferences involving important isotopes, e.g., see Cu-63 and Ag-107 in Figs. 3c and d of M-P 96. (Elements measured by SIMS, but *not* NAA, are termed **"non-NAA elements"**). Calibration for the SIMS sensitivity was done using the measured concentrations of the nine **NAA elements** as described in M-P 96. SIMS was used to determine isotope ratios except for the Cu and Ag ratios that were determined explicitly by NAA.

The EDX analysis used a Field Emission Electron Microscope (Hitachi S-800) operating in the energy dispersion analysis mode to detect elements with atomic concentrations above 1%. This measurement largely served as added confirmation of NAA measurements (e.g., see Table 2, M-P 96). AES was used in a sputtering mode to perform semi-quantitative depth profiling for the major element species above ~1 atom % (Fig. 5, M-P 96).

RESULTS

ELEMENT AND ISOTOPE CONCENTRATIONS

Results from NAA analyses of the *net* (final minus initial values) yields of high concentration elements in various runs are summarized in Table 3. Element yields as high as several μg/microsphere are obtained, representing roughly a mg of these high-yield elements per cell (1000 microspheres). The corresponding time average reaction rates are of order 10^{16} (atoms/cc film-sec).

To evaluate the concentrations of the **non-NAA elements** present and to obtain isotopic ratios, SIMS and NAA data are combined, e.g., see Table 3 in M-P 96 for run #8. Results for all elements observed in the six runs are shown later in Fig 2, which plots production rates vs. Z. NAA element values are thought to be quite accurate. The **non-NAA element** values are less certain due to uncertainties in the SIMS sensitivity calibration (i.e., "RSF" values) and the restricted location of the measurement on a single microsphere, but the results should still provide a good estimate of ***non-NAA*** isotopes. Further, note that the *isotopic yields* for **NAA elements** should be quite accurate, since the RSF values are constant

for isotopes of a given element, while the total concentrations of these elements are directly from NAA measurements.

ELEMENT DEPTH PROFILES

Data from AES profile measurements on a typical microsphere from PS/N run #8 were presented in Fig. 5 of M-P 96 for the higher concentration elements. Similar results have been obtained for other coatings. Most element profiles distinctly peak in the metal volume or near the metal-core interface, suggesting an internal source rather than diffusion in from the surface. However, the amount of peaking varies among elements and runs, complicating the interpretation of this measurement. Still, the results provide important support for the conclusion that the elements observed did not diffuse in from the surface.

Table 3. Yield for NAA Elements

Yield (micro-grams / microsphere)

Element	Z	Run #5	Run #7A	Run #8	Run #11	Run #13	Run #18C
Ag	47	7.14E-02	1.67E-04	1.60E+00	7.06E-02	2.04E-03	-2.09E-03
Al	13	1.09E-01	2.54E-02	1.39E-02	2.33E-01	-1.78E+00	3.16E-03
Cu	29	3.04E+00	1.24E-01	1.08E+00	2.77E-01	-4.26E-01	3.24E-02
V	23	2.39E-03	2.00E-04	1.05E-03	4.06E-03	-5.71E-03	3.71E-05
Cr	24	4.20E-02	4.46E-03	6.91E-01	6.04E-02	2.34E-02	1.93E-02
Ni	28	H	H	H	3.88E-01	H	H
Fe	26	2.98E-01	3.58E-03	1.78E+00	1.53E-01	5.19E+00	4.56E-02
Zn	30	2.17E+00	1.42E-02	2.99E-01	8.06E-01	3.97E-01	8.24E-02
Co	27	1.46E-03	1.79E-03	1.12E-02	2.18E-03	1.17E-02	4.89E-03

Production Rate (atoms / s - cc of microsphere)

Element	Z	Run #5	Run #7A	Run #8	Run #11	Run #13	Run #18C
Ag	47	3.42E+11	2.11E+09	1.28E+13	8.33E+11	1.74E+10	-1.45E+10
Al	13	2.08E+12	1.28E+12	4.44E+11	1.10E+13	-6.07E+13	8.79E+10
Cu	29	2.47E+13	2.65E+12	1.47E+13	5.55E+12	-6.15E+12	3.82E+11
V	23	2.42E+10	5.35E+09	1.77E+10	1.01E+11	-1.03E+11	5.46E+08
Cr	24	4.17E+11	1.17E+11	1.15E+13	1.48E+12	4.13E+11	2.78E+11
Ni	28	H	H	H	8.41E+12	H	H
Fe	26	2.75E+12	8.73E+10	2.75E+13	3.48E+12	8.53E+13	6.12E+11
Zn	30	1.71E+13	2.97E+11	3.95E+12	1.57E+13	5.57E+12	9.45E+11
Co	27	1.28E+10	4.13E+10	1.64E+11	4.72E+10	1.82E+11	6.22E+10

'H' : Host material

NUCLEAR RADIATION EMISSION

In view of evidence (in Table 3) that products are formed at a significant rate in an operating cell, measurable radiation emission would normally be expected. For example, assuming a rate of about (10^{13} reactions/s-cc ms) x (10^{-3} cc ms) x (10^{3} microspheres) x (1 gamma/reaction) indicates ~10^{13} gammas/sec. To date however, several attempts to measure nuclear radiation emission—neutrons, gammas, or x-rays—during cell operation have not detected any measurable quantities above background (M-P 96). Likewise, several attempts to

measure gamma-ray emission from microspheres removed from the cell after a run also failed to uncover signals above background.

Recently, several sets of PS/N microspheres (run ~4 months earlier) were exposed to high-speed ASA 3000 film (Klema, 1996) for a 4-day period with positive results (Fig. 4 in M-P 96). Unfortunately, these experiments are not very reproducible. A second positive exposure has been obtained, but three additional attempts failed. The technique is under study, and if verified, will demonstrate emission of low-energy beta rays or soft x-rays (estimated to be of the order of 20 keV). Clearly, much more study is needed to fully define possible radiation emission for these cells.

SYSTEMATICS

The yields for both **NAA** and **non-NAA elements** have been converted to element production rates (atoms/cc film-sec) to remove differences arising from variations in the length of runs and are plotted vs. Z in Fig. 2. The rates shown are average values over the run. (Other recent experiments indicate a somewhat faster initial rate and some element-to-element variations. Hence, the use of an average rate for comparisons is somewhat inaccurate, but should provide relative trends.)

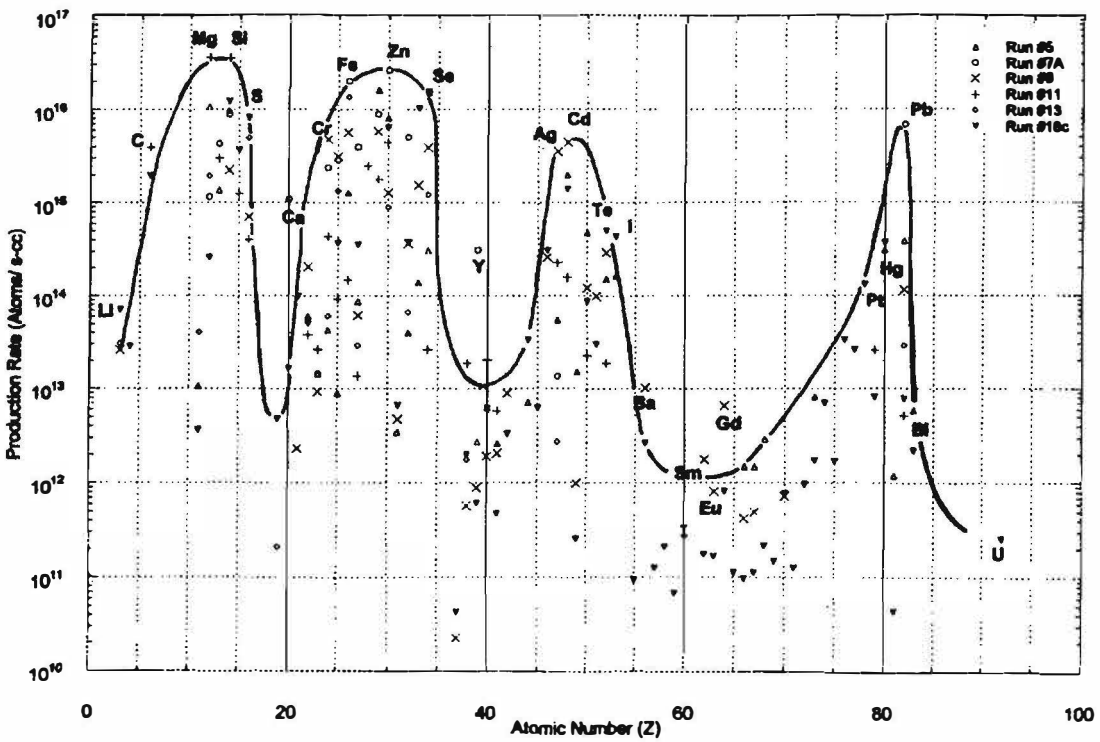

Figure 2. Comparison of atomic production rates for all runs

As indicated in the figure, the composite data of maximum production rates can be enclosed in an envelope with four distinct peaks at Z ~12, 30, 48, and 82. The largest production rates (hence, yields) lay in bands around each peak. This striking result has a close resemblance to the well known two-peak yield curve for neutron-induced fission of uranium (Katcoff, 1960). For that case, the peaks are associated with light and heavy fission products arising from the break-up (fission) of the neutron-uranium compound nucleus. Thus, one interpretation for the present result is that the peaks of Fig. 2 also represent the fission of compound nuclei, created in this case by proton-metal reactions. The startling fact that elements in the higher Z peaks lay above the host metals (Ni or Pd) would then require multi-atom fusion to form a compound nucleus capable of fissioning into these high-Z products. This view of the reaction mechanism is discussed in more detail later.

Comparison of the data for the individual runs in Fig. 2 provides further important insight. Runs #8 and #18c, both of which used 650-Å Ni film on a plastic core, are shown in Figs. 3a and b for clarity. However, they were done four months apart in different laboratories (U of Illinois and CETI, Florida, respectively) with different cells. The recent CETI run (#18c) used an ultra-pure cell (the only metal parts were the titanium electrodes) and the highest purity electrolyte (99.996% $LiSO_4$) with an additional pre-run with "sacrificial microspheres" for added purification. With these added precautions, impurity levels in the electrolyte in run #18c were reduced by a factor of 4-5 compared to the earlier run. But surprisingly, more reaction products were observed in #18c than in #8 (64 elements vs. 37 respectively), while the absolute rates for high-yield elements and the four-peak characteristic remains fairly similar. In that sense, the reproducibility of the experiment appears quite good. In the sense that products with characteristic four-peak behavior have been obtained in the dozen-plus experiments attempted to date, the reproducibility is excellent. This is in sharp contrast to the widely-recognized lack of reproducibility in conventional "cold fusion" experiments aimed at heat production. However, more experience with the thin-film concept by other independent researchers is needed before a final decision about reproducibility can be reached.

Run #13 (G/N) in Fig. 3c employed Ni on a glass (vs. plastic) core. As seen from the figure, this resulted in a distinct decrease in products in the third and fourth groups (higher Z) and slightly reduced the yields in the first and second groups. Concurrently, this run was unique in showing, cf Table 3, a decrease in Al, Cu and V levels. These results suggest that the core material plays a role in the mechanism. However, the basis for this effect requires more study—it could be attributed to differences in the swimming electron layer at the core-metal interface or to the interaction of the core material with the host matrix. These differences may be responsible for failure by other workers to obtain excess heat with independent G/P/N microsphere experiments (Schaffer, 1996).

The PS/P (palladium) core experiments (Fig. 4) also show a "four-peak" behavior, but, unlike the corresponding Ni runs, the amplitudes of the peaks decrease progressively in going to high-Z. Also, there appears to be a void of products between the third and fourth peaks. These results allow an interesting comparison with the solid Pd electrode (D_2O/Li_2CO_3 electrolyte) study by Mizuno et al., 1996. In that experiment, the products with non-natural isotopic abundance were observed in a thin region about 1 mm beneath the electrode source.

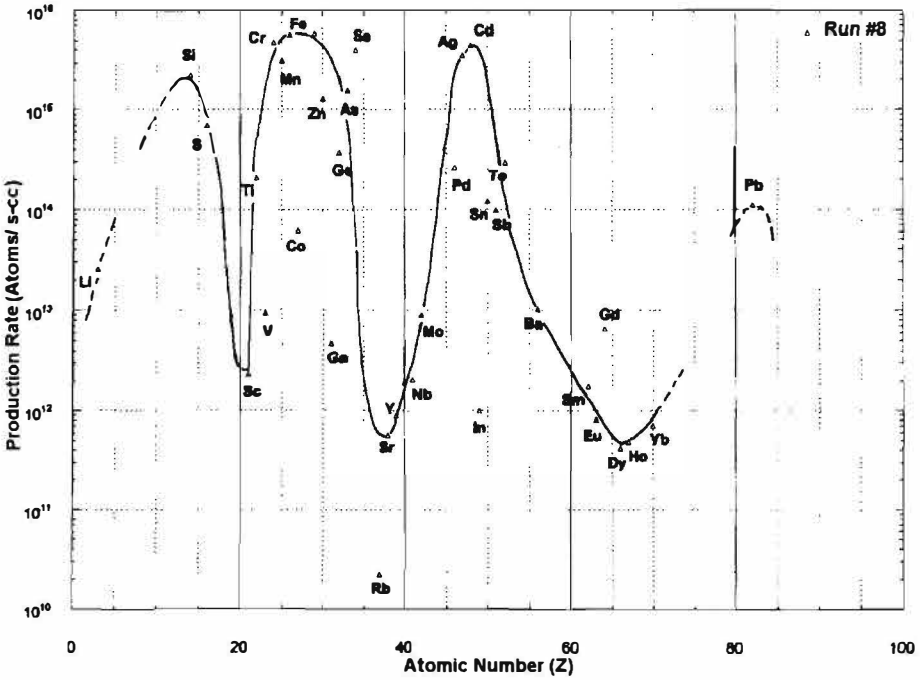

Figure 3a. Initial PS/N run done 3/96

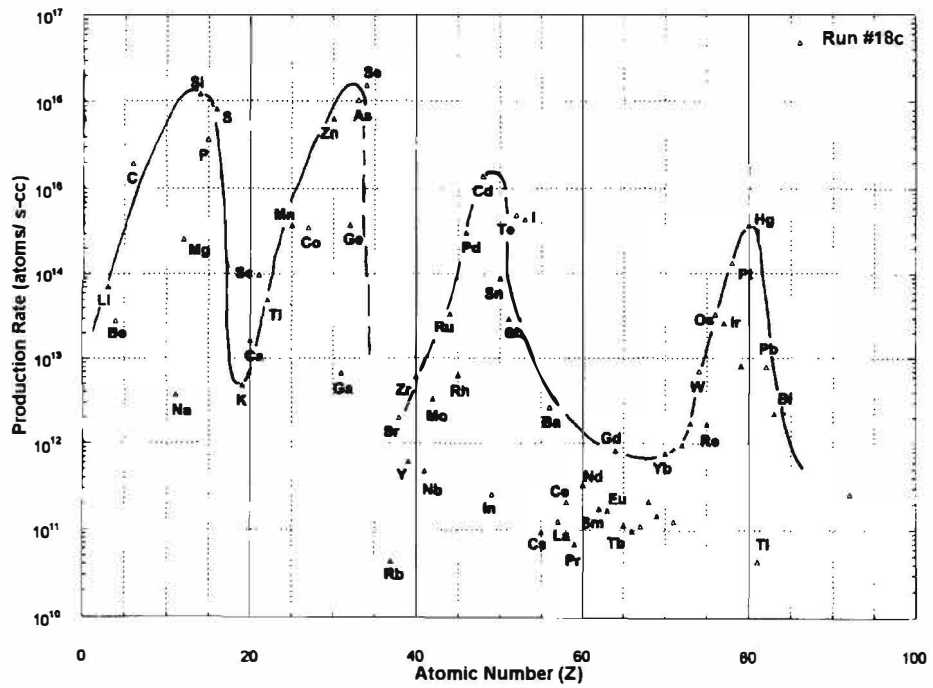

Figure 3b. Run #18c with PS/N microspheres - a duplication of run #8 using "ultra" clean cell conditions

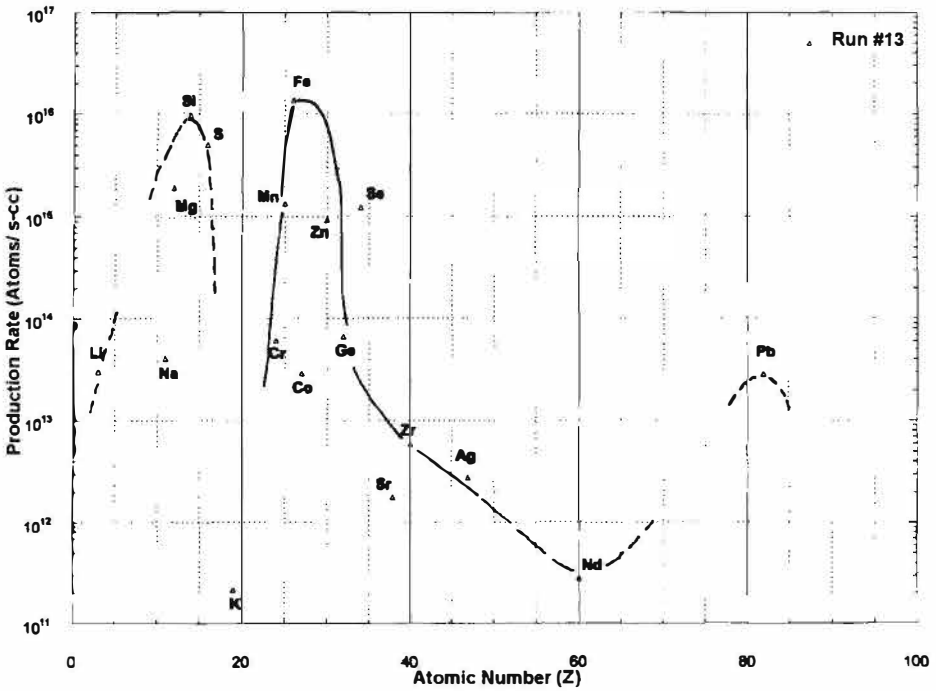

Figure 3c. Run #13 with GL/N (glass core) microspheres - compare with Figs. 3a and b for Ni on plastic cores

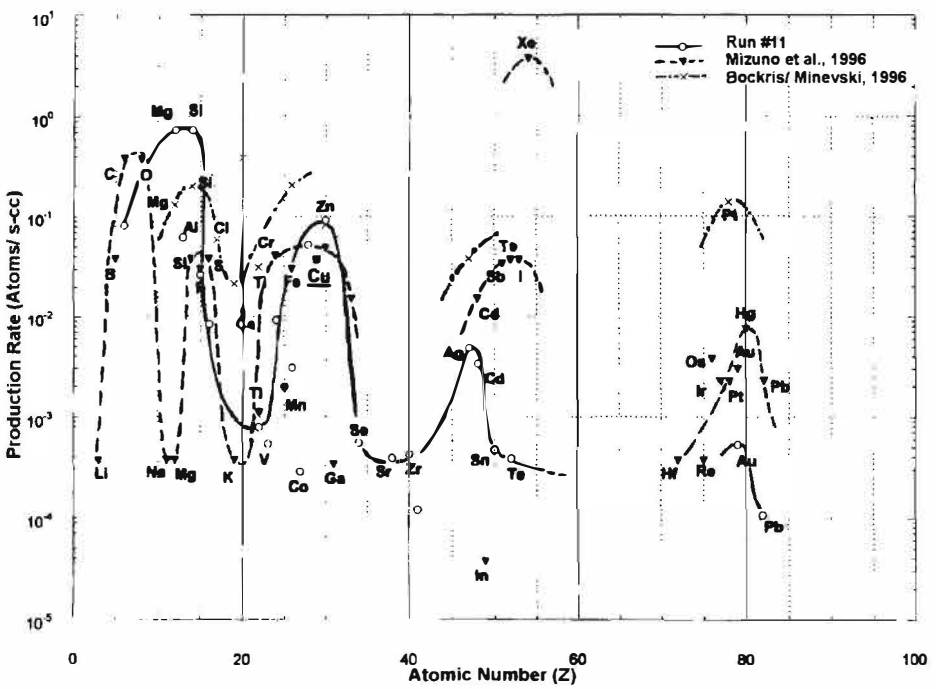

Figure 4. PS/P (palladium Run #11) and related to data for solid Pd D_2O electrolytic cell by Mizuno et al., 1996 and Bockris/Minevski, 1996 (both normalized to Cu data from Run #11)

Related results argued to be "too deep" to be impurities reported earlier by Bockris and Minevski, 1996, are also included in the figure. In contrast to present experiments, absolute production rates were not obtained in either of the solid electrode experiments; thus for comparison, yield data are normalized in Fig. 4 to the present Cu production rate. Again, the 4-peak structure is observed for both sets of data. A striking difference is observed in the third peak products where larger production rates, especially for Xe, are reported by Mizuno et al. and in the fourth peak where Mizuno reports a wider variety of elements and a high Pt rate is reported by Bockris/Minevski. A possible explanation for differences in gaseous products such as Xe is that in the present experiments gases rapidly diffuse out of the thin-films, preventing detection. In general, however, the similarity of results from independent experiments using radically different electrode design and electrolytes, suggests that the four-peak product curve is a general characteristic of this phenomenon. While amplitudes (yields) change with cell characteristics, the general shape of the curve remains intact. (Other product data appears to have this shape, but the results are less definite, e.g., see Karabut et al, 1991; Celani, et al, 1996; Ohmori and Enyo, 1996).

The two multi-layer runs (#5 and #7a included in Fig. 2) follow the same general trend as the single-layer runs. Physically #7a differed from #5 by having fewer layers (two vs. five), and used much thicker (~1μm vs. 300-500Å) layers made by electroplating. Run #5 in particular shows a rich array of products (similar to the PS/N run #18c) whereas #7a has few products in the region of the third and fourth yield peaks. Interestingly, consistent with SEL theory, the multiple layers also produced the most excess heat of all six runs; see Table 1. The depth probe scans for the multi-layer runs confirm that the product concentrations decrease with distance from the Pd/N interface(s), suggesting that the reaction occurs preferential there, in agreement with SEL theory.

Added runs are in progress to clarify the issue of heat production and its tie to the various yield curves. A general view, however, is that heavy elements generally involve low or negative Q-values (endothermic) reaction whereas light elements involve positive Q-values; the net energy produced, i.e., excess heat, involves the difference (or "net") of ±Q-values. This postulation could explain why reaction products apparently can occur without a large heat production. Since the net balance involves differences in large numbers, small changes can drastically affect the ability to produce excess heat, perhaps explaining why excess heat experiments appear to be so irreproducible.

Isotope Shifts

The change in % abundance of the various isotopes, as measured by SIMS, relative to natural abundance is summarized in Fig. 5 (changes <2% suppressed for clarity). From this result it is seen that a majority of the isotopes observed have measurable shifts. The larger values, marked with element symbols, are typically low-yield elements, although some high-yield elements have significant shifts. A pattern is not obvious, however, and the problem is further complicated by variations of the isotope ratios with depth into the film and location on the microspheres. Still, despite these variations, the many shifts observed add further strong

support to the conclusion that the elements observed are not impurities, which would be expected to exhibit natural abundances.

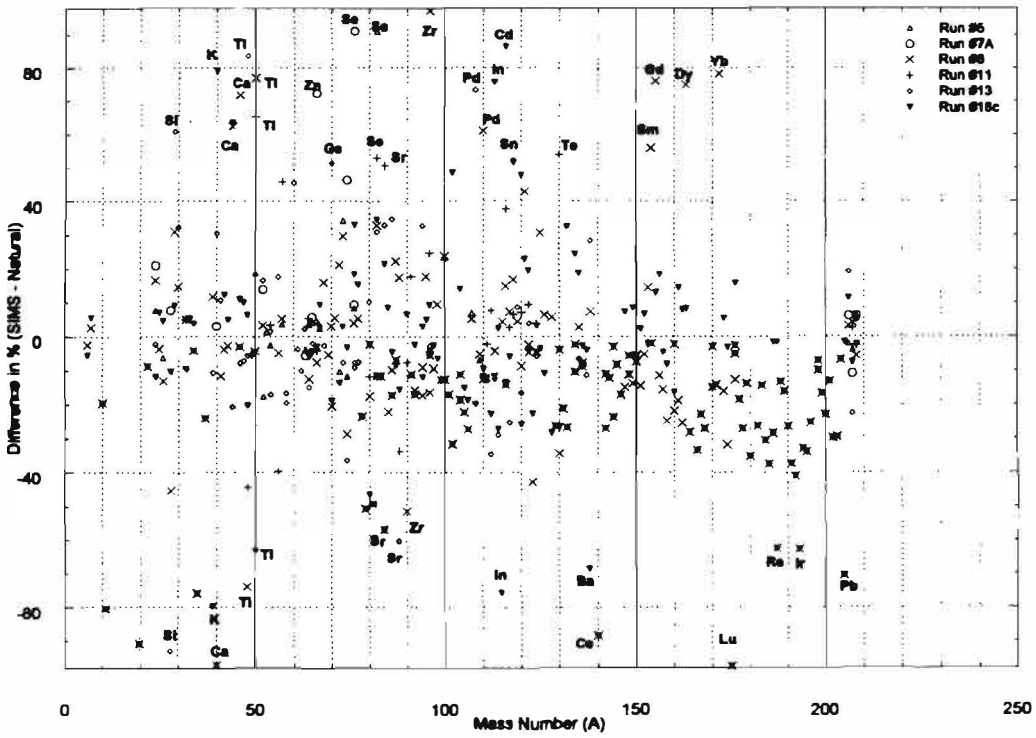

Figure 5. Summary of isotope shifts for all runs as measured by SIMS

Since Cu and Ag are key heavy elements, further confirmation for their shifts, obtained from NAA, is in progress. First results for Cu for run #8 with Pd/N gave Cu-63: +3.6 ±1.6%; Cu-65: -8.1 ±3.6% while corresponding SIMS values (Fig. 5) are Cu-63: +0.8%, Cu-65: -0.8%. While there are differences in magnitude, the positive and negative trends agree. The differences are thought to be due to the localized nature of the SIMS values compared to NAA results, which represent an average over the 10 microsphere samples employed.

In summary, despite variations in the individual runs, the data strongly supports the conclusion that significant deviations from natural abundance occurred.

IMPURITY ISSUES

The use of thin-films introduces a potential impurity problem in reaction product studies due to the small volume occupied by the film vs. the large volume of the electrolyte. Consequently, NAA measurements of the nine **"NAA elements"** were made on samples of microspheres, electrolytes and filter paper both before and after a run. (SIMS meaurements were also done on microspheres before and after runs.) Quantities of these **NAA elements** found prior to the run were consistently <10% of that found after the run (except for Al, which was initially higher); see Table 4a of M-P 96. Analysis of other cell components, i.e., the electrode and plastic components, did not uncover significant impurity concentrations of the

NAA elements. Other tests included a "null" run with electrically conductive sulfonated plastic beads used to simulate metal-coated beads (M-P 96). Substitution of platinum for the titanium anode did not affect results. Various runs presented here used three entirely different cells. The first PS/Ni run employed some metal fittings in the loop which were thereafter substituted out

in favor of plastic. Run #13 used an entirely new all plastic cell (the electrodes being the only metal components) with an electrolyte that was first run with "sacrificial" PS/N microspheres for a week (to collect impurities on the microspheres) before new microspheres were loaded and used for the actual run.

No impurity concentrations near the magnitude of the **NAA elements** found in the film following the runs were identified with these exhaustive tests, strongly supporting the conclusion that these elements were produced by nuclear transmutations. Results for the other **non-NAA elements** measured by the SIMS are less definite since their initial concentrations were measured in the microsphere, but not in the electrolyte, leaving impurity issues open. Still, there are other evidences (e.g., isotopic shifts from natural abundance) that most of these elements too, cannot be attributed to impurities.

In conclusion, the finding that the masses of the key isotopes following a run are large compared to possible sources of such isotopes from loop components, the negative results from simulation runs without Ni or Pd films, the observation of isotope shifts from natural abundance, and the observation that the isotopes vary with film material all combine to provide very strong evidence that the products reported are not caused by impurities.

REACTION MECHANISM CONSIDERATIONS

A nuclear explanation for the products requires an entirely new theory for chemically-assisted reactions in solids. Here it is possible only to point out some features that should be considered in such a theory. In the present case, the SEL theory cited earlier offers a possible explanation for overcoming the Coulombic barrier between ions in a multilayer thin-film electrode. However, this theory does not explain what reactions occur once barrier penetration is achieved. In view of the large yields obtained, the reactants must involve some of the key species present, namely: Li, S, or O from the electrolyte; C or H from the plastic microsphere core; Ni or Pd from the thin-films (cathode); and H, i.e., protons (p) from the light water. The following discussion assumes that the main reactions involve p-Ni or p-Pd interactions.

The concept that excess heat from electrolytic cells originates from reactions involving the electrode material is not new. Ragheb and Miley, 1989, originally proposed that in a Pd-D_2O cells, Oppenheimer-Phillips-type neutron-stripping reactions between the D and Pd might explain early observations. Later, Miley (Appendix B in Hoffman, 1995) summarized the status of such theories, and introduced a table of possible p-Pd reactions (including examples of fission-type reactions). The present results with high-Z products add a new dimension to these thoughts, however.

A key feature observed in Fig. 2 that must be accounted for is the four-peak curve, where the two higher Z peaks include elements significantly heavier than the host metal (Ni or

Pd). These heavy elements infer an endothermic reaction (-Q-value), which in turn suggests energy transfer to the reactants must occur to drive the reaction. (This is analogous to driving -Q-value reactions by colliding high-energy reactants using accelerated beams.) Consequently, the model must contain a mechanism for energy storage/transfer to reactions involved in high-Z element production.

The observed excess power and the estimated reaction rates for element production also pose a dilemma. Based on Table 3, present cells undergo about 10^{13} reactions/5-cm^3 ms. Thus, the single-layer runs with excess power of about 0.5 W correspond to an average energy release of ~6 x 10^{-2} MeV/atom reacting in the 1000-microsphere cell. That is considerably lower than the energy typically obtained from exothermic nuclear reactions expected in p-metal interactions (Miley, in Hoffman, 1995). This contradiction can possibly be explained if the excess energy released is reduced by endothermic reactions that "absorb" energy in the formation of heavier elements. As noted earlier, the view that excess energy involves a delicate balance between + and -Q reactions could partly explain why excess heat type experiments are often not reproducible. Conversely, this implies that transmutation product may be a more reproducible signal of reactions than heat, since products can be obtained, according to this view, even in a cell not producing significant excess heat.

The lack of intense high-energy radiation is another key characteristic that must be explained. This appears to be associated with energy transfer to the lattice via a coherent mechanism and "slow" reactions that allow relaxation to stable states, e.g., see Kucherov, 1996; Hagelstein, 1996.

A postulated reaction model, RIFEX (Reaction In a Film-Excited CompleX), is under development to satisfy these key characteristics. A major feature of RIFEX is that protons (p) interacting with the host Ni produce a relatively long-lived atom-p complex with excitation energies of orders of several MeV. This allows the production of heavy compound nuclei that subsequently fission. This model will be presented in detail in a future publication.

CONCLUSION

The use of thin-film electrodes has been shown to provide a unique and important method to study nuclear transmutations in electrolytic cells. By localizing the reaction, these films, combined with NAA and SIMS analyses, allow, for the first time, quantitative measurements of yields. As demonstrated by duplicate nickel-film runs, good reproducibility appears possible. However, as the authors stressed earlier (M-P 96), others are invited (and strongly encouraged) to investigate this new technique to provide full proof of reproducibility.

The most striking and unexpected result is the characteristic four-peak yield curve that appeared in all runs, but with various differences in numbers of products in various regions around the peaks. This curve, containing high-Z materials in the higher peaks, inescapably implies that multi-body reactions must occur. Since there is still debate about how deuteron ions can overcome the Coulombic barrier in "conventional" experiments, the implication that multi-body high-Z reactions occur greatly stretches the understanding of this phenomena. Various collective effects appear to be involved, although the initiation could still proceed via

swimming electron layer screening at interfaces. Theoretical studies are urgently needed to shed light on this amazing phenomenon, assuming that experimental reproducibility is confirmed by others.

REFERENCES

Bockris, J.O'M and G.H. Lin (organizers), 1996a. Proceedings of the First International Conference on Low Energy Nuclear Reactions Conference, *J. New Energy,* in press.

Bockris, J.O'M, G.H. Miley, and G.H. Lin (organizers), 1996b. Proceedings of the Second International Conference on Low Energy Nuclear Reactions Conference, *J. New Energy,* 1, 1, 111-118.

Bockris, J.O'M and Z. Minevski, 1996, "Two Zones of 'Impurities' Observed After Prolonged Electrolysis on Palladium," *Infinite Energy,* vol. 1, no. 5 & 6, 67-69.

Celani, F., 1996, Istituto Nazionale di Fisica Nucleare, Italy, personal communication.

Cravens, D., 1995, "Flowing Electrolyte Calorimetry," *Proc. 5th Intern. Conf. on Cold Fusion,* Valbonne, France, IMRA Europe, 79-86.

Hagelstein, P., 1996, "Lattice Induced Reactions," Abst. P-056, ICCF-6, Hokkaido, Japan

Hora, H., J. C. Kelly, J. U. Patel, M. A. Prelas, G. H. Miley, and J. W. Tompkins, 1993, "Screening in Cold Fusion Derived from D-D Reactions," *Physics Letters A*, 175, 138-143.

Karabut, A.B., Ya.R. Kucherov, and I.B. Savvatimova, 1991, "The Investigation of Deuterium Nuclei Fusion at Glow Discharge Cathode," *Fusion Technol., 20,* 924.

Karabut, A.B., Ya.R. Kucherov, and I.B. Savvatimova, 1992, "Nuclear Product Ratio for Glow Discharge in Deuterium," *Physics Letters A*, 170, 265.

Katcoff, S, 1960, "Fission-Product Yields from Neutron-Induced Fission," *Nucleonics,* 18, No. 11, 201.

Klema, E., 1996, Tufts University, Medford, MA. Private communication.

Kucherov, Y., 1996, "Slow Nuclear Excitation Model," Abs. P-006, ICCF-6, Hokkaido, Japan.

Landsberger, S., 1996, Dept. of NucE., U. of IL, Urbana, IL, private communication.

Schaffer, M., 1996, General Atomics Corp., San Diego, CA, personal communication.

Miley, G.H., M. Ragheb, and H. Hora, 1989, "Comments about Nuclear Reaction Products from Cold Fusion," Proceedings, NSF/EPRI Workshop, Washington DC, 16-18 October 1989.

Miley, G.H., J.U. Patel, J. Javedani, H. Hora, J.C. Kelly, and J. Tompkins, 1993, "Multilayer Thin-film Electrodes for Cold Fusion," *Proc. ICCF-3*, Frontiers In Science Series No. 4, ed. H. Ikegami, Universal Academy Press 659-663.

Miley, G.H., 1995; in Hoffman, N., *A Dialogue on Chemically Induced Nuclear Effects: A Guide for the Perplexed about Cold Fusion*, La Grange Park, IL, The American Nuclear Society, Appendix C, 146-154.

Miley, G.H., H. Hora, E.G., Batyrbekov, R.L. Zich, 1994, "Electrolytic Cell with Multilayer Thin-Film Electrodes," *Trans. Fusion Technol., 26*, 4T, Part 2, 313-320.

Miley, G.H. and J.A. Patterson, 1996. "Nuclear Transmutations in Thin-Film Nickel Coatings Undergoing Electrolysis," Proceedings of the 2nd International Conference on Low Energy Nuclear Reactions, Texas A & M, College Station Texas, September 13-14. (in press, J. New Energy). ***[Referred to as M-P 96]***

Mizuno, T., T. Ohmori, and M. Enyo, 1996, "Changes of Isotope Distribution Deposited on Palladium Induced by Electrochemical Reaction," *J. New Energy*, 1,1, 23-27.

Nix, J., 1996, "Revised Protocol for Patterson Cell Assembly and Operation," Memorandum, Clean Energy Technologies, Inc., 3 May 1996.

Ohmori, T., and M. Enyo, 1996, "Iron Formation in Gold and Palladium Cathodes", *J. New Energy*, 1, 1, 15-22.

Parry, S.J., 1991, *Activation Spectrometry in Chemical Analysis*, in *Chemical Analysis*, ed. J.D. Winefordner, Vol. 119, John Wiley and Sons, NY.

Patterson, J.A., 1996, "System for Electrolysis," U.S. Patent #5,494,559, 27 Feb. 1996.

Wilson, R.G., F.A. Stevie, C.W. Magee, 1989, *Secondary Ion Mass Spectrometry: A Practical Handbook for Depth Profiling and Bulk Impurity Analysis*, John Wiley & Sons, N.Y.

ACKNOWLEDGMENTS

This work was supported by a grant from CETI. S. Landsberger (UI) carried out the NAA analysis. J. Reding (CETI) coordinated the UI and CETI efforts. R. Twardock (UI), and E. Klema (Tufts U) carried out radiation measurements on microspheres. Valuable comments by M. McKubre (SRI) and P. Hagelstein (MIT) are also gratefully acknowledged.

CETI Session

ELECTROCHEMISTRY AND CALORIMETRY IN A PACKED-BED FLOW-THROUGH ELECTROCHEMICAL CELL

M. C. H. McKubre, S. Crouch-Baker and F. L. Tanzella, SRI International, Menlo Park, CA USA,
D. Cravens, CETI, New Mexico, USA

Abstract

Packed bed electrochemical cells have come to recent prominence as a convenient way to provide a large area cathode of nickel and/or palladium, in the search for "excess heat" production. In such cells, the electrolyte is constrained to flow axially, parallel to the direction of net current flow. Calorimetry can be performed by measuring the mass flow rate and temperature rise of the electrolyte in its transit through the cell.

This paper focuses on aspects of electrochemistry, electrochemical engineering and calorimetry that are peculiar to flow-through packed-bed cells. Results will be presented of calculations intended to characterize the distribution of electrochemical process: current, potential and composition, within the heterogeneous structure of the packed bed cathode. The interpenetrating, continuous conductive elements formed by the solid phase metallic conductor (coating) and the pore-filling electrolyte phase, extended in the dimension of current flow, form a system which can be modeled as an electrochemical transmission line. The results of such modeling can be used to predict the depth of electrochemical activity within a packed bed, and to estimate the profile of hydrogen activity.

1. Introduction

By far the most effective method of assessing the distribution of process inside an extended heterogeneous electrode is by making use of the transmission line analogy. Briefly, the interpenetrating solid and electrolyte volumes of the porous electrode are replaced by their resistivities per unit length in the direction of the imposed current flux, with the interfacial impedance distributed in between. The electrode may be treated[1] as "one-dimensional" provided that quantities such as the electrical potential, V, current flux, I, and reactant concentration, c, vary only with depth within the electrode (*i.e.*, in the direction of the imposed field), and not with lateral position. The local values of *V*, *I*, and *c* may then be replaced by their average values in a plane perpendicular to the applied electric field gradient.

The electrode may be represented by a finite transmission line of the form shown in Figure 1. A solution to this problem was first achieved by Lord Kelvin[2] and has been applied widely to membrane impedance problems since 1905.[3-5] Some 40 years later, this model was first used in electrochemistry by Coleman[6] and has subsequently been extended,[7-15] notably by deLevie.[9-11] Briefly, solutions are required to a set of differential equations of the form

$$\frac{\delta^2 I_s}{\delta x^2} + \frac{\delta \ln (1/Y)}{\delta x}\frac{\delta I_s}{\delta x} - Y (r_s + r_e) I_s = - Y r_e I \qquad [1]$$

$$\frac{\delta^2 I_e}{\delta x^2} + \frac{\delta \ln (1/Y)}{\delta x}\frac{\delta I_e}{\delta x} - Y (r_s + r_e) I_e = Y r_s I \qquad [2]$$

$$\frac{\delta^2 \zeta}{\delta x^2} - Y (r_s + r_e) \zeta = 0 \qquad [3]$$

where subscripts e and s refer to the electrolyte and solid phases, $I = I_s + I_e$, and $\zeta = V_s - V_e$.

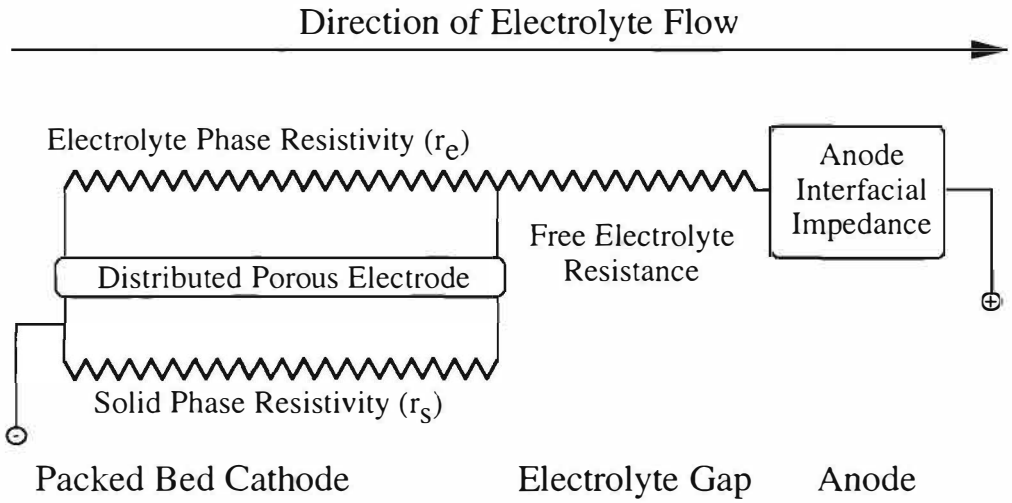

(a) Transmission line equivalent circuit

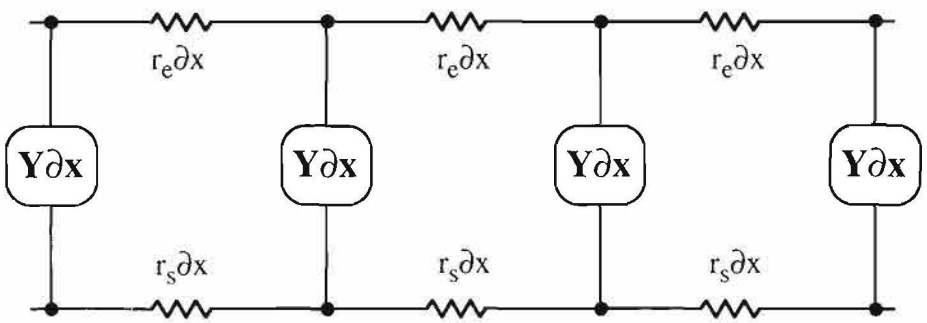

(b) Infinitesimally small section of the transmission line

JAM-350522-16

Figure 1 The transmission line model.

For the Patterson cell geometry shown in Figure 2, the current flows (in parallel to the electrolyte) through electrolyte and solid phase resistances that are effectively independent of the distance within the bed, x.

For this case, an analytical solution for the transmission line impedance, Z_{TL}, is easily obtained from equations [1] - [3], provided that the interfacial impedance can be considered also to be independent of x.

$$Z_{TL} = \frac{4r_s r_e + (r_s^2 + r_e^2)\,(e^{\gamma l} + e^{-\gamma l})}{\gamma(r_s + r_e)\,(e^{\gamma l} - e^{-\gamma l})} + \frac{r_s r_e\, l}{r_s + r_e} \qquad [4]$$

where $\gamma = [Y\,(r_s + r_e)]^{1/2}$ and l is the bed length.

Equation [4] is an extremely powerful tool to examine, by ac means,[14,15] the electrochemical characteristics of processes occurring within a packed-bed flow-through electrode.

The dc problem of the distribution of electrochemical activity with an extended bed electrode is more complex because of the intrinsic voltage non-linearity of electro-kinetic processes. One effective stratagem is to use a discrete transmission line model.[13-15] In this approach, the continuous transmission line shown schematically in Figure 1a, comprising an infinite number of infinitesimally small sections as shown in Figure 1b, is replaced by the series sum of a (large but finite) number of segments containing discrete circuit elements of the form shown in Figure 1b. In this way we can impose an arbitrary functionality on the three elements $Y\Delta x$, $r_e\Delta x$ and $r_s\Delta x$, as these change with current density, overvoltage, composition, temperature *etc*, along the axis of the bed, x. The advantage of the discrete approach is that it allows complete generality, and the use of standard formulae for the kinetics of electrochemical processes.

2. Model Parameters

The following assumptions, constraints, dimensions and equations were used in our model calculations:

- The bed is considered to be a cylinder of radius R = 0.75 cm, containing 1 cm^3 of coated resin beads. The beads are modeled as a hexagonally close packed (hcp) array of monodisperse spheres of diameter 0.075 cm (r = 0.0375 cm). The fraction of volume occupied by hcp spheres, $\phi = 74\%$ $(= \pi/3\sqrt{2})$, and the interfacial area presented in such an array is 29.6 $cm^2\ cm^{-3}$ $(\pi/3\sqrt{2}\ r)$, or 52.34 $cm^3\ cm^{-1}$ along the axis of the cylinder.

- The electrolyte phase resistivity is that for 1M Li_2SO_4 at 25°C ($\rho_e = 6.7\ \Omega$ cm). In the calculation we need to know the resistance per unit length, which is modified by the volume porosity (ϕ) and cross sectional area of the bed,

$$r_e = 2\,\pi\,R\,\rho_e\,(1 - \phi) \qquad [5]$$
$$= 14.5\ \Omega\ cm^{-1}$$

- The solid phase resistivity. The flow of electrons in a "Patterson" packed bed occurs via the thin conformal metal coating on the surface of each sphere. In a well packed bed for which inter-sphere contact resistances can be neglected, we can evaluate the resistivity of a hcp array of coated spheres. by direct integration. For a coating of thickness t,

$$\frac{\rho_{hcp}}{\rho_s} = \frac{0.89}{(q - q^2)} \quad \text{where } q = t/2r. \qquad [6]$$

and

$$r_s = 1.78\,\pi R/(q - q^2)\ \Omega\ cm^{-1} \qquad [7]$$

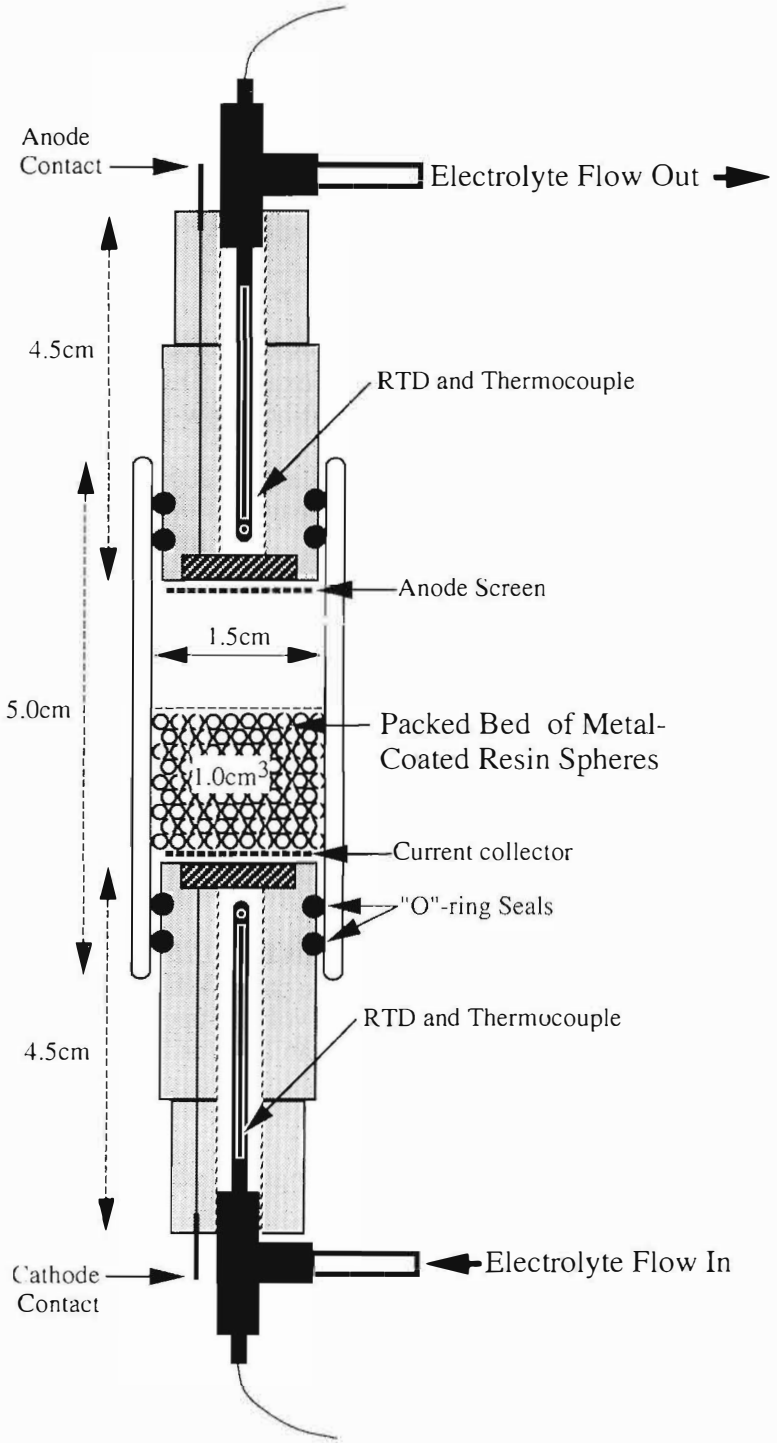

Figure 2 CETI/Patterson Packed-Bed Flow-Through Electrochemical Cell

For a coating thickness of 2 μm (t = 2 x 10^{-4} cm) of palladium and/or nickel ($\rho_s = 10^{-5}$ Ω cm),

$$r_s = 0.034\ \Omega\ cm^{-1}$$

• The electrochemical process. The hydrogen evolution reaction on Group 8 metal surfaces has been studied extensively. Nevertheless the detailed mechanisms remain little understood, and the kinetics poorly quantified. The use of ac impedance measurements in association with a discrete extension of equation [4] has the potential to greatly reduce the uncertainties of electrochemical mechanisms and rates in packed bed structures. Until this is completed we have chosen to employ a simple Butler-Volmer form for the expected voltage dependence of the electrochemical process;

$$i(x) = i^\circ \{ \exp [\alpha n F \zeta(x)/RT] - \exp [(\alpha-1)\, n F \zeta(x)/RT] \} \qquad [8]$$

where i° is the exchange current density
α is the barrier transfer coefficient
n is the number of electrons transferred
F is the Faraday constant
T is the absolute temperature
ζ is the kinetic component of the overvoltage

The use of equation [8] assumes that the hydrogen evolution rate within the bed is compositionally independent. This assumption has two parts; i° is independent of electrolyte composition, and i° is independent of the activity of hydrogen adsorbed onto the packed bed surface. In a flowing electrolyte system, and at modest or low current densities, the first assumption is likely to be valid as the electrolyte composition will change little during its transit through the bed. The effect of hydrogen atom activity on i° may require further examination and discussion.

The following values were used to calculate the results shown in Figures 3 and 4: $i^\bullet$ was varied from 10^{-4} to 3 x 10^{-3} A cm^{-2}, α = 1/2, n = 1, F = 96485 C mol^{-1}, and T = 25°C (278.15K).

3. Model Mechanics

In the transmission line model, as in the packed bed, the applied current enters the solid phase (via an appropriate current contact). At one end of the transmission line (the first element in a discrete model), all of the current is conveyed by electron motion in the solid. A local kinetic overvoltage is established between the solid and electrolyte phases which drives the electrochemical process. As a consequence of this overvoltage, an interfacial current flows between the solid and electrolyte phases such that, at the opposite end of the transmission line (the last discrete element), no current flows in the solid phase. All the current injected at one end into the solid electronic conductor, is carried at the other end by the motion of ions in the electrolyte.

Since there are no lateral leakage paths it is easy to see that the current, I, injected at one end, must flow either in the solid phase, $I_s(x)$, or in the electrolyte phase, $I_e(x)$, and nowhere else, so that these are complementary functions;

$$I = I_s(x) + I_e(x) \qquad [9]$$

As these currents flow, respectively, through the solid and electrolyte phase resistances, the potentials in these phases increase due to the accumulated IR drops;

$$V_s(x) = \int_0^x I_s\, r_s\, \delta x;\quad V_e(x) = \int_0^x I_e\, r_e\, \delta x \qquad [10]$$

In the discrete model, these integrals are replaced by summations.

At any position, x, the kinetic overvoltage between the solid and electrolyte phase drives the electrochemical process;

$$\zeta(x) = V_e(x) - V_s(x) \qquad [11]$$

The interfacial current density is given by equation [8].

Calculations were performed using a 1000 element discrete transmission line. The current and voltage distributions in this mesh were solved using equations [8] - [11], by adjusting the local overvoltage in the first element, $\zeta(0)$, iteratively to make the solid phase current in the last element, $I_s(L) = 0$.

4. Results

Figure 3 shows the results of a series of calculations made at constant cathodic current (0.1A), but varying exchange current density. The parameters plotted are the solid phase current, I_s, and the kinetic overvoltage, ζ, both as a function of distance, x, from the current collector at the bottom of the bed.

The current, I_s, is plotted as thinner lines referenced to the left axis of Figure 3. This current necessarily enters the bed at the imposed level, 0.1A, and declines monotonically to zero at the top of the packed bed where free electrolyte emerges in the direction of the anode. For all cases considered, the interfacial impedance is large; that is i° is small, reflecting the known sluggish kinetics of the hydrogen evolution reaction. Because of this, the profile of $I_s(x)$ is dominated by the (relatively large) electrolyte phase resistivity, and shows little variation with i°.

The overvoltage profile exhibits a much larger dependence on the exchange current density. For large values of i° (fast kinetics) very little of the bed, and very little voltage, is needed for the imposed current to traverse the interface. At $i^\circ = 3$ mA cm^{-2}, less than 0.2 cm of the bed can be considered to be active. At $i^\circ = 0.1$ mA cm^{-2}, the top of the bed is approximately twice as active as the bottom, but all of the bed will be in effective operation.

5. Discussion

Considerable attention has been focused in recent years on the appearance of anomalous excess heat in Pd/D systems, and the correlation of this heat with the level of loading of deuterium into the palladium lattice.[21] Anomalous excess heat has been reported for the Patterson cell[22] as well as for other light water experiments employing palladium and nickel cathodes.[19, 20] Very much less is known about the appearance and correlation of this thermal anomaly with proton loading, than is known from D/Pd experiments.

The direct measurement of hydrogen (or deuterium) loading in a packed bed cathode presents obvious difficulties. Nevertheless, we believe that it is important to estimate the probable distribution of this property. The following discussion which must remain speculative until further measurements are made, is an attempt to predict the distribution of hydrogen loading in a Pd coated packed bed cathode based on transmission line modeling.

We begin by noting that the loading of deuterium into palladium cathodes in alkaline environments exhibits a roughly logarithmic dependence on current density. This relationship is evident in the data of Hasegawa *et al.*,[23] from which we can deduce the following empirical relationship

$$m \approx m^* + \gamma \log_{10} (i/i^*) \qquad [12]$$

where: m is the D/Pd atomic ratio; $m = m^*$ at a selected reference current, $i = i^*$; and the slope $\gamma \approx$ 3%/decade from the Hasegawa data.

We also observe equation [12] to hold over a range of current densities, in our own experiments but we can distinguish two different modes of behavior. For electrodes that load

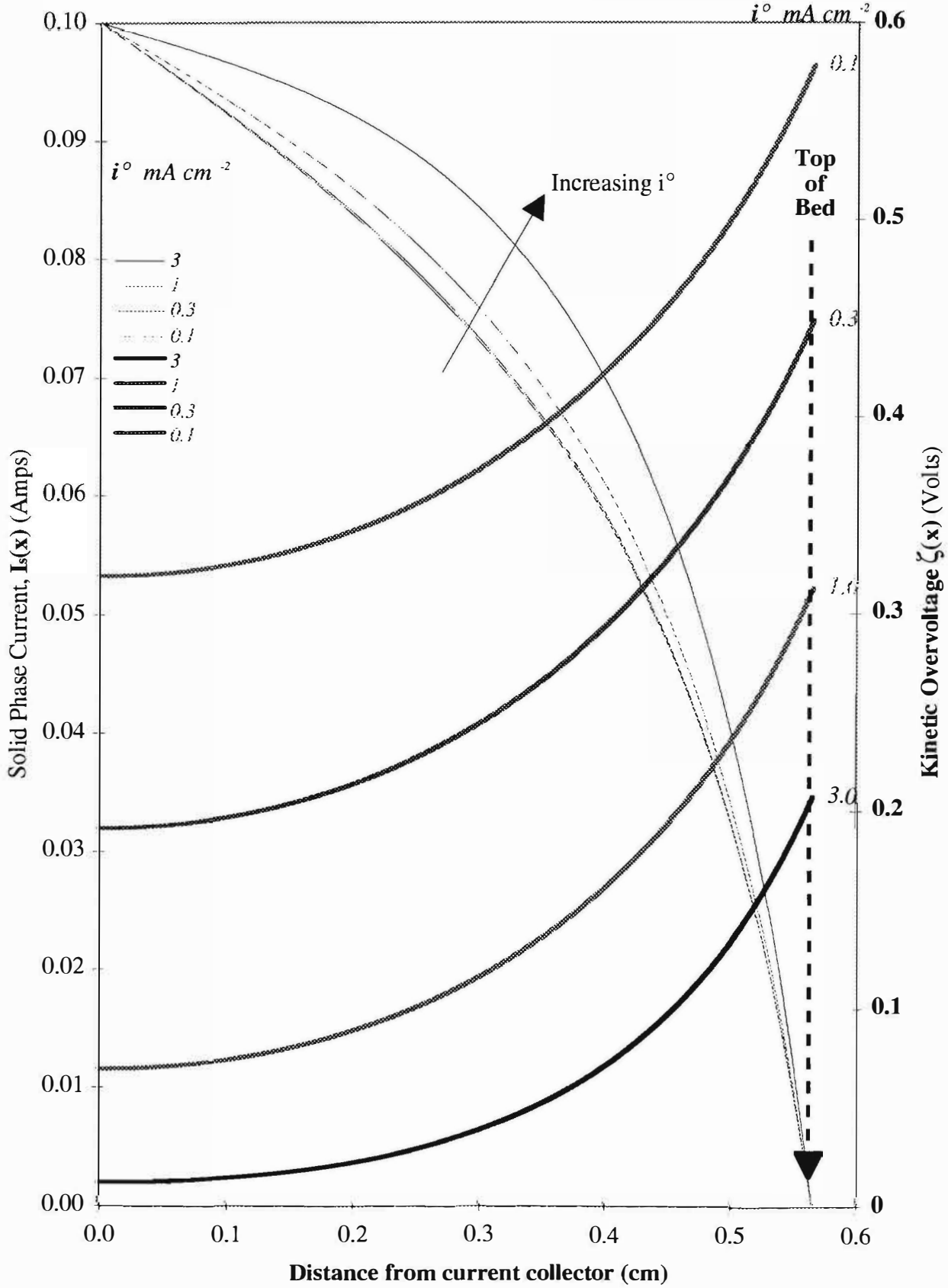

Figure 3 Distribution of Current and Voltage in a CETI Packed Bed at 0.1A cathodic.

"poorly", we measure a slope, γ, very similar to the 3% evidenced by Hasegawa.[23] For "better" loading electrodes, we see a much steeper functionality, with slope γ between 6% and 9% per decade.

Lacking further information, we make the following assumptions. That:

i) A palladium coating behaves similarly to bulk palladium with respect to interfacial kinetics and loading characteristics.
ii) Cathodes in light water electrolytes load similarly to those in heavy water electrolytes.
iii) The current density/loading functionality in 1M lithium sulfate is similar to that in 1M lithium hydroxide.

If this sequence of assumption is sound then we can use equation [12] in association with the interfacial current density calculated using the transmission line model, to estimate, approximately, the loading profile in the packed bed cathode. The heavy line in Figure 4 plots the interfacial current density, i(x), against distance within the bed, for one of the cases solved and presented in Figure 3 ($I = 0.1A$, $i^\circ = 0.001A$). This line is steeply curved, again suggesting that only the top millimeter or two of the bed show high levels of activity. Because of the logarithmic dependence with loading, however, the expected profiles of hydrogen loading are somewhat less steep. The two thin lines in Figure 4 show the profiles of loading calculated from equation [12] using two (approximately limiting) values of γ. The lower line is calculated for a value of $\gamma = 3\%$, and predicts a rather unimpressive profile of loading. The upper line, on the other hand, calculated for $\gamma = 6\%$, suggests that potentially interesting values of loading ($H/Pd \geq 0.9$) are attainable at the top of the packed bed cathode of Pd-coated spheres.

6. Summary and Conclusions

Using a discrete transmission line model, calculations were performed to estimate the profile of electrochemical parameters inside a single example of a CETI flow-through, packed-bed cathode. In this calculation the only significant uncertainty is in assigning the correct value to the interfacial exchange current density, i°. Four values were used covering the anticipated range of i° for a nickel or palladium surface coating in 1M Li_2SO_4.

In other electrolytes, the loading of hydrogen into palladium has been observed to depend approximately logarithmically on the interfacial current density. Based on the calculated profile of this parameter, we have been able to estimate a profile for the hydrogen loading within a Pd-coated packed bed cathode. This parameter is very difficult to measure experimentally.

Based on our calculation we are able to draw the following conclusions.

i) Calculations were performed for a relatively short bed (0.57 cm in the direction of current and electrolyte flow). This bed nevertheless exhibits a substantial dispersion of process. The end of the bed closest to the anode (furthest from the current contact) is the most active; this problem is exacurbated at high values of the exchange current density, i°.
ii) As a corollary to (i), the packed bed structure provides a convenient means to increase the area accessed by an electrochemical process. Because of the fall-off in activity with distance from the end of the bed, however, this accessed area does not increase substantially with bed length, for lengths greater than some critical value. The bed length employed by Patterson/CETI appears well matched to the expected electrochemical characteristics.
iii) Consistent with the assumptions used to transform the three-dimensional packed bed to its one-dimensional mathematical model, the radius of the bed is a free-scaling dimension. The accessed area can be increased without penalty, by increasing the bed radius.
iv) Even for relatively thin metal coatings, the solid phase conductivity is much greater than that for any aqueous electrolyte. Accordingly the profile of current within the bed, and overall bed impedance, is controlled by the electrolyte phase resistivity. Increased active area can be achieved by fluidizing the bed, effectively increasing the solid phase resistivity so that it matches more closely the electrolyte phase.

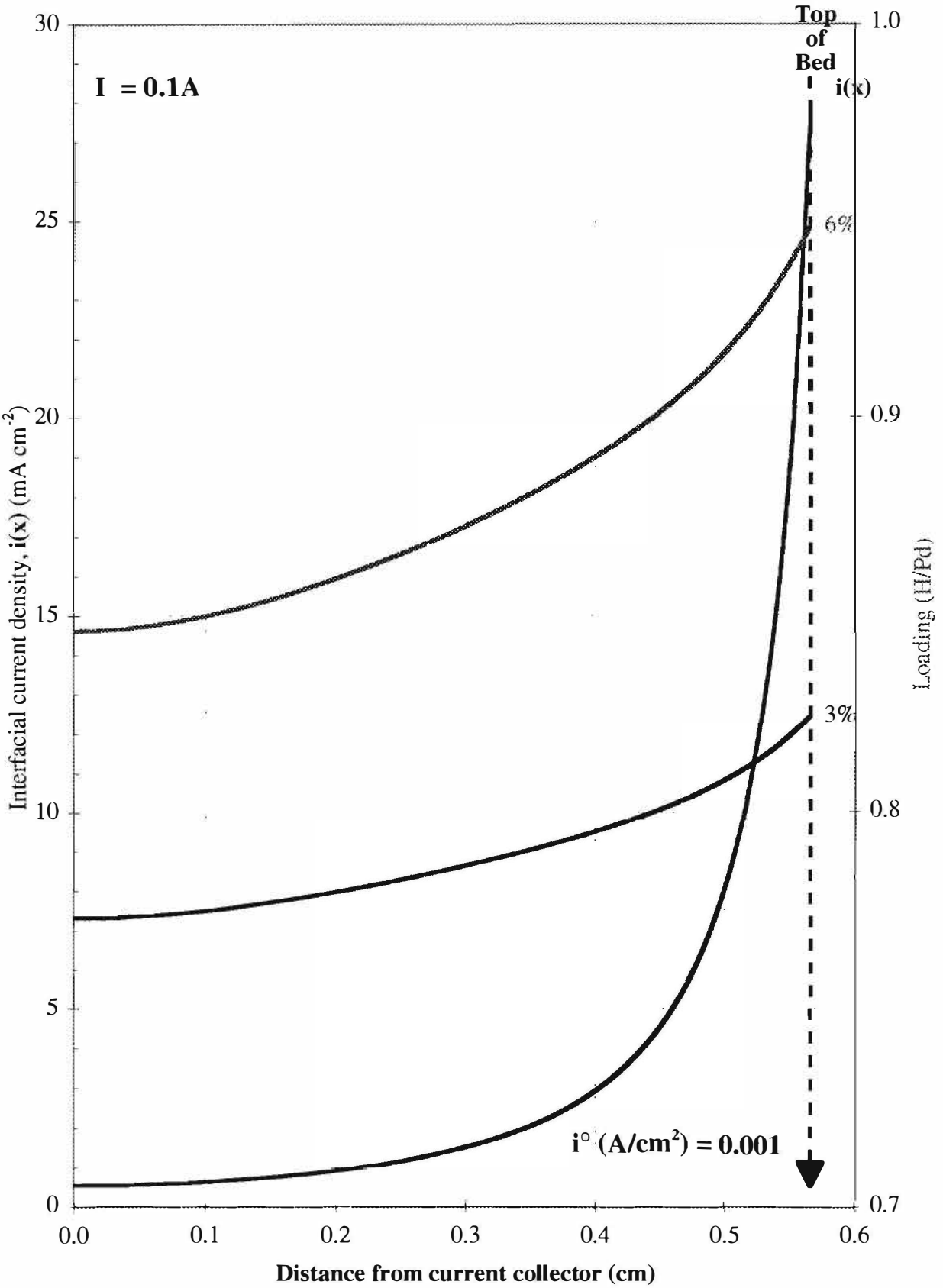

Figure 4 Distribution of Interfacial Current and Estimated Loading for a CETI Packed Bed at 0.1A Cathodic.

v) By making some assumptions about the dependence of hydrogen loading on current density, we have estimated approximate limits for H/Pd profiles within the CETI packed bed. These profiles suggest that, for a plausible set of electrochemical parameters, modest H/Pd loadings are to be expected throughout the bed. With the most favorable loading/current density functionality, we expect intensive loading (H/Pd ≥ 0.9) to be achieved only at the most active end of the bed.

Acknowledgments

The SRI authors wish to recognize the financial support and contributions of IAE and NEDO. CETI is recognized for providing cells, data and travel support for DC.

References

1. O. S. Ksenzheck and V. V. Stender, *Dokl. Akad. Nauk, SSSR* **106**, 487 (1976).
2. Lord (William Thompson) Kelvin, *Proc. R. Soc.* (London) **7**, 382 (1855).
3. I. G. Gurevich and V. S. Bagotskii, *Electrochim. Acta* **9**, 236 (1964).
4. L. Hermann, *Arch. Ges. Physiol.* **109**, 95 (1905).
5. G. Falk and P. Fatt, *Proc. R. Soc. (London) Ser. B* **160,** 69 (1964).
6. J. J. Coleman, *Trans. Electrochem. Soc.* **90**, 545 (1946).
7. V. S. Daniel'-Bek, *Zh. Fiz. Khim.* **20**, 567 (1946).
8. J. Euler and W. Nonnenmacher, *Electrochim. Acta* **2**, 268 (1960).
9. R. deLevie, *Electrochim. Acta* **8**, 751 (1963).
10. R. deLevie, *Electrochim. Acta* **9**, 1231 (1964).
11. R. deLevie, *Electrochim. Acta* **10**, 113 (1965).
12. G. G. Law and J. Newman, *J. Electrochem. Soc.* **126**, 2150 (1979).
13. M.C.H. McKubre, "Equilibrium and steady state studies of continuous flow-through electrode systems", report to The University, Southampton, England, 1978.
14. M.C.H. McKubre and D. D. Macdonald, "Impedance Measurements in Electrochemical Systems", in Modern Aspects of Electrochemistry, J. O'M. Bockris, B. E. Conway, and R. E. White, Eds., Vol. 15, p. 61, Plenum, New York, (1982).
15. M.C.H. McKubre and D. D. Macdonald, "Electronic Instrumentation for Electrochemical Studies", in A Comprehensive Treatise of Electrochemistry, J. O'M. Bockris, B. E. Conway, and R. E. White, Eds., Vol. 6, p. 1, Plenum, New York, (1984).
16. Proceedings of the First International Conference on Cold Fusion (ICCF1), National Cold Fusion Institute, Salt Lake City, UT, 1990, p. 20.
17. Proceedings of the Second International Conference on Cold Fusion (ICCF2),*"The Science of Cold Fusion,"* Eds. T. Bressani, E. Del Giudice, and G. Preparata, Conference Proceedings Vol. 33, Italian Physical Society, Bologna, 1992, p. 419.
18. Proceedings of the Third International Conference on Cold Fusion (ICCF3), *"Frontiers of Cold Fusion"*, ed. H. Ikegami, Universal Academy Press, Inc., Tokyo. p. 5 (1993).
19. *Proceedings of the Fourth International Conference on Cold Fusion* (ICCF4), EPRI TR-104188, Maui, Hawaii (1993).
20. Proceedings of the Fifth International Conference on Cold Fusion (ICCF5), Monte Carlo, Monaco (1995).
21. M. McKubre, S. Crouch-Baker, R. Rocha-Filho, S. Smedley, F. Tanzella, T. Passell, and J. Santucci "Isothermal Flow Calorimetric Investigations of the D/Pd System" J. Electroanal. Chem., **368** (1994) p. 55.
22. D. Cravens "Flowing Electrolyte Calorimetry," Proceedings of the Fifth International Conference on Cold Fusion (ICCF5), Monte Carlo, Monaco (1995).
23. N. Hasegawa, N. Hayakawa, Y. Yamamoto, K. Kunimatsu (IMRA Japan Co. Ltd., Sapporo, Japan), "Observation of Excess Heat During Electrolysis of 1M LiOD in a Fuel Cell Type Closed Cell," *Proceedings of the Fourth International Conference on Cold Fusion* (ICCF4), EPRI TR-104188, Maui, Hawaii (1993).

Transmutation

Analysis of Nickel - Hydrogen Isotope System on TNCF Model

KOZIMA Hideo, OHTA Masayuki, NOMURA Masahiro and HIROE Katsuhiko

Department of Physics, Faculty of Science, Shizuoka University
836 Oya, Shizuoka 422, JAPAN

Abstract

Experimental results obtained in the Ni - H and Pd - H systems generating the excess heat and/or with transmutated nuclei (NT) were investigated on Trapped Neutron Catalyzed Fusion (TNCF) model proposed by one of the authors (K.H.).

Experimental results, which are not able to be explained by d - d or p - p reaction, are explained by n - p or n - ^{6}Li and the following breeding reactions on TNCF model assuming the existence of the trapped thermal neutron. The trapped neutron works also as a key particle to transmute elements in the system. As same as the excess heat, it is difficult to understand the NT without thermal neutron.

On TNCF model, excellent experimental data of excess heat and NT in the Ni - H and Pd - H systems are explained consistently and quantitatively.

1. Introduction

In addition to Pd - D and Ti - D systems, the Cold Fusion (CF) phenomena in Ni - H and Pd - H systems were reported. The CF phenomena have shown the generation of the excess heat, ^{4}He, tritium (t), neutron (n), nuclear transmutation (NT) and so on. In those nuclear products, tritium and NT show apparent facts of occurrence of nuclear reaction in the sample.

From our point of view based on TNCF model[1,2], NT is the evidence that neutron is the key particle causing the nuclear reaction.

In this paper, we will compare the results obtained in the excellent experiments that one showed the NT and another showed the excess heat production, and will show the consistent interpretation of the phenomena by TNCF model.

2. Summary of Experimental Data

2 - 1) A Experiment Showing Nuclear Transmutation in Ni - H System[3]

The electrochemically induced nuclear transmutation in Ni - H system was reported[3]. In this experiment, generation of the excess heat and shift of Sr isotope ratio (^{86}Sr/^{88}Sr $\equiv$ η) were observed, using electrolyte Rb_2CO_3 and RbOH.

Transmutation

Before the experiment, in cathode material of Ni, the relative percentages of two Sr isotopes were determined as ^{86}Sr (10.51 ± 0.04 %) and ^{88}Sr (89.49 ± 0.04 %); this gave the original value $1/\eta = 8.515 \pm 0.004$.

After the Experiment (I) where the excess energy Q_1 was detected, the percentages changed to ^{86}Sr (22.20 ± 0.05 %) and ^{88}Sr (77.80 ± 0.05 %); the ratio became $1/\eta_1 = 3.504 \pm 0.002$.

After the Experiment (II) where the excess energy was $Q_2 = 5\ Q_1$, the percentages changed to ^{86}Sr (26.80 ± 0.05 %) and ^{88}Sr (73.20 ± 0.05 %); the ratio became $1/\eta_2 = 2.731 \pm 0.003$.

2 - 2) Another Experiment in Ni - H System of Gas Phase[4)]

We took another experiment which showed excess heat production in hydrogen - loaded Ni rod in H_2 gas. In this experiment, an excess heat of 44 W was detected for a period of twenty - four days (corresponding to about 90 MJ) and no penetrating radiation (neutron, γ - rays) was detected.

2 - 3) Experimental Data of Patterson Power Cell[5)]

Patterson Power Cell (PPC), using microspheres (beads) coated with Pd - Ni layers and Li electrolyte with light water, accomplished a good qualitative reproducibility. The experimental data[5)] showed the output power of 1.77 W ($= 1.1 \times 10^{13}$ MeV/s) using 1200 microspheres which had a diameter of 1 mm, with 2 μm thickness of all metal layers.

3. Analysis of Experimental Data on TNCF model

Let us analyze these experimental results by TNCF model.

This model assumes the stable existence of the trapped thermal neutrons in crystal. Inhomogeneous distribution of hydrogen in sample metal, produced by specific chemical or gas loading method, and surface layers of the electrolyte work to trap the thermal neutrons in the sample. The trapped thermal neutron exists stable against β - decay.

When the trapped thermal neutron suffers a strong perturbation induced by disorder of the crystal potential, the trapped neutron fuses with a proton (deuteron) to generate a deuteron (tritium) and gamma and also with minor elements to transmute the elements to show a change of isotope ratio.

Possible mechanisms of the neutron trapping were discussed in previous papers in detail[1,2)].

3 - 1) Analysis of the Experiment Showing Nuclear Transmutation in Ni - H System

We will give a result of analysis of the experiment[6)] showing nuclear transmutation[3)].

Assuming the existence of the trapped neutrons, there occurs nuclear reaction between the neutron and nuclei (hydrogen isotope or minor elements in Ni cathode). For nuclear reactions between neutron and nucleus of minor elements in Ni cathode, a nucleus absorbed the neutron forms an intermediate nucleus which may decay by β emission. In this case of nuclear transmutation, we can write down the reactions as follows:

$$n + {}^{85}\mathrm{Rb} = {}^{86}\mathrm{Rb} = {}^{86}\mathrm{Sr} + e^- + \bar{\nu}_e, \qquad (1)$$

$$n + {}^{87}\mathrm{Rb} = {}^{88}\mathrm{Rb} = {}^{88}\mathrm{Sr} + e^- + \bar{\nu}_e. \quad (2)$$

Denoting natural abundance of ^{85}Rb and ^{87}Rb as N_a (72.15 %) and N_b (27.85 %), ^{86}Sr and ^{88}Sr as n_a (10.51 %) and n_b (89.49 %), the ratio η after the n - Rb fusion reaction in the experiment will be given by a relation,

$$\eta = \frac{n_a + n_n v_n T_i \xi \sigma_a N_a}{n_b + n_n v_n T_i \xi \sigma_b N_b}. \quad (3)$$

where $n_n v_n$ is the flux density of the thermal neutron ($\mathrm{cm^{-3}s^{-1}}$), v_n is the thermal velocity of the trapped neutron, T_i is the time of electrolysis in the experiment i (i = 1, 2), ξ is ratio of number density of Rb and Sr, σ_j (j = a, b) is fusion cross section; σ_a = 0.7 and σ_b = 0.2 barns. The thermal velocity is given as $v_n = 2.7 \times 10^5$ cm/s (for 300K).

Using the relation (3), we can calculate the neutron density. With the numerical values corresponding to experiments (I) and (II), we obtain following values for $n_n v_n T_i \xi$; $n_n v_n T_1 \xi = 0.307 \times 10^{24}$ and $n_n v_n T_2 \xi = 0.459 \times 10^{24}$ $\mathrm{cm^{-2}}$, respectively.

Taking an average value for $n_n v_n T_i \xi$, ($< n_n v_n T > \xi = 0.38 \times 10^{24}$ $\mathrm{cm^{-2}}$), we can obtain the value $n_n T \xi$ as follows:

$$n_n T \xi = 1.4 \times 10^{18} \ \mathrm{cm^{-3}s}.$$

If we assume $\xi = 1$ and $T = 2.59 \times 10^6$ s (one month) arbitrarily, we obtain the density of trapped neutron in Ni cathode:

$$n_n = 5.4 \times 10^{11} \ \mathrm{cm^{-3}}.$$

3 - 2) Analysis of the Experiment in Ni - H System of Gas Phase

Next, we will give a result[7] of the case of Ni - H system in gas phase[4]. We assume a following reaction between the trapped neutron and occluded hydrogen in Ni:

$$n + p = d\ (1.3\ \mathrm{keV}) + \gamma\ (2.2\ \mathrm{MeV}). \quad (4)$$

If all of observed excess energy was generated by this reaction, the number of events is estimated as $\nu = 1.25 \times 10^{14}\ \mathrm{s^{-1}}$.

We can estimate the trapped neutron density n_n using the following relation,

$$\nu = 0.35 n_n v_n N_p \sigma_{n-p}, \quad (5)$$

where $0.35 n_n v_n$ is the flux density of the thermal neutron ($\mathrm{cm^{-3}s^{-1}}$), v_n is the thermal velocity of the trapped neutron as above, N_p is the number of occluded protons in the sample ($N_p = 3.0 \times 10^{21}$), σ_{n-p} is the fusion cross section of the thermal neutron and a proton; σ_{n-p} = 0.13 barns.

Thus, we obtain the value of the density of trapped neutron,

$$n_n = 3.6 \times 10^{12} \ \mathrm{cm^{-3}}$$

This value can be compared with the result we got in section 3 - 1). The assumption of the existence of a number of the trapped thermal neutron in Ni has given a consistent value of the density of the trapped neutrons $n_n \simeq 10^{12}$ and a unified interpretation of both of nuclear transmutation and excess heat generation.

If breeding reactions occur after the reaction mentioned above effectively, tritium will be produced by the following reaction:

$$n + d = t\ (6.98\ \text{keV}) + \gamma\ (6.25\ \text{MeV}). \tag{6}$$

In an optimum situation where the gamma is absorbed effectively in the sample[8], the excess heat becomes large, while tritium is only the detected byproduct in the situation where the absorption is scarce. In this experiment[4], however, tritium was not observed.

3 - 3) Analysis of the Patterson Power Cell

In the case of PPC, surface layers of $PdLi_x$ (or $NiLi_x$) alloy and Li metal will be formed on the surface of the microsphere. We assume only PdLi (NiLi) alloy layer with the thickness $l = 2\ \mu$m in the following analysis.

Then, we can obtain the density of trapped neutron n_n in PdLi layer. We will take up the main reaction of excess heat generation, as follows:

$$n + {}^6\text{Li} = {}^4\text{He}\ (2.1\ \text{MeV}) + t\ (2.7\ \text{MeV}). \tag{7}$$

The number of events per unit time denoted by ν is estimated as follows; $\nu = 1.1 \times 10^{13}$ (MeV/s) / 4.8 (MeV) $= 2.3 \times 10^{12}$ (/s).

On the other hand, the number of events per unit time ν is expressed as follows:

$$\nu = 0.35 n_n v_n \rho_{Li6} V \sigma_{nLi6}. \tag{8}$$

In this relation, ρ_{Li6} is the density of ^{6}Li in PdLi alloy. σ_{nLi6} is the fusion cross section. V is the total volume of PdLi alloy on the surface of 1200 microspheres.

In PdLi alloy, we can take the value of ρ_{Li} as follows; $\rho_{Li} = \rho_{Li6} + \rho_{Li7} = 3.4 \times 10^{22}$ cm^{-3}. The natural abundance of ^{6}Li and ^{7}Li are 7.5 % and 92.5 %, respectively, and therefore $\rho_{Li6} = 2.6 \times 10^{21}$ cm^{-3}.

Using the value $V = 1.6 \times 10^{-3}$ cm^3 and $\sigma_{nLi6} = 1.0 \times 10^3$ barns, the density of trapped neutron n_n is estimated as follows:

$$n_n = 6.0 \times 10^9\ \text{cm}^{-3}.$$

The detail including discussion about breeding of neutrons is reported in the previous paper[9] where an important role of deuterium in Pd - Ni - H_2O + LiOH system was pointed out.

4. Conclusion

In the experiments with hydrogen analyzed in this paper, it was observed that there occurred generations of excess heat and transmutated nuclei. While it has been considered that the hydrogen substitute the deuterium for a reference system, the experimental

data analyzed successfully and interpreted as real phenomena substantiate the cold fusion phenomena in the system with hydrogen.

As we have seen, both trapped neutron densities of two experiments in Ni - H system showed approximate coincidence.

Thus, if we allow to assume the existence of stable thermal neutron in crystal, we can explain various CF phenomena showing nuclear transmutation, excess heat generation, tritium production, He production and etc. occurred in several systems along conventional physics by only one adjustable parameter of trapped neutron density.

The TNCF model has been developed to fit various phases and systems of CF phenomena. We have got more than 15 results of analysis of experiments showing CF phenomena in several systems including Pd - D and Ti - D and so on, hitherto. The densities of the trapped thermal neutrons determined from analysis of experiments were in a range of $10^2 \sim 10^{12}$ cm^{-3} [10].

In reverse, the success of analysis on TNCF model shows the reality of trapped thermal neutron in crystal. The other three papers[11~13] given in this conference will help to understand the physics of the cold fusion.

References

(1) H. Kozima, *Trans. Fusion Technol.* **26**, 508 (1994).
(2) H. Kozima, *Cold Fusion* **16**, 4 (1996); *Proc. 3rd Russian Conference on Cold Fusion and Nuclear Transmutation (RCCFNT3)* (Sochi, Russia, Oct. 2 - 6, 1995), 224 (1996).
(3) R. Bush and R. Eagleton, *Trans. of Fusion Technol.* **26**, 344 (1994).
(4) S. Focardi, R. Habel and F. Piontelli, *Nuovo Cimento* **107A**, 163 (1994).
(5) D. Cravens, *Cold Fusion* **11**, 15 (1995) and also *Proc. ICCF-5* (1995) 79.
(6) H. Kozima, K. Hiroe, M. Nomura and M. Ohta, *Cold Fusion* **16**, 30 (1996).
(7) H. Kozima, *Cold Fusion* **8**, 5 (1995); M. Ohta, M. Nomura, K. Hiroe, H. Kozima, "On the Cold Fusion in Ni - H System (II)", *Cold Fusion* (to be published).
(8) H. Kozima, *Cold Fusion* **15**, 12 (1996).
(9) H. Kozima, *Cold Fusion* **17**, 8 (1996).
(10) H. Kozima, *Proc. 3rd Symposium of Basic Reseach Group in NHE Project* (July 3 - 4, 1996, Tokyo, Japan), 17 (1996) and also *Cold Fusion* **18**, 30.
(11) H. Kozima, "On the Existence of the Trapped Thermal Neutron in Cold Fusion Materials" (in this issue).
(12) H. Kozima, K. Hiroe, M. Nomura and M. Ohta, "Analysis of the Electrolytic Cold Fusion Experiments on TNCF Model" (in this issue).
(13) H. Kozima, M. Nomura, K. Hiroe and M. Ohta, "Nuclear Transmutation in Cold Fusion Experiments" (in this issue).

Transmutation

Nuclear Transmutation in Cold Fusion Experiments

KOZIMA Hideo, NOMURA Masahiro, HIROE Katsuhiko and OHTA Masayuki

Department of Physics, Faculty of Science, Shizuoka University, 836 Oya, Shizuoka 422, JAPAN

Abstract

Nuclear transmutation in chemical and biological systems are investigated with use of Trapped Neutron Catalyzed Fusion Model (TNCF model). In the TNCF model, it is possible to analyze experimental data consistently and quantitatively. We present the investigation of experimental results in cold fusion systems with various materials and methods in this paper.

1. Introduction

There are many experimental results in cold fusion research showing an existence of the nuclear transmutation, i.e. generation of new isotopic species or new elements in the experimental system. The nuclear transmutation has been difficult to understand in conventional physics, but if we take an assumption that the trapped thermal neutrons exist in the sample (TNCF model[1,6]), it is possible to analyze consistently and quantitatively in an accuracy of one or two orders of magnitude. In this paper we will give results of analysis on the various experimental results of the nuclear transmutation.

2. Theoretical Basis of the Analysis

If we take an assumption that the thermal neutron exists in the sample, the following reactions would be expected:

$$n + {}^{A}_{Z}\mathrm{M} = {}^{A+1}_{Z}\mathrm{M}, \tag{1}$$

$${}^{A+1}_{Z}\mathrm{M} = {}^{A+1}_{Z+1}\mathrm{M}' + e^- + \bar{\nu}_e, \tag{2}$$

$$n + {}^{A+1}_{Z}\mathrm{M} = {}^{A+2}_{Z}\mathrm{M}, \tag{3}$$

$${}^{A+2}_{Z}\mathrm{M} = {}^{A+2}_{Z+1}\mathrm{M}' + e^- + \bar{\nu}_e, \tag{4}$$

$$n + {}^{A+1}_{Z+1}\mathrm{M}' = {}^{A+2}_{Z+1}\mathrm{M}', \tag{5}$$

$${}^{A+2}_{Z+1}\mathrm{M}' = {}^{A+2}_{Z+2}\mathrm{M}'' + e^- + \bar{\nu}_e. \tag{6}$$

These reaction formulas begin with a thermal neutron and a nucleus ${}^{A}_{Z}\mathrm{M}$, where ${}^{A}_{Z}\mathrm{M}$ is a nucleus of the sample materials or a minor elements with mass number A and atomic number Z.

The number $d\nu_1(t)$ of the reaction (1) occurring in a short time duration dt at time t is expressed as follows:

$$d\nu_1(t) = 0.35 n_n v_n \rho_0(t) \sigma_1 dt. \quad (7)$$

Where $\rho_0(t)$ is the density of ${}^{A}_{Z}M$, n_n and v_n are the density and the thermal velocity of the trapped thermal neutron and σ_1 is the absorption cross section of the thermal neutron by the nucleus ${}^{A}_{Z}M$. And there is a following relation between $\nu_1(t)$ and $\rho_0(t)$;

$$\rho_0(t) = \rho_0 - \nu_1(t), \quad (8)$$

where ρ_0 is the density of ${}^{A}_{Z}M$ at $t = 0$. From the equation (8) and an integration of the equation (7) with time t, we obtain a relation,

$$\rho_0(t) = \rho_0 e^{-0.35 n_n v_n \sigma_1 t}. \quad (9)$$

So the density $\rho_1(t)$ of the nucleus ${}^{A+1}_{Z}M$ is expressed as follows:

$$\rho_1(t) = \rho_0(1 - e^{-0.35 n_n v_n \sigma_1 t}). \quad (10)$$

Next, in the reaction (3), the number $d\nu_3$ of the reaction (3) in a short time duration dt is given as

$$d\nu_3 = d\rho_3(t) = C\rho_1(t)\sigma_3 dt, \quad (11)$$

where $\rho_3(t)$ is a density of ${}^{A+2}_{Z}M$. In this reaction, the density $\rho_1(t)$ of the nucleus ${}^{A+1}_{Z}M$ changes as follows by the reaction (3):

$$\rho_1(t) = \rho_0(1 - e^{-C\sigma_1}) - \rho_3(t). \quad (12)$$

In these equations C is $0.35 n_n v_n$ and σ_3 is the absorption cross section of the thermal neutron by the nucleus ${}^{A+1}_{Z}M$.

Similarly, we obtain the density $\rho_3(t)$ of the nucleus ${}^{A+2}_{Z}M$:

$$\rho_3(t) = \rho_0[(1 - e^{-C\sigma_3 t}) - \frac{\sigma_3}{\sigma_3 - \sigma_1} \times (e^{-C\sigma_1 t} - e^{-C\sigma_3 t})]. \quad (13)$$

When the half life times of ${}^{A+1}_{Z}M$, ${}^{A+2}_{Z}M$ and ${}^{A+2}_{Z+1}M'$ in the reactions (2), (4) and (6) are very short, the number of β decay to ${}^{A+1}_{Z+1}M'$, ${}^{A+2}_{Z+1}M'$ and ${}^{A+2}_{Z+2}M''$ are equal to ν_1, ν_3 and ν_3. respectively, and densities of them are $\rho_1(t)$, $\rho_3(t)$ and $\rho_3(t)$.

3. Experimental Results and Analysis of the Data

Here we take up some experimental results and investigate them using the method explained above.

1) I.B. Savvatimova et al.[2].

In the glow discharge experiments with D_2 gas (and other gases) and Pd cathode (and other transition metal cathodes), they measured the excess heat and nuclear transmutation of various isotopes and elements with multi-layer cathode. After the discharge of 4 hours,

the sample was sent to mass spectrometry (SIMS) and was analyzed its isotope composition there about 3 ~ 6 months later. Here we take up two data.

1 - a) Decrease of ^{32}S

They detected a decrease of $^{32}_{16}S$ from 7 to 2 ~ 3 ppm through the glow discharge with D_2 gas using Pd cathode. We can assume that the density of $^{32}_{16}S$ was changed by the reaction (1) only, because $^{31}_{16}S$ is not exist (half life is 2.61s), and that $^{31}_{15}P$ was not exist in the Pd cathode. From the equation (9), we get a density of the trapped thermal neutron n_n as 2.2 $\times$ 10^{12} cm^{-3} using the values of the average speed of the thermal neutron $v = 2.2 \times 10^5$ cm/s, the absorption cross section $\sigma_1 = 0.53$ barn of n for $^{32}_{16}S$ and a duration of experiment $t = 10^7$s ($\simeq$ 4 month).

1 - b) Change of Isotopic Composition of Zr

Before the experiment, few $^{90}_{40}Zr$ and $^{91}_{40}Zr$ existed in Pd cathode, but after experiment they increased with a ratio of $^{90}_{40}Zr$: $^{91}_{40}Zr$ = 57 : 34 (in contrast with 51 : 11 by natural abundance). From the nuclear data, $^{89}_{40}Zr$ is unstable and natural abundance of $^{89}_{39}Y$ is 100 % , i.e. other Y is unstable. So, we can take there was a few $^{89}_{39}Y$ in the Pd cathode and following reactions would occurred:

$$n + {}^{89}_{39}Y = {}^{90}_{39}Y,$$

$${}^{90}_{39}Y = {}^{90}_{40}Zr + e^- + \tilde{\nu}_e,$$

$$n + {}^{90}_{40}Zr = {}^{91}_{40}Zr.$$

The absorption cross sections of neutron for $^{89}_{39}Y$ and $^{90}_{40}Zr$ are 1.0×10^{-3} and 5.0×10^{-2} barns, respectively. From the equations (12) and (13) and a relation $\rho_1(t) : \rho_3(t) = 57 : 34$, a density of the trapped thermal neutron was calculated as 2.6×10^{13} cm^{-3}.

2) V.A. Romodanov et al.[3].

Romodanov et al. measured a lot of tritium with cylindrical Mo cathode in a glow discharge with D_2 gas. The pressure of the gas was 1 atm in the cylinder and 0.2 atm outside. With a cylindrical cathode of 2.5 cmϕ $\times$ 10 cm with thickness of 5 mm, they measured tritium production of 10^7 s^{-1}. In this case, the temperature of the cathode was very high (up to 3000°C) and we may assume that following reaction would occurred in the whole volume of cathode material:

$$n + d = t\ (6.98\text{kev}) + \gamma\ (6.25\text{Mev}).$$

The fusion cross section of d for n is ~ 5.5×10^{-4} barns and a rate of tritium generation is 10^6 cm^{-3} s^{-1}. The number of the reaction can be expressed by the equation (9). Putting into the formula values obtained or determined in the experiment, we obtain a relation between n_n and n_d ;

$$n_n n_d \sim 3 \times 10^{27} \quad cm^{-6},$$

where n_d is the density of deuteron. If we assume for the average density of deuterium in the sample $n_d = 10^{20}$ cm^{-3} (10^{18}), then we have the density of the trapped thermal neutron $n_n \sim 3 \times 10^7$ cm^{-3} (3×10^9).

3) M. Okamoto et al.[4].

In an experiment in the series of works on Pd/D + LiOD system conducted hitherto, they determined distributions of Pd, D, Li, Al, and Si atoms in the Pd cathode. As we can see in these figures in Fig.1, densities of those elements changed drastically at near surface of a width $\sim$ 1 μm. Especially, Al decreased to $\sim$ 20 % of the original value and Si increased. We assume following reactions would occurred:

$$n + {}^{27}_{13}\mathrm{Al} = {}^{28}_{13}\mathrm{Al},$$

$${}^{28}_{13}\mathrm{Al} = {}^{28}_{14}\mathrm{Si} + e^- + \bar{\nu}_e,$$

because natural abundance of ${}^{27}_{13}$Al is 100 % and ${}^{28}_{13}$Al is unstable for β decay (half life time is 2.27 m). From the equation (9), we obtain a density of the trapped thermal neutron n_n as 4.9×10^{13} cm^{-3} with the values of the absorption cross section $\sigma_1 = 0.23$ barn of n for ${}^{27}_{13}$Al and a duration of experiment $t = 1.87 \times 10^6$ s.

4) Biotransmutation[5].

Finally we take up the Biotransmutation. From page 25 of kushi's book[5], the elemental transmutation in biological system is considered as " $\sim$ most likely taking place at the cellular level $\sim$ ", and " $\sim$ it was concluded that granted the existence of transmutation $\sim$ ". We investigate three transmutations observed in the biological system Na to Mg, P to S and Mn to Fe.

If we take the same assumption as above that the thermal neutron exist in a living body, we can assume that there occurs following reactions:

$$n + {}^{23}_{11}\mathrm{Na} = {}^{24}_{11}\mathrm{Na} = {}^{24}_{12}\mathrm{Mg} + e^- + \bar{\nu}_e,$$

$$n + {}^{31}_{15}\mathrm{P} = {}^{32}_{15}\mathrm{P} = {}^{32}_{16}\mathrm{S} + e^- + \bar{\nu}_e,$$

$$n + {}^{55}_{25}\mathrm{Mn} = {}^{56}_{25}\mathrm{Mn} = {}^{56}_{26}\mathrm{Fe} + e^- + \bar{\nu}_e,$$

where natural abundance of ${}^{23}_{11}$Na, ${}^{31}_{15}$P and ${}^{55}_{25}$Mn are all 100 % , and all intermediate nuclei produced from them (${}^{24}_{11}$Na, ${}^{32}_{15}$P and ${}^{56}_{25}$Mn) are unstable for β decay. Furthermore, we know the absorption cross sections of ${}^{23}_{11}$Na, ${}^{31}_{15}$P and ${}^{55}_{25}$Mn for thermal neutron are 0.534, 2.2 and 13.3 barn, respectively from data of nuclides. Comparing with the values of the absorption cross section used in the other analyses in this paper, we can recognize that these values are fairly large.

Therefore, if such elements as Na, P and Mn are in a living body with a lot of trapped neutron, it is possible to expect there occurs nuclear transmutations to Mg, S and Fe.

4. Conclusion

We took simple assumptions to investigate the experimental results that there were trapped thermal neutrons with the constance density n_n in the sample and they react with hydrogen isotope in the sample or minor elements, then we can determine the density n_n. The estimated values from other analyses[6] were in a range of $n_n = 10^3 \sim 10^{12}$ cm^{-3}. The results suggest that the TNCF model is one of the most realistic theory. The other three papers[6~8] given in this conference will help to understand the physics of the cold fusion.

Transmutation

References

(1) H. Kozima, "Trapped Neutron Catalyzed Fusion of Deuterons and Protons in Inhomogeneous", *Trans. FusionTechnol.* **24**, 508 (1994).
(2) I.B. Savvatimova, Ya.R. Kucherov, A.B. Karabut, "Cathode Material Change after Deuterium Glow Discharge Experiments", *Trans. FusionTechnol.* **26**, 389 (1994).
(3) V.A. Romodanov, V.I. Savin and Ya.B. Skuratnik, "The Demands to System Plasuma-Target for Obtaining a Balance Energy from Nuclear Reactions in Condensed Media", *Proc. RCCFNT2* (Sept. 1994, Sochi, RUSSIA), 99 (1995).
(4) M. Okamoto, H. Ogawa, Y. Yoshinaga, T. Kusunoki O. Odawara, "Behavior of Key Elements in Pd for the Solid State Nuclear Phenomena Occurred in Heavy Water Electrolysis" *proc. ICCF4*, **3**, 14 (1995).
(5) "Energy Development from Elemental Transmutations in Biological System", U.S. Army Material Technology Laboratory, 1978.
(6) H. Kozima, "On the Existence of the Trapped Thermal Neutron in Cold Fusion Materials" *Proc. ICCF6* (to be published).
(7) H. Kozima, K. Hiroe, M. Nomura, M. Ohta, "Analysis of the Electrolytic Cold Fusion Experiments on TNCF Model" *Proc. ICCF6* (to be published).
(8) H. Kozima, M. Ohta, M. Nomura, K. Hiroe, "Analyses of the Nickel-Hydrogen Isotope System on TNCF Model" *Proc. ICCF6* (to be published).

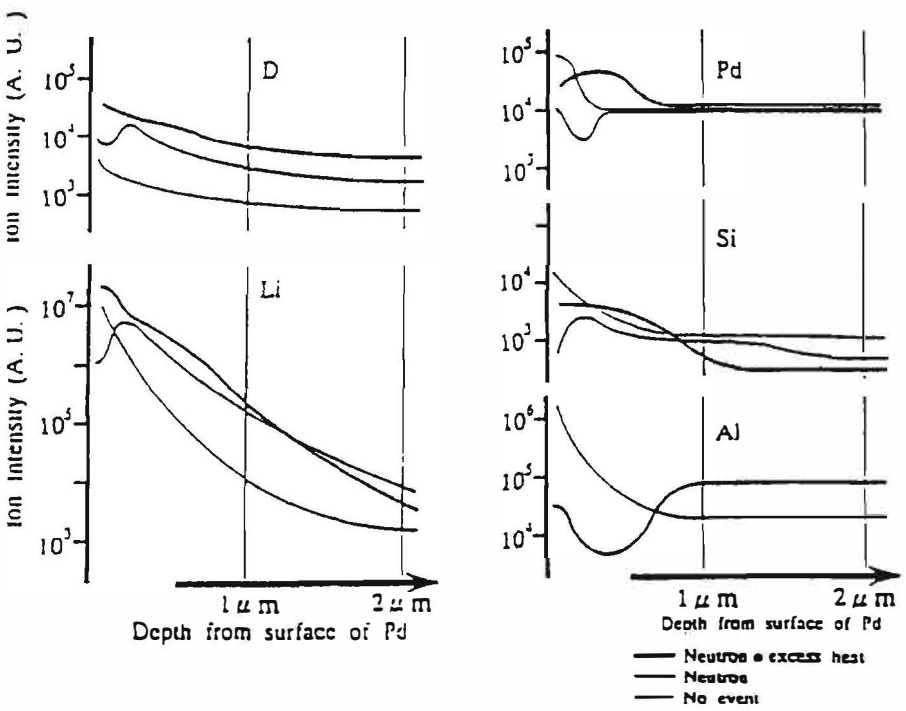

Fig.1 Examples of Depth Profiles for Each Element

Transmutation

ISOTOPIC DISTRIBUTION FOR THE ELEMENTS EVOLVED IN PALLADIUM CATHODE AFTER ELECTROLYSIS IN D_2O SOLUTION

T. Mizuno, T.Ohmori*, T.Akimoto, K.Kurokawa, M.Kitaichi,
K.Inoda, K.Azumi, S.Simokawa and M. Enyo**

Department of Nuclear Engineering, Faculty of Engineering, Hokkaido University, Kita-ku, North 13, West 8, Sapporo, 060 JAPAN,
*: Catalysis Research Center, Hokkaido University, Kita-ku, North 11, West 10, Sapporo, 060, JAPAN,
**: Hakodate National College of Technology, Tokura-cho 14-1, Hakodate, 042, JAPAN,

Abstract

It was confirmed by several analytic methods that reaction products with mass number ranging from 1 to 208 are deposited on palladium cathodes subjected to electrolysis in a heavy water solution at high pressure, high temperature, and high current density for one month. These masses were composed with many elements ranged from hydrogen and lead. Isotopic distributions for the produced elements were radically different from the natural ones.

1. Introduction

Many claimed that if nuclear reactions have been induced by electrochemical reaction occurring in solid electrodes, there must be clear evidence such as the evolution of radioisotopes and radiation. Moreover, the evolution rates of the reaction products should be quantitatively explained in terms of the proper nuclear reaction mechanisms. But such the claim could be held if the reaction mechanism had been consisted by proper theories. However, there is no proof that the conventional mechanism holds the reactions. It is difficult to detect the emission of the radiation and radioisotope if the mechanism was different from the proper ones. In this work, evidence which indicates the occurrence of some nuclear reactions is presented, in the form of isotopic changed elements in and on the cathode surface. These products have been obtained with a mechanism which had not

induced any detectable radiations. The anomalous isotopic distribution of these elements shows they do not come from contamination. We represent that the reaction mechanism was completely different from the proper nuclei formation process. However, we attempt to explain the process which produced these anomalous products by the mechanism within the framework of the proper theory(1).

2. Experimental

The experimental details for the sample, cell and electrolysis conditions have been described elsewhere(2). The sample electrodes were supplied to element detection after pull off the Teflon coat, washed by the Mill Q water for energy dispersive X-ray spectroscopy (EDX), Auger electron spectroscopy (AES), secondary ion mass spectroscopy (SIMS) and electron probe microanalyzer (EPMA).

3. Results

Many elements have deposited on the surface and distributed irregularly; these concentrations were changed with samples. The elements that have commonly been detected were C, O, S, Cl, Si, Ca, Ti, Cr, Mn, Fe, Co, Ni, Cu, Zn, Mo, Pd, Sn, Pt, Hg and Pb for all the samples. The amounts for Ca, Ti, Cr, Cu, Pt, Hg and Pb were abundantly existing and differed more than 3 times at the surface place compared with C, Cl, Si, Mn, Co, Ni, Zn and Sn which were existing rather uniformly. These changeable elements were also fluctuating with sample lot as 3 times deviations. It meaning that the uncontrollable factors such as surface conditions are the main importance for the reaction.

Several elements were detected in the Pd electrode by the EDX method; the measurements were taken to know the rough concentration for the elements because in the SIMS measurement the mass peaks have a possibility to contain other molecular peaks. Figure 1 shows typical results before and after electrolysis. Several peaks of Pt, Cr and Fe are clearly seen; these amounts were comparably with Pd bulk peak. And less amounts for Sn, Ti, Cu and Pb elements were also

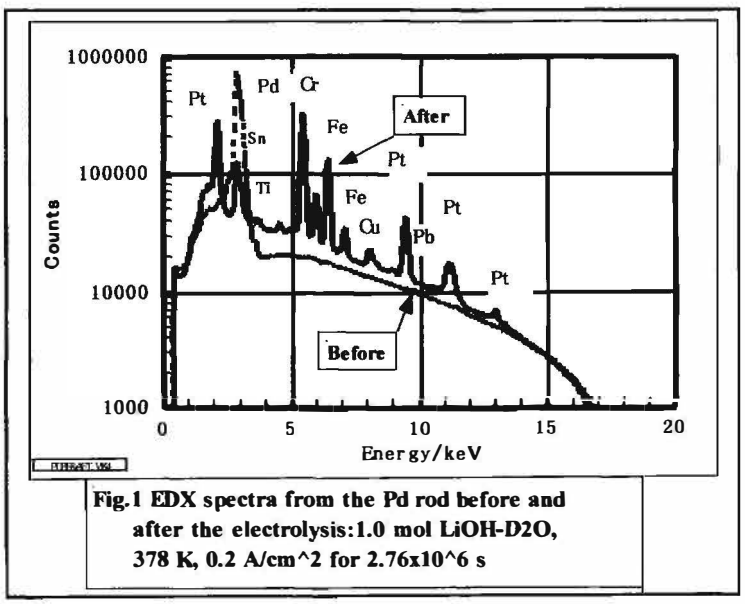

Fig.1 EDX spectra from the Pd rod before and after the electrolysis:1.0 mol LiOH-D2O, 378 K, 0.2 A/cm^2 for 2.76x10^6 s

clearly observed. The EDX analyses were repeated on various place of the sample; the deviation for the EDX counts sometimes reached to 10 times with the place. This change was depending on the scanning area. The amounts for the evolved elements were finally estimated by SIMS measurement. The EDX, AES and EPMA methods were complimentary used to correspond a mass Spectra to a certain atom and decide their isotopic distributions. The procedure is described as follows: (1); the mass number were decided in the first from light mass number. (2); the mass number were adjusted with the EDX and AES spectra. (3) the large count number of mass peaks was confirmed to existence of their molecular ion and oxide ion peaks. (4) the final mass spectra were estimated by multiplying the factors of counting correction to the original count of mass. The factor shows very high and low value at the inert gases and alkali metals respectively.

The ratios of atomic number for the mass were finally estimated with the procedures. The ratios were shown in fig.2 normalized with the total mass set as one. Typical counts by EDX and SIMS ranged from 10^2 to 10^6 and were 10 to 100 times higher than the background counts. Thus, the presence of Ca, Ti, Cr, Mn, Fe, Co, Cu, Zn, Cd, Sn, Pt and Pb was clearly confirmed. These elements are mostly grouped in four ranges of mass number:lightest elements under 50 mass number,light elements from 50 to 80;middle elements 100 to 140; and heavy elements from 180 to 208. The ratio of the mass number from 102 to 110 which correspond with Pd atom is under 1% of total even if it was bulk substance; the large ratio of existence for Oxygen and Xenon pull down their values. The reason for these high ratio can be considered that the many gas atoms may be released and succeeding contributes to the counting rate from the spot place heated up by ion bombardment.

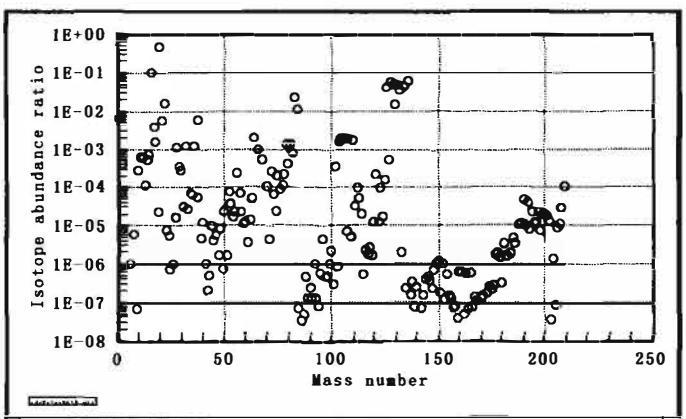

Fig.2 Count rates for Pd electrode electrolyzed in the heavy water solution observed by SIMS measurement.

The SIMS analysis showed other elements; As, Ga, Sb, Te, I, Hf, Re, Ir, Br and Xe. These elements, except Xe, were difficultly detected by AES and EDX because the peaks were very close and sometime overlapped with others and these were lower than the detection limits by the measurements. Xe atoms are naturally difficult to detect by EDX method because the such the gas atoms are easily escaped by ion bombardment from the spot area. The SIMS count numbers ranged from 10^3 to 10^6 where the background counts were as low as ~10, so we have confidence in these results. In Figure 2 we show the peak intensities normalized with the total peak. The intensity of Xe was 10 times larger than Pd; it may be that the gas was released by bombarding with O_2^- ions which

caused a temperature rise at the sample.

We have no peak except Pd been observed after pre-electrolysis Pd surfaces. Pt a Pd concentrations in the electrolyte after experiment were 10 and 15 ppm respectively by atomic absorption measurement and no other elements excepts for Li was observed. Total amount for the elements existed in one micro meter depth of Pd surface were calculated as follows; C: 0.37, S: 0.67, Ca: 0.55, Ti: 0.86, Cr: 7.0, Mn: 0.005, Fe: 0.17, Co: 0.0057, Ni: 0.0157, Cu: 0.026, Zn: 0.80, Mo: 0.005, Pd: 4.77, Cd: 0.105, Sn: 0.069, Pt: 0.025, Hg: 0.0375 and Pb: 0.021 atomic percentage. (The total deposited elements on the Pd and the calculated summation for the impurity in the electrolyte and Pd samples are less one and mere order than depositions.) Here, the total impurities except Ca are less than the deposition amounts; especially, Mn, Ti, Cd and Hg were not existing as the impurity.

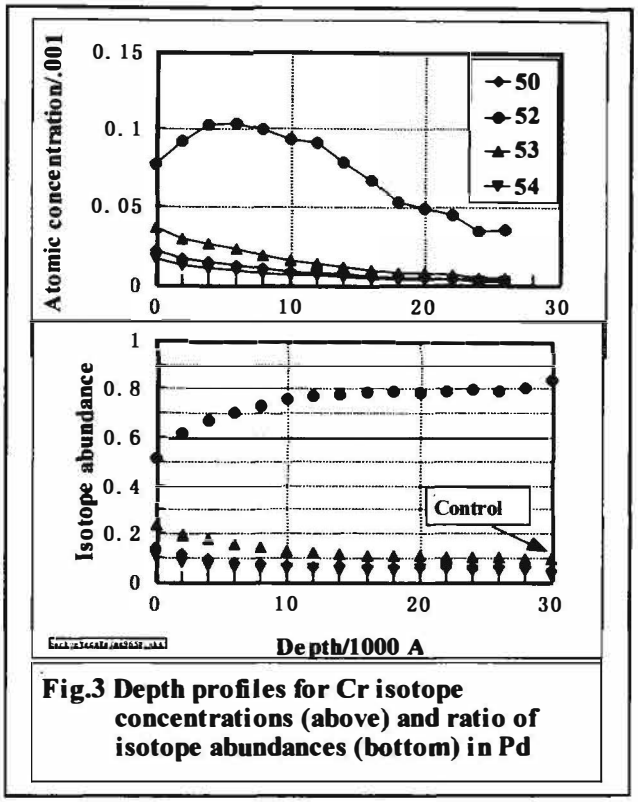

Fig.3 Depth profiles for Cr isotope concentrations (above) and ratio of isotope abundances (bottom) in Pd

Large differences in isotopic distributions compared with the natural distributions were observed by the SIMS method for Cr, Cu, Zn, Br, Xe, Pd, Cd, Hf, Re, Pt, Ir, Pb and Hg. The typical concentrations and their ratios for Chromium isotopes are shown in Fig.3 for an example; the concentrations except Cr52 decreased exponentially with depth but Cr52 has a peak at 0.5 micro meters and they showed largely shift in isotopic ratios: However, we can see large deviations for isotopic existence with natural ones, that means, these are higher than Cr52, i.e., Cr52 is less than others, in the figure where the natural isotope existence is plotted at the three micro meter depth positions. These isotopic distribution changes occurred mainly within the layer of most outer surfaces in one micro meter and their ratios approached into normal values toward the inner bulk layer. In Figure 4, for Pd is shown to have large shifts in abundances. Their concentrations are represented with the ratio to Pd106 which exists in natural as most abundant. Their atomic concentration increased with depth. This means the concentration of other deposition relatively decreased. Especially, amounts of Pd104 and 110 are higher value than the natural ones that values are shown at three micro meters depth in the figure.

4. Discussion

It can hardly be imagined that all of the elements found were impurities in electrolyte, electrode or cell. Even if we suppose that all impurities in the system accumulated in the cathode, the amount would be 10 to 100 times smaller than the total amount we detected. Furthermore, it is simple impossible to explain the shifts in the isotopic distribution. Therefore, it must be concluded that some novel reactions occurred, resulting in the reactants which were found abundant in the electrolyte and electrode material. We assume the cathode palladium was the starting material for these reactions, but it is possible that impurities and other cell components such as Li, D_2O, Pd, Pt, K, Na, Ca, B, C, Ag and Fe may have provided the starting material for the nuclear reactions. It must be admitted that these reactions have no solid, detailed theoretical basis yet, but in broad terms this can explain most of the elements which were observed. One may also imagine that as such transmutation reactions were presumably taking place during the electrochemical process, they are likely to be connected with other phenomena such as hydrogen embrittlement and local corrosion.

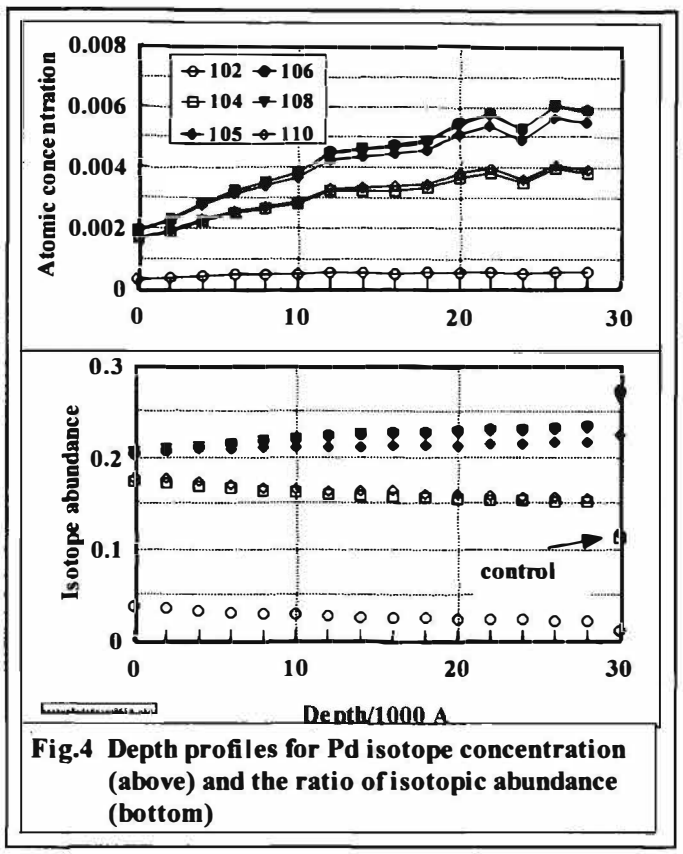

Fig.4 Depth profiles for Pd isotope concentration (above) and the ratio of isotopic abundance (bottom)

5. References

1. Tadahiko Mizuno, Tadayoshi Ohmori, Kazuya Kurokawa, Tadashi Akimoto, Masatoshi Kitaich, Koich Inoda, Kazuhisa Azumi, shigezo Shimokawa and Michio Enyo "Anomalous Isotopic Distribution of Elements Deposited on Palladium Induced by Cathodic Electrolysis", Denki Kagaku 64, No.11 (1996)

2. Tadahiko Mizuno, Tadashi Akimoto, Kazuhisa Azumi and Michio Enyo, "Diffusion Rate of Deuterium in Pd during Cathodic Charging", Denki Kagaku 60, no.5, 405 (1992)

Transmutation

PRODUCTION OF HEAVY METAL ELEMENTS AND THE ANOMALOUS SURFACE STRUCTURE OF THE ELECTRODE PRODUCED DURING THE LIGHT WATER ELECTROLYSIS ON Au ELECTRODE

T. OHMORI*, T. MIZUNO** and M. ENYO***

* Catalysis Research Center, Hokkaido University,
Kitaku Sapporo 060, JAPAN
** Faculty of Engineering, Hokkaido University
Kitaku Sapporo 060, JAPAN
*** Hakodate National College of Technology
Tokuracho Hakodate 042, JAPAN

ABSTRACT

Some 100 μ g of fine black porous powders were deposited at the bottom of the electrolytic cell during the electrolysis on Au electrodes for 20-30 days at current densities above 200 mA/cm^2. The main constituting elements of the deposits were Hg, Pt, Os, Fe Si and F other than Au. The isotopic distributions of Hg, Fe and Si containing in the deposits were evidently different from their natural ones. In addition, a lot of micro craters which are allowed to imagine the occurrence of some micro explosion were created on Au electrode surface during the electrolysis.

INTRODUCTION

In the previous study, we found that some 10 μ g of Fe, whose isotopic distribution was clearly different from its natural isotopic abundance, was formed on/in Au electrode during the electrolysis for 7 days at a current density of 100 mA/cm^2. In addition, there was a linear relationship between the amount of Fe and excess heat observed simultaneously [1-2]. This suggests strongly that Fe was produced by some nuclear transmutation. In the present study, we investigated whether there exist some elements other than Fe produced as a result of nuclear transmutation by noting the deposits obtained in the present electrolysis conducted at high current densities.

EXPERIMENTAL

The electrolytic cell was made of fused quiartz. The working electrodes were cold worked Au plates (2.0 cm^2 app. area; 0.1 mm thick; 99.99 % purity; Ag: 21 ppm, Pd: 3 ppm, Cu: 1 ppm, Fe, Si, Rh, Pt: < 1 ppm, no detectable for Hg, Os and Zn), whose surfaces were scraped with a cleaned glass fragment. The roughness factor of the electrode was around 2.0. The counter electrode was a 1 x 7 cm, 80 mesh Pt gauze (99.98 % purity; Rh: 18 ppm, Pd, Cr, Si: 2 ppm, no detectable for Hg, Os and Zn). The electrolytes used were Na_2SO_4 and Na_2CO_3 from Merck (sprapur grade; Fe, Zn: < 0.01 ppm, no detectable for Si, Hg, Os and F for Na_2SO_4; Si: < 0.5 ppm, Fe, Hg: < 0.05 ppm, Zn: < 0.01 ppm, no detectable for Os and F for Na_2CO_3). The volume of the electrolyte

solution was 100 ml and the concentration was adjusted to 0.5 M. The electrolysis was carried out at a constant current ranging from 1 to 3 A. During the electrolysis, Milli-Q water was supplied every 24 hours to maintain the total solution amount constant. The deposits obtained were washed with Milli-Q water and placed on Ni or Zr plates and the constituent elements of the deposits were analyzed by means of SIMS, AES, EPMA and EDX.

RESULTS AND DISCUSSION

Analysis of the deposits

The deposits were very porous with a lot of fine pores of nm order, look like pumices. Maximal constituent element of the deposits was Au, besides, considerable amounts of Hg, Pt, Os, Fe, Si, and F were contained. The yield of Si was increased significantly when electrolyzed in Na_2SO_4 at a high current density. The contents of Fe and F were increased in Na_2CO_3. Os was detected mainly in Na_2CO_3 at a high current density.

As a typical example, we show EPMA images of the deposits obtained after the electrolysis in Na_2SO_4 for 30 days at a current density of 800 mA/cm^2 in Fig. 1. As seen, in this case, fairly clear Hg, Pt and Os images were observed together with the strongest Au image. Fe image was also observed although it was a little weaker in this case than those of above elements. The fact that the major component of the deposits was Au suggests strongly that the deposits were produced at the Au electrode.

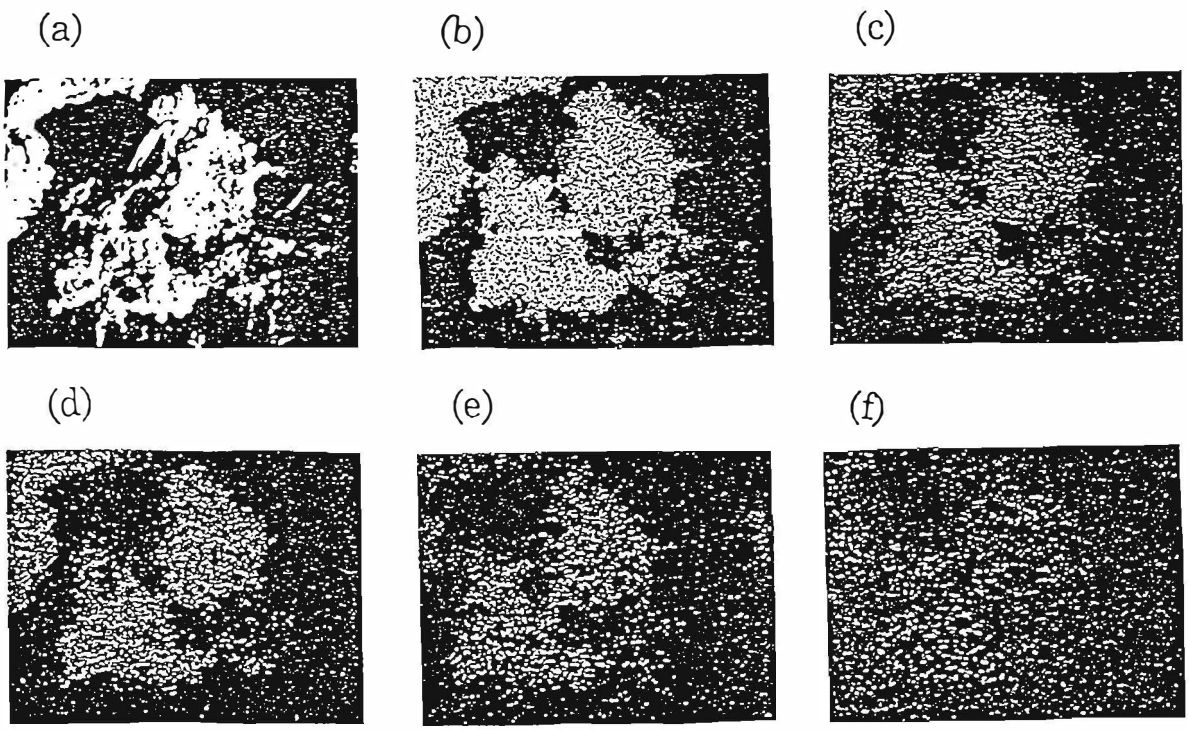

Figure 1. EPMA images of elements containing in the deposits. SEM image of the deposits (x 6,700) (a), EPMA images of Au (b), Hg (c), Pt (d), Os (e) and Fe (f). Wavelength of the specific X rays are 1.276, 1.241, 1.313, 3.163 and 1.937 Å for Au, Hg, Pt, Os and Fe, respectively.

Transmutation

Isotopic abundance

The isotopic distributions of Hg , Fe and Si containing in the deposits obtained by SIMS analysis are shown in Figs 2 - 4, respectively, over the scan range up to 15. The data of Hg and Fe were obtained in Na_2CO_3 and the datum of Si was obtained in Na_2SO_4 at a current density of 800 mA . The isotopic distributions of these elements reveal significant deviation from their natural isotopic abundance. Thus for Hg, Fig. 2, the isotopic content of ^{200}Hg is 35-50 %, evidently higher than its natural isotopic abundance of 23.13 %, while the content of ^{202}Hg, which being the major component in the nature, is reduced down to 15-20 % from its natural value of 29.8 %. The components of other isotopes change to some extent.

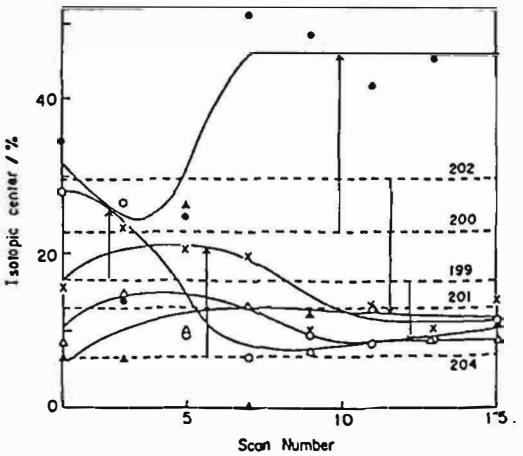

Figure 2. Isotopic distribution of Hg present in the deposits ranging from 1 to 15 scans. (○) : ^{199}Hg, (●): ^{200}Hg, (△): ^{201}Hg, (▲) : ^{202}Hg, (×): ^{204}Hg. Dashed lines mean individual natural isotopic abundance.

For Fe, Fig. 3, the content of ^{57}Fe drastically increases as in the case of Fe produced on/in Au electrode during the electrolysis at a current density of 100 mA/cm^2 [1-2], however, in this case, its ratio becomes much higher, exceeding 50 % particularly in the vicinity of the surface of the deposits. The ratio of ^{57}Fe has a tendency to decrease gradually with increasing the depth.

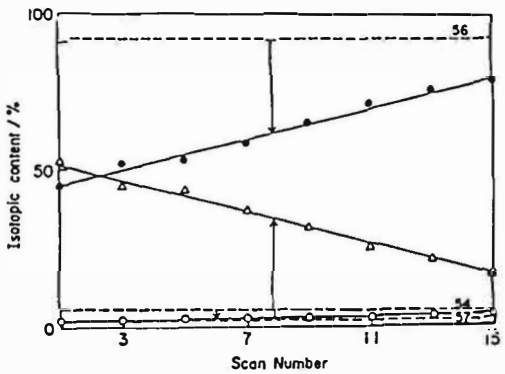

Figure 3. Isotopic distribution of Fe present in the deposits ranging from 1 to 15 scans. (○): ^{56}Fe, (●) ^{57}Fe.

As mentioned already, the content of Si in the deposits markedly increased when electrolyzed in Na_2SO_4 at a large current density (eg. 800 mA/cm^2), and, in this case, the color of the deposits turns white gray. From EDX measurement the major component was found to be Si, besides Au, Pt, Hg were also included. The isotopic content of ^{28}Si decreased down to ca. 58 % from its natural value of 92.2 % in the vicinity of the surface of the deposits.

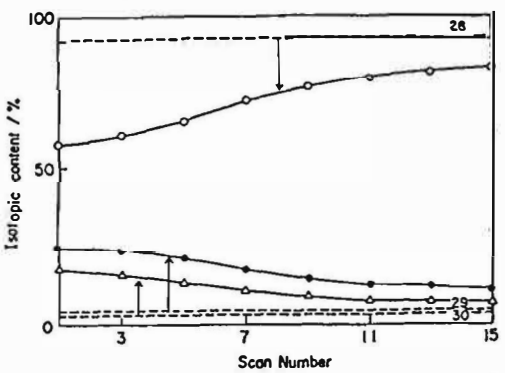

Figure 4. Isotopic distribution of Si present in the deposits ranging from 1 to 15 scans. (○): ^{28}Si, (●): ^{29}Si, (△): ^{30}Si.

On the contrary, the content of ^{29}Si and ^{30}Si increased. The extent of the decrease in the content of ^{28}Si of the deposits obtained by the electrolysis in Na_2CO_3 at a current density of 500 mA/cm^2 is somewhat smaller, the content is 70-75 % in the vicinity of the surface. These results show that ^{29}Si and ^{30}Si are produced preferentially by the electrolysis in Na_2SO_4 at a large current density. As have reported already, the isotopic distribution of Si present on/in Au electrode after the electrolysis in Na_2SO_4 at a current

density of 100 mA/cm^2 agreed closely with natural isotopic abundance [2], and, in the present experiment, the isotopic distribution of Si present on/in the Au electrode after the electrolysis in Na_2CO_3 at a current density of 500 mA/cm^2 was also in accord with its natural isotopic abundance. Such Si is considered to be the one of glass powder remained in the Au electrode after scraping. Hence, there would be no doubt that ^{29}Si and ^{30}Si were produced at Au electrode by some nuclear reaction occurring when the deposits were produced.

.Surface structure of Au electrode

The electrode surface after the electrolysis showed very anomalous structure. Fig. 5 shows the SEM images of the Au electrode surface after the electrolysis in Na_2CO_3 for 30 days at a current density of 500 mA/cm^2. A lot of craters with various sizes are created and developed along the scraped edge lines of the electrode surface (c,d). Each crater has a deep hole, looks like volcano. The size of the largest crater reaches ca. 20 μ m diam. and 30 μ m height (a,b). From the appearance of the craters, one can imagine that some micro explosion took place at that place. The outside walls of the craters consist of very fine porous substances, which are very alike to the structure of the deposits. In addition, the major element of the deposits is Au. Hence, there would be no doubt that the deposits were spewed out from these craters as the ashes as a result of some micro explosion, probably caused by some nuclear reactions.

The walls inside the craters are constituted by fine hexagonal crystallites which are assignable Au(111) (e,f). These crystallites may be considered to be produced by the reconstruction of Au polycrystals of the electrode material owing to the intense heat evolved locally resulting from the micro explosion. The amounts of Hg and Pt present on/in Au electrode after the electrolysis determined by SIMS were much smaller than those present in the deposits in every cases. Perhaps, O^+ irradiation of SIMS was not pin-pointed at the wall of the craters precisely.

Possible reactions

The amount of deposits obtained during the electrolysis was 0.5 - 1 mg. The content of Hg, Pt and Os in the deposit can be estimated at least at several percents from the results of EPMA measurement, from which the total amounts of Hg, Pt and Os produced yield at least some 10 μ g. On the other hand, even in 100 ml of the electrolyte solution of 0.5 M Na_2CO_3 containing 0.05 ppm of Hg as impurity, the amount of Hg which must be contained in the deposits as impurity would be at most 0.35 μ g. In addition, Os and F are completely free in the electrolysis system used. The deviation of the isotopic distribution of Hg, Fe and Si suggests that these elements were not mixed in the deposits as impurities but produced as a result of some nuclear transmutations. Hence, at least, Hg, Os, Fe, Si and F can be considered to be the products of the nuclear transmutation reaction

Although the reaction scheme of the nuclear transmutations is still ambiguous, we consider at the present stage that the reactions start by the following fusion reaction, $^{197}Au + n^1H \rightarrow {}^{198\text{-}204}Hg$. The Hg atoms thus produced would have very high nuclear energies, being unstable, splitting partly to produce Pt, Os and Fe. Si and F would be produced as a result of the split of Fe occurring successively.

It is very mysterious why such transmutations take place in Au electrode by the light water electrolysis at a room temperature. It is known that there are small amount of H

active sites on Au where the hydrogen evolution reaction occurs exclusively by slow recombination reaction [3-5]. Therefore, at that place where such sites are concentrated (perhaps, it corresponds to the lattice defect), the concentration of H would remarkably increase with increasing hydrogen overpotential, and, in addition, a considerable amount

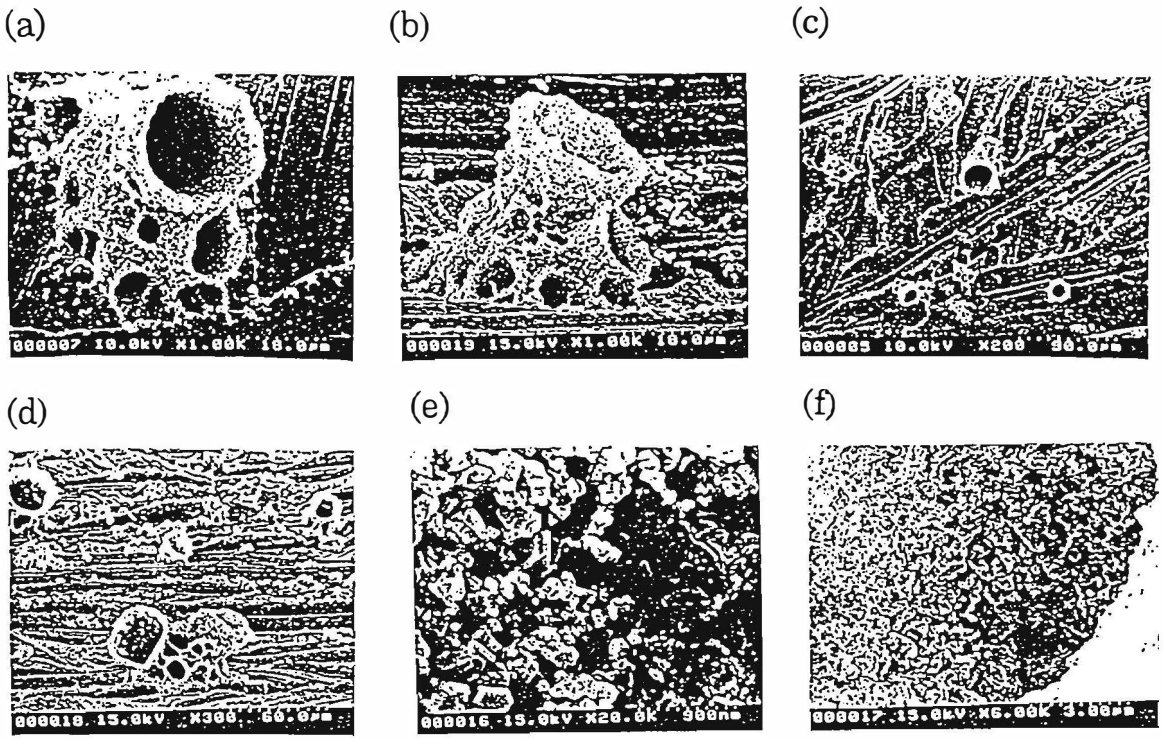

Figure 5. SEM images of the craters formed on Au electrode after the electrolysis in 0.5 M Na_2CO_3 for 30 days at a current density of 500 mA/cm². External views of the craters: (a)～(d), internal views of the crater: (e)～(f).

of micro cracks would be created with high loading of H. As a result of this, extremely strong electric field would be formed. Under such a condition, some H atoms would have a chance to acquire extremely high kinetic energy and become accessible to Au nuclei enough to cause the nuclear transmutation reaction even instantaneously.

Of course, our concepts concerning the reaction scheme are far from the completion. Nevertheless there is hardly any doubt that the nuclear transmutation reaction occurs in the electrolysis systems to produce Hg, Os, Fe, Si, F, etc. from the experimental results obtained here. To elucidate this problem, more extensive research would be necessary.

REFERENCES

1) T. Ohmori and M. Enyo, J. New Energy, 1, 15 (1996).
2) T. Ohmori, M. Enyo, T. Mizuno, Y.Nodasaka and H. Minagawa, Fusion Technology, (1996) in press.
3) T. Ohmori and M. Enyo, Electrochimica Acta, 37, 2021 (1992).
4) S. Schuldiner and J.P. Hoare, J. Phys. Chem., 61, 705 (1957).
5) A.T. Kuhn and M. Byrne, Electrochimica Acta, 16, 391 (1971).

Transmutation

Nuclear Reaction Caused by Electrolysis in Light and Heavy Water Solutions

Reiko Notoya, Toshiyuki Ohnishi and Yohichi Noya

Catalysis Research Center, Hokkaido University
Sapporo 060, JAPAN

Abstract

A series of analysis of the products of some nuclear reactions caused by electrolysis was performed by a gamma-ray or liquid scintillation spectroscopy. The electrolysis was carried out by use of the so-called thermally open cell which was equipped with the cathode made of porous nickel or platinized platinum, in 0.1～0.5 mole/liter Li_2CO_3, Na_2CO_3, K_2CO_3, Rb_2SO_4 and Cs_2SO_4 light and heavy water solutions. The result obtained by the analysis and that of our previous works indicated that;

i. gamma peaks due to ^{22}Na and ^{24}Na, ^{40}K, ^{89}Rb and ^{92}Sr, or ^{134}Cs and ^{135}Xe during each electrolysis of Na^+, K^+, Rb^+ or Cs^+ solution, respectively,

ii. gamma peaks due to ^{56}Co, ^{64}Cu and ^{65}Zn were shown in the cases of all electrolytes included even Li^+ solution,

iii. a gamma peak due to the positron annihilation was also observed in every solutions, at 511 k eV,

iv. liquid scintillation spectra showed the increment of tritium produced by electrolysis in all light and heavy solutions except for Rb^+,

v. some nuclear reactions were caused by electrolysis and occurring as the branching reactions of the hydrogen evolution reaction.

1.Introduction

The cold fusion occurring in the system of deuterium-palladium becomes gradually not-so curious owing to may scientists' efforts in the world, since Fleischmann and Pons proposed it on the basis of finding anomalous large heat evolution during electrolysis in heavy water solution of Li^+[1]. On the other hand, by use of the so-called low overvoltage metals for hydrogen electrode reaction, large heat evolution and some amount of tritium

production were observed during electrolysis even in light water solutions of various alkali-metallic ions M^+ [2]. Furthermore, a few methods of chemical analysis of the electrolytes used for electrolysis provides some evidence of nuclear reactions, for example, Ca in K^+[2] or 132-140X in Cs^+ solution[3] and so forth. For the last a few years, the evidence of the nuclear reactions caused by electrolysis has rapidly increased owing to accumulation of works experimental and theoretical. In particular, the simultaneous measurements of the excess heat and the radioactivity in an electrolytic cell are notable during electrolysis. In these systems, the reaction mechanism was determined as follows on the basis of the result of our studies using the galvanostatic transient method[4];

$$M^+ + e^- \Rightarrow M(I) \quad (1)$$
$$M(I) + H(a) \Rightarrow M(I) + H(a) + OH^- \quad (2)$$
$$H(a) + H(a) \rightarrow H_2, \quad (3)$$

where M(I), H(a), $\Rightarrow$ and $\rightarrow$ mean the inter-metallic compound between M and the electrode material, an adsorbed hydrogen, the rate not-determining and the rate determining steps, respectively.
The aim of this work is to find out the evidence for the nuclear reactions of M(I), which must be occurring even in light water solutions. The data concerning the positron annihilation is reported in the other place[5]. Therefore, it will be mentioned summarily in this paper.

2. Experimental Part

The electrolytic cell and electrodes were the same as described in the previous papers[2,3]. Namely, we used porous nickel or platinized platinum as a cathode(1.0 × 0.5 cm in size, $\leqq$ 0.1 cm in thickness). The same cathode was usually used a few times for electrolysis in the same kind of electrolyte. Twenty or thirty milliliters of 0.5 mole/l LiOH, Na_2CO_3, K_2CO_3 or 0.3 mole/l Rb_2SO_4, or 0.1 mole/l Cs_2SO_4 solution of light or heavy, or mixed water of them was used as the electrolyte. Some series of observation of excess heat and γ -ray spectra were performed simultaneously during electrolysis of 6~100 hours in a dark chamber made of lead walls of 10cm in thickness. After ele- ctrolysis, the electrolytes were analyzed by use of a liquid scintillation spectrometer. The procedure was the same as described also in previous paper[6].

3. Results and Discussion

3.1. γ -ray Spectra

Fig.1 shows the typical spectrum observed in K^+ solution by a γ -ray spectro meter equipped with a pure germanium detector (made by Nippon Atomic Industry Group Co.LTD).

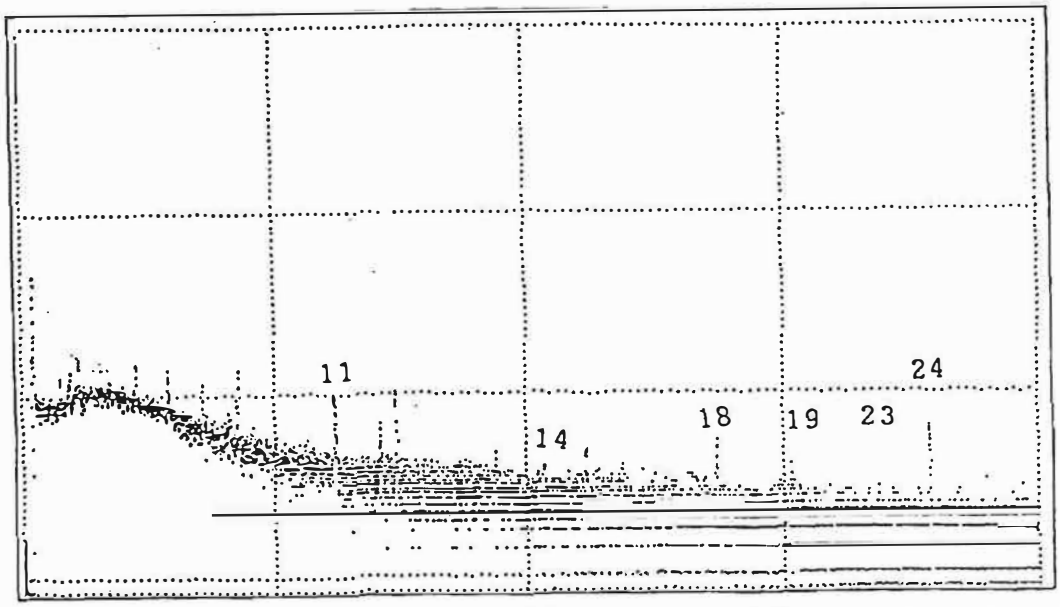

Fig.1. γ -ray spectrum observed in K^+solution on Ni: energy region, 0~1.6M eV, duration and input power of electrolysis, 50hr, 0.65w. Peaks are numbered in the same way in Table 1.

Table 1. Identified Nuclear Species and Their Amounts.

Nuclear Species	Energy (keV)	Amount (Bq)	Limit of Detected Value (Bq)	Peak No.
Th-234	63.33	2.11E-1 ± 1.21E-1	< 3.65E-1	2
Hg-197	77.11	1.22E-2 ± 6.51E-3	< 1.96E-2	3
Th-234	92.48	2.34E-1 ± 6.04E-2	1.81E-1	4
U -235	185.79	7.41E-3 ± 2.54E-3	< 7.64E-3	5
Ra-226	185.79	1.03E-1 ± 3.52E-2	< 1.06E-1	5
Pb-212	238.65	9.11E-3 ± 3.51E-3	< 1.05E-2	6
Pb-214	241.94	3.04E-2 ± 1.19E-2	< 3.60E-2	7
Tl-208	277.48	1.05E-2 ± 1.01E-2	< 3.08E-2	8
Pb-214	295.31	1.51E-2 ± 6.43E-3	< 1.93E-2	9
Pb-214	351.98	1.51E-2 ± 2.54E-3	7.59E-3	10
Cu- 64	511.26	2.53E-2 ± 6.70E-3	2.00E-2	11
Zn- 65	511.26	1.04E-1 ± 2.75E-2	8.23E-2	11
Co- 56	511.26	6.76E-3 ± 1.78E-3	5.35E-3	11
N - 13	511.26	3.35E-1 ± 8.86E-2	2.65E-1	11
F - 18	511.26	3.14E-2 ± 8.29E-3	2.48E-2	11
Tl-208	582.96	1.46E-3 ± 8.14E-4	< 2.45E-3	12
Co- 56	846.53	4.93E-4 ± 4.82E-4	< 1.46E-3	14
Zn- 65	1119.84	1.95E-3 ± 1.92E-3	< 5.80E-3	18
Co- 56	1238.00	8.87E-4 ± 3.90E-4	< 1.19E-3	19
Na- 24	1368.63	1.35E-3 ± 1.28E-3	< 3.91E-3	23
K - 40	1458.72	1.89E-2 ± 3.73E-3	1.11E-2	24

Transmutation

The amount of each nuclear species estimated from the peak value shown in Fig.1 was listed in Table 1, respectively.
These quantities estimated from the observation of γ -ray spectra are found in the region of 0.001~0.1 Bq. In Li^+ solution, merely the peaks due to the positron annihilation, ^{64}Cu and ^{65}Zn were increased by electrolysis. In the case of Na^+ , ^{22}Na (1,276 k eV) was often detected together with ^{24}Na(1,366keV).
In K^+ solution, ^{40}K(1,461 k eV) is increased always twice from 0.02Bq to 0.04Bq by 24 hours' electrolysis with 0.5~0.6 w.
In the case of Rb^+ solution, ^{89}Rb(1,032 and 1,250 keV) was produced by electrolysis and sometimes ^{92}Sr. In the case of Cs^+, a small amount of ^{134}Cs(609 and 794 keV)and ^{135}Xe(251 keV) were detected. But in Cs^+ solution, the peak due to positron annihilation showed the highest. The reason does not become clear in this time.

3.2. Liquid Scintillation Spectra
A liquid scintillation spectro-analyzer(Packard CA 2550) was used for determination of tritium concentration in electrolyte after electrolysis. Two types of a liquid scintillation spectra were exemplified in Fig.2a and Fig.2b observed by use of the samples of Li^+ and Rb^+ solutions. The maximum position shown in Fig.2a and those of the spectra of the samples of Na^+, K^+ and Cs^+ solutions, agree with that of the authentic sample of tritium. But, the maximum point of spectrum shown in Fig.2b moved towards higher energy, that was strongly affected by the presence of ^{87}Rb (the natural abundance: 27.835%). The rates of generation of tritium by electrolysis were determined in all kinds of electrolytes of right and heavy water except for Rb^+, which were listed in Table 2.

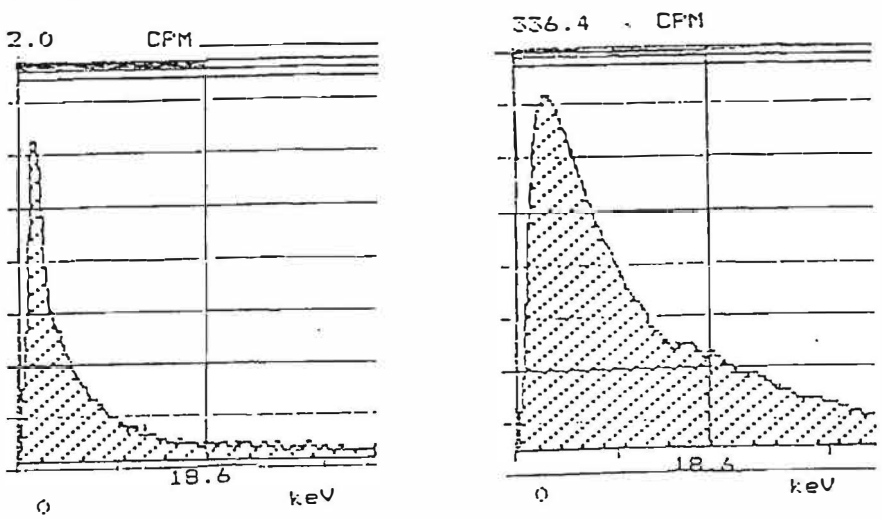

Figs.2a and 2b Liquid scintillation spectra observed by use of Li^+ and Rb^+ samples.

Table 2. Generation Rate of Tritium in Various Electrolytes on Porous Nickel.

Electrolyte Ion	Water	W_{input}[a] w	Excess Heat %	^3T[b] Bq/20ml · 24hr
1. Li^+	H_2O	0.75	53	0.25
2. "	"	0.73	52	0.032
3. Na^+	H_2O	0.61	134	1.92
4. "	"	0.77	59	0.222
5. "	H_2O+D_2O	-----	----	2.006
6. K^+	H_2O	0.47	97	0.89
7. "	H_2O+D_2O	------	-----	3.42
8. "	D_2O	0.65	110	393
9. Cs^+	H_2O	0.71	62	32
10. "	"	0.72	61	72
11. "	"	0.41	----	7

a: Input power

b: Bq denotes tritium amount generated in 20 ml electrolyte during 24hr's electrolysis

3.3. Nuclear Reactions Caused by Electrolysis

A clear peak was found at 511 keV, which must be due to the positron annihilation. In particular, it was remarkable that the peak appeared on all spectra which were observed during the electrolysis of all electrolytes used for this work. The increase of the peaks characterized by ^{64}Cu, ^{65}Zn and ^{56}Co with the increase of duration of electrolysis were common to all solutions. Besides, the increase of the products of some nuclear reactions as described above can be estimated on the basis of γ -ray spectral data. These radioactive species are well known to be produced easily in a nuclear furnace, for example, $^{23}Na(n,\gamma)^{24}Na$, $^{23}(\gamma,n)^{22}Na$, $^{39}K(n,\gamma)^{40}K$, $^{56}Fe(p,n \text{ or } d,2n)^{56}Co$, $^{63}Cu(n,\gamma)^{64}Cu$, $^{64}Zn(n,\gamma)^{65}Zn$ and $^{133}Cs(n,\gamma)^{134}Cs$. ^{89}Rb, ^{92}Sr and ^{135}Xe may be produced through a series of some elementary reactions. Ca and the elements of the mass number from 132 till 140 were produced in the same way, which had been detected in the electrolysis of K^+ and Cs^+ ions.

References

[1] M,Fleischmann and S.Pons, J.Electroanal.Chem.,261, 301(1989).

[2] R.Notoya, Fusion Technol., 24, 202(1993).

[3] R.Notoya, Y.Noya and T.Ohnishi, Fusion Technol., 26, 179(1994).

[4] A.Matsuda and R.Notoya, Denkikagaku, 34 169(1966).

[5] R.Notoya et al., in preparation.

[6] R.Notoya, Enviro.Res.Forum, V1-2(1996),127-140,Transtec Pub..

The Experimental Discovery of the Phenomenon of Controlling and Changing Probability and Time of Spontaneous Decay and Gamma-Transmutation of Excited Nuclei Statuses

Vladimir I. Vysotskii
Kiev Shevchenko University, Radiophysical dept., 252033, Kiev, Ukraine

Vladimir P. Bugrov, Alla A. Kornilova, Sergei I. Reiman
Moscow State University, 119899, Moscow, Russia

Abstract
The paper discusses the process of controlling the probability of spontaneous decay of radioactive and excited Mossbauer nuclei. For the first time two experiments have proved the possibility of changing the life time of radioactive nuclei by surrounding them with screens having resonant absorption frequency equal to the nuclear transition frequency. For the first time in the experiments with gamma sources $Co^{57}(Fe^{57*})$ and Sn^{119m} and with gamma absorbers Fe^{57} and Sn^{119} we have discovered the change of Mossbauer transition life-time by 20-100% and total life-time (including non- Mossbauer radiation and electron conversion) by 0.6-2%.

1. Theoretical model

The problem of controlling of nuclei decay is one of the most important in the physics. As far as we know, none of the previously conducted researches contain reliable data confirming the possibility of such controlling. We have carried out investigation aimed at experimental discovery (based on our original theory [1]) of this important phenomenon.

In [1] we have considered the possibility of controlling the probability of decay A_{ij} of excited Mossbauer nuclei by controlled mode restructuring of electromagnetic vacuum. The main idea of the spontaneous decay velocity control is in a strong influence of averaged modes density in a unit frequency interval

$$<\rho(\nu_{ij})> = \iint \rho(\nu_n) f(\nu_n,\nu_{ij},\Omega) d\nu_n d\Omega, \quad \rho(\nu_n) = 8\pi\nu_n^2/c^3 \qquad (1)$$

upon the final possible decay and radiation life-time τ of excited nuclei

$$A_{ij} \equiv 1/\tau = (8\pi^3\nu_{ij} \mid \mathbf{d}_{ij} \mid^2/3h) < \rho(\nu_{ij}) > \qquad (2)$$

Here $f(\nu_n,\nu_{ij},\Omega)$ is spectral-angular density of mode, having central frequency ν_n, spectral width γ_n and spreading in the direction of solid angle Ω. Usually

$$f(\nu_n,\nu_{ij},\Omega) = \gamma_n / 8\pi^2[(\nu_n - \nu_{ij})^2 + \gamma_n^2/4], \quad \gamma_n = \gamma_n(\nu_n,\Omega). \qquad (3)$$

In case of nuclei transition with high multipolity $L>1$ the dipole moment $\mathbf{d}$ ($L=1$) in (2) and other equations is replaced with multipole moment $\mathbf{Q}^{(L)}$. The rule for the substitution is

$$| \mathbf{d}_{ij} |^2 \rightarrow \{6\pi (L+1)/L[(2L+1)!!]^2\}(2\pi\nu_{ij}/c)^{2L-2}|\mathbf{Q}^{(L)}{}_{ij}|^2$$

Transmutation

Spectral width of mode γ_n is defined by time of life of photon $\Delta t_\gamma = Q_n/\nu_n$ in this mode. Here Q_n - quality of mode ν_n.

In case of free space time of life of photon is unlimited large and $\Delta t_\gamma \to \infty$. In result

$Q_n \to \infty$, $\gamma_n = \nu_n / Q_n \to 0$, $f(\nu_n, \nu_{ij}, \Omega) \to \delta(\nu_n - \nu_{ij})$ (Dirac δ-function) and from (1) - (3) we have

$$<\rho(\nu_{ij})> = \rho(\nu_{ij}), \quad \tau = A_{ij}^{-1} = 3hc^3/32\pi^3\nu_{ij}^3 \, | \, \mathbf{d}_{ij} \, |^2. \qquad (4)$$

In case of frequency non-selective absorption time of life of all photons Δt_γ decreases, $\gamma_n = \text{const} \neq \gamma_n(\nu_n)$ and for usual case $\gamma_{n\,(max)} << \nu_n$ we have the same result (4).

Another situation appears with presence of a frequency-selective (resonant) absorber (for instance, sphere of radius R or its part in solid angle $\Delta\Omega$) acting as a "black" screen in a narrow frequency band $\Delta\nu$ near ν_0 (for instance, near resonant frequency ν_0 of Mossbauer transition in source). In this case time of life of resonant photons is defined by their run $\Delta t_\gamma \approx 2R/c$ between frequency-selective absorber walls and $\gamma_n(|\nu - \nu_0| < \Delta\nu/2, \Delta\Omega) \approx c/2R$.

On the other hand, the nonresonant photons pass through the absorber freely and for them $\gamma_n(|\nu - \nu_0| > \Delta\nu/2, \Delta\Omega) \approx 1/\Delta t_\gamma << c/2R$. The decrease of quality $Q_n = \nu_n/\gamma_n \approx 2R\nu_0/c$ of modes lying within a small interval $\Delta\nu \leq c/2R$ of frequencies near ν_0 causes an essential change of averaged modes density

$$<\rho(\nu_{ij})> = \rho(\nu_{ij})F(\nu_{ij}), \quad F(\nu_{ij}) = \iint f(\nu_n, \nu_{ij}, \Omega) d\nu_n d\Omega$$

As a result it leads to change of time of decay (life-time)

$$\tau^* = 3hc^3/32\pi^3\nu_{ij}^3 \, | \, \mathbf{d}_{ij} |^2 / F(\nu_{ij}) \equiv \tau / F(\nu_{ij}) \qquad (5)$$

and to a decrease (at $\nu = \nu_0$) and increase (at $\nu \approx \nu_0 \pm \Delta\nu/2$) of the probability intensity of spontaneous decay.

This effect also leads to change (decrease at $\nu = \nu_0$) of the spectral widths of Mossbauer transition and radiation (in the radiation channel of nuclear decay) $\Gamma^* = 1/\tau^* = \Gamma F(\nu_{ij})$.

The similar situation takes place also in the more real case, when part of the space (where the excited nuclei are situated) is bounded by interval ([0, *l*], $\Delta\Omega$) between nonresonant absorber (for instance – basis or support for excited nuclei) and resonant one. In this case the domains of localization and the spectral properties of resonant and nonresonant modes are different - resonant mode is localized in bounded interval [0 , *l*] and has large width γ_n, while nonresonant one is localized in endless domain [0 , ∞] and has little width γ_n. It's also of great importance, that the results of effect on electromagnetic mode caused by only nonresonant absorber and by the combination of resonant absorber and nearly (with distance $\delta l \to 0$) nonresonant one are equal. The latter remarks are directly related to our experiments.

The equation for changes of population $n_2 \equiv n_e$ of excited nuclei (defined by partial probabilities of Mossbauer radiation in blocked angle $P^*_M = f\,\Delta\Omega/4\pi\tau^*$, Mossbauer radiation in non-blocked angle $P_M = f(1 - \Delta\Omega/4\pi)/\tau$, non-Mossbauer radiation

$P_{NM} = (1 - f)/\tau$ and electron conversion $P_\alpha = \alpha/\tau$) has a form

$$dn_2/dt = \Sigma_{i>2} \, n_i/\tau_{i2(tot)} - n_2/\tau^*_{tot},$$

$$\tau^*_{tot} = [P^*_M + P_M + P_{NM} + P_\alpha]^{-1} \equiv \tau/\{1 + \alpha - (1 - \tau/\tau^*) f \Lambda\Omega/4\pi\} \qquad (6)$$

Here α is a coefficient of electron conversion, f - parameter of recoil-free resonant radiation (parameter of Mossbauer), $\Delta\Omega$ - a solid angle blocked by the resonant absorber, $1/\tau_{i2(tot)}$ - total probability of transition from level $E_{i>2}$ to level E_2, τ^*_{tot} - total life-time of excited nuclei with present of resonant absorber. In equilibrium state $dn_2/dt = 0$ and the relation of

population of excited nuclei n_2^* for $\Delta\Omega \neq 0$ (with selective absorption) to population of excited nuclei n_2 for $\Delta\Omega = 0$ (without selective absorption) has a form

$$n_2^*/n_2 = 1/\{1 - (1 - \tau/\tau^*) f \Delta\Omega / 4\pi (1+\alpha)\}. \quad (7)$$

For optimal case ($\Delta\Omega \approx 4\pi$, $\tau << \tau^*$, $f \to 1$, $\alpha \to 0$) $n_2^*/n_2 \approx 1/\{1 - f/(1+\alpha)\} >> 1$.

Total intensity J_γ^* of Mossbauer radiation in non-blocked direction ($4\pi - \Delta\Omega$) also changes and $J_\gamma^* = J_\gamma n_2^*/ n_2$. Let's describe this change as $J_\gamma^* = J_\gamma/(1 - g)$. Then we have

$$g = 1 - J_\gamma/J_\gamma^* \equiv (1 - \tau/\tau^*) f \Delta\Omega / 4\pi (1+\alpha) \quad (8)$$

In this case

$$\tau^* = \tau/\{1 - 4\pi g (1+\alpha)/ f \Delta\Omega\}. \quad (9)$$

2. Experimental results and discussion

Two experiments on controlling of the nuclei decay were performed based on our theory.

The aim of the first experiment was to measure the changing of total intensity J_γ^* (8) of Mossbauer radiation (as a result of changing life-times τ^*_{tot} and τ^*) in non-blocked direction ($4\pi - \Delta\Omega$). The layout of the first experiment is presented on Fig. 1

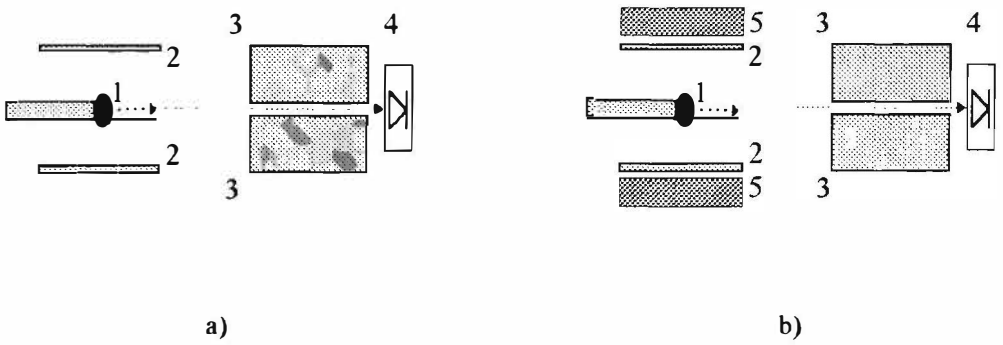

Fig. 1. Experimental layout for detecting of the effect of controlling the time of radiation nuclear decay based on the method for measurement of intensity direct beam change.

A $Co^{57}(Fe^{57*})$ isotope ($h\nu_0$=14,4 KeV, α=9) with activity of 10 mCi in a chromium matrix was used as a source of Mossbauer radiation 1. This source had a spectrum in the form of single line of natural width.

The source was fixed in the Plexiglas disc and put in the center (l=2.5 cm) or near the diaphragm-oriented edge (l=1 cm) of the resonant absorber 2, having a form of cylinder with diameter D=2 cm and length L=5 cm, made of stable Fe^{57} isotope (200 mg) in stainless steel (100 mg). The thickness (surface density) of absorber $\sigma_m \approx 7$ mg/cm^2 provided the requirement of total absorption of resonant radiation (for $|\nu - \nu_0| < \Gamma/2$ the coefficient of transparency equals $K \approx 10^{-3}$) and almost full transparency for non-resonant radiation ($K \approx 0{,}95$ for $|\nu - \nu_0| >> \Gamma/2$).

The lead diaphragm 3 had a hole with diameter D_0 = 1 cm and length L_0 = 2,5 cm. Behind the diaphragm there was amplitude detector 4 - NaJ(Tl) crystal with width 10^{-2} cm and photo-

electronic multiplier. The signal processing system picked out the part of amplitude specter close to the gamma-line with $E_\gamma \approx 14{,}4$ KeV.

The measurements of the quanta counts N with direct gamma-beam (traveling from source 1 through diaphragm 3 to amplitude detector 4) were performed in two regimes.

In the first regime (see Fig. 1, case a) the quanta count $N^* = J_\gamma^* \Delta t$ corresponds to presence of resonant absorber cylinder 2 only .

In the second regime (see Fig.1, case b) another cylinder 5 made of lead with diameter $D_1=2{,}2$ cm, length $L_1=5$ cm and thickness $\Delta D_1=0{,}2$ cm was put around the resonant absorber cylinder. It totally absorbed both resonant and non-resonant radiation in the range of energies close to $E_\gamma \approx 14{,}4$ KeV. This corresponds to completely non-selective absorber and leads to the intensity of registered flux of gamma-quanta J_γ and the quanta count $N = J_\gamma \Delta t$. Such method excludes the uncontrolled influence of reverse scattering of resonant gamma-quanta after changing resonant absorption to non-resonant (which would occur when resonant absorber cylinder is simply taken off the source).

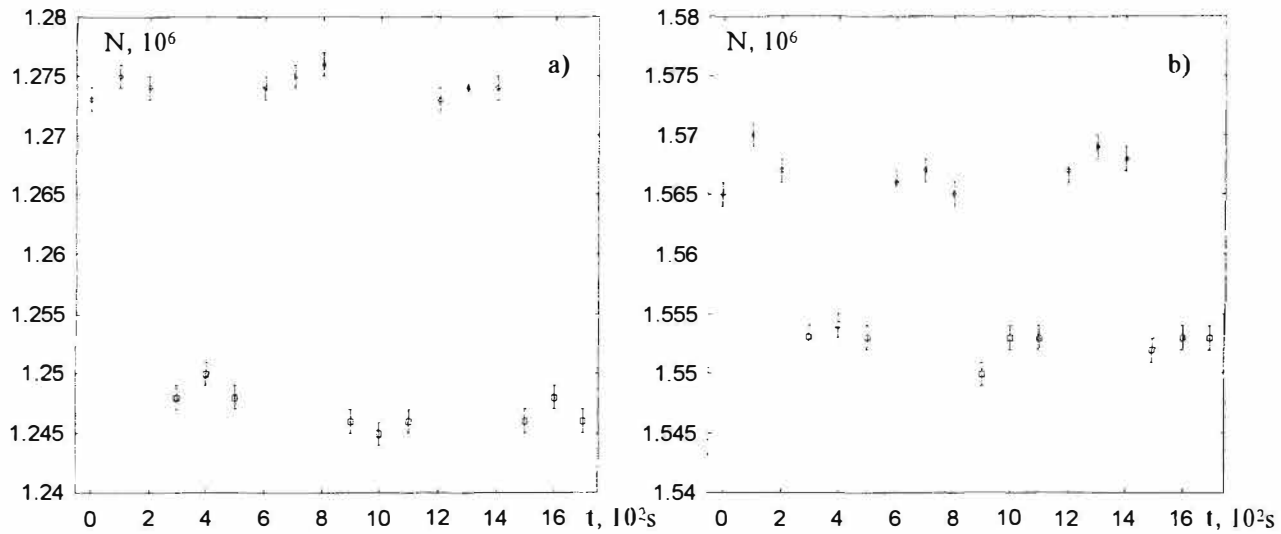

FIG. 2. The influence of spatial position of non-resonant totally absorbing screen 6 upon the intensity (the quanta count $N = J_\gamma \Delta t$) of direct beam of gamma-quanta: circles (upper points) – screen is put around the resonant absorber, squares (lower points) – screen is taken off. The case a) corresponds to the source 1 situated in the center of the resonant absorber (l=2.5 cm), the case b) - the source is at l=1 cm.

Each measurement lasted $\Delta t=100$ s. The results of measurements are presented on Fig.2.

It can be seen, that the presence of additional non-selective absorber in side direction reduced the intensity of radiation coming from the source in the direction of detector. It fully agrees with the theory described in [1] and above. The change in count rate $(N^*- N) / N = g / (1-g)$ is defined by $g = 0.022 \pm 0.002$ for l=2.5 cm and $g = 0.008 \pm 0.002$ for l=1 cm, with corresponding changes (increases) of radiation time (9) of nuclear decay (life-time) of Fe^{57*} (E_γ=14,4 KeV) for Mossbauer component $\tau^* \approx 2\tau$ for l=2.5 cm and $\tau^* \approx 1.4\tau$ for l=1 cm.

In fact, considering the scattering of non-resonant gamma-quanta (in region $E_\gamma \approx 14{,}4$ KeV) from lead absorber, which increases J_γ, this increase of life-time τ^* is even greater.

Changed total life-time for Fe^{57*} equals $\tau^*_{tot} = \tau_{tot} / (1- g)$. Here $\tau_{tot} = \tau / (1+\alpha) = 9{,}8.10^{-8}$ s — standard total life-time for Fe^{57*}. For both cases the change of total life-time $(\tau^*_{tot}- \tau_{tot})/\tau_{tot}$ equals 2,2% and 0,8%.

Transmutation

The aim of the second experiment was to measure the changing (decreasing at $\nu = \nu_0$) of the spectral width of Mossbauer radiation (as a result of changing life-times τ^*_{tot} and τ^*).

The anticipated change in natural and total widths of gamma-spectrum increases with the decrease of life-time. In order to reduce the influence of technical fluctuations the isotope Sn^{119m} with $\tau_{tot} = 1{,}85.10^{-8}$ s, $\alpha = 5{,}5$ and $\tau = 1{,}2.10^{-7}$ s was used instead of Fe^{57*} with $\tau = 10^{-6}$ s.

The layout of the second experiment is presented on Fig. 3.

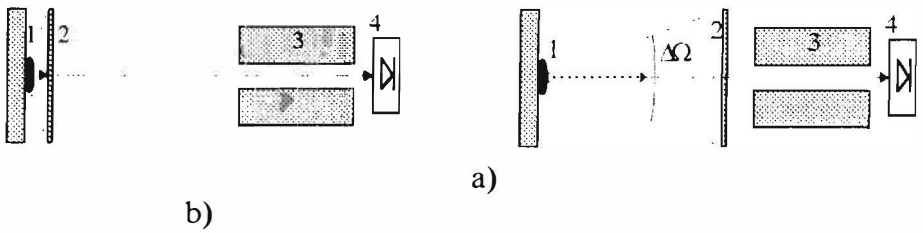

Fig. 3. Experimental layout for detecting of the effect of controlling the time of radiation nuclear decay based on the method for measurement of width of gamma-spectrum in the system source - absorber - resonant detector.

The excited Sn^{119m} isotope (chemical compound $CaSn^{119m}O_3$) with activity of 5 mCi was used as a source of Mossbauer radiation 1 with the energy of quanta $E_\gamma = 23{,}8$ KeV. This source had a spectrum in the form of single line of nearly natural width.

The resonant absorber 2 had a form of disk with diameter $D \approx 3$ cm, made of stable Sn^{119} isotope (chemical compound $Sn^{119}O_2$, surface density $\sigma_m \approx 1{,}39$ mg/cm^2). This absorber has a spectrum of absorption in the form of nearly natural width. The thickness (surface density) of resonant absorber satisfied two contradictory requirements. First it is necessary to have $\sigma_m \to \infty$ and $K \to 0$ to maximize the influence upon resonant electromagnetic mode. But to lower the statistical errors the quanta count has to be increased, thus requiring $\sigma_m \to 0$, $K \to 1$. The value $\sigma_m \approx 1{,}39$ mg/cm^2 (for which a coefficient of resonant transparency equals $K \approx 0{,}5$) is nearly optimal.

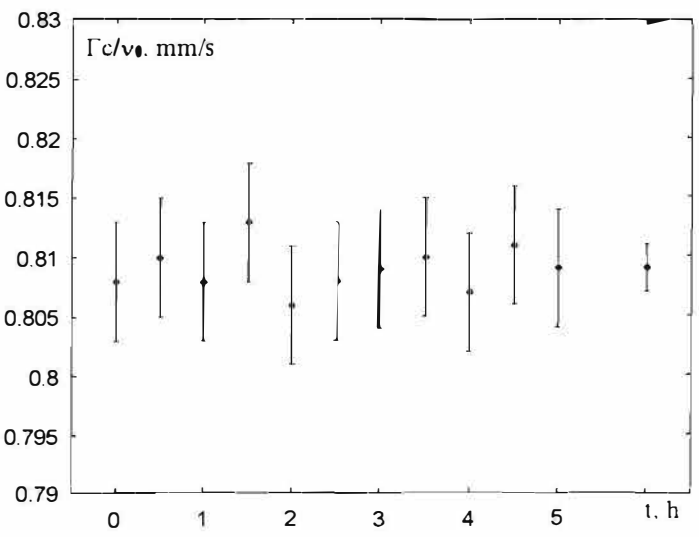

FIG. 4. Width of gamma-spectrum in the system source – resonant detector. The rightmost point represents the average value.

The lead diaphragm 3 had a hole with diameter $D_0 = 1$ cm and length $L_0 = 2{,}5$ cm. Behind the diaphragm there was a resonant detector 4 (a compound $CaSn^{119}O_3$ was used as a resonant detector) and a system for changing the Doppler velocity of detector 4.

The measurements with gamma-beam (traveling from source through resonant absorber and diaphragm to resonant detector) were performed in two regimes too.

In the first regime (Fig. 3, case a) the resonant absorber 2 was fixed in position near source 1. For this regime the solid angle blocked by the reso-

nant absorber equals $\Delta\Omega \approx 2\pi$ and $F(\nu_{ij}) < 1$, $\tau^* > \tau$.

In the second regime (Fig. 3, case b) the resonant absorber 2 was fixed at l=3 cm from source in position near diaphragm 3. For this regime $\Delta\Omega \approx (D_0/16\, l\,)^2 \approx 7.10^{-4}$ and $F(\nu_{ij}) \approx 1$, $\tau^* \approx \tau$.

In the regimes (a) and (b) the total widths $\Gamma^* = \Gamma_s^* + \Gamma_d + \Delta\Gamma$ and $\Gamma = \Gamma_s + \Gamma_d + \Delta\Gamma$ of gamma-spectrums including both the sum of source (Γ_s) and resonant detector (Γ_d) resonant-line widths, and a broadening $\Delta\Gamma$ (as a result of resonant absorption) in absorber 2.

In order to verify the stability of gamma-line position and width the measurement of gamma-spectrum was performed in the system source 1 - detector 4 without the resonant absorber 2. The results of this measurement are presented on Fig. 4.

The resulting value $\Gamma_s + \Gamma_d = \Gamma_{s0} + \Delta\Gamma_{so} + \Gamma_{d0} + \Delta\Gamma_{do} \approx 0.809$ mm/s (in Doppler velocity units $v = c\Gamma/\nu_0$) demonstrates that the broadening $\Delta\Gamma_{so} \approx \Delta\Gamma_{do} \approx 0.081$ mm/s small in relation to natural widths $\Gamma_{s0} = \Gamma_{do} = 1/\tau_{tot} \approx 0{,}323$ mm/s takes place in the source and detector.

For the regime (a) we have $\Gamma_{do} = 1/\tau_{tot}$, $\Gamma_{s0} \rightarrow \Gamma_{s0}^* = 1/\tau_{tot}^* \equiv \Gamma_{s0}\,[1 - (\tau_{tot}^* - \tau_{tot})/\tau_{tot}^*]$ and

$\Gamma^* = \Gamma_{s0} - \Gamma_{s0}(\tau_{tot}^* - \tau_{tot})/\tau_{tot}^* + \Delta\Gamma_{so} + \Gamma_{d0} + \Delta\Gamma_{do} + \Delta\Gamma$.

For the regime (b) we have $\Gamma_{do} = 1/\tau_{tot}$, $\Gamma_{s0} = 1/\tau_{tot}$ and $\Gamma = \Gamma_{s0} + \Delta\Gamma_{so} + \Gamma_{d0} + \Delta\Gamma_{do} + \Delta\Gamma$.

Then (from (6), using the obtained results for Γ^* and Γ) we find

$\tau_{tot}/\tau_{tot}^* = 1 - \tau_{tot}(\Gamma - \Gamma^*)$,

$$\tau/\tau^* = 1 - \tau_{tot}(\Gamma - \Gamma^*)\,[4\pi\,(1+\alpha)/f\,\Delta\Omega\,] \equiv 1 - (1 - \tau_{tot}/\tau_{tot}^*)\,[4\pi\,(1+\alpha)/f\,\Delta\Omega\,] \qquad (9)$$

Each measurement of Γ (or Γ^*) in both cases lasted Δt=0,5 hour. The results are presented on Fig. 5 for two series of experiments (each with a duration about one or two days). The average values measured were $\Gamma = (1{,}184 \pm 0{,}003)$ mm/s , $\Gamma^* = (1{,}167 \pm 0{,}003)$ mm/s, with corresponding changes (increases) of total life-time of Sn^{119m} $(\tau_{tot}^* - \tau_{tot})/\tau_{tot} = (0{,}63 \pm 0{,}12).10^{-2}$ and life-time for Mossbauer component of Sn^{119m} $\tau^* = (1{,}20 \pm 0{,}04)\tau$.

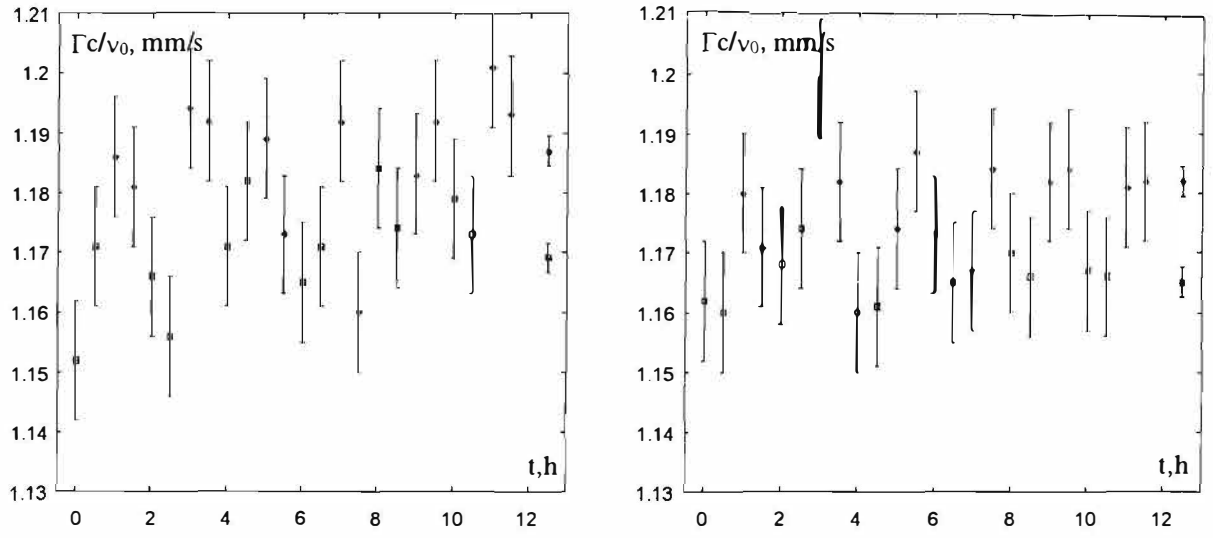

FIG. 5. The influence of position of resonant absorber upon the width of gamma-spectrum for gamma-quanta passing through this absorber, for two series of independent measurements: squares — absorber is situated near source; circles — absorber is situated near diaphragm. The points to the right are the result of averaging the data for all measurements.

The results of all experiments are approximately corresponding to estimations based on the theoretical model for $F(\nu_{ij})$.

When the experiment is performed in vacuum (which increases the quality Q_n of non-resonant modes compared to experiments described here, that were performed in air) with only resonant absorber present, $\Delta\Omega = 4\pi$ and the gamma-transitions with $f \cong 1$ and $\alpha \cong 0$ are employed, it is possible to increase $\tau^*_{tot} >> \tau_{tot}$ by several orders of magnitude .

We would like to acknowledge useful discussion with R.N.Kuz'min.

Reference

1. V.I.Vysotskii, V.I. Vorontsov, R.N. Kuz'min . Pis'ma Zh. Tekh. Fiz. (Soviet Phys.-J.T.P. Letters) 10, 300 (1984).

Transmutation

Experimental Discovery of the Phenomenon of Low-Energy Nuclear Transmutation of Isotopes ($Mn^{55} \Rightarrow Fe^{57}$) in Growing Biological Cultures

Vladimir I. Vysotskii
Kiev Shevchenko University, Radiophysical Dept., 252033, Kiev, Ukraine

Alla A. Kornilova
Moscow State University, Physical Faculty, 119899, Moscow, Russia

Igor I. Samoylenko
Gamaleya Institute of Epidemiology and Microbiology, Moscow, Russia

Abstract
For the first time the experimental study of cold nuclear transmutation of isotopes was carried out in growing microbiological culture with controlled conditions of growth. With the help of Mossbauer effect the formation of Fe^{57} isotope from Mn^{55} in nutrient medium based on heavy water was observed. The possible mechanism of low-temperature nuclear transmutation is discussed.

1. Introduction

Hypothesis of possibility of nuclear transmutation of elements and isotopes in biological and geological structures has been repeatedly discussed during the last decades. The interest to this topic considerably increased after large-scale researches of the cold nuclear fusion phenomenon on the basis of dd-reactions in solids.

As far as we know, none of the previously conducted researches contains reliable data confirming the possibility of such transmutations.

We have carried out investigations aimed at discovery of nuclear transmutation of elements in microbiological cultures. We believe that this aim can be achieved only if an isotope obtained in the process of transmutation does not have any analogues in the nutrient medium where the culture is growing (along with inevitably present admixtures of this isotope). Therefore all experiments like [1] are hardly convincing because they don't meet this condition.

We have conducted a series of experiments based upon new technology employing the precise methods of Mossbauer spectroscopy. The experiments are based on the expected

$$Mn^{55}+d^2=Fe^{57}$$

reactions in growing microbiological culture in heavy-hydrous (D_2O) sugar-salt nutrient medium deficient in Fe but additionally containing Mn. The reaction results is generation of stable rare Fe^{57} isotope, concentration of which in the natural iron (mainly Fe^{55}) is very low.

The Fe^{57} isotope obtained in small quantities can be easily discovered by means of the Mossbauer effect. The Mossbauer effect allows to monitor the isotope contents of all components

of the nutrient medium, the initial culture and all samples of initial culture after its growth has finished, taking into account all varieties of experiments.

2. Experimental method and procedures

The researches were carried out on the basis of bacterial cultures ***Deinococcus radiodurans M-1, Bacillus subtilis GSY 228, Escherichia coli K-1*** and yeast culture ***Saccharomyces cerevisiae T-8***, selected according to the possibility of their growth in light and heavy water media. The course of the experiments was as follows.

Previously obtained cultures after centrifuging, washing and post-growth were placed in a flask with sugar-salt nutrient medium containing salts of Mg , Ca, K, ammonium tartrate, sucrose and 10 ml of pure water (D_2O in transmutation experiments, H_2O in control experiments).

The composition of medium is shown in the table.

Components	Concentration in medium (%)	Admixture of Fe (no more) relative (%)	Admixture of Fe (no more) absolute (g)
Sucrose	3	10^{-4}	3.10^{-7}
$(NH_4)_2$ tartrate	1	5.10^{-4}	5.10^{-7}
$MgSO_4 \cdot 7H_2O$	0,25	2.10^{-4}	5.10^{-8}
$CaHPO_4 \cdot 7H_2O$	0,008	$1,5.10^{-3}$	$1,2.10^{-8}$
K_3PO_4	0,5	5.10^{-4}	$2,5.10^{-7}$
$MnSO_4 \cdot 7H_2O$	0,01	5.10^{-4}	5.10^{-9}
Pure water (D_2O or H_2O)	100 (10 ml)	10^{-7}	10^{-8}

In accordance with degree of purification of all nutrient medium ingredients (chemically pure category), the possible content of Fe as an admixture does not exceed $\Delta m \approx 1.1 \times 10^{-6}$g. In accordance with natural content of Fe^{57} isotope (2,2 per cent of the total Fe), its possible quantity as an admixture does not exceed $\delta m \approx 2.5 \times 10^{-8}$g.

In transmutation experiments, $MnSO_4$ containing less than $\Delta m_1 \approx 10^{-8}$g of Fe admixture and $\Delta m_0 \approx 2 \times 10^{-4}$g of basis stable Mn^{55} isotope ($N_0 = 1.8 \times 10^{18}$ of Mn^{55} atoms) was added to the sugar-salt nutrient medium.

All initial dry ingredients of the sugar-salt nutrient medium were investigated on Mossbauer spectrometer. The same investigation was held with a part of the inoculum in the nutrient medium of previously dried culture.

A typical series of experiments concerning nuclear transmutation of elements consisted in growing of certain microbiological culture in 3 disks simultaneously (see Fig.1)

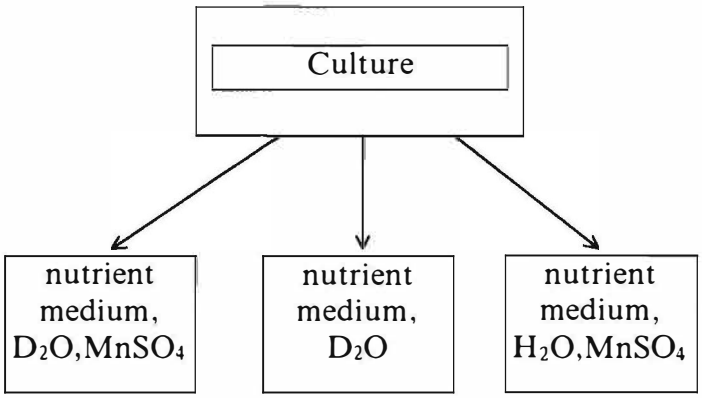

Fig.1 The scheme of experiment.

The first disk contained full-compounded heavy-hydrous (D_2O) nutrient medium with $MnSO_4$, the second one — also heavy-hydrous (D_2O) nutrient medium without $MnSO_4$, and the third one — light-hydrous (H_2O) full-compounded (with $MnSO_4$) nutrient medium.

Such series of experiments was held for different cultures, different time of growth Δt (24, 48 and 72 hours) and different growth modes (in still disks and media and in suspension stirring mode using magnet stirring device). Bacteria and yeast were grown in a thermostat at optimal temperature 32^0 C.

After completing each series, the obtained biological substance was collected using a centrifuge, cleaned in distilled water (H_2O) and dried. The dried substance in the form of a thin film was separated using non-iron containing instrument, ground to a powder and placed in the Mossbauer spectrometer. To increase the possibility of resonant absorption in some of the experiments a sample was cooled to T=78 K.

A Co^{57} isotope with activity of 40 mCi in a chromium matrix was used as a source of Mossbauer radiation. This source has a spectrum in the form of a single line of natural width. The measurements in each of 256 channels of spectrometer were carried out till the required number of counts $N_\infty=3.5\times10^6$ was achieved in channels remote from gamma-resonance line. Calibration of gamma-spectrometer was carried out with standard Fe^{57}-containing absorber.

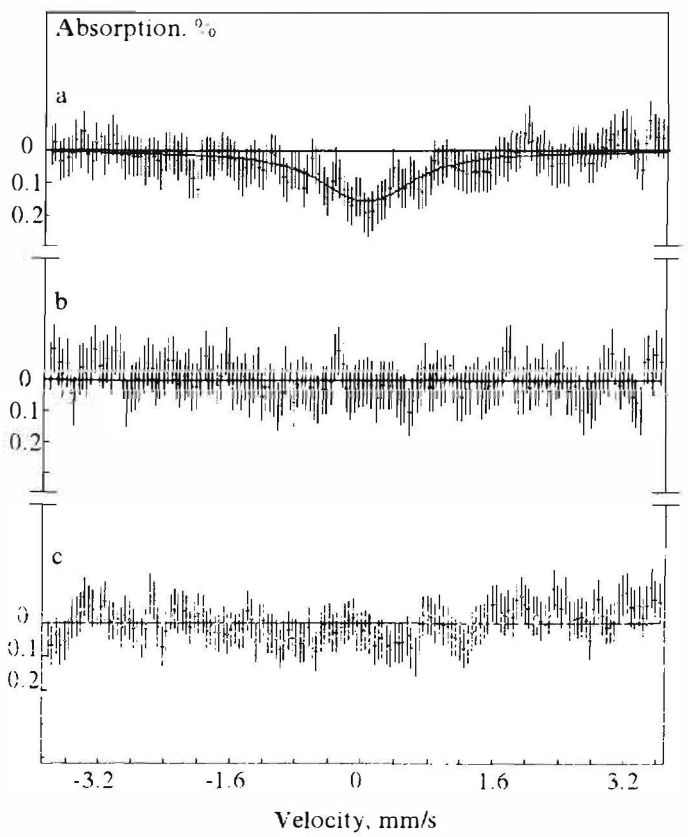

Fig. 2. Mossbauer spectra of grown cultures. Culture *Saccharomyces cerevisiae T-8* grown: a) in D_2O with present Mn^{55}; b) in H_2O with present Mn^{55}; c) in D_2O without Mn^{55}

3. Results and discussion

The figure 2a presents the Mossbauer spectrum of ***Saccharomyces cerevisiae T-8*** culture grown during Δt = 72 hours in nutrient medium of optimal composition, containing D_2O and $MnSO_4$. The total mass of the culture was 0.28 g. The spectrum 2b corresponds to the same culture grown in the medium containing H_2O and $MnSO_4$, and the spectrum 2c - the medium with D_2O, but without $MnSO_4$. The natural width of Fe^{57} Mossbauer resonance (in Doppler velocity units) equals Γ=0.19 mm/s. In case 2a the gamma resonance line is widened by $p_a=\Delta\omega_a/\Gamma \approx 10$ times.

The total number of resonant Fe^{57} atoms for a Lorentz-widened line was calculated by the equation

Transmutation

$$N = \eta S(1+p)/\sigma_0 f$$

obtained for a thin resonant absorber. Here $\eta = (N_\infty - N_0)/N_0$ - relative depth of absorption resonance, N_∞ and N_0 - number of counts in non-resonant and central resonant channels, $S \approx 0.63$ cm^2 - area of gamma-spectrometer disk, filled with the studied culture, $f \approx 0.6$ - probability of Mossbauer effect in the absorber, σ_0 - cross-section of resonance absorbtion in Fe^{57} isotope.

The full numbers of Fe^{57} atoms and their mass are the following:

$$\eta_a=(1.9\pm0.53).10^{-3},\ N_a=(0.87\pm0.24).10^{16},$$
$$m_a=(1\pm0.28).10^{-6}\text{g}.$$

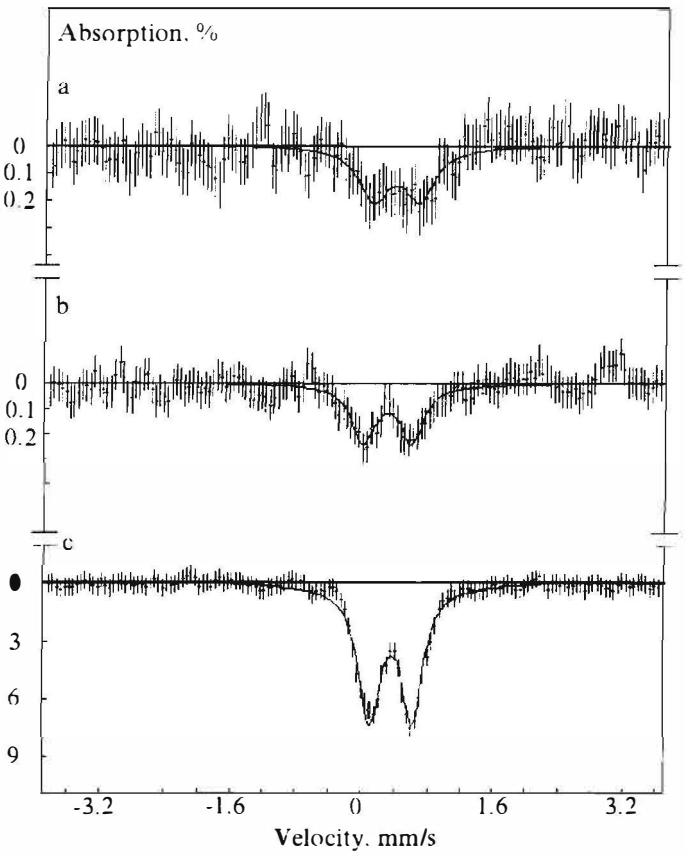

Fig. 3. Mossbauer spectra of grown cultures. Culture *Deinococcus radiodurans* grown: a) and b) in D_2O with present Mn^{55}; c) in H_2O with present Mn^{55} and small quantity of Fe^{57}

The amount of Fe^{57} isotope in cultures grown in non-optimal conditions, with consideration of measurement , approximately corresponds to the concentration of Fe^{57} admixture in the nutrient medium and water. The significantly larger amount of Fe^{57} in the culture grown at optimal conditions, in the presence of D_2O and Mn^{55} is a result of low-temperature nuclear reaction of Mn^{55} transmutation into Fe^{57} taking place in this culture. The transmutation coeffitient equals

$$\lambda_a = N_a/N_0\Delta t = (1.9\pm0.52).10^{-8}\ Fe^{57} \text{ nuclei per s and per single } Mn^{55} \text{ nucleus.}$$

The similar results were obtained during the growing of other cultures in optimal conditions. In some cases (for example, for ***Deinococcus radiodurans***) the structure of Mossbauer resonanse for created Fe^{57} in grown culture has a form of doublet, what corresponds to spatial or phase structure of the substance. Fig. 3a, 3b presents the results of investigation of Mossbauer spectrum of culture ***Deinococcus radiodurans*** in optimal medium (D_2O with $MnSO_4$). For case 3a

$$N = 2\eta S(1+p)/\sigma_0 f$$

and $p_{3a}\approx3.4$, $\eta_{2a}=(1.53\pm0.57).10^{-3}$, $N_{3a}=(0.59\pm0.21).10^{16}$, $m_{3a}=(0.67\pm0.24).10^{-6}$g,

$$\lambda_{3a} = (1.3\pm0.46).10^{-8}\ s^{-1} \text{ per single } Mn^{55} \text{ atom.}$$

It is necessary to point out that the average power

$$\langle P_a \rangle \approx N_a\,[M(Mn^{55}) + M(d^2) - M(Fe^{57})]\,c^2/\Delta t$$

that is produced in the process of reaction $Mn^{55}+d^2=Fe^{57}$ is small and doesn't exceed 50 mW per total volume $V=10cm^3$ of nutrient medium with growing culture (here $M(Mn^{55})$, $M(d^2)$, $M(Fe^{57})$ - mass of nucleus Mn^{55}, d^2 and Fe^{57}).

As a result of connecting the main experiments 2a, 3a, 3b and control experiments 2b,2c (nonoptimal nutrient medium ingradients on the basis of H_2O with $MnSO_4$ and on the basis of D_2O without $MnSO_4$) one can say:

1) in D_2O there isn't admixture Fe^{57};

2) in sugar-solt components of nutrient medium there is no Fe^{57};

3) during the growing of cultur Fe^{57} isn't extrated from the glass of flask.

One of the theoretically possible effects causing the appearance of absorption peak in cultures grown in the medium with D_2O and $MnSO_4$ (and absence of this peak in control experiments), could be connected with possible splitting of Mossbauer line due to Fe^{57} admixtures in experiments 2b (H_2O with $MnSO_4$) and 2c (D_2O without $MnSO_4$) and localization (narrowing) of this line (with its increasing) in the main experiments 2a, 3a, 3b (D_2O with $MnSO_4$). To ensure that such effect doesn't take place the additional control experiments were performed, when small amounts of Fe^{57} were added to media 2b and 2c. These experiments (the results presented on fig. 3c) with culture ***Deinococcus radiodurans*** have shown that the appearing resonances of absorption by their width and energy approximately correspond to the cases 3a and 3b. Therefore the appearance of absorption resonance on Fe^{57} in main experiments is not connected with elimination (transformation) of hyperfine splitting and redistribution of resonance line positions, but manifests the appearance of Fe^{57}, which is absent in the control experiments.

Concluding the mentioned results and discussion of the experiments, we can state, that creation of Fe^{57} isotope as a result of nuclear transmutation in growing biological medium was observed and verified using precise Mossbauer spectroscopy methods.

4. Theoretical model

In conclusion let's consider briefly the possible mechanisms of nuclei interaction, contributing to effective nuclear transmutation reaction with formation of Fe^{57} isotope.

Obviously, no modification of micro-accelerating mechanisms connected with formation of microcrack, accelerating plasma waves and similar processes can take place in a liquid nutrient medium. It is also evident that tunneling quantum processes can't provide a great probability of nuclear transmutation. We assume that the most effective action in this case would be the one provided by the mechanism suggested in [2] (and in [3]), which is capable of providing a short-term elimination of the Coulomb barrier of the pair reaction in micro-potential hole with the structure that is close to parabolic. In such holes the structure of quantum levels is equidistant and characterized by the spectrum

$$E_n=\hbar\omega_0(n+3/2),\ n=0,\ 1,\ 2,\ldots$$

Let the Mn atom be in the center of such a hole. Due to dissociation processes, high-hydrous compound has a great quantity of free d-deutons (at T = 300 K dissociation probability is $\eta\approx10^{-10}$). When a deuton gets into the hole due to diffusion, a complex Mn+d appears in the hole. In the free space this complex would correspond to quasimolecule $(MnD)^+$. In the

Transmutation

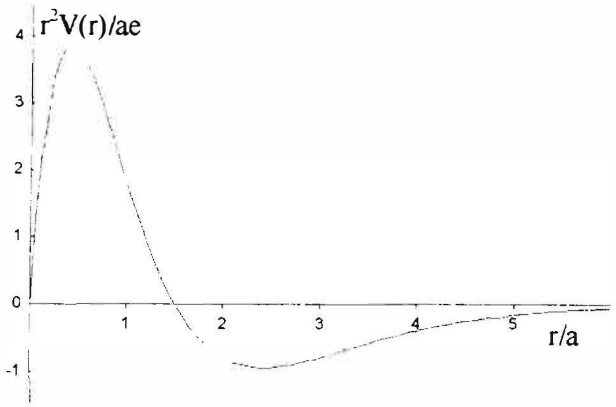

Fig. 4. Structure of interaction energy $r^2V(r)$ in system Mn-d.

quantum system the situation is more complicated.

The matter is that in such a system energy of nucleus interaction V(r) is a sign-variable distance function (see fig. 4 for a plot of function $r^2V(r)$ which is important for calculation of diagonal matrix elements). For distances $r \geq a \equiv \hbar^2/me^2$ this energy V(r) is similar to the energy of p-e-d system and $V(r) < 0$. In the region of intermediate distances $a/Z < r < a$ this energy is defined by the Thomas-Fermi approximation

$$V(r) = \frac{Ze^2}{r}\chi\left(rZ^{1/3}/0.885a\right) \text{ and } V(r) > 0.$$

In the region of small distances $r < a/Z$ nucleus interaction corresponds to pure Coulomb repulsion of bare nuclei and $V(r) = Ze^2/r > 0$.

Can this energy be a small amendment and not influence the character of nuclei movement in quantum system?

For that purpose, the diagonal elements of interaction energy matrix should be small and probability of interlayer transition because of this interaction should also be small.

Probability of interlayer transition in the regarded parabolic potential becomes equal to zero automatically at the moment $\tau = 2s\pi/\omega_0, s = 1,2,3\ldots$, when frequencies of all possible interlayer transitions $\omega_{nk} = (n-k)\omega_0$ will correspond to zeroes of spectral density of perturbation energy (see fig. 5)

$$|V(\omega)|^2 = \left|\int_0^{\tau} V_{nk}(t)\exp(i\omega t)\,dt\right|^2 = V_{nk}[\sin(\omega\tau/2)/(\omega/2)]^2$$

Here nucleus interaction completely disappears and deuton wave function is determined only

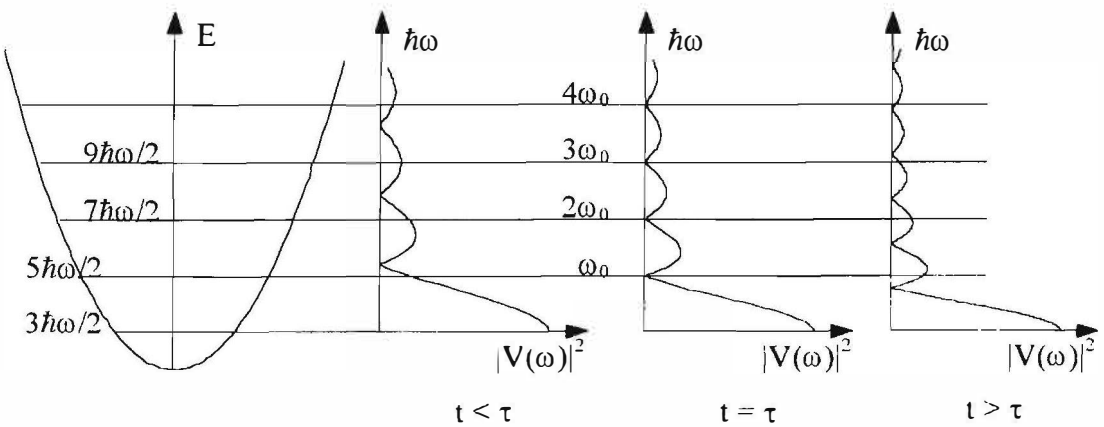

Fig. 5. Correlation between energy spectrum of quantum levels E_n and spectral density $|V(\omega)|^2$ of perturbation energy V(t) for $t < \tau$, $t = \tau$, $t > \tau$.

by quantum potential field properties.

For zeroing of diagonal matrix elements of interaction energy (which is a sign-variable function of inter-nucleus distance)

$$V_{nn} = \int 4\pi |\psi_n(r)|^2 V(r) r^2 dr$$

it is essential that the size of the hole be optimal. In the paper [2] it is shown that in case of d-e-d system this size corresponds to $2R \approx 3A$ and the optimal slope of the walls of the hole is $U_{max}/R^2 \approx 0.1 eV/A^2$. For the system Mn-d this size is $2R \approx 8A$.

If all the above-mentioned conditions are met, the independent from Mn quantizing of the deuton in the hole takes place. In this case the wave function of deuton $\psi_n(0)$ in all even states will be different from zero in the center of the hole, where the Mn nucleus is located. This leads to a high probability of nuclear fusion, $\lambda = C|\psi_n(0)|^2$, C - constant of purely nuclear Mn^{55}-d^2 interaction.

As it can be seen from the given scenario of the process, quantizing structures of optimal size and shape are necessary for such non-barrier nucleus interaction [4]. The exact parameters of these structures are very hard to calculate. The situation substantially improves when the hole parameters are slowly changing inevitably passing through optimal value. This situation is realized in growing microbiological cultures. In the growth process the replication of DNA and other biomolecules takes place. In this case in the field of growth inter-atomic potential holes with slowly changing sizes are consistently appearing. If a Mn atom and a deuton are in such a changing hole, conditions for a new Fe^{57} isotope fusion will be created.

We believe that the given mechanism completely describes the basic properties of the process of nuclear transmutation, which is observed in experimental course.

References.

1. H. Komaki. Frontiers of Cold Fusion (Proc. Third International Conference on Cold Fusion) (Nagoya, October 1992), Ed. H. Ikegami (Universal Academy Press, 1993), p.555.

2. V.I.Vysotskii. Proc. Fourth International Conference on Cold Fusion (Lahaina, Hawaii, December 1993), Ed. T.O.Passell (EPRI, 1994), v. 4, p. 20-1.

3. V.I.Vysotskii, R.N.Kuz'min. Intern. Symposium "Cold Fusion and Advanced Energy Sources" (Minsk,1994), Ed.H.Fox, 1994, p. 288.

4. V.I.Vysotskii, A.A.Kornilova, I.I.Samoylenko. Vestnik novikh meditsinskih tekhnologii (in Rusian) (Bulletin of new medical technologies), v.3, n.1, p. 28 (1996)

COLD FUSION ACTIVITIES IN RUSSIA

Nikolai Samsonenko

Russian Peoples' Friendship University
119198 Moscow, Miklukho-Maklaya str., 6, Russia

Vladimir Tsarev

Lebedev Physical Institute, Russian Academy of Sciences
117924 Moscow, Leninsky Prospect 53, Russia

Abstract

A review of Cold Fusion researches in Russia during last two years is presented.

1. Introduction

Four years ago at the Nagoya ICCF4 one of us (V.T.) described the decay of the USSR and a new geography of CF studies in the ex-Soviet Union [1].

Unfortunately all "final state products" of the decay, the new independent countries, are still in the "excited state". There is no stabilization of the economy, and as a result nowadays our society does not want or is unable to support our science properly. Since 1991 the number of scientists in our country reduced 3.5 times. Nevertheless our CF community is still alive and active. In the period of 1993-1996 four Conferences on CF have been organized in Russia with participation of scientists from other former Soviet republics and France, Italy, Japan, Spain and USA (see Table 1).

Table 1

Title of Conf.	1st (and last) All-Union CF Conf.	1st Russian CF Conf.	2nd Russian CF Conf.	3rd Russian CF Conf.	4th Russian CF Conf.
Place	Dubna JINR	Abrau-Durso Novorossiisk	Burevestnik Sochi	Dagomys Sochi	Dagomys Sochi
Date	March 1991	September 1993	September 1994	October 1995	May 1996
Number of participants	117	42	44	39	30

The modest number of participants last years is due to the poor financial support and a scanty salaries of Russian scientists, which is often even not payed at all. In 1990 at Como ICCF2 the results of more than 80 papers from about 45 Russian Institutes and laboratories have been presented [1]. In 1992 at Nagoya ICCF3 these numbers were about four times less. Almost the same situation is at present. There are now about 15 Institutes where enthusiasts of CF carry out their researches usually without any financial support. The total number of Russian papers submitted to the ICCF6 or published just before the Conference is about 25. It is impossible to discuss all of them in this report in detail. Luckily many of them are presented at this Conference. Thus the main aim of this review is to show a landscape of Russian CF activity and to mention some of the recent results, which have not been submitted to the ICCF6.

2. Experimental results

2.1. CF in gas discharge.

The most ambitious results are presented by two research groups from "LUCH" (Podolsk, Moscow District), which are continuing their studies of CF with gas discharge.

Romodanov et al. [2] carry out mainly tritium measurements. During the last few years they accumulated the following evidences from experiments with metallic cathodes: (a) the rate of nuclear reactions in condensed matter for deuterium ion energy range 10-10^4 eV exceeds the calculated rate of the ordinary thermonuclear fusion reactions by several orders of magnitude, (b) the neutron-to-tritium branching ratio is less than 10^{-7}, (c) the rate of nuclear reactions is increasing with increasing the atomic number of target and with concentration of hydrogen in deuterium, (d) the energy dependence of tritium yield has a threshold at about 100 eV of deuteron energy, (e) the linear dependence of the tritium production rate R upon ion current density j is observed (see Fig. 1), (f) the "nuclear interaction coefficient" Q (the number of tritium atoms produced per one deuterium ion) as a function of plasma gas pressure has a maximum in the range of 1000-3000 Pa.

In experiment with ceramic targets (TiC, VC, ZrC, ZrN, ZrB_2, LaB_6) this group measured both tritium production and gamma ray radiation. They reported rather large tritium production rate of (3.6-3.9) 10^7 T/s for ZrB_2 cathode in the temperature interval 1650-2240 K. The rate of gamma emission was very low: less than 10-1000 1/s, so the ratio gamma/T was less than 10^{-4} - 10^{-6}.

This group also studied tritium generation at transfusion of hydrogen isotopes through the target during plasma glow discharge. For V, Nb, Ta cathodes deuterium transfusion did not produce any detectable effect on the tritium production rate R. For Mo cathode it led to about 2 times increase in R. For the same cathode the hydrogen transfusion resulted in decrease of R.

The other group (Karabut, Savvatimova et al.) measured both transmutation phenomenon and excess heat generation in gas discharge [3]. In Pd cathode after irradiation by D, H, Ar, Xe ions in glow discharge they observed many new elements: Na, Mg, Ti, Fe, Ni, Cu, Rb, Zr, Nb, Ag, etc. with relative concentration 10^{-6} - 10^{-8} of the matrix element (Fig. 2). The amount of new elements was shown depending upon the kind of gas used: it was the largest for D and the smallest for Ar and Xe.

In the other experiment they used the continuous flow calorimeter to measure heat effect, and various detectors to record reaction products. The results are: (a) excess heat up to 20W with $\Delta Q/Q$=115-190%, (b) neutron emission, (c) gamma emission with energies 100-3000 keV up to 1000 sec after switching off the current, (d) beta emission from the samples with energy 1-1000 keV and intensity of (1-10)/s. These effects were found correlating with production of stable isotopes up to 10^{16} - 10^{17} atoms during 10^4sec run, and with atomic mass numbers from 4 to 140.

The new results with glow discharge have been also presented by the group from the Tomsk Polytechnical Institute [4]. In the series of their experiments samples of Ni, Nb, Pd, Ti and stainless steel were stimulated with D or H ions by glow discharge, HRF discharge or electrolysis of D_2O+LiOD. Neutron signals of up to 100 times the background level and acoustic signals were recorded intermittently. Specific feature of the experiment is "after switch-off" detection of signals of gamma and phonons 40 s to 10 min after the switch-off the discharge voltage with no neutrons at all.

2.2 Nuclear phenomena in deuterated ferroelectrics.

The idea of using strong electric field of ferroelectrics (FE) was proposed in [5], and later specified [6] in the form of polarization reversal. Last years FE became popular materials in CF studies in Russia.

In experiment performed at the Russian Peoples' Friendship University in collaboration with the

Russian Activities

Theoretical Physics Department of the Russian Academy of Sciences [7] $LiTaO_3$ and DTGS crystals $(ND_2CD_2COOD)3D_2SO_4$ were used. After preparation by degassing at 450-500°C in a vacuum of 10^{-5} Torr, the samples were saturated with deuterium at a pressure of 0.6-1.2 atm. The deuterated samples were subjected to a.c. field at operated time of 10 min and total neutron yield was recorded. The control experiment consisted in the neutron background detection before, during and after operating cycles. The neutron emission activity of $LiTaO_3$ sample was found to be (0.30 ± 0.12)n/s for the thick (10x10x5mm) and (0.49 ± 0.17)n/s for the thin (5x5x1mm) samples (Fig.3). This corresponds to the fusion rate of $(6.0 \pm 2.4)10^{-22}$ and $(7.8 \pm 1.4)10^{-21}$ reactions per second for the thick and the thin samples respectively, the higher rate being seemingly due to higher electric field (70kV/cm) which is more favorable for polarization reversal.

The group of the Institute of Physical Chemistry presented results on the experimental study of the influence of thermal neutron background level, D-H substitution and crystal mass on a neutron emission intensity in ferroelectrics in the vicinity of the Curie temperature T_c [8]. About 40 thermal cycles were done with DKDP crystals (DTGS) near T_c, and a decrease and an increase of the neutron emission was measured at different phases of the cycle (Fig4). A remarkable phenomenon, the shift of T_c by 4°C under irradiation by a very weak neutron flux (0.1-10n/cm^2 s) was reported.

2.3 CF in tungsten-bronze structure and in protonic conductors.

The group from the Institute of High-Temperature Electrochemistry (Ekaterinburg) submitted to the Conference the following results [9].

(a) Using X-ray measurements before and after the experiment they claimed the observation a correlation between neutron activity of the Na_xWO_3 samples and their structural changes. The neutron signals were detected only in those samples, where changes from perfect to mosaic structure have been found in the surface layer after the experiment.

(b) They also confirmed the earlier results of the Liaw's group on excess heat generation in the electrolysis of molten salt eutectics. The specific feature of this experiment was parallel electrolysis in two cells: one with LiD and another with LiH, which allows them to measure the temperature difference in D- and H-electrodes. The excess heat was found at elevation of current density from 4 mA to 290 or 420 mA.

(c) Electrolysis in D and H atmosphere at elevated temperature (200-800 C) was studied with SrCeO3 ceramic tablets. An excess heat $\Delta Q/Q_{in}$ = 10-1000% was measured in correlation with phase transition. However, the absolute value of the excess power was very small $\Delta P = 2 \cdot 10^{-3}$ W), which may rise some preoccupations.

Some new results on CF with Na_xWO_3 have been also reported recently at the RCCFNT4 [10]. In this experiment the single crystal multi-layers (1mkm thickness) of Na_xWO_3 (x=0.8 to 0.9) were deposited on the surface of tungsten wire of a diameter 200 mkm from Na_2WO_4+WO3 melt at a high temperature. For loading of these structured films with sufficient value of deuterium this wire was dragging out at a very small velocity through the electrolyte with a heavy water. Neutron bursts of 20-25 neutrons were measured.

2.4 CF studies during electrolysis.

The Lebedev Physical Institute group have investigated particle emission from PdO-Pd-PdO and PdO-Pd-Ag samples [11], prepared and electrolytically loaded with D or H in the Institute of Physical Chemistry.The main feature of this experiment was the study of charged particles emission by 3 different methods: a) by plastic scintillation detector, b) by CR-39 plastic track detector, and c) by Si-SSD. The proton and neutron emission were observed in the process of deuterium escaping from deuterized samples (see an example of the signal in Si-SSD in Fig.5).

The ratio of proton-like and neutron-like events was estimated as about 1. The charged particle emission was also observed in the experiments with light water, when hydrogen was escaping from hydrogenized samples. These particles may be interpreted as protons and/or alpha-particles. The influence of the weak thermal neutron flux (emitted by Cf-source throughout a moderator) on "CF" process in the samples loaded with D was also investigated, and the fast neutron flux emitted from deuterized samples exposed by thermal neutrons was found to be 300 times more of unexposed samples.

The emission of neutrons and gamma were observed by the "Erzion" Center group (Moscow) in solution H_2O+1.5M LiOD with Ti, Ni, and Zr cathodes, and Pt anode [12].

The other group [4] detected neutrons, gamma and acoustic signals during electrolysis of D_2O on Ni and stainless steel cathodes. In some cases the correlation between the signals was recorded.

The influence of tritium on hard emission generation during electrolysis of heavy water on Pd cathode was studied by the group from Semenov Institute of Chemical Physics [13]. The presence of tritium in the electrolyte was found resulting in sharp increase of hard emission (mainly neutrons) in comparison with the experiments without tritium, which is attributed by the authors to the CF reaction T + D --> He + n. The full reproducibility of the results is claimed.

2.5. **Miscellaneous.**

(a) Nuclear transmutation of isotopes in growing biological cultures was reported by the collaboration of Kiev Shevchenko University, Moscow State University and Gamaleya Institute of Epidemiology and Microbiology [14]. They claimed the CF transmutation Mn55--> Fe57 in nutrient medium based on a heavy water.

(b) The other amazing result reported by the Kiev group [15] is the "Discovery of the phenomenon of controlling and changing probability and time of spontaneous decay and gamma-transmutation of excited nuclear states". Both results are too puzzling to comment them.

(c) Transmutation of elements via nuclear mechanofusion. In an experiment of the Institute of Physical Chemistry group [16] graphite powder with and without 5% H_2O or 5% D_2O was rotated in a drum containing stainless steel balls. An increase of C^{14} concentration was recorded. The other group from the Russian Peoples' Friendship University failed to detect neutron emission in experiment with mechanical demolition of deuterated ferroelectrics [17].

(d) A large collaboration of 5 research groups ("Erzion", "Vizor", "Energiya", Institute of Physical Chemistry, Institute of Nuclear Physics of Moscow State University) has done a series of experiments with the hydro-aggregate "Yusmar" [18]. Electrolytic solutions H_2O+(LIOH,D_2O, H_2SO_4) and organic solutions were compressed cyclically with different periods of time. Tritium excess [(5.0 ± 0.7)Bq/ml], neutrons up to (304 ± 21)n/2.5h and radiocarbon excess [(3.0 ± 0.03)Bq/ml after 1.5h were registered during the aggregate running.

3. **Theory**

All published models aimed to understand the CF phenomena are based on some assumptions. Depending on how much radical these assumptions are we will divide (somehow arbitrary) theoretical papers on CF, published recently by Russian authors, into three categories.

Three papers published last year by the Lebedev Physical Institute group [19] fall into the first category being based on well known phenomena. In the first one the authors call attention to some physical phenomena related to nonlinear influence of electric field on current carrier mobility, which could manifest themselves in CF experiment. Similar phenomena are well known in gas and semiconductor plasma physics. In electrolytic or gas discharge experiments they could result both in heat effects and triggering off nuclear reactions in highly loaded hydrides. The arguments are presented that at high x>1 PdH_x can transform into a new phase with semimetallic (semiconducting) properties. It is shown that in this case the negative differential conductivity can

arise leading to various current instabilities of the Gunn-effect type, current filamentation, pinch effect, etc. which could initiate nuclear reactions due to the ion acceleration or current compression, and also imitate excess heat effects.

In the second paper it is emphasized that all CF experiments with ferroelectrics have been carried out so far in far from being optimal conditions, and some possibilities to increase the reaction rate are suggested. The conditions are indicated under which strong electric field in ferroelectrics can exist over large distances (10^{-4} cm) producing very effective ion acceleration.

The third paper shows the possibility of nonequilibrium heating of electron and vibration degrees of freedom of crystals and heterogeneous solids during pulsed laser pumping. In this case the effective temperature for selected modes may exceed 10^9 K. Changing of some properties of solids is expected. Possible applications include: laser "cleaning" of crystals off defects produced during crystallization process, heterogeneous catalysis of solid state chemical reactions and diffusion processes, and possibly the initiation of nuclear reactions in solids.

The less orthodox claims are presented in the second group of papers.

An explicit non-relativistic analysis of the Barut-Vigier model is presented in [20]. The model is based on the assumption of existence of a new "tight" quantum orbit in the hydrogen atom with energy of few keV.This orbit is confirmed in [20] using the approximation which neglects the anomalous magnetic moment of particles.

In [21] the origin of CF is attributed to some hypothetical nuclear-chemical transformations involving electron capture by deuteron with formation of "bineutron", or three-particle electron capture with participation of D and H nuclei. The solid state matrix acts as a nonlinear active medium, and CF occurs presumably in "submicrocracks".

Yu.Bazhutov et al. continue to develop various aspects of their "erzion" model. (The "erzion" is a hypothetical heavy stable particle which could catalyze CF). In the new papers [22] they discuss transmutation of elements in radioactive wastes of nuclear reactors and conclude that nearly all radionuclides may be utilized. The other paper deals with the catalytic nuclear transmutation, ball-lighting and some other anomalous geophysical phenomena, which according to the authors, could be explained by "erzion".

And finally, the most radical approach to the CF explanation is presented by L.Sapogin [23]. It is based on his earlier research in the field of unitary quantum theory. A particle is described not as a point-like object as in conventional quantum mechanics, but as a wave packet. It periodically spreads out across the space (disappears) and assembles (appears), the envelope of the process coinciding with the conventional quantum mechanics wave function. On this basis the author is able to explain the tunnel effect, the suppression of the proton channel in CF, the excess energy and nuclear transmutation.

4. Conclusion

In spite of considerable efforts during 7 years after the first announcement, CF still remains to be rather illusive. This is especially relevant to the "on-line" registration of nuclear products (neutrons, protons, gamma). Neutron bursts are now doubtful. Other signals are reported typically at the level of less than 1.5-2 times the background. The experiments reported by two groups from "Luch" with accumulation of tritium and transmuted elements seem to be the most powerful , reproducible and clear (many standard deviation above the background level) proof of CF. However, the attempts to replicate these results by P.Hagelstein's group from MIT failed for 3 years.Well, one can say that both Russian groups have a 20-year experience in glow discharge experiments. But the consulting with an ex-Luch expert, Dr. Ya.Kucherov, did not helped to solve the problem. (P.Hagelstein, private communication). During the Conference the negotiations started on a possible collaboration between Hagelstein's and Romodanov's groups, which hopefully may bring a

conclusive result. The situation in theory is also unclear. No theoretical formulation of CF has succeeded so far in quantitatively or even qualitatively description of reported experimental results. But some new claims have been presented and it remains to verify how justified they are. In any case this activity could clarify many problems related to CF and beyond and may initiate new experimental approaches.

Acknowledgements.

One of us (V.T.) would like to thank the Organizing Committee of the ICCF6 for financial support, and Physical Department of Kochi University for hospitality during preparation of this report.

References

1. V.A.Tsarev, Proc. ICCF2, Como, 1991, 319; Proc. ICCF3, Nagoya, 1992.
2. V.A.Romodanov et al., papers P-045, P-070, P-071 submitted to this Conference.
3. A.B.Karabut et al., papers P-001, P-002, P-003, P-067 submitted to this Conference.
4. I.Chernov et al., reports at the RCCFNT3 and RCCFNT4, see Reviews H.Kozima, Cold Fusion 15, 18 (1995), Cold Fusion, 1996.
5. P.I.Golubnichii et al., Dokladi Akademii Nauk 307, 99 (1989).
6. A.A.Kouticov, G.V.Fedorovich, Proc. RCCFNT2 p.133 (1994).
7. N.V.Samsonenko et al., paper submitted to this Conference.
8. A.G.Lipson et al., paper P-011 submitted to this Conference.
9. A.L.Samgin, S.V.Vakarin et al., papers O-037, P-074 submitted to this Conference.
10. K.Kaliev, V.Filimonov et al., report at the RCCFNT4 (1996).
11. A.S.Roussetski, paper P-046 submitted to this Conference.
12. Yu.N.Bazhutov et al report at the RCCFNT3 (1995) .
13. R.A.Stukan et al., High Energy Chemistry, V.30 (5) p. 343 (1996).
14. V.I.Vysotskii et al., paper TS-007 submitted to this Conference.
15. V.I.Vysotskii et al., paper TS-006 submitted to this Conference.
16. A.G.Lipson et al., Proc. RCCFNT3, p.61 (1995).
17. N.V.Samsonenko et al., report at the RCCFNT4 (1996).
18. Yu.N.Bazhutov et al., paper P-057 submitted to this Conference.
19. Yu.M.Aliev et al., Kratkie Soobsheniya po Fizike 1995, 5/6,68, G.M.Guro, V.A.Tsarev, ibid. 1995, 5/6, 62. V.S.Gorelik et al., Proc. Italian Conf. on Cold Fusion, Siena, 1995, ed. B.Stella.
20. N.V.Samsonenko et al., Phys. Lett. A220 (1996) 297.
21. S.F.Timashev Russian Journal of Physical Chemistry, V.69(8), p.1259 (1995).
22. Yu. N.Bazhutov et al., papers P-058 and P-059 submitted to this Conference.
23. L.G.Sapogin, paper P-072 submitted to this Conference.

Russian Activities

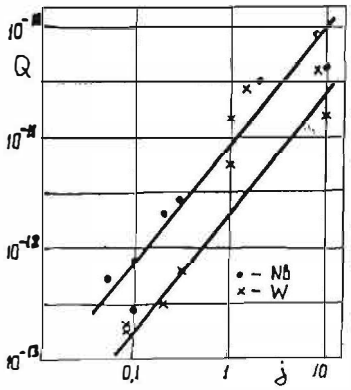

Fig.1

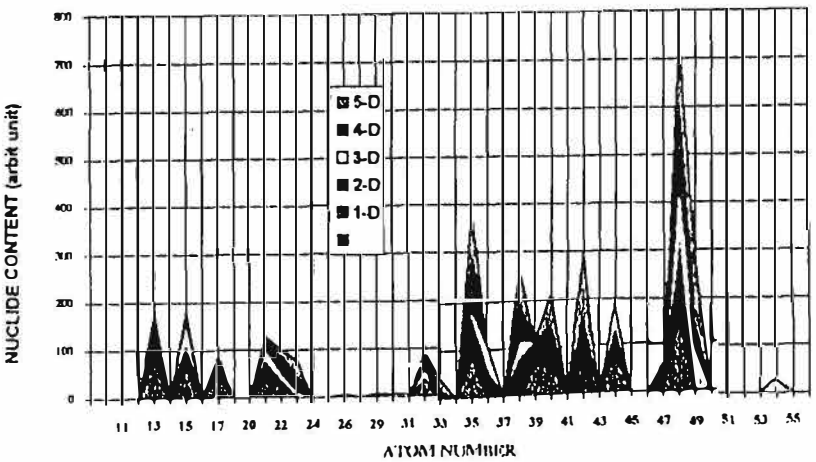

Fig.2

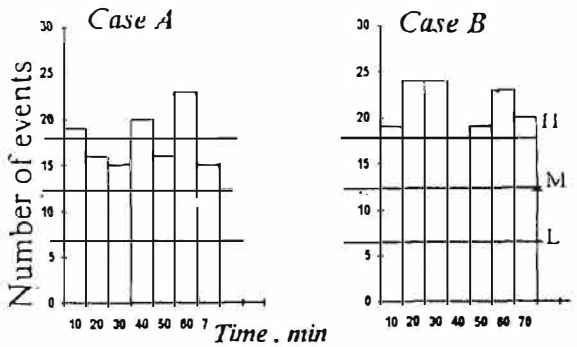

Fig.3

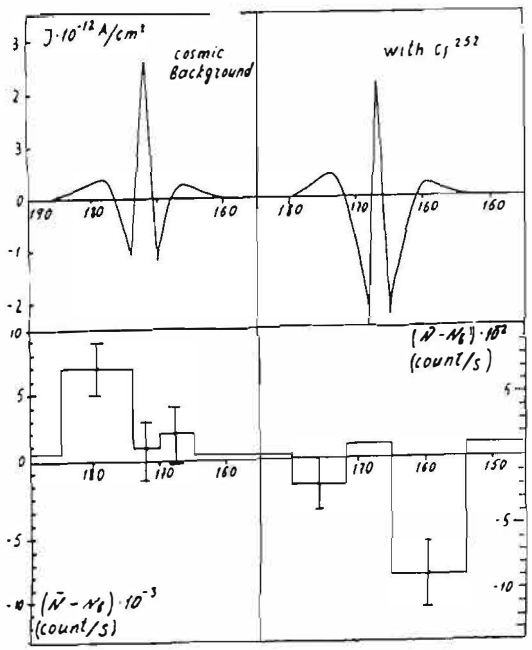

Fig.4

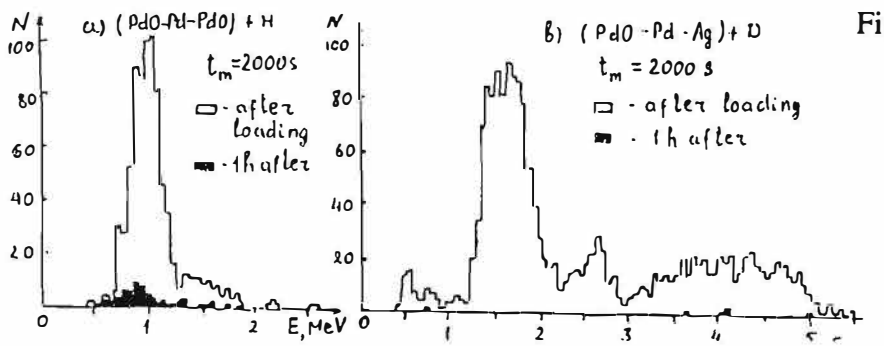

Fig.5

Fig.1 Nuclear interaction coefficient Q (atom/ion) vs j (A/cm^2) [2]
Fig.2 Concentration of new elements on Pd after irradiation by D-ions [3]
Fig.3 Number of events recorded by He^3 detector during 10 min-intervals (A-thick sample)
M - average background level, H and L - the limits of BG variation at 90% CF [7]
Fig.4 Transition the Curie temperature T_c during cooling in correlation with neutron measurements. Left - with cosmic background, right - under irradiation with Cf-source [8]
Fig.5 Signal in Si-SSD from hydrogenized (left) and deuterized (right) samples [11]

Summary

Nuclear Products in Cold Fusion Experiments Comments and remarks after ICCF–6

T. Bressani

Dipartimento di Fisica Sperimentale dell'Università degli Studi di Torino
I 10125 Torino (Italy)
and
Istituto Nazionale di Fisica Nucleare. Sezione di Torino (Italy)

1 Introduction

From the first beginning two major problems have affected the scientific development of the Cold Fusion and related phenomena. They are:

- the lack of reproducibility of most of the experimental observations (in particular the Excess Power in given conditions)
- the lack of a substantial amount of nuclear ashes that could validate the hypothesis that the sometimes observed Excess Power could be the result of nuclear reactions occurring in the metal lattice. Nuclear origin was inferred in an indirect way. by the observation that the sometimes measured Excess Powers were at least three orders of magnitude greater than those produced by any known chemical reaction.

I think that. by the time of ICCF-6. one of these two problems has been solved in a positive way. following the accepted cryterion of the scientific methodology. that is SEVERAL INDEPENDENT CONFIRMATIONS BY DIFFERENT GROUPS AT DIFFERENT LABORATORIES. The nuclear product which is observed to be emitted in correlation with the Excess Power and in quantity of the expected order of magnitude is ^{4}He.

One could ask himself why so much time elapsed before reaching such a conclusion. The main reason. to my opinion. is the experimental difficulty. coupled to the well known general discredit in which Cold Fusion was put by the majority of the scientific establishment. This circumstance discouraged a substantial part of the Groups to follow the ^{4}He detection approach.

I remind that Fleischmann. Hawkins and Pons [1] from the first beginning. noticed that the neutron and ^{3}H production in their cells. even if measured with rudimentary tools. was lower by 10^8 to 10^{10} orders of magnitude than what expected by the measurement of the Excess Heat. in the hypothesis that it was of nuclear origin. following the fusion of two deuterons. In the Pd lattice the $d + d$ fusion reaction had to proceed in a way substantially different than in free space. in which case the $(n +^3 H\epsilon)$ and $(p +^3 H)$ channels almost equally probable. are the well known final products. It must also be noticed that. from the first beginning. the channel with ^{4}He in the final state. known to occur with a frequency lower by a factor 10^{-6} with respect to

Summary

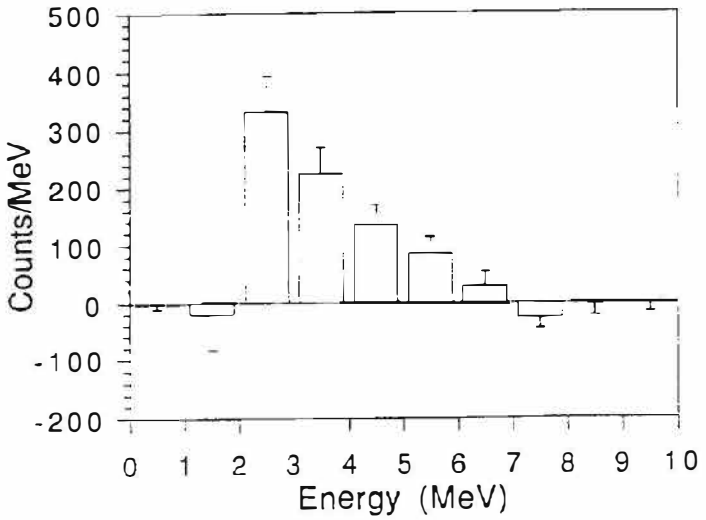

Figure 1: Neutron spectrum observed from a Ti/D_2 system. loaded in gas phase [3].

the $(n + {}^3He)$ and $(p + {}^3H)$ ones in free space. was supposed to be the most important one in $(d + d)$ fusions in a metal lattice by some authors [2].

Notwithstanding these facts. tens of experimental Groups in many Laboratories in the world started to set up in a hurry neutron detection systems. more or less sophisticated. and also. in a reduced number. ^3H detection devices. Why such a big experimental effort. in spite of the lack of observation of substantial amounts of neutron and ^3H by Fleischmann. Hawkins and Pons? The reason is quite simple. Many groups knew the techniques of neutron detection and had at home more or less complete apparatuses. Their hope was that of observing in a clear–cut way even a few neutrons (at 2.5 MeV). that were the simpler signature for ascertaining that "something nuclear" occurred in a Cold Fusion cell. The problem of the discrepancy of the orders of magnitude (10^8!) was left over. implicitely assuming that some other reaction. not producing neutrons. was responsible of the Excess Heat.

Now. after several years of experiments (more than 100) on neutrons and ^3H detection from Cold Fusion cells. quite general conclusions can be drawn. There is a weak emission of neutrons. completely unable to explain the amount of Excess Heat. with a statistical significance exceeding hardly a few standard deviations. Fig.1 shows. as an example. a neutron spectrum observed from a Ti/D_2 system. loaded in gas phase [3]. The neutron detector was constructed ad hoc for Cold Fusion experiments. not recuperated from scratch. and is rather sophisticated in controlling background and environmental effects. It is in fact based on the time–of–flight. double scattering method and incorporates the state–of–art techniques of electronics and data acquisition. The statistical significance of the signal reaches at best 5 standard deviations.

The low statistics prevented also to observe in a convincing way correlations between the weak neutron emission and the occurrence of Excess Heat. However. in some cases. correlations were reported: last examples were discussed at this Conference by Okamoto [4] and Sanchez [5].

2 Measurements of ^4He from Cold Fusion Cells

I said in the introduction that experiments on ^4He detection were started rather late. Fig.2 shows the evolution with time of dedicated experiments on ^4He production: in abscissa

Summary

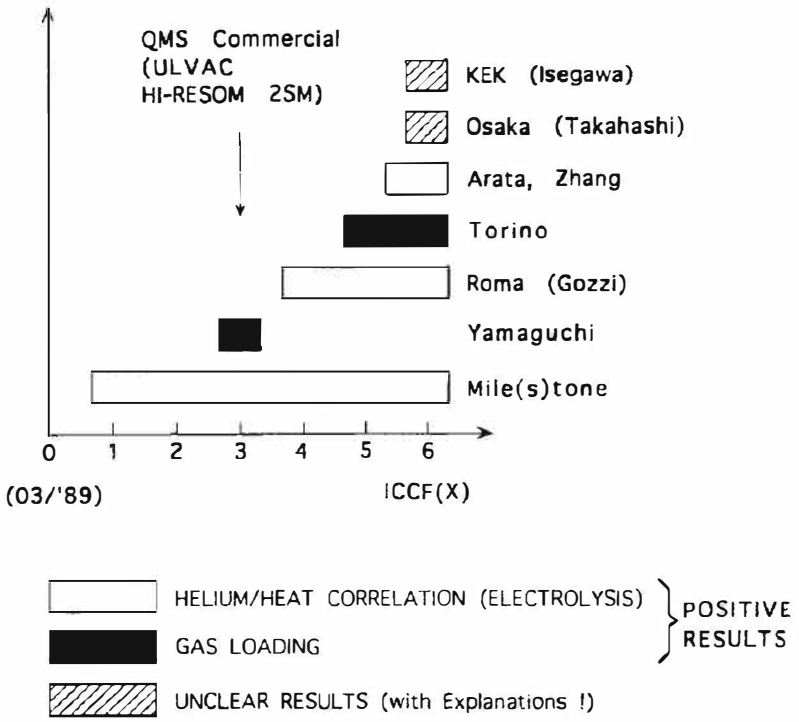

Figure 2: Evolution of dedicated experiments on ^{4}He production: the abscissa scale indicates the edition of the subsequent ICCF's held until now.

I used the time at which subsequent ICCF's were held. The time interval between each ICCF is, in average, fifteen months. At ICCF-1 (Salt Lake City, March 28-31, 1990) no dedicated experiments on ^{4}He were presented. However it is quite instructive to notice that a qualitative test at ETEC/Rockwell showed anomalous ^{4}He presence in Pd samples previously electrolysed and having produced a weak Heat Excess [6].

At ICCF-2 (Como, June 29-July 4, 1991), the first dedicated experiment on ^{4}He production was presented and discussed by Miles et al. [7]. They used open isoperibolic calorimetric cells with Pd rod cathodes in D_2O solutions. Effluent gas samples were collected in flasks and sent to the University of Texas for analysis by mass spectrometry. The results were striking. ^{4}He was observed in large quantities in experiments in which Excess Heat was measured. No ^{4}He was observed in experiments without Excess Heat or with H_2O solutions (blank). From ICCF-2 to ICCF-6 Miles et al. continued their impressive series of measurements, carried out in a sometimes hostile scientific environment, producing at the end a final report [8] which summarizes six years of experiments. Their main conclusions are: 30 of 33 experiments showed a correlation between either Excess Power and ^{4}He production or no Excess Power and no ^{4}He. The ^{4}He production rate is (10^{11}-10^{12}) He atoms/sec per watt of Excess Power, which is the correct magnitude for $d + d$ reaction that yield ^{4}He as a final product. The probability that these observations are the results of random correlations is $\sim 10^{-6}$.

At ICCF-3 (Nagoya, October 21-25, 1992) an advanced set-up for the detection of ^{4}He released from a heterostructure of Pd deuterated in gas phase was presented by Yamaguchi and Nishioka [9]. The apparatus was completely built in stainless steel pieces, avoiding glass or other materials that could induce the suspicion of contamination from atmospheric ^{4}He, and a high resolution electric quadrupole mass (Q-mass) spectrometer allowed the separation of the peaks due to $^4He^+$ and D_2^+. The measurements showed a close correlation between the production of ^{4}He and the Heat Excess released by the Pd sample (a few watt for 10^3 seconds).

Summary

and the amount of detected ^{4}He was in the order of magnitude of that expected. Unfortunately Yamaguchi and Nishioka did not continue their experiments beyond ICCF-3. I notice that a quite important fact occurred at ICCF-3. that might explain the trend of the experiments on ^{4}He detection. as shown by Fig.2: the commercialization of a relatively simple high resolution Q-mass spectrometer (ULVAC HI-RESOM 2SM). rather largely used in the following by several Groups.

At ICCF-4 (Maui. December 6-9. 1993) first results on ^{4}He content of effluent gas from electrolytic cells were presented by Gozzi et al. [10]. They used open cells with different Pd electrodes. ^{4}He was measured not "in situ" but at a nearby Laboratory. equipped with a high resolution magnetic mass spectrometer. They found a quite nice correlation between ^{4}He and Heat production. but control measurements of the $^{20}Ne^{2+}$ content in the samples. indicator of a possible contamination from atmosphere. were somehow puzzling. They continued their improvements on the apparatus. by the use of a Q-mass spectrometer directly coupled to the apparatus (ICCF-5). and results were presented at ICCF-6 [11]. I am personally very impressed by the completeness of the apparatus and the cleverness of the data handling. During the years. the apparatus of Gozzi et al. was continuously improved. adding time-by-time new detectors of nuclear ashes and new controls. At present. it is the most complete of all Cold Fusion experiments. featuring simultaneously: calorimetry. neutron. ^{3}H. ^{4}He and X-rays on-line detection. ^{4}He detection also for melted electrolysed cathodes. complete control of all possible sources of contamination (atmospheric He). Owing to this unique potentiality. Gozzi et al. tried to obtain not only a Yes/No correlation between ^{4}He and Excess Heat. which is quite good in their experiments. but also a time correlation between the evolution of these two quantities. This goal required a lot of experimental efforts and the preliminary results show an indication of a time correlation. even though not yet completely established. Incidentally. I notice that at ICCF-6 Gozzi et al. reported a very convincing measurement of hard X-ray emission. a clear-cut proof that a nuclear phenomenon is at work.

At ICCF-5 (Monte Carlo. April 9-13. 1995) a new experiment (Botta et al. [12]) entered in the arena of ^{4}He apparatuses. The set-up is dedicated to the on-line measurement of ^{4}He from Pd. loaded with D_2 in gas phase. The loading ratio is enhanced by electromigration: measured values of α up to 0.83 were reported. The entire apparatus is made of stainless steel to avoid atmospheric contamination. with on-line careful controls at all the stages of the experiment. Evidence for ^{4}He production was reported. but the results were affected by a quite large value of background. In the following year the set-up was improved. in particular the gas sampling could be performed by the Q-mass spectrometer in static vacuum conditions instead of with the turbomolecular pump on. and at ICCF-6 a quite impressive result was reported (see Fig.3) [13]. A peak corresponding to $^4He^+$ is clearly observed after several days of D_2 loading. enhanced by electromigration. The amount of produced ^{4}He is large: $(5.3\pm0.2)\times10^{18}$ atoms. Unfortunately no correlated calorimetric measurement was done.

At ICCF-6 (Toya. Hokkaido. 13-18 October. 1996) three new groups using ^{4}He detection by Q-mass spectrometer reported their results. The experiment of Arata and Zhang is really impressive for cleverness and completeness [14]. They use closed electrolytic cells with special cathodes (Pd fine powder). Considerable amounts of Excess Heat are measured by careful calorimetry and several runs with D_2O and H_2O (blanks) were performed. The produced ^{4}He. which was supposed to reside in the Pd cathodes. was thermally desorbed at high temperatures (1300 K) in a sealed-off apparatus including two Q-mass spectrometers. reference samples for ^{4}He and D^+ and getter pumps to lower the D_2 percentage of the gas composition. The two Q-mass spectrometers were set around the masses 3 and 4 respectively in order to determine the time evolution of the $^4He^+$ and D_2^+ and HD^+ ions. the last two lowered by the getter pump

Summary

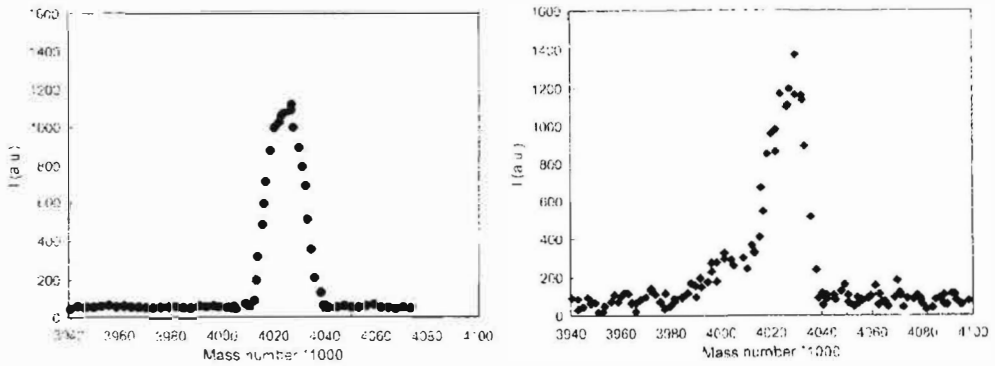

Figure 3: Spectra of "mass 4" gases as measured by the Q mass. Left: spectrum at the beginning of the experiment: only the peak corresponding to D_2^+ is visible. Right: spectrum at the end of the experiment: a second peak, corresponding to $^4He^+$ is clearly visible.

action. This control was very effective in obtaining the certitude that $^4He^+$ was really desorbed by the electrolysed Pd. No $^4He^+$ was measured in blank runs.

Yasuda et al. [15] presented at ICCF-6 a quite complete set-up. They use closed electrolytic cells, with on-line measurement of Heat Excess, loading ratio of the cathodes and neutron emission. Production of ^3H and ^4He is measured off line, by sampling. Correlation of ^4He production with Excess Heat was not clearly ascertained, but the authors underlined some calibration problems of their spectrometer, operative since a short time.

Isagawa et al. [16] too presented a quite complete set-up. They use open type cells: Heat Excess, neutron, ^3H and ^4He emission were measured. A large amount of ^4He was detected with a Pd sample heated above 1000°C. The authors cannot avoid however that it is due to permeation from air.

3 Conclusions and Perspectives

Production of large amounts of ^4He, whose order of magnitude is compatible with that expected in the hypothesis of Excess Heat due to $(d + d)$ fusion was measured by at least five different experimental Groups. Four of them report also a convincing evidence of the correlation of ^4He production with the Excess Power. All the Groups working on ^4He production are well experienced in Cold Fusion experimental research, being active from the first beginning. The different settings are quite complete and expensive (from 0.5 to 1 Million of U.S. $): apparently those Groups did not suffer from severe budgetary cuts from the funding agencies. A further remark concerns the order of magnitude of ^4He production. Since the ^4He detection device (Q-mass spectrometer) works on a minimun ionization current, not on single particle counting like neutron and ^3H detection, it is clear that a current signal, when observed, corresponds to a large amount of ^4He atoms. Therefore in judging the quality of the results, it is important to evaluate the signal/noise ratio. It appears to be from 10 to 100 in the different experiments.

THESE EXPERIMENTAL FACTS SEEM TO ME LARGELY ENOUGH TO CONCLUDE THAT THE EXCESS POWER RELEASED IN COLD FUSION CELLS IS OF NUCLEAR ORIGIN ($d + d \rightarrow {}^4He$ + heat).

A related conclusion is that the claims of Fleischmann, Hawkins and Pons in 1989 were substantially correct. Starting from these considerations it is important to continue vigorously

Summary

the experimental effort on ^{4}He detection with Q-mass spectrometers. To that purpose it is necessary to start a coordinated work for normalizing the procedures of operation with these devices, still quite difficult. In particular it would be necessary to agree protocols on:

- operation with dynamic or static vacuum:
- effect of getter pumps:
- precise determination of the detection sensitivity:
- precise determination of residual gases pressures
- other items.

In parallel it will be necessary to continue the experimental work necessary to solve still some open problems like, for example:

- the precise relation between ^{4}He amount and Excess Power (at present it is determined only as order of magnitude !)
- the determination of the percentage of ^{4}He directly desorbed from the electrodes during the Cold Fusion occurrence with respect to that remained in the metal.

The solution of these problems will probably convince all the Groups working on Cold Fusion to use ^{4}He detection as a standard tool in all experiments, as a sort of microcalorimetry.

I am grateful to Prof. F. Iazzi and Dr. E. Botta for their useful discussions and comments.

References

[1] M. Fleischmann, M. Hawkins and S. Pons, *J. Electromol. Chem.* **261** (1989), 301.

[2] T. Bressani, E. Del Giudice and G. Preparata, *Il Nuovo Cimento* **101 A** (1989), 845.

[3] E. Botta *et al.*, *Il Nuovo Cimento* **105 A**,11 (1992), 1663.

[4] M. Okamoto *et al.*, these Proceedings

[5] C. Sanchez *et al.*, these Proceedings

[6] D. Worledge, in Proc. of the First Annual Conference on Cold Fusion (Salt Lake City, March 28–31, 1990), 252.

[7] M. H. Miles *et al.*, in The Science of Cold Fusion (T. Bressani, E. Del Giudice and G. Preparata Editors, Società Italiana di Fisica, 1991), 363.

[8] M. H. Miles *et al.*, Rep. NAWCWPNS TP 8302 (Dept. of Navy, USA, Unclassified), September 1996.

[9] E. Yamaguchi and T. Nishioka, in Frontiers of Cold Fusion (H. Ikegami editor, Universal Academy Press, Tokyo, 1993),179.

[10] D. Gozzi *et al. J. Electroanal. Chem.* **380** (1995), 108.

[11] D. Gozzi *et al.*, these Proceedings.

[12] E. Botta *et al.* in Proc. 5th Int. Conf. on Cold Fusion (Monte Carlo, Monaco, April 9–13, 1995), 233.

Summary

[13] E. Botta *et al.*, these Proceedings.

[14] Y. Arata and Y. C. Zhang, Proc. Japan Acad., Vol. 71 (B), (1995), 304.

[15] K. Yasuda *et al.*, these Proceedings.

[16] S. Isagawa *et al.*, these Proceedings.

Appendix

Authors' Index

Authors' Index

Authors' Index

Authors' Index

First printing :	December, 11, 1996
Name of the proceedings :	Progress in New Hydrogen Energy Vol. 2
Published by :	New Energy and Industrial Technology Development Organization (NEDO) The Institute of Applied Energy (IAE)
Supported by :	The Agency of Natural Resources and Energy of the Ministry of International Trade and Industry
Edited by :	Makoto Okamoto (Tokyo Institute of Technlogy)